The University Of Sheffield.

Characterising the internalisation of theranostic agents via membrane heat shock protein 70 (Hsp70) by cancer cells using flow cytometry and image analysis platforms

Gemma Ann Foulds

Thesis submitted for the degree of Doctor of Philosophy

Academic Unit of Surgical Oncology

Department of Oncology

The Medical School, University of Sheffield

AUGUST 2015

Copyright statement

Acknowledgements

This study was only made possible by way of funding from Deutsche Forschungsgemeinschaft, as part of Sonderforschungsbereiche (SFB) Program 824 (*Imaging for the selection, monitoring and individualization of cancer therapies*), and for this I am most grateful.

I wish to thank my supervisor Professor Graham Pockley for being a source of inspiration, the best mentor I could hope for and for the time he has sacrificed to this project.

I would also like to offer particular thanks to Professor Gabriele Multhoff for her teachings, guidance, patience and assistance.

At the University of Sheffield, I give thanks to Professor Nicola Brown for her help and support especially through the final year of my time, to Dr Colin Grey for providing unrivalled microscopy tuition and to both Sue Clark and Kay Hopkinson for their training and guidance in all aspects of flow cytometry. Special mention goes to the ladies of K floor – Kim, Sapna, Abi and Rachel – for keeping me sane and for all showing me that whatever the ups and downs it is possible to reach the end of a thesis.

At the Technische Universität München I wish to thank everyone with whom I have worked over the years, with particular mention to Dr Mathias Gehrmann, Stefan Stangl and Stephanie Breuninger, not only for the technical assistance and training I have received, but for always making me so welcome in a foreign laboratory and for giving me a taste for German beer.

I thank all my family and friends for their unwavering support and encouragement, without which I doubt this process could have reached a final conclusion.

And finally I thank Alex, my wonderful partner, for his incredible support and love which has seen me through the hardest part of this writing. Be ready to get to know me without the constant stress!

Table of Contents

List of Figures

List of Tables

List of Abbreviations

ADCC Antibody-dependent cellular cytotoxicity

ALDH1 Aldehyde dehydrogenase

Bak Bcl-2 homologous antagonist/killer

Bax Bcl-2-like protein 4

Bcl B cell lymphoma 2

Bid BH3 interacting-domain death agonist

CA4P Combretastatin A-4 phosphate

CSC(s) Cancer stem cell(s)

CTLA Cytotoxic T lymphocyte-associated protein

CXCL C-X-C chemokine ligand

CXCR C-X-C chemokine receptor

DNAM DNAX-accessory molecule

ER Oestrogen receptor

FDA Food and Drug Administration

HER2 Human epidermal growth factor 2

IFN Interferon

Ig Immunoglobulin

IL Interleukin

iTreg Induced regulatory T (cell)

LAMP Lysosomal associated membrane protein

LPS Lipopolysaccharide

mAb Monoclonal antibody

MICA MHC class I polypeptide-related sequence A

MICB MHC class I polypeptide-related sequence B

MHC Major histocompatibility complex

N-CAM Neural cell adhesion molecule

NK Natural killer (cell)

nTreg Natural regulatory T (cell)

PARP Poly ADP-ribose polymerase

PBMC(s) Peripheral blood mononuclear cell(s)

PI3K Phosphoinositide 3-kinase

PR Progesterone receptor

PRR Pattern Recognition Receptor

PTEN Phosphatase and tensin homolog

STAT Signal transducer and activator of transcription

tBid truncated Bid

TGF Transforming growth factor

TLR Toll-like receptor

TNF Tumour necrosis factor

Treg Regulatory T (cell)

ULBP UL16-binding protein

uNK Uterine natural killer (cell)

VEGF Vascular endothelial growth factor

Abstract and Summary

Introduction: A unique, membrane form of the 70 kDa heat shock (stress) protein Hsp70 is expressed on large proportion of tumours and cancer cells, but not on their non-malignant counterparts. Although the expression of this membrane Hsp70 expression has been associated with poor outcome in some cancers and is associated with aggressive disease (e.g. metastatic disease), its expression is enhanced by radiation and certain chemotherapeutics and so it might serve as the basis for the development of adjunct therapeutics. Previous studies have shown that membrane Hsp70 acts as a targeting structure for activated natural killer (NK) cells, and that the NK cell cytotoxicity is mediated via the membrane Hsp70-specific uptake of NK cell-derived serine protease granzyme B. The administration of a membrane Hsp70-specific monoclonal antibody (mAb, cmHsp70.1) to animals bearing tumours expressing membrane Hsp70 reduces the growth of these tumours *in vivo* via the induction of antibody-dependent cellular cytotoxicity (ADCC). In addition, preliminary data suggest that a 14-mer Hsp70-derived peptide (TKDNNLLGRFELSG) interacts with membrane Hsp70, and this therefore provides a potential tool for tumour imaging and targeting. The mechanism, route, kinetics and consequence of cmHsp70.1 mAb, 14-mer peptide and granzyme B interaction with, and internalisation via, membrane Hsp70 have yet to be fully explored, elucidated and compared.

Aims of the Study: The aim of the study is to use imaging technology to define the kinetics and pathway of internalisation of cmHsp70.1 mAb, the TKDNNLLGRFELSG 14-mer peptide and granzyme B) with a view to better understanding their theranostic potential for targeting and imaging memHsp70^{+} breast cancer cell lines.

Experimental Approach: The binding and internalisation of fluorescently-conjugated cmHsp70.1 mAb, the Hsp70-derived TKDNNLLGRFELSG 14-mer peptide and human recombinant granzyme B by human (MDA-MB-231, MCF7, T47D) and mouse (4T1) breast cancer cell lines expressing varying degrees of memHsp70 was analysed using flow cytometry, confocal microscopy and image analysis platforms. Recombinant human granzyme B was generated using transfected HEK293 cells, purified using FPLC, and its purity and activity confirmed using Western blotting and colorimetric enzymatic activity assays. The yields of enzymatically active granzyme B were high (1-4mg/L of cell supernatant). The intracellular trafficking path taken by internalised mAb, the TKDNNLLGRFELSG 14-mer peptide and granzyme B was interrogated using novel image processing approaches that determined the uptake kinetics and quantify the co-localisation of these molecules with intracellular structures (endosomes, lysosomes and mitochondria). The influence of granzyme B on cell death-mediated events was explored by examining its impact on the expression of Annexin V and active caspase-3 expression using flow cytometric assays.

Results: All breast cancer cell lines expressed some degree of memHsp70; the level of which was higher in cells those lines which represent a more aggressive, 'likely-to-metastasise' phenotype. Cells were able to bind and internalise the cmHsp70.1 mAb, the TKDNNLLGRFELSG 14-mer peptide and granzyme B, with the amount of each being bound and internalised increasing in line with the level of memHsp70 expressed increasing. The cmHsp70.1 mAb, the TKDNNLLGRFELSG 14-mer peptide and granzyme B were internalised through a similar pathway of late and recycling endosomes (as demonstrated by co-localisation, which was observed using confocal microscopy imaging and quantified through correlative and Manders image analyses), with only a proportion co-localising with lysosomes. Visual and quantitative analyses of z-stack confocal images revealed the strong vesicular association and that the route of internalisation showed a preference for the adhered surface of cells. The latter finding suggests a link between memHsp70 and membrane reorganisation, such as that which occurs at adhesive interfaces. A proportion of the memHsp70-mediated uptake of antibody, the TKDNNLLGRFELSG 14-mer peptide and granzyme B was co-localised to the mitochondria, and this could be evidence for a specific route of internalisation which is associated with this

manner of molecular uptake. The close association of internalised granzyme B with mitochondria may offer a way for it to exert cytotoxic effects without the need for perforin.

The pathway and speed of internalisation was similar for all three molecules, thereby suggesting conservation in the mechanism of memHsp70-mediated internalisation. Although the uptake of granzyme B promoted cell death on the basis of cell numbers, viability and expression of Annexin V, it had no apparent effect on the measurable activation of caspase-3. It might therefore be that memHsp70-mediated, granzyme B-induced cell death may occur as a result of a different route of internalisation when compared to perforin-dependent uptake of granzyme B.

Discussion: Membrane Hsp70 positive breast cancer cell lines take up the cmHsp70.1 mAb, the TKDNNLLGRFELSG 14-mer peptide and granzyme B via memHsp70, and the extent of this uptake is proportional to the level of memHsp70 expression on the cell surface. The lack of memHsp70 on non-cancerous cells makes this a suitable molecular target on which to base new imaging and therapeutic strategies. The antibody or peptide could be used to deliver cytotoxic drugs as a direct therapy, or as a way of better imaging the tumour in order to allow for prognostic and/or diagnostic improvements.

Membrane Hsp70 positive breast cancers take up granzyme B, which in turn leads to cell death exhibiting apoptotic features. This could be developed as a complimentary therapeutic for use in patients undergoing standard care. Granzyme B therapy does not require an active immune system to induce apoptosis, and so its use could prove beneficial to immunocompromised patients as part of an 'adjuvant'-based approach which is used in conjunction with current therapies. It is also possible that the induction of cell death through granzyme B mediated apoptosis could in turn lead to presentation of released tumour antigens and therefore promote protective, adaptive anti-tumour immune responses.

Conclusion: Membrane Hsp70 is widely, and selectively, expressed on tumours and could therefore provide an invaluable platform on which to develop new imaging and targeted therapies for the large proportion of patients with tumours that express membrane Hsp70. This is a particularly exciting area, given that membrane Hsp70 expression is associated with aggressive disease and is highly expressed on metastatic disease. Membrane Hsp70 therefore has great potential as a platform on which to base new theranostics that can improve the management and treatment of patients with cancer.

CHAPTER ONE: Introduction

1.1 The human system and cancer

1.1.1 Anti-tumour immunity

The immune system plays an essential role in tumour surveillance and eradication. Meta-analyses conducted on published data involving almost 1 million people have revealed an increased risk of cancer in people in an immunosuppressed state [1, 2], be that as a consequence of taking immunosuppressive drugs following organ transplantation [3, 4] or due to HIV/AIDS infection [5]. This risk is more pronounced for those cancers that are driven by viral infections such human papillomavirus (HPV) infection [2] (which has a well-documented association with cervical cancer [6], but has also been implicated in oesophageal squamous carcinoma [7], non-small cell lung carcinoma [8] and non-melanoma skin cancers [9]) or Epstein-Barr virus (EBV) [1] (which is associated with a range of B and T lymphomas [10]). However, there is also evidence that some spontaneous tumours are more common in immunosuppressed individuals, including prostate, kidney, thyroid, brain and colorectal cancer [1], and also cancers of the stomach and liver [2]. Another common finding has been that the rate of commonly arising cancers of epithelial origin does not appear to correlate with an immunosuppressed state [1, 2], thereby suggesting that cancers can suppress potentially protective anti-tumour immune mechanisms.

The concept that the avoidance of the immune system by tumours might be key to their establishment and continued growth is a relatively recent one. Noticeably absent from a list of as six hallmarks of cancer which Hanahan and Weinberg proposed in a seminal paper which was published in 2000 [11] was any mention of the immune system.

- self-sufficiency in growth signals
- insensitivity to anti-growth signals
- the ability to invade tissues and metastasise
- limitless replicative potential
- sustained angiogenesis
- capacity to evade apoptosis

In a revised model published a decade after their initial proposal, Hanahan and Weinberg included an additional four traits listed below [12]:

Additional hallmarks of cancer

- deregulation of cellular energetics
- avoiding immune destruction

Enabling characteristics

- tumour-promoting inflammation
- genome instability and mutation

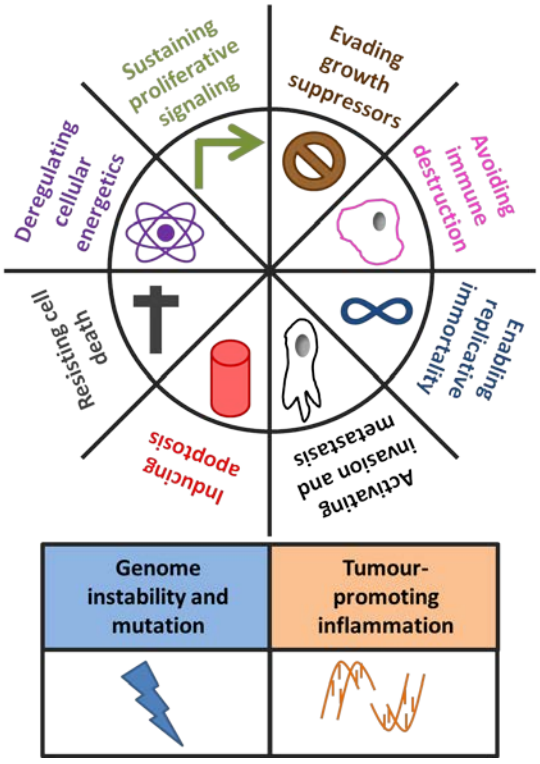

Figure 1.1 The Hallmarks of Cancer and Enabling Characteristics

The hallmarks of cancer are eight capabilities acquired during the development of human tumours. They explain the methods by which tumours can undergo their defining property of unrestricted growth. More recently proposed are the two 'enabling characteristics; traits that promote the hallmark characteristics.

Figure has been adapted from Hanahan and Weinberg [11, 12].

In response to the original hallmarks publication, and appearing at the same time as the revised version, Cavallo *et al* published their own suggestions of possible immune-based hallmarks of cancer [13]:

- withstanding a chronically inflamed environment
- evading recognition
- being able to suppress immune reactivity

The inclusion of avoidance of the immune system as one of Hanahan and Weinberg's revised Hallmarks, in addition to these traits proposed at the same time by Cavallo, demonstrate the growing recognition of the importance of tumour immunity. Having this framework defining hallmarks of cancer enables research efforts to be focussed on targeting specific features of cancer.

1.1.1.1 Role of NK cells in anti-tumour immunity

As indicated above, NK cells comprise 5-20% of human peripheral blood lymphocytes and can be categorised into distinct functional subsets based on the expression of CD56 (Neural Cell Adhesion Molecule, N-CAM) and CD16 (FcγRIII) [14]. The vast majority (~90%) of peripheral blood NK cells are $CD56^{low}CD16^{+}$. These cells are also termed effector NK cells, as they contain cytotoxic granules comprising of granzymes (cytotoxic agents) and perforin which are released to induce apoptosis in target cells. Around 10% of peripheral blood NK cells are $CD56^{high}CD16^{-}$ NK cells [15]. These NK cells are weakly cytotoxic when resting, however they obtain similar cytotoxic capabilities after activation with IL-2 or IL-12 [16]. This subset of NK cells is also a prolific producer of IFN-γ, TNF-β, GM-CSF, IL-10 and IL-13 [15]. A negligible proportion of peripheral blood NK cells (~1%) are $CD56^{high}CD16^{+}$ [17], although there is currently little insight into whether these represent a subset of cells functionally distinct from $CD56^{high}CD16^{-}$, with some publications linking all $CD56^{high}$ NK cells into one subset [15].

The traditional view of NK cell maturation proposed that different NK cell subsets comprise points along a single maturation lineage, with $CD56^{high}CD16^{-}$ NK cells becoming $CD56^{low}CD16^{+}$ via an intermediary $CD56^{high}CD16^{+}$ phenotype [17]. However, another view is that the different NK cell subsets represent endpoints of maturation lineages [15]. Observations following bone marrow transplantation in humans have demonstrated an early appearance of $CD56^{high}CD16^{-}$ NK cells, with a subsequent decline in the prevalence of this population being accompanied by a gradual emergence of $CD56^{low}CD16^{+}$ NK cells [18, 19]. Although this supports the notion that all NK subsets are derived from a single lineage, further studies are required in order to confirm if this is indeed the case.

$CD56^{high}CD16^{-}$ NK cells represent a minority population in the periphery, although this situation is reversed in lymph nodes, in which they are the predominant NK cell population (~90%) [15]. Current understanding suggests that this occurs during development rather than simply by cell migration [20]. Full details of NK cell precursors and their sites of development have yet to be totally elucidated, but knowledge is growing. Although NK cells arise from $CD34^{+}$ hematopoietic progenitor cells, the phenotype of these progenitors differs between different sites. Although the majority (>90%) of those NK cells in lymph nodes express low levels of CD34 ($CD34^{dim}$), this $CD34^{dim}$ phenotype constitutes a small minority of $CD34^{+}$ progenitor cells in blood (~6%) and bone marrow (<1%) [21]. *Ex vivo* human culture experiments have shown that $CD34^{dim}$ progenitor cells isolated from lymph nodes differentiate into $CD56^{bright}CD16^{-}$ NK cells in the presence of CD3/CD28 monoclonal antibody (mAb)-activated T cells [21], and that $CD34^{dim}$ progenitors isolated from peripheral blood and cultured with IL-2 and IL-15 also differentiate into $CD56^{bright}CD16^{-}$ NK cells [21]. Those progenitor cells expressing higher levels of CD34 ($CD34^{+}$) differentiated into $CD56^{low}CD16^{+}$ NK cells [21]. Since their activation leads to high secretion of the NK activating cytokine IFN-γ, these $CD56^{bright}CD16^{-}$ NK cells serve to maintain a pro-NK environment. This subset of NK cells constitutively express the IL-2 receptor (CD25) and are activated by T cell derived IL-2 [22], thereby providing a link between innate and adaptive immunity.

Another NK cell population is found in the uterus (uNK) and although on the basis of their surface marker expression these bear some resemblance to cytokine-releasing NK cells in the periphery ($CD56^{high}CD16^{-}$) [23], gene microarray analysis suggests that they are a distinct subtype by highlighting large increases in expression of over 200 genes in uNK cells, particularly relating to surface proteins including lectin-like receptors, killer cell Ig-like receptors and integrins [24]. The numbers of uNK cells are linked to menstruation, with only sparse numbers being found in the uteri of foetuses, neonates [25] or post-menopausal women [26]. The prevalence of uNK cells fluctuates over the uterine cycle, reaching a peak by the late secretory phase, when uNK cells can comprise 30% of all endometrial cells [27]. It is currently unclear whether uNK cells are the result of the migration and subsequent differentiation of peripheral NK cells [23, 28], or if they arise from local progenitor cells that are resident in the endometrium [29-31] - current opinion favours the latter [32]. NOD/SCID/γc^{null} mice which received subcutaneous implants of human endometrium that were in the proliferative phase of the uterine cycle, followed by 28 days of hormone administration (17β-estradiol (E_2) and progesterone) to progress the implants to the secretory phase, were found to exhibit a significant increase to $CD56^{bright}CD16^{-}$ NK cell numbers in the endometrial stroma [29]. Since NOD/SCID/γc^{null} mice lack NK cells, the observed

$CD56^{bright}CD16^{-}$ NK cells are proposed to have originated in the endometrium implant. Further evidence in support of *in situ* proliferation comes from immunohistochemical staining of human endometrium samples which found that during the secretory phase, up 40% of uNKs can be found to express the proliferation marker Ki67 [33]. uNK cells have very low cytotoxic capacity, but are prolific secretors of cytokines, including IFN-γ, TGF-β, TNF-α, IL-1β, Ang-2, PlGF, VEGF and GM-CSF [34, 35]. As for the role of NK cells in the uterus, there is no definitive conclusion as yet. Being prolific secretors of pro-angiogenic cytokines, some of which also inhibit trophoblast invasion (Ang-2, TNF-α, IFN-γ, TGF-β), it has been speculated that they have a role in aiding successful implantation and vascularisation of the embryo, and studies have attempted to find a link between uNK cells and spontaneous recurrent miscarriage. Findings have been inclusive and contradictory, with both an increase in uNK cell numbers [36, 37] and a decrease in uNK cell numbers [38, 39] being positively correlated to the occurrence of spontaneous miscarriage.

NK cell populations express a wide variety of surface receptors, the majority of which recognise ligands on the surface of potential target cells. Broadly, their surface receptors fall into one of two categories; those which trigger NK cell activation (activating receptors) and those which prevent action (inhibitory receptors). Whether an NK cell responds to a particular target cell is dependent on a balance of the signals received to the two classes of receptor. If the greatest signal comes from inhibitory receptors, then the NK cell will not respond, however if activating receptors provide the majority of the signal then the NK cell will be activated to either release cytokines or cytotoxic granules depending on NK cell type. The number of described NK receptors continues to increase, and for human cells currently stands at 22 [40]. The receptors are characterised into different groups current understanding is summarised in **Table 1.1**.

In terms of tumour immunology, a key class of NK receptors are the killer cells immunoglobulin-like receptors (KIRs). A primary ligand for these receptors is the MHC class I molecule, the binding of which provides an inhibitory signal which promotes non-reactivity to self-cells. However, given sufficient additional activation signals, NK cells are still able to kill target cells which express MHC class I. A large proportion of tumours (40-70%) either lack, or have down-regulated MHC class I expression, which can impair/prevent the clearance of tumour cells by $CD8^{+}$ T cells (as recognition of specific peptides on MHC class I is required for their activation). The effect on NK cells is simply a loss of an inhibitory ligand so, providing the tumour cells also offer some activating ligands, NK cells can kill tumour cells.

		Signal provided
C-type Lectin-like receptors	CD161	-
	CD85j	-
	KLRG1	-
	NKG2A	-
	NKG2C	+
	NKG2D	+
	NKG2E	+
	NKp65	+
	NKp80	+
Fc receptor	CD16 (FcγIIIA)	+
Glycoprotein	DNAM-1	+
Killer cells immunoglobulin-like receptors	KIR2DS1	+
	KIR2DS4	+
	KIR2DL4	+
	KIR2DL1	-
	KIR2DL2	-
	KIR2DL3	-
	KIR3DL1	-
Natural cytotoxicity receptors	NKp30	+
	NKp44	+/-
	NKp46	+
Other	2B4	+/-

Table 1.1 Examples of NK receptor family members and the signals they provide

Natural killer cells express a wide variety of surface receptors capable of binding a diverse selection of target cell ligands. The outcome of successful receptor-ligand binding results in either an activation signal (+), whereby NK cells are induced to release cytotoxic granules, or an inhibitory signal (-) where NK cells are not compelled into action. As NK cells express many receptors it is possible to recognise multiple different ligands at once, in which case the sum total of activation and inhibitory signals received will determine the NK cell action.

In addition to recognising ligands on the surface of target cells directly, NK cells can also act in conjunction with B cells via Antibody Dependent Cellular Cytotoxicity (ADCC). The high expression of CD16 (low affinity Fc receptors FcγRIIIa (CD16a) and FcγRIIIb (CD16b) by effector NK cells allows recognition of the Fc region of antibodies that are bound on the surface of potential target cells. Activation of the CD16 receptor results in the release of cytotoxic granules, in the same manner as recognition of target ligands to activating receptors, and subsequent apoptosis of the target.

Cytotoxic granules contain apoptosis-inducing serine proteases (granzymes), as well as the pore forming protein perforin. Prior to their release, the granules are held along intracellular microtubule networks. Target recognition and the subsequent formation of an immunological synapse triggers intracellular signalling which directs the polarisation of the microtubule organising centre (MTOC) and rearrangement of filamentous actin [41] in order to direct the release of granules in a highly focused locale just at the immunological synapse [42]. The majority of this process is well characterised and has been the subject of in depth review [43]. Upon first contact with target cells, the suggestion is that NK cells weakly adhere through ligation of CD2 and activation receptors [41, 44, 45], with potential involvement of molecules of the selectin family [46], although full details of this first-step interaction have not yet been fully described [43]. The next stage is a higher affinity adherence between NK cell and target cell, largely involving molecules in the integrin family [41] which contributes to NK cell activation [47, 48]. Once these initial steps are complete, reorganisation and polarisation processes take place within the NK cell. Surface receptors move to cluster at the synapse with macro-clusters of receptors observed at the site of the synapse [49]. The microtubules upon which the cytotoxic granules are held are polarised to the synapse, allowing trafficking of the granules first to the microtubule-organising centre (MTOC) and then onto the site of release. This polarisation occurs under the control of ERK (extracellular-signal-regulated kinase) phosphorylation, PYK2 (protein tyrosine kinase 2) and activation of VAV1 [50-52]. Intracellular reorganisation of F-actin mediated by Wiskott-Aldrich syndrome protein (WASP) also occurs, and this provides a final necessary step in the granule delivery network from the microtubules [50] and the creation of a channel at the plasma membrane through which granules can secreted [53, 54]. The exact mechanisms of granule docking to the plasma membrane and subsequent release remain to be fully elucidated [43].

The main constituents of cytotoxic granules are serine proteases from the granzyme family. There are five known granzymes in humans; granzyme A, B, H, K and M. Of these, the best

characterised, and also the most abundant, is the 32kDa granzyme B. It acts by preferentially cleaving at the C-terminal side of aspartic acid residues [55] and has a large number of substrates within the intrinsic apoptosis pathway (intracellularly triggered apoptosis characterised by mitochondrial membrane permeabilisation, and in contrast to the extrinsic pathway which is triggered by signalling through cell surface death receptors such as FAS). Caspase-3 was the first substrate to be identified [56, 57]. Caspase-3 exists in the inactive precursor (zymogen) form procaspase-3 and is activated as a two-stage process. Granzyme B acts in the first of these, by cleaving procaspase-3 into two subunits (p20 and p10). However, as apoptosis can occur for numerous reasons and in the absence of granzyme B, upstream molecules can also initiate this activation (caspase-8 for example).

After the initial cleavage of caspase-3, the molecule can self-catalyse p20 to p17 and become fully active [58]. Granzyme B has also been shown to act further upstream. This activates the zymogen procaspase-8 [59] which can then act to activate capsase-3. Granzyme B can also act on substrates downstream of caspase-3, including the Inhibitor of Caspase Activated DNase (ICAD) [60], poly(ADP-ribose) polymerase (PARP) [61] and the DNA-dependent protein kinase catalytic subunit (DNA-PK_{cs}) [61]. Another substrate for granzyme B is the Bcl-2 family member Bid [62], and this is also a substrate for caspase-8. After cleavage, truncated Bid (tBid) locates to the mitochondria and in conjunction with Bax and Bak results in mitochondrial membrane permeabilisation. One of the many results of mitochondrial membrane permeabilisation is the activation of caspase-3. Additionally, granzyme B has been shown capable of cleaving caspase-7 and caspase-10 [63]. It would also appear that a number of granzyme B substrates have yet to be defined, as recent protease proteomics experiments have indicated at least 20 possible substrates [64].

The next best characterised is granzyme A. Although there have been reports of granzyme A exhibiting similar perforin-dependent, apoptosis inducing effects as granzyme B [65], granzyme A has also been shown to induce non-apoptotic death that is independent of caspase activation via the direct disruption of the mitochondria and nuclear damage [66, 67]. Granzyme A does not cleave Bid and acts independently of Bcl-2 [67], but it does lead to accumulation of reactive oxygen species (ROS) and causes a loss in mitochondrial membrane potential [67]. Granzyme A is trafficked to the mitochondria via intracellular hsp27 and hsp70 and is able to cleave the mitochondrial protein NDUFS3, which triggers disruption sufficient to induce cell death [66].

The remaining granzymes (H, K and M) are much less well understood. Although they are able to mediate cell death and all are reported to induce DNA damage [68-70], there are conflicting

reports as to the mechanisms involved. For granzyme H, while reported that it is able to induce apoptosis through cleavage of Bid and the subsequent mitochondrial damage [68], other findings have shown that apoptosis can be induced through a Bcl-2 mediated pathway and in the absence of Bid cleavage [71]. Granzyme H does lead to a loss in mitochondrial membrane potential, although there is conflict as to whether this is coupled with the release of cytochrome c and activation of caspases [68] or is independent of these [72]. Granzyme K has been reported to lead to mitochondrial swelling and to depolarisation of the mitochondrial membrane, but the question of cytochrome c release with its occurrence [73] and its absence [74] being observed. With respect to caspase activation, there is consensus, with granzyme K inducing apoptosis in a caspase-independent manner [75]. Conflicting reports are also evident for granzyme M, with discussion as to whether induced cell death is caspase-independent [76] or caspase-dependent [70, 77]. Much of the study of these molecules has been conducted *in vitro*, using recombinant proteins derived in a range of sources, and this might account for at least some of the variability and apparent inconsistency of results.

Granules also contain the pore-forming protein perforin. Although perforin is commonly thought to facilitate the internalisation of granzyme B into target cells, debate surrounding its actual mechanism continues. The initial proposal was that perforin could form pores in the plasma membrane of target cells, through which granzyme B (and other lytic components of the cytotoxic granules) could pass [78, 79]. Observations that granzyme B could internalise into Jurkat and HeLa cells in the absence of perforin [80] challenged this notion and led to another suggested mechanism for the involvement of perforin. If cells that had taken up granzyme B were treated with perforin 60 minutes later, then granzyme B was seen to translocate to the nucleus [80] and fragmentation of the nucleus (a classic sign of apoptosis) occurred. This led to the endosomolysin model, which proposed that although cells are capable of endocytosing granzyme B (via an as yet unknown mechanism), perforin is required to trigger the release of granzyme B from intracellular vesicles [81]. There is much speculation to this model, with no clear evidence as to how perforin enters the cell or the mechanism by which endosomal membranes are affected.

A third model of perforin involvement has been proposed. The 'hybrid model' [82] suggests that perforin forms pores in the plasma membrane which promotes Ca^{2+} influx. The subsequent membrane repair response [83], via which pores are repaired using donated membrane from intracellular vesicles such as lysosomes and endosomes, may facilitate the endocytosis of perforin and granzymes (although the authors offer no specific suggestions as to how this would occur). Perforin could then trigger the release of granzymes from the endosomes (again no specifics are given). A study conducted by Veugelers *et al* which

demonstrated that T cell cytotoxicity against HeLa cells was reduced when cells were transfected with mutated form of human dynamin cDNA has led to the proposition that the endocytosis of granzyme B from cytotoxic granules is facilitated by the GTPase dynamin [84]. Dynamin is activated by GTP hydrolysis, and forms a ring which 'pinches' the invaginated membrane to produce a separate vesicle [85]. It is known to be instrumental in a number of endocytic processes that are mediated by caveolae and clathrin, as well some independent of either, as well as phagocytic pathways [86]. Consequently, there remains uncertainty as to which is/are involved in the uptake of granzyme B and there is still much to be elucidated regarding the role of granzymes and perforin from cytotoxic lymphocytes in the induction of apoptosis.

Although classified as being part of the innate immune system, there has been much debate about whether NK cells could be better described as bridges between the innate and adaptive systems [87] [88-92]. As discussed by Sun et al [87], NK cells have many characteristics that are common with T cells. They derive from the same progenitor cells and exhibit many of the same surface receptors (including CD25, CD69 and CD62L). Both NK cells and T cells depend on cytokines from the IL-2R common-γ-chain family and produce IFN-γ and TNF-α after stimulation. The key defining feature of adaptive immunity is the ability to mount a stronger, faster response to previously encountered antigen, due to the creation of memory cells. The traditional view of NK cells is that they are incapable of this, however some authors are proposing evidence as a suggestion of the possible existence of NK cell memory.

Mice exhibiting hapten-induced contact hypersensitivity (using 2,4-dinitrofluoobenzene and oxazolone) then experienced up to four weeks resistance to the same hapten [93]. This was true for mice lacking T and B cells (BALB/c SCID), but no resistance was apparent in mice that also lacked NK cells (BALB/c SCID beige). In a separate study conducted by Sun *et al*, NK cells from naïve C57BL/6 mice or C57BL/6 mice challenged with murine cytomegalovirus were adoptively transferred into neonates who were subsequently themselves challenged with murine cytomegalovirus [94] and the result was a significantly increased survival rate in those neonates that had received NK cells from previously challenged mice. By adjusting the number of transferred NK cells, the authors found that 10-fold more NK cells transferred from naïve mice were required to confer protection. Although these studies highlight the overall importance of NK cells, they do not offer definitive evidence of memory.

A key to confirming memory is to show an altered cell phenotype which persists. As Sun et al [87] discuss, we do not yet know how 'memory NKs' may differ from other NK populations, in terms of surface marker expression, cytokine requirement and release, or the specific

conditions that are required for the induction and maintenance of these cells. In a mouse model of murine cytomegalovirus [94], Sun *et al* examined NK cells *ex vivo* and observed an increased proportion of virus-specific Ly49H (activating receptor) occurring in the first week after infection (from ~50% of circulating NK cells being $Ly49H^+$ to ~ 90%). As the infection was cleared, the proportion of virus-specific Ly49H NK cells decreased, returning to a frequency similar to that pre-infection after 30-40 days. Interestingly, after 70 days, virus-specific $Ly49H^+$ NK cells were detected which differed in surface antigen phenotype to MCMV-naïve $Ly49H^+$ NK cells in terms of presenting a 'more mature' receptor repertoire having higher expression of KLRG1, CD43 and Ly6C along with reduced CD27. Sun *et al* propose that this altered phenotype and longevity could be indicative of NK cell memory, and went on to demonstrate that these 'memory' NK cells were functional *ex vivo* and even showed enhanced responses in terms of increased IFN-γ production and greater degranulation assessed by proxy of LAMP-1 expression [94]. Whist these findings are interesting, Ly49H is a mouse-specific NK receptor so could not be used to distinguish human memory NK cells. Indeed, the majority of memory NK cell experiments have been performed in mice and there is currently little known about whether a memory component of NK cells can be found in humans.

The supposition is that memory NK cells would have distinguishing characteristics from other NK cells. A large proportion of humans (60%) come into contact with human cytomegalovirus and seroconvert (produce specific antibodies). Seroconverted individuals exhibit a greater proportion of peripheral blood $CD56^{low}$CD94:NKG2C$^+$ NK cells than individuals who are sero-negative for human cytomegalovirus [95]. This could indicate an expansion of NK cells which exhibit a surface marker phenotype which is specific for an encountered pathogen, and their retention in order to boost future responses to a repeat infection. Sun *et al* have proposed that this phenotype could be the human equivalent of the increased Ly49H density on the proposed murine memory NK cells [87]. However, as human cytomegalovirus becomes a chronic latent infection it could simply be confirmation of a continual battle by the NK cells to keep the infection under control.

Another cell surface marker that has been proposed as potentially indicating memory NK cells in humans in CD57. The acquisition of CD57 on peripheral blood NK cells correlates to their transition from a $CD56^{high}$ to $CD56^{low}$ phenotype [96], and overall CD57 expression of all NK cells increases with age [97, 98]. This could potentially occur via the steady accumulation of memory over time. It is difficult to discern whether these observations do actually relate to memory or simply NK cell maturation. CD57 expression on T cells correlates with cell maturation and memory and a similar situation might exist in the case of NK cells [99]. The observation that CD57 expression increases with age could be explained on the basis that it is a

memory marker, the expression of which is fostered by accumulated exposure to challenges. However, as NK cell maturation is proposed to involve a transition from $CD56^{high}$ to $CD56^{low}$, then the increased expression of CD57 on $CD56^{low}$ NK cells could solely be associated with maturation. The concept of memory NK cells is interesting and of potential biological significance. If indeed human NK cells can retain a memory leading to a more robust response this could potentially be exploited in targeting tumours.

1.1.1.2 Role of T cells in anti-tumour immunity

T cells are the most abundant of all circulating lymphocyte populations and are classified into different groups on the basis of surface marker expression as well as the profile of cytokines that they are capable of releasing and responding to. Classically, T cells were described as falling into either $CD4^+$ helper or $CD8^+$ cytotoxic populations, although the division is not that easily defined. T cell populations with a surface expression of CD4 comprise around 60% of the circulating T cells. Whilst the majority do exhibit 'helper' functions, promoting other immune responses through the release of cytokines, they are also capable of acquiring cytotoxicity. There are three widely accepted classifications for helper T cell populations (T_H1, T_H2 and T_H17), as well the emerging, but still little understood, T_H22 population. A number of naturally-occurring and inducible immunosuppressive $CD4^+$ populations (regulatory T (Treg) cells) have also been reported [100]. The remaining 40% of circulating T cells express the co-stimulatory molecule CD8 and are often described as cytotoxic effector T cells, however a subset of $CD8^+$ T cells exhibit immunoregulatory properties similar to the $CD4^+$ Treg cells.

The distinction between T_H1 and T_H2 cell populations comes from them exhibiting different transcription factor activation patterns following activation and their distinct cytokine secretion profiles. The concept of distinct helper T cell sub-populations was first described by Mosmann *et al* in 1986, following the observation of different patterns of cytokine secretion in mouse T cells [101]. Differentiation of naïve T cells into T_H1 is driven by the presence of IL-2 and IL-12, which triggers the transcription factors STAT4 (Signal Transducer and Activator of Transcription 4), then T-bet [102]. T-bet serves to promote the *Ifnγ* gene leading to production of IFNγ [103]. This can help stabilise the T_H1 phenotype, as T_H1 cells also respond to IFNγ through a positive feedback loop by way of STAT1 activation [104]. The release of IFNγ is capable of stimulating macrophages, which aid in clearance of the target cells as well as offering further promotion of the T_H1 cells via the release of IL-12. Broadly speaking, a T_H1 response involves pro-inflammatory cytokines, promotes macrophage activation and is typically described as providing a more anti-tumorigenic environment.

The primary driver of differentiation to a T_H2 phenotype is the anti-inflammatory cytokine IL-4 [105]. Appropriate stimulation of naïve T cells through antigen recognition induces activation of the transcription factor NFAT (nuclear factor of activated T cells) which activates STAT6 and subsequently promotes GATA3 [106]. Through enhancement to the promotors of *il4*, *il5* and *il13* genes there is a vast increase to the production and release of the anti-inflammatory cytokines IL-4, IL-5 and IL-13 [107]. The production of IL-4 creates a positive feedback loop promoting the maintenance of the T_H2 phenotype [105]. T_H2 $CD4^+$ T cells promote a humoral (antibody-mediated) immune response by the activation of plasma B cells

Once naïve T cells are undergoing the process of differentiation into either T_H1 or T_H2, then various mechanisms exists to inhibit the other. For example, the promotion of the transcription factor GATA3 [108] in the conversion of T_H2 leads to silencing of the *IL12R* gene inhibiting the response to the T_H1 driving cytokine IL-12 [105]. Conversely, promotion of T-bet during T_H1 differentiation subsequently silences the *Gata3* gene and inhibits T_H2 differentiation [109].

T_H17 cells were described by two different research groups in 2005 [110, 111]. The majority of T_H17 cells are described as being inducible, as naïve immature $CD4^+$ T cells develop the T_H17 phenotype in response to cytokines released in sites of inflammation. This acquisition of phenotype occurs over multiple stages, beginning with initiation of the transcription factor STAT3 (signal transducer and activator of transcription factor 3), primarily in response to the presence of the pro-inflammatory cytokine IL-6 [112] which is secreted by a variety of cells including macrophages, monocytes, T cells, B cells and some tumour cells [113, 114]. However, *in vitro* experiments have also demonstrated the ability for intermediate levels of TGF-β to mediate conversion to a T_H17 phenotype [115] (although at high concentrations TGFβ becomes inhibitory to conversion to T_H17, due to its ability to suppress IL-23R). STAT3 serves to increase transcription of *Rorc, Il17* and *Il23r* genes producing RORγt (retinoic acid receptor related orphan receptor), IL-17 and IL-23 receptor respectively [116]. The expression of the IL-23 receptor allows the cells to respond to IL-23 (another pro-inflammatory cytokine) and this completes their transition to full T_H17 phenotype [117]. IL-23 can also protect the T_H17 phenotype. The *Il17* gene promoter is activated by STAT3, but STAT5 (which would silence the gene) can compete for STAT3 binding sites [118]. IL-2 activates STAT5, but IL-23 is able to suppress IL-2 signalling [117] and prevent the competition of STAT3 by STAT5 thereby maintaining IL-17. By producing IL-17, T_H17 cells promote the recruitment of monocytes and neutrophils which aids clearance of infection. Once the inflammation has been cleared, the loss of IL-23 can trigger the reversal to a naïve phenotype [119]. As well as acquiring a T_H17 phenotype in response to an inflammatory environment (inducible T_H17), a population of

helper T cells that constitutively express a T_H17 phenotype that is RORγt$^+$ and IL-23R$^+$, as well as being able to produce IL-17 (natural T_H17, nT_H17) exist [120] [117]. These nT_H17 cells develop in the thymus, from weakly self-reactive thymocytes [121], and are maintained by TGF-β and IL-23 [122].

Circulating T_H17 cell numbers are low, but comparatively a disproportionately high number are found to infiltrate a range of tumours including colorectal carcinoma [123], gastric cancer [124], head and neck cancer [125], non-small cell lung cancer [126], prostate cancer [127] and breast cancer [128]. For the most part, TH17 cells are reported to play an immunosuppressive role and contribute to the promotion of a pro-tumourogenic environment. Indeed in the case of colon and pancreatic cancer at least, the infiltration of T_H17 cells correlates with poor prognosis of patients [129, 130]. Conversely, an increased tumour infiltrate of T_H17 cells correlates with improved survival of patients with ovarian cancer, thereby suggesting that T_H17 cells are able to act in an anti-tumourgenic manner, depending on the context of the immunological environment and the cancer type [131].

The full role that these cells play in tumour immunity has yet to be elucidated, but current evidence proposes an overall pro-tumourogenic effect, as a combination of the suppression of anti-tumour immunity and the promotion of tumour angiogenesis [132]. T_H17 cells are prolific secretors of the pro-inflammatory cytokine IL-17A, as well as IL-23, both of which have been demonstrated to promote tumour growth in colorectal cancer mouse models after neutralisation of both cytokines led to a reduction in tumour development after implantation [133]. The role of T_H17 cells on angiogenesis is less well defined. T_H17 cells are known for being prolific secretors of the pro-angiogenic cytokine IL-17A and *in vivo* experiments in mouse models have shown, through the use of implantation of tumours transfected with IL-17A as well IL-17A knockdowns, that IL-17A contributes to an increased pattern of angiogenesis as well as more rapid tumour growth [134]. Conversely, T_H17 cells also secrete the anti-angiogenic cytokines IL-17F, IL-21 and IL-22 [135-137].

Populations of CD4$^+$ T cells can also suppress immune responses of a wide range of immune cells (regulatory (Treg) cells), including both CD4$^+$ and CD8$^+$ T lymphocyte populations [138-140], NK cells [141], B lymphocytes [142], monocytes/macrophages [143] and DCs [144]. There are no unique surface markers of Treg cells in humans, although they are described as constitutively expressing high levels of surface CTLA-4 and CD25, as well as the intracellular transcription factor FoxP3 and a low surface expression of CD127. There are naturally-occurring Treg (nTreg) cells, which develop and retain the Treg phenotype within the thymus, as well naïve CD4$^+$ T cells which develop the phenotype, the induced Treg (iTreg) cells [145]. In

order for iTreg cells to form, the naïve cells require stimulation of the TCR at a low affinity, and this can be in response to a self or non-self-peptide [146]. Phenotypic conversion is also dependent on co-stimulation via CTLA-4 [147], as well as stimulation from IL-2 [148] and immunosuppressive cytokines such as IL-10 [149] or TGF-β1 [150]. Circulating Treg cell populations can be formed of a mixture of both nTreg and iTreg cells, although much of the published literature continues to refer simply to 'Treg cells' and identifies the cells using common markers such as CD3, CD4, CD25 and Foxp3. Indeed, it has been proposed that there is no reliable surface marker for distinguishing between the two [151], although a variety of publications claim there are numerous phenotypic differences to be found [100, 152]. These include co-stimulation markers (necessity of CD28 on nTreg cells and CTLA-4 on iTreg cells), a higher expression of PD-1 and CD73 on nTreg cells than iTreg cells and the specific expression of neuropilin-1 [153] and Helios [154, 155] on nTregs, although the specificity of Helios at least is disputed [156].

Both nTreg and iTreg cells are capable of exerting immunosuppression through a wide range of mechanisms (reviewed in detail by [157] and [158]). They are able to produce and release immunosuppressive cytokines including TGF-β1 [159], IL-10 [160], IL-35 [161] and IL-9 [162]. These cytokines can encourage a positive feedback loop of suppression as they, particularly TGF-β1 [163], also cause the transformation of iTreg cells, thereby boosting the overall Treg cell population. As well as mediating suppression via the release of immunoregulatory molecules, Treg cells are also capable of suppressing via cell-contact mechanisms. Treg cells express CD39 and CD73 on their surface which allows for direct inhibition of proliferation of T responder populations through adenosine signalling [164, 165]. In mice, Treg cells have been shown to utilise surface CTLA-4 to mediate suppression [166], although the exact mechanism is not yet fully understood. It is unclear whether this molecule is also involved directly in the suppressive properties of human Treg cells. Treg cells are also capable of exerting suppression through the induction of apoptosis in effector populations, by way of releasing cytotoxic granules in a similar manner to cytotoxic effector lymphocytes. This apoptosis is perforin-dependent and is mediated by granzymes, with nTreg cells predominantly utilising granzyme A [167] and iTreg cells granzyme B [168]. Activated effector T cell populations (both $CD4^+$ and $CD8^+$) as well as monocytes and DCs have been shown to be susceptible to apoptosis by Treg cells [167].

Due to their constitutively high expression of CD25 (the alpha chain of the IL-2 receptor), nTreg and iTreg cells are potent consumes of exogenous IL-2 and so are able to deprive other cells (T effectors and NK cells) of this vital cytokine [169]. Treg cells themselves do not produce IL-2, so rely on their target cells to provide this stimulation, and this creates a feedback loop between

the Treg cells and their targets [170]. IL-2 is crucial to the proliferation of T cells, as IL-2 binding to the IL-2 receptor triggers progression through the cell cycle.

$CD8^+$ 'cytotoxic T cells' have the capability to elicit cytotoxic responses directly via the release of cytotoxic granules and recognised through their surface expression of the co-receptor CD8. The expression of the CD8 receptor confers an ability to recognise peptides presented in the context of MHC class I molecules that are expressed on the surface of target cells. This involves peptide derived from within the cytosol of cells, and can demonstrate when a cell has been infected, as virally infected cells will present virus-derived peptides within their MHC class I. $CD8^+$ T cells recognising the peptides will initiate release of cytotoxic granules in order to kill the infected cell. The cause of around 20% of humans cancers can be attributed to viral infections (such as Epstein-Barr or HPV) [171] and it is the $CD8^+$ T cells which are most effective, as virus derived peptides are found intracellularly in infected cells and are present on MHC class I molecules.

1.1.1.3 Immunoregulatory effects of tumours and the tumour microenvironment

Tumours are not simply malignant cells within the environment of an organ of the body, but rather entities which create their own micro-environment within the body. For the tumour to support any large size it must have a vascular network to deliver adequate respiratory and metabolic requirements. The creation of new blood vessels on an existing network is termed angiogenesis and is driven by endothelial cells, and is triggered by binding of soluble, pro-angiogeneic factors (the most potent being vascular endothelial growth factor VEGF, but others include fibroblast growth factor FGF, platelet-derived growth factor PDGF, Angiopoietin (Ang) -1 and -2) that are released in response to an hypoxic environment binding to tyrosine kinase receptors on their surface. Solid tumours are capable of producing VEGF and therefore can directly promote the generation of the vasculature which is necessary for sustained tumour growth.

In addition, tumours have been shown to boost angiogenesis by inducing/up-regulating VEG-F secretion by local cell populations within the tumour microenvironment [172]. There are several factors in the tumour microenvironment which can drive the immune response towards one of a pro-tumour, pro-angiogenic manner, including TGF-β, PGE-2, VEG-F, lactic acid and adenosine [172]. These can be released by tumours themselves as self-preservation and contribute to the conversion of iTreg cells, a reduction in NK cell cytotoxicity by polarising towards a $CD56^{bright}CD16^-$ phenotype [28, 173] and the promotion of an inflammatory environment. Macrophages secrete pro-angiogeneic growth factors such as VEGF, FGF and PDGF [174, 175] and are actively recruited by tumours through both CCL2 and CXCL12/CXCR4

axes [174-176]. Neutrophils have been found to produce both pro-angiogeneic growth factors [177] and vasculature remodelling agents such as MMP-9 [178]. These remodelling agents are important, as they disrupt localised areas of the existing vasculature, which is necessary for the formation of new vasculature structures. Tumours can promote the infiltration of neutrophils through release of CXCL8 [179]. Whilst dNK cells are well documented to secrete pro-angiogeneic growth factors [180, 181], peripheral NK cell populations do so to a much lower degree, but have been shown to up-regulate secretion when infiltrated into non-small cell lung cancer environment [182]. In ovarian cancer, tumour infiltrating Treg cells have been shown to secrete more VEGF, thus promoting angiogenesis [183]. Myeloid derived suppressor cells (MDSCs) are also capable promoting angiogenesis through the secretion of growth factors such as VEGF, as well as the secretion of remodelling factors such as MMP9 [184] and will be recruited to a pro-inflammatory tumour microenvironment by way of GM-CSF, IL-1β and IL-6 [185]. Although a highly vascularised network is beneficial to the tumour in terms of delivering necessary metabolic requirements for adequate growth, better vascularisation allows immune cells, and indeed administered therapeutics, better access to the tumour.

The activation of both $CD4^+$ effector and $CD8^+$ cytotoxic T cells are augmented by the addition of a secondary signal through the co-stimulatory receptor CD28, the main ligands to which are members of the B7 family. These have been found capable of providing a stimulatory signal (in the case of B7-1/CD80 or B7-2/CD86) or an inhibitory signal (for example, B7-H1 (also known as PD-1), B7-H2, -H3, -H4, or -H6). A wide range, between 10 and 95%, of tumour entities have been found to present inhibitory B7 family members on their surface [186, 187]. Whilst B7-H2 and B7-H6 are seen primarily on haematological tumours, the other B7 family members have been reported on tumours from different origins. The speculation is that tumours expressing ligands which can inhibit T cell activation would present a less favourable clinical prognosis and there are a large number of publications surrounding patient observations which support this theory. The most widely studied of the B7 inhibitory ligands is B7-H1 (PD-1), the expression of which correlated with tumour progression, invasiveness, grade and advanced stage, as well as poor patient prognosis, poor survival and increased death across bladder carcinoma [188], oesophageal squamous cell carcinoma [189], gastric cancer [190], breast cancer [191], ovarian cancer [192], glioma [193], pancreatic cancer [194] and renal cell carcinoma [195]. The expression of B7-H2 on AML has been shown to correlate with poor patient survival [196]. High expression of B7-H3 correlates with advanced tumour grade and progression in colorectal [197] and prostate cancer [198]. Expression of B7-H4 correlates with poor patient survival, tumour size, tumour stage and cancer recurrence in gastric cancer [199], non-small cell lung cancer [200], oesophageal squamous cell carcinoma [201], melanoma [202], prostate cancer

[203] and renal cell carcinoma [204]. The strong correlation between inhibitory ligand expression and poor clinical outcome has stirred interest in the possibility of targeted therapy to block the inhibition.

Early experiments using murine models for *in vivo* investigation of melanoma demonstrated that tumour rejection could be achieved if implanted melanoma cells have been transfected to express stimulatory B7 ligands [205, 206]. When thinking in terms of translational medicine in the clinical setting, it appears that more than just a modification of B7 stimulatory ligands would be required to achieve tumour regression. In addition to serving as CD28 ligands, members of the B7 family also bind to Cytotoxic T-lymphocyte Antigen 4 (CTLA-4) and programmed death ligand 1 (PD-L1), both of which act to suppress T cell function [207]. The idea behind the therapeutic targeting of inhibitory ligands such as PD-1 is to remove the T cell checkpoint blockade and current headway in this area will be discussed later.

It has been known that tumours are able to downregulate the expression MHC class I molecules on their surface since the 1970's [208, 209]. Depending on tumour location, up to 90% have been shown to exhibit either a downregulated MHC class I expression or total loss of the molecule [210, 211]. For breast cancers, the frequency of reduced or lost MHC class I expression is around 50% [212, 213]. Since $CD8^+$ T cell recognition of target cells can only occur via the presentation of relevant peptides in the context of MHC class I, an alteration in the expression of these molecules on tumours effectively allows escape from $CD8^+$ T cell-mediated cytotoxicity. The altered MHC class I expression on tumours can be categorised into one of six different phenotypes ranging from the loss of one haplotype or even the total loss of any MHC class I, to the tumour exhibiting a down regulated MHC class I expression [210], and can be either irreversible or reversible [214].

The irreversible (hard) changes are caused by genetic alterations in genes encoding structural information for MHC class I. Most often these result from mutations, deletions or loss of heterozygosity in the *HLA-ABC* genes on chromosome 6 [215] or the *β2-microglobulin* (*β2m*) on chromosome 15 [216]. Reversible (soft) alterations arise through defects in *HLA* and *β2m* gene transcription, and have been shown to be driven by oncogenes such as p53 or Her2/Neu [217, 218]. An interesting point to note is that the presence of MHC class I provides a major inhibitory signal to NK cells through the inhibitory KIRs. The loss of MHC class I on tumour cells should theoretically render them more susceptible to NK cell-mediated cytotoxic responses. Observations in colorectal cancer suggest that the prognosis is less favourable for those tumours which have downregulated MHC class I expression. Histological investigation of tumour biopsies from 336 patients with colorectal carcinoma who had not received any

radiotherapy showed positive correlation between loss of MHC class I and a reduced expression of transporters associated with antigen presentation (TAP1 and TAP2) as well as a reduction in infiltrating $CD8^+$ T cells [219]. This infiltration of $CD8^+$ T cells is an indicator of patient prognosis, with high infiltration correlating with a more favourable prognosis [219]. Also in colorectal cancer, it has been reported that downregulated, but not totally lost MHC class I expression [220], and the authors proposed that this could be due to the level of MHC class I being too low to allow efficient peptide recognition, but too high for an effective loss of NK cell inhibition [220]. A small observational study in 10 patients with metastatic melanoma who were receiving immunotherapy found that those whose tumours had high expression of MHC class I showed regression after treatment and those people with tumour MHC class I downregulation showed disease progression [221]. As the patient size is so small it is not possible to infer too much from the observed traits, but it would warrant further investigation in a larger group. One potential confounding factor to take into account is the observation that NK cell infiltration into tumours can be vastly reduced compared to the levels seen in surrounding normal tissue [222] [223].

It is apparent that NK cells are important for tumour surveillance, as has been demonstrated by an 11-year follow-up study looking at NK activity in the general population in Japan which found that low NK cell activity correlated to increased risk of cancer development [224]. Furthermore, the importance of NK cells for preventing the progression of metastatic disease has been demonstrated using NOD/SCID mice which lack T and B lymphocytes and NOD/SCID/γc^{null} (NSG) mice which also lack NK cells [225]. Breast cancer cells (MDA-MB-231, MCF-7 and T47) implanted into NSG mice formed primary tumours within 3 weeks with the MDA-MB-231 cells also showing metastases [226]. In comparison, although primary tumours were present in NOD/SCID mice, they were much smaller and there were no metastases [226]. A greater understanding of the relationship between NK cells and metastasis might provide a better basis on which to develop new tumour targeted therapies.

NK cell function is tightly controlled via a complex profile of signals that are delivered by the triggering of inhibitory and stimulatory receptors and ligands and evidence suggests that tumours and tumour-derived factors might influence the phenotype and function of NK cells. There is a large degree of heterogeneity in the expression of different NK cell receptors between individuals and there is some evidence that alterations in this might be contributing factor in cancer development and progression. Overall there is an increasing body of literature comparing the phenotype of NK cells from cancer patients to those of healthy people which suggests that the expression of NK activating receptors is lower in patients with cancer. However, data are limited across different cancers and need to be confirmed in more studies.

Studies from both gastric and cervical cancer patients have shown that their NK cells express lower levels of the activating receptor NKG2D [227, 228], with NK cells in cervical cancer patients also expressing lower levels of NKp30 and NKp46 [228]. In patients with acute myeloid leukaemia, NK cells express significantly lower levels of multiple activating receptors, namely NK30, NKp46, DNAM-1, CD244 (otherwise known as 2B4) and the CD94/NKG2C complex [229]. NK cells from patients with oesophageal squamous cell carcinoma have been found to express significantly lower levels of the Fc receptor CD16 than those from healthy individuals [230]. Investigating the effect of *ex vivo* incubation with IL-12 and IL-18 on NK cells derived from patients with non-small cell lung cancer found that they expressed lower levels of the activating receptors NKp46 and CD25 on the cell surface than NK cells from healthy individuals [231], as well as producing lower levels of IFNγ, the main NK cell stimulatory cytokine. In an observational study involving 677 breast cancer patients, between 50% and 99% of tumours expressed MIC-A, MIC-B and/or ULPB-2 [232], all of which are ligands for the NK cell activating receptor NKG2D, and the presence of these ligands correlates with a longer relapse free period (RFP) following chemotherapy or hormone therapy [232]. However, a separate study looking at 140 breast cancer patients found that the density of NKG2D expression, as well as other NK cell activating receptors NKp30, DNAM-1, CD16 and 2B4, were lower in patients with invasive breast cancer compared to those with *in situ* disease or healthy volunteers [233]. This apparent down regulation of activation receptors may be due to modulation of NK cells by tumour-associated factors, or may be indicative of a naturally occurring phenotypic profile that is more likely to allow tumour escape. Investigation into the effect of administering oestrogen on the phenotype of mouse NK cells showed that the activating receptors CD69, NKp46, NKG2D and 2B4 were all down regulated in response to oestrogen [234]. Since oestrogen is important for a large proportion of breast cancers, this finding offers one possible explanation for the observed down regulation in receptor expression.

Far fewer studies have commented on the expression of inhibitory receptors on NK cell populations in patients with cancer, other than to discuss the genetic distribution of the many different KIRs through different populations. One study has reported that NK cells in patients with lung cancer express significantly higher levels of two inhibitory KIRs, CD158b and CD158e, than healthy individuals [231]. Although other publications have made direct comments on the *ex vivo* cytotoxicity of the NK cells, these have almost always assessed cytotoxicity on the basis of the capacity of NK cells to kill the highly NK-sensitive erythroleukaemic cell line K562.

Target cell death can be measured via different methods. These include analysing the viability of target cell populations by flow cytometry using viability stains such as 7-AAD and propidium iodide, the release of ^{51}chromium or by measuring the release of cytotoxic granules from NK

cells on the basis of surface expression of LAMP-1 (lysosome associated membrane protein 1) as a proxy, or using ELISPOT assays which measure the release of the serine protease granzyme B. NK cells from patients with lung [231], gastric [227] and breast [235] cancer all exhibit lower cytotoxicity than NK cells from corresponding healthy individuals. Dewan *et al* further characterised the breast tumours from the patients, and showed that NK cytotoxic activity was higher in patients with $HER2^+$ tumours than those with HER^- (correlating with the more favourable prognosis of $HER2^+$ over $HER2^-$). They also found that NK cytotoxicity in patients exhibiting only a primary tumour was higher than that in patients with metastatic disease [235]. It remains unclear whether individuals that express NK cells with lower levels of activating receptors and/or higher levels of inhibitory receptors are more predisposed to the development of cancer, or whether something about a tumour (the microenvironment, soluble factors released from the tumour, or even an indirect factor such as the resulting treatment) modifies NK cell receptor expression towards a more pro-tumourogenic environment.

Using the NK cell line NKL and several cervical cancer lines (C33A, SiHa, HeLa), Jimenez-Perez *et al* have showed that co-culturing NK cells with tumour cells for only 4 hours leads to a reduction in the expression of the stimulatory receptor NKG2D [236]. In the case of SiHa and HeLa cell lines, this translated into a reduced cytotoxicity against K562 cells. Further investigations revealed different profiles of NKG2D ligand expression on the cell lines which correlated to the observed functional changes [236]. NK cytotoxicity was inhibited when co-cultured with the lines expressing higher levels of the NK cell activating ligands MHC class I polypeptide-related sequence A (MIC-A) and UL binding protein 2 (ULBP2), both of which bind to the NK cell surface receptor NKG2D [236]. No cytotoxic change was observed after incubation with the cell line expressing high levels of another NKG2D ligand MHC class I polypeptide-related sequence B (MIC-B) [236]. Further investigations are required in order to clarify the potential modulating effect of tumours, or the significance of individual NK receptor expression on the development, progression and clearance of tumours.

Whilst these are interesting observations, the evidence for tumours directly modulating the expressed receptor repertoires of NK cells is not conclusive. Another possibility (which could also occur in parallel with any potential tumour-mediated changes and is not necessarily an alternative explanation) is that the heterogeneity of the NK receptor and cytotoxicity profile between individuals could mean that some people are naturally pre-disposed to more easily allow the immune escape of tumours. For this to be the case, then there would need to be a large degree of heterogeneity in NK cell receptor repertoire profiles between individuals in addition to there being a stability of phenotypes within individuals. There is little published

evidence focusing on this potential aspect of NK cell biology, apart from that focusing on the Killer cell Immunoglobulin-like receptor (KIR) family [237]. There is broad diversity in KIR due to multiple haplotypes with allelic polymorphism, to such an extent that there is less than 1% chance of unrelated individuals exhibiting identical KIR profile [238]. At least one KIR gene is expressed by every NK cell, although during cell development different numbers and combinations of KIR genes are expressed by individual cells, creating a diverse, heterogeneous repertoire within an individual [239]. The KIR profile of individual NK cells is mediated by DNA methylation, with the hypermethylated genes being transcribed and the receptors expressed, whereas hypomethylated genes are not transcribed [240, 241]. This expression within a cell is stable, and is maintained for numerous generations of cell division [239-242]. This diversity may well contribute to potential immune escape of developing tumours, and is undoubtedly an interesting area of study.

Another leukocyte population which is found to infiltrate tumours, and which is the subject of much attention, are regulatory T cells, as these cells can potentially offer protection to the tumour. As detailed previously, the phenotype of nTreg cells and iTreg cells are similar in many ways, with both exhibiting a $CD3^+$, $CD4^+$, $CD25^{high}$, $FoxP3^+$ profile. In a large number of publications, this receptor profile has been used to identify simply 'Treg cells' without attempt to further distinguish them, and consequently it can be difficult to fully elucidate their infiltration into tumours. Treg cells have been shown to infiltrate a wide range of human tumours, including ovarian cancer [243], gastric cancer [244], renal cell carcinoma [245], tongue squamous cell carcinoma [246], hepatocellular carcinoma [247], pancreatic cancer [248], colorectal carcinoma [249], non-small cell lung carcinoma [250] and breast cancer [251]. Observations in ovarian, gastric and breast cancer suggest that Treg cells infiltrate the tumours in response to trafficking signals mediated by CCL17 and CCL22 [243, 252, 253]. A positive correlation between increased numbers of Treg cells infiltrating tumours and higher tumour grade/stage in humans was initially described in ovarian carcinoma [243], but was also observed in early gastric cancer [252]. The presence of tumour-infiltrating Treg cells has also been found to be a positive correlative factor for poor patient prognosis in colorectal cancer [249], pancreatic cancer [248], squamous cell carcinoma [246] and breast cancer [251].

One difficulty lies in determining whether the tumour is able to provide its own protection via the recruitment of immunosuppressive Treg cells to the area, or whether the tumour flourishes because it arises in an environment which is rich in Treg cells. Evidence that tumour-derived TGF-β1 induces the formation of $CD4^+CD25^+$ iTregs supports the former proposition [163]. There is evidence to show that Treg cells may exhibit greater suppressive potential within a tumour microenvironment, as the amount of granzyme B which they possess is higher

than their counterparts in the peripheral circulation [254, 255]. Treg cells isolated from patients with colorectal cancer have been found to specifically respond to a limited number of tumour antigens *ex vivo* [256], thereby revealing another way in which tumours might contribute to the creation of a protective environment. As Treg cells are able to respond to much lower concentrations of antigen (10-100 fold) than T effector cells [257], it might be that tumours can drive a pro-tumourogenic environment by increasing their numbers within the tumour microenvironment and promoting their suppressive capacity.

In addition to their infiltration into tumours, a significantly higher prevalence of Treg cells (determined as either $CD4^{+}CD25^{high}$ or $Foxp3^{+}CTLA\text{-}4^{+}$) in the peripheral blood of patients with a wide range of cancers (pancreatic, breast, lung, colorectal, gastric, oesophageal, cervical, ovarian and of the gall bladder) has also been observed [258-260]. This also appears to be the case in patients with early stage/low grade non-metastatic tumours [260]. This evidence suggests that targeting Treg cells and/or inhibiting their function might enhance protective anti-tumour immunity and the efficacy of immunotherapeutic strategies.

1.1.2 Influence of cancer therapies on anti-tumour immunity

The use of cytotoxic anti-neoplastic drugs (chemotherapy) is one of the main lines of defence in the treatment of cancer, particularly in the case of metastases. These treatments target proliferating cells and cause DNA/RNA damage, thereby resulting in the inhibition of mitosis and induction of apoptosis. They can affect both tumour and healthy cells, and one side-effect is leukocyte depletion which results in immunosuppressive consequences. Compromising the immune system in this way therefore poses a risk to patients. Cancer patients undergoing chemotherapeutic treatment often experience increased susceptibility not only to bacterial infection as a result of drug-induced neutropenia, but also to viral, fungal and parasitic infection as a consequence of lymphopenia. Cell depletion can be rapid - in the case of the commonly used drug cyclophosphamide, a single dose can lead to significant T and B cell depletion [261, 262]. The cell populations do recover once the treatment regimen is complete, albeit slowly. NK and B cell populations return to pre-clinical levels within 3 months of treatment cessation [263]. T cell populations have the longest recovery time, with $CD8^{+}$ populations returning 3-6 months after treatment and $CD4^{+}$ populations taking even longer [263]. In addition to reducing immune cell numbers, chemotherapeutic drugs can impair their mechanisms of action. The effect on NK cells includes impaired tumour recognition due to ligand shedding, as well as a reduction to NK cytotoxicity, and has been reviewed by Rosental *et al* [264].

Despite the immunosuppressive properties of chemotherapeutic drugs, evidence suggests that they could boost the anti-tumourogenic immune response under certain conditions (reviewed by [265]), particularly through the removal of immunosuppressive cell populations such as Treg cells. Although observations as to the potential capacity of cyclophosphamide to promote immune responses were recorded in guinea pigs 50 years ago [266], at the time the immunosuppressive mechanistics of Treg cells were not understood. A single dose of cyclophosphamide has been shown to induce a marked reduction in the prevalence of $CD4^+CD25^+$ T cells in mice [267] and humans [268], and appears to correlate with an increase in anti-tumour immune activity. Although the authors refer to the $CD4^+CD25^+$ T cell population as 'regulatory' cells this is not entirely accurate. CD25 is not a definitive marker for Treg cells, as it is also expressed on activated T cells. However, the authors do state that the depletion of these $CD4^+$ cells is followed by an increase in macrophage cytotoxic activity. As Treg cells are capable of suppressing multiple cell types, the removal of additional T cell populations does not seem to be as important as the loss of suppression acting on other cell types. A reduction in Treg cell numbers (identified as $CD45^+$ $CD4^+$ $CD25^{high}$ $Foxp3^+$) as a result of a single dose of cyclophosphamide has been shown in a phase I/II trial of renal cell cancer patients with IMA901, a cancer vaccine developed from a combination of multiple tumour-associated peptides [269]. Patients receiving this combination of a single dose of cyclophosphamide with the vaccine also had significantly longer survival times [269]. The use of cancer therapies also boosting the immune system of patients is an interesting idea, although as yet our understanding is insufficient to allow for this to be effectively manipulated in the clinical setting.

Radiotherapy is a commonly used, standard-care treatment which involves the localised administration of ionising radiation in an effort to induce apoptosis through DNA damage. As well as directly affecting tumour cells, other cells within the tumour microenvironment will also receive a radiation dose [270, 271]. The outcome of this is somewhat of a double-edged sword, with radiation inducing both pro- and anti-tumour immune effects [272], as both effector and regulatory cell populations will be affected and whilst the loss of a regulatory population may allow increased anti-tumourogenic responses from local effector cells, they themselves could be reduced in number as a direct effect of induced cell death caused by ionising radiation. As well as directly induced death, another effect seen after irradiating solid tumours is for them to release pro-inflammatory cytokines such as TNF-α [273] and IL-1 [274], which will promote the infiltration of leukocytes (both effector and regulatory populations) into the tumour microenvironment. In a mouse model examining the effect of ionising radiation on macrophages, the authors demonstrated that whole body irradiation with as little

as 0.075 Gy was sufficient to produce a 50% increase in the concentrations of the pro-inflammatory cytokines IL-12 and IL-18 within 30 minutes [275].

As well as the direct effects on immune cells, radiotherapy may also have a number of indirect immunomodualtory effects. One of these is via the promotion of leukocyte infiltration into the tumour microenvironment. Irradiation (2 doses of 12Gy) of 4T1 breast cancer cell-derived tumours in BALB/c mice has been shown to upregulate the expression of the chemokine CXCL16 on the tumour, as well as trigger the release of soluble CXCL16 [276]. The consequence of this is an increase in the infiltration of $CXCR6^+$ $CD8^+$ T cells (as confirmed by a reduced level of infiltration following CXCL16 blocking) which correlates with tumour regression. Although the authors primarily focussed on $CD8^+$ T cells, other leukocytes including $CD4^+$ T cells, NK cells and NKT cells can express CXCR6 and could therefore be induced to infiltrate an irradiated tumour microenvironment as a consequence of CXCL16. With there being no specificity for either anti-tumoural or immunosuppressive populations the consequence of CXCL16 expression following irradiation may prove to be either pro- or anti-tumoural. The upregulation of surface expression of CXCL16 occurs in other cancer cell lines in response to ionising radiation, including in the prostate carcinoma TRAMP-C1, the fibrosarcoma MC57, the colon carcinoma MCA38 and the mouse melanoma B16/F10. The release of CXCL16 from the majority of cell lines suggests that this could be a common consequence of radiotherapy.

Irradiation can also influence the infiltration of leukocytes by modifying the tumour vasculature, specifically by increasing the presence of adhesion molecules (including ICAM and P-/E-selectins) that bind integrins and P-selectin glycoprotein ligand 1 which is expressed on the surface of leukocytes. These interactions facilitate the extravasation of these leukocytes into the tumour microenvironment [277]. A similar issue relating to the possibility that such effects on leukocyte infiltration could result in anti-tumoural effects that are mediated by effector populations, or immunosuppressive effects that are mediated by the selective infiltration of regulatory immune populations.

Irradiation can also influence tumour target recognition by way of tumour antigens. Tumour cell death following irradiation results in the release of soluble tumour antigens which can result in a boost to anti-tumour immunity, via the presentation of these antigens to immune effector cells by APCs. Endogenous proteins that are released upon cell damage are termed ‘alarmins’ [278]; a prevalent human alarmin is high mobility group box protein 1 (HMGB1). Tumour-derived HMGB1 binds to TLR-4 on the surface of DCs and is necessary to trigger the processing of soluble tumour antigens by DCs. This is exemplified by the observation of early relapse in breast cancer patients who exhibit a TLR4 polymorphism which impairs HMGB1

binding [279]. One class of molecules with particular interest as tumour antigens are heat shock (stress) proteins. Despite them historically being considered as purely intracellular molecules, there is increasing evidence for these proteins to be found as soluble factors released in the periphery [280], and that the circulating heat shock proteins might serve as biomarkers for a range of diseases, including cancer [281]. Extracellular heat shock proteins also have the potential to act as intercellular signalling molecules, an example of which is the fact that Hsp70 is capable of interacting with APCs through a number of cell surface receptors including LOX-1 [282], and Toll-like receptors [283]. It is also of note that released heat shock proteins have been shown to activate Treg cells through TLR-4, thus triggering an immune-suppressive response [284]. As well as being released, a proportion of tumours present Hsp70 within the plasma membrane [285-289], and this expression can be up-regulated by certain chemotherapeutic agents and also following irradiation [290]. This membrane form of Hsp70 has been shown to act as a target recognition structure for activated NK cells, and hence the therapy (chemotherapy, radiation)-induced increase in membrane Hsp70 expression on tumours has the potential to increase their vulnerability to NK cell-mediated cytotoxicity. The membrane expression of Hsp70 on tumour cells and its implications for tumour targeting possibilities will be further discussed in section 1.3.

As both effector and regulatory lymphocytes are capable of being influenced by factors resulting from tumours following therapy, it is difficult to predict whether such therapies will lead to a more pro- or more anti-tumourogenic environment. However, if it could be possible to harness irradiation that also provides an anti-tumourogenic immune environment, then patients could gain an additional benefit.

With the various immunosuppressive or evasive mechanisms employed by tumour cells, any immunotherapy-based treatment must be able to overcome tumour-mediated endogenous immunoregulatory mechanisms and also the immunosuppressive effects of currently available chemo- and radio-therapies. A favourable approach could be the development of a highly specific tumour-targeted therapy which is able to act independently of the patient's immune system.

1.2 Breast Cancer

Breast cancer remains one of the greatest health burdens in the world, with 1 in 8 women developing breast cancer at some point in their lifetime. Data published by the World Health Organisation in 2008 showed that in the UK alone, female breast cancer was responsible for more than 14,300 deaths per year with around 44,000 women diagnosed with the disease in the same time frame (WHO data, 2008). However data from the United Kingdom and Ireland Association of Cancer Registries published in 2011 suggest that although the incidence of breast cancer is rising (almost 50,000 new cases of female breast cancer in 2010), mortality is falling (~11,500 in 2010). This could be attributable to the recent advances in therapies that target the primary tumour which are discussed below. The majority of breast cancers are of epithelial origin (carcinomas) and glandular (adenocarcinoma). Cancers remaining within the tissue in which it originated is described as *in situ* or non-invasive.

A major barrier to the successful management of breast cancer is the development of metastasis - roughly 44% of women who are diagnosed with breast cancer will go on to develop some form of metastatic disease [291]. Although the disease remains classified as 'treatable' under such circumstances, it is no longer deemed 'curable' [292, 293]. The 5-year survival for all breast cancer is approximately 85%, however this drops to below 20% for patients with metastatic disease (Cancer Research UK, 2010). Furthermore, the median survival of patients after diagnosis for metastatic disease is only 31 months [294, 295]. This clearly highlights the fact that metastatic disease is more aggressive and resistant to current treatments and that there is an urgent need for better understanding and treating metastatic disease.

Over one hundred years ago, Paget published the 'seed and soil' hypothesis [296] which proposed that metastatic cancer cells (which he likened to seeds) grow best in certain organs (soils), and he based his proposition on observations that the location of metastatic disease from different primary tumours did not match that expected from a truly random occurrence from over 900 autopsy records.

A number of publications have revisited this hypothesis, and the general principle continues to be applicable [297]. The suggestions from these are that effective clearance of metastasis will come from targeting both the cancer cells themselves, as well as disrupting the favourable, or preferred, environmental features of the target organ. The most likely sites of metastasis from primary tumours are well characterised - for breast cancer these are the brain, bone, liver and lung (National Cancer Institute data, 2013). Targeting brain metastases with therapy poses its own difficulties, as the blood-brain barrier prevents accumulation of many molecules in the

brain. Another avenue of study has been to better elucidate the mechanism of metastasis formation from the primary tumour in order to attempt to find appropriate points at which to apply targeted therapy.

Unfortunately, many of the specific mechanisms that underlie the establishment of metastatic disease remain elusive. The general process has been described as involving the release of tumour cell(s) from the primary tumour, followed by invasion of the vasculature and their circulation in the body. After some time, the tumour cell(s) adheres to vessel walls and extravasate into nearby tissue. This establishes as a new tumour site via the proliferation and expansion of tumour cells, and also encourages the formation of new blood vessels (angiogenesis). We do not yet know the timescale of these stages, exactly how the decision is taken for a cell/cells to disassociate from the primary or what causes the cells to stop circulating and extravasate where they do.

Tumours are known to be formed of heterogeneous populations of cells, with only a small subset of the cells having the capacity to initiate tumour growth. In addition these are able to self-replicate and self-renew and consequently these cells have been called cancer stem or tumour initiating cells (or cancer stem-like cells, CSCs). This concept was first described in acute myeloid leukaemia (AML) following the observations that only a minority subset of human AML cells that expressed a $CD34^{+}$ $CD38^{-}$ phenotype (<1%) were capable of initiating AML in NOD/SCID mice [298]. The first CSCs in solid tumours were found six years later in breast cancer [299]. As with AML, this discovery was made following *in vivo* implantation of human tumour samples into NOD/SCID mice. For these studies, human breast carcinoma samples were digested to provide single cell suspensions, which were then stained for the expression of cellular adhesion molecules and sorted into purified populations using flow cytometry, before being injected into the mammary fat pad of NOD/SCID mice. All implantations with $CD44^{+}CD24^{-/low}$ breast tumour cells were capable of initiating tumour growth. Although a small proportion of $CD24^{+}$ cell implantations (2 of 12) were also observed to give rise to growths, these were much smaller in size than those from $CD24^{-/low}$ implantations. The authors suggested that this might have resulted from limitations of the sorting process and an incomplete depletion of $CD24^{-/low}$ cells [299].

Three hypotheses for the emergence of CSCs have been proposed [300]. Firstly, that mutations arising in existing stem cells could give rise to tumourigenic progeny [301]. The long life span and self-renewing capability of stem cells could result in increased accumulation of mutations and their pluripotent capacity could offer a mechanism via which tumour heterogeneity could be generated and maintained [302]. A second proposition is that CSCs are an intermediate cell

type between progenitor cells and fully differentiated progeny which retain self-renewing capacities of stem cells [303]. Finally, it has been suggested that cancer cells arise from mature fully-differentiated cells, but that a proportion of these cells can de-differentiate and re-acquire stem cell-like properties [304]. The addition of four transcription factors (SOX2, NANOG, LIN28 and OCT4) to human somatic cells *in vitro* has been shown to be sufficient to induce them to mimic embryonic stem cells in both surface marker and gene expression, as well as confer an ability to differentiate pluripotently [304].

Although the existence of breast CSCs is widely accepted, studying them has been hampered by the failure to find unique surface markers. They have been described in terms of adhesion molecule expression (being $CD44^+$ while lacking CD24) [299], an overexpression of aldehyde dehydrogenase 1 (ALDH1) [305], and also by their ability to pump out Hoechst 33342 stain [306]. An *in vitro* method of culturing breast cancer stem cells which has been successfully used for cell lines as well as primary tumour tissue was described by Ponti *et al* [307]. The authors found that culturing cells in serum-free DMEM-F12 growth medium containing fibroblast growth factor, epidermal growth factor, insulin and bovine serum albumin (BSA) led to a proportion of cells developing into non-adherent clusters (termed 'mammospheres'). These mammospheres were found to exhibit the phenotype of breast CSCs ($CD44^+CD24^-$) and could initiate tumour growth in immunedeficient SCID mice following the implantation of as few as 10^3 cells into the mammary fat pad.

Despite the marked advances in breast cancer treatments and improving survival rates, 30-50% of patients who are diagnosed with early stage disease go on to develop metastatic disease despite receiving treatment. Furthermore, around 40% of patients relapse at some point after previously successful therapy [308]. The resistance of disease to current therapeutic strategies could possibility be due to the persistence of small numbers of breast CSCs. Indeed, breast CSCs have been shown to possess increased resistance to the classical first-line treatments of chemo- [309, 310] and radio-therapies [311, 312]. If treatments were able to specifically target breast CSCs, then it may be possible to reduce tumour recurrence rates. The rapid increase in understanding of CSCs and their biology within the last 10 years is likely to underpin improved treatments and outcomes over the next 10-20 years.

1.2.1 Characterising tumours

It has long been established that breast cancer is not a homogeneous disease, with differences in disease phenotype contributing to treatment responsiveness [313, 314] and patient survival [315-317]. High throughput gene expression analysis has been used to categorise tumours into groups [315]. This approach was subsequently expanded to define tumours into one of five

intrinsic molecular subtypes; Luminal A, Luminal B, HER2+, Triple Negative or normal-like [315, 316, 318], on the basis of their hormone and tyrosine kinase receptor expression, tumour stage and grade. Discussion surrounding the true existence of normal-like breast cancer subtype (so called due to the morphological similarity with normal breast tissue) resulted in a revised description of these entities simply having a large contamination of normal tissue [318], and consequently this subtype has been lost from the literature. Characteristics of the remaining four subtypes are shown below (**Table 1.2**).

	ER	PR	HER2
Luminal A	++	++	+/-
Luminal B	++	++	+/-
HER2+	+	+	++
Triple negative	--	--	--

Table 1.2 Receptor expression on breast cancer subtypes

Breast cancers subtypes exhibit differential expression of a variety of known surface markers. The presence of markers allows for the use of specific targeted therapies to be employed. (ER) Oestrogen receptor. (PR) Progesterone receptor. (HER2) Human epidermal growth factor receptor 2

Having a classification system is highly important, as it is one of the current methods of deciding upon the clinical care strategy [292]. Luminal A and Luminal B tumours are both oestrogen receptor (ER) and typically progesterone receptor (PR) positive. They differ in prognoses, with survival rates being much more favourable for the former [319]. Around 25% of breast cancer is described as being $HER2^+$ [320]; these are tumours which over-express the tyrosine kinase receptor human epidermal growth factor receptor 2 (HER2) while lacking the hormone receptors. Although the prognosis of $HER2^+$ breast cancer is typically worse than with Luminal A or Luminal B tumours [321, 322], with a median survival of 4 years, the survival of patients bearing such tumours has been improved with the advent of HER2 targeting strategies such as trastuzumab and pertuzumab.

Triple negative breast cancers (TNBC) account for up to 20% of breast cancers and do not express oestrogen or progesterone receptors, nor do they overexpress HER2. With their definition arising from the lack of expression/overexpression of a range of markers, there are no current targeted therapies that can specifically act on TNBCs, and consequently the only available treatment options are surgery, chemotherapy and radiotherapy. The prognosis for patients with these tumours is poor, even those who do respond to therapy typically relapse within months and the median survival after diagnosis of distant metastasis is only 13 months

[323]. Triple negative breast cancers are of great interest in terms of developing novel therapies, as there are currently very limited treatment options.

Breast cancers which resemble normal breast basal tissue (tissue in the outer layer of breast ducts), by way of expression of the filament protein vimentin, the cell-cell adhesion molecule p-cadherin, the small heat shock protein αβ-crystallin, the integral membrane proteins caveolin 1 and 2, basal cytokeratins (CK5/6, CK17 and CK14) and epidermal growth factor receptor (EGFR) are described as basal-like tumours. There is a large overlap between those tumours classified as triple negative and those which are basal-like (~75%, [324, 325] however there is not perfect concordance between these classifications. Around 20% of TNBCs do not express any basal-like markers [319, 326], and up to 30% of basal-like breast cancers are not triple-negative [327]. Despite this, the presence of basal-like markers being entirely synonymous with a triple-negative phenotype continues to be discussed in the literature [328, 329], thereby leading to difficulties in interpreting some published data.

Another subtype of breast cancer - Claudin-low - has also been proposed [319, 330], however this has not yet been adopted for clinical diagnosis. In a study published in 2012, genetic copy number aberration (CNA) information was used to cluster 2000 tumour biopsies into similar groups, resulting in the description of 10 different subgroups of disease [331]. Although the prognosis for patients in the different subgroups is different, further studies are required in order to better understand how these genetic differences might influence treatment strategies and outcomes.

Patients are also assessed for their expression of mutations within the *BRCA1* and *BRCA2* genes, as these account for the vast majority of familial breast cancer. Historically, although this meant that genetic profile was used to assess the risk of developing the disease, treatment strategies continued to be based on the receptor expression of the tumour. However, this concept is changing and genetics is increasingly being used to assist the shaping of treatments that are offered to patients (reviewed by [332]). Tumours with *BRCA* mutations express higher levels of the DNA repair molecule polyadenosine diphosphate ribose polymerase (PARP), leading to speculation that this might make them more susceptible to PARP inhibitors. However, this possibility requires further investigation [333, 334]. Using phosphoinositide 3-kinase (PI3K) inhibitors in combination with PARP inhibitors could improve the effectiveness of the latter, since *BRCA* mutations often correlate with loss of phosphatase and the tensin homolog (PTEN) which promotes cell survival by conferring resistance to apoptosis which is triggered via PI3K/AKT signalling [335].

Bioinformatic approaches have also lead to the proposition of a further classification of breast cancer patients. The Nottingham Prognostic Index Plus (NPI+) [336] is enables the stratification of patients with breast cancer into one of seven classes of predicted survival prognosis. This was based initially on the expression levels of a combination of 25 biomarkers [337] although the classification was also found to remain true for a reduced selection of 10 of the most significantly influential markers [338]. This index has evolved out of a desire to improve on the previously published Nottingham Prognostic Index [339], in which data from 387 patients were used to produce an algorithm for stratifying patients in terms of survival prognosis based on data from only three factors; tumour size, lymph node stage and histological tumour grade. This was subsequently verified by a prospective long-term followup of separate patient cohorts, one comprising 320 patients and another 1629 patients [340] and has since been implemented as a clinical tool for aided the decision-making surrounding adjuvant treatment application.

1.2.2 Targeted therapies

The strategy employed for the treatment of breast cancer will depend on the characteristics of the tumour, its stage and grade of the tumour and the medical history of the patient. Surgery is typically the first treatment, often in conjunction with chemotherapy and/or radiotherapy. Those tumours which express oestrogen receptor can also be targeted using endocrine therapy, either preceding surgery or as a follow up. Over-expression of HER2 has allowed the development of monoclonal antibody-based therapies and small molecule tyrosine kinase inhibitors for the treatment of $HER2^{+}$ breast tumours [341, 342].

1.2.2.1 Endocrine therapies

Approximately 80% of breast tumours express the oestrogen receptor (ER^{+} tumours) [343] and the vast majority of breast cancers depend on oestrogen for growth. Two endocrine therapy approaches are available; inhibiting the synthesis of oestrogen using aromatase inhibitors (e.g. amastrozole and letrozole) and blocking the binding of oestrogen to the oestrogen receptor using tamoxifen (reviewed in [344]). In general, tamoxifen is the first line treatment for pre-menopausal women and aromatase inhibitors are used for the treatment of post-menopausal women. The latter is often given in the form of 'neo-adjuvant' therapy (therapy given as a precursor to the primary therapy, for example with the view to shrinking a tumour to an operable size). However, if a patient presents with a particularly aggressive tumour, then chemotherapy, and not endocrine therapy, will be first choice. Although no clinical trial has yet assessed the possibility of using a combination of chemotherapy and endocrine therapy, it is possible to follow a course of chemotherapy with an endocrine therapy.

As ER^+ tumours depend on oestrogen for growth, a link between the use of hormone replacement therapies (HRT) and the incidence of breast cancer incidence has been proposed. Indeed, since 2002, the use of HRT has declined by 75% and the incidence of breast cancer has fallen by approximately 18% [343]. Although there may be a link, as yet there is insufficient evidence to show causality. Improved screening by mammography has also been cited as being a possible contributor to this falling incidence of disease [343]. There is also a good correlation between the presence of oestrogen receptors and much higher survival rates, which indicates the overall success of treatments that specifically target the primary tumour [345].

Around 50% of ER^+ breast tumours also express the progesterone receptor (PR^+) and are dependent on progesterone for growth [346]. This area is less well studied than that relating to oestrogen receptor expression, and is consequently less well understood. Approaches for specifically treating PR^+ tumours are therefore not as advanced. Clinical trials in the 1990s investigated the possibility of using progesterone receptor antagonists as a therapy for breast cancer, but the results were not encouraging. In a group of 28 women with PR^+ breast cancer given mifepristone, only 3 exhibited a partial response [347]. Although another Phase II study using onapristone showed better response rates (56% having partial response, 11% with static disease), recruitment had to be halted due to abnormal liver function tests [348]. Although focus therefore moved away from progesterone receptor targeting, interest is once more growing with the advent of new generation anti-progestins. A Phase I/II clinical trial involving lonaprisan is currently underway [349]. Although early *in vitro* investigations have been conducted on two more anti-progestin compounds [350] the lack of any follow-up publications suggest that little progress was made.

1.2.2.2 Monoclonal antibody therapy

The development of monoclonal antibody (mAb) therapies relies on the discovery of a suitable candidate marker for targeting - one that is uniquely or overexpressed on a tumour surface. The main focus of mAb therapy in breast cancer has been targeting the epidermal growth factor receptor HER2/neu, which is overexpressed in around 25% of patients. The first mAb against HER2 was the humanised murine antibody trastuzumab (also known as Herceptin®), and this was approved for use in 1998. Trastuzumab treatment has significantly improved the prognosis for patients with $HER2^+$ breast cancer, with reports of 50% reduction in disease recurrence in patients treated with trastuzumab for one year post-surgery [351], and a 44% reduction in risk of death when including those patients who also received trastuzumab as a first line treatment [352]. Trastuzumab exerts multiple anti-tumour mechanisms of actions. One is the direct effect of reducing tumour proliferation via G1 cell cycle arrest, in that binding of trastuzumab to extracellular HER2/neu leads to disruption of HER2/HER3 interactions

resulting in uncoupling of PI3K-AKT signalling [353] as well as accumulation of the cyclin-dependent kinase inhibitor $p27^{Kip1}$ [354]. This significantly increases in association with cyclin-dependent kinase 2 (CDK2), but not other CDKs [355]. Secondly, given that trastuzumab is a humanised IgG1 antibody, its binding to HER2/neu facilitates ADCC [356] via coupling of the F_c region of the antibody to $F_c\gamma$RIII on NK cells [357, 358]. However, resistance to trastuzumab can develop over time, as demonstrated by the observations that there is a significant reduction in response rates in those patients who had previously been treated (39%) compared to patients naïve for trastuzumab (71%), despite overexpressing HER2. One possible strategy to help with the appearance of resistance is to target the tumour with several therapies in tandem at the start of treatment. Already the use of trastuzumab administered as neoadjuvant therapy to chemotherapy and then again as adjuvant follow up has shown to be superior to chemotherapy alone (5 year event free survival being 43% for patients receiving chemotherapy but 58% for those who also received trastuzumab) [359].

However, trastuzumab treatment is associated with significant cardiotoxicity and congestive heart failure in around 1% of patients [360]. Furthermore, around 50% of patients with $HER2^+$ breast tumours fail to respond to, or become resistant to trastuzumab treatment [361]. With this in mind, other HER2 targeting therapies are arriving to the market. The recombinant humanised mAb pertuzumab has been approved for use in patients with $HER2^+$ metastatic or locally advanced breast cancer in patients who have not received either chemotherapy or anti-HER2 targeted therapies [362]. Pertuzumab binds to HER2, but at a different epitope than trastuzumab. Similar to trastuzumab, binding of pertuzumab induces ADCC [363] and prevents the dimerization of HER2 with other EGFRs. Due to the different binding sites of pertuzumab and trastuzumab, combination therapy is possible [364]. The pivotal Phase III trial which led to the clinical approval of pertuzumab compared the outcome of 806 patients with locally recurrent or metastatic breast cancer when given trastuzumab plus docetaxel plus either pertuzumab or placebo [364]. The addition of pertuzumab into the treatment regime increased the proportion of patients achieving a response (80.2% compared to 69.3%), and those patients who exhibited progression-free survival maintained this status for longer (median of 18.5 months compared to 12.4 months). As yet there is insufficient data available yet to comment on whether, as with trastuzumab, eventual pertuzumab resistance will occur.

Recently approved for use as a single agent therapy against $HER2^+$ breast cancer is the antibody-drug conjugate trastuzumab emtansine (also referred to as T-DM1 or Kadcyla©) [365]. This preparation of trastuzumab is conjugated to the cytotoxic, microtubule disrupting drug DM1 (a derivative of maytansinoid) using a non-reducible thioether linker [366]. Investigations *in vitro* confirm that T-DM1 retains the mechanisms of unconjugated

trastuzumab (the induction of ADCC and disrupting HER2/HER3 interactions leading to reduced cell proliferation [367]. A Phase III trial comparing the effect of giving patients lapatinib alongside capecitabine or giving T-DM1 has demonstrated a significant benefit to receiving T-DM1, in terms of the proportion of patients having a partial or complete response (30.8% compared to 43.6%) and in the median duration of the response (6.5 months compared to 12.6 months) [368]. This trial enrolled only those patients whose disease had progressed after having previously received treatment with trastuzumab. A later Phase II trial compared the effect of trastuzumab plus docetaxel compared to T-DM1 in patients with previously untreated, locally advanced breast cancer [369]. There was a statistically significant benefit to receiving T-DM1, in terms of median duration of progression-free survival (14.2 months compared to 9.2 months) and the proportion of patients responding to treatment (64.2% compared to 58.0%). This is a promising new development for patients with $HER2^+$ breast cancer.

1.2.2.3 Small molecule tyrosine kinase inhibitor

An additional approach for the selective therapy of $HER2^+$ breast cancer is to use the small molecule tyrosine kinase inhibitor lapatinib. Lapatinib is a dual HER2/EGFR tyrosine kinase inhibitor, inhibiting phosphorylation of the intracellular C-terminus kinase domain which leads to inhibition of both PI3K-AKT and MAPK-ERK1/2 pathways and a reduction in cell proliferation due to G1-phase cell cycle arrest [370, 371], and the downstream effects of lapatinib are similar to those seen following binding of anti-HER2 mAbs. A Phase II clinical trial of patients with advanced breast cancer, who had previously been treated with chemotherapy and trastuzumab regimes, has shown that lapatinib provides a clinical benefit (partial response or stable disease) to 64% of patients [372]. A Phase III clinical trial randomised patients with metastatic breast cancer who had previously received anthracyclines, taxanes and/or trastuzumab to receive capecitabine chemotherapy alone or in combination with lapatinib [373]. The addition of lapatinib into the regime increased median overall survival from 64.7 to 75.0 weeks. Another similarity with anti-HER2 mAb therapies is that disease resistance occurs, typically around 1 year after starting treatment, and from this point the disease progresses rapidly [374]. Clinical trials have been conducted to assess the potential benefit of combination treatments targeting HER2. A randomised, Phase III trial compared the outcome of receiving lapatinib and trastuzumab alone or in combination in 455 patients with $HER2^+$ breast tumours, who had no evidence of metastases and had received no prior treatment, who were undergoing surgical resection with adjuvant chemotherapy [375]. A significantly higher proportion of patients who received the trastuzumab/lapatinib combination were observed to undergo a complete response (51.3% compared to 29.5% of those who received only

trastuzumab and 24.7% who received lapatinib). The benefit was slightly more pronounced if the data from only those patients with small tumours (≤5cm) was compared (55.2% vs 28.4% vs 26.1%), thereby suggesting that this may be of particular benefit as a first-line therapy option.

1.2.2.4 Vaccination therapy

The idea of developing a vaccine to boost a patient's own immune response to a tumour has been a focus of study for many years. Despite much on-going research in this field, there are as yet no clinical vaccines for breast cancer available [376]. In fact, there is only one vaccine approved by the US Food and Drug Administration (FDA) for any cancer therapy; Sipuleucel-T for use in prostate cancer patients [377]).

There are different strategies for delivering cancer vaccines [378], with possibilities being employing the use of:

- a peptide or protein (typically with an adjuvant)
- a recombinant virus, or other recombinant microorganism
- tumour lysate, or dead tumour cells
- DCs activated using peptide or protein
- DNA plus a vector - the sequence for the peptide of interest is included in a delivery vector, and the peptide is produced and then processed within APCs

The majority of current breast cancer vaccine trials are conducted using peptides, or DCs pulsed with peptides. The benefits of using peptides are the relative ease and low-cost with which they can be produced, and the low risk of associated toxicity. One drawback is that the potential pool of patients for which a given peptide vaccine may be effective could be small due to the HLA restriction of the peptide. The majority of peptides under investigation are HLA-A2 restricted and so cannot be used for patients who do express this particular haplotype. Although it is relatively easy to induce a $CD8^+$ T cell response with single peptide vaccines, these responses are typically short-lived [379, 380]. A more robust and sustained response can been observed if both $CD8^+$ and $CD4^+$ T cells are triggered [381]. To this end, vaccinating with longer peptides that can be processed via both MHC class I and MHC class II pathways, or with combinations of peptides that are specific for $CD4^+$ and $CD8^+$ T cells is considered as being a more viable strategy [382, 383].

The success of a vaccine therapy depends on finding a suitable tumour antigen which is selectively expressed or over-expressed by tumours, is absent (or expressed at very low levels)

in normal tissue, is immunogenic and, ideally, is prevalent in different patient groups and sub-groups. Current molecules under consideration for use against breast cancer include mucin-1 (MUC-1) [384, 385], HER2/neu [379, 386, 387], carcinoembryonic antigen (CEA) [388] and telomerase reverse transcriptase (hTERT). Vaccinating against MUC-1 has progressed as far as Phase III, with a trial involved over 1000 women with metastatic breast cancer being recently completed. However, the results were disappointing with no patient benefit derived from vaccination in terms of disease progression or overall survival [389]. Another cancer vaccine currently under investigation is PANVAC™, which provides antigens to both MUC-1 and CEA [390]. So far it has just been used in pilot studies to confirm vaccine safety, and has only been used in patients with metastatic carcinoma [391] [392]. There were encouraging observations with a proportion of patients showing partial responses and others having stable disease so the outcome of future larger trials will be interesting. Multiple peptides are being considered as the basis for vaccinating against HER-2 tumours, with the best studied being E75, AE37 and GP2. E75 has been used in a Phase II trial which involved 195 women with HER-2^+ breast cancer who had already completed the standard treatments of surgery, chemotherapy and radiotherapy [393, 394]. Although there was a trend for vaccinated patients to have better 5-year disease-free survival rates (89.7% compared to 80.2%), this result was not significant. There was, however, a correlation between vaccination and risk of recurrence, with a 48% reduction in vaccinated patients [395]. As yet, AE37 has only been investigated in a pilot study involving 15 breast cancer patients, however it did elicit a specific response and this would be interesting to follow up on. GP2 has also been looked at in a Phase II trial of 172 women with newly diagnosed breast cancer. There was a strong specific cell response which also showed a trend (albeit non-significant) towards a reduced risk of disease recurrence [396]. There has been relatively little published data regarding the use of hTERT. A small study involving 19 patients with metastatic breast cancer found that hTERT vaccination resulted in a $CD8^+$ T cell response (but no $CD4^+$ T cell response) in just over 50% of patients, and that this correlated with an increase to overall survival (from 17.5 months in non-responders to 32.2 months in those with a high $CD8^+$ T cell response) [397]. The development of cancer vaccines is an exciting area of research, in which interest has been renewed and developed over the last few years. However, a number of significant challenges exist and it will be interesting to see what arises in the near future.

1.2.2.5 Targeting the tumour vasculature

A common feature which is crucial for the establishment and proliferation of both primary tumours and distant metastases is the creation of a vascular network. Tumours are prolific producers of pro-angiogenic factors such as Vascular Endothelial Growth Factor (VEGF) [398].

Tumours can overexpress receptors for pro-angiogenic growth factors (8-15% of breast cancers express amplified Fibroblast Growth Factor receptor (FGFR) [399, 400] and consequently promote the development of their own vascular network. The development of large metastases also requires the establishment of vasculature. This dependence on adequate vascularisation has promoted interest into the potential for a new family of cancer therapies. There are two classes of agents which can target the tumour vasculature; anti-angiogenic drugs which prevent the formation of new vessels and vascular disrupting agents (VDAs) which destroy previously formed vessels. VDAs can be further classified into two groups, with respect to their mechanism of action; ligand-based agents (targeted delivery of toxins or pro-apoptotic factors via ligands specifically expressed in tumour vessels) or small molecule VDAs (which themselves fall into two categories; flavonoids and tubulin binding).

The most widely reported VDA in the literature is the small-molecule combretastatin A-4 disodium phosphate (CA4P), which acts through inhibition of tubulin polymerisation [401, 402]. Although the most commonly investigated tumours are NSCLC (non-small cell lung cancer), some trials of VDAs have been undertaken in patients with breast cancer. CA4P analogues are also under investigation and have been shown to induce apoptosis in MCF7 breast cancer models [403]. As the outer rim of tumours is able to diffuse oxygen and nutrients from the surrounding environment, VDA treatment is thought to be best administered in combination with other therapy. Promising *in vivo* data (specifically detail and reference some of this promising data) has not translated as well as hoped. Phase II trials of the flavonoid small molecule VDA ASA404 administered in conjunction with standard chemotherapy of 175mg/m^2 paclitaxel plus 6mg/mL/min carboplatin to patients with NSCLC did result in a modest increase in patients showing a partial response (from just over 22% in those receiving standard chemotherapy alone, to almost 38%in those also receiving the highest dose of ASA404 [404, 405], as well as an increase to median survival time from 9 to almost 15 months. Early investigations using an *in vivo* SKBR3 breast cancer model have shown that CA4P received in conjunction with chemotherapeutic drugs (cisplatin and cyclophosphamide) induced a 10-fold increase in tumour cell death than chemotherapy only [406]. The lack of follow up from this into human clinical trials suggests that attempts to translate this therapy for breast cancer have been unsuccessful

The concept of using inhibitors of angiogenesis and/or vascular disrupting agents is an attractive one, as it targets a feature which is common to all malignancies and could therefore be developed for a large number of patients. It could be used against both primary and secondary malignancies, and it has particular promise for those tumours for which no specifically targeted treatments exist, such as TNBC [407]. Indeed, current trials have

predominantly focussed on TNBC due to the current lack of any other targeted therapies for these patients. However, the angiogenesis inhibitors bevacizumab or polyadenosine diphosphate ribose polymerase inhibitors have not improved disease-free survival in patients with TNBC [329].

Current progress has been hampered by a variety of issues. There is a large interspecies variation in tolerance [408] necessitates intensive and time-consuming toxicity investigations for the translation of findings from rodent models to human trials [409]. There are also reports of toxicity in patients which occurs either as a result of effects on the non-tumour vasculature (through a lack of specificity to that within the tumour) or due to downstream effects from the release of cytokines [410]. VDAs including CA4P and other tubulin-binding drugs AVE8062 and ZD6126, as well as the flavonoid-based VDA ASA404 have all been found to cause cardiac toxicities including ischaemia (oxygen restriction), dyspnea (shortness of breath) and hypertension in patients [410-413], as well as pain at the infusion and tumour sites and motor-, sensory and visual neurotoxicity [412, 414].

Promising data arising from Phase I and Phase II clinical trials using inhibitors of poly(ADP-ribose) polymerase (PARP, a DNA repair molecule found in the nucleus) has since been followed up by failings at Phase III, in which no significant improvements in disease progression or patient survival have been observed. However, it was subsequently discovered that the drug used, iniparib, could not inhibit PARP when used as at the doses used [415]. Trials are ongoing with other drugs.

1.2.2.6 Checkpoint Inhibitors

A popular avenue of current investigation is the potential for boosting patients' anti-tumour immune responses by removing 'checkpoint inhibition'. T cells require both antigen recognition and co-stimulation in order to respond; however responses can also be hindered if T cells receive a co-inhibitory signal, referred to as checkpoint inhibition. Evidence now suggests that tumours have the capacity to trigger these inhibitory events and so that concept underlying checkpoint inhibition as a therapeutic strategy is that its 'removal' promote a more robust T cell response and anti-tumour immunity. The two mechanisms of checkpoint inhibition that have been most well studied are signalling through the T cell surface receptors CTLA-4 (cytotoxic T lymphocyte-associated molecule 4) and PD-1 (programmed death 1).

CTLA-4 expression is induced on the surface of both $CD4^+$ and $CD8^+$ T cells after stimulation with MHC-presented antigen peptide, and it is constitutively expressed on the surface of Treg cells [416]. There is high sequence homology between CTLA-4 and the co-stimulatory receptor CD28 [417-419], and consequently it is of little surprise that CTLA-4 is capable of binding to the

same ligands (CD80 and CD86) [420, 421]. It is interesting to note that CTLA-4 binds with higher avidity than CD28 [422], highlighting that competitive binding could favour T cell inhibition. Interestingly, soluble CTLA-4, which could block available CD80 and CD86 and thus prevent T cell co-stimulation through CD28 has been found in the plasma of patients with breast cancer [260].

PD-1 (also referred to as B7-H1) is expressed on T cells and binding to its ligand PD-L1 results in signalling which inhibits T cell activation. PD-L1 has been found to be highly expressed in a large proportion of breast cancers and breast cancer cell lines [416]. Furthermore, there is a correlation between the expression of PD-L1 and tumour grade [423] The expression of PD-L1 has also been shown to be increased in those patients undergoing chemotherapy (including regimes of paclitaxel, etoposide and fluorouracil) [424, 425], indicating that whilst these treatments have direct anti-tumour effects there could be indirect pro-tumour effects due to an increased potential for T cell inhibition.

Current therapy for blocking CTLA-4 binding involves the administration of an anti-CTLA-4 blocking mAb. Promising results with a mouse model of breast cancer in which animals treated with anti-CTLA-4 therapy were able to reject tumours that are derived from implanted SM1 mammary carcinoma cells, and even reject subsequent tumour challenges despite receiving no further antibody therapy were obtained over 15 years ago [426]. However, Phase I and Phase II trials assessing anti-CTLA-4 treatments in humans have not been so effective. At Phase I, approximately 40% of patients were observed to maintain stable disease [427], whereas no observed benefit to receiving the anti-CTLA-4 treatment was observed at Phase II (clinical trials.gov NCT0083278). It is worth noting that these trials were considering the use of anti-CTLA-4 therapy alone. As this does not appear to be effective in this setting, there could be benefit in combining anti-CTLA-4 treatments with other, conventional therapeutics. Therapies to block the PD-1 pathway also rely on the administration of a blocking antibody and the safety of anti-PD-1 mAb therapy has so far been assessed in Phase I trials. The therapy was found to be well tolerated with the maximum tolerated dose not reached in almost 300 patients suffering from a range of solid tumours, and 36% of patients with PD-L1^{+} tumours demonstrated some response [428]. A second Phase I trial involving 207 patients also found the treatment well tolerated, but a reduced observed response in patients, with 6-17% showing some response depending on tumour entity [429]. As these trials involved patients with a range of tumours, it is difficult to comment on the potential effectiveness of approach in breast cancer, and further studies to confirm whether they will prove clinically effective, be it alone or in combination with existing therapies are required.

1.2.2.7 Future considerations

As metastases currently pose the biggest threat to overall patient survival, strategies that can more effectively target the establishment and progression of metastatic disease are of the highest priority. This could occur at any stage in the process of metastatic growth, be it after cells have disseminated from the primary tumour and are circulating in the vasculature, or once they are establishing in distant tissues. Targeted therapies, such as mAb treatments and / or the induction of protective adaptive and innate anti-tumour immunity, have the potential to effectively eradicate primary and metastatic disease and establish long-term protection against disease recurrence.

The development of new immunotherapeutic or other targeting strategies for cancer would be greatly enhanced by the identification of features that are common to tumours, as this would reduce the profile of therapeutics which needs to be developed and tested. One such molecule might be a unique membrane form of the 70kDa heat shock (stress) protein family, Hsp70, which was discovered by Professor Gabriele Multhoff [285-289].

1.3 Heat Shock (Stress) Proteins

The discovery of heat shock (stress) proteins can be attributed to a serendipitous moment in 1962, when an incubator containing *Drosophila melanogaster* larva was inadvertently left at an above optimal temperature overnight. The resulting unusual puffing patterns in gene expression were noticed by Professor Ferruccio Ritossa (25 February 1936 – 9 January 2014) [430]. However, it was not until 1974 that the products of these genes were identified and the term 'heat shock protein' was attributed to them [431]. It is now known that this term is somewhat of a misnomer, as intracellular levels of such proteins are upregulated in response to a variety of cell stresses in addition to heat shock, including, but not limited to, oxidative stress [432, 433], nutritional stress [434], infection [435], UV irradiation [436] and chemotherapeutic drugs [437]. Consequently, some of the literature has begun to refer to these as 'stress proteins', although the vast majority still retain the original 'heat shock' nomenclature.

1.3.1 The 70kDa Family of Stress (Heat Shock) Proteins

Heat shock proteins (Hsps) are highly conserved across species, and are found in all prokaryotes and eukaryotes. There are over 30 mammalian heat shock proteins, and these are divided into six families based on their molecular weight. The 70kDa family currently has 13 known members. The term 'Hsp70' has been used to describe multiple members of the 70kDa family, making it difficult to fully interpret and compare some of the literature. The nomenclature of heat shock protein families is complex, with multiple terms given to individual molecules. Although a standard nomenclature has been suggested [438], inconsistencies and confusion in the literature remain. This study concerns the most widely studied of the 70kDa family, which will be referred to here as Hsp70, but is also referred to in the literature as HSP1A1.

1.3.2 Intracellular Role of Hsp70

Hsp70 is constitutively expressed at relatively low levels and acts as an ATP-dependent intracellular molecular chaperone [439-443] which promotes the folding and trafficking of nascent polypeptides and proteins [444]. In times of cellular stress, Hsp70 expression can be increased to much higher levels via the activation of heat shock factors (HSF) in the cytoplasm, their trimerisation and relocation to the nucleus, and their binding to heat shock protein gene promoter regions. This upregulation of expression helps to confer some transient resistance to apoptosis by stabilising and refolding proteins [445-447]. It can also block intracellular apoptotic pathways by inhibiting Bax on mitochondrial membranes [448], inhibit the production of the apoptosome by binding Apaf-1 [449] or by inhibiting JNK activation by binding to JNK-1 [450]). Hsp70 also plays a role in cell proliferation, with healthy cells

expressing Hsp70 during G1/S and S phase [451, 452]. Hsp70 expression can be induced by a number of oncogenes, including p53 [453], c-myc [454] and adenovirus E1A [455]. Intracellular Hsp70 is therefore over-expressed in many cancers, and this reduces the cell growth doubling time. The influence of Hsp70 on cell growth has been confirmed by the observation that MCF7 cells that have been transfected to further increase intracellular Hsp70 expression exhibit a significantly shorter doubling time (39 hours) than those with lower expression (54 hours) [456].

Many tumour cell lines express constitutively high intracellular Hsp70 and this could therefore contribute to their survival ability [457]. The Hsp70 expression in tumours can have implications for disease prognosis, and there is a general agreement that an increased expression of Hsp70 correlates with a less favourable prognosis [458]. Examination of primary human breast cancer samples has revealed that an overexpression of intracellular Hsp70 is correlated to both the expression of oestrogen receptor [459] and an increased rate of cellular proliferation [460], both of which are features of invasive breast cancer. Intracellular Hsp70 may also be useful as a prognostic factor in human breast cancer, with the overexpression of Hsp70 inversely correlating with both disease-free survival [461] and overall survival [462]. However, other proteins within the Hsp70 family are not so clearly correlated with disease status. For example, although Hsp70-2 overexpression positively correlates with overall survival, its expression shows no association with disease-free survival [463].

1.3.3 Extracellular Hsp70

Although widely considered as being an intracellular protein, Hsp70 can be released from cells and the presence of Hsp70 in the blood of healthy humans was first reported in 1998 [280]. Other studies have subsequently shown that a variety of different cell types and isolated peripheral blood mononuclear cells (PBMCs) grown in culture medium can also release Hsp70 [464, 465]. Cells undergoing stress have been shown to upregulate Hsp70 release, with extracellular levels positively correlating with increasing temperature/heat stress [465] and mycobacteria infection status [466]. Disease states can also be linked to increased levels of soluble Hsp70, in particular patients with vasculature disease. Increased levels of soluble Hsp70 have been observed in patients with peripheral and renal vascular disease [467]. In addition, levels of soluble Hsp70 could potentially be used as a biomarker for disease severity in atherosclerosis patients, as circulating Hsp70 levels have been shown to positively correlate with calcification score [468]. Circulating Hsp70 levels are also elevated in patients with colorectal cancer [469], prostate cancer [470] and leukaemia [471, 472]. The finding that there is a correlation between higher levels of Hsp70 in the circulation and poor prognosis in patients with leukaemia has prompted speculation as to the possible use of soluble Hsp70

levels as a biomarker for tumour progression [471, 472]. Further evidence as to the potential of circulating Hsp70 as a cancer biomarker has been provided from a mouse model head and neck cancer [473], in which tumours increasing levels of circulating Hsp70 positively correlated with the size of FaDu spheroid-derived tumours. Furthermore, a radiation-induced reduction in tumour size correlated with decreases in circulating levels of Hsp70, and complete tumour regression was associated with the return of circulating Hsp70 levels to those in control animals [473].

1.3.3.1 Mechanism of Release

Despite numerous reports of Hsp70 being found in the extracellular compartment, the mechanism for the release of Hsp70 from cells is still not fully understood. Hsp70 release has been suggested to be the result of a non-classical pathway [474], due the fact that Hsp70 lacks an inherent secretory leader sequence [475] and that its release is not prevented by treatment with Brefeldin A [464] which prevents transport of proteins from the Endoplasmic Reticulum to Golgi. Prior to its release, Hsp70 is found to translocate to the plasma membrane where it integrates into the lipid bilayer within ion channel openings [286]. This concurs with previous research which demonstrated an affiliation between Hsp70 and lipids in the membrane [476], particularly phosphatidylserine [477]. The actual release of Hsp70 may be via inverse evagination of the membrane, exocytosis or membrane shedding [286]. The observation that Hsp70 release correlates with the cell surface expression of LAMP1 [475] is further evidence of release via exosomes/exolysosomes and therefore exocytosis, as is the observations that exosomes collected from both heat stressed and mycobacteria infected cells contain significantly higher levels of Hsp70 than those from normal cells [465, 466].

1.3.3.2 Extracellular Hsp70 can bind to cells

Evidence is also growing to support the idea that Hsp70 can bind to cells and thereby act as an intercellular signalling molecule. *In vivo* experiments in which monocytes were cultured in the presence of Hsp70 showed that Hsp70 could bind via Toll-like receptors (TLR) 2 and 4, the result of which was the release of the pro-inflammatory cytokine IL-6 [283]. To date, the seven cell surface receptors which have been identified as probable candidates for binding heat shock proteins are CD91, CD40, LOX-1, TLR-2, TLR-4 and SR-A, with all but SR-A proposed to bind recombinant Hsp70, as reviewed by Binder [478]. Other groups have also shown that Hsp70 can bind to DCs via CD91 [479] or TLR4 [480] and human endothelial cells (HDMECs) [481], possibly via LOX-1 [282]. A study which isolated both the ATPase domain and the substrate binding domain of Hsp70 has shown that although both could bind to DCs, they did so via distinct binding sites [482].

1.3.4 Immunological properties of extracellular Hsp70

1.3.4.1 Inducing immunity to tumours

Over two decades ago, Pramod Srivastava and colleagues showed that mice could be protected against tumour challenge if they had previously been injected / immunised with proteins that had been isolated from those same tumour cells [483]. The proteins conferring protection against tumours were isolated and found to include the heat shock proteins Hsp70, Hsp90 and gp96. Subsequent work showed that it was not actually the heat shock proteins themselves, but peptides bound to the heat shock proteins that were inducing the immunity, as peptide-free heat shock proteins conferred no protective effect [484, 485]. As indicated above, although heat shock proteins are primarily found intracellularly, they are also frequently released from tumours and this might offer a mechanism via which tumour-specific T cell responses can be generated [486, 487].

As a molecular chaperone, Hsp70 possesses the ability to bind a plethora of peptides from the original host cell. Hsp70-peptide complexes formed *in vitro* are able to elicit an immune response *in vivo* via the induction of peptide-specific $CD8^+$ cytotoxic T cells [488]. For this, Hsp70-peptide complexes bind to APCs such as DCs and are internalised via endocytosis [489]. The Hsp70-peptide complex is trafficked within different compartments of the APC and the peptide is transferred to MHC class I molecules and expressed by these on the cell surface. This process is known as 'cross-presentation' and has been reviewed by Berwin [490]. Antigen specific activation of $CD8^+$ T cells occurs via the recognition of peptide-MHC class I complexes on the APC by appropriate T cell receptors on the surface of the responding $CD8^+$ T cell, concomitant with the delivery of essential co-stimulatory signals by the APC.

Evidence also links extracellular Hsp70 to $CD4^+$ T effector cell mediated immunity. Findings published in 2009 show that Hsp70 binding to DCs causes upregulation of IL-15 production and release, which consequently, indirectly, leads to enhanced proliferation of $CD4^+$ T effector cells [480]. Work from a different group found a direct link, with Hsp70-peptide complexes being used in not only the MHC class I pathway, but also the MHC class II pathway, thereby enhancing antigen-specific $CD4^+$ T effector cell responses [491].

This strategy has been employed in a number of studies that were focussed on the creation of personalised vaccines for cancer patients which used heat shock proteins derived from a patient's own tumour to elicit an immune response against the tumour [492, 493]. A significant step forward has been made with another of the heat shock proteins, gp96. However, Phase III clinical trials in patients with melanoma, colorectal cancer or renal cell carcinoma, have not been as conclusive as early *in vitro* and experimental *in vivo* studies might

have suggested [494-496]. One potential issue relating to the use of tumour-derived gp96 as an anti-cancer vaccine is that there is a dose-dependent switch in the elicited immune response, in that low doses induce protective anti-tumour immunity, whereas high doses do not [497]. These findings have been confirmed using *in vivo* models of cardiac allograft transplantation (in Lewis and Wistar rats) [498] and skin grafts (in C57BL/6 mice) [499] which have demonstrated that high doses (100μg) administered intradermally can be anti-inflammatory and reduce rejection responses. It might therefore be difficult to identify the correct dosage to be used in the clinical setting.

In an effort to produce more effective Hsp70-based vaccines, the possibility of using Hsp70 derived from DC-tumour fusions has been considered. Following on from studies that used the colon adenocarcinoma cell line MC38 fused to bone marrow-derived DCs in a murine model [500], the same group translated findings into the clinical setting [501]. For this, Hsp70-peptide complexes extracted from fusions generated from DCs isolated from healthy donor blood packs and tumour cells (either patient-derived ovarian cancer cells or breast cancer cell lines MCF7, BT20, ZR75 or SKBR3) were used to stimulate healthy donor T cells *in vitro* and were found to result in higher levels of cytotoxicity against specific targets than when T cells were stimulated with Hsp70 from the cells alone [501].

One point open for discussion is the effect that internalisation of the Hsp70-peptide complex has on the APC. Studies have shown that DCs mature, both phenotypically and functionally, in response to internalising Hsp70-peptide complexes [502]. Much of the work in this area has made use of recombinant Hsp70 derived from *E. coli* systems, which can carry lipopolysaccharide (LPS) contamination. LPS is known for its ability to activate APCs via the CD14 surface receptor and Bausinger and colleagues argue that it is high levels of LPS contamination that result in APC maturation [503]. Their data show that Hsp70 with no LPS contamination, or with very low levels (<10IU/mg) do not show any capacity to induce the maturation of APCs. The issue of LPS contamination was addressed in a review published in 2010, in which the authors discussed not only Hsp70, but also other stress proteins including Hsp60 and gp96 [504]. This review of the growing body of evidence which supports the theory of heat shock proteins and not LPS contamination being responsible for various immunological effects showed that support far outweighs the criticism. That is not to say that LPS is not an issue, however it does highlight the necessity of taking steps to ensure LPS contamination is minimal and that experiments are adequately controlled in order to ensure that effects are attributable to Hsp70.

1.3.4.2. Immunity to pathogens

Evidence also suggests that a similar Hsp70-peptide complex-mediated mechanism can induce immunity to infectious agents [489, 505]. Ciupitu and colleagues showed that mice immunised with Hsp70 complexes formed with peptides from lymphocytic choriomeningitis virus (LCMV) withstood later challenge with LCMV, and exhibited reduced virus titres and the presence of peptide-specific cytotoxic T cells [506]. Similarly, other stress proteins can form peptide complexes that are capable of eliciting immune responses to infectious agents. Mice immunised with gp96-peptide complexes from *Mycobacterium tuberculosis* or Listeria have been shown to exhibit a significant expansion of cytotoxic T lymphocytes when compared to control mice [507]. Mycobacterial Hsp70 fused with proteins can also elicit an immune response, with mice immunised with HIV-1 p24 expressing anti-p24 IgG1 antibodies for over a year [508].

1.3.4.3. Autoimmunity

As Hsp70 is highly conserved between species, and immune responses can be directed against pathogen-derived Hsp70, is it also possible to see a response against self-Hsp70? Healthy individuals have anti-Hsp70 antibodies in their serum [280] and although immune reactivity towards Hsp60 has been implicated in the progression of arthritis [509], multiple sclerosis and diabetes mellitus [510], there is evidence that immune reactivity against self-Hsp can be immunoregulatory and control inflammatory responses [511]. *Ex vivo* observations of BALB/c mice that received various doses of the heat shock protein gp96 (between 0.5 and 200 µg) found that inhibition in the T cell response increased with increasing dose of gp96, and that this inhibition was mediated via an increased activation of Treg cells [512]. Using isolated $CD4^+$ T cells and Treg cells from healthy human donors, *in vitro* investigations have demonstrated that treating Treg cells with 10µg/mL can enhance their suppressive capabilities on $CD4^+$ T cells by increasing the secretion of the suppressive cytokines IL-10 and TGF-β [513]. In a rat model of breast cancer, tumour radiofrequency ablation has been shown to increase the levels of circulating heat shock proteins, thereby leading to speculation that a bystander effect may be enhanced immunosuppression [514]. The clinical implication of the immunomodulation which is mediated by heat shock proteins is clearly an important point for consideration.

1.3.5 Membrane Hsp70 (memHp70)

In addition to being an intracellular and extracellular protein, studies in the mid-1990s by Gabriele Multhoff and Claus Botzler demonstrated the selective localisation of Hsp70 within the plasma membrane of tumour cells [285-289]. These studies revealed that Hsp70 can be integrated into the membrane, with only a small sequence of the substrate binding domain being exposed on the cell surface.

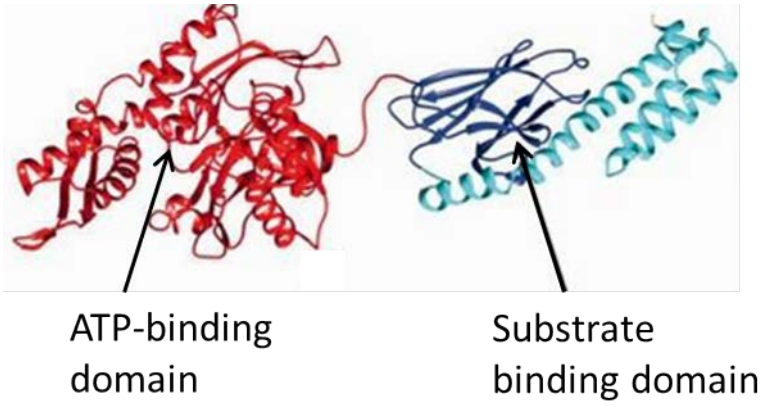

Figure 1.2 Structure of Hsp70

Diagram showing the structure of Hsp70. The N-terminal or ATP-binding domain is shown in red, and the C-terminal or substrate binding domain is shown in blue. The substrate binding domain is comprised of two parts, a two layered twisted β sheet (dark blue) which can actually bind substrate and an α helical subdomain (light blue) which acts as a lid closing over any bound substrate.

Imaged adapted from hsp70.com/structure

The definitive distinction of the membrane form of Hsp70 from Hsp70 which has bound to the cell surface either via plasma membrane- or receptor-mediated interactions is only possible using a specific mAb [289]. The cmHsp70.1 mAb has been generated using hybridoma cells by multimmune GmbH (Munich, Germany), with specificity confirmed by way of immunoprecipitation using Hsp70 protein from heat shocked cells. The antibody epitope was determined using perspot membrane epitope mapping analysis, utilising 13-mer peptides of the C-terminal domain set up with 11-mer overlaps; the epitope of the cmHsp70.1 mAb is amino acid residues 453-461 within the β-sheet of the substrate binding domain [285]. When Hsp70 is held within the membrane, only a portion of the substrate-binding domian of the protein is exposed on the cell surface and is therefore accessible to the cmHsp70.1 mAb. All other commercial antibodies to Hsp70, including a mAb supplied by StressMarq Biosciences (clone C92F3A-5, Victoria, Canada) recognise epitopes that are outside of this region and do not, therefore, recognise the membrane form of Hsp70. Binding of the cmHsp70.1 mAb, but not the C92F3A-5 antibody therefore definitively distinguishes the membrane form of Hsp70 from extracellular Hsp70 which has bound to the cell surface. This is an important control of which to be aware, as there are reports of membrane Hsp70 expression in the literature by other investigators which, as they have not used the cmHsp70.1 mAb, reflects Hsp70 which has bound to the membrane, and not the membrane form of the molecule which was first described by Multhoff and Botzler.

1.3.5.1 Membrane Hsp70 expression on Tumour Cells

Ongoing screening of tumour biopsies taken from a variety of primary tumours including breast, colon, gastric, lung, prostate, head and neck, ovarian, pancreatic and haematological malignancies (currently standing at over 1,300 samples) indicates that around 40-60% of the tumours are positive for the membrane form of Hsp70, whereas corresponding normal tissue is membrane Hsp70 negative [285]. The potential relationship between membrane Hsp70 expression and the prognosis of patients was investigated by Pfister *et al* [515]. In total, 150 patients suffering from colon cancer, gastric cancer, lower rectal carcinoma or squamous cell carcinoma were assessed for memHsp70 expression and followed up for 5 years. Despite a similar proportion of patients with each cancer type expressing memHsp70 (37-43%), there were clear differences in disease prognosis; the memHsp70 status of tumours correlated with a significantly improved *survival* of patients with colon or gastric cancer, but to a significantly *reduced* survival of patients with lower rectal or squamous cell carcinoma. The authors hypothesise that this difference stems from different patterns of metastatic spread. Both colon and gastric cancers preferentially metastasise through the liver, thus exposing them to hepatic NK cells. Having previously demonstrated the ability of activated NK cells to recognise and kill memHsp70$^+$ tumour cells (see below) [516], the authors suggest that a hepatic NK response to memHsp70$^+$ metastases leads to tumour cell death and subsequent improvement in patient survival.

The mechanism via which Hsp70 is selectively integrated into the plasma membranes of tumour cells is currently unclear. However, evidence suggests that membrane lipid composition might be involved, at least for some cancer cells. Release of Hsp70 from Caco-2 epithelial cells is reduced by treatment with methyl-β-cyclodextrin, a drug which disrupts lipid rafts (now more commonly termed cholesterol rich microdomains or CRM) [517]. If CRMs are involved in Hsp70 release, then perhaps they also play a role in anchoring Hsp70 into the membrane. Gehrmann *et al* profiled lipids from plasma membranes of two human cancer cell lines (colon-derived CX2 and pancreas-derived Colo357) and they found significantly higher expression of the glycosphingolipid Gb3 in membrane Hsp70 positive cells, along with co-localisation of the Hsp70 with Gb3 [518].

Given that the vast majority of normal tissue is Gb3 negative, the authors suggested that this could help explain the high incidence of membrane bound Hsp70 in tumour cells. However, it appears that Gb3 is not an absolute requirement for memHsp70 expression, as recent studies involving breast cancer cell lines (MCF7, MDA-MB-436 and T47D) have shown high expression of membrane Hsp70, despite none of the cell lines being positive for Gb3 (unpublished data). The mechanisms by which Hsp70 locates and anchors into the plasma membrane are not yet

fully elucidated and it could be that the involvement of Gb3 is cell type dependent. Another interesting point to note is that memHsp70 expression is increased in response to gamma irradiation, as well as a number of chemotherapeutic agents [290, 519, 520]. The fact that membrane Hsp70 appears to be selectively expressed on a large proportion of tumours suggests that it might act as a useful and widely applicable structure and target for immunotherapies. Furthermore, the potential of this molecule as a targeting structure is further enhanced by the observations that its expression can be increased following conventional therapies.

1.3.5.2 MemHsp70 as a target recognition structure for NK cells

A key discovery by the Multhoff laboratory [289] has been that membrane Hsp70 acts as a target recognition structure for activated NK cells. Their studies have shown that NK cells which have been activated *ex vivo* with low dose IL-2 (100 U/ml over 3-4 days) recognise membrane Hsp70 positive tumour cells via CD94 molecule.

Focusing around the 8-mer epitope of the cmHsp70.1 mAb (as this is the region which is available on the surface of memHsp70$^+$ tumour cells and therefore the part available for recognition by NK cells), the Multhoff laboratory trialled a variety of Hsp70-derived peptides for their ability to activate NK cells. Using peptides from 8 to 14-mer, that match the cmHsp70.1 mAb epitope or that were extended towards the N-terminal, the C-terminal or both, as well as peptides matching equivalent regions in Hsp70hom, Hsc70 and DnaK, the authors found that whilst most failed to elicit NK activity, the 14-mer peptide TKDNNLLGRFELSG (abbreviated to TKD peptide) was able to stimulate both cytolytic and proliferative activity of NK cells [523]. The effect was confirmed using anti-Hsp70 mAbs to block the interaction [522]. The Multhoff group also showed that an increased expression of the membrane form of Hsp70 on tumour cells correlates to the cell having an increased sensitivity to killing by IL-2/TKD-activated NK cells [522]. Another interesting point to note is that NK cells which have been activated by Hsp70 or TKD peptide show increased expression of granzyme B, thereby leading to enhanced cytotoxic potential of NK cells [524].

Investigation of human NK cells *in vitro* showed that stimulation with TKD peptide increases their migration towards, as well as cytolytic activity against, memHsp70$^+$ cancer cells [525]. The action of NK cells on memHsp70 tumour cells has also been studied *in vivo*, using a pancreatic cancer model, in which Colo357 cells injected into SCID/beige mice (which lack T lymphocytes and NK cells). NK cells which had been incubated with low dose IL-2 (100IU/mL) and TKD peptide (2µg/mL) for 4 days were administered to the mice, with the result being a decrease to tumour burden, delayed appearance of metastases and an increase to life expectancy [526].

Other studies have reported on the capacity of NK cells purified from peripheral blood samples of both healthy donors and patients with leukaemia that had been stimulated *ex vivo* with a 14-mer peptide matching the sequence of the NK cell recognition site on Hsp70 (2µg/mL), together with a low dose of IL-15 (10µg/mL) for 5 days (or with one or neither stimulant as a control) to increased density of CD56 and CD94 on the NK cells' surface and boosted the cytolytic activity against memHsp70^{+} K562 cells or autologous/allogenic leukaemic blasts *in vitro* on the basis of their release of granzyme B using an ELISpot [527].

1.3.6 Clinical Application of Membrane Hsp70 targeted tumour immunotherapy

As a large proportion of tumours express memHsp70, it is plausible to attempt to exploit this unique and selective expression for the therapeutic targeting of tumours. This could be achieved via a variety of approaches.

1.3.6.1 Tumour targeting with NK cells

A phase I clinical trial looking at the feasibility and safety of infusing cancer patients' own *ex vivo* IL2/TKD-stimulated NK cells in an effort to increase cytolytic activity against tumour cells has been conducted [528]. The patients involved were suffering from either non-small lung cell carcinoma or metastasised colorectal cancer. NK cells from the majority of the patients (10 out of 12) exhibited an increased surface density of CD94 expression and an upregulation of NK cell cytolytic activity directed against membrane Hsp70 positive tumour cells following *ex vivo* stimulation. Of the 5 patients who received more than four cycles of treatment, two showed clinically measurable improvement.

Following the Phase I trial, the same group also published a case report of a male patient with colorectal carcinoma who was given similar treatment. Peripheral blood mononuclear cells obtained using leukapheresis were activated *ex vivo* with a combination of IL-2 and TKD peptide for four days before being re-infused to the patient [529]. This patient received monthly treatment for six months, was given a three month break, then returned for a further three months. After treatment, there was an infiltration of NK cells to metastatic sites, and a reduction in expression of the colon carcinoma marker carcino-embryogenic antigen (CEA). These are encouraging results, as both scenarios correlate with better prognosis. Cytotoxicity of the NK cells was assessed *in vitro* which had been generated from the patient's own tumour as the target [529].

Multiple infusion treatments resulted in increased NK cytotoxicity, and although this abated during the break from treatment, once the infusions recommenced NK cytotoxicity quickly returned to the previous level. Overall, the findings of these studies are very encouraging and this avenue potentially offers a novel treatment in cancer therapy. A multi-centre randomised

control Phase II trial in patients with non-small cell lung carcinoma commenced in Germany in early 2015 (Gabriele Multhoff, personal communication).

1.3.6.2 Tumour targeting with granzyme B

An affinity column conjugated with a 14-mer peptide corresponding to a region within the extracellular portion of memHsp70 was used to determine which component(s) of NK cell lysates bound to the solid phase. This approach identified that a 32kDa protein bound to the Hsp70-derived peptide, and this was identified as being granzyme B. The discovery that memHsp70 could act as a conduit for the internalisation of the serine protease granzyme B was highly significant, as this suggested another approach for the therapeutic targeting of tumours expressing membrane Hsp70 [530]. To confirm whether granzyme B could also bind to the membrane form of Hsp70 on tumour cells, the ability of memHsp70^{+} CX-2 (colon carcinoma) and Colo357 (pancreas carcinoma) cell lines to bind and take up granzyme B was examined. Both cells lines took up granzyme B and it was shown that granzyme B uptake resulted in apoptosis, despite the absence of perforin in the system [530].

Investigations into the effect of a human recombinant form of granzyme B on a mouse colorectal cancer model using the CT26 cell line have showed similar results [531]. The treatment of cells grown in a monolayer and as spheroids with granzyme B results in caspase-3 activation, the killing of cultured cells and a reduction in the size of spheroids [532]. Granzyme B has also been shown to significantly reduce the size of implanted CT26 tumours expressing memHsp70 in BALB/c mice [532]. No adverse side effects were recorded, nor was there any accumulation of granzyme B in healthy organs. The treatment therefore appears to be well tolerated. Further studies are now required in order to assess the feasibility of this potential treatment in humans.

Whether memHsp70 expressed on breast cancer cells allows this internalisation of granzyme B, and if so whether knowledge pertaining to the internalisation pathway can give information about the ability to induce apoptosis, will be the subject of this thesis. The ability to directly target tumour cells on the basis of their memHsp70 expression could prove to be a valuable clinical tool. With around 50% of tumours expressing this molecule to some degree [285], and with metastatic disease expressing even higher levels than their memHsp70 expressing primary tumour counterparts [532], granzyme B has great potential as a therapeutic molecule which would be a highly specific and effective in a large proportion of patients with cancer. Theoretically, granzyme B could be an excellent combination treatment for cancer patients, as its targeting molecule (memHsp70) is widely expressed, induced by radio(chemo)therapy and would continue to be effective in individuals that have been rendered as being

immunosuppressed either as a consequence of disease or the treatments that they have received. Furthermore, the *in situ* killing of tumours is likely to induce the release of tumour specific antigens which might promote the development of protective anti-tumour immunity either alone, or in combination with an appropriately configured vaccination strategy.

1.3.6.3 Tumour targeting with the cmHsp70.1 monoclonal antibody

Stangl and colleagues have demonstrated that the cmHsp70.1 mAb can also be used *in vivo* to target tumours derived from the CT26 memHsp70 positive murine colorectal cancer cell line [533]. Three doses of the cmHsp70.1 mAb has been shown to significantly reduce tumour volume and increase the survival of BALB/c mice bearing subcutaneous CT26 cells. The cmHsp70.1 mAb binds to memHsp70 on tumour cells and promotes ADCC by NK cells. That the targeting is specific for memHsp70 and involves the induction of ADCC has been confirmed using a memHsp70$^-$ cell line (small cell lung carcinoma 1048) and treatment with C92F3A-5 mAb (specific for an epitope unavailable in the membrane form of Hsp70) or a Fab fragment of cmHsp70.1 (cannot induce ADCC), none of which had any effect on tumour progression.

The possibility of using the cmHsp70.1 mAb to better image tumours has also been considered, and investigated by Stangl and colleagues, again using CT26 tumours in BALB/c mice [534]. For these studies, mice were injected with Cy5.5-labelled cmHsp70.1 mAb 14 days after receiving the tumour cells. Using intraoperative fluorescent imaging it was possible to detect localisation of the antibody to the tumour within 30 minutes. This localisation was highly selective, as a similarly labelled isotype control was not detected in the tumour, and nor was the cmHsp70.1 mAb detected in healthy surrounding tissue. By overlaying a standard optical image of the tumour region with the fluorescent image, the authors showed that cmHsp70.1 mAb binding was restricted to an area with the tumour boundary. The antibody was endocytosed via mechanisms which the authors suggest involves the rapid turnover of membrane Hsp70, and accumulated within the tumour whilst retaining fluorescence. The fluorescence intensity remained at a detectable level for up to 96 hours. The implications of this study to future treatment possibilities are exciting. As well as offering improvements to tumour imaging, this specific tumour targeting and subsequent internalisation of the cmHsp70.1 mAb could enable the selective delivery of chemotherapeutic drugs or radio-nuclides to tumours, whilst avoiding damage to healthy tissue.

Although it is clear that memHsp70 positive CT26 cells are capable of internalising fluorescently-labelled cmHsp70.1 mAb, the precise intracellular trafficking pathway has yet to be elucidated. In order to be able to exploit this effect for drug delivery it is essential to fully understand the subsequent intracellular movements of internalised antibody. The most

effective way to do this would be to undertake microscopical analysis of cells after cmHsp70.1 mAb internalisation. The selectivity, kinetics and route(s) of cmHsp70.1 mAb internalisation into tumour cells will be investigated in this thesis.

1.3.6.4 Tumour targeting with the TKDNNLLGRFELSG 14-mer peptide

The NK cell recognition site of Hsp70 is a 14 amino acid sequence within the substrate binding domain (aa 450-463) [523, 525], which is within the region that is exposed extracellularly when Hsp70 is in the cell membrane. Although the use of the peptide to direct and boost NK cell mediated cytotoxicity towards memHsp70^{+} tumours could prove to be a powerful tool in tumour therapeutics, it might also have value for tumour imaging and targeting.

Peptides have many advantages over antibodies as targeted imaging and therapeutic agents [535]. They are relatively easy and quick to generate in large quantities and typically have low associated toxicities. They are stable, exhibit better distribution than antibodies and being small molecules have an enhanced ability to penetrate tissues. Peptides are already under investigation for targeting HER2^{+} breast cancer in pre-clinical mouse models. A combination of two peptides, one derived from the B cell epitope of HER2 and the other as a VEGF mimic, have been shown to inhibit the *in vivo* growth of TUBO tumours in BALB/c mice [536]. The expression of membrane Hsp70 on a large proportion of tumour entities opens up a potentially powerful small molecule targeting strategy. The 14-mer peptide derived from the C-terminal substrate binding domain of Hsp70 which is capable of binding to membrane Hsp70, both *in vitro* and in vivo, could offer an avenue to provide greater tumour imaging potential [535].

1.4 Hypotheses

- Membrane Hsp70 on breast cancer cell lines offers a route of specific tumour targeting.
- Granzyme B internalised via memHsp70 leads to apoptosis in human breast tumour cells.

1.5 Aims and Objectives

The aim of the proposed study is to use multi-parameter flow cytometry and fluorescent confocal microscopy imaging technology to define the kinetics and pathway of internalisation of three potential theranostics (cmHsp70.1 mAb, TKDNNLLGRFELSG 14-mer peptide and granzyme B) into breast cancer cell lines expressing the membrane form of Hsp70, with a view to better understanding their targeting and imaging potential. Specifically, this study will

- Use imaging technology platforms to determine the uptake of cmHsp70.1 mAb, TKDNNLLGRFELSG 14-mer peptide and granzyme B and elucidate the pathways that are involved and utilised.
- Use different imaging platforms to compare uptake pathways and kinetics in relation to membrane Hsp70 expression.
- Develop novel analytical approaches that better enable uptake kinetics and co-localisation to be interrogated from fluorescent images.

As a secondary aim, the project will also use flow cytometry to determine whether lymphocyte populations express memHsp70 and whether any expression can be upregulated in response to factors consistent with a tumour microenvironment.

CHAPTER 2 Materials and Methods

2.1 Background

The primary aim of this study is to use imaging technology (multi-parameter flow cytometry and confocal microscopy) to characterise and quantify the selective internalisation of cmHsp70.1 mAb, granzyme B and an Hsp70-derived peptide (TKDNNLLGRFELSG) by breast cancer cells expressing membrane Hsp70.

Although flow cytometry can give high-throughput results and can be used to acquire and analyse many different fluorescent signals in a single cell, it cannot provide any insight into the localisation of the signal, nor can it provide a definitive insight into the surface binding, internalisation and intracellular localisation of given molecules. In contrast, confocal microscopy provides information on localisation of target molecules on and within cells. Combining these two techniques permits a comprehensive analysis of cell-molecule interactions and their dynamic relationship(s).

2.2 Tumour Cell Lines

Five cancer cell lines were used in this work. Three are derived from human breast cancer metastasis (MDA-MB-231, MCF7, T47D), whereas the other two are derived from murine mammary carcinoma (4T1) and murine colon carcinoma (CT26). MDA-MB-231, MCF7, T47D and 4T1 cells were purchased from the European Collection of Cell Cultures (ECACC) whereas the CT26 cells were provided by Professor Gabriele Multhoff (Technische Universität München, Munich). The three human lines were selected, as they represent a range of disease states and severity. 4T1 cells were used to assess whether a mouse model behaved in the same way as human cells. The CT26 cells were used as a comparison to previously published data which have demonstrated that the cmHsp70.1 mAb can specifically bind*, in vivo*, to tumours derived from colorectal cancer cells expressing memHsp70.

Cell Line	HER2	ER	PR	Classification	Disease severity represented
MDA-MB-231	-	-	-	TNBC	+++
MCF7	-	+	Low	Luminal A	++
T47D	-	+	High	Luminal A	+

Table 2.1 Characteristics of the human breast cancer cell lines selected

A summary of the key differences between the three human-derived breast cancer cell lines used in this study, in terms of receptors expressed and disease severity represented. HER2 (also HER2/neu) = Human epidermal growth factor receptor 2. ER = Oestrogen receptor. PR = Progesterone receptor.

MDA-MB-231: This epithelial cell line was derived from pleural effusion of a 51-year old Caucasian female with mammary adenocarcinoma [537]. It expresses receptors for both epidermal growth factor and transforming growth factor alpha (TGFα). These cells are adherent, and have a doubling time of less than 24 hours.

MCF7: This epithelial cell line was also originally derived from the pleural effusion of a 69-year old Caucasian female patient with a mammary carcinoma [538]. The cell line differs from the MDA-MB-231, in that cells express the oestrogen receptor [539], and cell growth is inhibited by exogenous TNFα.

T47D: This epithelial cell line was originally isolated from the pleural effusion of a 54-year old female with a ductal carcinoma and expresses a range of hormone receptors, including those for androgen, oestrogen, progesterone and prolactin [540].

4T1 is a tumourogenic cell line derived from the mammary gland of BALB/c mice [541]. It is a commonly used cell line for studying metastatic breast cancer *in vivo* and is an animal model for stage IV human breast cancer. After implantation, the primary tumour quickly and spontaneously metastasises to many sites, including the lung, liver, brain and lymph nodes.

CT26 is a tumourogenic cell line derived from a transplantable colon carcinoma in BALB/c mice [542]. Although not a breast tumour model, this line was included, as the cmHsp70.1 mAb has previously been shown to bind to memHsp70^{+} tumours *in vivo* [534].

2.2.1. Cell Culture – Maintenance

All tumour cell lines were grown in RPMI 1640 growth medium, supplemented with foetal bovine serum (5% v/v in the case of the CT26 cells, 10% v/v for all the others), 6mM glutamine, 100IU/mL penicillin and 100µg/mL streptomycin (termed RPMI^{complete}) (all reagents supplied by Lonza).

All of the cell lines are adherent and therefore require trypsin-EDTA (Lonza) treatment in order to passage. The growth medium was decanted from the flask and cells were washed twice with 8-10 mL PBS (Lonza), taking care to gently bathe the PBS over the whole surface of the flask before decanting. This is important, as it ensures removal of as much of the remaining RPMI^{complete} as possible. This has a high content of protein which can block the action of the trypsin-EDTA. After washing, 2.5 mL trypsin-EDTA was added to the flask and bathed over the

cells before removing with a pipette. The flask was replaced in the incubator for an appropriate duration for the particular cell line (see **Table 2.2**). Once completed, the cells were checked for rounded edges (to show they were beginning to detach) and the flask was gently tapped to dislodge cells, after which the activity of the trypsin-EDTA was neutralised by adding 5 mL of fresh $RPMI^{complete}$. This medium was gently pipetted a few times over the bottom of the flask to ensure collection of all cells, and to encourage cells into a single cell suspension rather than aggregating. Usually, those cell lines which require longer incubation times with trypsin-EDTA are also more prone to cellular aggregation. A proportion of the cells was added to fresh $RPMI^{complete}$ in a new T75 flask, making a total volume of 10 mL. The proportion of cells added was dependent on cell line (see **Table 2.2**).

	Incubation time with trypsin-EDTA	Passage Proportion
MDA-MB-231	>30 seconds	1/10
MCF7	>90 minute	1/6
T47D	>3 minutes	1/5
4T1	>3 minutes	1/10
CT26	>30 seconds	1/20

Table 2.2 Cell culture - maintenance

Whilst trypsin-based cellular detachment is highly effective, its action is to cleave at any lysine or arginine sites and therefore it is not specific for surface adherins. The cells need sufficient incubation time for the adherence to be disrupted, but not so long that all other surface antigens are also cleaved. This Table list the incubation times that are required for effective cell detachment using trypsin-EDTA incubation, as well as the proportion of cells that were used to seed T75 flask at each passage.

2.3 Determining memHsp70 status of tumour cells

The expression of membrane Hsp70 by the cell lines that were used in the study was determined by flow cytometry using fluorescently-labelled antibodies specific for different Hsp70 epitopes. For this, cells were first passaged and reseeded at cell numbers that would produce confluent cultures after 48 hours.

2.3.1 Cell Culture – Experimental Set Up

Trypsinised cells were harvested and cells were counted on a haemocytometer using trypan blue (Sigma Aldrich) exclusion to determine viability. One grid block from each side was counted, the counts were averaged and then converted to $\chi*10^6$ cells/mL format. The appropriate number of cells that would result in confluent cultures after 48 hours (**Table 2.3)** were suspended in 10 ml of $RPMI^{complete}$ and cultured in T75 flasks until being harvested, stained and analysed by flow cytometry, as described below.

	T75 Flasks
MDA-MB-231	$1.25x10^5$
MCF7	$2.50x10^5$
T47D	$5.00x10^5$
4T1	$1.25x10^5$
CT26	$1.25x10^5$

Table 2.3 Seeding densities into T75 flasks

To compensate for different growth rates, cell lines were seeded into T75 flasks at different densities which allow for comparable levels of confluency after 48 hours. This table details the starting number of each cell line.

2.3.2 Staining of tumour cells

The expression of memHsp70 by cultured cells was determined every 24 hours for up to four days, or until the cells had reached confluency. MemHsp70 was determined using the cmHsp70.1 mAb (multimmune GmbH, Germany) which is specific to an epitope within the substrate binding domain of Hsp70 which is exposed when in the membrane form [289]. The cmHsp70.1 mAb is the only antibody which can recognise this unique membrane form of Hsp70. The specificity of the staining for membrane Hsp70 expression was confirmed using a second anti-Hsp70 mAb (clone C92F3A-5 clone, Stressgen via Enzo Life Sciences) which is specific for an epitope towards the N terminus of the molecule which is inaccessible on viable, membrane Hsp70 positive cells. As a consequence, if cells are positive for cmHsp70.1 mAb staining, but not for C92F3A-5 mAb staining, then Hsp70 is present in the membrane form. Positivity for both antibodies indicates that the entire Hsp70 molecule is present on the cell surface, and this is not reflective of the presence of the unique membrane form. This is an essential control for such experiments, as many cells and cell lines can release Hsp70 into the extracellular environment. This could then bind to the cell surface and give a false positive indication as to the memHsp70 status.

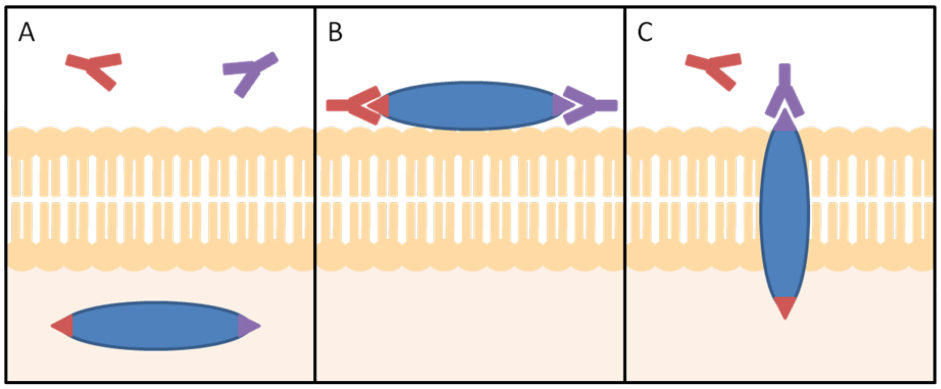

Figure 2.1 Different specificities of the cmHsp70.1 and C92F3A-5 anti-Hsp70 mMAb clones

(A) When Hsp70 only expressed intracellularly neither antibody (cmHsp70.1 in purple; C92F3A-5 in red) can bind. If Hsp70 is bound to the cell membrane **(B)** then both antibodies are capable of binding the molecule, but when the membrane form of Hsp70 is present, **(C)** then only the cmHsp70.1 can bind.

At the appropriate time, cells were harvested using Trypsin-EDTA as described above and viable cells counted. Cells were rested for 15 minutes before starting the staining in order to allow for the recovery of any memHsp70 that has been potentially cleaved during the trypsinisation process (Gabriele Multhoff, personal communication), after which $1x10^5$ cells were transferred into 1.5 ml microfuge tubes and washed with 1 ml staining buffer (phosphate buffered saline (PBS) containing 10% v/v FCS). After centrifugation (300g, 4°C, 5 minutes), the supernatant was removed using a vacuum aspirator and cells were resuspended being placed on ice. Cells were resuspended in 15 µL staining buffer containing 0.2µg of either FITC-conjugated cmHsp70.1 mAb (provided pre-conjugated by multimmune GmbH), FITC-conjugated C92F3A-5 mAb (Stressgen via Enzo Life Sciences) or an appropriate FITC-conjugated IgG1 isotype control (Biolegend). The concentration of the cmHsp70.1 mAb was as recommended by the supplier, and the other reagents were used at the same concentration. Unstained cells were included as a further negative control in all assays.

Samples were vortex mixed and incubated at 4°C protected from light for 30 minutes, after which cells were washed with 1mL staining buffer, the supernatant aspirated and cells resuspended in staining buffer. Cells were then transferred into 12x75 mm tubes and stored on ice protected from light until they could be analysed by flow cytometry, but this was always conducted within 1 hour. Propidium iodide (Sigma Aldrich, used at 0.5 µg in 10µL) was added to each sample no more than 5 minutes prior to flow cytometric data acquisition, in order to enable the exclusion of non-viable cells from all of the analyses. In some of the cell lines, there was some variation in the expression of memHsp70 over time after cell seeding (**Fig. 2.2**). As

the highest intensity expression was observed 48 hours after seeding this was the time-point selected for experimental use.

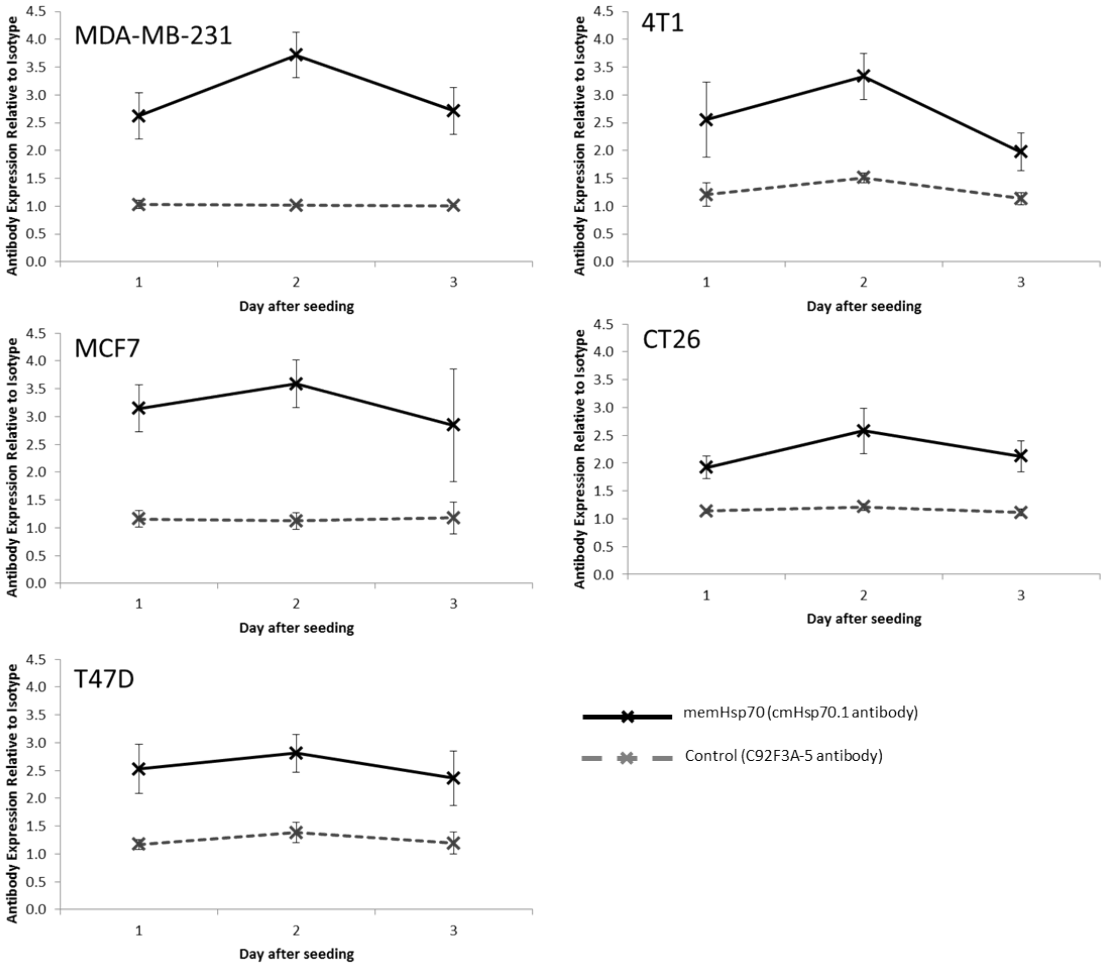

Figure 2.2 Membrane Hsp70 expression of cell lines over time

Cells were seeded into T75 flasks and their expression of memHsp70 was monitored over a period of 72 hours. The solid lines show the staining intensity with cmHsp70.1 (and therefore the expression of membrane Hsp70), whilst the dashed lines show staining intensity with the control C92F3A-5 antibody. The maximal intensity of expression was observed 48 hours after seeding, so this time-point was used for subsequent experiments. Data shown are the mean (±SEM) of at least three independent experiments.

2.4 Flow Cytometry

2.4.1 Introduction to Flow Cytometry

Flow cytometry is a technique for analysing the size, intracellular granularity and the fluorescent characteristics of cells in a single cell suspension using lasers and optics. Individual cells pass through the laser beams, with the subsequent scattered and emitted light being collected by detectors which convert the light into quantifiable electrical signals.

This study used a BD™ LSRII flow cytometer equipped with four excitation lasers (355nm, 405nm, 488nm, 633nm) and FACSDiva™ acquisition and data analysis software (BD Biosciences). Theoretically, it is possible to measure 13 fluorescent parameters, although in reality fewer are possible due to spectral overlap which is caused by the emission of one fluorophore 'leaking' into the detection channel for a second fluorophore. Although some degree of spectral overlap can be corrected by compensation (see below), this can reduce the sensitivity of detection. It is therefore essential that an appropriate panel of conjugated antibodies is selected in order to minimise spectral overlap issues. In addition, detectors measure the light which is scattered in line with the 488nm laser (Forward Light Scatter, FSC) and light which is scatted to the side of the laser (Side Light Scatter, SSC). These parameters provide information about the size and intracellular complexity/granularity respectively, thereby providing information which allows cell populations to be visualised (**Fig 2.3**). Three size and three granularity measurements can be taken, relating to the area, height and width of a cell, denoted by –A, –H or –W following the description at acquisition. The acquisition of at least the area and one other parameter enables additional analyses to be conducted subsequently.

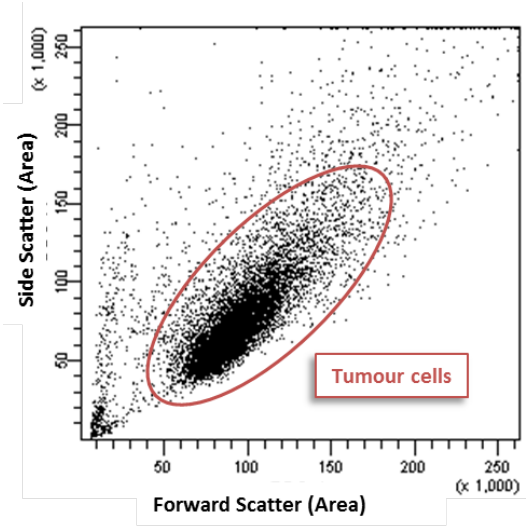

Figure 2.3 Visualising cell populations by flow cytometry

The extent of forward and side scattered light provides information about the size and granularity of cells respectively. In this instance MCF7 cells are shown as a distinct population in the centre of the dot plot (circled in red).

2.4.2 Isotype controls

In addition to excluding background auto-fluorescence from the analysis by including unstained cells in all experiments, appropriate isotype controls were also included. It is essential to confirm that mAbs are binding to cells via the specific receptor/marker of interest, and not non-specifically (e.g. via Fc receptors). In humans, antibodies fall into one of five classes (IgG, IgM, IgA, IgD, IgE). The inclusion of non-reactive isotype-matched controls (the

same class of antibody as the one of interest labelled with same fluorescent marker) in all experiments and the setting of analysis gates that are defined on the basis of the isotype control samples allows any non-specific, background binding to be excluded. In this study, such binding was minimised by incubating samples with normal mouse serum prior to the mAbs of interest. Isotype controls were included, as the expression of memHsp70 is typically represented as a shift in the fluorescence histogram rather than a defined separate population of cells. Further details on the approaches that were used for analysing the data are presented below.

2.4.3 Compensation

As indicated above, one of the difficulties that can be encountered when undertaking multi-colour flow cytometry is the issue of spectral overlap (spillover) between the emission spectra of different fluorochromes. Spectral overlap occurs when the emission of one fluorophore 'leaks' into the detection channel for a second fluorophore (**Fig 2.4**). The potential for spectral overlap can be minimised with careful selection of fluorochromes; i.e. selecting those which require different excitation sources and/or have distinct and non-overlapping emission spectra. However, fluorochrome options can be limited, and so in very large experiments some degree of spectral overlap is always unavoidable. The only approach to consider and avoid erroneous data is to apply 'compensation', the aim of which is to 'remove' the spectral overlap signal from the detection channel for the second fluorophore.

The principle behind setting up compensation is to run through single colour samples for each fluorochrome in the panel, check the output into all of the other channels and adjust the percentage deductions until data are only received into the correct channel. The figures for compensation are quoted as percentages, and there is one for every possible pair of fluorochromes. It is worth noting that compensation ceases to be as effective over 50%, as the consequence could be an increase in false negative signals, and any fluorochrome pairs that produce such a high compensation requirement should not be used together in the same experiment.

Applying compensation manually is difficult, especially when more than two fluorochromes are involved. To simplify the process some acquisition software, including BD FACSDiva™, allows users to apply compensation calculations automatically. FACSDiva™ allows this to be done at any time, although with some software it is only possible to apply compensation at the time of acquisition.

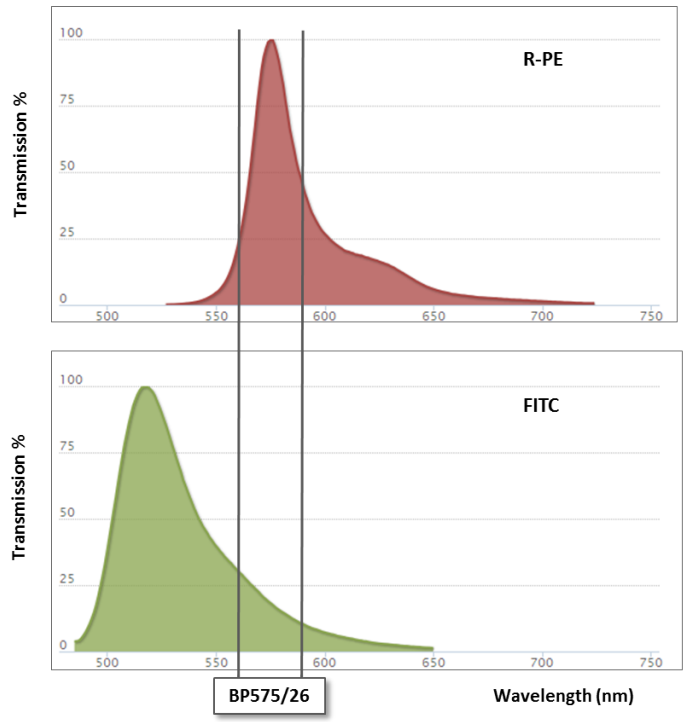

Figure 2.4 Spectral overlap

Spectral overlap is caused by the emission from different fluorochromes being detected in the same channel and can be illustrated with the emission spectra from two of the most commonly used fluorochromes; FITC and R-PE. The maximum emission of R-PE occurs at 576nm which is perfectly captured using a band pass (BP) 575/26 filter (a range of 26nm around a mid-point of 575nm). Whilst the emission peak of FITC is at 518nm, 15-30% emission still occurs at the longer wavelength region covered by the BP575/26 filter. Therefore, if these two fluorochromes are used in conjunction, a proportion of data recorded as R-PE emission will actually be from FITC emission. A process of compensation can be applied. This involves removing an appropriate percentage of acquired data from any detector channel, and is dependent on the fluorochrome combination and individual instrument voltages. Compensation values must be calculated for every analysis conducted. Emission curves were generated using CurvoMatic software (Omega Optical, Inc (USA): www.omegsfilters.com/Products/Curvomatic).

Compensation was set up using the BD™ CompBeads system (BD Biosciences). This comprises polystyrene microparticles, half of which have been coated in an anti-mouse Ig antibody and the other half uncoated. When antibody and beads are incubated together, coated beads can bind the antibody non-specifically through the F_c region whilst the uncoated beads cannot. This provides a sample with both positive and negative signals for the given fluorochrome. The benefits for using this bead system are twofold. Firstly, cell samples can be used for the experimental analyses rather than for the instrument set up procedures, thereby maximising data from a single experiment. Secondly, accurate compensation relies on having a reasonably sized positive population for each fluorochrome in question. Therefore, using cells with rare populations and/or inducible markers can make compensation very difficult. Although the acquisition software is used to calculate the actual compensation settings, it is important to know how correctly compensated data appear on screen (**Fig 2.5**), and also to check every

possible pair of fluorochromes in each experiment to ensure that the compensation has been applied appropriately.

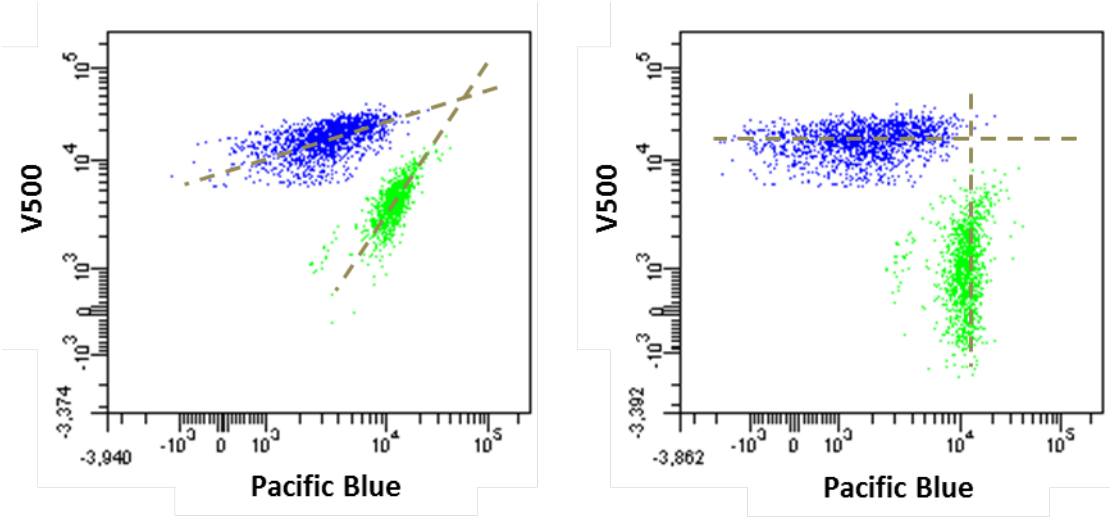

Figure 2.5 Applying compensation

Although the actual compensation calculations are applied by the acquisition software, it is important to be aware of how this appears on screen in order to see whether it has been applied correctly. The left hand plot shows data before compensation, with the cell populations exhibiting a dragging, diagonal shape across the plot and seeming to converge in the top left corner. After compensation has been applied (right) the populations follow a more regular formation clearly separated from each other.

2.4.4 Data acquisition

To minimise the effect of photo-bleaching on the fluorochromes, cells were kept on ice and in the dark until the time to acquire data. Data acquisition took place as soon as possible, and always within 1 hour of staining the cells. To enable exclusion of non-viable cells, propidium iodide was added to the cells, but not more than 5 minutes before running the acquisition. For these particular experiments, all acquisitions took place on a BD™ LSRII using the 488nm excitation laser and acquiring through the 530/30, 575/26 and/or 610/20 nm band pass filter channels, depending on the specific requirements of each experiment. Data acquisition was automatically stopped when data on 10,000 tumour cells (or as many cells as possible) were collected.

2.4.5 Post acquisition analysis

All analysis was undertaken using FACSDiva™ software by creating a hierarchy of regions of interest around cells (**Fig 2.6**). It always began with setting up plots to first choose the population of interest, using forward (FSc) and side (SSc) light scatter profiles to define the relevant population. The population often appears as a dragged diagonal shape towards the top right corner. Generally a "population" is also seen in the lower left hand corner of the display, but this is in fact cellular debris and is excluded from the analysis. Drawing a gate around the lymphocyte population enables only these cells to be carried onto the next level of

the analytical hierarchy, in which any aggregated cells (doublets) are excluded. To this end, area and height measurements from the forward light scatter parameter are compared. Area and width, or the same pairings using the side scatter data would also provide an equivalent output. Keeping the area measurement on the x-axis ensures that single cells are shown as the top diagonal population, and any aggregates will appear as a ghost population below. It is essential to exclude any aggregated cells, as they can give false results. A gate drawn around the single cells enables only these to be taken onto the next step in the hierarchy, which is the selection of viable cells. As with aggregates, non-viable cells can give false results during fluorescence analysis. The viability assessment is conducted using propidium iodide (or other stains such as 7-AAD), with any dead cells becoming positive for the stain and viable cells remaining negative. Those viable cells can be gated and carried onto the analysis of the markers of interest.

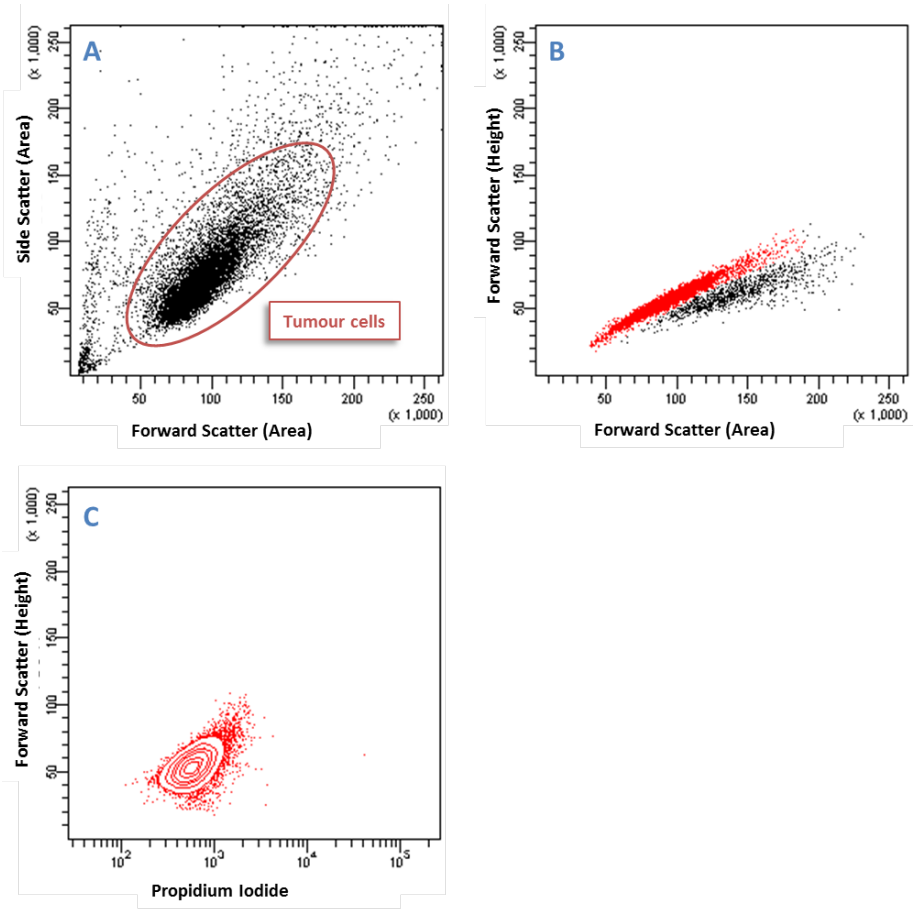

Figure 2.6 Identification of viable tumour cells for analysis

It is essential that flow cytometric analysis is only conducted on viable, single cell populations, as debris, cell aggregates and non-viable cells can all provide false positive data. Tumour cells can be seen on a forward scatter vs side scatter plot (A) and a region to exclude the debris which is found in the lower left corner was applied. By comparing cell height and area (B) single cells (red) can be separated from cell aggregates (black). Finally, the cells are checked for propidium iodide (PI) staining (C). Any non-viable (PI positive) cells appear on the right of the plot.

Once the single, viable cell population has been confirmed, then it is possible to begin analysis of the surface markers of interest, although the analytical approach is very much dependent on the expression profile of the marker. Traditionally, a gate is applied using either an unstained or isotype control sample as a guide then by recording the proportion of cells which have sufficiently high expression intensities to fall outside of the control region. A median value for the intensity of these positive cells is also usually recorded. However, depending on the profile of marker expression, this approach might not be the most appropriate. There are some markers for which cells are definitely either positive or negative, and in these instances it is perfectly reasonable to assess the percentage of cells in the population which are positive for marker expression. Markers for which this approach is not suited are those which result in a shift of the entire population, rather than the identification of two distinct populations. Staining cells for memHsp70 expression using the cmHsp70.1 mAb results in a single fluorescence peak which does not fully separate away from fluorescence profile of the corresponding isotype control (**Fig. 2.7**). When cells are exhibited as a single fluorescence population they are essentially all behaving in the same way, in that they might all be considered as being positive, but to varying degrees. In such instances, it is might be better to quantify results in the context of the median fluorescent intensity of the whole cell population.

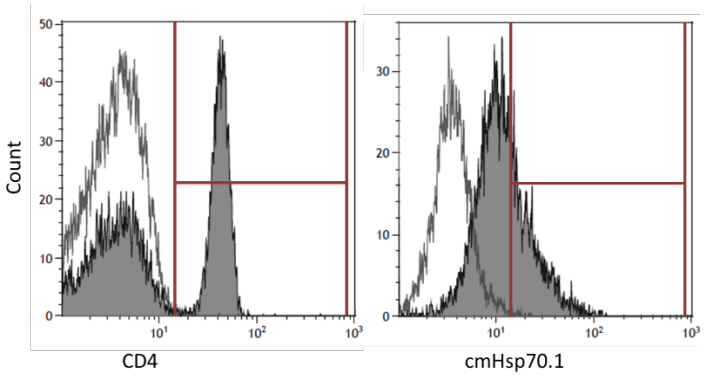

Figure 2.7 Flow cytometric analysis of cell surface marker expression

Representative staining patterns for two different surface molecules (solid histograms) and their appropriate isotype control staining (open histograms) **Left panel***:* PBMCs stained for CD4 expression. CD4 is expressed to a high degree on a subset of T cells, but is absent from other PBMC populations, creating a clear bi-population expression pattern that is easily gated for those cells which are positive. **Right panel***:* 4T1 cells stained with cmHsp70.1 *mAb* do not exhibit a clear positive/negative divide*,* but rather show an overall increase in fluorescence intensity to the whole population. If the same gating strategy were employed here as *for the staining for* CD4 *expression,* then the population would be effectively cut in two by the gate. *A* median fluorescence *intensity* of the entire population is *therefore* recorded.

A higher median intensity equates to greater expression of the marker on question, whereas fluorescent values close to those of the isotype (or unstained) control indicate very low to no expression. Variations in isotype between experiments must be accounted for, and the easiest

way to do this to divide the median fluorescence intensity of staining which is generated following staining with the cmHsp70.1 mAb by the median fluorescence intensity of the isotype. The closer this number is to 1, the less memHsp70 is present. The data for C92F3A-5 were analysed in the same way, and this would typically be expected to result in a measurement close to 1, as this antibody does not bind to memHsp70 positive tumour cells (**Fig. 2.1**).

2.4.6 Limitations of flow cytometry

Although flow cytometry is an excellent technique for high-throughput analysis of overall intensity of antigen expression, and enables effective comparison of treatments in a range of populations, it cannot be used to determine the localisation and / or co-localisation of labelled molecules.

2.5 Membrane Hsp70-mediated uptake of cmHsp70.1 mAb, recombinant human granzyme B and TKDNNLLGRFELSG peptide into tumour cells

Although tumour cells have been found to express memHsp70 [287, 543, 544], relatively little is known about the mechanism of its appearance, why it is expressed in this form, or indeed its functional role (if any). However, the selective expression of memHsp70 has the potential to provide a tumour-specific targeting structure that can be exploited for the imaging and potentially the delivery of therapeutics [533]. Previous evidence has shown that memHsp70 can act as a target recognition structure for activated NK cells, and also that a monoclonal antibody which is specific for the Hsp70 epitope which is expressed on the plasma membrane (cmHsp70.1 mAb) can be used to detect and target cancer cells *in vitro* and *in vivo* tumours [287]. Out of these latter studies came the evidence that NK cell-mediated killing involved the release of granzyme B, and its interaction with, and internalisation by, this membrane form of Hsp70 [516]. Cancer cells expressing memHsp70 are therefore susceptible to granzyme B mediated cell lysis, even in the absence of perforin [530-532]. Furthermore, data obtained using the mouse colorectal cell line CT26, which expresses memHsp70, has demonstrated that granzyme B is internalised into, and kills, these cells *in vitro* and *in vivo* [531].

The goal of the present study is to use flow cytometry and confocal microscopy to further investigate the interaction of the cmHsp70.1 mAb, a recombinant form of human granzyme B and a 14-mer peptide (TKDNNLLGRFELSG) having a sequence which is derived from the oligomerisation domain of Hsp70 which is expressed on the cell surface of tumor cells with cancer cells that express memHsp70.

For these studies, purified cmHsp70.1 mAb was obtained from Professor Multhoff's laboratory at the Technische Universität München. Recombinant human granzyme B was generated following a protocol developed by Professor Multhoff's group at Technische Universität München [531]. Carboxyfluorescein (CF-) labelled 14-mer peptides TKDNNLLGRFELSG and a 'scrambled' peptide having an identical amino acid composition, but different sequence (NGLTLKNDFSRLEG) at a purity >97% were obtained from EMC microcollections (Tübingen, Germany). Lyophilized peptides were reconstituted to a stock concentration of 1 mg/ml using distilled water and stored at 4°C for a period of no more than two weeks following reconstitution.

2.5.1 Production of granzyme B

Recombinant human granzyme B was generated in Professor Multhoff's laboratory at the Technische Universität München following an established protocol [531], as follows.

2.5.1.1 Transfection of HEK293 cells

A vector construct of His-tag joined to the human granzyme B gene via an enterokinase domain was developed and transfected into Human Embryonic Kidney 293 (HEK293) cells. The transcript also included the *Sh ble* gene which confers resistance to zeocin, a copper-chelated glycopeptide antibiotic (InvivoGen, USA) [545, 546], to act as a selection marker for those cells successfully transfected. Cells were frozen in FCS containing 10% v/v DMSO and stored under liquid nitrogen until required. Although these details are provided for completeness of the method, the transfection procedure was actually undertaken by members of Professor Multhoff's laboratory at Technische Universität München.

2.5.1.2 Defrosting and cellular expansion

The transfected HEK293 cells were defrosted quickly and washed in 50mL ice cold growth medium (RPMI 1640 containing 5% v/v FCS, 6mM ι-glutamine, 1mM sodium pyruvate, 100IU/mL penicillin and 100µg/mL streptomycin) by centrifugation at 300g for 5 minutes then resuspended in growth medium containing 300µg/mL zeocin. Successful transfection means that cells possess the *Sh ble* gene which confers zeocin resistance, therefore the addition of zeocin into the growth medium allows for selection of transfected cells. All cells were added to one T75 flask and allowed to rest until confluent (typically around 3 days). After this time, cells were harvested with trypsin and all cells were reseeded into 2 x T162 flasks, again in growth medium supplemented with 300µg/mL zeocin. Cells were left until confluent (typically another 3-4 days), at which time they underwent another expansion, this time into 5 x T162 flasks. From this point onwards, cells were left in growth medium without the addition of zeocin.

After 3-4 days, when cells have once again reached full confluency, they were expanded for the final time into 20 x T162 flasks. Once they were approximately 80% confluent (after 2 days), the medium was removed and cells were washed once gently with 10mL PBS. From this point onwards, only unsupplemented OptiMEM® medium (Life Technologies) was used. Each flask received 25ml of OptiMEM® medium and was returned to the incubator. The supernatant was harvested for processing as described below every 3-4 days, with the flasks being replenished with fresh OptiMEM® on each occasion. The harvesting of supernatants could be conducted up to four times before the cells began to detach in sufficient numbers to negatively impact on the production of granzyme B.

2.5.1.3 Processing the supernatant

Twenty T162 flasks typically generated 500mL of supernatant and this had to be processed immediately. Supernatant was decanted into 250mL Falcon tubes (BD Biosciences) and centrifuged at 500g for 7 minutes in order to ensure removal of cellular debris. Supernatants from all tubes were combined for use in the next stage of the purification process. A small aliquot (1mL) was taken and stored at 4°C to allow later analysis as to the presence and activation status of granzyme B. Imidazole (Sigma Aldrich) was added to the supernatant, to a final concentration of 20mM. Supernatant was then sterile filtered using a Surfactant-Free Cellulose Acetate (SFCA) filter (Nalgene) and another small aliquot (1mL) was saved for use later in protein determination and granzyme B activation assays.

The granzyme B was purified using an Äkta-prime automated liquid chromatography system (GE Healthcare Life Sciences). After the system has been washed with 20% v/v ethanol followed by distilled water, a HisTrap™ FF Nickel column (GE Healthcare Life Sciences) was put in place and prepared with Nickel Column binding buffer (20mM TRIS, 20mM imidazole, 500mM NaCl; pH 8.0, 4°C). An aliquot was saved (time point C, 1mL) then the supernatant was applied through the column. Granzyme B binds to the column via the his-tag, whilst other proteins pass through to the waste. Although other proteins which contain available histamine residues may also bind, these are removed in a subsequent purification (see later). Once the supernatant had been processed, 35mL of NC binding buffer was also applied to the system in order to ensure that all of the supernatant has passed through the column. To elute the granzyme B an increasing concentration of Nickel Colum elution buffer (20mM TRIS, 500mM imidazole, 500mM NaCl; pH 8.0, 4°C) was applied to the column, by way of a linear gradient beginning with 100% Nickel Column binding buffer: 0% Nickel Column Elution Buffer and finishing with 0% Nickel Column binding buffer: 100% Nickel Column Elution buffer after 80ml. The gradient was eluted into 4ml fractions (i.e. 20 fractions in total). Previous experiments

have found the granzyme B to be eluted in fractions 8-15. After elution, the system was washed first with distilled water and then with 20% v/v ethanol. The eluted fractions are stable at 4°C and were stored until all supernatant harvests were complete (typically two-four weeks).

2.5.1.4 Determination of granzyme B content in eluted fractions

Multiple assays were used to determine the overall protein content of the fractions, as well as confirm which fractions contained granzyme B.

2.5.1.4.1 Bicinchoninic Acid

A Bicinchininic Acid (BCA) Protein Assay kit (Pierce) was used to determine the total protein content of each eluted fraction, and the assay was set up in accordance with the manufacturer's protocol. From the kit, solutions A and B were diluted 49 parts A and 1 part B and then pipetted into a flat-bottomed 96 well plate (200µL per well). A standard curve was created by diluting bovine serum albumin (BSA) in distilled water. The standards, blank (distilled water) and samples were added to the plate, 25µL to each well as appropriate. The plate was incubated for 30 minutes at 37°C then analysed using a BioTek EL808 Plate Reader set to 533nm. The protein content of samples was calculated by reference to the standard curve.

2.5.1.4.2 Bradford Assay

The total protein content of the eluted fractions was also determined using a Bradford Assay. For this, Bradford Solution (Sigma Aldrich) was prepared by diluting 1 part of the stock solution in 4 parts distilled water. Any remaining working solution was stored at 4°C for up to two weeks. A standard curve was created using BSA diluted in distilled water, and water only was used as a blank. Bradford Solution pipetted into a flat bottomed 96 well plate (200µL per well), then 10µL of standards, water or elution fractions were added as appropriate. In the presence of proteins, the Bradford Solution turns from brown to blue. The colour change is immediate and the plate was read on a BioTek EL808 Plate Reader using 570nm wavelength. The protein content of each sample (µg/ml) was determined by reference to the standard curve.

2.5.1.4.3 SDS-PAGE

Polyacrylamide gels (5% w/v) were stored at 4°C for up to two weeks until required. To prevent the gels from drying out, they were wrapped in running buffer (25mM Tris, 192mM glycine, 0.1% v/v sodium dodecyl sulphate (SDS)) soaked paper towels inside sealed plastic bags. When ready to use, the gel was unpacked and loaded into the electrophoresis chamber. Running buffer was poured into the space behind the gel and into the base compartment, and the whole unit was cooled with flowing tap water. Based on the results from the BCA or

Bradford assay, only those fractions containing proteins were analysed by SDS-PAGE. The volume of each sample used provided 20µg of protein and was made up to 30µL with distilled water. This was mixed with 10µL bromide blue stain (Sigma Aldrich) which enables samples to be seen more easily when loading into the gel. Previously generated granzyme B of a known concentration was included as a positive control. Samples were then denatured by incubating on a heating block at 95^{o}C for 10 minutes. Samples were then transferred to ice, then directly to a chilled centrifuge and pulsed up to 5000g twice in order to retrieve the evaporate into the sample. A rainbow ladder marker was used to show the position of proteins of known sizes. The ladder, fraction samples and positive control were pipetted into the wells and the current was applied to the unit. A maximum of 30mA per gel was applied, and the gel was run until the ladder was fully spread. It typically took 60-90 minutes and after this time the gel was used in either a Coomassie Blue stain or Western Blot, as detailed below.

2.5.1.4.4 Coomassie Blue Stain

Gels were stained using the Coomassie Blue Assay in order to provide insight into the purity of the preparation. For this, the stain was prepared as 30mL distilled water, plus 10mL methanol and 10mL Coomassie stain (5x stock, Biorad). The Coomassie stain required mixing for at least 10 minutes prior to use, in order to ensure all of the particulates were resuspended. The gel was transferred into a suitable vessel, and 50ml of the prepared stain was poured to the side. Gentle agitation was applied to ensure the stain covered the gel, then the vessel was left on a plate shaker (40 rpm) overnight. Once the bands had developed then gel was transferred to a fresh vessel and washed twice in Coomassie Blue wash buffer (3 parts distilled water to 1 part methanol), by pouring 50mL into the vessel and returning to the shaker for 5 minutes. After washing, the gel was placed into stabilisation buffer (1.5M ammonium sulphate). In order to dry the gels for imaging and storage, they were placed into drying buffer (30% v/v methanol and 5% v/v glycerol in water) for 30 minutes then left at room temperature in a drying chamber made of the gel wrapping in distilled water-soaked cellophane sheets inside a plastic frame. Typically drying required around 48 hours. After this time the gels were removed from the frame, but kept in the cellophane, and stored at room temperature protected from light.

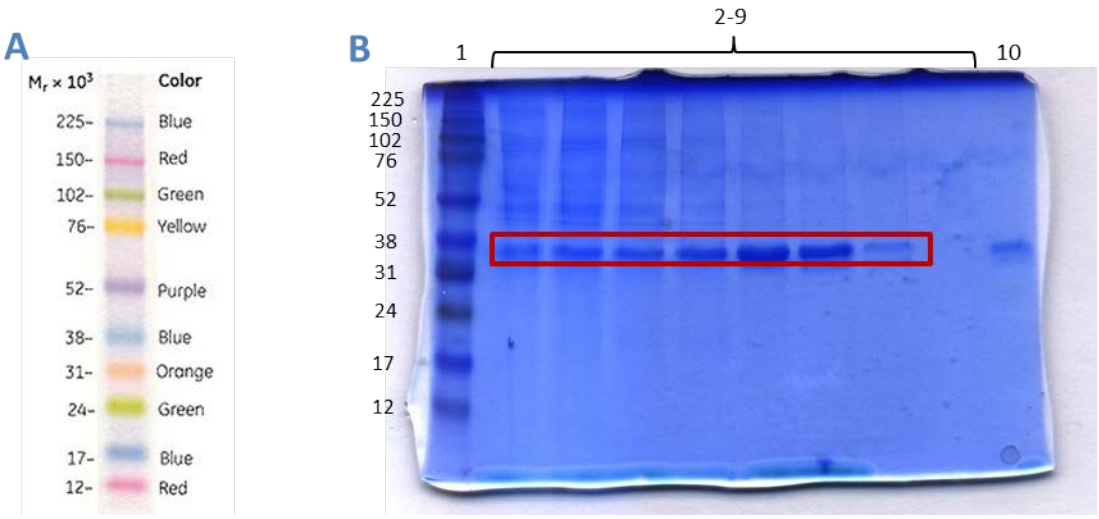

Figure 2.8 Coomassie Blue staining

A Coomassie Blue stain is a visualisation tool, to determine the purity of preparations based on the number of visible bands. The grey box shows the expected position of granzyme B. A rainbow ladder (stock image of which shown in A) was used in the gels to help estimate the size of the proteins. B The gel itself was stained then dried before being digitally scanned. The rainbow ladder was always loaded into the first column and the image has been annotated with the molecular weights of each marker. Columns 2-9 contained consecutive eluted fractions, some of which are expected to contained granzyme B, which would be found in the area highlighted with the red box, between markers of 31 and 38 kDa. In this instance, columns 5-7 contained the largest amount of potential granzyme B. To aid with calculating the placement of proteins, a positive control was placed into column 10. This is a sample from a previously prepared batch of granzyme B.

2.5.1.4.5 Western Blot

Western blot analyses were used confirm the presence of granzyme B. After samples had been run through SDS-PAGE, the proteins were transferred to a polyvinylidene fluoride (PVDF) membrane (GE Healthcare Life Sciences) via a semi-dry Western blot protocol. The gel was removed from the SDS-PAGE unit, and soaked in PBS containing 0.1% v/v Tween for at least 5 minutes. The PVDF membrane was cut to the same size as the gel, and four sheets of blotting paper were also soaked for at least 5 minutes in PBS-Tween (0.1% v/v). After this time, everything was placed in the semi-dry blotter with the gel placed on top of the membrane, and two sheets of blotting paper above and below, all carefully pressed to avoid air bubbles becoming trapped between any of the layers. The unit was closed and current applied (55mA, but limited to 50V) for 45 minutes. Next, the membrane was stained for the presence of granzyme B. For this, the membrane was washed in a 5% w/v solution of milk powder for 1 hour in order to block potential non-specific staining. Next, the membrane was transferred into a solution of 1% w/v milk powder containing the unconjugated primary mouse anti-human antibody recognising granzyme B (IgG2a, clone 2C5/F5 BD Biosciences, used at 1:2000) and left on a plate shaker overnight. The next morning, the membrane was washed three

times in PBS-Tween (0.1% v/v, 15 minutes, 5 minutes, 5 minutes) and then incubated in 1% w/v milk powder containing a horseradish peroxidase (HRP)-conjugated rabbit anti-mouse secondary antibody (Dako, used at 1:2000) for 1 hour at room temperature. After this time, the membrane was washed three times in PBS-Tween (0.1% v/v), each for 10 minutes. The membrane was briefly incubated in ECL (enhanced chemiluminescence) substrate (Pierce) for 5 minutes, after which time the membrane was imaged via film exposure, conducted in a dark room and beginning with an exposure time of 15 seconds. After viewing the film development, the membrane exposure to film could be repeated with adjustments to exposure time as necessary.

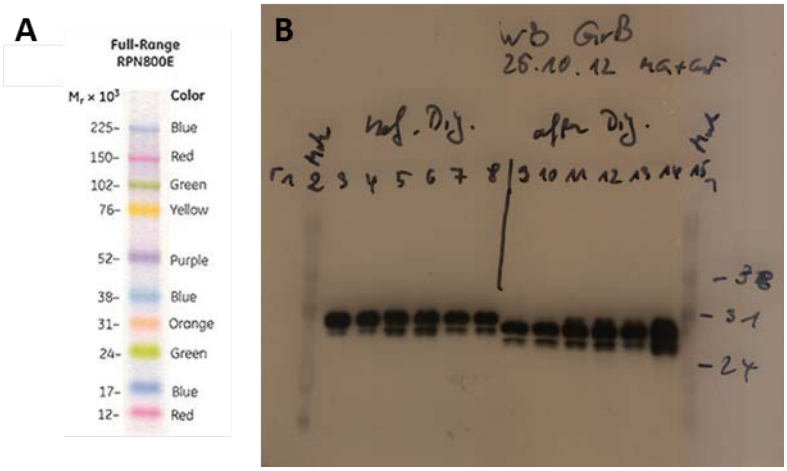

Figure 2.9 Representative Western blot for granzyme B

A. Molecular weights and colours of each band in the ladder used. B. Western blot using aliquots from different steps in the granzyme B purification. The step decrease in size indicates the point at which the enterokinase cleavage occurs and the granzyme B is activated.

2.5.1.5 Activation of granzyme B

All fractions which contained granzyme B were pooled together, and an estimation as to the total protein content was made using the BCA and Bradford assays. Only fractions containing very high amounts of granzyme B, or those fractions which contained less, but were particularly pure, were taken forward. This meant that the total protein content could be used as an estimation of the total granzyme B content.

Granzyme B is produced in an inactive form due to the attached histidine $(His)_6$ tag, which is linked via an enterokinase digestion site. By applying enterokinase and cleaving the $(His)_6$ tag, the granzyme B becomes active. For this, granzyme B was transferred to a suitable buffer (enterokinase buffer; 50mM Tris-HCl, 1mM $CaCl_2$, adjusted to pH 8.0) and concentrated to 1.5mg/mL by centrifuging the pooled granzyme B fractions in Amicon Ultra tubes (Millipore) at 14,000g for 10-12 minutes per 10mL of sample. After the granzyme B had been processed, enterokinase buffer was applied to the membrane and the centrifugation was repeated. This

ensured that all remnants of the NC Binding Buffer and NC Elution Buffer were exchanged with enterokinase buffer. Granzyme B was thoroughly resuspended from the membrane by pipetting and transferred to a 15ml Falcon tube and diluted to 1.5mg/mL with enterokinase buffer. Enterokinase (Life Technologies) was added at 1U per mg of granzyme B and the mixture was rotated for 16 hours at room temperature.

The enterokinase digestion, and therefore activation of granzyme B, was confirmed using an activity assay. For this, 95µL of activation detection buffer (10mM HEPES, 140mM NaCl, 2.5mM $CaCl_2$, adjusted to pH 8.0) containing 200mM colorimetric granzyme B substrate Ac-IEPD-ρNA (N-acetyl-Ile-Glu-Pro-Asp-ρ-nitroanilide, Merck KGaA) was added to 5µl of the aliquots taken at different time stages of the granzyme B purification procedure in flat-bottomed 96 well plates. Previously generated granzyme B was included in the assay as a positive control, and enterokinase buffer alone was used as a blank. The plate was read in a BioTek EL808 plate reader, maintained at 37°C. Readings were made at 405nm every 5 minutes to provide information regarding the kinetics of granzyme B activity. Once granzyme B activity was confirmed, the sample could be further purified.

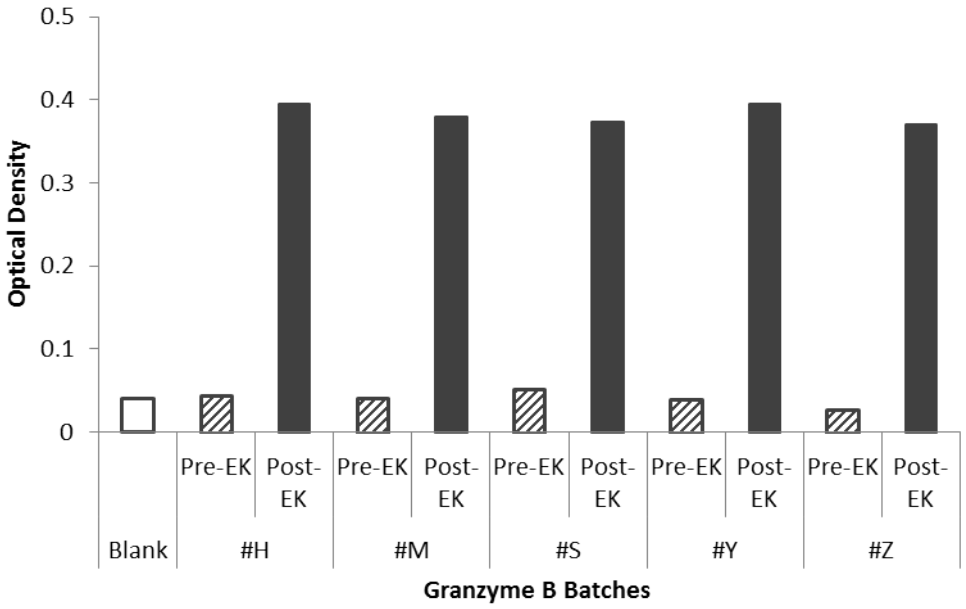

Figure 2.10 Granzyme B activity data

Granzyme B is produced in an inactive form due to the addition of a $(His)_6$ tag, which is joined by an enterokinase digest site and is only active following incubation with enterokinase, as confirmed in the increase in optical density. Granzyme B activity before and after incubation with enterokinase was assessed using a colorimetric activity assay. Five batches of granzyme B were used in this work, all exhibiting similar optical density results from the activity assay, showing that the activity of granzyme B generated following this method is highly conserved.

2.5.1.6 Heparin purification of granzyme B

Following the activation of granzyme B it was necessary to remove the enterokinase from the preparation. This was achieved by conducting a second automated liquid chromatography step on the Äkta-prime system, this time using a HiTrap™ Heparin HP column (GE Healthcare Life Sciences) and exploiting the natural high affinity binding between granzyme B cationic binding sites and heparin. To begin, the system was primed with granzyme B Heparin Binding Buffer (binding buffer, 10mM Tris-HCl, 0.1M NaCl, adjusted to pH 8.0) and then the granzyme B preparation, diluted in binding buffer, was applied. The column was equilibrated by washing with 50mL binding buffer after which time granzyme B was eluted using an increasing concentration of granzyme B elution buffer (10mMTris-HCl, 1.5M NaCl, adjusted to pH 8.0) by way of a linear gradient beginning with 100% granzyme B heparin binding buffer : 0% granzyme B elution buffer and ending with 0% granzyme B herparin binding buffer : 100% granzyme B elution buffer over 20mLs and being separated into 20 elution fractions. Typically granzyme B is present in fractions 10-15. Fractions were assessed by protein determination assays (Bradford Assay and/or BCA), and those fractions containing protein further examined by Coomassie Blue and/or Western blot to confirm the presence of granzyme B cleaved from the His(6)-tag. The granzyme B activity assay was repeated in order to confirm that the heparin purification steps had not interfered with the granzyme B functionality.

For long term storage, the granzyme B was put through a buffer exchange process. For this, granzyme B was centrifuged multiple times in 10kDa molecular weight cutoff Amicon Ultra tubes and at 14,000g, each time discarding the old buffer and resuspending the granzyme B in PBS. The granzyme B was resuspended at a final concentration of 1.5mg/mL and then sterilised by passing through a 0.22µm filter. After aliquoting into sterile microfuge tubes the granzyme B was stored at -80^{o}C until required.

2.5.2 Fluorescent labelling of antibodies and proteins

The cmHsp70.1 mAb (and the alternative Hsp70 antibody clone C92F3A-5) and granzyme B were conjugated to the highly photo-stable fluorochrome ATTO-488 (excitation 488nm, emission 523nm) in house using the Lightning-Link® labelling kit (Innova Biosciences) following the manufacturer's instructions. BSA (as a control for granzyme B internalisation) was similarly conjugated. The antibody/protein to be labelled was diluted to be within the range 1-4mg/mL, to which was then added the Lightning-Link® modifier reagent (1µL for every 10µL of antibody/protein). The solution was gently mixed by pipetting then transferred directly into the vial containing the lyophilised fluorochrome. The solution was gently mixed, after which it

was incubated at room temperature whilst protected from light. The minimum suggested incubation time is 3 hours and that was found to be suitable for both antibody and protein labelling. After the incubation period, Lightning-Link® Quenching Solution was added (1µL for every 10µL of initial antibody/protein) which negates the necessity of further purification steps. The labelled product was stored at 4°C, protected from light.

The TKDNNLLGRFELSG peptide and the scrambled NGLTLKNDFSRLEG control peptide were labelled with carboxyfluorescein during their synthesis. Fluorescein has relatively low photostability [547] and consequently is liable to photo-bleaching when exposed to extended periods of light (as experienced during confocal microscopy analysis). This was the reason for labelling the antibodies and proteins with the highly photo-stable ATTO488, and in the future this would be a consideration with the peptide.

2.5.3 Capacity of granzyme B to kill membrane Hsp70 positive cells *in vitro*

Tumour cell lines were assessed for their susceptibility to the human recombinant granzyme B. Previously published data have shown that granzyme B can induce apoptosis in CX-2 colon and Colo357 pancreatic carcinoma cell lines expressing memHsp70, even in the absence of perforin [530]. To investigate whether human breast cancer cell lines expressing memHsp70 at a variety of intensities also undergo apoptosis in response to granzyme B (both purified and fluorescently-labelled), cells were incubated for up to 48 hours in growth medium containing 4µg/ml granzyme B. Cells were removed at different time points and analysed using two flow cytometry-based approaches for determining cellular apoptosis – the exposure of phosphatidyl serine on the plasma membrane (as detected on the basis of Annexin V staining) and the activation of caspase 3. Optimisation experiments demonstrated that the inclusion of serum hampered the uptake of granzyme B, and that the most efficient uptake occurred when cells were incubated with granzyme B in PBS (F**ig 2.11**). As PBS would not sufficiently maintain cells over a prolonged period of time the decision was made to incubate cells in PBS containing granzyme B for the first hour, then growth medium would be added to the cells for the remaining duration of the incubation.

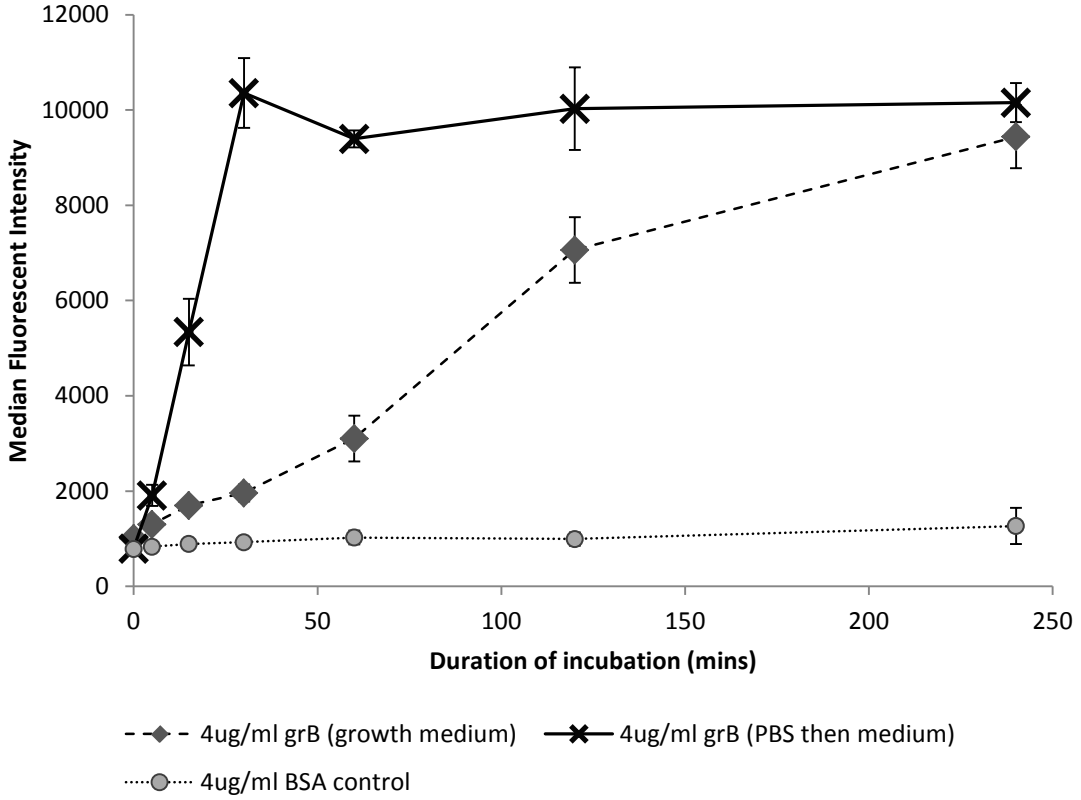

Figure 2.11 Optimisation of granzyme B uptake protocol

CT26 cells were incubated with ATTO488-granzyme B in growth medium, or beginning in PBS with the addition of growth medium after an hour. The uptake of granzyme B was more efficient when the incubation began in PBS. Cells incubated with ATTO488-BSA were used as control and did not show any uptake over time.

Firstly, for Annexin V staining, cells were counted, and $1x10^5$ cells washed in Annexin V Binding Buffer (PBS containing 10% v/v FCS, 1.0mM $MgCl_2$ and 2.5mM $CaCl_2$) before being centrifuged for 5 minutes at 400g. The supernatant was removed using a vacuum aspirator and cells were resuspended in 100µL of Annexin V Binding Buffer. Alexa Fluor 647 Annexin V (Biolegend) was added (5µL), and samples vortex mixed in order to ensure even distribution of the stain, after which samples were incubated for 15 minutes at room temperature whilst protected from light. Cells were then washed in Annexin V Binding Buffer and the supernatant aspirated before cells were resuspended in 250µL fresh buffer. Cells were transferred to 12x75 mm polypropylene tubes, stored on ice protected from light before being analysed by flow cytometry. Immediately before analysis, 10µL Propidium Iodide (diluted from stock 1:19, Sigma, UK) was added to allow identification, and exclusion, of any non-viable cells. Early apoptotic cells were defined as being Annexin V^+ PI^- and were calculated as a percentage of the whole population.

The influence of granzyme B on the activation of caspase-3 (an instrumental molecule in cellular apoptotic pathways) was determined by flow cytometry using a Caspase-3 kit (BD Biosciences) and following the manufacturer's protocol. For this, cells were counted and washed (400g, 5 minutes) in BD Cytofix/Cytoperm Fixation and Permeabilisation Solution (BD Biosciences), after which they were resuspended in BD Cytofix/Cytoperm Fixation and Permeabilisation Solution for 20 minutes to allow cell fixation. Cells were washed twice in BD Perm/Wash Buffer (BD Biosciences) and then resuspended in BD Perm/Wash Buffer containing the appropriate volume of caspase-3 antibody for the cell number and incubated for 30 minutes at room temperature protected from light. Cells were washed in BD Perm/Wash Buffer again, transferred to 12x75 mm polypropylene flow cytometry tubes and put on ice protected from light until immediate analysis by flow cytometry. Cells expressing active caspase-3 are deemed to be apoptotic, and the proportion of positive cells was determined as a percentage of the whole population.

2.5.4 Flow cytometric assessment of uptake into memHsp70^{+} tumour cells

To ensure standardised practices, all cells were seeded in T75 flasks and grown for 48 hours prior to use in the uptake assessments. Seeding densities were selected based on the proliferation rate of the different cell lines and are detailed in **Table 2.4**. This resulted in cells being ~70% confluent at the time of use.

	T75 Flasks
MDA-MB-231	$1.25x10^5$
MCF7	$2.50x10^5$
T47D	$5.00x10^5$
4T1	$1.25x10^5$
CT26	$1.25x10^5$

Table 2.4 Seeding densities into T75 flasks

To compensate for different growth rates, cell lines were seeded into T75 flasks at different densities which allow for *a* comparable *level of confluency* after 48 hours growth. The *T*able details the starting number of each cell line.

After the 48 hour growth period, cells were gently washed twice with 10mL PBS then with 2mL trypsin-EDTA. Cells were incubated for 1-2 minutes at 37^{o}C then 10mL of fresh growth medium was applied and gently pipetted over the cells in order to fully detach them from the flask surface. As it was necessary for the uptake assessment to be conducted in staining buffer in

order to block non-specific binding, cells were centrifuged (300g, 5 minutes), the supernatant was decanted and cells were resuspended in 1mL staining buffer. Cells were counted on a haemocytometer and viable cell number ascertained using trypan blue exclusion. For each condition (unstained, control or fluorescently-labelled molecule of interest), $0.5x10^6$ cells were transferred into a 1.5mL microfuge tube. As the staining volume was required to be low, cells were centrifuged (300g, 5 minutes), the supernatant was vacuum aspirated, and cells resuspended in 20μL staining buffer containing fluoresecently labelled molecule of interest (cmHsp70.1 mAb, TKDNNLLGRFELSG peptide or granzyme B) or control molecule (C92F3A-5 mAb, IgG isotype, NGLTLKNDFSRLEG peptide or BSA) as appropriate. Cells used as the unstained control were resuspended in 20μL staining buffer alone. Immediately after resuspension, a 2μL aliquot was removed as the 'time 0' measurement and placed into a 12x75mm tube containing 3mL chilled staining buffer. Half of the remaining 18μL cell/molecule mixture was transferred into a clean, chilled 1.5mL microfuge tube and kept on ice and protected from light, and the original microfuge tube was incubated at 37°C. At each time-point (5, 15, 30 and 60 minutes), cells were gently mixed and a 2μL aliquot was transferred into a 12x75mm tube containing 3mL chilled staining buffer. Once transferred to 12x75mm tubes, cells were centrifuged immediately (300g, 5 minutes, 4°C) then the supernatant was decanted and cells were resuspended in 250μL staining buffer. Tubes were kept on ice and protected from light until all time-points were completed, then analysed via flow cytometry. In order to exclude non-viable cells from the analysis, 10μL of 50μg/mL propidium iodide was added to each tube immediately prior to data acquisition. The median fluorescent intensity of cells was used as a measurement of the uptake of fluorescently-labelled molecules. The use of control molecules can confirm the specificity of the uptake, whilst the two different temperatures allow for a comparison between binding (on ice) and uptake (occurs when the cells are metabolically active at 37°C).

2.5.5 Confocal microscopic assessment of uptake of into memHsp70$^+$ tumour cells

For assessments involving confocal microscopy, cells were set up in 35mm glass bottom dishes (MatTek™ Corporation) and grown for 48 hours before staining. The seeding densities for each line are detailed in **Table 2.5**, and these were selected in order to ensure that all cell lines exhibited a similar degree of confluency at the time of assessment.

	MatTek dishes
MDA-MB-231	$0.625x10^5$
MCF7	$1.250x10^5$
T47D	$2.500x10^5$
4T1	$0.300x10^5$
CT26	$0.625x10^5$

Table 2.5 Seeding densities for MatTek™ glass bottom dishes

The total number of cells seeded into a single MatTek™ glass bottom dish is dependent on the rapidity of cell division, cell size and the propensity for cell aggregation/clumping. The seeding densities selected allowed for each line to be at approximately the same confluence after 48 hours, when cells were stained.

After the cells have grown for 48 hours they were removed from the incubator, the medium was aspirated using a vacuum pump, after which cells were washed with 2mL chilled PBS which was also vacuum aspirated to ensure that no medium remained. The fluorescently-labelled molecules (either cmHsp70.1 mAb, granzyme B protein or the TKDNNLLGRFELSG 14-mer peptide, or the appropriate controls) were diluted in buffer and 100µL of this solution was added to the central well of the dish. Dishes were then replaced in the 37^{o}C incubator for 5, 15, 30 or 60 minutes. After this time, dishes were washed with 2mL PBS and all liquid was removed using a vacuum aspirator. To enable mounting onto microscopy slides, as well as subsequent intracellular staining when necessary, cells were fixed using 100µL of either 4% w/v paraformaldehyde (PFA) or 'Solution A' from a Fixation and Permeabilisation Kit (Life Technologies). Cells were incubated with the fixation solution at room temperature and protected from light for 15 minutes, then washed in 2mL staining buffer. If cells did not require further staining, then the coverslips were detached by soaking the base of the glass bottomed dishes in Cover Slip Removal Fluid (MatTek Corporation), by standing the dish in an inverted dish lid containing 750µL of the fluid. Although the manufacturer's datasheet suggests an incubation time of 45 minutes, 25 minutes was found to be sufficient. The incubation was conducted at room temperature and the dishes were kept protected from light for the duration. After this time, excess fluid was removed by standing the dishes on paper towels and then the coverslips were removed by applying very gentle pressure with fine tipped forceps to the edge of the coverslip. There may be adhesive residue remaining on the coverslip which must be removed, as the best images will only be obtained when the coverslip lies as flat and close to the microscopy slide as possible. The easiest method of removing the residue is to scratch it carefully with a scalpel, taking care to avoid the adhered cells. Coverslips were then mounted onto polysine microscope slides (VWR International) that were pre-cleaned with 70% v/v ethanol and allowed to fully dry, using one of VECTASHIELD® Mounting Medium (Vector Laboratories) containing DAPI. Care was taken to minimise the creation of air bubbles, and

coverslips were sealed along all edges with clear nail varnish. Slides were stored at 4°C and protected from light until imaging could take place (not longer than 24 hours). If cells were to be used for further staining, this was carried out as described below.

2.5.5.1 Confocal microscopic assessment – co-localisation of internalised cmHsp70.1 mAb, granzyme B and TKDNNLLGRFELSG peptide with intracellular vesicles

To study the pathway of uptake in more detail intracellular structures were also stained, and this required the cells to be fixed and permeabilised. The intracellular vesicles selected for examination were endosomes (early, late and recycling), lysosomes and mitochondria. As previous investigations have excluded the possibility of Golgi involvement, this range of markers was felt to provide a reasonable covering of the other possibilities.

For this, cells were permeabilised and stained using 100µL solution B (Invitrogen Fix/Permeabilisation kit) containing the appropriate concentration of primary antibody for one intracellular structure of interest immediately after the fixation step (described in **Table 2.6**).

Primary abs	Raised in	Specific for	Dilution	Supplier
Rab4a	Rabbit	Early endosome	1 in 50	Santa Cruz Biotech
Rab5a	Rabbit	Early endosomes	1 in 50	Santa Cruz Biotech
Rab7	Rabbit	Late endosomes	1 in 50	Santa Cruz Biotech
Rab9	Goat	Late endosomes	1 in 50	Santa Cruz Biotech
Rab11	Goat	Recycling endosomes	1 in 50	Santa Cruz Biotech
LAMP1	Mouse	Lysosomes	1 in 50	Biolegend
LAMP2	Rabbit	Lysosomes	1 in 50	Sigma Aldrich

Table 2.6 Primary antibodies used in confocal microscopy investigations

Primary antibodies specific for a range of intracellular vesicles were used to help elucidate the intracellular trafficking pathway of molecules internalised through memHsp70. They were used in combination with appropriate secondary antibodies, specific for the species in which the primary was raised. The dilutions used were within the range suggested by the manufacturers.

Cells were incubated at room temperature, again in the dark, for 20 minutes. After this time, cells were washed in 2mL PBS then stained with 100µL of an appropriate fluorescently labelled secondary antibody diluted in staining buffer as described in **Table 2.7**. Cells were incubated at 4°C, again in the dark, for 20 minutes and then washed with 2mL staining buffer. Cells were then mounted onto microscopy slides as described below.

Secondary abs	Dilution	Supplier (specificity)
Cy3 Goat anti-Rabbit	1 in 100	Jackson ImmunoResearch (IgG H+L)
Cy3 Rabbit anti-Goat	1 in 100	Jackson ImmunoResearch (IgG H+L)

Table 2.7 Secondary antibodies used in confocal microscopy investigations

The primary antibodies which required fluorescently-labelled secondary counterparts were all either raised in rabbit or goat. Two secondary antibodies were used, an anti-rabbit IgG polyclonal and an anti-goat IgG polyclonal both of which were conjugated to Cy3™. As only one intracellular vesicle was stained for at any one time, these secondary antibodies were never used together.

2.5.5.2 Confocal microscopic assessment – co-localisation of internalised molecules with mitochondria

Particularly when investigating the internalisation of granzyme B, another intracellular structure of interest was mitochondria. The co-localisation of internalised granzyme B with mitochondria could provide some insight into how apoptosis could be initiated. The staining of mitochondria was conducted in a different way as to the other intracellular structures. Instead of antibodies, mitochondrial-selective dyes were used. These are membrane permeable, so there is no need to permeabilise cells, although not all of the dyes can withstand fixation so the uptake and staining protocols had to be modified for these changes.

However, mitochondrial staining proved to be more problematic. Fixation can affect the membrane potential of mitochondria, which can lead to loss of staining. Consequently, cells that are stained for mitochondria had to be imaged live, meaning that it was necessary to make some modifications to the uptake protocol. The mitochondrial staining is conducted at 37°C, and as the cells are live they will be metabolically active during this time. It was not possible to conduct the molecule uptake and mitochondria staining concurrently, as different durations were required for each. The cells will remain metabolically active during the mitochondria staining, meaning that if the molecule uptake was undertaken first the cells could continue to traffic internalised molecules during the staining. Therefore the intracellular placement of internalised molecules would no longer represent that of the incubation time-point, but a longer duration incorporating the time of the mitochondrial staining. To account for this, the order of the protocol was reversed, with the mitochondria staining preceding the incubation with the relevant fluorescently-labelled molecule (Hsp70 mAb, granzyme B, peptide).

Cells were set up in 35mm MatTek™ glass bottom dishes as described previously in **Table 2.5** and grown for 48 hours. After this time the medium was aspirated and replaced with

mitochondria stain. Two different mitochondrial stains were used, MitoTracker® Green (MTG) (Molecular Probes®, Life Technologies) and MitoID™® Red (Enzo Life Sciences).

MitoTracker® Green is stored desiccated at -20°C, and reconstituted to 1mM in DMSO. The reconstituted preparation was stored in 15µL aliquots (to reduce the need for repeated freeze-thaw cycles) at -20°C for up to 3 months. For cell staining, the MitoTracker® Green was diluted to 100nM in growth medium then 1mL was added to the dishes. Cells were incubated for 30 minutes at 37°C then the MitoTracker® Green medium was vacuum aspirated and cells were washed three times with 1mL fresh growth medium.

MitoID™® Red is supplied in the form of a kit and staining was conducted as per the manufacturer's instructions. The suppliers do not provide information relating to the concentration of the reagent, and so the amounts used are stated in terms of dilutions. The MitoID™® Red dye is stored at -20°C and a working stock is prepared as a 10-fold dilution in DMSO. The working stock can be stored at -20°C for up to one month. For staining cells, the working stock is further diluted 50-fold in 1x assay buffer (prepared as a 10-fold dilution in deionised water of the supplied 10x assay buffer). MitoID™® Red was added to the cells, as 500µL to the centre of the dish. Cells were incubated for 30 minutes at 37°C then cells were washed twice in 1x assay buffer.

After the mitochondria staining was complete, cells were washed once with staining buffer to ensure removal of the mitochondrial buffer. Cells then received 100µL of the fluorescently-labelled molecule (staining buffer containing fluorescently labelled cmHsp70.1, TKDNNLLGRFELSG peptide, granzyme B or one of the appropriate controls) and were incubated for 5, 15, 30 or 60 minutes at 37°C. After the incubation, cells were washed with 1mL staining buffer which was vacuum aspirated to ensure complete removal. Cells were covered with fresh staining buffer and kept in a chilled box, to minimise any further metabolic activity, and protected from light, to prevent photo-bleaching of the fluorescent molecules, until imaging could take place. Immediately prior to imaging the staining buffer was aspirated and cells were covered with PBS (to avoid background interference of the fluorescent imaging by serum). Cells were imaged within 1 hour of the molecule uptake incubation being completed. Imaging was conducted as quickly as possible as the environment within the chamber was not controlled and higher than the preferable 4°C.

2.5.5.3 Confocal Microscopy Image Acquisition

Samples were analysed using an Inverted Zeiss LSM 510 NLO, running Zeiss Browser software and equipped with an argon laser (capable of 458, 477, 488 or 514nm), two helium-neon lasers (one emitting at 543nm and the other at 633nm) and a mercury lamp for imaging DAPI staining

of the nucleus. A variety of objectives that are suitable for water or oil immersion were available, thereby allowing for the best possible imaging of cells either in PBS suspension or mounted in a suitable medium (such as VECTASHIELD®). The slides were laid upside-down in the imaging chamber, with the mounted glass coverslip closest to the objective. By altering the size of the pinhole situated before the photomultiplier detectors it is possible to control the depth of focus in the sample, essentially imaging thin slices of a single cell. The total height of the cell can be set into the mechanised controls and multiple scans of the same cell can be conducted, working from bottom to top, and these images can be reassembled in order to generate an overall picture of the entire cell and allowing accurate distinction as to the cellular localisation of the fluorescent signal.

Multi-colour images can be obtained, although the set up works best with fluorochromes which are fairly well spread along the light spectrum. To minimise any potential spillover between markers, each laser was only used to excite up to one fluorochrome and, with the exception of transmitted light, every marker was detected in a separate scan of that particular cellular plane. The trade off with this approach was that the scan times for cells were vastly increased, which increased any potential for fluorochrome bleaching. The potential impact of this was assessed by repeating single plane images after producing full cell stacks in order to ensure that fluorescent intensities had not significantly dimmed or been lost. The excitation lasers and filters for emission data was specific to each individual experiment dependent on exactly which fluorochromes were in use, but followed the description in **Figure 2.12** shown over.

For every experiment, the images were taken by scanning full frame shots, but cycling through each colour individually. Using one excitation laser at a time, and an appropriate optical set up, removes the need for compensation. Before image analysis commenced, the laser power, detector gain, and amplifier offset were adjusted to fit the minimum and maximum measureable fluorescent intensity into the colour palette. As these measurements were set with each experiment, it means that the settings are not always identical, although the adjustments always serve to put the minimum and maximum values at the same level, meaning that all the images are comparable. Predominantly the confocal images are used to place internalisation of specific molecules through the cells and intensity is not recorded or analysed so any variation of actual intensities between samples is not important, however if the aim were to quantify the fluorescence this would need to be addressed.

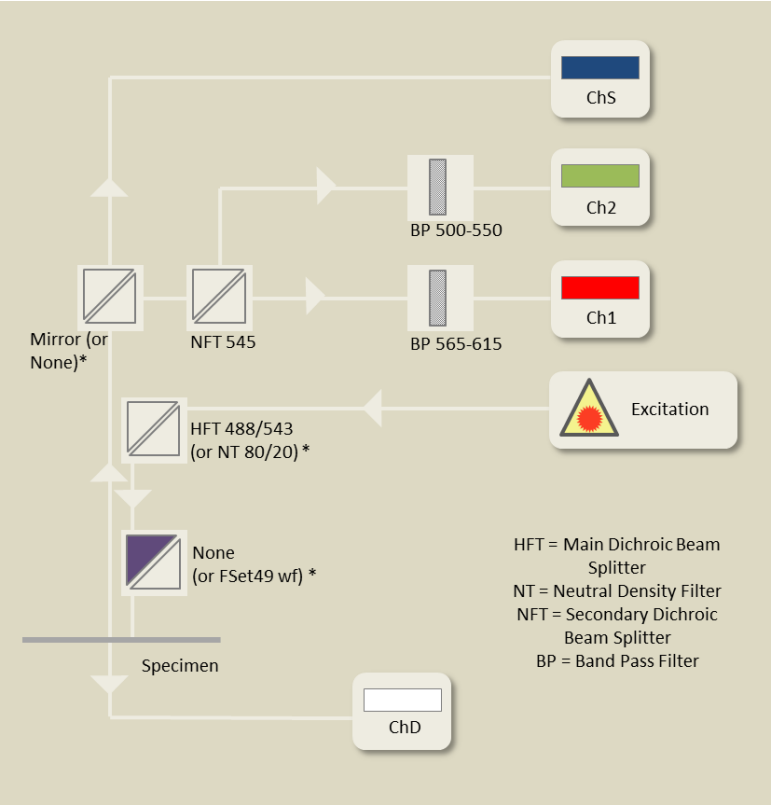

Figure 2.12 Schematic diagram of confocal microscope set-up.

Different combinations of optical filters and splitters are required to acquire data from different fluorescent markers. Each fluorescent marker is imaged on a separate track (an entire frame is scanned for the first colour only, then scanned again for the next colour, repeating for as many colours as necessary). This increases the time taken for a complete scan, but minimises the chance of any colour spillover. The filters can be switched as necessary between tracks, but they are set up to reduce the number of changes necessary within a scan. The set up below was found to work well for the imaging conducted here. *Components* listed in brackets and marked with an asterix are required when imaging DAPI staining. These can be computer controlled so are switched automatically between tracks as necessary. This image has been adapted from the configuration control window screen on the LSM 510 software (Carl Zeiss MicroImaging GmbH, Germany).

Initially, cells were imaged using the 20x objective, with the pinholes fully open. This provided an overview and allowed those cells for closer imaging to be identified. This would be undertaken using the 63x objective, with the size of the pinhole being dependent on the specific experiment. Higher intensities of fluorescence required the use of a smaller pinhole in order to create clear images, whereas a larger pinhole maximised the capture of fluorescence signals when low levels were present. Specific information regarding pinhole sizes are provided in the Results. Each cell imaged with the 63x objective was imaged as a z-stack, with single images taken in different planes throughout the cell. When setting up, the focus was adjusted to find the top and bottom of the cell, these stage heights are stored in the software and the z-stack is performed over the distance. The thickness of the plane slices is determined by the size of the pinhole – with a larger pinhole leading to a thicker slice and *vice versa*. The software

automatically overlaps the slices slightly in order to better enable subsequent 3D reconstruction of the images.

2.5.6 Confocal Microscopy Image Analysis

After consideration of the other options available, ImageJ (http://imagej.nih.gov/ij/) was selected as being the most suitable image analysis tool for this project. ImageJ is freely available in the public domain, and plugins which cover a wide range of additional applications available are available to download. It is possible to save any changes into the lossless compression .tiff format (a small file size, but all information remains). Any image manipulations/analyses were conducted on duplicated files so that the original always remained intact as a backup. The false colour overlays can be adjusted with ease and there are many powerful analysis tools built in to the program.

All images analysed were subjected to adjustment of brightness and contrast, beginning with the 'auto' suggestions for settings and fine adjustments to reduce the background noise. All fluorescent channels, as well as the brightfield channel, were adjusted before further analysis could take place. Careful consideration was taken to ensure that any manipulations only enhanced the clarity of the original image.

2.5.6.1 Making composite images

One of the difficulties of confocal imaging is that the natural consequence of restricting the height of the cell from which data are obtained is that the amount of fluorescence available in any one frame is also restricted and images can therefore be dim. ImageJ was therefore used to combine multiple slices of the same z stack together in one single composite image in some of the images during the post-acquisition analysis in order to compensate for this. These composites were saved as separate .tiff files, which could be reanalysed in ImageJ if necessary. Where composites have been shown instead of single images, this is stated in the figure legend.

2.5.6.2 Red to magenta change

Colour blindness affects approximately 10% of a Caucasian male population, with by far the most frequent affliction being the difficulty to distinguish red and green. Owing to the large distance between these two on the light spectrum, fluorochromes that emit in these regions are often used in combination as they require very little or no compensation. The detectors in the confocal microscope record intensity of received light, rather than an actual colour, but for ease, and in the case of multi-colour images necessity a false colour overlay is applied to the results of each of the detector channels.

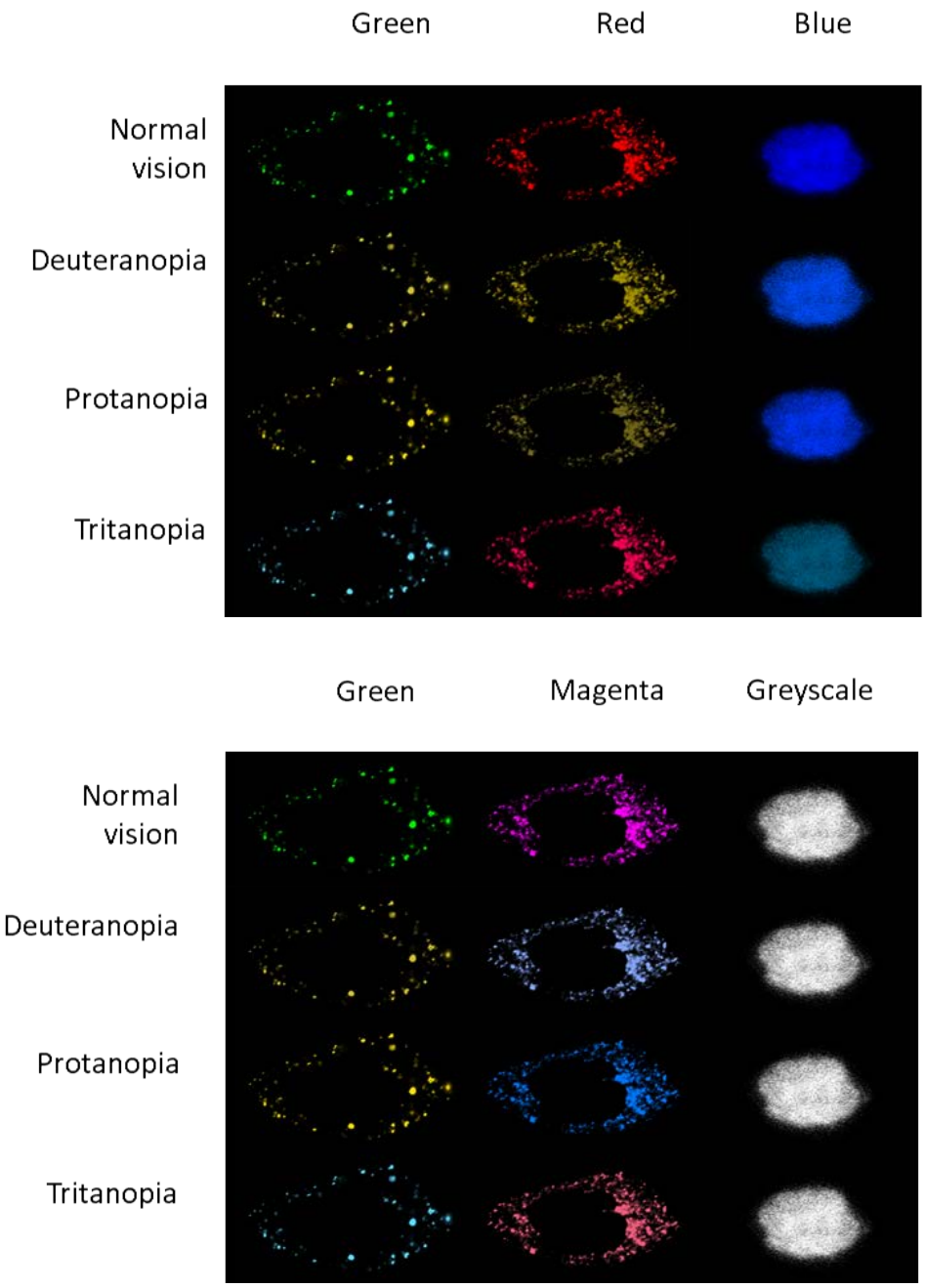

Figure 2.13 Colour blind considerations for image presentation

The vast majority of multi-colour images presented or published make use of a red/green/blue colour combination which leads to dichromatic and trichromatic colour blindness sufferers being unable to make distinctions between some of the colours. When looking for colocalisation this is highly important. However, by using a magenta overlay in the place of a red one, all colours are easily distinguished by sufferers and those of normal sight, as demonstrated by the above reconstructions of how different colours are viewed by sufferers of different conditions.

Tradition dictates that the choice of false colour overlay mimics the emission wavelength of the fluorochrome as closely as possible, a consequence being that red and green are often presented – this poses a problem for people with red-green distinction difficulties. In fact,

three-colour microscopy images are not unusual and the typical third choice for colour overlay is blue. These three colours in combination means that sufferers of all forms of dichromatic and trichromatic colour blindness will be unable to distinguish two of the colours presented. A solution has been suggested – abandon the red overlay and use magenta instead. This one simple change to traditional practice would mean that three colour microscopy images can be distinguished by sufferers of all types of dichromatic and trichromatic colour blindness (**Fig 2.13)**. There is also monochromatic colour blindness, but as this means that the sufferer can distinguish no colour at all, as opposed to having a deficiency at only some point in the spectrum, there is no solution to presenting multicolour images for these individuals. The colour change from red to magenta can be easily accomplished in ImageJ by highlighting the colour channel of interest and selecting 'magenta' from the Lookup Table drop down menu.

2.5.6.3 Quantification of image data

The distinct fluorescent spots relating to the internalisation of the cmHsp70.1 mAb, granzyme B and the peptides were counted manually. The spotted pattern of internalisation, indicating vesicular association, particularly lent itself to quantification in this manner. Cells were quantified over each frame of the z-stack, and any fluorescent spots present in multiple frames were counted in the one containing the greatest intensity. All frames from the adherent surface to the cell's apex were included.

Although other quantification approaches would have been useful, the nature of the confocal microscopy images does not allow these to be applied. Without having appropriate control measures to standardise the fluorescence obtained on different days it was not practical to attempt to quantify the fluorescent intensity. Although calculating the area of the fluorescence relating to the internalised molecules (cmHsp70.1 mAb, granzyme B, peptide, as appropriate) would have been a useful measurement, the nature of the confocal data made this impractical. Adjusting the brightness and/or contrast of the images also resulted in modifications to the size of the fluorescence spots. Without the ability to standardise the fluorescence across images acquired on different days, it is not possible to accurately compare spot size.

2.5.6.3.1 Quantifying molecule distribution

On examination, the fluorescence throughout the cell appeared to be asymmetric, and this was examined by counting spots at different vertical levels. As the dimensions of cells varied within an experiment and between cell lines, relative, rather than absolute, distances from the adherent surface was used as a parameter. The data were examined in two different ways. Firstly scatter plots of spot count against percentage distance, with every cell represented as a

single line. Secondly, each cell was separated into quartiles of height and the total spot count in each quartile was calculated.

2.5.6.3.2 Co-localisation analysis

The co-localisation of cmHsp70.1 mAb, granzyme B, and peptides with intracellular vesicles was also examined. For this, cells were incubated in the presence of the fluorescently conjugated molecules for a range of time points, at which time cells were stained using antibodies specific for endosomal or lysosomal markers, or using a mitochondrial dye. Colocalisation analyses were then performed on the microscopy images to confirm whether the molecule of interest was present in the same location as the vesicular staining. There is no definitive method of quantitating the extent of colocalisation. Rather, there is a wide selection of different equations, all requiring different assumptions to be made about the data. It was therefore necessary to assess which statistics are the most appropriate for the dataset. Preferably more than one statistic should be used, as this will provide a more robust description of the data.

Herein, both the Pearson's coefficient and Manders' M1 & M2 coefficients [548] were calculated. The Pearson's coefficient provides a description of the correlative variance between two colour channels. The output value can be anywhere between -1 (a perfect negative correlation) and 1 (a perfect positive correlation). If there is no relationship between the two channels, the value will be 0. The Manders' M1 & M2 coefficients provide a measure of the proportion of one channel which overlaps the other, thereby providing information about each channel separately (M1 describes the proportion of channel A which overlaps with channel B, and *vice versa* for M2). As the output describes a proportion, values are only possible between 0 and 1.

All co-localisation statistics were calculated using the '*Just Another Co-localisation Plugin (JACoP)*' add-on for ImageJ [549]. For this, a region of interest was drawn around additional cells within the frame of view and the surrounding area was cleared to match the colour of the background. The image was split by colour channel, brightness/contrast adjustments were performed and up to one noise reduction algorithm was conducted as necessary. Images were loaded into the JACoP program and the threshold levels were adjusted as required. One benefit to using this plugin is that co-localisation statistics can be calculated as a total across all frames within the stack, giving a more accurate description of what is occurring in the entire cell.

2.5.7 Limitations

In most respects, confocal microscopy provides distinctly different analytical approaches to flow cytometry. The data acquisition is highly labour intensive with the possibility to obtain data on only a small number of cells. However, the data that are obtained are highly informative with regards to special information and the co-localisation of the molecules of interest with other cellular features. For example, it can show how a specific marker is clustered or spread over the cell surface, or how it sits intracellularly. Especially useful is how co-localisation of multiple markers can be used to show, for example, in which intracellular compartments lays a fluorescently labelled marker of interest after a certain incubation time.

2.6 Membrane Hsp70 expression on lymphocytes?

The vast majority of published literature demonstrates the presence of memHsp70 on tumour cells but not on healthy tissue. In fact there is only one published paper that has reported any expression of memHsp70 on non-tumour cells, which was that peripheral blood lymphocytes in healthy individuals showed 10.4% expression of memHsp70 compared to a mean of 35.2% in three individuals with juvenile idiopathic arthritis. It is difficult to infur too much from this, since the authors made no use of the C92F3A-5 Hsp70 antibody and therefore the reported 'memHsp70' may in fact turn out to be Hsp70 which has bound to the surface of the lymphocytes. If indeed, memHsp70 is expressed at all on lymphocytes then this may provide a mechanism for Treg-mediated suppression. One way by which Treg cells exert suppression on other lymphocytes is through the release of granzyme B. Although this occurs alongside perforin in cytotoxic vesicles, granzyme B can also be taken up by memHsp70 so any expression on lymphocytes would increase the possibility of granzyme B-induced, Treg-mediated cell death.

In addition, the expression of memHsp70 is not static and its expression on the surface of cancer cells can be upregulated by a variety of chemotherapeutic agents and radiotherapy [290, 519, 520]. Furthermore, evolving data suggest that the tumour microenvironment can impact on the phenotype and function of systemic and localised immunity. As yet, no studies have investigated the potential influence of the tumour microenvironment on the possible induction and/or upregulation of memHsp70 on lymphocytes, and if this occurs whether it exhibits any functionality which is consistent with its expression on tumour cells. If indeed memHsp70 can be induced on lymphocytes, and memHsp70 serves as a conduit through which granzyme B can pass into cells and induce apoptosis, then employing granzyme B as a treatment for memHsp70 tumours could in turn lead to adverse influences on the development of effective, protective anti-tumour immunity. Although this is unlikely given the

fact that lymphocyte populations express high levels of natural inhibitors such as SerpinB9, the possibility should be examined.

2.6.1 Volunteers and Ethics

Healthy volunteers were recruited from the University of Sheffield Medical School at the Royal Hallamshire Hospital, Sheffield. Donors were required to be over 18, generally fit and well, and not to have taken any medication within the previous week. Volunteers were given an information sheet prior to giving blood and were given the opportunity to ask any questions they had regarding the study or blood taking procedure. If the volunteers were happy to proceed, they were asked to sign a consent form. All volunteers were aware that they could withdraw from the study at any time, even after having given consent. The study was granted ethical approval by the Sheffield University Ethics Committee (SMBRER109).

Blood was obtained by venepuncture and blood was collected into Lithium-Heparin (Li-Hep) BD Vacutainer® tubes (BD Biosciences). Tubes were gently inverted twice and kept at room temperature until required (typically for 10 minutes and not longer than 30 minutes). Volunteers were observed for a few minutes after giving blood to be sure of no adverse effects. All volunteers were provided with contact details should they wish to discuss anything after their donation.

In order to assess whether the conditions found within a tumour microenvironment could affect membrane expression of Hsp70 in lymphocytes, peripheral blood mononuclear cells (PBMCs) were isolated from whole blood and subjected to the treatments described below. After treatment, the PBMCs were stained with a range of fluorescently-labelled antibodies to allow for flow cytometric analysis of cell subset, activation status and Hsp70 expression.

2.6.2 Expression of memHsp70 on lymphocytes in peripheral blood

The first assessment of memHsp70 was conducted *ex vivo* on lymphocytes in peripheral blood samples. As the blood samples were generally used for multiple experimental setups time constraints meant that the blood could not be stained immediately. Instead, 1mL was aliquotted from the Li-Hep BD Vacutainers® into sterile 7mL bijous containers and kept on ice until staining could take place (no longer than 3 hours from the time of the blood donation). The phenotype and activation state of cells in whole blood and isolated PBMCs was determined using a panel of fluorescently labelled mAbs (**Table 2.8**).

2.6.2.1 Whole blood staining

Whole blood samples were stained directly in 12x75 mm polypropylene flow cytometry tubes, using 50µL whole blood per tube. Prior to staining, samples were incubated for 10 minutes at

room temperature with mouse serum (2% v/v) in order to prevent potential non-specific antibody binding. Both unstained and isotype controls were always included. The monoclonal antibodies and isotypes were added as described in **Table 2.9** along with 10µL staining buffer (PBS containing 10% v/v FCS) containing Blue Live/Dead Fixable Dead Cell Stain (Molecular Probes, USA). Cells were vortex mixed and then incubated at 4^{o}C protected from light for 30 minutes.

Antigen	Description	Clone
CD3	The TCR co-receptor, expressed by all T cell subpopulations. Formed of four distinct chains (CD3γ, CD3δ and two CD3ε). Comprises the TCR complex together with CD3ζ (also known as CD247) and the TCR which allows signal transduction and cellular activation.	UCHT1, specific for an epitope with CD3ε
CD4	CD4 is a member of the immunoglobulin superfamily and has four immunoglobulin domains, designated D_1-D_4. It interacts with the β2-domain of MHC Class II through D_2. It is found on the surface of T helper cells as well as regulatory T cells.	RPA-T4, specific for the D_2 domain
CD8	CD8 is a transmembrane glycoprotein which acts as a co-receptor for the T cell receptor and binds to MHC Class I. It is expressed on the surface of cytotoxic T cells.	RPA-T8
CD56	CD56 is a single transmembrane glycoprotein known also as N-CAM (Neural Cell Adhesion Molecule). It is involved in cellular adhesion, capable of binding to itself (homophilic) and to heparin sulphate (heterophilic) binding and is expressed by NK and NK-T cells.	MEM-188
Hsp70	When Hsp70 is expressed within the plasma membrane, the bulk of the protein remains intracellular whilst the substrate binding domain is in an extracellular position. This form of Hsp70 has been documented on tumour cells, and its expression can be upregulated in response to a variety of stresses, although its expression on healthy lymphocytes is unknown.	cmHsp70.1 and C92F3A-5 (specific for different epitopes within the substrate binding domain)
CD69	CD69 is a type II transmembrane protein, sometimes called very early activation antigen (VEA). Presence of CD69 indicates cellular activation on T cells, B cells, NK cells, neutrophils and eosinophils.	FN50
CD25	CD25, also known as low affinity IL-2 receptor α chain, is a type I transmembrane glycoprotein, expressed on the surface of activated T cells, B cells, macrophages and monocytes. It is also constitutively expressed on regulatory T cells regardless of activation status.	BC96
Phosphatidylserine (PS)	PS is a phospholipid component of the plasma membrane. In viable cells it is restricted to the intracellular side of the membrane, but becomes exposed on the extracellular surface when cells become apoptotic.	4B6

Table 2.8. Antigens of interest for the phenotypic analysis of whole blood and PBMCs.

Cells populations were determined on the basis of CD3, CD4, CD8 and CD56 expression, and assessed with regards to memHsp70 and cellular activation (using CD69 and CD25). Phosphatidylserine expression enabled apoptotic cells to be excluded.

Antigen	Fluorochrome	Excitation laser and detector channel
CD3	QDot605 Alexa Fluor 700	Blue 610/20 Red 730/50
CD4	Pacific Blue	Violet 450/50
CD8	V500 Alexa Fluor 700	Violet 550/50 Red 730/50
CD56	Phycoerythrin	Blue 575/26
Hsp70	Fluorescein ATTO 488	Blue 530/30 Blue 530/30
CD69	PE/Cy7	Blue 780/60
CD25	PerCp/Cy5.5	Blue 695/60
Phosphatidylserine	Alexa Fluor 647 ATTO 633	Red 660/40 Red 660/40

Table 2.9 Fluorescently-labelled reagents used in flow cytometric analyses.

Details of the antibodies used in flow cytometric analyses. For each antibody the antigen recognised is given, the fluorochoromes used (for some antibodies multiple fluorochrome conjugates were used, in order to form spectorally compatible multi-antibody panels depending on the staining being conducted), the laser of excitation, the channel for emission detection and the volumes used in each staining procedure.

After this time, samples were washed with 3mL chilled staining buffer and centrifuged (300g, 5 minutes, 4^{o}C). The supernatants were decanted and cells resuspended by gentle agitation of the tubes. Erythrocytes were lysed using BD Lysis Buffer (BD Biosciences) which was diluted to a 1x working solution from the stock (nine parts distilled water and one part Lysis Buffer Stock Solution). This working solution was stored at room temperature in glass bottles for up to 1 month. For the lysis itself, 2mL working solution lysis buffer was added to each tube and then well mixed by vortexing. Cells were stored at room temperature protected from light for 20 minutes then centrifuged (300g, 5 minutes, 4^{o}C). The supernatant was decanted and cells were washed twice with 3mL staining buffer and centrifuged as before. Finally, cells were resuspended in 250µL staining buffer before being analysed by flow cytometry.

2.6.2.2 Activation of lymphocytes in whole blood

The potential influence of polyclonal activation on the expression of membrane Hsp70 by CD4^{+} T cells, CD8^{+} T cells and CD56^{+} NK cells in whole blood was determined by activating cells with the polyclonal mitogenic lectin Concanavalin A (ConA). For this, whole blood was diluted 1:4 with growth medium containing ConA (5µg/ml final concentration, #C5275 Sigma) and cultured for 24 hours in 96-well plates (200µl/well) in a humidified incubator at 37°C. As a control, blood was incubated for 24 hours after being diluted with medium in the absence of ConA. The contents of each well were then transferred into 12x75mm polypropylene tubes and washed with staining buffer (PBS containing 10% v/v FCS) then centrifuged (300g, 5

minutes). The supernatant was decanted to leave approximately 50µl of sample and this was stained for memHsp70 expression as described previously.

2.6.3 Expression of memHsp70 on isolated peripheral blood mononuclear cells (PBMCs)

Whole blood samples were not suitable for examining all of the treatments that were used in order to reflect elements of the tumour microenvironment. For these experiments PBMCs were isolated from whole blood using density gradient separation and exposed to range of different conditions. The influence of these conditions on membrane Hsp70 expression was then determined by multi-parameter flow cytometry.

2.6.3.1 Isolation of PBMCs

PBMCs were isolated by density gradient, either with NycoPrep™ 1.077 (Axis-Shield PoC AS, Norway) or Lymphocyte Separation Medium LSM 1077 (PAA Laboratories GmbH, Pasching, Austria). Blood samples were diluted 1:1 with PBS and the diluted blood carefully layered onto the density gradient medium of choice (3mL blood mixture onto 6mL NycoPrep™ 1.077 in 15mL conical tubes or 8mL blood mixture on 8mL LSM 1077 in 25mL conical tubes), after which samples were centrifuged (400g for 30 minutes when using NycoPrep™ 1.077 and 1200g for 20 minutes when using LSM 1077) at 4^{o}C with no brake applied. The PBMCs at the interphase layer were harvested using a Pasteur pipette and transferred into 25ml tubes, with no more than 5mL in one tube. In order to ensure removal of platelets, and thus reduce the potential for cell clumping within the preparation and also the possible effects of platelet-derived growth factors (which can inhibit the functional capacity of PBMCs) on the responsiveness of PBMCs, a second density gradient isolation step was performed. For this, the density medium was diluted 1:3 with phosphate buffered saline (PBS) to create a relative density of 1.068. This was then layered underneath the cells using a 21G needle and 20ml syringe. The samples were then centrifuged again, this time for 15 minutes. The change in density means the PBMCs will form a pellet and the platelets will collect at the interphase layer. To retrieve the PBMCs, the supernatant was decanted and the cell pellet was resuspended in 10ml PBS. Cells were washed twice in PBS (300g, 5 minutes, brake on) then resuspended in 1ml of complete growth medium prior to undertaking a viable cell count using a haemocytometer on the basis of trypan blue dye exclusion. Cells were then used for staining of memHsp70 expression or to set up treatments to investigate the possibility of memHsp70 induction.

2.6.3.2 Staining of PBMCs

The same panel of mAbs were used to stain PBMCs as were used in the whole blood samples (**Table 2.8**). PBMCs ($1.5x10^{6}$) were placed into microfuge tubes and washed with 1mL of

staining buffer (PBS + 10% v/v FCS + 1.0mM $MgCl_2$ + 2.5mM $CaCl_2$) by centrifugation at 300g for 5 minutes at 4°C. The supernatant was aspirated and the cells resuspended in 100µL staining buffer containing 7.5µL Alexa Fluor 647-conjugated Annexin V (Biolegend). After vortexing, the cells were incubated at room temperature for 20 minutes. The cells were washed in 1mL staining buffer and centrifuged at 300g for 5 minutes at 4°C. After aspiration of the supernatant, cells were resuspended in 10µL of staining buffer and 1µL mouse serum and incubated at 4°C for 10 minutes before the addition of fluorescently-labelled antibodies. The total volume of suspension was made up to 50µL with staining buffer containing Blue Live/Dead Fixable Dead Cell Stain (Molecular Probes, USA), and the cells were incubated at 4°C, protected from light, for 30 minutes. Cells were then washed with 1mL staining buffer and centrifuged at 300g for 5 minutes at 4°C and supernatants were aspirated.

If the sample was to be analysed for intracellular expression of Hsp70, then the cells were resuspended in 50µL Fix/Perm Solution A (Life Technologies) and incubated at 4°C for 20 minutes. The samples were then washed in staining buffer (1mL, centrifugation at 300g for 5 minutes) before being resuspended in 50µl Fix/Perm Solution B (Life Technologies) and the C92F3A-5 anti-Hsp70 mAb, and incubated at 4°C for 20 minutes. The samples were then washed one final time with staining buffer (1mL, centrifugation at 300g for 5 minutes). All samples were washed once with PBS (300g, 5 minutes) and then resuspended in 200µL PBS with 100µL CellFix™ (BD Biosciences), mixed well and transferred into 12x75mm polypropylene tubes. Cells were stored at 4°C, protected from light, until flow cytometric analysis could be conducted.

2.6.3.3 Influence of non-lethal heat

It is well documented that heat stress upregulates the expression of intracellular Hsp70 as well as upregulating the expression of memHsp70 on tumour cells [287]. However, it is not known whether heat stress can induce memHsp70 expression on lymphocytes. To investigate whether increased temperature can induce expression of memHsp70, isolated PBMCs were incubated at an above optimal temperature environment and then stained for memHsp70 expression as described previously. To set up the incubation, $1x10^6$ PBMCs suspended in 1mL growth medium were placed in 12x75mm polypropylene tubes then incubated in a temperature controlled water bath at 42°C for 2 hours. This duration was selected as it was sufficient to induce a peak in expression of intracellular Hsp70 whilst remaining non-lethal to the lymphocytes (see **Fig 2.14**). After this time, cells were centrifuged (300g, 5 minutes), the supernatant was decanted and cells were resuspended in 1mL fresh medium before being placed into the 37°C incubator to recover for a period of 2 hours (short recovery) or 22 hours

(long recovery). After the recovery period, cells were stained for memHsp70 expression as previously described.

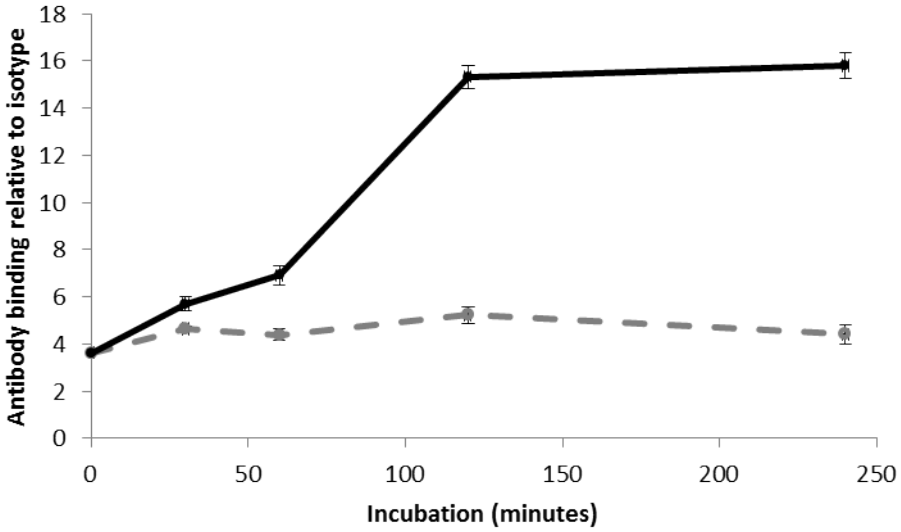

Figure 2.14 Intracellular Hsp70 response to heat stress

Intracellular Hsp70 content is stable under optimal incubation conditions (37°C, dashed line), but is increased in response to incubation at 42°C (solid line). This increase peaks after 2 hours and then remains stable. For longer durations (18-24 hours), incubation at 42°C is lethal. Data are presented as mean ± SEM, n = 3.

2.6.3.4 Influence of polyclonal activation

The effect of activation on the expression of memHsp70 by lymphocytes was assessed in two ways, firstly using ConA and secondly using polystyrene beads coated with anti-CD3 and anti-CD28 mAbs. These beads polyclonally activate cells by binding to the T cell receptor (via the anti-CD3 mAb), and the binding of the anti-CD28 mAb mimics the delivery of essential co-stimulatory signals that are delivered by APCs. This mode of activation closely mirrors the physiological events that occur following cell activation by APCs.

To activate using ConA, PBMCs were suspended in medium containing 5µg/mL ConA and placed into 12x75mm polypropylene tubes ($1x10^6$ PBMCs in 1mL). Cells were incubated for 24 hours at 37°C before being stained for memHsp70 expression as described earlier. For the second method, two different activation beads were used, Dynal Expander beads (Life Technologies) and Suppression Inspector beads (Miltenyi Biotec). Dynal Expander beads deliver a more potent stimulatory signal, as they are coated with a higher concentration of mAbs, and so comparing the effects of both bead populations should enable any correlation between the degree of cell activation and membrane Hsp70 expression to be assessed. Control (unstimulated) samples were cultured without beads. For the culture, $1x10^6$ PBMCs were placed in 12x75mm polypropylene tubes and suspended in 1ml of medium at a 1:1 ratio with one or other of the beads. Cells were mixed thoroughly and then incubated at 37°C for 24

hours. After this time the cells were agitated to aid disruption of the bead binding. The beads are magnetic so samples were placed into a magnetic rack and once the beads had aggregated the supernatant containing the cells was transferred into a fresh tube. Cells were then stained for memHsp70 expression as described previously.

2.6.3.4.1 Influence of supernatant derived from polyclonally activated cells

To confirm whether soluble factors released during lymphocyte activation could also have any effect on memHsp70 expression, supernatant was collected from cells after incubation with the activation beads and stored in microfuge tubes at -80°C. As a control, supernatant was also harvested from unstimulated cells. When required, aliquots were defrosted and added to Isolated PBMCs ($1x10^6$ cells in polypropylene 12x75mm tubes). Cells were either set up with supernatant only (100% v/v) or in supernatant with growth medium (50% v/v) and then incubated for 24 hours at 37°C. After this time cells were stained for memHsp70 expression as described previously.

2.6.3.5 Influence of hypoxia

Vascularisation can be inadequate when tumours grow rapidly and regions become hypoxic. To assess whether the hypoxia that tumour infiltrating lymphocytes could experience can induce memHsp70 expression, PBMCs were examined after incubation in a hypoxic chamber. $1x10^6$ PBMCs suspended in 1mL growth medium and placed into 12x75mm polypropylene tubes were incubated for 20 hours at 37°C and 0.1% v/v oxygen. After this time the cells were stained for memHsp70 expression as described previously.

2.6.3.5.1 Influence of hydrogen peroxide

Hydrogen peroxide (H_2O_2) served as a chemical approach to the administration of oxidative stress. To this end, $1x10^6$ PBMCs n 12x75mm polypropylene tubes were suspended in medium containing 1000, 100, 50, 25, 10 or 1µM H_2O_2 (Sigma) and incubated at 37°C for 1 hour. Cells were then centrifuged (300g, 5 minutes) and resuspended in 1mL fresh growth medium, after which they were incubated for a further 22 hours at 37°C before being stained for memHsp70 expression, as described previously.

2.6.4 Data acquisition

Data from stained PBMCs were acquired on a BD™ LSRII flow cytometer, in the same way as for the tumour cell samples. The fluorochromes and the corresponding detector channels are summarised in **Table 2.9**. Samples were run until 10,000 lymphocytes had been acquired or, if there were insufficient cells to obtain this number, until the whole sample volume had been processed.

2.6.5 Post Acquisition Analysis

The analysis was conducted using FACSDiva™ software and follows the same principles as the analysis of tumour cell samples. Hierarchical plots are drawn to first enable selection of different cell types and then allow examination of inducible marker expression. Before starting, the compensation settings were applied and checked by comparing every pair of fluorochromes on scatter plots.

The first step in the analysis was to identify the cell populations of interest, beginning with selection of lymphocytes. This was conducted in a similar manner to the tumour cell analysis using forward and side light scatter profiles (FSC vs SSC), which correlate to the size and granularity of cells respectively. In the whole blood samples this allowed distinction, and therefore exclusion, of neutrophils and monocytes from the lymphocyte population. In the isolated PBMC samples only mononuclear cells were present (**Fig 2.15**).

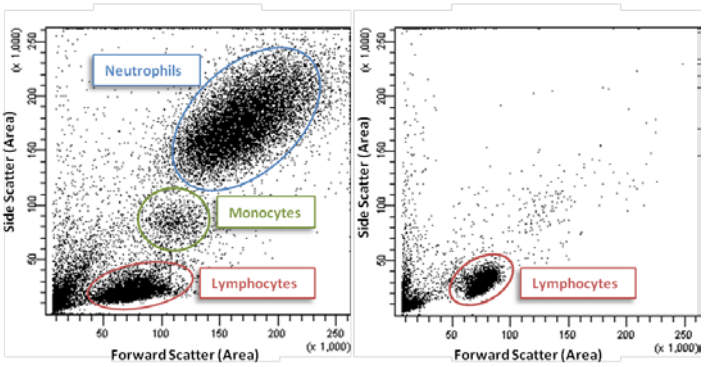

Figure 2.15 Identification of cell populations

A portion of the laser light hitting the cells will be scattered and this gives information about certain physical properties of the cell. The angle of light scattered in front of the cell (Forward Scatter) is proportional to the size of the cell. The angle of light scattered to the side (Side Scatter) is proportional to the granularity. These measurements allow distinction of multiple populations within the same sample, as long as the relative physical properties are known. This is illustrated by separation of cell populations in a whole blood sample (left). After density gradient separation of lymphocytes the profile is very different (right). The dense region in the lower left of both plots shows the debris in the sample.

The next step was the exclusion of cell aggregates, and this was achieved as described previously using the FSC-area and FSC-height parameters, from which can be selected the viable, non-apoptotic cells (**Fig 2.16**). The viability of cells was determined by exclusion of the blue fixable live/dead stain and non-apoptotic cells by the lack of surface expression of phosphatidylserine (PS). Expression of PS was determined using an anti-phosphatidylserine antibody (whole blood samples) or Annexin V (PBMC samples).

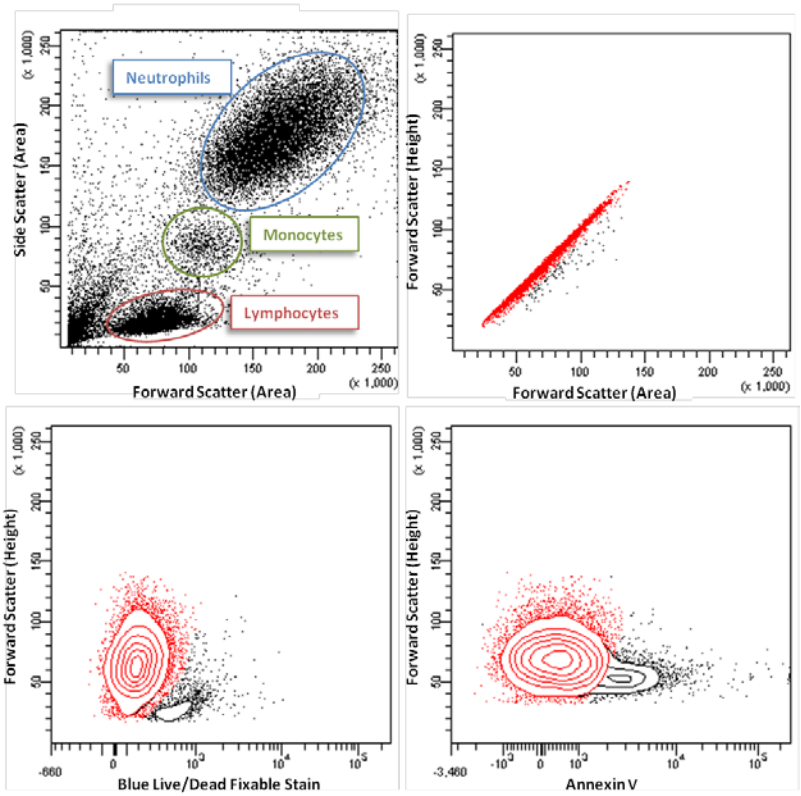

Figure 2.16 Selection of viable cell populations to analyse.

It is essential to analyse the correct cells to get accurate results. Dead and dying cells can autofluoresce, whereas clumped cells can lead to multiple phenotypes being recorded for a single cell. Starting with the FSC against SSC plots, the population of interest is selected. From these, the cells are displayed on a plot comparing the FSC giving information about cell area with that of cell height. Single cells will show as a perfectly correlated line, with any clumped cells below. These single cells are checked for viability, using a Blue Live/Dead Fixable stain. This stain detects amine residues, so while viable cells will bind a small amount to the membrane the compromised membrane of dead cells allows the stain to permeate into the cell resulting in much brighter staining. Finally, the viable cells are also checked for the early signs of apoptosis using Annexin V staining. In each plot the cells that will be selected are highlighted in red.

The next stage was separating the different lymphocyte populations of interest (T cells and NK cells) on the basis of phenotypic cell surface marker expression (**Fig 2.17**). Initially, CD3 expression enabled the identification of T cells ($CD3^+$) from other lymphocytes ($CD3^-$). The T cells were further divided into $CD4^+$ and $CD8^+$ expression (predominantly helper and cytotoxic populations). The $CD3^-$ lymphocyte population contains the NK cells of interest, and B cells which must be excluded. This is achieved using the NK cell marker CD56, for which all NK cells will be positive, but for which B cells are negative. By comparing CD56 with CD8 it is possible to distinguish two NK populations, $CD8^+$ and $CD8^-$.

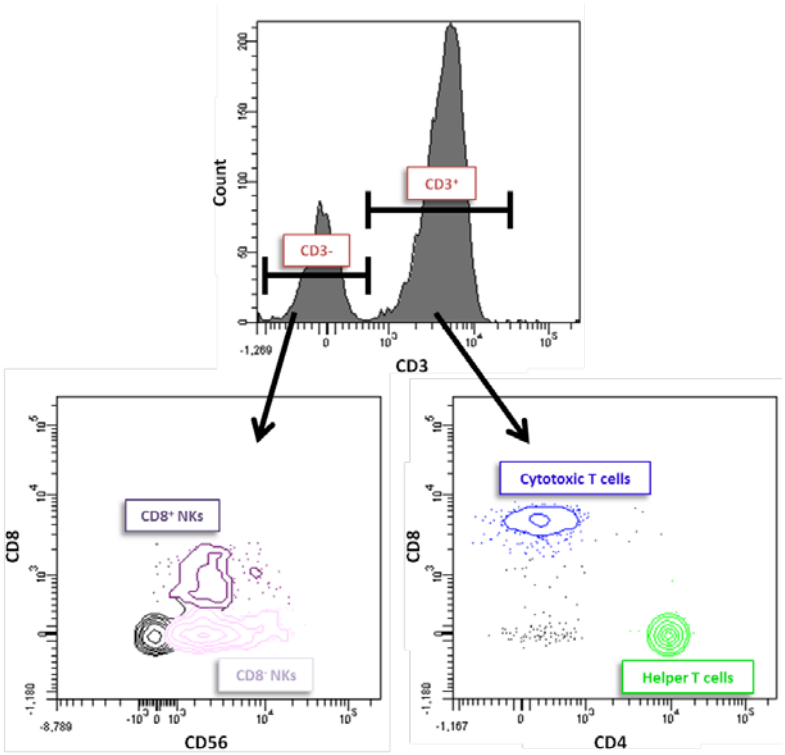

Figure 2.17 Selection of lymphocyte sub-populations

Lymphocyte sub-populations can be distinguished on the basis of different surface markers. T cells can be identified on the basis of their expression of CD3, and the major subpopulations on the basis of CD4 (shown in green) and CD8 (shown in blue) expression. NK cells arte $CD3^-$, but $CD56^+$. Although $CD56^+$, NK cell sub-populations express low and high intensities of this antigen. $CD3^-$ lymphocytes do not express CD56. A proportion of NK cells were also found to express CD8, which was a very interesting finding as this is not found in the published literature.

Once the T cell and NK cell populations had been identified, the expression of memHsp70 and cellular activation markers by these populations was assessed by comparing the fluorescent intensity of the whole population to that of the isotype. Both CD69 and CD25 exhibited a two peak positive/negative profile, and so assessment was conducted into the proportion of cells which expressed the markers (activated cells) and the intensity of the positive expression.

2.6.6 Response to exogenous granzyme B

Exogenous granzyme B has been shown to lead to induction of apoptosis in the $memHsp70^+$ cell line CT26 [532]. To investigate whether apoptosis can also be induced in lymphocytes by granzyme B, lymphocytes were incubated in the presence of granzyme B in the same way as tumour cell lines then assessed in terms of active caspase-3 expression and apoptosis determined by Annexin V binding.

2.7 Statistical analysis

All statistical analyses were conducted using SPSS v20. The appropriateness of parametric tests was assessed by comparing mean and median measurements (for small experimental numbers), as well as test of normality. Paired and unpaired Student's T tests were used to

compare data from two groups when these were normally distributed, with the Wilcoxon signed-rank test and the Mann Whitney U test being used if the data were non-parametric. A one-way or repeated measures ANOVA was employed for the analysis of data three or more groups. ANOVA tests were conducted along with *post hoc* comparisons; the Games-Howell comparison if the assumption of homogeneity was violated, otherwise a Bonferroni comparison if all groups had equal numbers of subjects or a Gabriel comparison if the subject numbers varied slightly. All analyses were performed with two-tailed hypotheses, at a 0.05 significance level and any significant results are described as * ($p<0.05$), ** ($p<0.01$) or *** ($p<0.001$). Potential correlations were assessed using two-tailed Pearson's Correlation Coefficients. Power calculations to determine necessary assay sample sizes were conducted using the freely available G*Power software (distributed by Heinrich Heine Universität Düsseldorf, www,gpower.hhu.de).

CHAPTER 3: Results I – Internalisation of the cmHsp70.1 mAb by cancer cells expressing membrane Hsp70

3.1 Introduction

Heat shock protein 70 (Hsp70) is found in all eukaryotic cells and is primarily considered as being an intracellular molecule. However, it is now known that approximately 50% of all tumours express a membrane form of this protein (memHsp70, [285]). The presentation of an Hsp70-derived sequence on the plasma membrane of tumour cells can be detected by flow cytometry using a fluorescently labelled antibody (clone cmHsp70.1 mAb) that binds to a site located in the epitope which is available at the cell surface [289]. However, the cmHsp70.1 mAb is unique, as all other commercially-available anti-Hsp70 antibodies (including clone C923F5-A) recognise an epitope which is not accessible on the surface of tumour cells when Hsp70 is in its membrane form, but which can be recognised if extracellular Hsp70 has bound to the surface of tumour cells. The staining of cells using clone C923F5-A has therefore been used as a control to define the form of Hsp70 expression throughout this study.

Given that such a large proportion of tumours, but not normal tissue, selectively express memHsp70, then this molecule could act as a valuable targeting structure for agents and molecules that specifically recognise and interact with this epitope. The studies presented herein have investigated the interaction of 3 such molecules: the cmHsp70.1 mAb [289, 533], a 14-mer peptide (sequence TKDNNLLGRFELSG) which has been found to exhibit binding potential similar to that of the cmHsp70.1 mAb [535], and a recombinant form of human granzyme B [530, 532]. This chapter will address the interaction of the cmHsp70.1 mAb with breast cancer cell lines.

The cmHsp70.1 mAb (multimmune GmbH, Munich, Germany) was originally generated by immunising mice with the 14-mer peptide TKDNNLLGRFELSG, comprising amino acids 450–461 ($aa_{450–461}$) in the C terminus of the inducible Hsp70. Since the human and murine sequences only differ in one amino acid ([550]; human TKDNNLLGRFELSG; mouse TRDNNLLGRFELSG), the cmHsp70.1 mAb shows a cross-reactivity for human and mouse tumours [533]. The capacity of this antibody to selectively bind to tumour cells via memHsp70 and induce antibody-dependent cytotoxicity (ADCC) *in vitro* and *in vivo* [533] suggests that it might have clinical value as a tumour targeting agent and/or an immunotherapeutic agent. The following studies further examine the interaction of cmHsp70 mAb with human and murine cancer cells and its

internalisation. These properties will then be compared to those of the TKDNNLLGRFELSG peptide and recombinant granzyme B which are examined subsequently.

3.2 Membrane Hsp70 expression by human and murine cancer cell lines

The expression of memHsp70 by three human breast cancer cell lines (MDA-MB-231, MCF7 and T47D) and two murine cell lines – CT26 (colorectal cancer) and 4T1 (mammary carcinoma) was determined by flow cytometry using a FITC-labelled cmHsp70.1 mAb. Using the median fluorescence intensity of the whole cell population relative to that of the isotype provides a relative measurement of the expression of memHsp70 of that cell line (**Fig 3.1**). A second Hsp70 antibody clone was also used, C92F3A-5, which binds to an epitope that is inaccessible when the molecule is held within the cell membrane. In the absence of cell fixation and permeabilisation, the C92F3A-5 antibody would only be able to bind to Hsp70 that was bound to the surface of cells and consequently its lack of binding can be used to confirm the presence of memHsp70 only. In all tumour cell lines used, the fluorescence intensity of C92F3A-5 is not significantly different to the isotype control, demonstrating that there is no surface bound Hsp70 and therefore cmHsp70.1 staining is indicative of memHsp70 only.

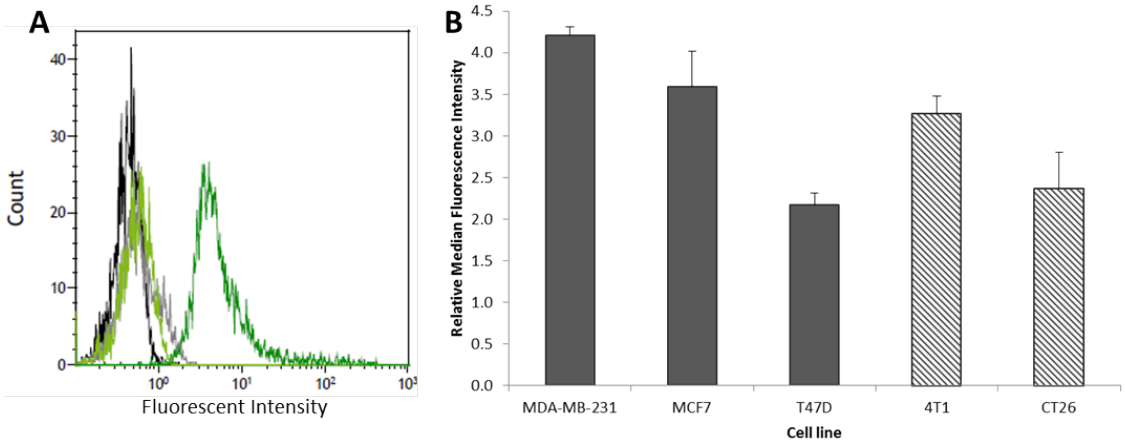

Figure 3.1 Binding of cmHsp70.1 mAb antibody to tumour cell lines

A. Representative flow cytometry plots showing the fluorescent intensity of MDA-MB-231 cells incubated for 30 minutes at 4^{o}C in staining buffer (black line), with isotype antibody (grey line), with C92F3A-5 mAb (light green line) and with cmHsp70.1 mAb (dark green line). B. The binding of FITC-labelled cmHsp70.1 mAb to both human (solid bars) and mouse (dotted bars) cancer cell lines, expressed as the intensity of fluorescence in the whole population relative to cells that were unstained. A measurement of greater than 1 indicates specific binding of cmHsp70.1 mAb and the higher the value the more antibody is bound, indicating a greater surface density of memHsp70. Data are presented as mean ± SEM and are the result of 4-7 independent experiments.

Of the human lines examined, MDA-MB-231 cells expressed the greatest amount of memHsp70, with MCF7 cells only slightly lower and T47D expressing around 50% of this expression. Of the mouse-derived cell lines, 4T1 expressed the highest level of memHsp70. The availability of cell lines which express memHsp70 to varying degrees allowed the potential relationship between expression of memHsp70 and the binding/internalisation of memHsp70-specific reagents to be investigated.

3.3 Internalisation of cmHsp70.1 mAb by cancer cells expressing memHsp70

To investigate the influence of memHsp70 on the internalisation of cmHsp70 mAb by the different cancer cell lines, cells were incubated in the presence of FITC-labelled cmHsp70.1 mAb at 37°C (to allow metabolic activity and therefore antibody internalisation) or 4°C (to allow binding only). An aliquot was saved at different time points up to 60 min, and these were analysed by flow cytometry. In addition, cells were also incubated at 37°C with FITC-conjugated C92F3A-5 mAb in order to confirm the specificity of any observed effects and responses (**Fig 3.2**).

All cells internalised the antibody, with significant differences between the median fluorescence intensity (mfi) of cells incubated with cmHsp70.1 mAb at 4°C and 37°C (one-way ANOVA. MDA-MB-231: $F = 32.918$, $p < 0.001$; MCF7: $F = 41.859$, $p < 0.001$; T47D: $F = 19.259$, $p < 0.001$; CT26: $F = 19.606$, $p < 0.001$; 4T1: $F = 6.828$, $p < 0.001$). The extent of cmHsp70.1 mAb internalisation was related to the intensity of memHsp70 which they expressed on their plasma membrane, with cell lines expressing the lowest levels of memHsp70 (T47D and CT26) internalising the least amount of antibody (mfi at the 60 minute, 37°C incubation time-point of 1015 ± 64 and 1346 ± 85 respectively), compared to the lines expressing higher memHsp70 (MDA-MB-231: 3006 ± 348; MCF7: 3835 ± 204; 4T1: 2996 ± 649). The lack of binding/internalisation of C92F3A-5 mAb provides a baseline measure of non-specific fluorescence, with the difference between this and the cmHsp70.1 at 4°C again confirming the specific binding of the antibody clone.

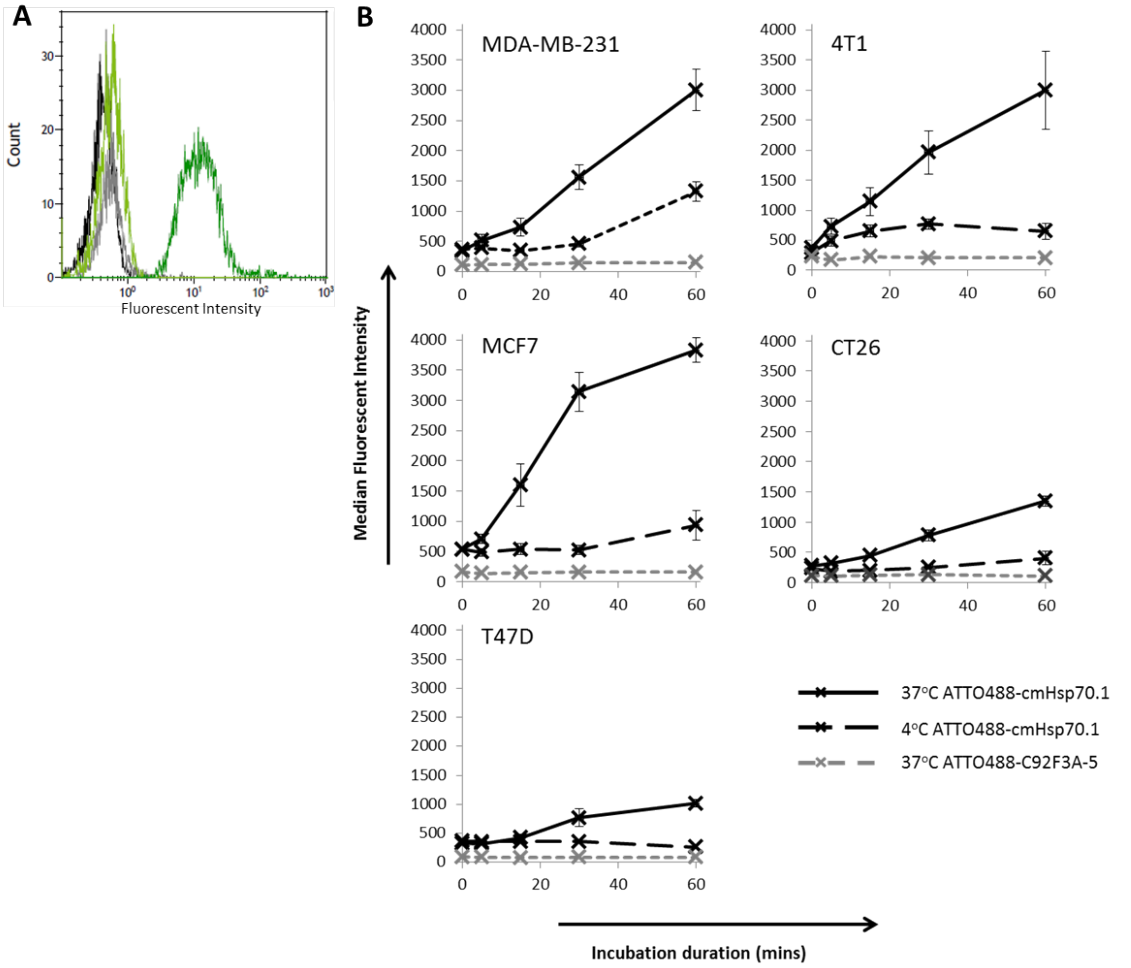

Figure 3.2 Uptake of fluorescently-labelled cmHsp70.1 mAb antibody into human and murine cancer cell lines expressing differing levels of memHsp70

A. Representative flow cytometry plots showing the fluorescent intensity of MDA-MB-231 cells incubated for 60 minutes at 37°C in medium (black line), with isotype (grey line), C92F3A-5 (light green line) and cmHsp70.1 (dark green line). B. Cells were incubated in the presence of FITC-cmHsp70.1 with samples saved at different time points, for up to an hour. The median fluorescent intensity of the whole population was recorded by flow cytometry. The intensity after 4°C incubation relates to the binding of antibody to the cell surface (dashed black lines), while the 37°C incubation allows for inclusion of antibody internalisation (solid black lines). All cell lines are capable of binding and internalising the cmHsp70.1 mAb, albeit to varying degrees. As a control, cells were also incubated with the C92F3A-5 mAb, which did not stain cell, even after incubation at 37°C (dashed grey lines). Data are presented as mean ± SEM of at least three independent experiments.

In addition to using flow cytometry, the uptake of ATTO488-cmHsp70.1 mAB was assessed using fluorescent microscopy images of cells at multiple time-points after incubation with the fluorescently-labelled antibody (**Fig 3.3 and 3.4**). Tile scan images were produced by way of fluorescence microscopy rather than confocal microscopy in order to ensure the total fluorescence of cells was captured.

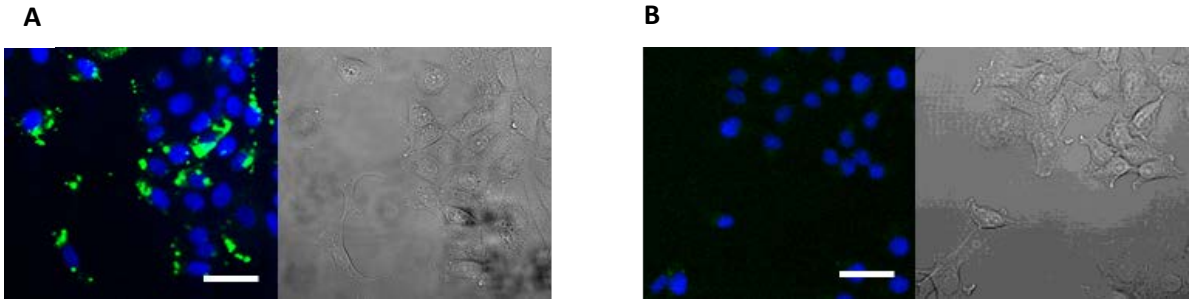

Figure 3.3 Representative tile scan images showing antibody uptake into MDA-MB-231 cells

Tile scan images were produced for MDA-MB-231, MCF7, T47D, 4T1 and CT26 cells, across different time-points of incubation with Hsp70 antibodies. Representative tile scan images of MDA-MB-231 cells incubated with cmHsp70.1 (A) and C92F3A5 (B) antibodies for 60 minutes are shown. Antibodies are shown in green and the nucleus stained with DAPI is shown in blue. Scale bar represents 50µm.

Using the analysis software package ImageJ, the fluorescent intensity of every imaged cell was determined (normalised to the background intensity). The mean fluorescent intensity of cells increased over time, thereby demonstrating uptake of the fluorescently-labelled mAb. The level of uptake varied between cell lines, but in line with memHsp70 expression, mimicking the flow cytometric data shown earlier and confirming that using the in-house conjugate with microscopy was a robust method of examining cmHsp70.1 mAb uptake.

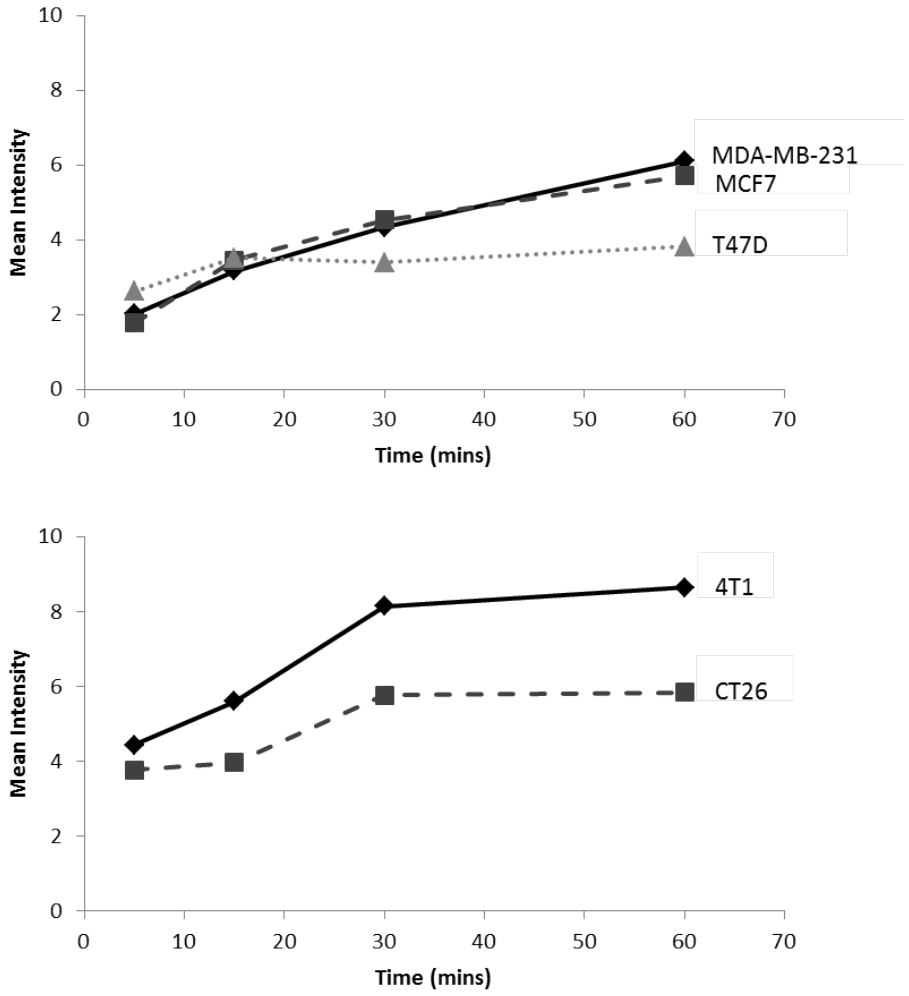

Figure 3.4 Uptake of ATTO488-labelled cmHsp70.1 mAb into human and murine cancer cell lines expressing differing levels of memHsp70

Cancer cell lines from human (A) and mouse (B) grown in MatTek™ glass bottom dishes were incubated in the presence of ATTO488-cmHsp70.1 mAb for up to an hour, after which cells were imaged using fluorescent microscopy. Mean fluorescent intensity values were calculated and normalised to the background fluorescence. All cell lines are capable of internalising the cmHsp70.1 mAb, but to varying degrees and in line with the memHsp70 expression of cell lines. Data are presented as mean ± SEM of a minimum of 80 cells from at least three independent experiments.

The internalisation of cmHsp70.1 mAb was also studied using confocal microscopy image analyses in order to better understand cmHsp70.1 mAb internalisation events (**Fig 3.5-3.9**). Cells were imaged at a number of time points up to 60 min, and z-stack images covering the entire cell generated. It is interesting to note that internalisation of the cmHsp70.1 mAb resulted in the appearance of distinct fluorescent 'spots', thereby suggesting that the internalised antibody was associated with intracellular vesicles, rather than being 'free' and distributed in the cytoplasm. Although the lack of inter-experimental controls relating to fluorescence intensity rendered it impossible to compare the intensity of images obtained at different times and in different experiments, the distribution of cmHsp70.1 mAb did enable

quantification in the form of counting the number of distinct spots. When a spot appears over more than one z-stack frame it was counted in the stack in which the greatest fluorescence intensity was apparent.

The data gained using this quantification from microscopy images tracks with the flow cytometry quantification of the population intensity. Simply by viewing the confocal images, it appears that the size of the fluorescent spots varied between the different cell lines. The fluorescent spots reflecting cmHsp70.1 mAb internalisation in the two murine cancer cell lines were much smaller than those that were apparent in the human cells lines, for reasons that are currently unclear but may simply be indicative of smaller sized vesicles in mouse. There also appear to be differences in the sizes of spots between the human cell lines, again for reasons that are currently unclear. It was not possible to accurately quantitate the size of the fluorescent spots in this setting, as the area containing fluorescence is altered as brightness/contrast/threshold values are adjusted, thereby meaning that any size calculation is entirely dependent on the image settings. Without reliable methods of calibrating the settings when acquiring, as well as processing, images it is therefore not possible to calculate size values which can be compared.

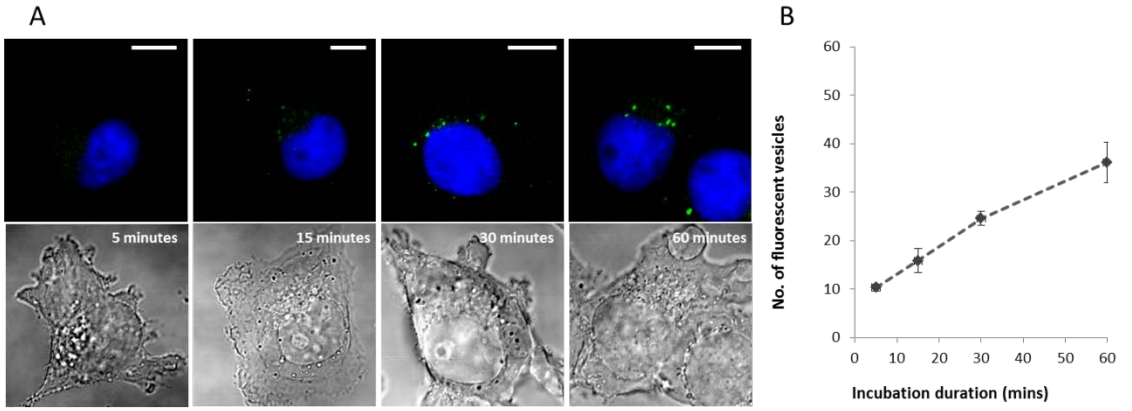

Figure 3.5 Kinetics of cmHsp70.1 mAb uptake by MDA-MB-231 cells

A. Representative single frame images showing ATTO488-labelled cmHsp70.1 mAb internalised into MDA-MB-231 cells. Frames were selected from the mid-point of cells (25-75% of distance from adhered surface). ATTO488-cmHsp70.1 mAb (green) appears in well-defined vesicles rather than free in the cytosol. The frames depict a region 0.88µm thick. Scale bars are 10µm. For clarity, the nucleus was stained with DAPI and is shown here in blue. **B.** The number of distinct fluorescent spots in cells after different incubation times. This is a total count including spots within the cell and at the membrane. Data are presented as mean ± SEM for 10-24 individual cells, from at least two independent experiments.

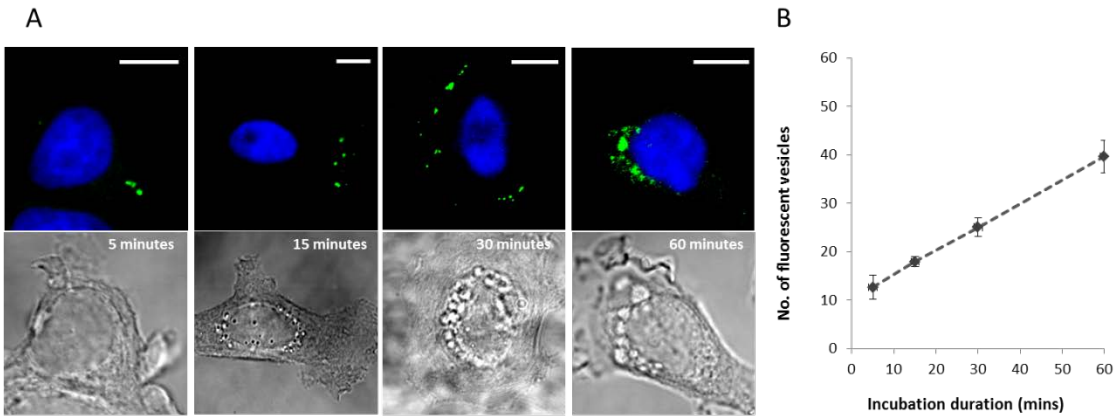

Figure 3.6 Kinetics of cmHsp70.1 mAb uptake by MCF7 cells

A. Representative single frame images showing ATTO488-labelled cmHsp70.1 mAb internalised into MCF7 cells. Frames were selected from the mid-point of cells (25-75% of distance from adhered surface). ATTO488- cmHsp70.1 mAb (green) appears in well-defined vesicles rather than free in the cytosol. The frames depict a region 0.88µm thick. Scale bars are 10µm. For clarity, the nucleus was stained with DAPI and is shown here in blue. **B.** The number of distinct fluorescent spots in cells after different incubation times. This is a total count including spots within the cell and at the membrane. Data are presented as mean ± SEM for 13-24 individual cells, from at least two independent experiments.

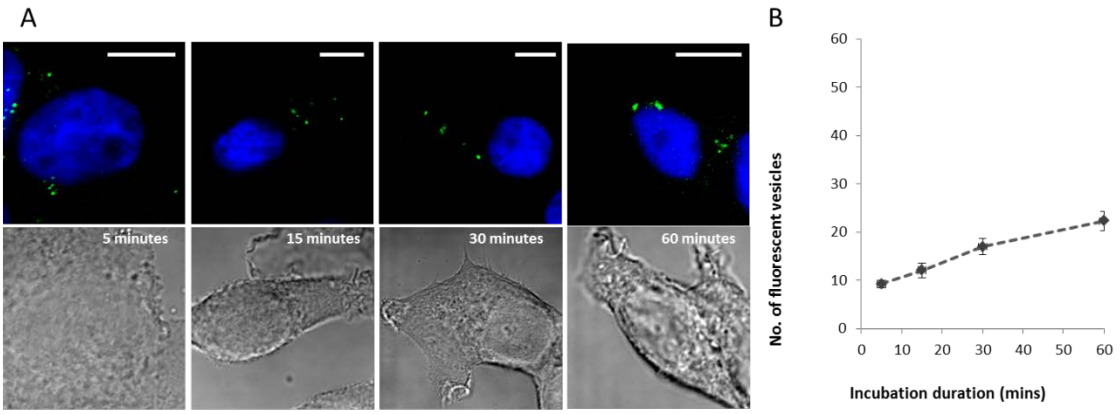

Figure 3.7 Kinetics of cmHsp70.1 mAb uptake by T47D cells

A. Representative single frame images showing ATTO488-labelled cmHsp70.1 mAb internalised into T47D cells. Frames were selected from the mid-point of cells (25-75% of distance from adhered surface). ATTO488- cmHsp70.1 mAb (green) appears in well-defined vesicles rather than free in the cytosol. The frames depict a region 0.88µm thick. Scale bars are 10µm. For clarity, the nucleus was stained with DAPI and is shown here in blue. **B.** The number of distinct fluorescent spots in cells after different incubation times. This is a total count including spots within the cell and at the membrane. Data are presented as mean ± SEM for 8-19 individual cells, from at least two independent experiments.

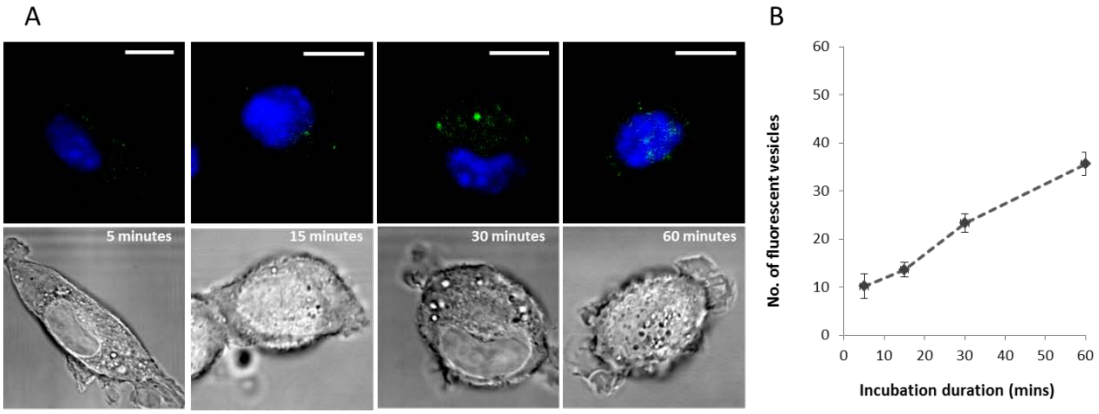

Figure 3.8 Kinetics of cmHsp70.1 mAb uptake by 4T1 cells

A. Representative single frame images showing ATTO488-labelled cmHsp70.1 mAb internalised into 4T1 cells. Frames were selected from the mid-point of cells (25-75% of distance from adhered surface). ATTO488- cmHsp70.1 mAb (green) appears in well-defined vesicles rather than free in the cytosol. The frames depict a region 0.88µm thick. Scale bars are 10µm. For clarity, the nucleus was stained with DAPI and is shown here in blue. **B.** The number of distinct fluorescent spots in cells after different incubation times. This is a total count including spots within the cell and at the membrane. Data are presented as mean ± SEM for 7-18 individual cells, from at least two independent experiments.

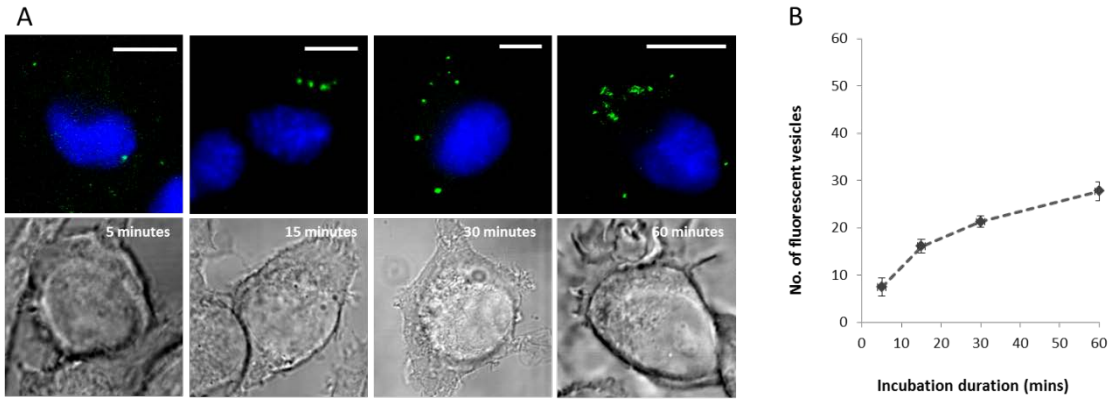

Figure 3.9 Kinetics of cmHsp70.1 mAb uptake by CT26 cells

A. Representative single frame images showing ATTO488-labelled cmHsp70.1 mAb internalised into CT26 cells. Frames were selected from the mid-point of cells (25-75% of distance from adhered surface). ATTO488- cmHsp70.1 mAb (green) appears in well-defined vesicles rather than free in the cytosol. The frames depict a region 0.88µm thick. Scale bars are 10µm. For clarity, the nucleus was stained with DAPI and is shown here in blue. **B.** The number of distinct fluorescent spots in cells after different incubation times. This is a total count including spots within the cell and at the membrane. Data are presented as mean ± SEM for 9-23 individual cells, from at least two independent experiments.

3.3.1 Distribution of cmHsp70.1 mAb after internalisation into human and murine cell lines expressing memHsp70

Utilising z-stack images and counting the cmHsp70.1 fluorescent spots per frame, allowed the intracellular distribution of cmHsp70.1 mAb-containing vesicles to be described through the

vertical axis (i.e. from the adherent surface to the apex). A representative montage of frames from a z stack is shown in **Fig 3.10**).

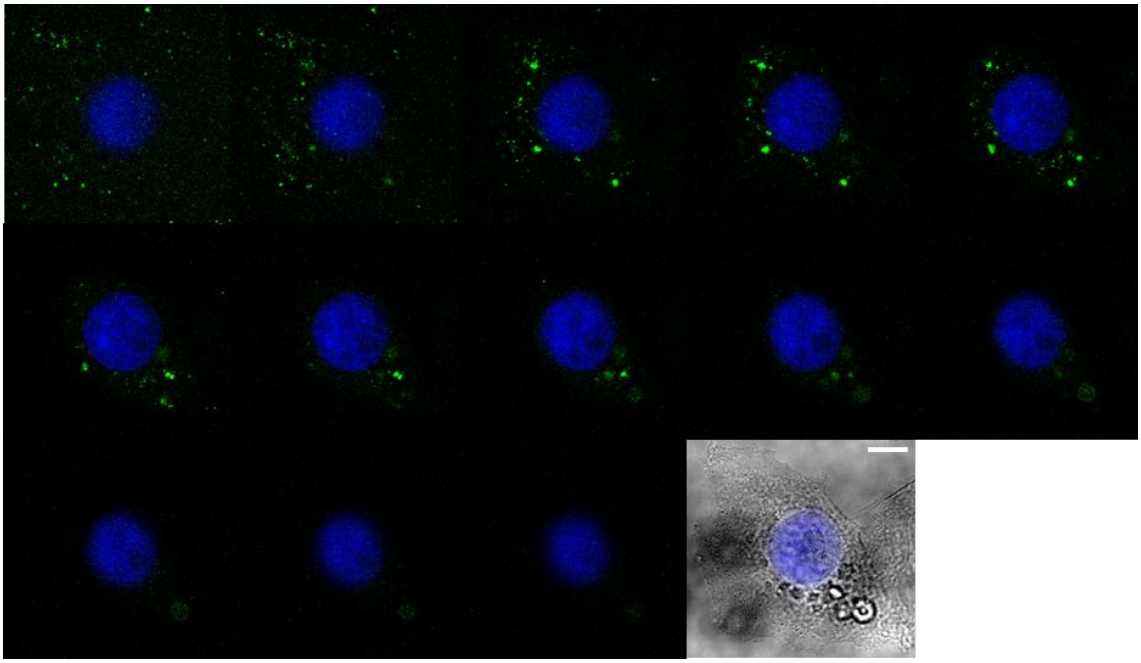

Figure 3.10 Representative montage of z-stack confocal images showing cmHsp70.1 mAb internalised into MDA-MB-231 cells.

Z-stack frames from the full height of a single MDA-MB-231 cell demonstrating distribution of cmHsp70.1 mAb following 60 minutes incubation time. Single frame images start at the adhered surface and finish at the apex of the cell. Brightfield imaging is included to help with orientation. Internalised cmHsp70.1 mAb is shown in green, DAPI staining of the nucleus is in blue. The scale bar represents 10µm.

Due to the differing sizes and morphology of cells, the use of absolute distances was not possible. As a consequence, the percentage of the overall height from adhered surface (0%) to the apex of the cell (100%) was calculated. This analysis revealed that the fluorescence spots preferentially localised towards the adherent surface in all of the human and murine cell lines (**Fig 3.11 and Fig 3.12**).

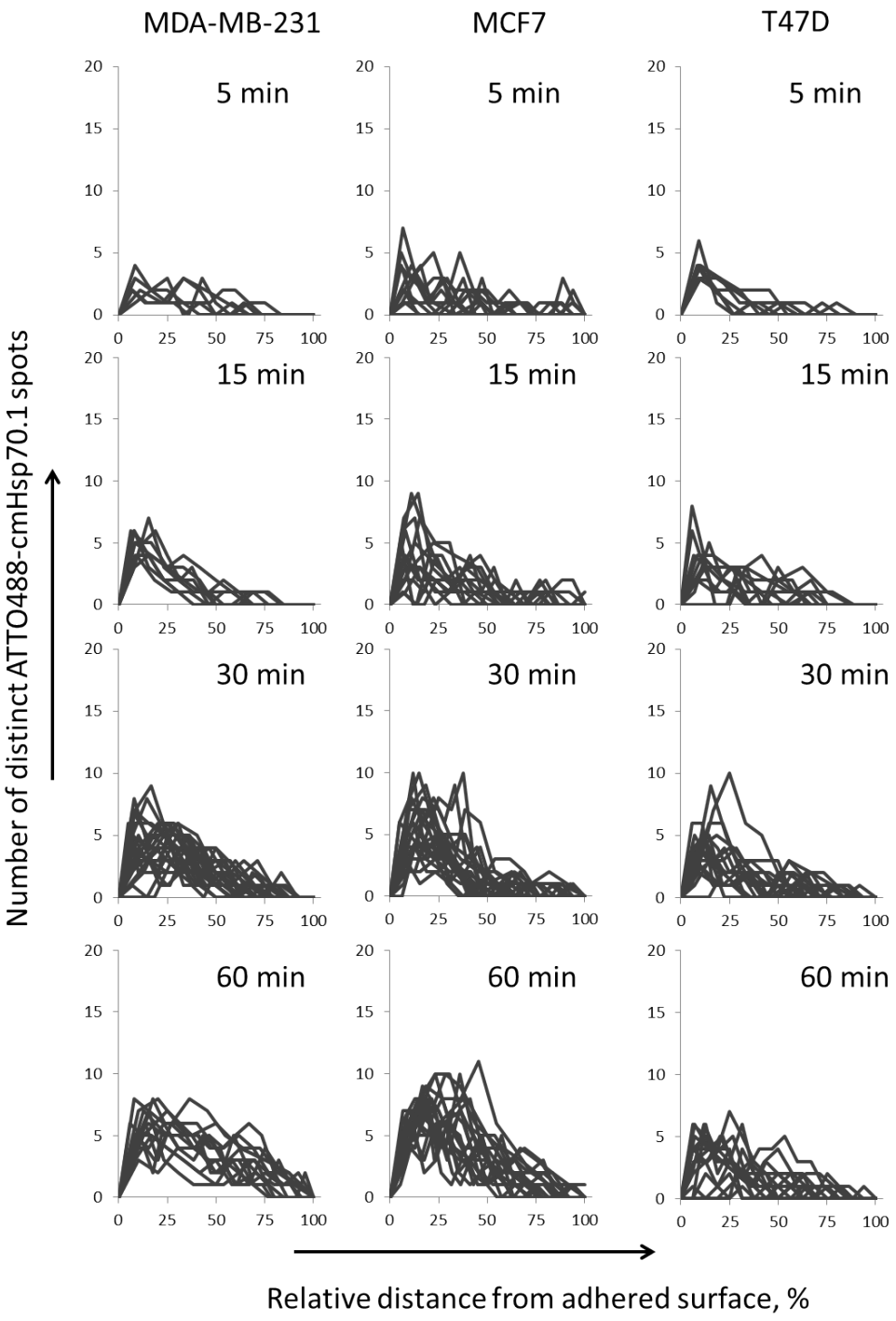

Figure 3.11 Distribution of internalised cmHsp70.1 mAb in human cancer cell lines

Line graphs of the distribution of internalised ATTO488-labelled cmHsp70.1 mAb in every cell imaged for MDA-MB-231, MCF7 and T47D cell lines at each time point, up to 60 minutes. Although ATTO488-cmHsp70.1 mAb appears throughout the full height of the cells, there is a clear bias towards the antibody being present close to the adhered surface of the cells. This asymmetrical distribution was observed in all cell lines and at all time- points. Each line represents the profile of an individual cell, with a minimum of four cells per condition.

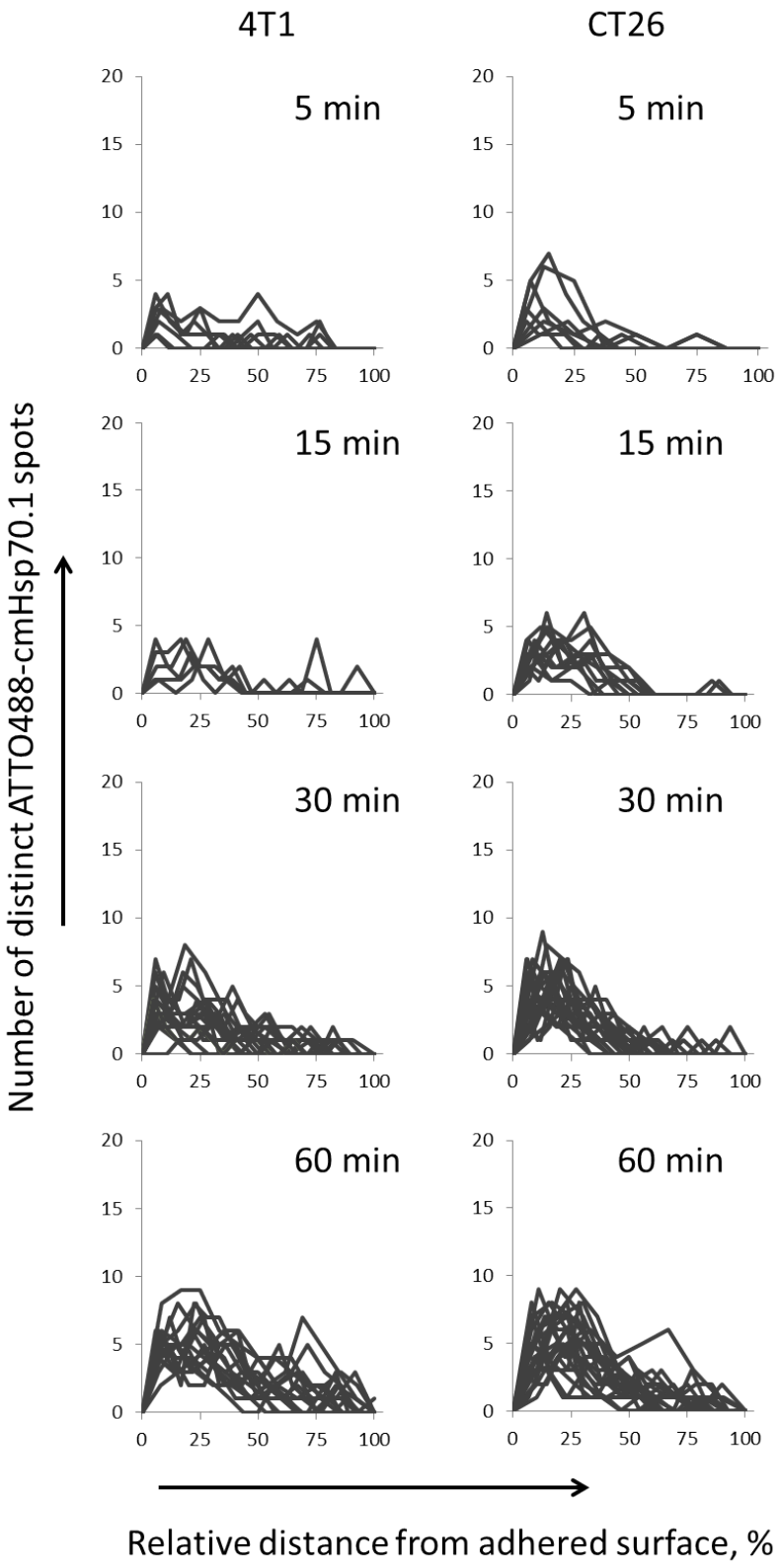

Figure 3.12 Distribution of internalised cmHsp70.1 mAb in murine cancer cells

Line graphs of the distribution of internalised ATTO488-labelled cmHsp70.1 mAb in every cell imaged for 4T1 and CT26 cell lines at each time point, up to 60 minutes. Although ATTO488-cmHsp70.1 mAb appears throughout the full height of the cells, there is a clear bias towards the antibody being present close to the adhered surface of the cells. This asymmetrical distribution was observed in all cell lines and at all time- points. Each line represents the profile of an individual cell, with a minimum of four cells per condition.

Over time, the number of spots found closer to the apex (up to ~75% of the cell's height) increased. Although these data provide some insight into the location of internalised cmHsp70.1 mAb at each time point, cumulative totals of fluorescent spots over quartiles of the cell height (0-25%, 25-50%, 50-75%, 75-100%) were calculated. These data are shown for all time points (**Fig 3.13A-3.17A**) and each cell line is presented separately. Representative images for each height quartile are provided for both the 5 and 60 minute time points (**Fig 3.13B-3.17B**), and these are in the form of composites composed of all frames within that quartile.

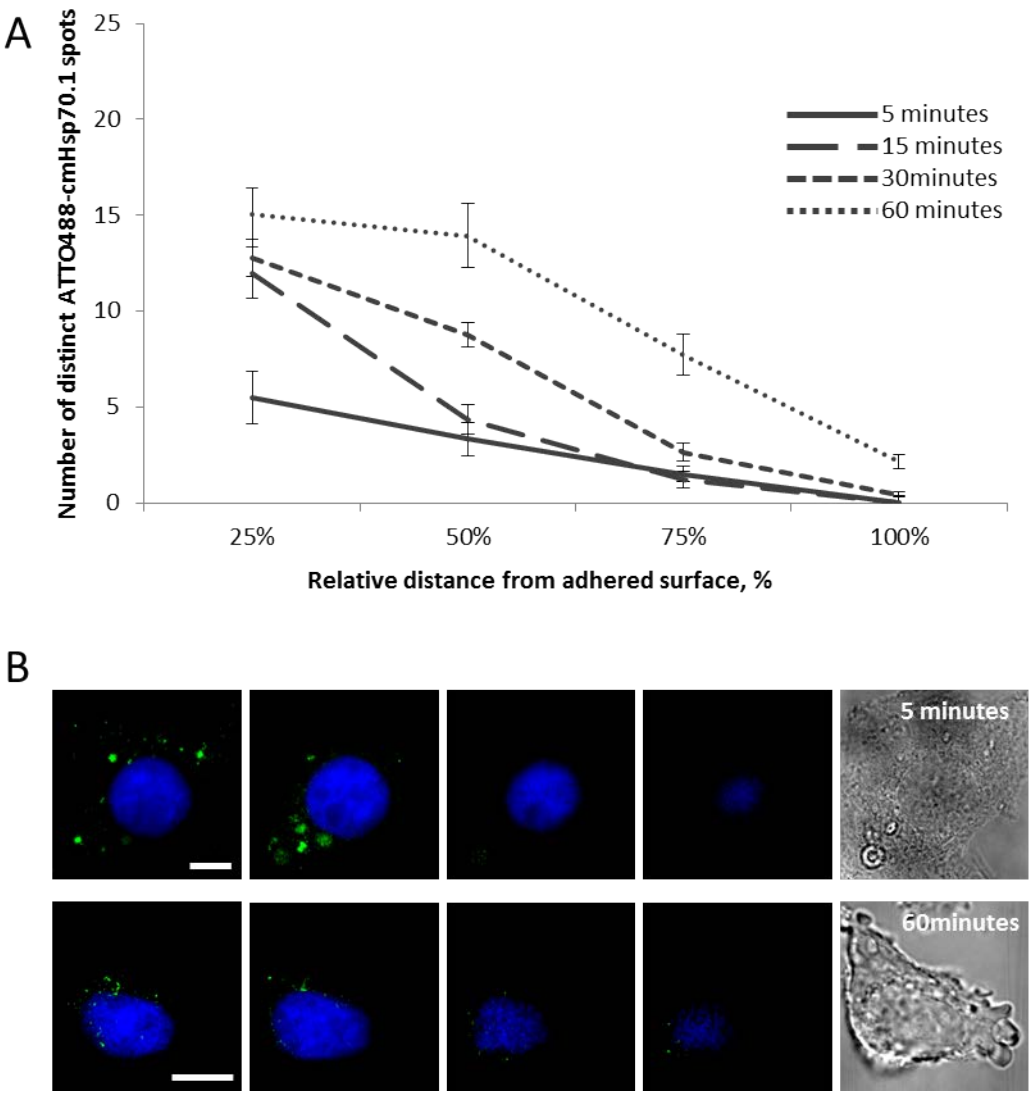

Figure 3.13 Distribution of internalised ATTO-cmHsp70.1 mAb in MDA-MB-231 cells

A Line graph of the mean ATTO488-labelled cmHsp70.1 mAb spot counts over the full height of cells at all incubation time points. The quartile containing the adherent surface consistently holds the greatest number of ATTO-cmHsp70.1 mAb spots. As the incubation time, increases spot counts increase over the middle quartiles (25-50% and 50-75%) whilst the spot count remains very similar in the quartile containing the apex (75-100%). Data are presented as mean ± SEM, n = 24. **B** Representative fluorescence images of the first and last quartiles (0-25% and 75-100%) after 5 minutes and 60 minutes incubation with ATTO488-cmHsp70.1 mAb. These are composite images of all frames that make up the quartile. Bright-field images are included to confirm placement of cell boundaries.

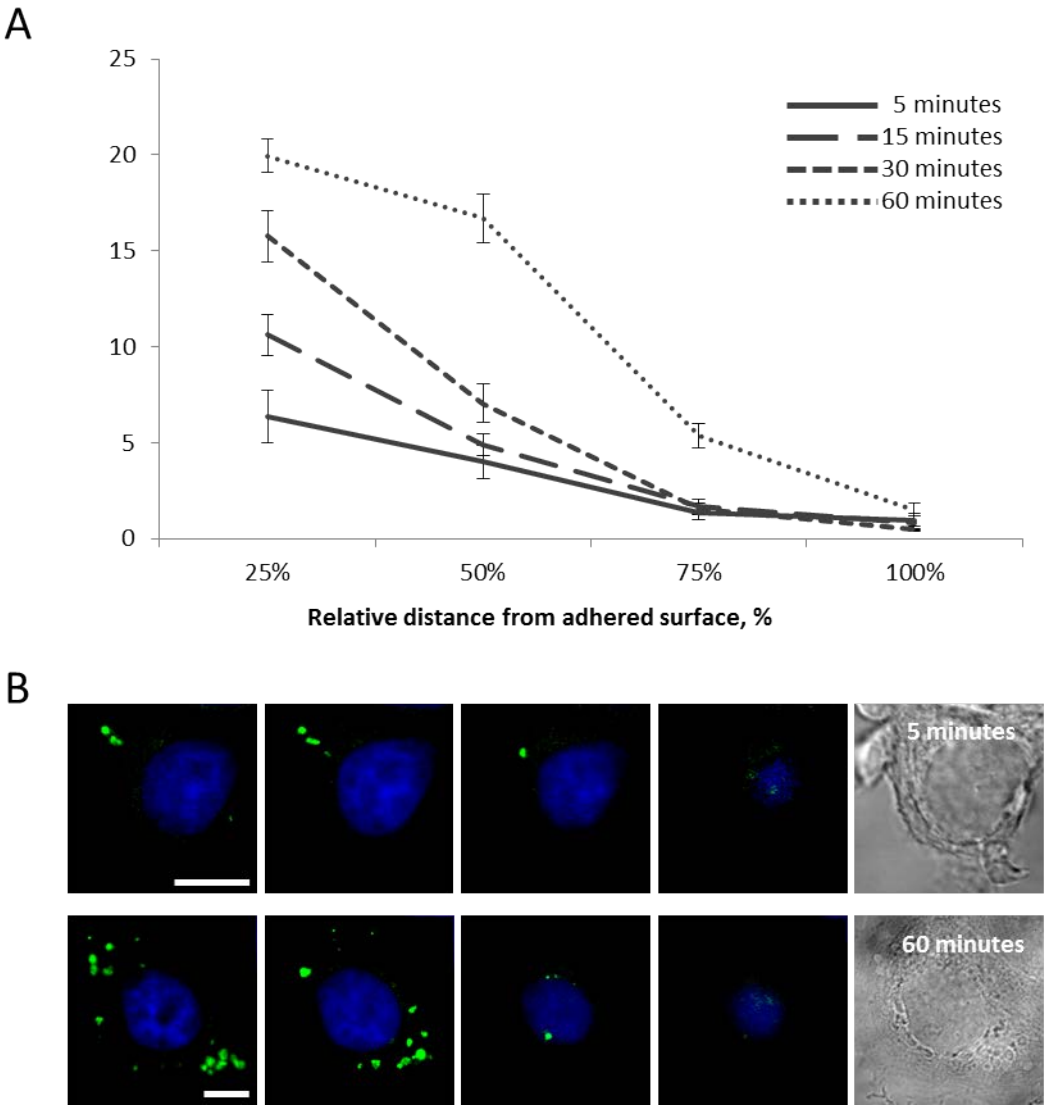

Figure 3.14 Distribution of internalised ATTO488-cmHsp70.1 mAb in MCF7 cells

A Line graph of the mean ATTO488-labelled cmHsp70.1 mAb spot counts over the full height of cells at all incubation time points. The quartile containing the adherent surface consistently holds the greatest number of ATTO-cmHsp70.1 mAB spots. As the incubation time, increases spot counts increase over the middle quartiles (25-50% and 50-75%) whilst the spot count remains very similar in the quartile containing the apex (75-100%). Data are presented as mean ± SEM, n = 29. **B** Representative fluorescence images of the first and last quartiles (0-25% and 75-100%) after 5 minutes and 60 minutes incubation with ATTO488-cmHsp70.1 mAb. These are composite images of all frames that make up the quartile. Bright-field images are included to confirm placement of cell boundaries.

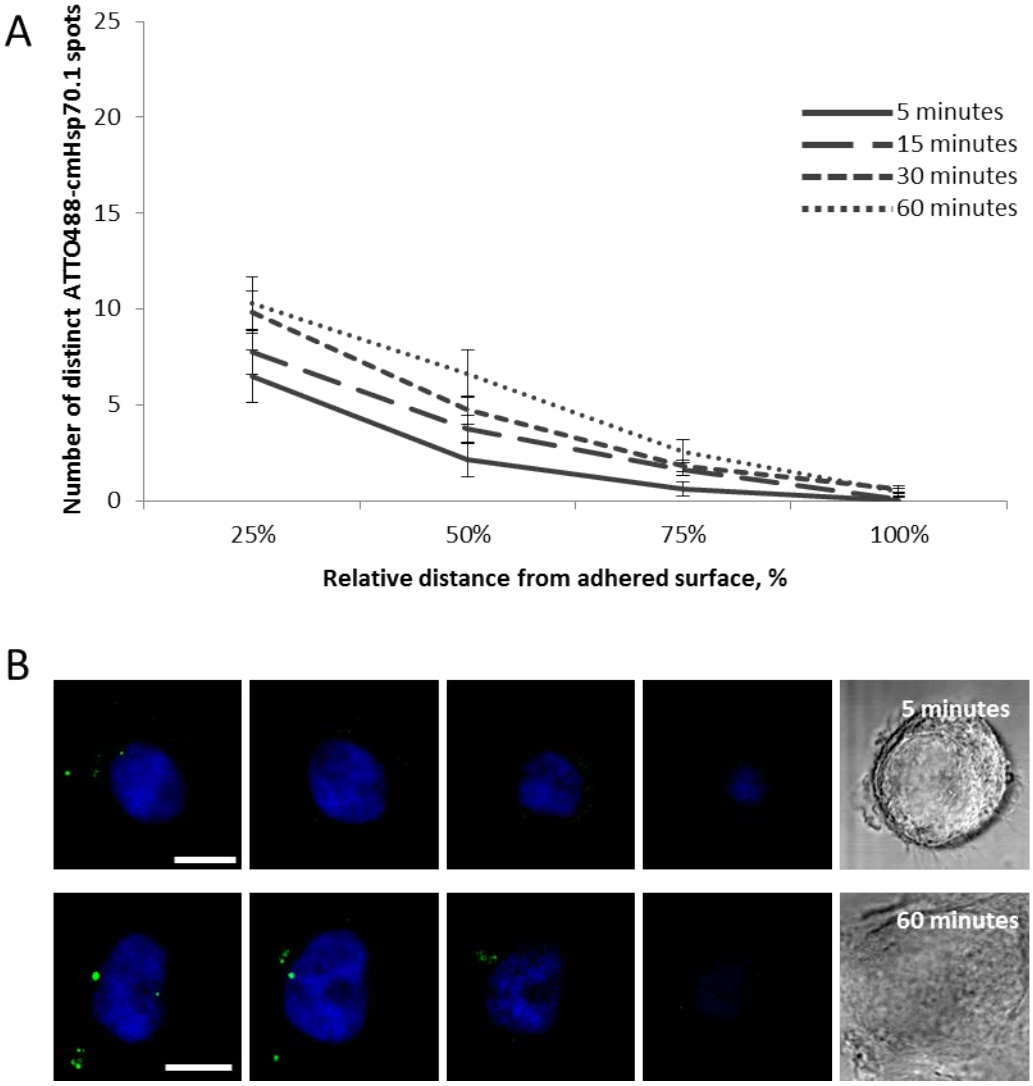

Figure 3.15 Distribution of internalised ATTO488-cmHsp70.1 mAb in T47D cells

A Line graph of the mean ATTO488-labelled cmHsp70.1 mAb spot counts over the full height of cells at all incubation time points. The quartile containing the adherent surface consistently holds the greatest number of ATTO-cmHsp70.1 mAB spots. As the incubation time, increases spot counts increase over the middle quartiles (25-50% and 50-75%) whilst the spot count remains very similar in the quartile containing the apex (75-100%). Data are presented as mean ± SEM, n = 19. **B** Representative fluorescence images of the first and last quartiles (0-25% and 75-100%) after 5 minutes and 60 minutes incubation with ATTO488-cmHsp70.1 mAb. These are composite images of all frames that make up the quartile. Bright-field images are included to confirm placement of cell boundaries.

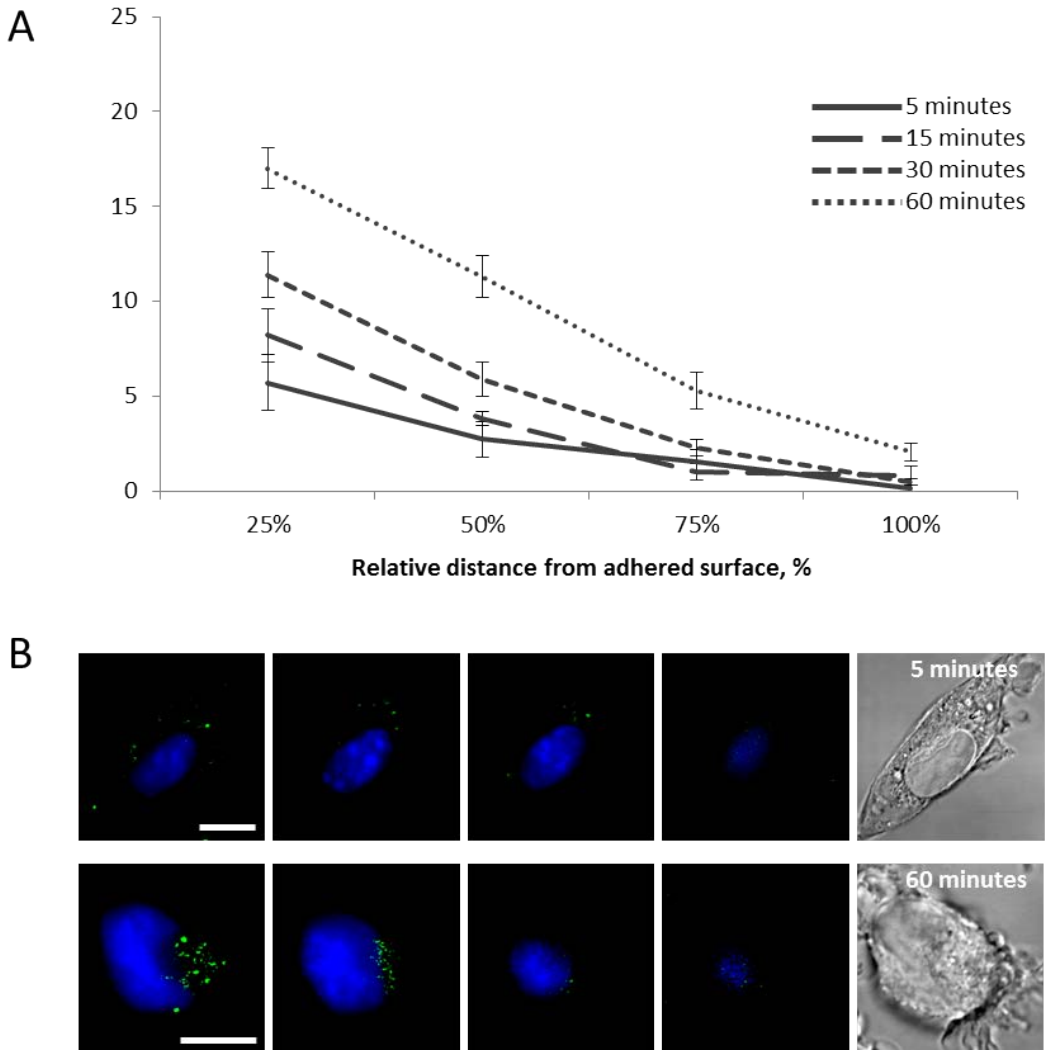

Figure 3.16 Distribution of internalised ATTO488-cmHsp70.1 mAb in 4T1 cell

A Line graph of the mean ATTO488-labelled cmHsp70.1 mAb spot counts over the full height of cells at all incubation time points. The quartile containing the adherent surface consistently holds the greatest number of ATTO-cmHsp70.1 mAb spots. As the incubation time, increases spot counts increase over the middle quartiles (25-50% and 50-75%) whilst the spot count remains very similar in the quartile containing the apex (75-100%). Data are presented as mean ± SEM, n = 20. **B** Representative fluorescence images of the first and last quartiles (0-25% and 75-100%) after 5 minutes and 60 minutes incubation with ATTO488-cmHsp70.1 mAb. These are composite images of all frames that make up the quartile. Bright-field images are included to confirm placement of cell boundaries.

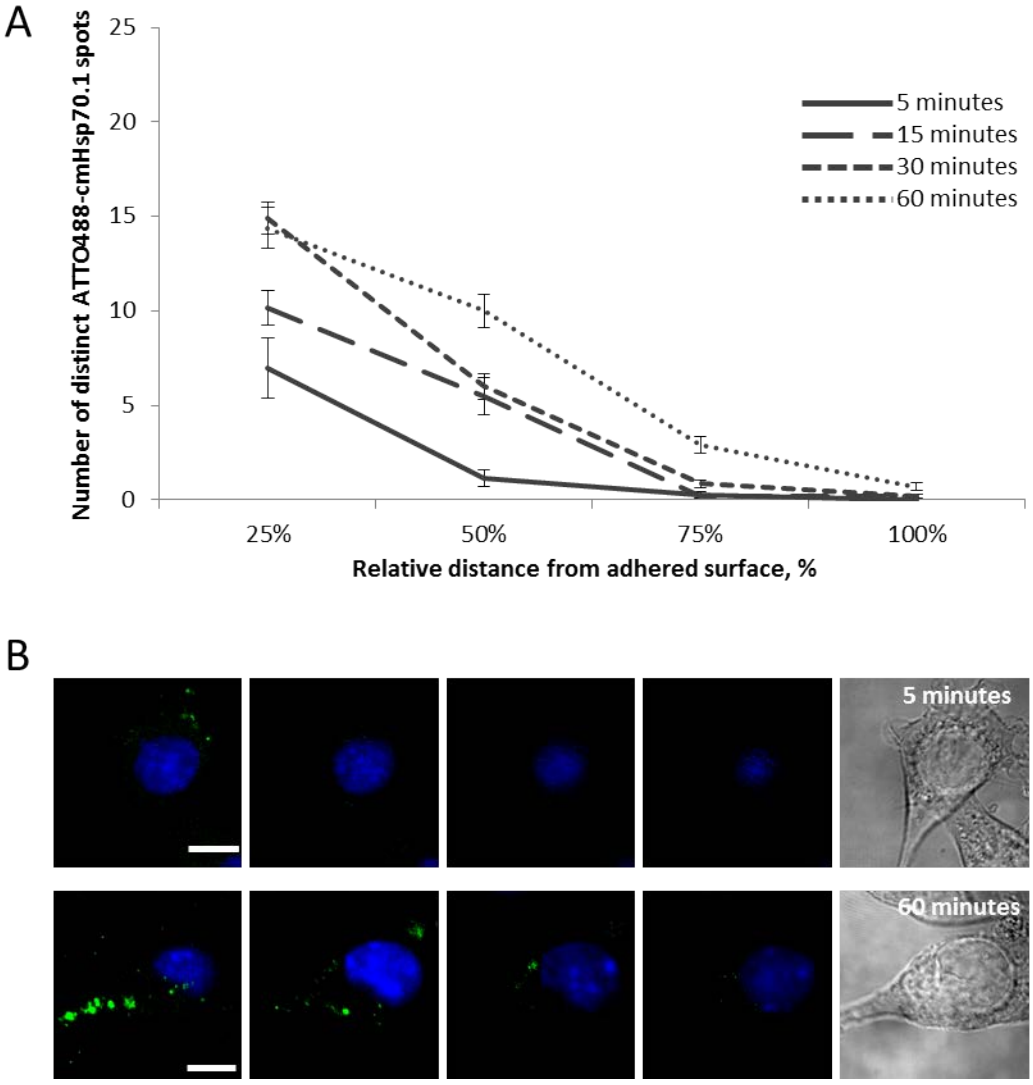

Figure 3.17 Distribution of internalised ATTO488 cmHsp70.1 mAb in CT26 cells

A Line graph of the mean ATTO488-labelled cmHsp70.1 mAB spot counts over the full height of cells at all incubation time points. The quartile containing the adherent surface consistently holds the greatest number of ATTO-cmHsp70.1 mAb spots. As the incubation time, increases spot counts increase over the middle quartiles (25-50% and 50-75%) whilst the spot count remains very similar in the quartile containing the apex (75-100%). Data are presented as mean ± SEM, n = 23. **B** Representative fluorescence images of the first and last quartiles (0-25% and 75-100%) after 5 minutes and 60 minutes incubation with ATTO488-cmHsp70.1 mAb. These are composite images of all frames that make up the quartile. Bright-field images are included to confirm placement of cell boundaries.

As the greatest number of cmHsp70.1 mAb spots are seen close to the adhered surface it could be proposed that this could be the region which enables the greatest amount of cmHsp70.1 mAb internalisation. Little is known about the presentation of Hsp70 within the membrane of cells and one possibility could be that it is restricted to, or more abundant at, the adhered surface. However this would need to be further investigated to be confirmed. Another possibility is that adhesion can in some way promote endocytic activity. Recent data examining neural maturation in a C57Bl/6J mouse model has demonstrated a link, whereby the

expression of neural cell adhesion molecule (NCAM) is required for the maturation of endocytic machinery in neurons while this maturation is impossible in NCAM knockout mice [551]. It may also be that there is a greater abundance of vesicles in the vicinity of adherent surfaces.

It is worth noting that these data rely on the absolute counts of fluorescent spots, uncorrected for cell area. This introduces difficulties in the interpretation of data, although the situation was unfortunately unavoidable. Without the inclusion of a membrane-specific fluorescent stain, the only avenue for determining cell area lies with calculating it from the bright-field image. As it is not possible to conduct confocal microscopy for bright-field images the only in-focus image sits in the centre of the z-stack. All others display varying degrees of blurring and therefore making accurate determination of cell boundaries close to the adherent surface and cell apex impossible.

3.3.2 Association of internalised cmHsp70.1 mAb with intracellular vesicles

The pattern of internalised cmHsp70.1 mAb was highly distinctive across all of the cell lines that were studied, in that it was present in well-defined spots that did not overlap with the nucleus. The most likely explanation is that the antibody is associated with intracellular vesicles, and additional studies were performed in order to better define the intracellular location of internalised cmHsp70.1 mAb.

For these studies, cells were incubated with ATTO488-labelled cmHsp70.1 mAb for different time points, up to 60 min, after which cells were formaldehyde fixed and permeabilised. They were stained using primary antibodies that were specific for one of a number of markers of intracellular vesicles, followed by staining with an appropriate secondary antibody. The coverslips were detached from the culture dishes and mounted onto microscopy slides with VECTASHIELD® Mounting Medium containing DAPI (enabling staining of the nucleus). Cover slips were sealed using clear nail varnish and stored at 4°C protected from light, until such time as they could be imaged (and not longer than 24 hours).

Using fluorescently labelled antibody and fluorescently stained vesicles, co-localisation of the two fluorescence signals can be used as confirmation of association of the antibody with that particular vesicle. As well as simply observing overlap of the two fluorescent signals on the acquired images, a more robust method of calculation is to use co-localisation algorithms. There is a wide variety of these, each of which have specific criteria for their use. The analyses conducted in the following experiments were Pearson's coefficient and Manders' M1 coefficient, using the Just Another Co-localisation Program plugin on ImageJ.

The association of cmHsp70.1 mAb with early endosomes in the three human-derived cell lines, MDA-MB-231, MCF7 and T47D was determined using antibodies specific for Rab4a and Rab5a. Although all of the cell lines exhibited large numbers of $Rab4a^+$ and $Rab5a^+$ vesicles, no co-localisation of internalised cmHsp70 mAb with these was observed (**Table 3.1**, representative images in **Fig 3.18**).

A. Pearson Coefficient		5 minutes	15 minutes	30 minutes	60 minutes
MDA-MB-231	Rab4a	0.540 ± 0.021	0.345 ± 0.167	0.393 ± 0.102	0.489 ± 0.036
	Rab5a	0.795 ± 0.018	0.274 ± 0.126	0.159 ± 0.061	0.475 ± 0.109
MCF7	Rab4a	0.292 ± 0.071	0.417 ±0.085	0.372 ± 0.108	0.482 ± 0.084
	Rab5a	0.378 ± 0.027	0.387 ±0.074	0.327 ± 0.050	0.431 ± 0.055
T47D	Rab4a	0.864 ± 0.010	0.886 ± 0.019	0.777 ± 0.068	0.501 ± 0.017
	Rab5a	0.744 ± 0.013	0.669 ± 0.011	0.664 ± 0.013	0.044 ± 0.035

B. Manders M1 Coefficient		5 minutes	15 minutes	30 minutes	60 minutes
MDA-MB-231	Rab4a	4.2 ± 2.1 %	1.5 ± 0.8 %	13.0 ± 4.7%	3.3 ± 2.9 %
	Rab5a	2.1 ± 1.5 %	2.7 ± 0.9 %	21.2 ± 4.5 %	9.0 ± 2.0 %
MCF7	Rab4a	13.7 ± 3.2 %	11.0 ± 4.0 %	8.1 ± 3.6 %	13.3 ± 2.5 %
	Rab5a	9.7 ± 5.8 %	5.9 ± 2.0 %	8.5 ± 4.8 %	16.0 ± 3.2 %
T47D	Rab4a	1.0 ± 0.2 %	11.9 ± 4.0 %	14.9 ± 6.1 %	3.7 ± 1.4 %
	Rab5a	5.2 ± 0.3 %	9.4 ± 2.1 %	3.7 ± 1.9 %	16.9 ± 1.1 %

Table 3.1 Internalisation of ATTO488-cmHsp70.1 mAb into human breast cancer cell lines may not utilise an early endosome pathway

A Pearson coefficient of the correlation between internalised ATTO488-cmHsp70.1 mAb and staining for the early endosome markers Rab4a and Rab5a in human breast cancer cell lines MDA-MB-231, MCF7 and T47D. At all time-points there was a positive correlation suggesting some degree of co-localisation between the markers of interest. **B** Manders' M1 measurement calculating the percentage of internalised ATTO488-cmHsp70.1 mAb which was co-localised with staining for the early endosome markers Rab4a and Rab5a over different time-points. The proportion of co-localisation is low; indicating that at each time very little cmHsp70.1 mAB is within early endosomes. Data are presented as mean ± SEM from 5–8 imaged cells, from at least two independent experiments.

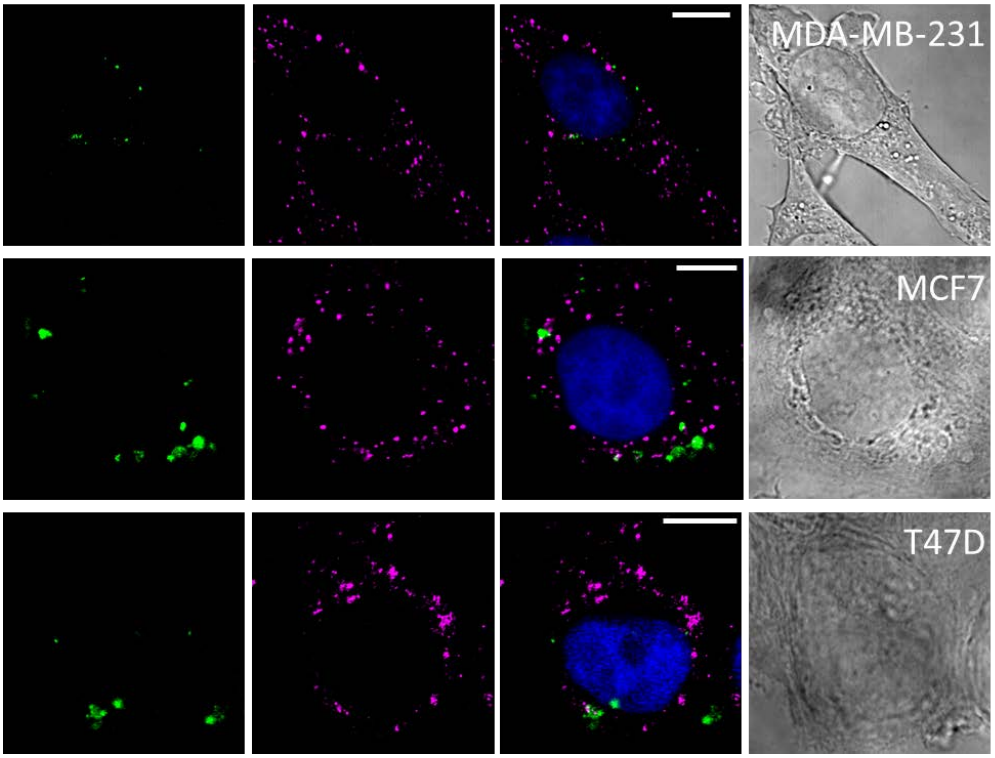

Figure 3.18 Trafficking of internalised ATTO488-cmHsp70.1 mAb to early endosomes in human breast cancer cell lines

MDA-MB-231, MCF7 and T47D cells grown in MatTek glass bottom dishes and incubated with ATTO488-cmHsp70.1 mAb for 5, 15, 30 or 60 minutes were fixed, permeabilised and stained for the localisation of early endosomes using Rab4 and Rab5 as markers. Any co-localisation of ATTO488-cmHsp70.1 mAb fluorescence (green) and endosome staining (magenta) could be confirmation of involvement of an early endosome pathway of cmHsp70.1 mAb internalisation. Co-localisation was assessed using both Pearson's and Manders' M1 coefficients of co-localisation, as well as visual overlap of the intensity channels. Images shown are representative single frames taken from the middle region (2nd or 3rd quartile) of cells incubated with ATTO488-cmHsp70.1 mAb for 30 minutes and subsequently stained for the presence of Rab5. No co-localisation was found, nor using the Rab4 marker. Scale bars are 10µm.

Despite not finding any co-localisation between cmHsp70.1 mAb and early endosome markers, it is not possible to conclude a definite lack of early endosomal involvement. Previous knowledge of the mechanisms of early endosome trafficking would presume involvement only in the initial stages of internalisation. It may be that an individual early endosome was associated with such a small amount of cmHsp70.1 mAb that detection above the background level of fluorescence was not possible, or that any association is so brief that at the specific moment cells are fixed the proportion of cmHsp70.1 mAb which is associated with early endosomes is negligible. Confirmation of these suggestions would require additional experiments.

The association of cmHsp70.1 mAb with late and recycling endosomes endosomes was examined using antibodies for Rab7, Rab9 and Rab11, and co-localisation was observed in

some instances (**Table 3.2 and Fig 3.19-3.21**). Although cmHsp70.1 mAb was not co-localised with Rab7$^+$ vesicles in any of the cell lines, some co-localisation with Rab9$^+$ endosomes was observed. The proportion of cmHsp70.1 mAb fluorescence which was co-localised to Rab9 was similar at the 30 and 60 minute time points (MDA-MB-231: 30 min 25.3 ± 4.4% and 60 min 27.0 ± 3.8%. MCF7: 30 min 28.0 ± 5.5% and 60 min 33.3 ± 5.7%) for the MDA-MB-231 and MCF7 cells. In contrast, co-localisation with Rab9 over these times was markedly different in T47D cells (from 1.4 ± 0.8% to 16.5 ± 2.1%), and this difference could reflect the lower expression of memHsp70 by these cells.

A. Pearson Coefficient		**30 minutes**	**60 minutes**
MDA-MB-231	Rab7	0.541 ± 0.025	0.483 ± 0.039
	Rab9	0.299 ± 0.015	0.530 ± 0.023
	Rab11	0.586 ± 0.100	0.310 ± 0.041
MCF7	Rab7	0.352 ± 0.071	0.314 ± 0.034
	Rab9	0.647 ± 0.049	0.518 ± 0.025
	Rab11	0.442 ± 0.064	0.661 ± 0.077
T47D	Rab7	0.514 ±0.013	0.457 ± 0.051
	Rab9	0.780 ± 0.021	0.568 ± 0.070
	Rab11	0.694 ± 0.049	0.523 ± 0.017

B. Manders M1 Coefficient		**30 minutes**	**60 minutes**
MDA-MB-231	Rab7	7.0 ± 2.5 %	2.2 ± 0.2 %
	Rab9	25.3 ± 4.4 %	27.0 ± 3.8 %
	Rab11	15.2 ± 3.3 %	17.7 ± 2.4 %
MCF7	Rab7	7.0 ± 0.9 %	3.3 ± 1.1 %
	Rab9	28.0 ± 5.5 %	33.3 ± 5.7 %
	Rab11	9.1 ± 2.2 %	24.5 ± 2.1 %
T47D	Rab7	5.8 ± 1.4 %	4.8 ± 2.5 %
	Rab9	1.4 ± 0.8 %	16.5 ± 2.1 %
	Rab11	5.3 ± 3.0 %	12.1 ± 6.3 %

Table 3.2 Trafficking of internalised ATTO488-cmHsp70.1 mAb to late and recycling endosomes in human breast cancer cell lines

A Pearson coefficient of the correlation between internalised ATTO488-cmHsp70.1 mAb and staining for the late endosome markers Rab7 and Rab9 as well the recycling endosome marker Rab11, in human breast cancer cell lines MDA-MB-231, MCF7 and T47D. At all time-points there was a positive correlation suggesting some degree of co-localisation between the markers of interest. **B** Manders' M1 measurement calculating the percentage of internalised ATTO488-cmHsp70.1 mAb which was co-localised with staining for the late endosome markers Rab7 and Rab9 as well as the recycling endosome marker Rab11 over different time-points. The proportion of co-localisation with both Rab9 and Rab11 in all cell lines increases over time; indicating that the internalisation of cmHsp70.1 mAb could utilise endosomal pathways at this time. Data are presented as mean ± SEM from 4-9 imaged cells, from at least two independent experiments**.**

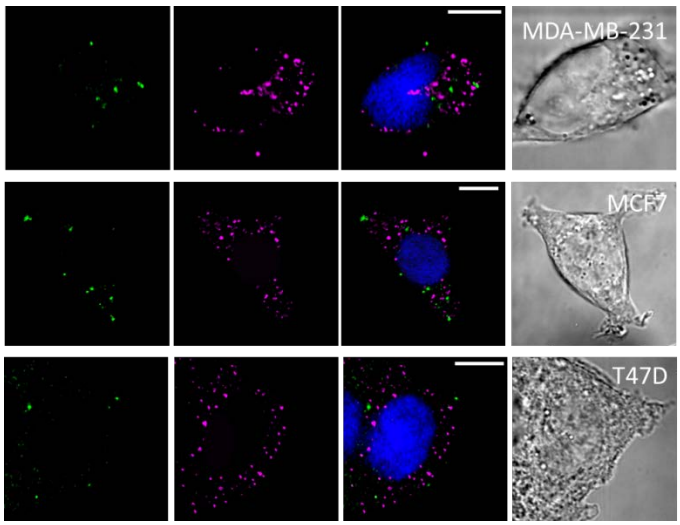

Figure 3.19 Trafficking of internalised ATTO488-cmHsp70.1 mAb to Rab7^{+} late endosomes in human breast cancer cell lines

MDA-MB-231, MCF7 and T47D cells grown in MatTek™ glass bottom dishes and incubated with ATTO488-cmHsp70.1 mAb for either 30 or 60 minutes were fixed, permeabilised and stained for Rab7 to indicate late endosomes. Any co-localisation of ATTO488-cmHsp70.1 mAb fluorescence (green) and endosome staining (magenta) could be confirmation of involvement of a late endosome pathway of cmHsp70.1 mAb internalisation. Co-localisation was assessed using both Pearson's and Manders' M1 coefficients of co-localisation, as well as visual overlap of the intensity channels. No co-localisation was found in any of the cell lines. Images shown are representative single frames taken from the middle region (2nd or 3rd quartile) of cells incubated with ATTO488-cmHsp70.1 mAb for 60 minutes. Scale bars are 10µm.

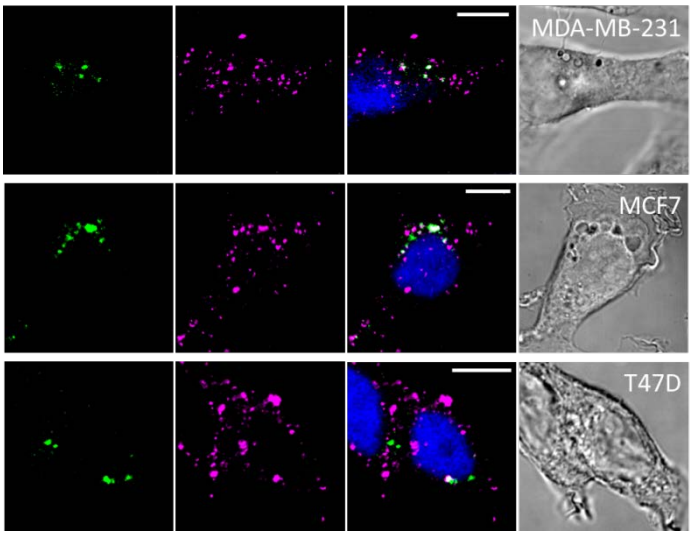

Figure 3.20 Trafficking of internalised ATTO488-cmHsp70.1 mAb to Rab9^{+} late endosomes in human breast cancer cell lines

MDA-MB-231, MCF7 and T47D cells grown in MatTek glass bottom dishes and incubated with ATTO488-cmHsp70.1 mAb for either 30 or 60 minutes were fixed, permeabilised and stained for Rab9 to indicate late endosomes. Any co-localisation (white) of ATTO488-cmHsp70.1 mAb fluorescence (green) and endosome staining (magenta) could be confirmation of involvement of a late endosome pathway of cmHsp70.1 mAB internalisation. Co-localisation was assessed using both Pearson's and Manders' M1 coefficients of co-localisation, as well as visual overlap of the intensity channels. Co-localisation was found in all of the cell lines, increasing over time and increasing in line with the expression of memHsp70. Images shown are representative single frames taken from the middle region (2nd or 3rd quartile) of cells incubated with ATTO488-cmHsp70.1 mAb for 60 minutes. Scale bars are 10µm.

The co-localisation of cmHsp70.1 mAb with Rab11$^+$ vesicles was much the same as with Rab9$^+$ in MDA-MB-231 cells. The proportion of cmHsp70.1 mAb accounted for in terms of co-localisation remains consistent between the 30 minute and 60 minute incubation time points (from 15.2 ± 3.3% to 17.7 ± 2.4%). However, the accumulation of cmHsp70.1 mAb in Rab11$^+$ vesicles between 30 and 60 minute time-points was slower in MCF7 and T47D cells (MCF7: 30 min 9.1 ± 2.1%, 60 min 24.5 ± 2.1%. T47D: 30 min 5.3 ± 3.0%, 60 min 12.1 ± 6.3%). These data also suggest that the level of memHsp70 expression impacts on the kinetics of cmHsp70 mAb uptake.

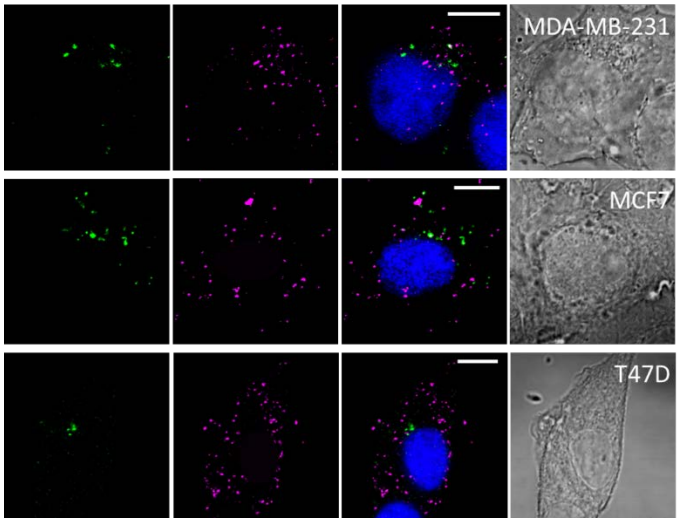

Figure 3.21 Trafficking of internalised ATTO488-cmHsp70.1 mAb to Rab11$^+$ recycling endosomes in human breast cancer cell lines

MDA-MB-231, MCF7 and T47D cells grown in MatTek glass bottom dishes and incubated with ATTO488-cmHsp70.1 mAb for either 30 or 60 minutes were fixed, permeabilised and stained for Rab11 to indicate recycling endosomes. Any co-localisation (white) of ATTO488-cmHsp70.1 mAb fluorescence (green) and endosome staining (magenta) could be confirmation of involvement of a late endosome pathway of cmHsp70.1 mAb internalisation. Co-localisation was assessed using both Pearson's and Manders' M1 coefficients of co-localisation, as well as visual overlap of the intensity channels. Co-localisation was found in all of the cell lines, increasing over time. Images shown are representative single frames taken from the middle region (2nd or 3rd quartile) of cells incubated with ATTO488-cmHsp70.1 mAb for 60 minutes. Scale bars are 10µm.

The co-localisation of cmHsp70.1 mAb with lysosomes was determined using antibodies for the lysosomal associated membrane protein markers, LAMP1 and LAMP2 (**Table 3.3 and Fig 3.22**). These data show a remarkably different pattern to that with the other assessed markers. Although a gradual increase in the co-localisation of cmHsp70.1 mAb over time was observed in MCF7 and T47D cells (LAMP2 co-localisation; MCF: 5 min 2.8 ± 1.2%, 15 min 12.9 ± 2.3%, 30 min 29.4 ± 6.5 %, 60 min 35.1 ± 5.9%. T47D: 15 min 12.1 ± 2.0%, 30 min 16.1 ± 4.5%, 60 min 24.3 ± 6.2%), there was a negligible co-localisation of cmHsp70.1 mAb with LAMP1$^+$ or

LAMP2^{+} vesicles in MDA-MB-231 cells (LAMP2 co-localisation; 5 min 6.3 ± 4.1%, 15 min 5.9 ± 3.2 %, 30 min 7.7 ± 3.2%, 60 min 5.3 ± 3.2%).

A. Pearson Coefficient		5 minutes	15 minutes	30 minutes	60 minutes
MDA-MB-231	LAMP1	0.329 ± 0.044	0.402 ± 0.107	0.465 ± 0.065	0.310 ± 0.041
	LAMP2	0.560 ± 0.051	0.459 ± 0.039	0.590 ± 0.038	0.346 ± 0.083
MCF7	LAMP1	0.449 ± 0.075	0.760 ± 0.113	0.858 ± 0.060	0.113 ± 0.013
	LAMP2	0.450 ± 0.044	0.594 ± 0.112	0.682 ± 0.061	0.283 ± 0.029
T47D	LAMP1	-	0.361 ± 0.021	0.443 ± 0.050	0.109 ± 0.027
	LAMP2	-	0.414 ± 0.046	0.445 ± 0.076	0.392 ± 0.030

B. Manders M1 Coefficient		5 minutes	15 minutes	30 minutes	60 minutes
MDA-MB-231	LAMP1	2.4 + 1.5 %	1.0 ± 0.7 %	3.8 ± 1.4 %	2.6 ± 1.7 %
	LAMP2	6.3 + 4.1 %	5.9 + 3.2 %	7.7 ± 3.2 %	5.3 ± 3.2 %
MCF7	LAMP1	1.9 ± 1.6 %	8.9 ± 4.2 %	13.8 ± 4.7 %	21.2 ± 5.2 %
	LAMP2	2.8 ± 1.2 %	12.9 ± 2.3 %	29.4 ± 6.5 %	35.1 ± 5.9 %
T47D	LAMP1	-	30.2 ± 7.7 %	11.2 ± 5.5 %	13.5 ± 3.6 %
	LAMP2	-	12.1 ± 2.0 %	16.1 ± 4.5 %	24.3 ± 6.2 %

Table 3.3 Trafficking of internalised ATTO488-cmHsp70.1 mAb to lysosomes in human breast cancer cell lines

A Pearson coefficient of the correlation between internalised ATTO488-cmHsp70.1 mAb and staining for the lysosome markers LAMP1 and LAMP2, in human breast cancer cell lines MDA-MB-231, MCF7 and T47D after 5, 15, 30 and 60 minutes incubation with cmHsp70.1 mAb. At all time-points there was a positive correlation suggesting some degree of co-localisation between the markers of interest. **B** Manders' M1 measurement calculating the percentage of internalised ATTO488-cmHsp70.1 mAb which was co-localised with staining for the lysosome markers LAMP1 and LAMP2 over different time-points. In general, the proportion of ATTO488-cmHsp70.1 mAb co-localisation with both LAMP1 and LAMP2 increases over time in all cell lines, indicating an accumulation of cmHsp70.1 mAb in lysosomes, and that this appears to inversely follow the expression of memHsp70. Data are presented as mean ± SEM from 5-9 imaged cells, from two independent experiments**.**

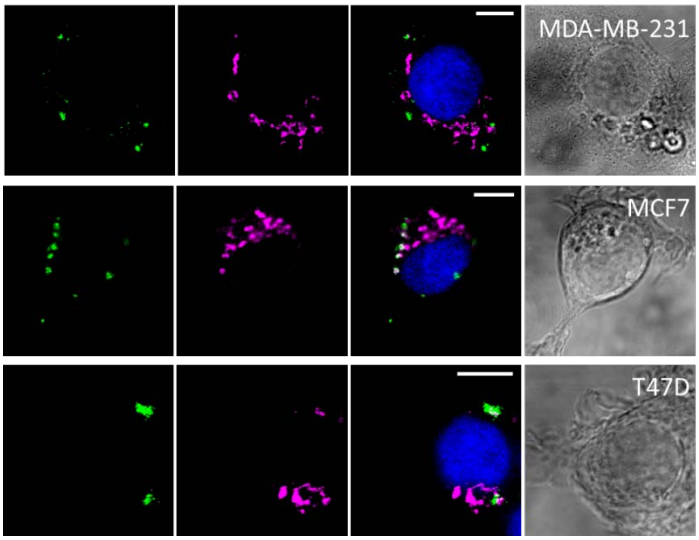

Figure 3.22 Trafficking of internalised ATTO488-cmHsp70.1 mAb to lysosomes in human breast cancer cell lines

MDA-MB-231, MCF7 and T47D cells grown in MatTek glass bottom dishes and incubated with ATTO488-cmHsp70.1 mAb for 5, 15, 30 or 60 minutes were fixed, permeabilised and stained for LAMP1 and LAMP2 to indicate lysosomes endosomes. Any co-localisation (white) of ATTO488-cmHsp70.1 mAb fluorescence (green) and lysosome staining (magenta) could be confirmation of involvement of a late endosome pathway of cmHsp70.1 mAb internalisation. Co-localisation was assessed using both Pearson's and Manders' M1 coefficients of co-localisation, as well as visual overlap of the intensity channels. Co-localisation was found in all of the cell lines, increasing over time. Images shown are representative single frames taken from the middle region (2^{nd} or 3^{rd} quartile) of cells incubated with ATTO488-cmHsp70.1 mAb for 60 minutes and stained for LAMP2 expression. Scale bars are 10µm.

The co-localisation of cmHsp70.1 mAb with mitochondria was determined using a mitochondrial dye which diffuses into live cells. This approach required a different experimental protocol, as cells cannot be fixed. A preliminary optimisation of the staining protocol showed that the most reliable mitochondria staining occurred when conducted after the cmHsp70.1 mAb incubation period. However, since the mitochondria staining must be conducted at 37°C, cells will remain metabolically active and could therefore continue to internalise and traffic the cmHsp70.1 mAb. Care must therefore be taken when interpreting the mitochondria data in comparison with other co-localisation data. The time points for assessing mitochondria co-localisation are 30 minutes with cmHsp70.1 mAb followed by 30 minutes with the mitochondria dye (denoted as 30+30) and 60 minutes with cmHsp70.1 mAb followed by 30 minutes with the dye (60+30) (**Table 3.4 and Fig 3.23**). All of the human-derived cell lines exhibited a progressive co-localisation of cmHsp70.1 mAb with mitochondria (MDA-MB-231: 30+30 min 28.8 ± 8.9%, 60+30 min 41.1 ± 7.6%. MCF7: 30+30 min 22.3 ± 1.7 %, 60+30 min 41.1 ± 7.7%. T47D: 30+30 min 16.3 ± 2.9%, 60+30 min 28.0 ± 5.1%).

A. Pearson Coefficient	30+30 minutes	60+30 minutes
MDA-MB-231	0.775 ± 0.072	0.788 ± 0.018
MCF7	0.840 ± 0.034	0.833 ± 0.048
T47D	0.731 ± 0.032	0.735 ± 0.028

B. Manders M1 Coefficient	30+30 minutes	60+30 minutes
MDA-MB-231	28.8 ± 8.9 %	41.1 ± 7.6 %
MCF7	22.3 ± 1.7 %	41.1 ± 7.7 %
T47D	16.3 ± 2.9 %	28.0 ± 5.1 %

Table 3.4 Trafficking of internalised ATTO488-cmHsp70.1 mAb to mitochondria in human breast cancer cell lines

A Pearson coefficient of the correlation between internalised ATTO488-cmHsp70.1 mAb and staining for the mitochondria in breast cancer cell lines MDA-MB-231, MCF7 and T47D after 30 and 60 minutes incubation with cmHsp70.1 mAb. At all time-points there was a positive correlation suggesting some degree of co-localisation between the markers of interest. **B** Manders' M1 measurement calculating the percentage of internalised ATTO488-cmHsp70.1 mAb which was co-localised with staining for the mitochondria over different time-points. The proportion of ATTO488-cmHsp70.1 mAb co-localisation with the mitochondria increases over time in all cell lines, and positively correlates to the expression of memHsp70. Data are presented as mean ± SEM from 5-10 imaged cells, from two independent experiments**.**

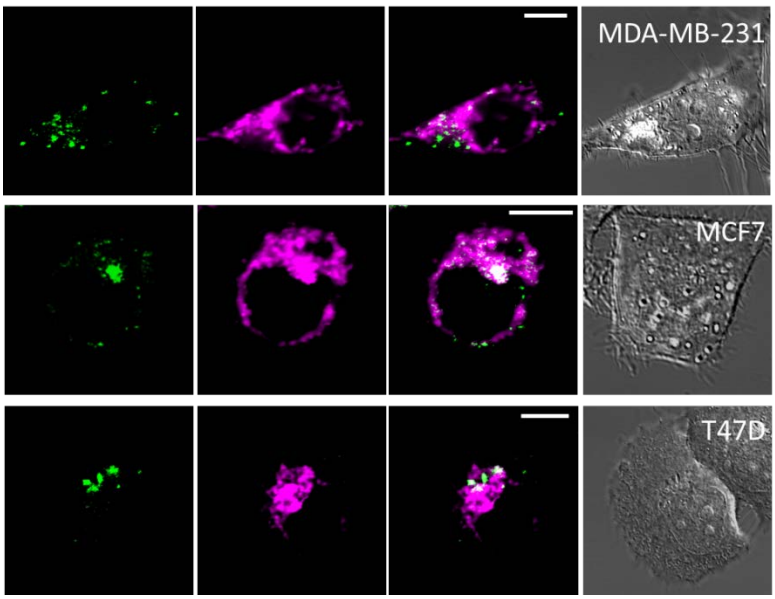

Figure 3.23 Trafficking of internalised ATTO488-cmHsp70.1 mAb to mitochondria in human breast cancer cell lines

MDA-MB-231, MCF7 and T47D cells grown in MatTek™ glass bottom dishes and incubated with ATTO488-cmHsp70.1 mAb for 30 or 60 minutes were stained with MitoID™ red to show the mitochondria. Any co-localisation (white) of ATTO488-cmHsp70.1 mAB fluorescence (green) and mitochondrial staining (magenta) could be confirmation of trafficking of cmHsp70.1 mAB to mitochondria. Co-localisation was assessed using both Pearson's and Manders' M1 coefficients of co-localisation, as well as visual overlap of the intensity channels. Co-localisation was found in all of the cell lines, increasing over time. Images shown are representative single frames taken from the middle region (2nd or 3rd quartile) of cells incubated with ATTO488-cmHsp70.1 mAb for 60 minutes. Scale bars are 10µm.

A. Pearson Coefficient		5 minutes	15 minutes	30 minutes	60 minutes
4T1	Rab4a	0.516 ± 0.006	0.635 ±0.092	0.588 ± 0.038	0.654 ± 0.046
	Rab5a	0.471 ± 0.080	0.671 ± 0.011	0.490 ± 0.025	0.629 ± 0.015
CT26	Rab4a	0.213 ± 0.086	0.195 ± 0.074	0.465 ± 0.093	0.654 ± 0.011
	Rab5a	0.162 ± 0.076	0.199 ± 0.041	0.490 ± 0.062	0.420 ± 0.080

B. Manders M1 Coefficient		5 minutes	15 minutes	30 minutes	60 minutes
4T1	Rab4a	5.1 ± 4.5 %	3.9 ± 0.5 %	4.5 ± 1.6 %	4.4 ± 3.5 %
	Rab5a	2.6 ± 1.4 %	2.9 ± 0.5 %	1.5 ± 0.6 %	0.8 ± 0.4 %
CT26	Rab4a	7.9 ± 4.1 %	12.2 ± 7.1 %	14.6 ± 3.7 %	7.4 ± 1.6 %
	Rab5a	25.9 ± 10.5 %	8.9 ± 7.1 %	11.3 ± 3.4 %	8.1 ± 2.8 %

Table 3.5 Trafficking of internalised ATTO488-cmHsp70.1 mAb to early endosomes in murine cancer cell lines

A Pearson coefficient of the correlation between internalised ATTO488-cmHsp70.1 mAb and staining for the early endosome markers Rab4a and Rab5a, in mouse cancer cell lines 4T1 and CT26. At all time-points there was a positive correlation suggesting some degree of co-localisation between the markers of interest. **B** Manders' M1 measurement calculating the percentage of internalised ATTO488-cmHsp70.1 mAb which was co-localised with staining for the early endosome markers Rab4a and Rab5a over different time-points. The proportion of co-localisation is low; indicating that at each time very little cmHsp70.1 mAb is within early endosomes. Data are presented as mean ± SEM from 7-13 imaged cells, from at least two independent experiments**.**

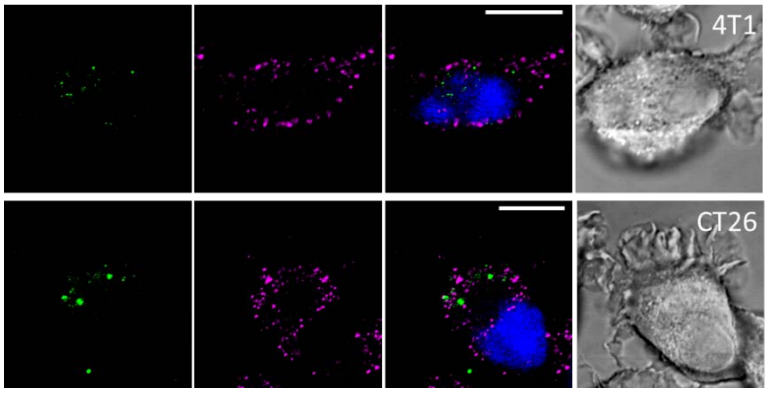

Figure 3.24 Trafficking of internalised ATTO488-cmHsp70.1 mAb to early endosomes in murine cancer cell lines

Murine 4T1 and CT26 cells grown in MatTek glass bottom dishes and incubated with ATTO488-cmHsp70.1 mAb for 5, 15, 30 or 60 minutes were fixed, permeabilised and stained for the localisation of early endosomes using Rab4 and Rab5 as markers. Any co-localisation of ATTO488-cmHsp70.1 mAb fluorescence (green) and endosome staining (magenta) could be confirmation of involvement of an early endosome pathway of cmHsp70.1 mAb internalisation. Co-localisation was assessed using both Pearson's and Manders' M1 coefficients of co-localisation, as well as visual overlap of the intensity channels. Images shown are representative single frames taken from the middle region (2nd or 3rd quartile) of cells incubated with ATTO488-cmHsp70.1 mAb for 30 minutes and subsequently stained for the presence of Rab5. No co-localisation was found, nor using the Rab4 marker. Scale bars are 10µm.

Similar analyses were conducted for the mouse-derived cell lines. Both Rab4a and Rab5a markers were used to assess the co-localisation of internalised cmHsp70.1 mAb with early endosomes. In both lines, at all time-points, and across both markers, there are very low levels of co-localisation (data for Rab4a at 5 min, similar for other marker/time combinations 4T1: 5.1 ± 4.5%. CT26: 7.9 ± 4.1%) (**Table 3.5 and Fig 3.24**). As discussed with the human-derived lines, the lack of co-localisation observed does not allow for the conclusion that early endosomes are not involved. It may be that the techniques employed here simply do not allow for detection.

A. Pearson Coefficient		**30 minutes**	**60 minutes**
4T1	Rab7	0.438 ± 0.022	0.728 ± 0.022
	Rab9	0.532 ± 0.031	0.550 ± 0.058
	Rab11	0.529 ± 0.008	0.689 ± 0.016
CT26	Rab7	0.591 ± 0.019	0.462 ± 0.020
	Rab9	0.497 ± 0.027	0.372 ± 0.018
	Rab11	0.582 ± 0.048	0.355 ± 0.052

B. Manders M1 Coefficient		**30 minutes**	**60 minutes**
4T1	Rab7	0.438 ± 0.022	0.728 ± 0.022
	Rab9	0.532 ± 0.031	0.550 ± 0.058
	Rab11	0.529 ± 0.008	0.689 ± 0.016
CT26	Rab7	0.591 ± 0.019	0.462 ± 0.020
	Rab9	0.497 ± 0.027	0.372 ± 0.018
	Rab11	0.582 ± 0.048	0.355 ± 0.052

Table 3.6 Trafficking of internalised ATTO488-cmHsp70.1 mAb to late and recycling endosomes in murine cancer cell lines

A Pearson coefficient of the correlation between internalised ATTO488-cmHsp70.1 mAb and staining for the late endosome markers Rab7 and Rab9 as well the recycling endosome marker Rab11, in mouse cancer cell lines 4T1 and CT26. At all time-points there was a positive correlation suggesting some degree of co-localisation between the markers of interest. **B** Manders' M1 measurement calculating the percentage of internalised ATTO488-cmHsp70.1 mAb which was co-localised with staining for the late endosome markers Rab7 and Rab9 as well as the recycling endosome marker Rab11 over different time-points. The proportion of co-localisation with both Rab9 and Rab11 in all cell lines increases over time; indicating that the internalisation of cmHsp70.1 mAb could utilise endosomal pathways at this time. Data are presented as mean ± SEM from 5-6 imaged cells, from two independent experiments**.**

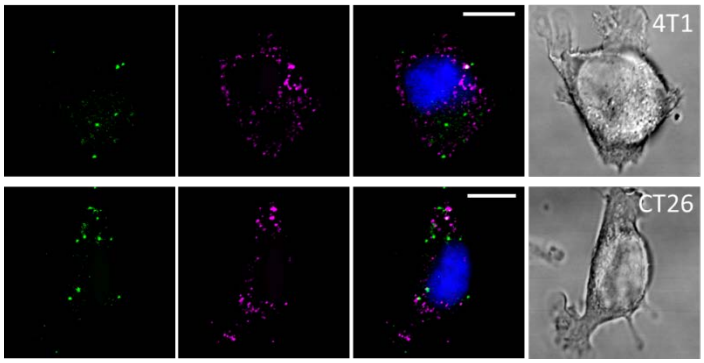

Figure 3.25 Trafficking of internalised ATTO488-cmHsp70.1 mAb to Rab7^{+} late endosomes in murine cancer lines

Murine 4T1 and CT26 cells grown in MatTek™ glass bottom dishes and incubated with ATTO488-cmHsp70.1 mAb for either 30 or 60 minutes were fixed, permeabilised and stained for Rab7 to indicate late endosomes. Any co-localisation of ATTO488-cmHsp70.1 mAb fluorescence (green) and endosome staining (magenta) could be confirmation of involvement of a late endosome pathway of cmHsp70.1 mAB internalisation. Co-localisation was assessed using both Pearson's and Manders' M1 coefficients of co-localisation, as well as visual overlap of the intensity channels. No co-localisation was found in any of the cell lines. Images shown are representative single frames taken from the middle region (2nd or 3rd quartile) of cells incubated with ATTO488-cmHsp70.1 mAb for 60 minutes. Scale bars are 10µm.

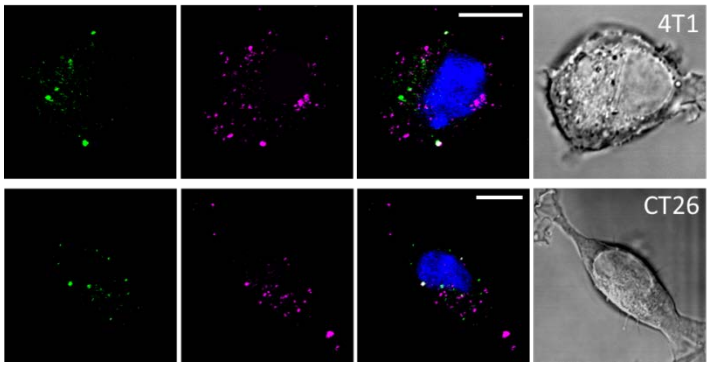

Figure 3.26 Trafficking of internalised ATTO488-cmHsp70.1 mAb to Rab9^{+} late endosomes in murine cancer lines

Murine 4T1 and CT26 cells grown in MatTek glass bottom dishes and incubated with ATTO488-cmHsp70.1 mAb for either 30 or 60 minutes were fixed, permeabilised and stained for Rab9 to indicate late endosomes. Any co-localisation (white) of ATTO488-cmHsp70.1 mAb fluorescence (green) and endosome staining (magenta) could be confirmation of involvement of a late endosome pathway of cmHsp70.1 internalisation. Co-localisation was assessed using both Pearson's and Manders' M1 coefficients of co-localisation, as well as visual overlap of the intensity channels. Co-localisation was found in all of the cell lines, increasing over time and increasing in line with the expression of memHsp70. Images shown are representative single frames taken from the middle region (2nd or 3rd quartile) of cells incubated with ATTO488-cmHsp70.1 mAb for 60 minutes. Scale bars are 10µm.

In a similar result to that with the human-derived lines, there was no appreciable co-localisation of cmHsp70.1 mAb with Rab7^{+} vesicles in either of the mouse-derived lines (4T1: 30 min 1.7 ± 0.6%, 60 min 3.3 ± 1.1%. CT26 30 min 3.3 ± 1.4%, 60 min 11.7 ± 3.3%). However, some co-localisation with Rab9^{+} vesicles was apparent, in that there was a progressive increase in co-localisation, with the greater expressor of memHsp70 (4T1), also exhibiting the greater

co-localisation (4T1: 30 min 14.4 ± 6.4%, 60 min 25.8 ± 5.5%. CT26 30 min 9.3 ± 4.3%, 60 min 21.6 ± 2.9%) (**Table 3.6 and Fig 3.25-3.27**).

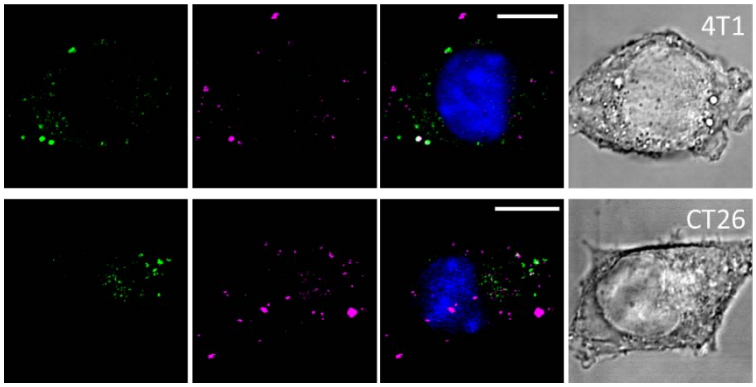

Figure 3.27 Trafficking of internalised ATTO488-cmHsp70.1 mAb to Rab11^{+} recycling endosomes in murine cancer cell lines

Murine 4T1 and CT26 cells grown in MatTek glass bottom dishes and incubated with ATTO488-cmHsp70.1 mAb for either 30 or 60 minutes were fixed, permeabilised and stained for Rab11 to indicate recycling endosomes. Any co-localisation (white) of ATTO488-cmHsp70.1 mAb fluorescence (green) and endosome staining (magenta) could be confirmation of involvement of a late endosome pathway of cmHsp70.1 mAb internalisation. Co-localisation was assessed using both Pearson's and Manders' M1 coefficients of co-localisation, as well as visual overlap of the intensity channels. Co-localisation was found in all of the cell lines, increasing over time. Images shown are representative single frames taken from the middle region (2nd or 3rd quartile) of cells incubated with ATTO488-cmHsp70.1 mAb for 60 minutes. Scale bars are 10µm.

A. Pearson Coefficient		**5 minutes**	**15 minutes**	**30 minutes**	**60 minutes**
4T1	LAMP2	-	-	-	-
CT26	LAMP2	0.620 ± 0.024	0.160 ± 0.094	0.604 ± 0.068	0.412 ± 0.026

B. Manders M1 Coefficient		**5 minutes**	**15 minutes**	**30 minutes**	**60 minutes**
4T1	LAMP2	-	-	-	-
CT26	LAMP2	1.4 ± 0.7 %	25.4 ± 3.2 %	26.8 ± 7.3 %	38.2 ± 3.7 %

Table 3.7 Trafficking of internalised ATTO488-cmHsp70.1 mAb to lysosomes in murine cancer cell lines

A Pearson coefficient of the correlation between internalised ATTO488-cmHsp70.1 mAb and staining for the lysosome marker LAMP2, in the mouse cancer cell line CT26 after 5, 15, 30 and 60 minutes incubation with cmHsp70.1 mAb. At all time-points there was a positive correlation suggesting some degree of co-localisation between the markers of interest. **B** Manders' M1 measurement calculating the percentage of internalised ATTO488-cmHsp70.1 mAb which was co-localised with staining for the lysosome marker LAMP2 over different time-points. In general, the proportion of ATTO488-cmHsp70.1 mAb co-localisation with LAMP2 increases over time, indicating an accumulation of cmHs70.1 mAb in lysosomes. Data are presented as mean ± SEM from 7-12 imaged cells, from two independent experiments.

The pattern of co-localisation with Rab11^{+} vesicles in CT26 and 4T1 cells was different, in that co-localisation progressively increased over time in CT26 cells, but remained constant in 4T1 cells (4T1: 30 min 19.4 ± 5.7%, 60 min 15.1 ± 8.9%. CT26: 30 min 7.8 ± 1.1%, 60 min 20.3 ± 2.7%). The more rapid internalisation of cmHsp70.1 mAb into 4T1 cells likely reflects their greater expression of memHsp70.

For technical reasons, it was only possible to determine the co-localisation of cmHsp70 mAb with LAMP2^{+} lysosomes in CT26 cells. The cmHsp70.1 mAb was observed to be found co-localised with LAMP2 as soon as the 15 minute incubation time point, and this progressively increased (5 min 1.4 ± 0.6%, 15 min 25.4 ± 3.2%, 30 min 26.8 ± 7.3%, 60 min 38.2 ± 3.7%) (**Table 3.7**).

With regards to co-localisation with mitochondria, the co-localisation of cmHsp70.1 mAb in 4T1 and CT26 cells different markedly. Although co-localisation at the first time point as well as an increased proportion at the later time point was apparent for 4T1 cells, there was only a negligible level of co-localisation at either time in the CT26 cells (4T1: 30+30 min 24.9 ± 7.4%, 60+30 min 36.9 ± 3.3%. CT26: 30+30 min 2.1 ± 0.6%, 60+30 min 4.5 ± 1.9%) (**Table 3.8 and Fig 3.28**).

A. Pearson Coefficient	**60 minutes**	**60+30 minutes**
4T1	0.851 ± 0.029	0.847 ± 0.012
CT26	0.195 ±0.047	0.192 ± 0.059

B. Manders M1 Coefficient	**60 minutes**	**60+30 minutes**
4T1	24.9 ± 7.4 %	36.9 ± 3.3 %
CT26	2.1 ± 0.6 %	4.5 ± 1.9 %

Table 3.8 Trafficking of internalised ATTO488-cmHsp70.1 mAb to mitochondria in murine cancer cell lines

A. Pearson coefficient of the correlation between internalised ATTO488-cmHsp70.1 mAb and staining for the mitochondria in murine 4T1 and CT26 cells after 30 and 60 minutes incubation with cmHsp70.1 mAb. At all time-points, there was a positive correlation suggesting some degree of co-localisation between the markers of interest. **B.** Manders' M1 measurement calculating the percentage of internalised ATTO488-cmHsp70.1 mAb which was co-localised with staining for the mitochondria over different time-points. The proportion of ATTO488-cmHsp70.1 mAB co-localisation with the mitochondria increases over time in all cell lines, and positively correlates to the expression of memHsp70. Data are presented as mean ± SEM from 5-6 imaged cells, from two independent experiments**.**

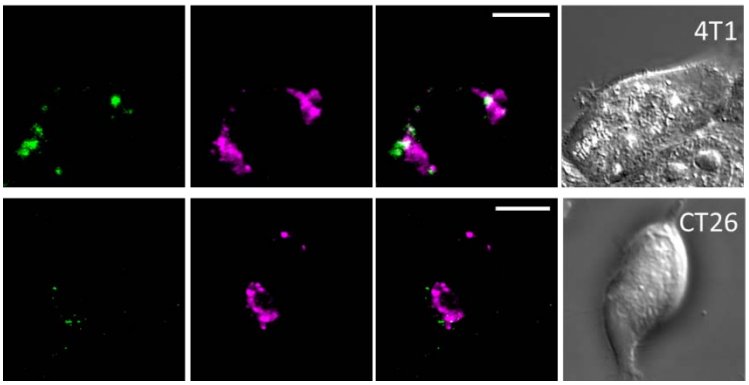

Figure 3.28 Trafficking of internalised ATTO488-cmHsp70.1 mAb to mitochondria in murine cancer cell lines

Murine 4T1 and CT26 cells grown in MatTek™ glass bottom dishes and incubated with ATTO488-cmHsp70.1 mAb for 30 or 60 minutes were stained with MitoID™ red to show the mitochondria. Any co-localisation (white) of ATTO488-cmHsp70.1 fluorescence (green) and mitochondrial staining (magenta) could be confirmation of trafficking of cmHsp70.1 to mitochondria. Co-localisation was assessed using both Pearson's and Manders' M1 coefficients of co-localisation, as well as visual overlap of the intensity channels. Co-localisation was found in all of the cell lines, increasing over time. Images shown are representative single frames taken from the middle region (2^{nd} or 3^{rd} quartile) of cells incubated with ATTO488-cmHsp70.1 mAb for 60 minutes. Scale bars are 10µm.

3.4 Summary

Although Hsp70 is typically considered as being a purely intracellular molecule, studies have shown that it can be actively released from cells as a soluble molecule, and also that it can be expressed on the plasma membranes of cancer cells (membrane Hsp70, memHsp70). Previously published data have demonstrated that the mouse colorectal cell line CT26 expresses memHsp70 [534] and consequently it was included as a positive control in the studies that are described herein. Three human cell lines representing different degrees of disease severity (in descending order: MDA-MB-231, MCF7 and T47D) were examined, as was a murine mammary cancer cell line (4T1). Whilst all cell lines were found to express memHsp70, the expression levels increased with increasing severity of disease, from which the cells lines were derived.

The cmHsp70.1 mAb was shown to be effective for the imaging of memHsp70^{+} cell lines using both flow cytometry and fluorescence microscopy. It was possible to observe the uptake of fluorescently-labelled cmHsp70.1 mAb into the cell lines and see a pattern of vesicular involvement, as well as to observe that some of the antibody was free in the cell cytoplasm. Interrogation of confocal microscope image stacks showed the preferential presence of the cmHsp70.1 mAb towards the adhered surface, suggesting that this may be a favoured point of uptake. Intracellular vesicles were identified through the application of specific primary antibodies and fluorescently-labelled appropriate secondary antibodies, or through the use of localised dyes, enabling co-localisation measurements to track the movement of the

fluorescently-labelled cmHsp70.1 mAb through the cells over time. There was no observed co-localisation of internalised cmHsp70.1 mAb with early endosomes, although this may be an artefact of time-point choice and speed of trafficking rather than confirmation of a non-endocytic pathway. Involvement of late endosomes and recycling endosomes was found for all cell lines, with the amount of cmHsp70.1 mAb in these vesicles increasing in line with increasing memHsp70 expression on the cell lines. Although cmHsp70.1 mAb was also found in lysosomes, the amount was inverse to the memHsp70 expression of the cells. Some internalised cmHsp70.1 mAb was also found to traffic to the mitochondria, and again the proportion co-localised here increased in line with increasing expression of memHsp70 by the cell line under investigation.

The uptake of cmHsp70.1 mAb by breast cancer cells is in line with published data for uptake of the antibody into the memHsp70^{+} cell line CT26. Employing the use of confocal imaging and detailed image analysis has allowed for further understanding of the trafficking of cmHsp70.1 mAb internalised in memHsp70^{+} breast cancer cell lines.

CHAPTER 4: Results II – Internalisation of the TKDNNLLGRFELSG peptide by cancer cells expressing membrane Hsp70

4.1 Introduction

A monoclonal antibody which specifically binds to and is taken up by memHsp70$^+$ breast tumour cells has potential as a therapeutic vehicle for the targeting of tumours. Indeed human monoclonal antibodies engineered with radio-labels to deliver therapeutic treatment in a highly selective and targeted manner is being investigated in a wide range of malignancies [552-556]. However, the use of antibodies does have drawbacks. Their production and purification are labour-intensive and highly expensive. In addition, when the antibodies have been derived in other species (very often in mice) they cannot be directly applied due being immunogenic in humans and consequently they are first transformed through a process of chimeric humanisation, after which there can be changes in the affinity, avidity or specificity.

An alternative strategy is to use small molecules, such as peptides, as they are easier and cheaper to produce than antibodies, and can be generated in large quantities at high purity. In addition, peptides typically exhibit good stability *in vivo* and better biodistribution than antibodies, and are better at penetrating tissues. Therapeutic peptides are already in use in breast [557] as well as other cancers [558] and can be used as a tool to aid diagnostic imaging or to specifically deliver radionuclide therapy.

In order for peptide-based therapies to be applicable to the widest number of patients it is necessary that their cellular recognition structure is widely expressed. Membrane Hsp70 offers such a structure, with around half of breast cancer patients having tumours which are positive for memHsp70 expression [285, 287-289, 543]. The capacity of a 14-mer peptide derived from Hsp70 (TKDNNLLGRFELSG) which had been identified as being capable of binding to memHsp70$^+$ tumour cell lines to bind to, and be internalised by, cancer cell lines expressing memHsp70 was therefore investigated in this study.

4.2 Binding of TKDNNLLGRFELSG peptide to cancer cells expressing memHsp70

The binding of TKDNNLLGRFELSG peptide to memHsp70$^+$ tumour cells was assessed by flow cytometry using a carboxy-fluorescein labelled preparation of the peptide (CF-TKDNNLLGRFELSG) and a correspondingly labelled 'scrambled' peptide having an identical amino acid composition, but different sequence (NGLTLKNDFSRLEG, termed NGL).

Cells previously grown for 48 hours were harvested, counted and incubated with 75µg/mL CF-TKDNNLLGRFELSG at 4°C for 30 min. Cells were washed once with staining buffer (PBS containing 10% v/v FCS) then analysed on a BD™ LSRII flow cytometer. Cells which had been incubated in staining buffer without CF-TKDNNLLGRFELSG were used as a control, as well as cells incubated with a carboxy-fluorescein labelled scrambled version of the peptide (CF-NGL). The median fluorescent intensity of the whole population was used to calculate a relative intensity of each sample compared to the unstained control cells. Any relative value above one is indicative of specific binding, with greater values corresponding to more CF-TKDNNLLGRFELSG bound to cells (**Fig 4.1**).

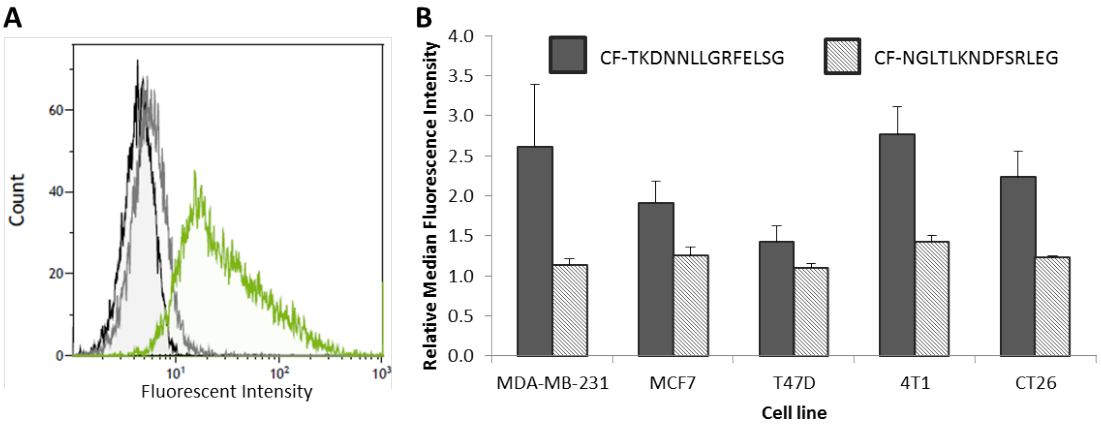

Figure 4.1 Binding of CF-TKDNNLLGRFELSG and CF-NGLTLKNDFSRLEG peptides to cancer cell lines

A. Representative flow cytometry plots showing the fluorescent intensity of MDA-MB-231 cells incubated for 30 minutes at 4°C in staining buffer (black line), with CF-NGLTLKNDFSRLEG peptide (grey line) and with CF-TKDNNLLGRFELSG peptide (green line). The binding of CF-TKDNNLLGRFELSG peptide (solid bars) and the scrambled control CF-NGLTLKNDFSRLEG peptide (slashed bars) to both human and mouse cancer cell lines, expressed as the intensity of fluorescence in the whole population relative to cells that were unstained. A measurement of greater than 1 indicates specific binding of CF-TKDNNLLGRFELSG and the higher the value the more peptide is bound. The cell lines which express more memHsp70 bind more CF-TKDNNLLGRFELSG, whilst binding of CF-NGLTLKNDFSRLEG was negligible. Data are presented as mean ± SEM and are the result of 4-7 independent experiments.

CF-TKDNNLLGRFELSG bound to all of the cell lines, in a manner which was similar to that which was observed for the cmHsp70 mAb. Of the three human breast cancer cell lines, the lowest expresser of memHsp70, T47D, also showed the lowest binding of CF-TKDNNLLGRFELSG (1.42 ± 0.20 relative to unstained cells). The greatest expresser of memHsp70, MDA-MB-231, showed the greatest capacity to bind CF-TKDNNLLGRFELSG (2.61 ± 0.78 relative to unstained cells). MCF7 cells exhibited an intermediate capacity to bind CF-TKDNNLLGRFELSG (1.92 ± 0.27). A similar situation was observed in the two mouse cancer cell lines, with the greatest expresser of memHsp70 (4T1), exhibiting higher relative CF-TKDNNLLGRFELSG binding (2.76 ± 0.33) than CT26 cells (2.23 ± 0.34). Overall, there were no significant differences between the

CF-TKDNNLLGRFELSG binding of the cell lines (one way ANOVA F=1.749, p=0.167), although there was a significant difference in the binding of CF-TKDNNLLGRFELSG peptide to the highest and lowest binding cell lines (4T1 and T47D respectively; p=0.025 Games-Howell post hoc comparison).

4.3 Internalisation of CF-TKDNNLLGRFELSG peptide by cancer cells expressing memHsp70

As CF-TKDNNLLGRFELSG peptide is able to bind to memHsp70^{+} tumour cells, the next step was to confirm whether the peptide can also be internalised by these cells. For this, cells were grown for 48 hours then harvested, counted and incubated in staining buffer in the presence of 75µg/mL CF-TKDNNLLGRFELSG at 37°C (allowing cells to remain metabolically active) for up to 60 min. As a control, cells were also incubated with carboxyl-fluorescein labelled scrambled peptide (CF-NGL). Cells were washed in staining buffer and the median fluorescent intensity of the whole population of cells was analysed by flow cytometry. The fluorescent intensity of cells that had been maintained at 4°C over the same time period reflected cell surface CF-TKDNNLLGRFELSG binding, with the additional fluorescence seen in cells incubated at 37°C reflecting the internalisation of CF-TKDNNLLGRFELSG (**Fig 4.2**).

All cell lines were capable of internalising CF-TKDNNLLGRFELSG, as demonstrated by a significant difference between the mfi of cells incubated with CF-TKDNNLLGRFELSG at 37°C and incubated at 4°C (One-way ANOVA. MDA-MB-231: F=22.331, p<0.001; MCF7: F=11.087, p<0.001; T47D: F=19.146, p<0.001; CT26: F=10.905, p<0.001; 4T1: F=79.815, p<0.001). The greatest internalisation for each line was observed after 60 minutes, although no cell line appeared to have reached saturation by this time. Although the internalisation of CF-TKDNNLLGRFELSG is mediated through memHsp70, the observed memHsp70 expression and CF-TKDNNLLGRFELSG internalisation was not entirely as expected. Although the MDA-MB-231, MCF7 and CT26 cell lines internalised more CF-TKDNNLLGRFELSG than T47D cells (the lowest memHsp70 expresser) after 60 minutes (mfi: 6,415 ± 733, Gabriel post-hoc comparisons: with MDA-MB-231 p=0.003, with MCF7 p=0.024, with 4T1 p=0.032, with CT26 p=0.0001), the MDA-MB-231 and MCF7 cells did so in reverse of their memHsp70 expression (MDA-MB-231: 17,341 ± 2,463. MCF7: 22,305 ± 5,769. Data presented as mean ± SEM). The same was true of the mouse lines, with the lower memHsp70 expresser CT26 internalising more CF-TKDNNLLGRFELSG (18,614 ± 4,299. Data presented as mean ± SEM) than the 4T1 cells which expressed higher levels of memHsp70 (14,317 ± 1,457. Data presented as mean ± SEM). However, there were no significant differences in the amount of CF-TKDNNLLGRFELSG which was internalised by MDA-MB-231, MCF7, 4T1 or CT26 cells. This suggests that there could be a

threshold level for an amount of memHsp70 required for adequate internalisation of CF-TKDNNLLGRFELSG. T47D cells, which express less memHsp70 than any other cell line investigated here, were the only cells found to internalise significantly less CF-TKDNNLLGRFELSG peptide.

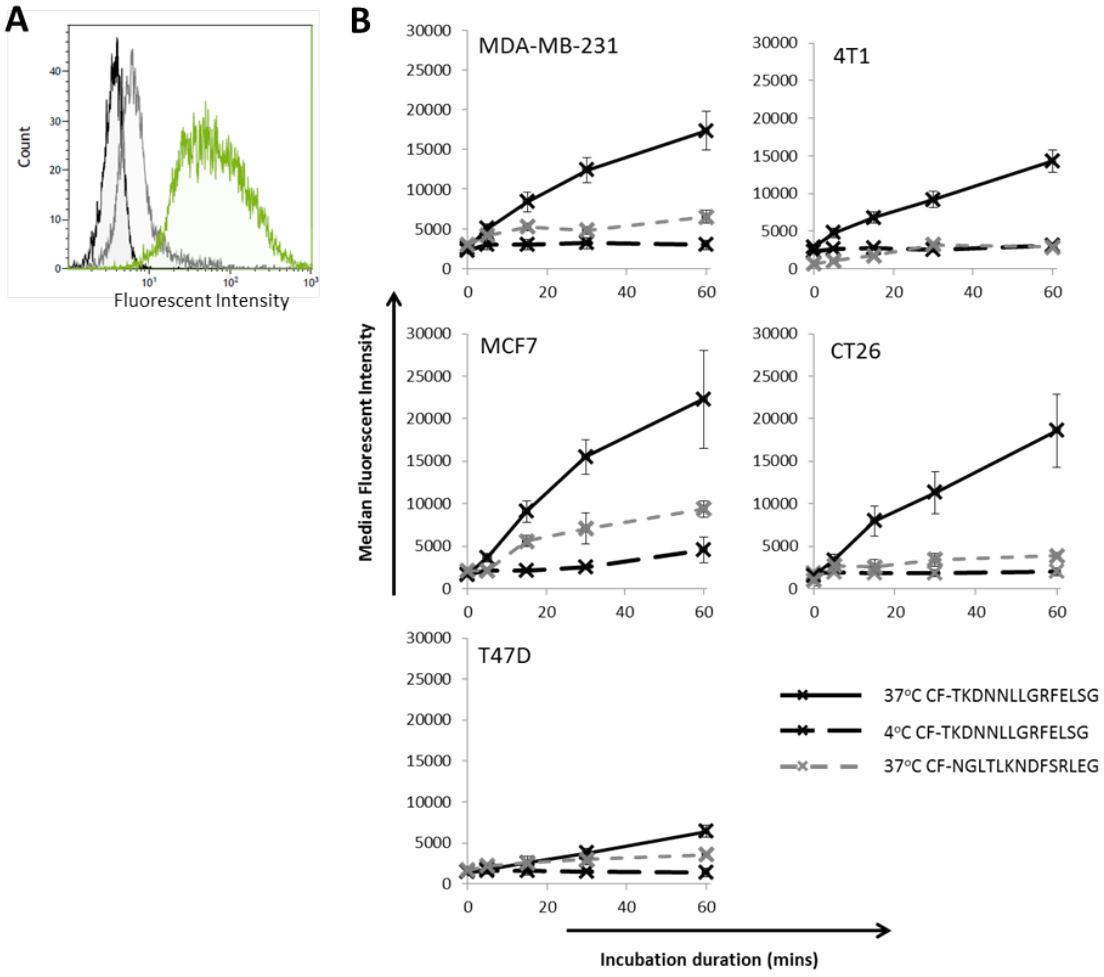

Figure 4.2 Flow cytometric assessment of CF-TKDNNLLGRFELSG peptide uptake into cancer cell lines

A. Representative flow cytometry plots showing the fluorescent intensity of MDA-MB-231 cells incubated for 60 minutes at 37°C in medium (black line), with CF-NGLTLKNDFSRLEG peptide (grey line) and with CF-TKDNNLLGRFELSG peptide (green line). B. Cells were incubated in the presence of CF-TKDNNLLGRFELSG peptide with samples saved at different time points, for up to an hour. The median fluorescent intensity of the whole population was recorded, as a relative measure of the amount of CF-TKDNNLLGRFELSG. The intensity after 4°C incubation relates to the binding of peptide to the cell surface, while the 37°C incubation allows for inclusion of peptide internalisation. All cell lines are capable of binding and internalising CF-TKDNNLLGRFELSG peptide, although the internalisation was much lower in T47D cells (the line which expresses the least memHsp70). Significantly more CF-TKDNNLLGRFELSG is associated with cells after incubation at 37°C (One-way ANOVA, $F=11.066$, $p<0.001$), thereby demonstrating that all cell lines are capable of internalising CF-TKDNNLLGRFELSG. Data are presented as mean ± SEM of at least three independent experiments.

Cells were also imaged using fluorescent and confocal microscopy to produce wide angle tile scans as well as z-stack images of the full height of cells. This way it was possible to confirm the

presence of CF-TKDNNLLGRFELSG peptide within the cells. Initially fluorescent microscopy images were used to demonstrate the selective uptake of CF- TKDNNLLGRFELSG peptide over the scrambled control CF-NGLTLKNDFSRLEG peptide (**Fig 4.3**).

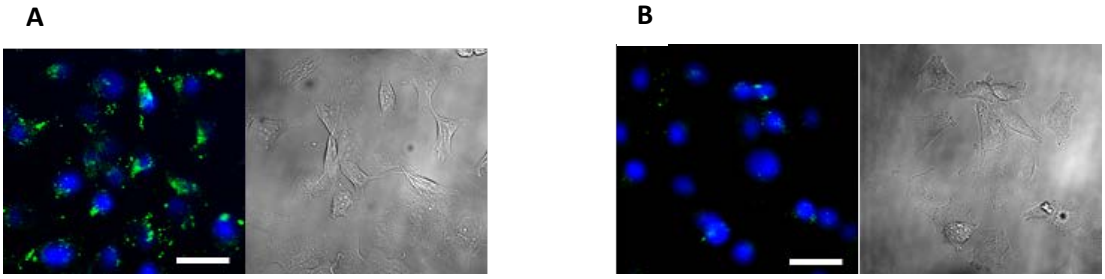

Figure 4.3 Representative tile scan images showing peptide uptake into MDA-MB-231 cells

Tile scan images were produced for MDA-MB-231, MCF7, T47D, 4T1 and CT26 cells, across different time-points of incubation with Hsp70 antibodies. Representative tile scan images of MDA-MB-231 cells incubated with CF-TKDNNLLGRFELSG (A) and CF-NGLTLKNDFSRLEG (B) antibodies for 60 minutes are shown. Peptides are shown in green and the nucleus stained with DAPI is shown in blue. Scale bar represents 50µm

Fluorescent tile scan images were analysed using the software package ImageJ, in order to calculate the mean fluorescent intensity (normalised to the intensity of the background) of all imaged cells. Over time, the intensity from CF-TKDNNLLGRFELSG peptide increased in all cell lines, thereby confirming the flow cytometry data. Furthermore, the maximum observed fluorescent intensity for each cell line positively tracked to the level of memHsp70 expression of the cells (**Fig 4.4**). This was not exactly mimicked when cells were examined using flow cytometry, although still the cell lines expressing most memHsp70 were observed to uptake the most amount of antibody.

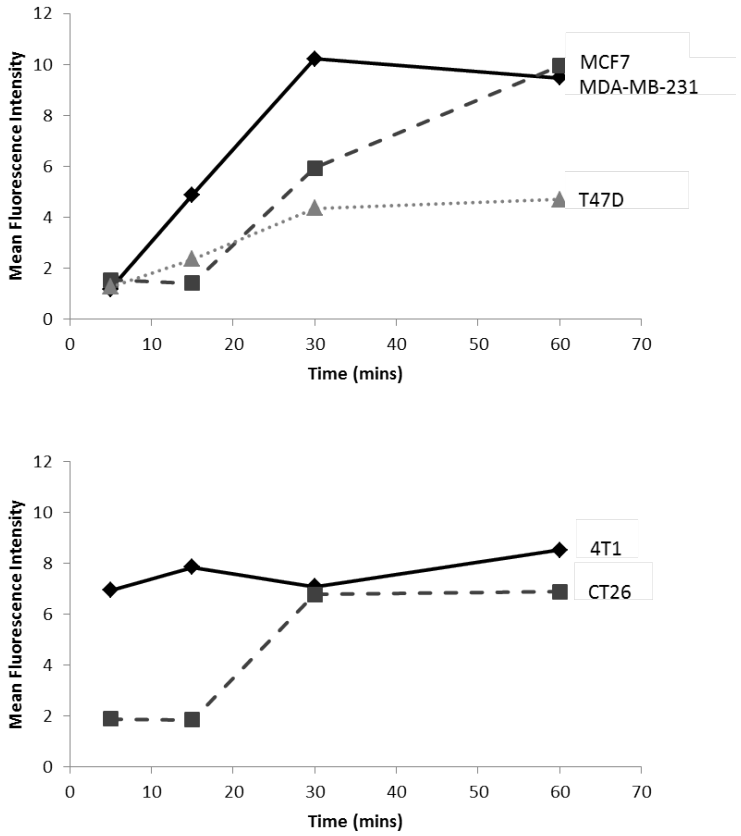

Figure 4.4 Uptake of CF-TKDNNLLGRFELSG peptide into human and murine cancer cell lines expressing differing levels of memHsp70

Cancer cell lines from human (A) and mouse (B) grown in MatTek™ glass bottom dishes were incubated in the presence of CF-TKDNNLLGRFELSG peptide for up to an hour then imaged using fluorescent microscopy. Mean fluorescent intensity values were calculated, normalised to background fluorescence. All cell lines are capable of internalising the CF-TKDNNLLGRFELSG peptide, albeit to varying degrees, and the level of internalisation positively increased with increasing memHsp70 expression of cell lines. Data are presented as mean ± SEM of a minimum of 80 cells from at least three independent experiments.

As neither flow cytometry nor fluorescent microscopy can make any distinction between fluorescence on the surface of cells or inside cells, using these techniques it is not possible to confirm whether cells incubated at 37°C do indeed internalise the peptide or just allow for greater surface binding. In order to further investigate which occurs, it was necessary to use another imaging technique – namely confocal microscopy.

4.3.1 Distribution of CF-TKDNNLLGRFELSG peptide after internalisation into memHsp70$^+$ cancer cells

The intracellular distribution of internalised CF-TKDNNLLGRFELSG was examined using confocal microscopy. For this, cells were grown for 48 hours in glass-bottomed dishes before the growth medium was aspirated and replaced with staining buffer containing 75µg/mL CF-

TKDNNLLGRFELSG. Cells were incubated for up to 60 minutes at 37°C to allow internalisation of CF-TKDNNLLGRFELSG to occur. Afterwards, cells were washed with staining buffer, formaldehyde fixed and mounted onto microscopy slides with VECTASHIELD® containing DAPI. Slides were kept cool and protected from light until imaging could be completed. Initially, single frame tile scan images of a large area of cells were imaged using an open pinhole setting, after which a minimum of four separate cells were imaged by confocal z-stack. Representative mid-stack, single frame images from one cell at each time point are shown (**Fig 4.5A-4.9A**). Bright-field images are also provided in order to confirm the internalisation of the CF-TKDNNLLGRFELSG (shown in green). The number of spots was determined for every cell imaged and data are presented as the mean number of fluorescent spots per cell at each time point (**Fig 4.5B – 4.9B**).

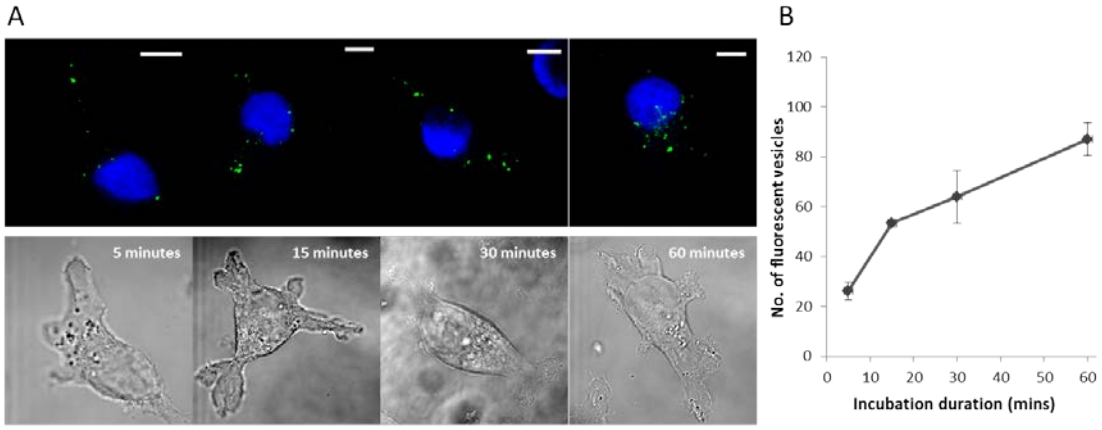

Figure 4.5 Kinetics of CF-TKDNNLLGRFELSG peptide uptake into MDA-MB-231 cells

A. Representative single frame images showing CF-TKDNNLLGRFELSG peptide internalised into MDA-MB-231 cells. Frames were selected from the mid-point of cells (25-75% of distance from adhered surface). CF-TKDNNLLGRFELSG peptide (green) appears in well-defined vesicles rather than free in the cytosol. The frames depict a region 0.88µm thick. Scale bars are 10µm. For clarity, the nucleus was stained with DAPI and is shown here in blue. B. The number of distinct fluorescent spots in cells after different incubation times. This is a total count including spots within the cell and at the membrane. Data is presented as mean ± SEM for at least four individual cells, from two independent experiments.

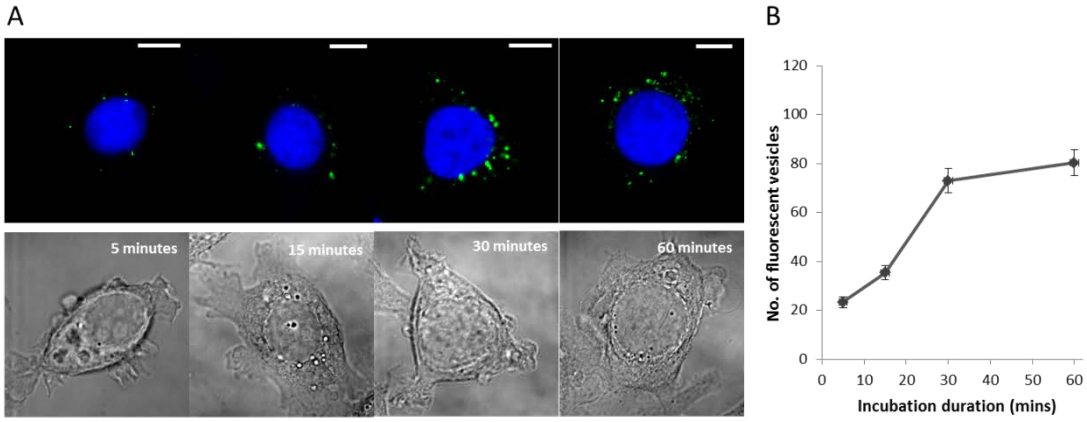

Figure 4.6 Kinetics of CF-TKDNNLLGRFELSG peptide uptake into MCF7 cells

A. Representative single frame images showing CF-TKDNNLLGRFELSG peptide internalised into MCF7 cells. Frames were selected from the mid-point of cells (25-75% of distance from adhered surface). CF-TKDNNLLGRFELSG peptide (green) appears in well-defined vesicles rather than free in the cytosol. The frames depict a region 0.88µm thick. Scale bars are 10µm. For clarity, the nucleus was stained with DAPI and is shown here in blue. B. The number of distinct fluorescent spots in cells after different incubation times. This is a total count including spots within the cell and at the membrane. Data is presented as mean ± SEM for at least six individual cells, from two independent experiments.

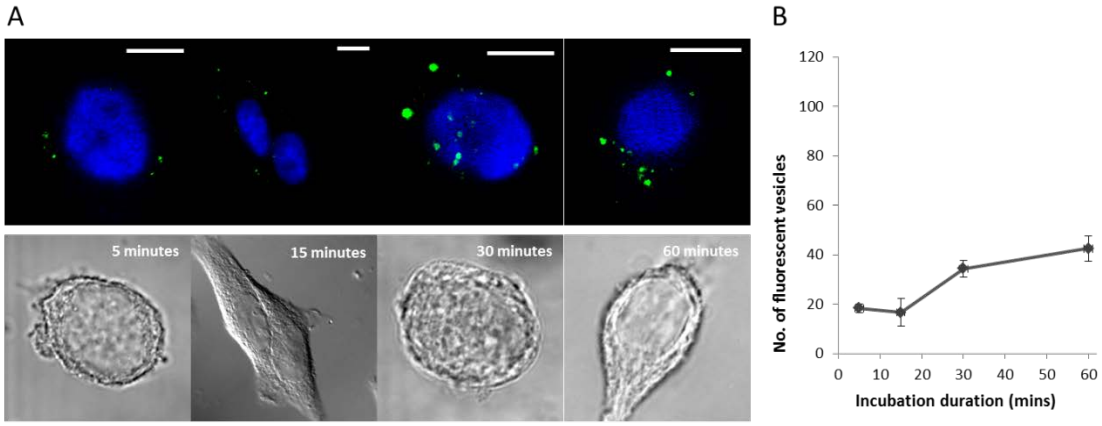

Figure 4.7 Kinetics of CF-TKDNNLLGRFELSG peptide uptake into T47D cells

A. Representative single frame images showing CF-TKDNNLLGRFELSG peptide internalised into T47D cells. Frames were selected from the mid-point of cells (25-75% of distance from adhered surface). CF-TKDNNLLGRFELSG peptide (green) appears in well-defined vesicles rather than free in the cytosol. The frames depict a region 0.88µm thick. Scale bars are 10µm. For clarity, the nucleus was stained with DAPI and is shown here in blue. B. The number of distinct fluorescent spots in cells after different incubation times. This is a total count including spots within the cell and at the membrane. Data is presented as mean ± SEM for at least six individual cells, from two independent experiments.

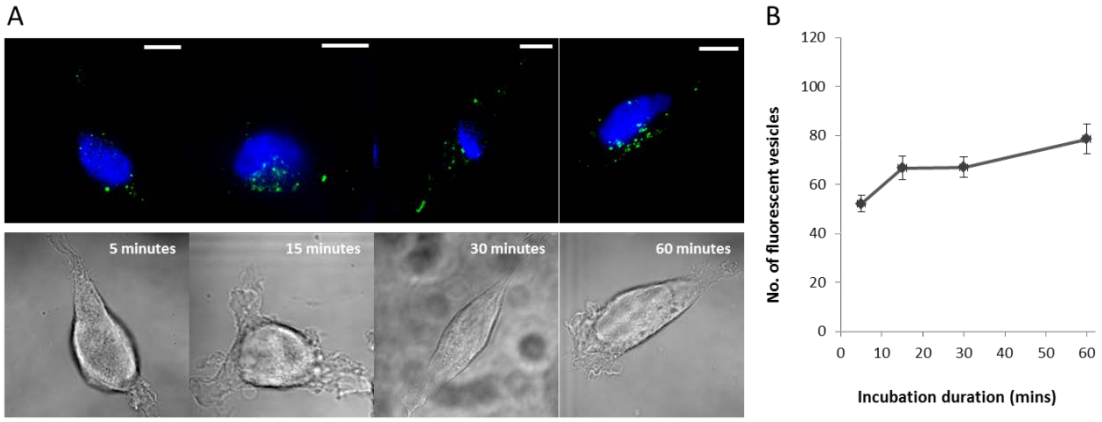

Figure 4.8 Kinetics of CF-TKDNNLLGRFELSG peptide uptake into CT26 cells

A. Representative single frame images showing CF-TKDNNLLGRFELSG peptide internalised into CT26 cells. Frames were selected from the mid-point of cells (25-75% of distance from adhered surface). CF-TKDNNLLGRFELSG peptide (green) appears in well-defined vesicles rather than free in the cytosol. The frames depict a region 0.88µm thick. Scale bars are 10µm. For clarity, the nucleus was stained with DAPI and is shown here in blue. B. The number of distinct fluorescent spots in cells after different incubation times. This is a total count including spots within the cell and at the membrane. Data is presented as mean ± SEM for at least five individual cells, from two independent experiments.

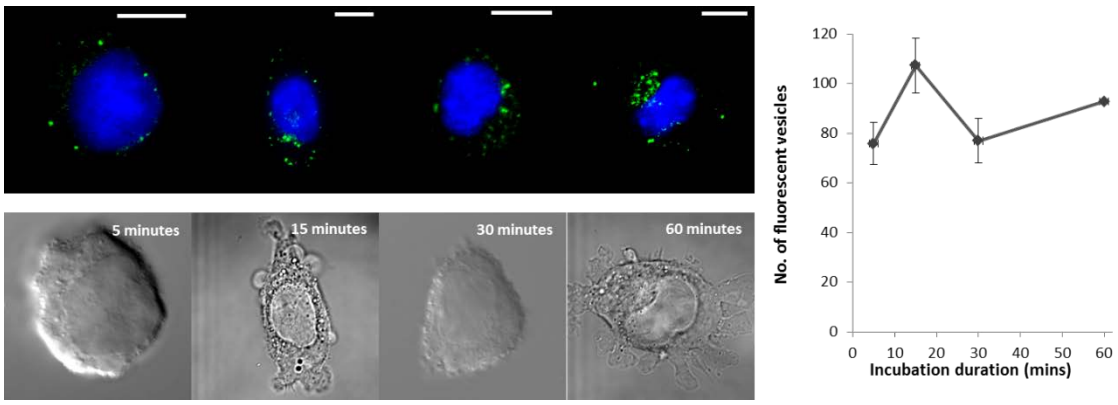

Figure 4.9 Kinetics of CF-TKDNNLLGRFELSG peptide uptake into 4T1 cells

A. Representative single frame images showing CF-TKDNNLLGRFELSG peptide internalised into 4T1 cells. Frames were selected from the mid-point of cells (25-75% of distance from adhered surface). CF-TKDNNLLGRFELSG peptide (green) appears in well-defined vesicles rather than free in the cytosol. The frames depict a region 0.88µm thick. Scale bars are 10µm. For clarity, the nucleus was stained with DAPI and is shown here in blue. B. The number of distinct fluorescent spots in cells after different incubation times. This is a total count including spots within the cell and at the membrane. Data is presented as mean ± SEM for at least four individual cells.

For all of the cell lines, the majority of CF-TKDNNLLGRFELSG appeared to be at the surface during the very early time points and intracellularly after 60 minutes incubation. CF-TKDNNLLGRFELSG was not found to locate in the nucleus in any of the five cell lines at any of the time points assessed. As was observed for the cmHsp70 mAb, all cell lines investigated exhibited multiple clear, distinct spots of CF-TKDNNLLGRFELSG fluorescence. The number of

spots progressively increased in all of the cells lines, with MDA-MB-231 and MCF7 cells showing similar CF-TKDNNLLGRFELSG spot counts and an increase of almost four-fold from the 5 minute to 60 minute time point (MDA-MB-231: 5 min = 26 ± 4 spots, 60 min = 87 ± 7 spots. MCF7: 5 min = 23 ± 2, 60 min = 80 ± 5. Data presented as mean ± SEM). There was a rapid increase in the spot count during the first 15 minutes in MDA-MB-231 cells, which was followed by a more consistent, steady increase thereafter. Almost all of the internalisation into MCF7 cells occurred between 15 and 30 min, with virtually no additional accumulation being apparent between 30 and 60 min. The internalisation of CF-TKDNNLLGRFELSG into T47D cells was less rapid (5 min = 18 ± 8, 60 min = 43 ± 5), but showed a similar internalisation pattern to MCF7 cells, with the largest increase in spot number occurring between 15 and 30 min. The level of CF-TKDNNLLGRFELSG internalisation appears to correlate with memHsp70 status, as T47D cells express the least memHsp70 and were found to present fewer spots of internalised CF-TKDNNLLGRFELSG, whereas the lines expressing more memHsp70 (MDA-MB-231 and MCF7) exhibited almost twice as many spots of internalised CF-TKDNNLLGRFELSG.

In contrast to the human cell lines, there was little change in accumulation of CF-TKDNNLLGRFELSG spots in the murine cells lines between the 5 minute and 60 minute incubation times (4T1: 5 min= 76 ± 9, 60 min = 93 ± 9. CT26: 5 min = 52 ± 3, 60 min = 79 ± 6). After only 5 min, both mouse cell lines exhibited CF-TKDNNLLGRFELSG spot counts that were at least twice that seen in any of the human breast cancer cell lines, indicating that these cells have an even greater and faster capability for internalising CF-TKDNNLLGRFELSG.

As well as a total spot count per cell, CF-TKDNNLLGRFELSG spots were counted per frame of each cell stack, as has been described previously, making use of z-stack images (**Fig 4.10**). Across all cell lines, there was a trend for the bulk of the CF-TKDNNLLGRFELSG to be present at or near to the adhered surface of the cell. This holds across all time points, despite the amount of CF-TKDNNLLGRFELSG in other regions of the cell increasing (**Fig 4.11 and 4.12**).

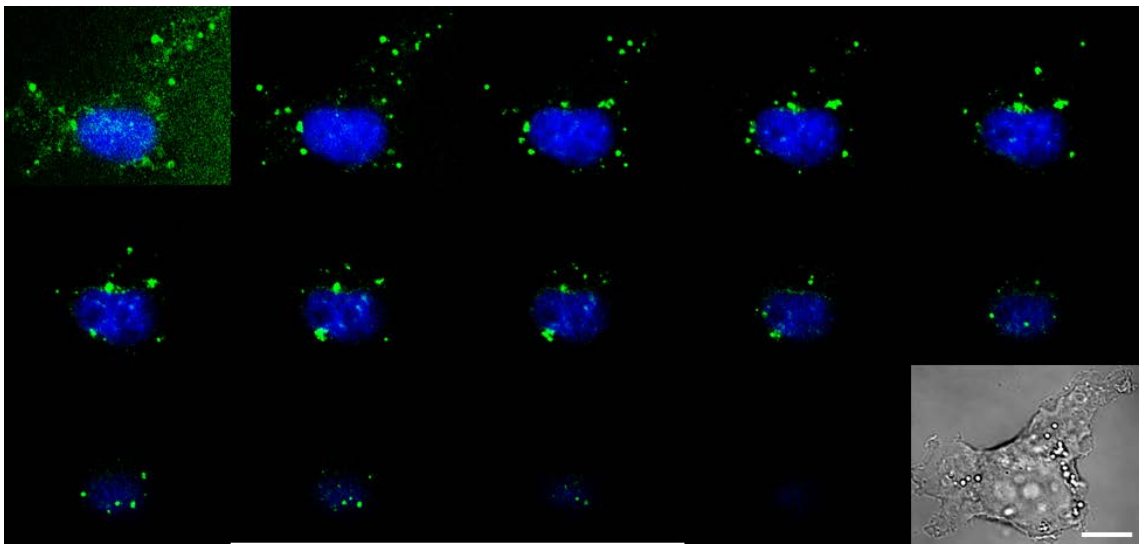

Figure 4.10 Representative montage of z-stack confocal images showing CF-TKDNNLLGRFELSG internalised into MDA-MB-231 cells.

Z-stack frames from the full height of a single MDA-MB-231 cell demonstrating distribution of CF-TKDNNLLGRFELSG following 60 minutes incubation time. Single frame images start at the adhered surface and finish at the apex of the cell. Brightfield imaging is included to help with orientation. Internalised cmHsp70.1 mAb is shown in green, DAPI staining of the nucleus is in blue. The scale bar represents 10µm.

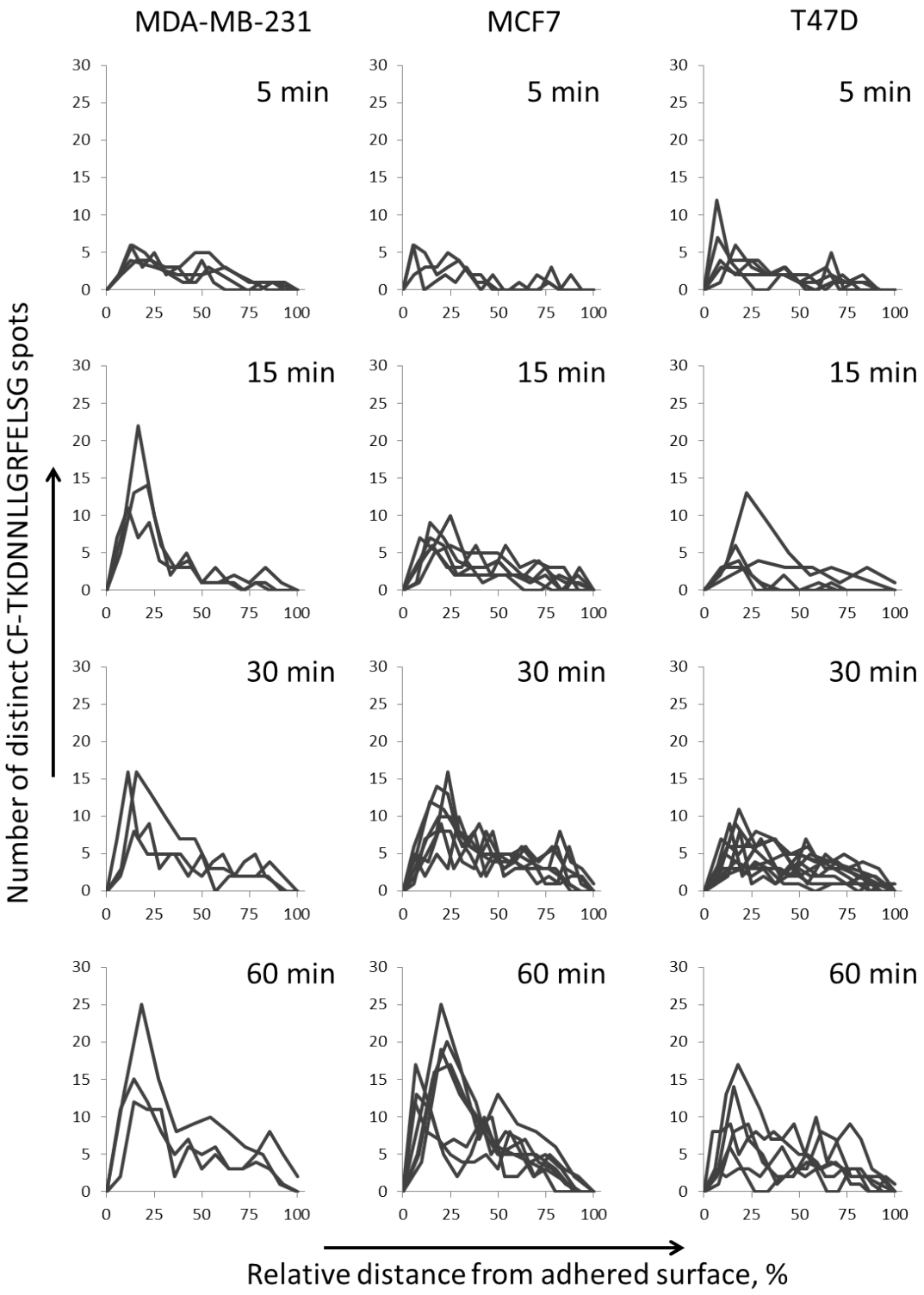

Figure 4.11 Distribution of internalised CF-TKDNNLLGRFELSG in human breast cancer cell lines

Distribution of internalised CF-TKDNNLLGRFELSG spots in every human breast cancer cell imaged at each time point up to 60 minutes. Although CF-TKDNNLLGRFELSG appears throughout the full height of the cells, there appears to be a greater accumulation towards the adhered surface of the cells. Cells which were incubated with CF-TKDNNLLGRFELSG for the longest periods showed a greater number of spots in the middle region of cells. Each line represents the profile of an individual cell, with a minimum of three cells per condition.

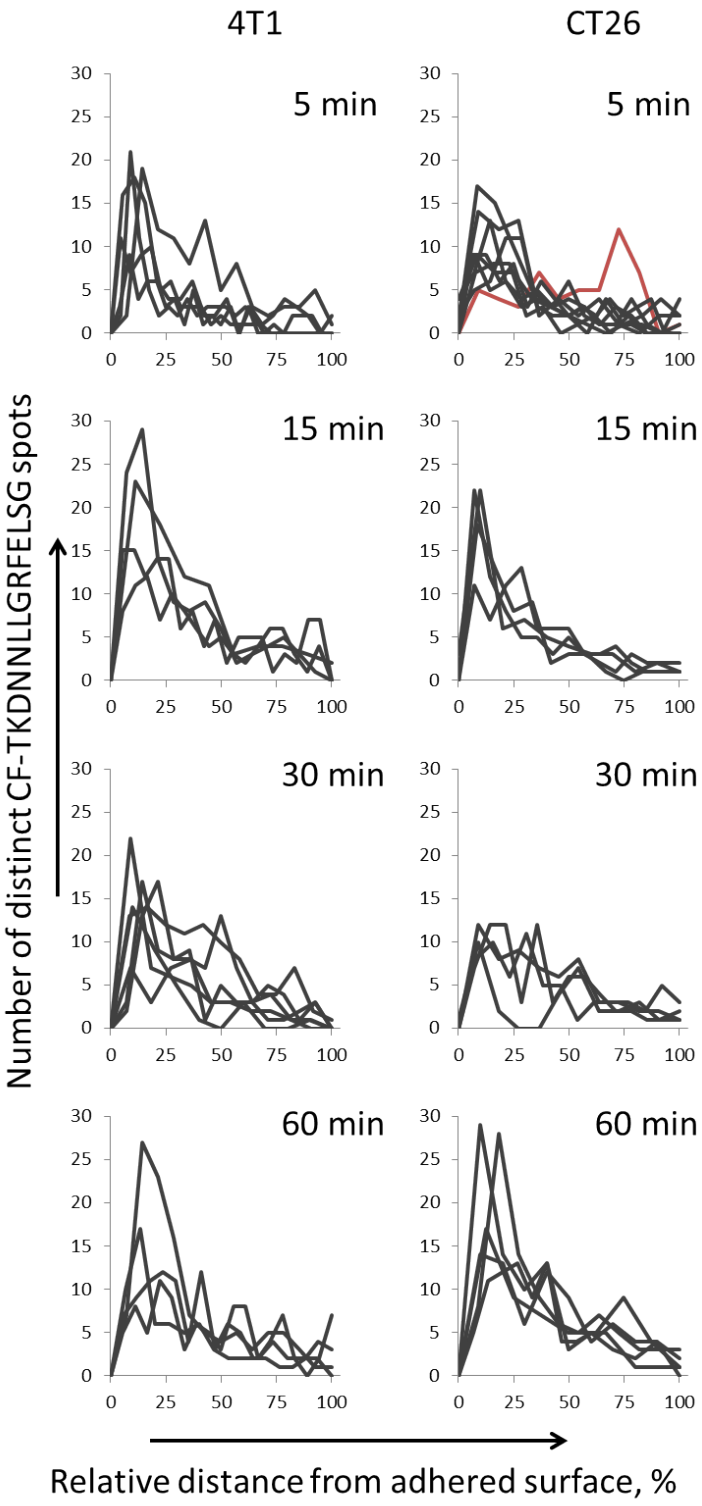

Figure 4.12 Distribution of internalised CF-TKDNNLLGRFELSG in mouse cancer cell lines

Distribution of internalised CF-TKDNNLLGRFELSG spots in every 4T1 and CT26 cell imaged at each time point up to 60 minutes. Although CF-TKDNNLLGRFELSG appears throughout the full height of the cells, there is a clear bias towards the peptide being present close to the adhered surface of the cells. This asymmetrical distribution was observed at all time-points. Each line represents the profile of an individual cell, with a minimum of four cells per condition.

To better allow interrogation of the CF-TKDNNLLGRFELSG distribution data, spot counts were totalled over quartiles of the cells' height (**Fig 4.13A–4.17A**). This allowed average measurements to be made, rather than relying on raw data for all of the individual cells. Across all cell lines the quartile which contained the most CF-TKDNNLLGRFELSG spots was 0-25% from the adhered surface. These data confirm that CF-TKDNNLLGRFELSG is also preferentially internalised through the adhered surface. Represented composite stack images are displayed to show the number of spots in the upper most and lower most quartiles of each cell line after 5 minutes and 60 minutes incubation with the CF-TKDNNLLGRFELSG peptide (**Fig 4.13B-4.17B**).

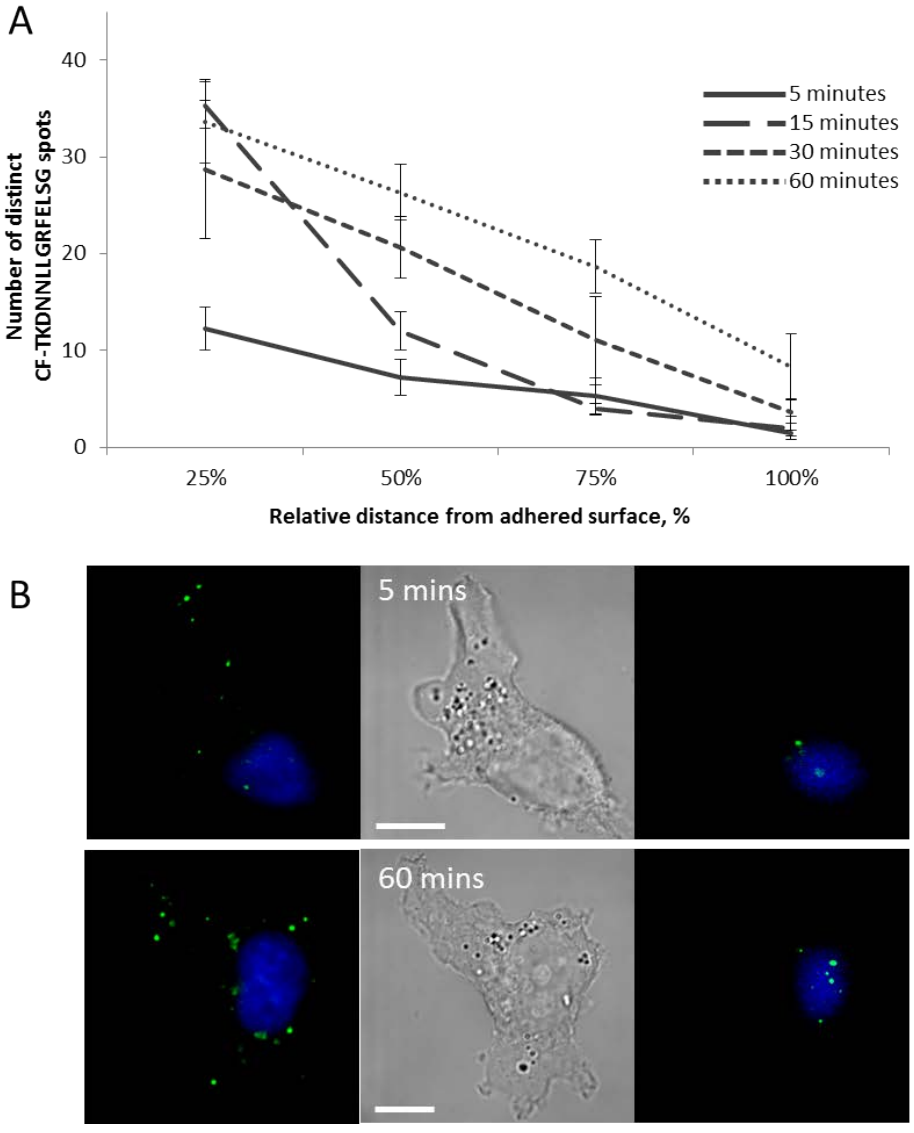

Figure 4.13 Distribution of internalised CF-TKDNNLLGRFELSG in MDA-MB-231 cells

A CF-TKDNNLLGRFELSG spot counts over the full height of cells at all incubation time points. The quartile containing the adherent surface consistently holds the greatest number of CF-TKDNNLLGRFELSG spots. As the incubation time increases spot counts increase over the middle quartiles (25-50% and 50-75%). The spot count remains very similar in the quartile containing the apex (75-100%). Data are presented as mean ± SEM, n = 5. **B** Representative fluorescence images of the first and last quartiles (0-25% and 75-100%) after 5 minutes and 60 minutes incubation with CF-TKDNNLLGRFELSG. These are composite images of all frames that make up the quartile. Bright-field images are included to confirm placement of cell boundaries.

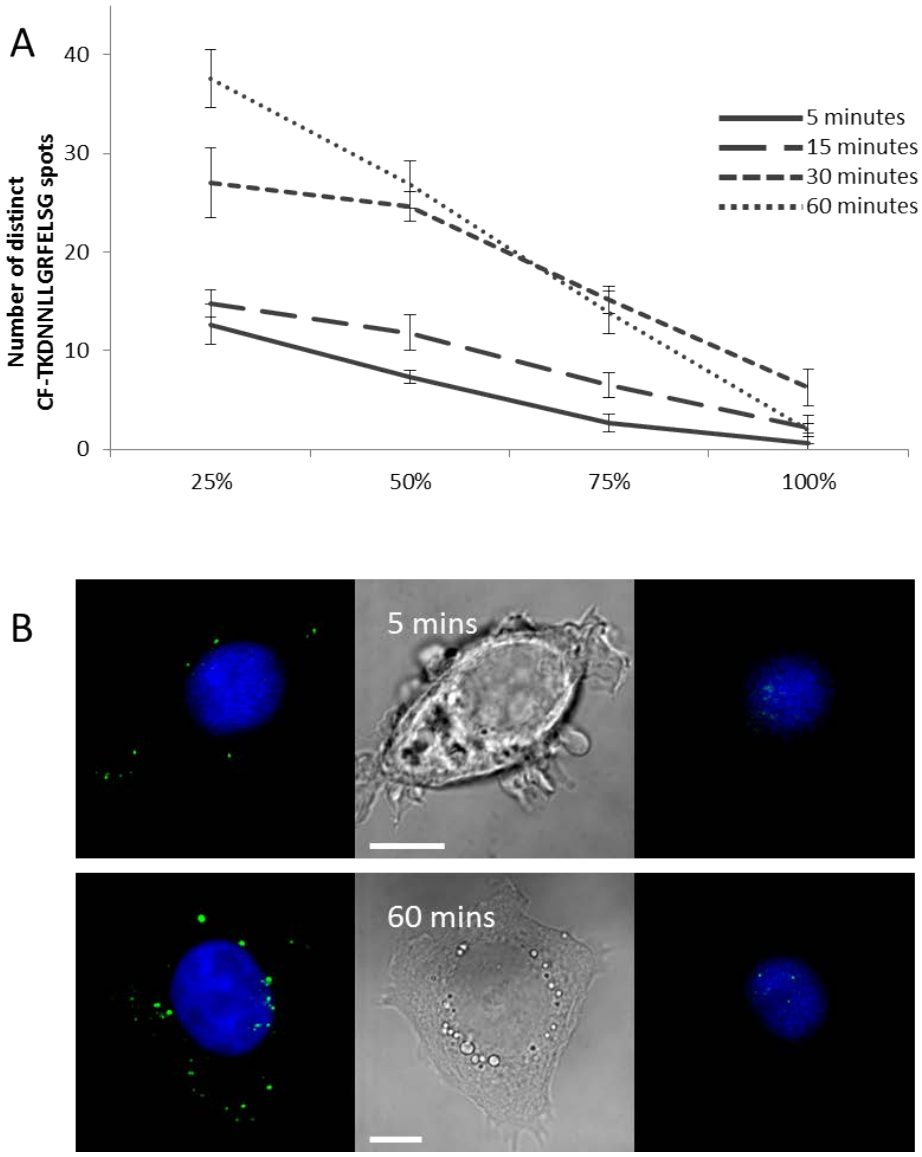

Figure 4.14 Distribution of internalised CF-TKDNNLLGRFELSG in MCF7 cells

A CF-TKDNNLLGRFELSG spot counts over the full height of cells at all incubation time points. The quartile containing the adherent surface consistently holds the greatest number of CF-TKDNNLLGRFELSG spots. As the incubation time increases spot counts increase over the middle quartiles (25-50% and 50-75%). The spot count remains very similar in the quartile containing the apex (75-100%). Data are presented as mean ± SEM, n = 7. **B** Representative fluorescence images of the first and last quartiles (0-25% and 75-100%) after 5 minutes and 60 minutes incubation with CF-TKDNNLLGRFELSG. These are composite images of all frames that make up the quartile. Bright-field images are included to confirm placement of cell boundaries.

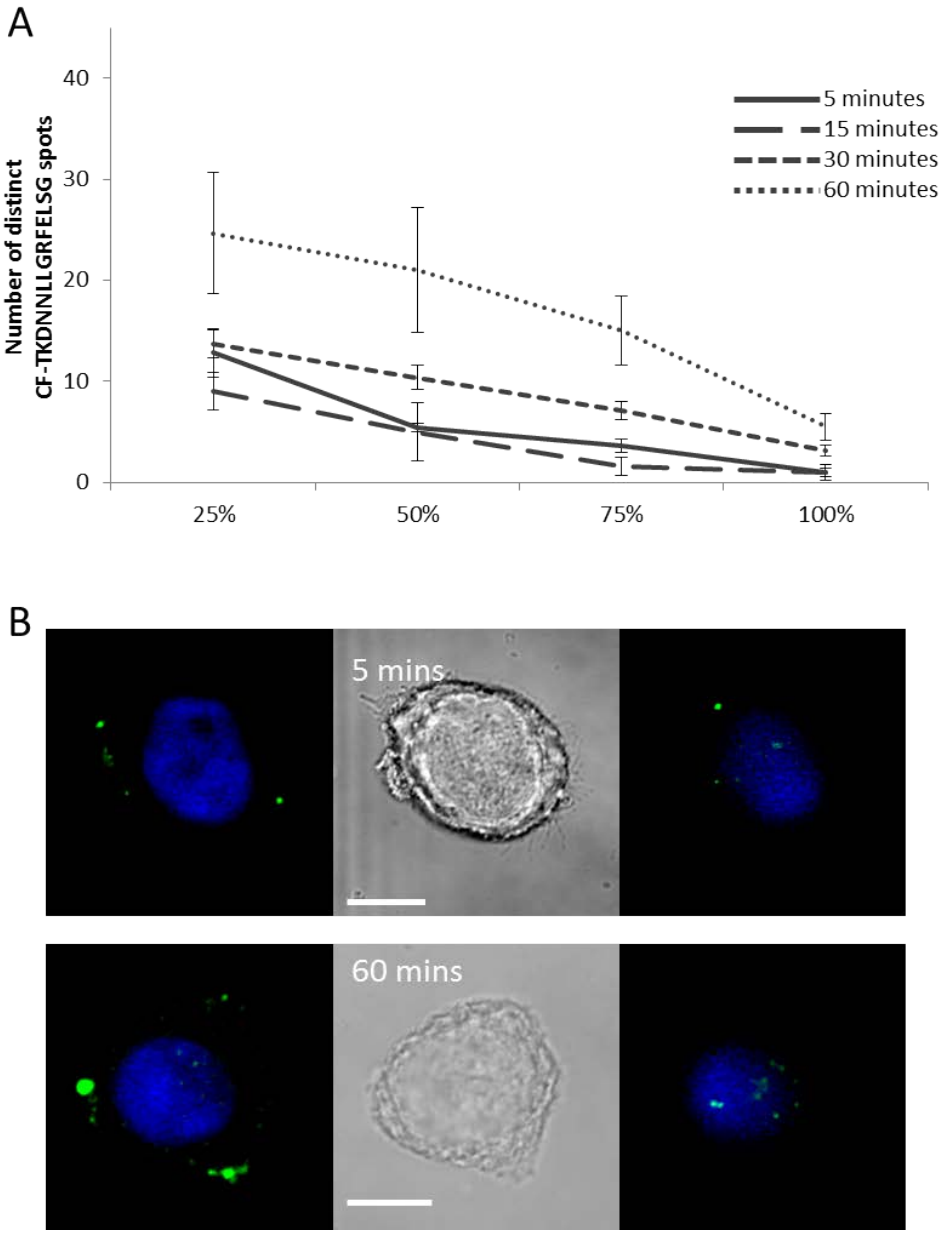

Figure 4.15 Distribution of internalised CF-TKDNNLLGRFELSG in T47D cells

A CF-TKDNNLLGRFELSG spot counts over the full height of cells at all incubation time points. The quartile containing the adherent surface consistently holds the greatest number of CF-TTP spots. As the incubation time increases spot counts increase over the middle quartiles (25-50% and 50-75%). The spot count remains very similar in the quartile containing the apex (75-100%). Data are presented as mean ± SEM, n = 11. **B** Representative fluorescence images of the first and last quartiles (0-25% and 75-100%) after 5 minutes and 60 minutes incubation with CF-TKDNNLLGRFELSG. These are composite images of all frames that make up the quartile. Bright-field images are included to confirm placement of cell boundaries.

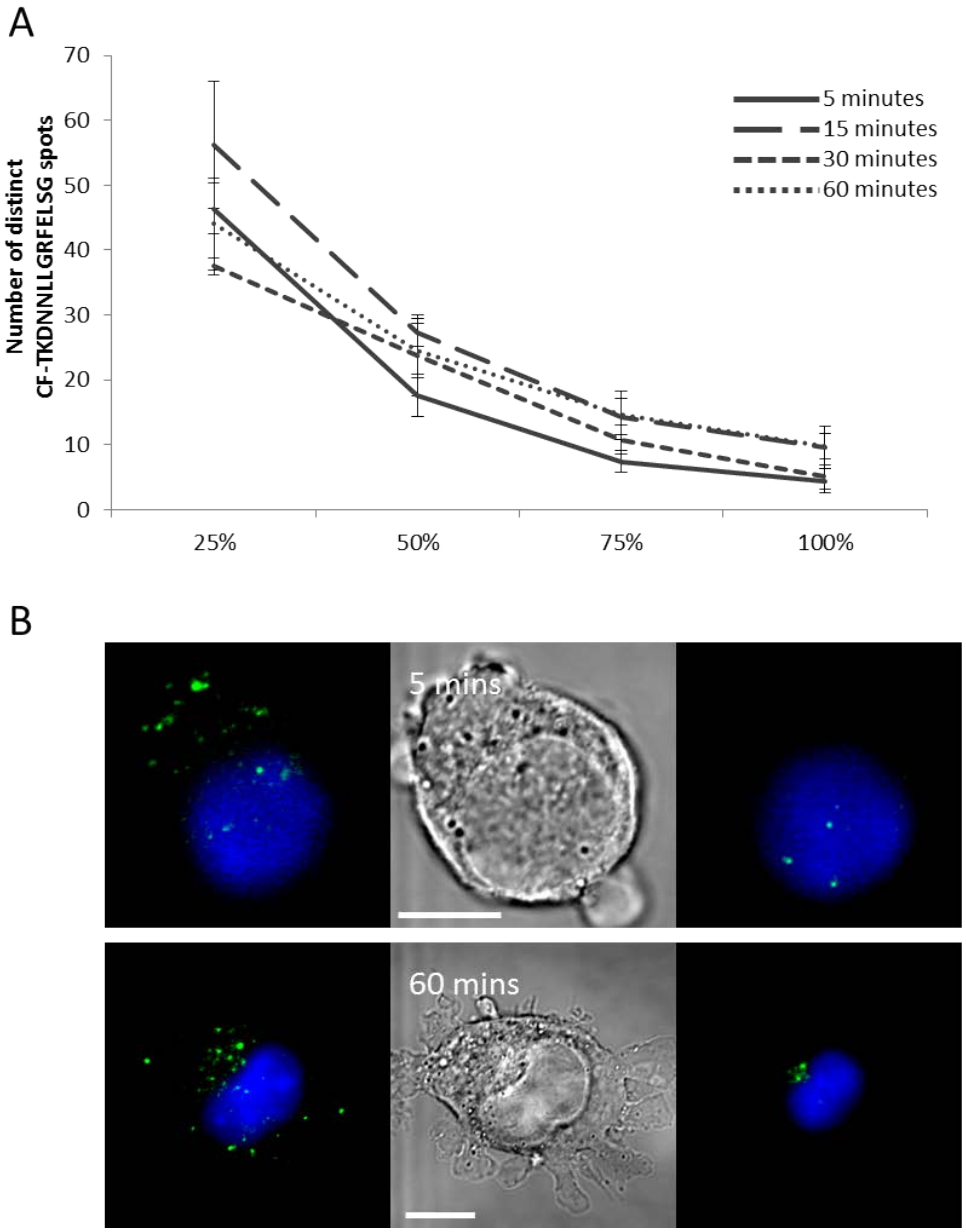

Figure 4.16 Distribution of internalised CF-TKDNNLLGRFELSG in 4T1 cells

A CF-TKDNNLLGRFELSG spot counts over the full height of cells at all incubation time points. The quartile containing the adherent surface consistently holds the greatest number of CF-TKDNNLLGRFELSG spots. As the incubation time increases spot counts increase over the middle quartiles (25-50% and 50-75%). The spot count remains very similar in the quartile containing the apex (75-100%). Data are presented as mean ± SEM, n = 6. **B** Representative fluorescence images of the first and last quartiles (0-25% and 75-100%) after 5 minutes and 60 minutes incubation with CF-TKDNNLLGRFELSG. These are composite images of all frames that make up the quartile. Bright-field images are included to confirm placement of cell boundaries.

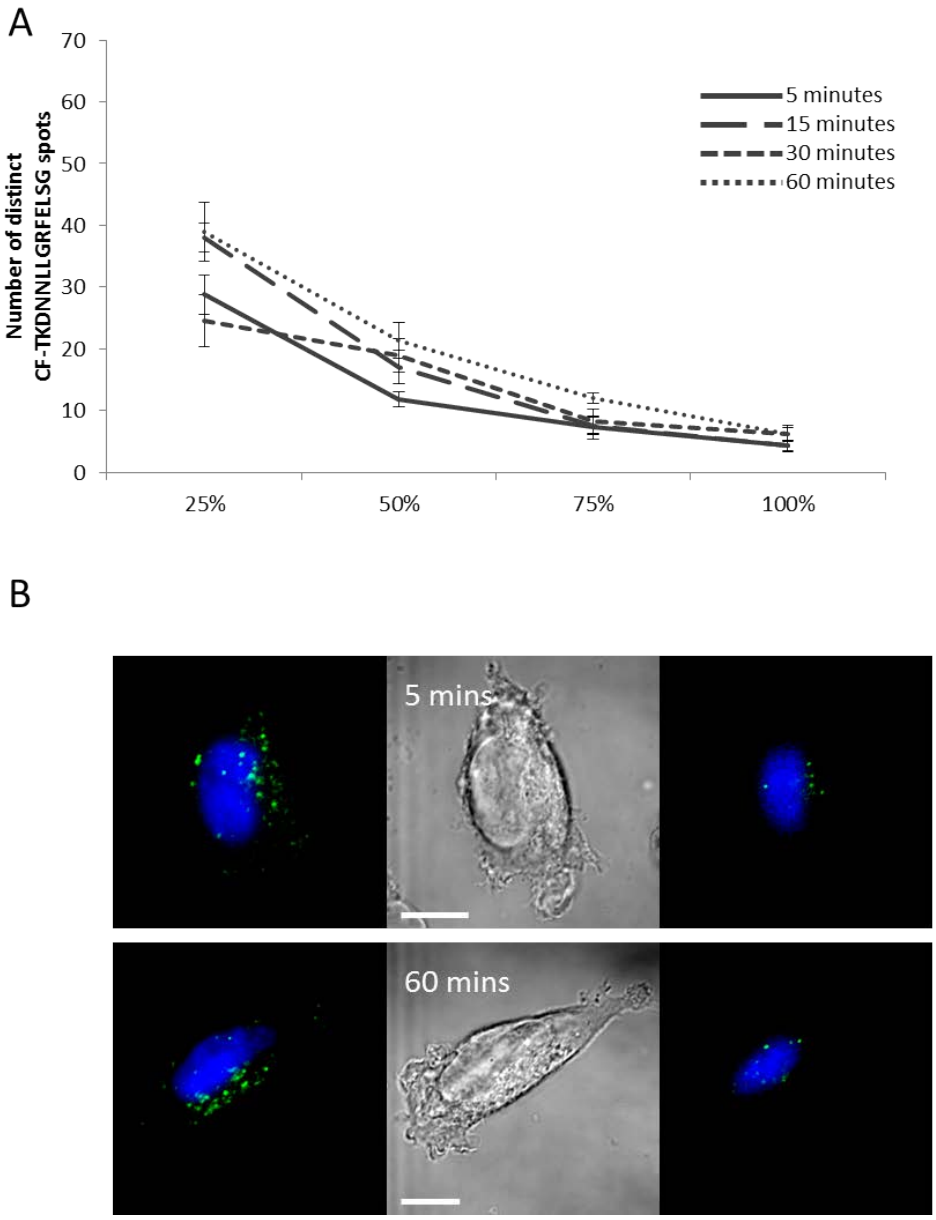

Figure 4.17 Distribution of internalised CF-TKDNNLLGRFELSG in CT26 cells

A CF-TKDNNLLGRFELSG spot counts over the full height of cells at all incubation time points. The quartile containing the adherent surface consistently holds the greatest number of CF-TKDNNLLGRFELSG spots. As the incubation time increases spot counts increase over the middle quartiles (25-50% and 50-75%). The spot count remains very similar in the quartile containing the apex (75-100%). Data are presented as mean ± SEM, n = 9. **B** Representative fluorescence images of the first and last quartiles (0-25% and 75-100%) after 5 minutes and 60 minutes incubation with CF-TKDNNLLGRFELSG. These are composite images of all frames that make up the quartile. Bright-field images are included to confirm placement of cell boundaries.

In the three human cell lines, as the incubation duration increases so does the mean spot count of CF-TKDNNLLGRFELSG, particularly evident in the first three quartiles (0-75%) thereby demonstrating an accumulation of CF-TKDNNLLGRFELSG throughout the cells over time. At all time-points, very little CF-TKDNNLLGRFELSG is found within the apex quartile of the cells. The situation in the mouse cell lines differs, with the CF-TKDNNLLGRFELSG distribution through the cells remaining similar across the time-points, with the vast majority of CF-TKDNNLLGRFELSG

being found in the quartile at the adherent cell surface. This could be due to CF-TKDNNLLGRFELSG being trafficked more slowly in the mouse cell lines, and thus the accumulation of CF-TKDNNLLGRFELSG takes longer than the durations examined here. The large number of CF-TKDNNLLGRFELSG spots in the adherent surface quartile, even after the shortest duration, suggests a potential preferential route of internalisation around the point of cell adhesion.

4.3.2 Internalised CF-TKDNNLLGRFELSG peptide associates with mitochondria

As was observed for cmHsp70 mAb, internalised CF-TKDNNLLGRFELSG appears as well defined, distinct spots throughout the cell, thereby leading to the proposition that is associated with intracellular vesicles. Attempts were therefore made to stain the intracellular vesicles of cells incubated with CF-TKDNNLLGRFELSG in order to determine co-localisation profiles. For these experiments, cells were grown for 48 hours in glass bottomed dishes and then incubated in staining buffer containing 75µg/mL CF-TKDNNLLGRFELSG. After the desired incubation period, cells were formaldehyde fixed, permeabilised and stained with appropriate primary and secondary antibodies, as described previously. However, fluorescence signals could be detected. In an attempt to solve this problem, different permeabilisation agents were tried (saponin, Triton X and methanol), but all with the same result. The conclusion is that permeabilisation results in the peptide being washed out from cells, however the reason for this is unclear. Unfortunately it was not possible to generate Biacore data relating to peptide binding affinity, however a peptide ELISA demonstrated that the TKDNNLLGRFELSG peptide bound specifically to Hsp70 in a concentration-dependent manner [535]. In the future it would be of interest to obtain Biacore data to establish with what affinity the peptide binds to Hsp70.

Due to the observed peptide leaching it was not possible to fully elucidate the internalisation pathway of CF-TKDNNLLGRFELSG. A different protocol would need to be employed, such as labelling the vesicles of live cells rather than having to fix and then permeabilise cells, and this would be the strategy adopted in the future. There was just one intracellular structure for which co-localisation investigations could be conducted; the mitochondria. This is because the MitoID staining protocol involves using live cells, with the stain diffusing in rather than requiring cell permeabilisation. Co-localisation of the CF-TKDNNLLGRFELSG peptide and stained mitochondria was assessed following 60 minute incubation with the CF-TKDNNLLGRFELSG peptide with subsequent 30 minute mitochondrial staining, for the human breast cancer cell lines MDA-MB-231, MCF7 and T47D (**Table 4.1 and Fig 4.18**) and the mouse cancer cell lines 4T1 and CT26 (**Table 4.2 and Fig 4.19**).

A. Pearson Coefficient	60+30 minutes
MDA-MB-231	0.585 ± 0.065
MCF7	0.855 ± 0.010
T47D	0.813 ± 0.010

B Manders M1 Coefficient	60+30 minutes
MDA-MB-231	43.3 ± 7.0 %
MCF7	40.7 ± 5.6 %
T47D	14.1 ± 4.1 %

Table 4.1 Trafficking of internalised CF-TKDNNLLGRFELSG peptide to mitochondria in human breast cancer cell lines

A. Pearson coefficient of the correlation between internalised CF-TKDNNLLGRFELSG peptide and staining for the mitochondria in breast cancer cell lines MDA-MB-231, MCF7 and T47D after 60 minutes incubation with CF-TKDNNLLGRFELSG. The positive correlation suggests some degree of co-localisation. **B.** Manders' M1 measurement calculating the percentage of internalised CF-TKDNNLLGRFELSG which was co-localised with staining for the mitochondria. The proportion of CF-TKDNNLLGRFELSG co-localising with the mitochondria is increases with the expression of memHsp70. Data are presented as mean ± SEM, n = 7-14 from at least two independent experiments.

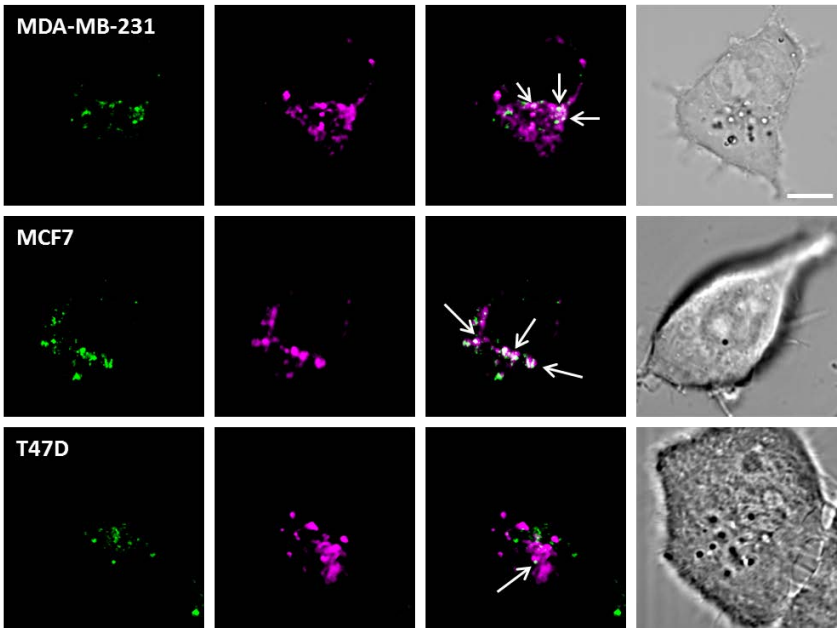

Figure 4.18 Trafficking of internalised CF-TKDNNLLGRFELSG peptide to mitochondria in human breast cancer cell lines

MDA-MB-231, MCF7 and T47D cells grown in MatTek™ glass bottom dishes and incubated with CF-TKDNNLLGRFELSG peptide for 60 minutes were stained with MitoID™ red to show the mitochondria. Any co-localisation (white) of CF-TKDNNLLGRFELSG fluorescence (green) and mitochondrial staining (magenta) could be confirmation of trafficking of CF-TKDNNLLGRFELSG to mitochondria. Co-localisation was assessed using both Pearson's and Manders' M1 coefficients of co-localisation, as well as visual overlap of the intensity channels. Co-localisation was found in all of the cell lines, increasing in line with increased memHsp70 expression. Images shown are representative single frames taken from the middle region (2^{nd} or 3^{rd} quartile) of cells incubated CF-TKDNNLLGRFELSG for 60 minutes. Scale bars are 10µm.

A. Pearson Coefficient	60+30 minutes
4T1	0.822 ± 0.011
CT26	0.778 ± 0.011

B. Manders M1 Coefficient	60+30 minutes
4T1	31.2 ± 4.8 %
CT26	4.2 ± 2.1 %

Table 4.2 Trafficking of internalised CF-TKDNNLLGRFELSG peptide to mitochondria in murine cancer cell lines

A. Pearson coefficient of the correlation between internalised CF-TKDNNLLGRFELSG peptide and staining for the mitochondria in cancer cell lines 4T1 and CT26 after 60 minutes incubation with CF-TKDNNLLGRFELSG. There was a positive correlation suggesting some degree of co-localisation. **B.** Manders' M1 measurement calculating the percentage of internalised CF-TKDNNLLGRFELSG which was co-localised with staining for the mitochondria. The proportion of CF-TKDNNLLGRFELSGco-localisation with the mitochondria positively correlates to the expression of memHsp70. Data are presented as mean ± SEM, n = 5-11 from at least two independent experiments。

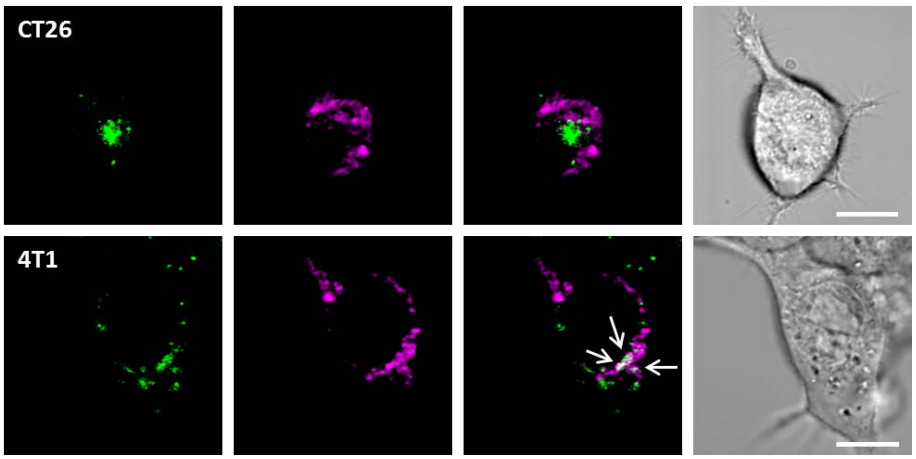

Figure 4.19 Trafficking of internalised CF-TKDNNLLGRFELSG to mitochondria in murine cancer cells lines

4T1 and CT26 cells grown in MatTek™ glass bottom dishes and incubated with CF-TTP for 60 minutes were stained with MitoID™ red to show the mitochondria. Any co-localisation (white) of CF-TTP fluorescence (green) and mitochondrial staining (magenta) could be confirmation of trafficking of TTP to mitochondria. Co-localisation was assessed using both Pearson's and Manders' M1 coefficients of co-localisation, as well as visual overlap of the intensity channels. Co-localisation was found in both of the cell lines. Images shown are representative single frames taken from the middle region (2nd or 3rd quartile) of cells incubated with ATTO488-cmHsp70.1 mAb for 60 minutes. Although hoechst staining of the nucleus was also conducted the strength of the signal was insufficient to obtain images under confocal conditions. Scale bars are 10μm.

Some degree of co-localisation between internalised CF-TKDNNLLGRFELSG and mitochondria was apparent in all of the human breast cancer cell lines. Using the Manders' M1 coefficient, it was possible to calculate the proportion of CF-TKDNNLLGRFELSG co-localising at the mitochondria. The proportion of co-localisation appears to correlate with the memHsp70

status, with the greatest co-localisation being apparent in MDA-MB-231 cells (43.3 ± 7.0%), followed by MCF7 (40.7 ± 5.6%) and T47D cells (14.1 ± 4.1%). The two mouse cancer cell lines exhibited vastly different degree of CF-TKDNNLLGRFELSG co-localisation with the mitochondria (4T1: 31.2 ± 4.8% CT26: 4.2 ± 2.1%), but this still followed in line with their memHsp70 expression.

4.4 Summary

The Hsp70-derived 14-mer peptide TKDNNLLGRFELSG was found to bind to memHsp70^{+} breast cancer cell lines, in a manner which positively tracked with the expression density of memHsp70. When cells were incubated with the CF-TKDNNLLGRFELSG peptide at 37^{o}C, and were therefore metabolically active, the peptide was rapidly internalised. The accumulated intracellular quantities of peptide also increased with increasing levels of memHsp70 expression on cell lines. There is a good degree of specificity to the binding and internalisation, although a 'scrambled' version of the peptide (NGL) did exhibit a small amount of binding and internalisation as well. The NGL peptide comprises the same 14 amino acids, and so will have the same overall charge as the TKDNNLLGRFELSG peptide, and this may explain the low levels of binding and uptake exhibited.

When cells were fixed and permeabilised any internalised peptide was found to leak from the cells, making staining of intracellular vesicles difficult. The mitochondrial stain, which passively diffuses into live cells, did not pose this problem and the CF-TKDNNLLGRFELSG peptide was found to co-localise to mitochondria in the same manner as the cmHsp70.1 mAb. Due to time constraints it was not possible to use other similar diffuse dyes to study co-localisation with other intracellular structures, however this is something which could be looked into in the future.

Since TKDNNLLGRFELSG is part of the oligomerisation domain of Hsp70, it was hypothesized that the binding of the peptide to Hsp70 involves mechanisms that are related to the oligomerisation domain of Hsp70. Furthermore, it appeared that the uptake and intracellular transport of TKDNNLLGRFELSG follows similar pathways as those for the cmHsp70.1 mAb.

CHAPTER 5

Results III – Internalisation of recombinant human Granzyme B by cancer cell lines expressing membrane Hsp70

5.1 Introduction

The serine protease granzyme B is one of the primary constituents of cytotoxic granules released by NK cells and cytotoxic $CD8^+$ T cells. In this setting, granzyme B is released in conjunction with perforin which facilitates its delivery into target cells. Granzyme B preferentially cleaves substrates at aspartic acid residues [55] and acts on many components of the apoptotic pathway. Granzyme B is capable of activating the zymogens procaspase-3 [56, 57] and procaspase-8 [59], as well as directly acting downstream on caspase substrates, including the Bcl-2 family member Bid [62], inhibitor of caspase-activated DNase (ICAD) [60, 559], poly (ADP-ribose) polymerase (PARP) [61] and the catalytic subunit of DNA-dependent protein kinase ($DNA\text{-}PK_{cs}$) [61]. Granzyme B therefore has great potential as a therapeutic agent, if strategies for effectively (and selectively) delivering it to tumour cells could be developed.

Two human cell lines which express memHsp70, the colon carcinoma line CX-2 and the pancreas carcinoma Colo357, have been shown to bind and internalise recombinant human granzyme B in the absence of perforin [530]. It has also been demonstrated that internalisation is mediated via memHsp70, and that it leads to apoptotic cell death [530]. The following studies are aimed at learning more about the mechanism of memHsp70-mediated internalisation of granzyme B so that its potential as a cancer therapeutic can be better evaluated. For these experiments, the potential internalisation of exogenous recombinant human granzyme B by three human breast cancer cell lines and two murine cancer cell lines, and the biological consequences have been studied.

5.2 Internalisation of granzyme B by cancer cells expressing memHsp70

The ability of granzyme B to bind to $memHsp70^+$ tumour cells was investigated by flow cytometry using ATTO488-labelled granzyme B. As a control, cells were also incubated with ATTO488-labelled bovine serum albumin (BSA). There is a clear difference between the results for cells incubated with granzyme B and those incubated with BSA, indicating specific uptake of granzyme B (**Fig 5.1**).

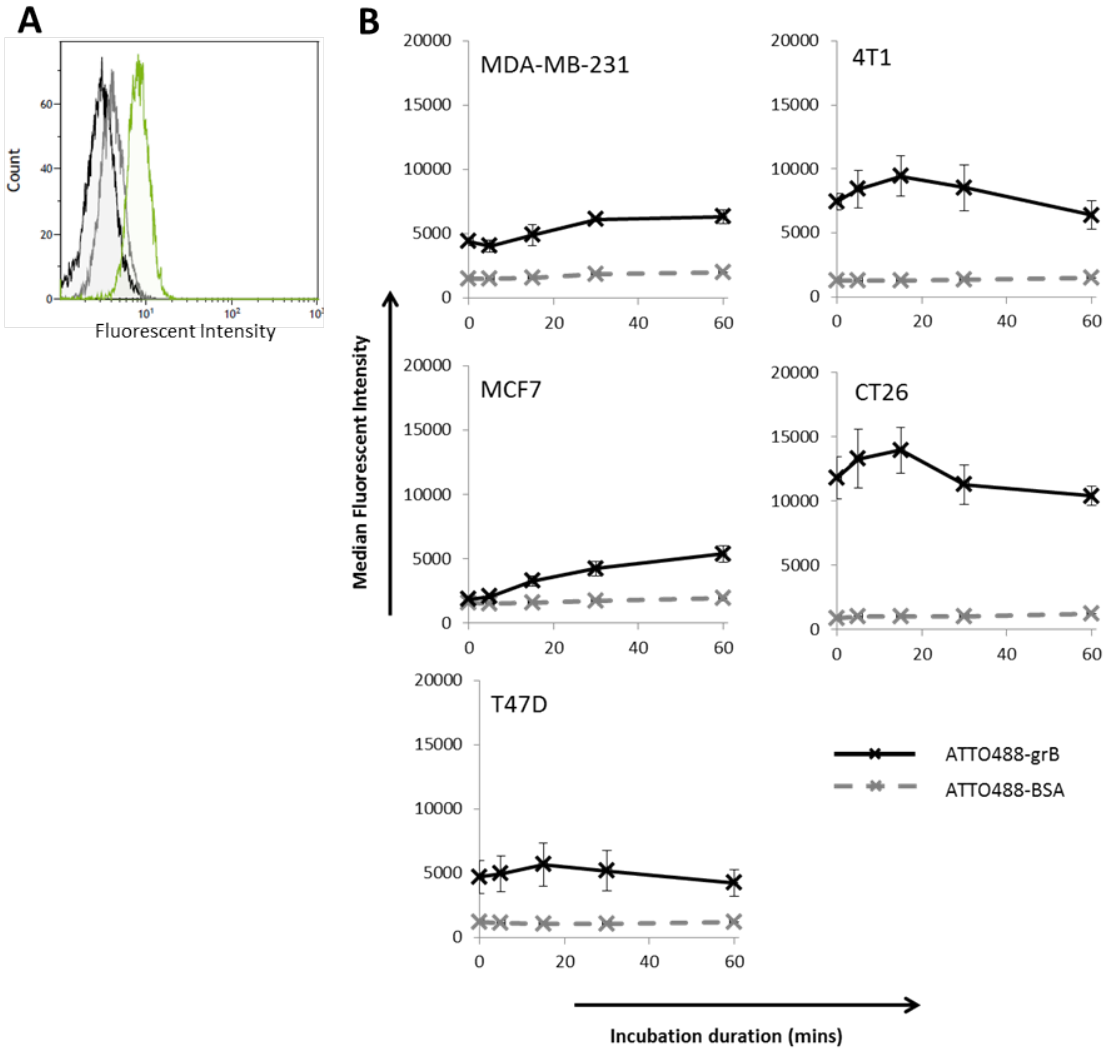

Figure 5.1 Flow cytometric assessment of uptake of fluorescently-labelled granzyme B into cancer cell lines

A. Representative flow cytometry plots showing the fluorescent intensity of MDA-MB-231 cells incubated for 60 minutes at 37^{o}C in medium (black line), with ATTO488-labelled BSA (grey line) and with ATTO488-labelled granzyme B (green line). B. Cells were incubated in the presence of ATTO488-labelled granzyme B with samples saved at different time points, for up to an hour. The median fluorescent intensity of the whole population was recorded, as a comparative measure of the amount of granzyme B (solid black line). The intensity after incubation with similarly ATTO488-labelled BSA serves as a control (dashed grey line). All cell lines are capable of specifically binding and internalising granzyme B. Data are presented as mean ± SEM of at least three independent experiments.

Although there was a progressive increase in the internalisation of granzyme B by the human cell lines over time, the internalisation of granzyme B into the murine cells was more rapid, peaked earlier and declined thereafter. The reasons for this different profile remain unclear and further studies are required.

The internalisation of fluorescently-labelled granzyme B into memHsp70^{+} tumour cells was also confirmed using confocal microscopy. As the flow cytometry data indicated that the intensity of granzyme B appeared to reduce after 30 minutes in the mouse cell lines, the

confocal microscopy was conducted at longer time points. Serum was shown to interfere with granzyme B uptake so these incubations were conducted in PBS only. Cells were grown in glass bottomed dishes for 48 hours then washed and incubated with PBS containing 4µg/mL ATTO488-labelled granzyme B for up to 60 min. Cells receiving longer incubation times were provided with 1mL fresh growth medium then replaced in the 37°C incubation environment for the remaining incubation period. As a consequence, incubation times are denoted as 60+30 and 60+210 minute time points. After incubation, cells were formaldehyde fixed and mounted onto microscopy slides using VECTASHIELD® mounting medium containing DAPI to enable staining of the nucleus, except at the latest time point of 60+210 min. This time point was used to determine the co-localisation of granzyme B with mitochondria and was conducted using live imaging. At this time Hoechst staining was conducted, although the fluorescence was insufficient to be detected in the single frames of confocal microscopy.

Cells were imaged using fluorescent and confocal microscopy to produce wide angle tile scans as well as z-stack images of the full height of cells. Fluorescent tile scan images were obtained demonstrating the specificity of internalisation of ATTO488-labelled granzyme B compared to ATTO488-labelled BSA, with images analysed using ImageJ in order to calculate the mean fluorescent intensity (normalised to the intensity of the background) of all imaged cells. Representative tile scan images are shown below (**Fig 5.2**)

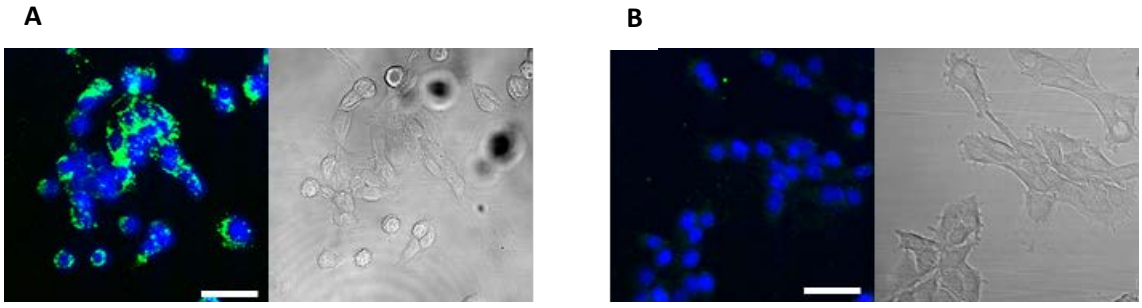

Figure 5.2 Representative tile scan images showing antibody uptake into MDA-MB-231 cells

Tile scan images were produced for MDA-MB-231, MCF7, T47D, 4T1 and CT26 cells, across different time-points of incubation with ATTO488-labelled granzyme B and ATTO488-labelled BSA. Representative tile scan images of MDA-MB-231 cells incubated with ATTO488-labelled granzyme B (A) and ATTO488-labelled BSA (B) for 60+30 minutes are shown. Granzyme B and BSA are shown in green and the nucleus stained with DAPI is shown in blue. Scale bar represents 50µm.

Over time, the intensity from ATTO488-granzyme B increased in all cell lines, thereby confirming the flow cytometric analysis, and the maximum observed fluorescent intensity for each cell line positively tracked with the level of memHsp70 expression of the cells (**Fig 5.3**).

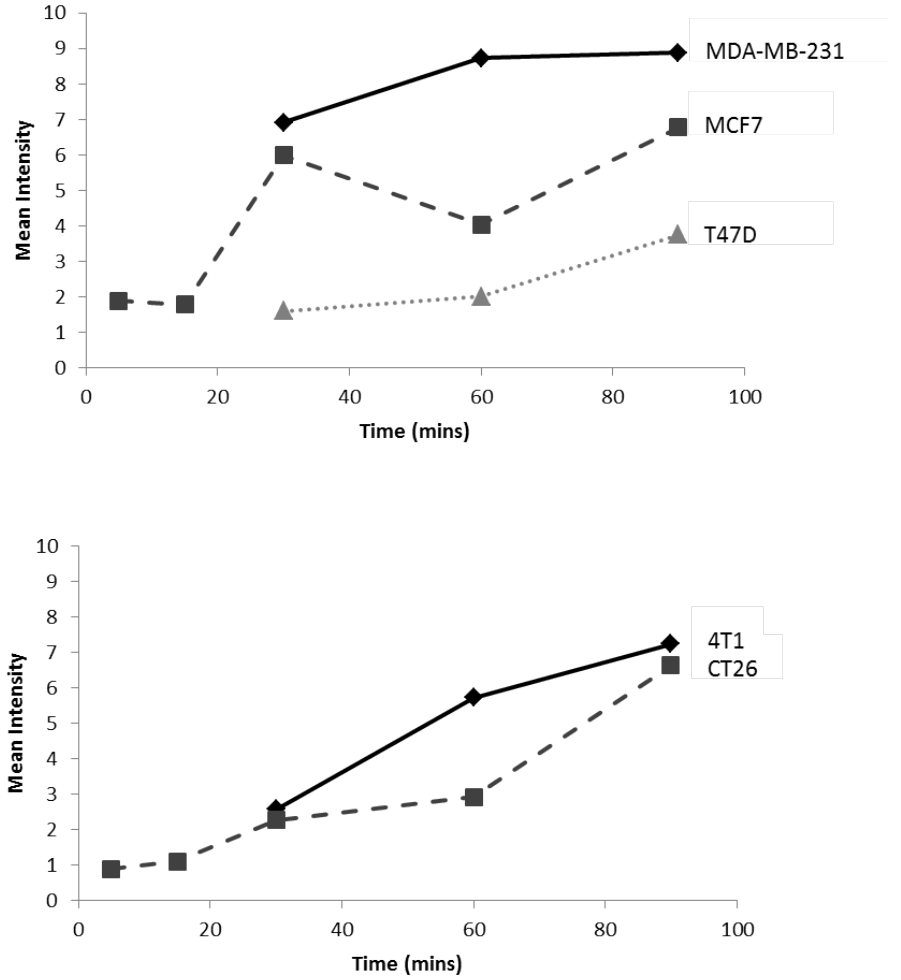

Figure 5.3 Uptake of ATTO488-labelled granzyme B into human and murine cancer cell lines expressing differing levels of memHsp70

Cancer cell lines from human (A) and mouse (B) grown in MatTek™ glass bottom dishes were incubated in the presence of ATTO488-granzyme B for up to an hour then imaged using fluorescent microscopy. Mean fluorescent intensity values were calculated, normalised to background fluorescence. All cell lines are capable of internalising the granzyme B but to varying degrees, with increasing internalisation occurring in line with increasing memHsp70 expression in cell lines. Data are presented as mean ± SEM of a minimum of 80 cells from at least three independent experiments.

Representative single frame images taken from around the midpoint of cells height (within 25-75% from the adhered surface) are shown at each time point (**Fig 5.4A-5.8A**). Internalised granzyme B presents as distinct spots of fluorescence (green), indicating association with intracellular vesicles. Bright-field images are provided to show the placement of cell boundaries. In all cell lines, it is clear to see an increase in the internalised granzyme B from 30 minutes to the other time points.

In order to also provide some quantitative analysis of granzyme B internalisation, the fluorescent spots of granzyme B where counted over the full height of every z-stack imaged, to

produce a measure of spots per cell. If a spot was present in more than one frame, it was counted only in the one where the greatest fluorescent intensity was observed (**Fig 5.4B-5.8B**). When interpreting these quantifications it is very important to keep the experiment protocol in mind. Cells were incubated with PBS containing granzyme B for up to 60 minutes, but at this time cells on longer incubation times received fresh growth medium. This would have provided serum as well as diluting any remaining granzyme B. Both of these procedures would be expected to reduce the rate of uptake of granzyme B. It is then reasonable to assume that from 60 minutes onwards, cells were merely trafficking granzyme B that had already been internalised rather than continuing to increase their intracellular granzyme B content. Any changes to spot count after this point should only relate to the continuing trafficking of previously internalised granzyme B.

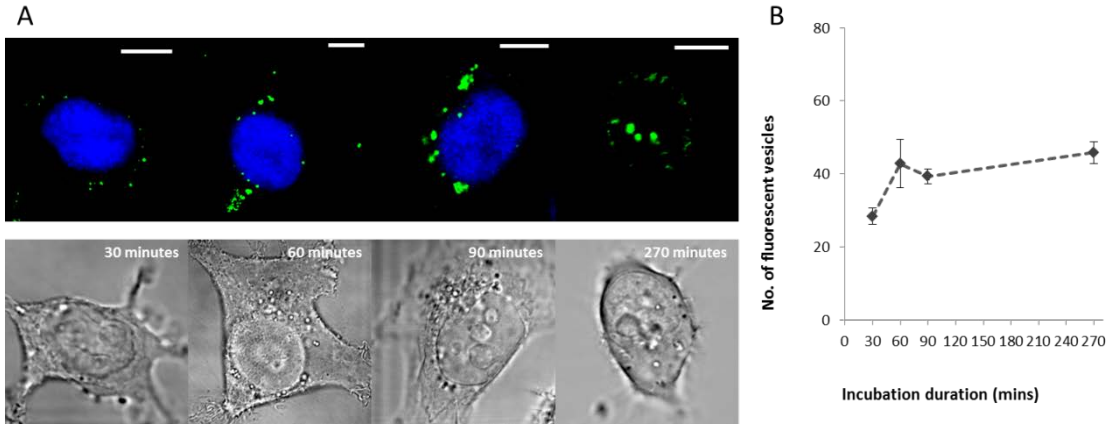

Figure 5.4 Kinetics of granzyme B uptake by MDA-MB-231 cells

A. Representative single frame images showing ATTO488-labelled granzyme B internalised into MDA-MB-231 cells. Frames were selected from the mid-point of cells (25-75% of distance from adhered surface). After 30 minutes incubation time the majority of granzyme B (green) appears to be surface bound (with a ring formation following the edge of cell seen in the bright-field image). At longer incubations, the granzyme B can be seen within the cell boundary and therefore has been internalised. Granzyme B appears as well-defined spots suggesting vesicular association rather than being free in the cytosol. The images shown depict a region 0.88µm thick. Scale bars represent 10µm. For clarity, the nucleus was stained with DAPI (blue). B. The number of distinct fluorescent spots in cells after different incubation times. This is a total count including spots within the cell and at the membrane. Data is presented as mean ± SEM for 9-30 individual cells, from at least two independent experiments.

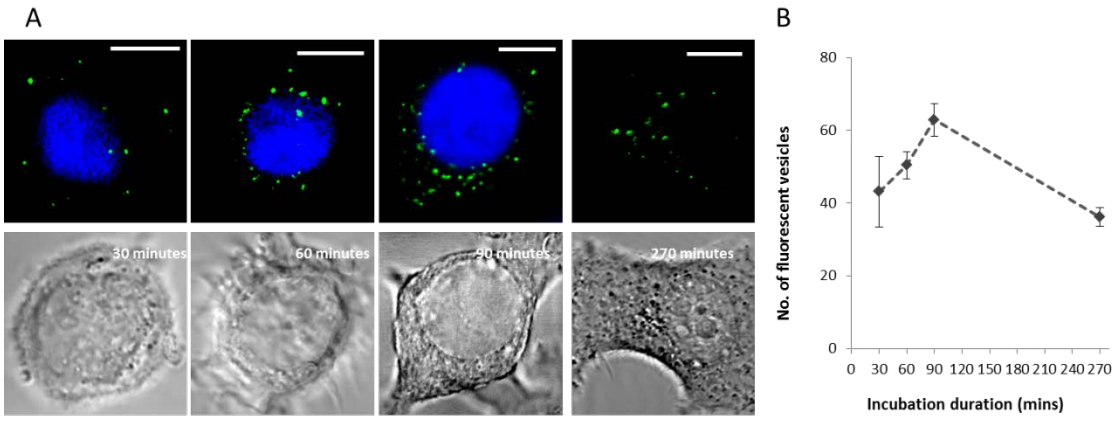

Figure 5.5 Kinetics of granzyme B uptake by MCF7 cells

A. Representative single frame images showing ATTO488-labelled granzyme B internalised into MCF7 cells. Frames were selected from the mid-point of cells (25-75% of distance from adhered surface). After 30 minutes incubation time the majority of granzyme B (green) appears to be surface bound (with a ring formation following the edge of cell seen in the bright-field image). At longer incubations the granzyme B can be seen within the cell boundary and therefore has been internalised. Granzyme B appears as well-defined spots, suggesting vesicular association rather than being free in the cytosol. The images shown depict a region 0.88µm thick. Scale bars represent 10µm. For clarity, the nucleus was stained with DAPI (blue). B. The number of distinct fluorescent spots in cells after different incubation times. This is a total count including spots within the cell and at the membrane. Data is presented as mean ± SEM for 10-24 individual cells, from at least independent experiments.

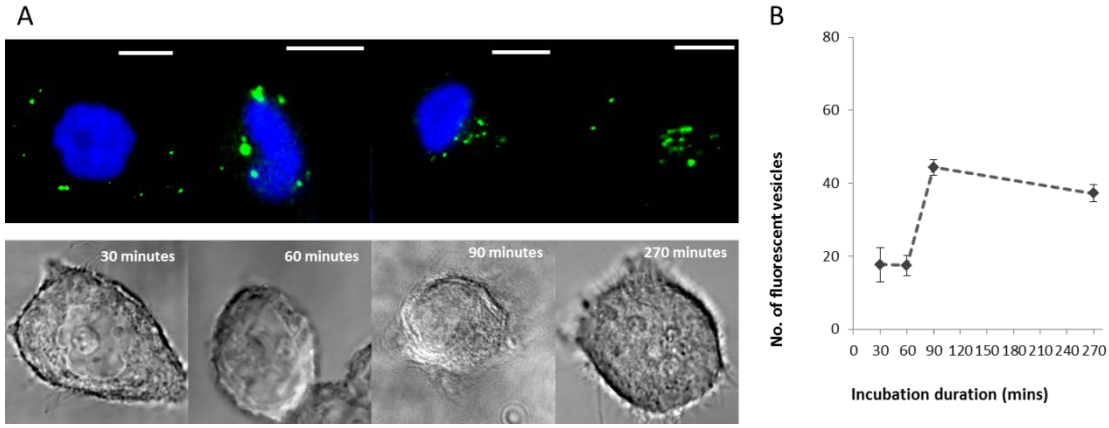

Figure 5.6 Kinetics of granzyme B uptake by T47D cells

A. Representative single frame images showing ATTO488-labelled granzyme B internalised into T47D cells. Frames were selected from the mid-point of cells (25-75% of distance from adhered surface). After 30 minutes incubation time the majority of granzyme B (green) appears to be surface bound (with a ring formation following the edge of cell seen in the bright-field image). At longer incubations the granzyme B can be seen within the cell boundary and therefore has been internalised. Granzyme B appears as well-defined spots, suggesting vesicular association rather than being free in the cytosol. The images shown depict a region 0.88µm thick. Scale bars represent 10µm. For clarity, the nucleus was stained with DAPI (blue). B. The number of distinct fluorescent spots in cells after different incubation times. This is a total count including spots within the cell and at the membrane. Data is presented as mean ± SEM for 13-28 individual cells, from at least two independent experiments.

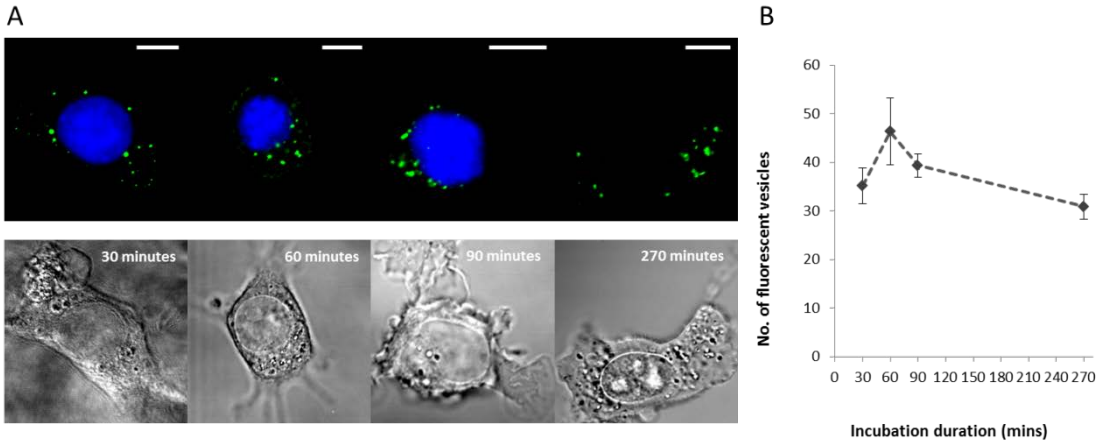

Figure 5.7 Kinetics of granzyme B uptake by 4T1 cells

A. Representative single frame images showing ATTO488-labelled granzyme B internalised into 4T1 cells. Frames were selected from the mid-point of cells (25-75% of distance from adhered surface). After 30 minutes incubation time the majority of granzyme B (green) appears to be surface bound (with a ring formation following the edge of cell seen in the bright-field image). At longer incubations the granzyme B can be seen within the cell boundary and therefore has been internalised. Granzyme B appears as well-defined spots, suggesting vesicular association rather than being free in the cytosol. The images shown depict a region 0.88µm thick. Scale bars represent 10µm. For clarity, the nucleus was stained with DAPI (blue). B. The number of distinct fluorescent spots in cells after different incubation times. This is a total count including spots within the cell and at the membrane. Data is presented as mean ± SEM for 11-37 individual cells, from at least two independent experiments.

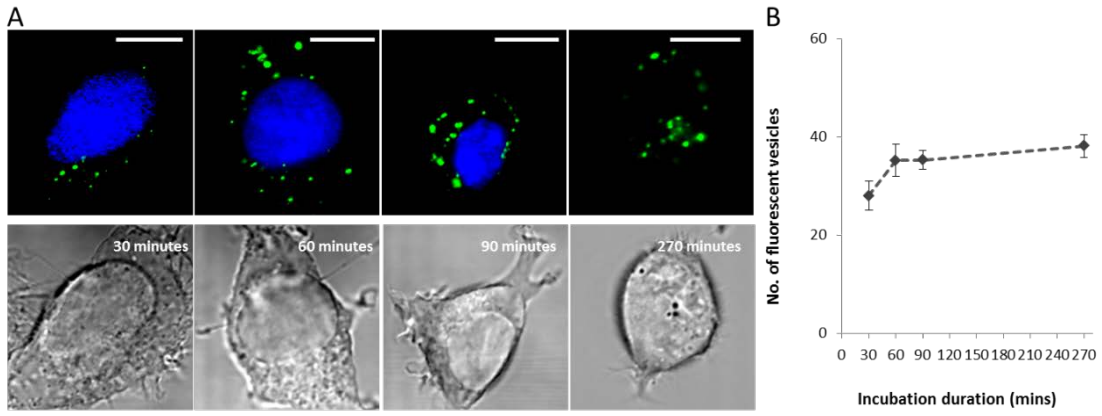

Figure 5.8 Kinetics of granzyme B uptake by CT26 cells

A. Representative single frame images showing ATTO488-labelled granzyme B internalised into CT26 cells. Frames were selected from the mid-point of cells (25-75% of distance from adhered surface). After 30 minutes incubation time the majority of granzyme B (green) appears to be surface bound (with a ring formation following the edge of cell seen in the bright-field image). At longer incubations the granzyme B can be seen within the cell boundary and therefore has been internalised. Granzyme B appears as well-defined spots, suggesting vesicular association rather than being free in the cytosol. The images shown depict a region 0.88µm thick. Scale bars represent 10µm. For clarity, the nucleus was stained with DAPI (blue). B. The number of distinct fluorescent spots in cells after different incubation times. This is a total count including spots within the cell and at the membrane. Data is presented as mean ± SEM for 9-28 individual cells, from at least two independent experiments.

The MDA-MB-231 cells showed consistent spot counts between 60 minutes (43 ± 7) and 60+210 minutes (46 ± 3), but the other human breast cancer cell lines behaved differently. The MCF7 cells showed a reduction in spot count (60 minutes = 50 ± 4, 60+210 minutes = 36 ± 3), which could indicate an accumulation of granzyme B from multiple intracellular vesicles. In contrast, there was an increase in spot count from 60 minutes (18 ± 3) to 60+30 minutes (44 ± 2) and then a slight decline at 60+210 minutes (37 ± 2) in T47D cells. One way to explain this large increase in count between 60 and 60+30 minutes could be that, during trafficking, granzyme B from one vesicle is dispersed into many. Alternatively, granzyme B may be internalised in such a low concentration that the emitted fluorescence is below the confocal detection threshold. Perhaps only after granzyme B has been trafficked to a particular part in the internalisation pathway does it accumulate to such an extent for there to be a sufficient fluorescent signal to be distinguished from the background. Of the mouse cell lines, 4T1 cells show some reduction in spot number from 60 minutes (46 ± 7) to 60+210 minutes (31 ± 3), whereas CT26 cells were remarkably consistent (60 minutes = 35 ± 3, 60+210minutes = 38 ± 2).

5.2.1 Distribution of internalised granzyme B

Spots were counted for each frame of the z-stack (**Fig 5.9**), it was possible to examine the distribution of granzyme B in cells, as has been described above for the cmHsp70 mAb and the TKDNNLLGRFELSG peptide. As for these, the majority of the internalised granzyme B was localised near to the adherent surface initially, after which it appeared to be more evenly distributed (**Figs 5.10-5.11**).

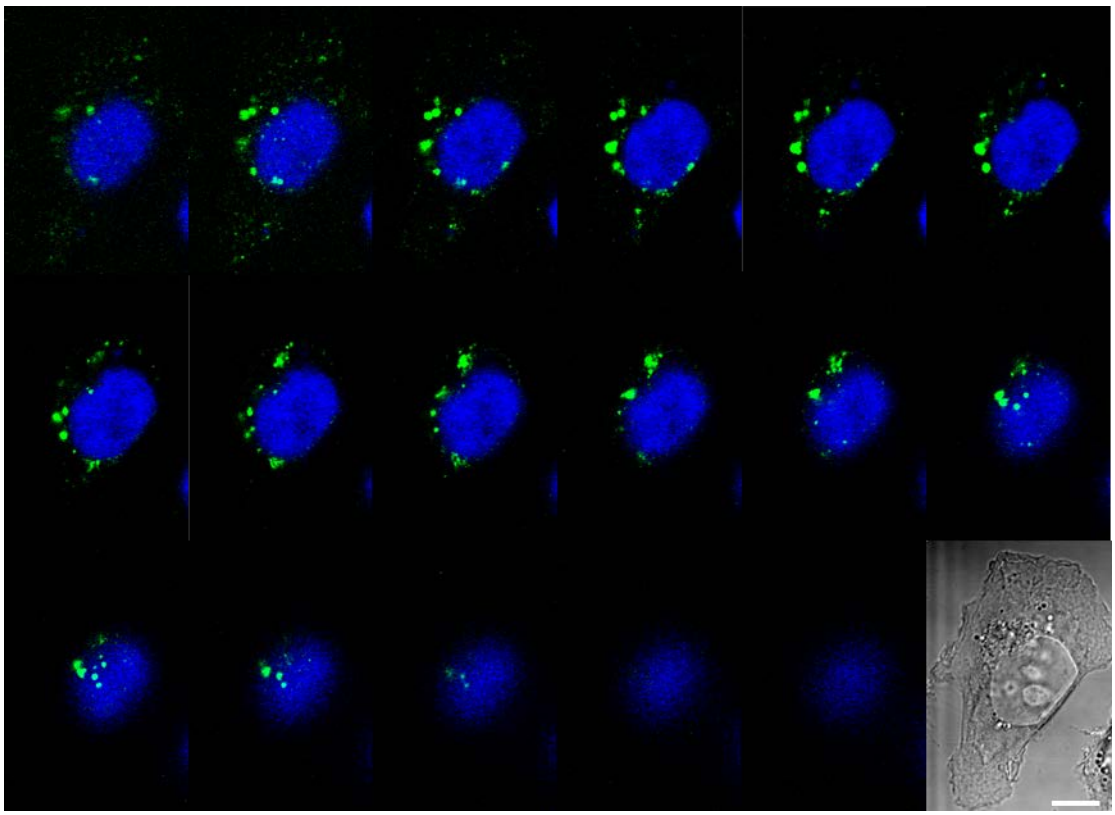

Figure 5.9 Representative montage of z-stack confocal images showing ATTO488-grB internalised into MDA-MB-231 cells.

Z-stack frames from the full height of a single MDA-MB-231 cell demonstrating distribution of ATTO488-grB following 60 minutes incubation time. Single frame images start at the adhered surface and finish at the apex of the cell. Brightfield imaging is included to help with orientation. Internalised cmHsp70.1 mAb is shown in green, DAPI staining of the nucleus is in blue. The scale bar represents 10µm.

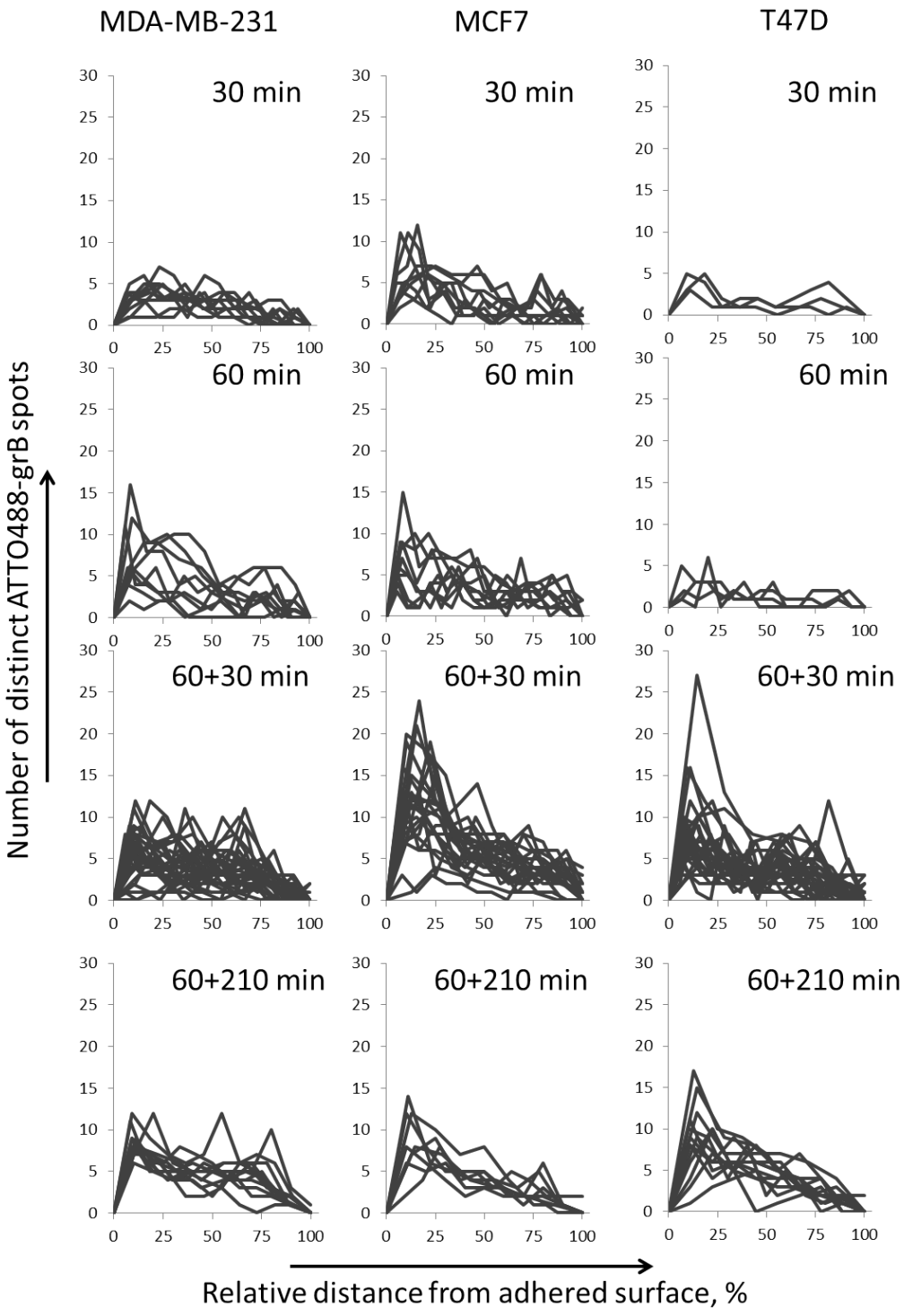

Figure 5.10 Distribution of internalised ATTO488-granzyme B In human breast cancer cell lines

Line graphs of the distribution of internalised ATTO488-labelled granzyme B in every cell imaged for MDA-MB-231, MCF7 and T47D cell lines at each time point, up to 60+210 minutes. Although ATTO488- granzyme B appears throughout the full height of the cells, there is a clear bias towards the antibody being present close to the adhered surface of the cells. This asymmetrical distribution was observed in all cell lines and at all time- points. Each line represents the profile of an individual cell, with a minimum of three cells per condition.

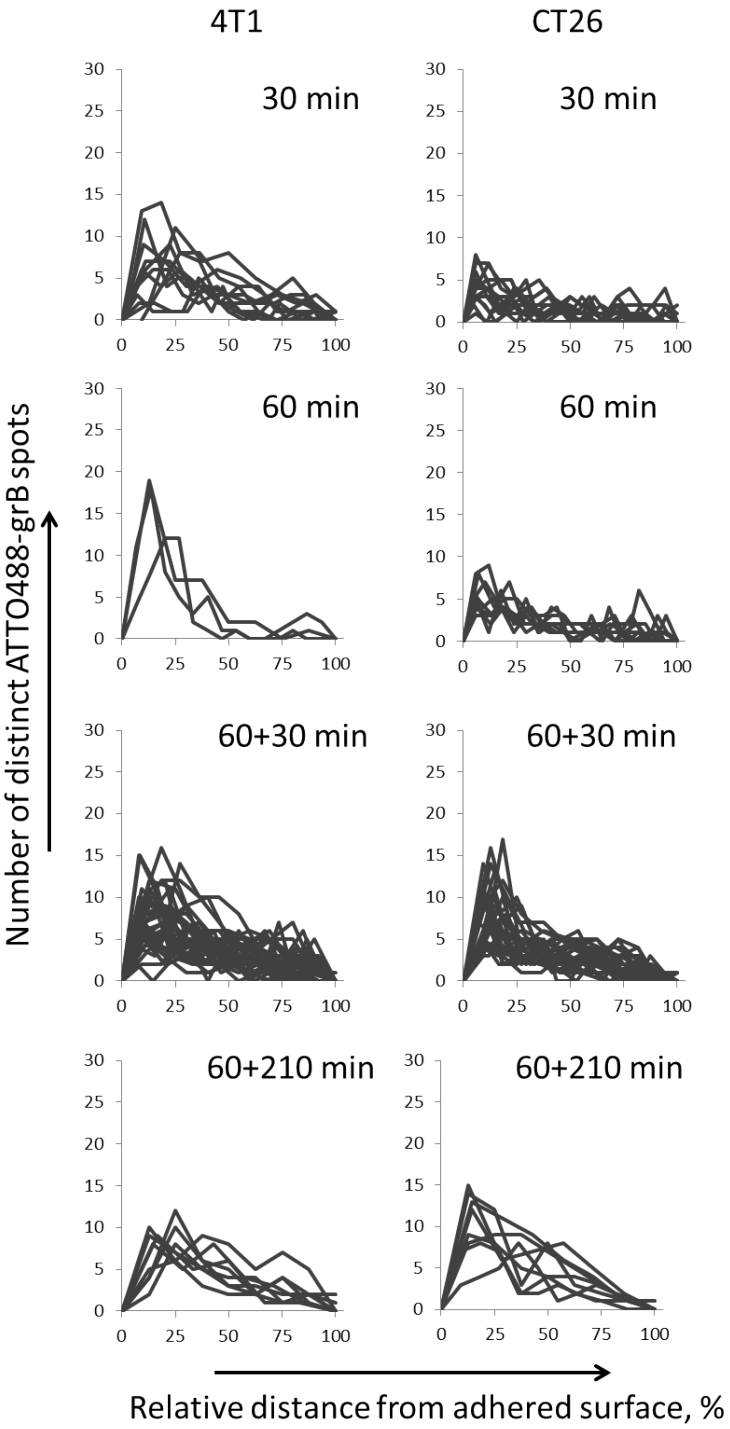

Figure 5.11 Distribution of internalised ATTO488-granzyme B In mouse cancer cell lines

Line graphs of the distribution of internalised ATTO488-labelled granzyme B in every cell imaged for 4T1 and CT26 cell lines at each time point, up to 60+210 minutes. Although ATTO488-granzyme B appears throughout the full height of the cells, there is a clear bias towards the antibody being present close to the adhered surface of the cells. This asymmetrical distribution was observed in all cell lines and at all time- points. Each line represents the profile of an individual cell, with a minimum of three cells per condition.

Granzyme B spots were also quantified, not per frame, but according to their vertical position in the cell height. Cell lines are presented separately, with all time points indicated (**Fig 5.12A-5.16A**). The amount of granzyme B in the first quartile, towards the adhered surface, was

always greater than in any other quartile, however within each cell line all time points gave very similar results. Representative images from the 60+30 minute time point are included (**Fig 5.12B-5.16B**), and presented as composite images to accurate display data included in each quartile. A single frame brightfield image is included to allow determination of the cell boundary.

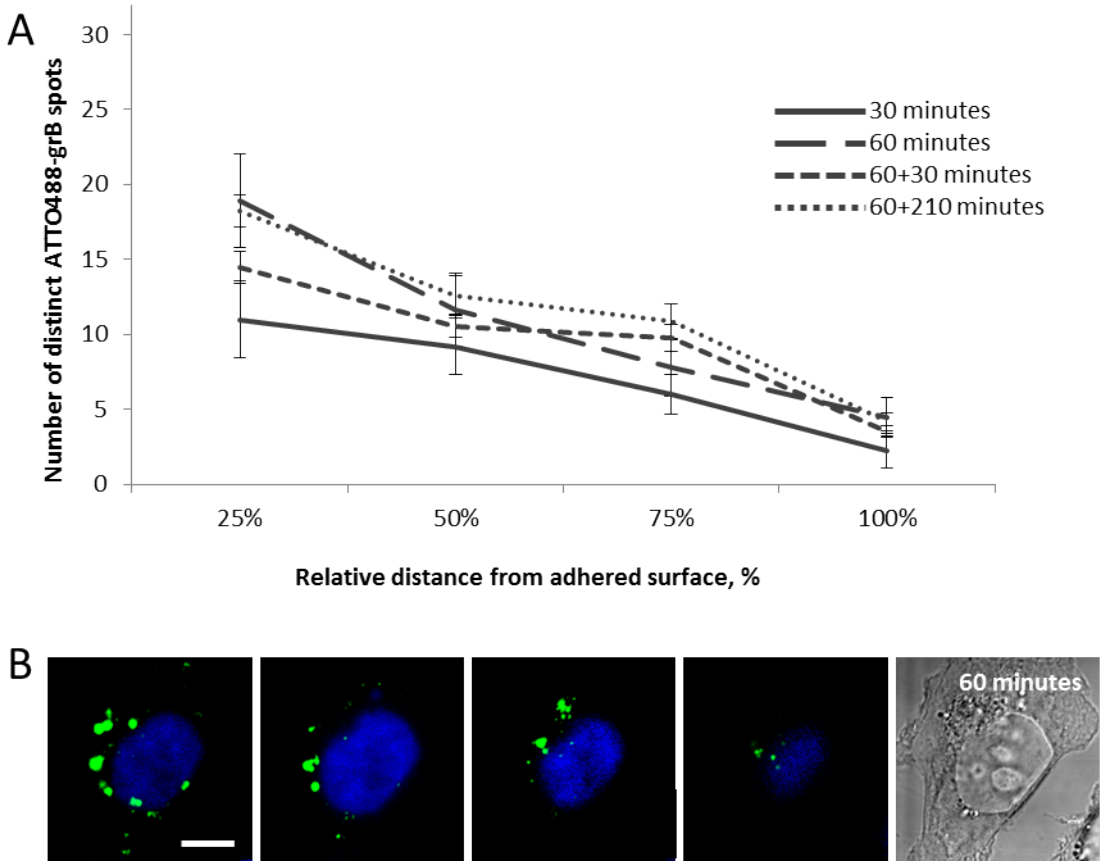

Figure 5.12 Granzyme B is pre-dominantly internalised through the adhered surface of MDA-MB-231 cells.

A. Using confocal microscopy z-stack images, the number of distinct fluorescent granzyme B spots was calculated over quartiles of the cell height. At all-time points the quartile containing the most granzyme B was the first, from the adhered surface to 25% of the cells height. The cross-sectional area of adhered cells is always greatest in this quartile and is a possible confounding factor, however due to the difficulty in calculating area accurately from bright-field images obtained on a confocal microscope it was not possible to normalise the results for area. Data are presented as mean ± SEM, n = 31. **B.** Representative images to highlight the difference between the first and last quartile (matching the adhered point and apex of the cell). It is clear to see that the first quartile contains vastly more granzyme B than the top of the cell. Fluorescent images shown are representative composites, formed as a sum of the intensity in all frames within the quartile of interests. Bright-field images are single frames from the middle of the cell. Scale bars are 10µm.

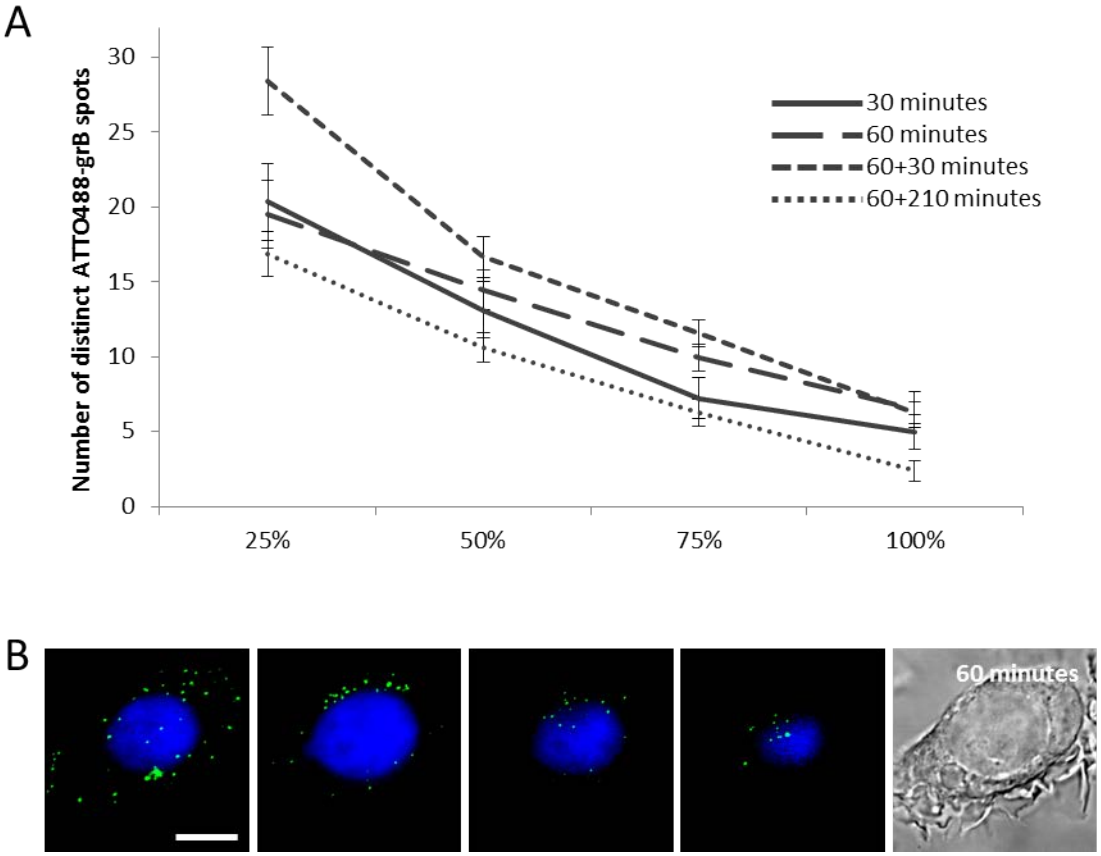

Figure 5.13 Granzyme B is pre-dominantly internalised through the adhered surface of MCF7 cells

A. Using confocal microscopy z-stack images, the number of distinct fluorescent granzyme B spots was calculated over quartiles of the cell height. At all-time points the quartile containing the most granzyme B was the first, from the adhered surface to 25% of the cells height. The cross-sectional area of adhered cells is always greatest in this quartile and is a possible confounding factor, however due to the difficulty in calculating area accurately from bright-field images obtained on a confocal microscope it was not possible to normalise the results for area. Data are presented as mean ± SEM, n = 24. **B.** Representative images to highlight the difference between the first and last quartile (matching the adhered point and apex of the cell). It is clear to see that the first quartile contains vastly more granzyme B than the top of the cell. Fluorescent images shown are representative composites, formed as a sum of the intensity in all frames within the quartile of interests. Bright-field images are single frames from the middle of the cell. Scale bars are 10µm.

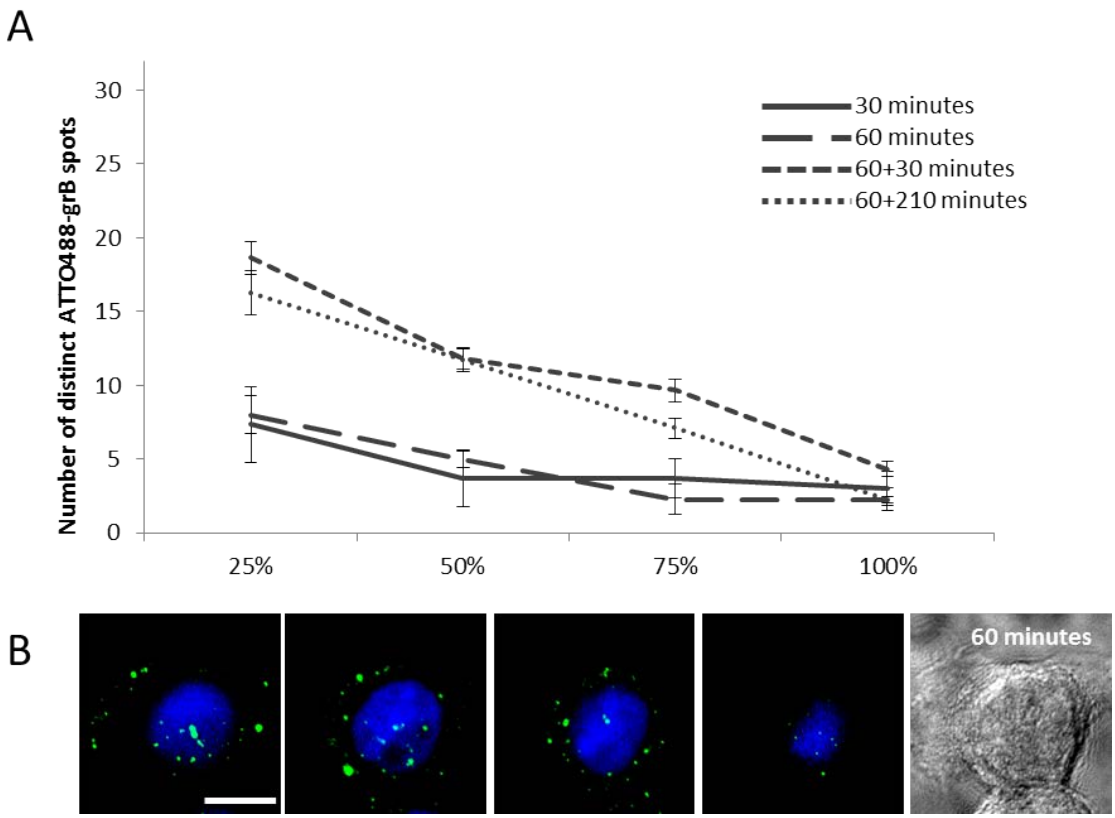

Figure 5.14 Granzyme B is pre-dominantly internalised through the adhered surface of T47D cells.

A. Using confocal microscopy z-stack images, the number of distinct fluorescent granzyme B spots was calculated over quartiles of the cell height. At all time-points the quartile containing the most granzyme B was the first, from the adhered surface to 25% of the cells height. The cross-sectional area of adhered cells is always greatest in this quartile and is a possible confounding factor, however due to the difficulty in calculating area accurately from bright-field images obtained on a confocal microscope it was not possible to normalise the results for area. Data are presented as mean ± SEM, n = 28. **B.** Representative images to highlight the difference between the first and last quartile (matching the adhered point and apex of the cell). It is clear to see that the first quartile contains vastly more granzyme B than the top of the cell. Fluorescent images shown are representative composites, formed as a sum of the intensity in all frames within the quartile of interests. Bright-field images are single frames from the middle of the cell. Scale bars are 10µm.

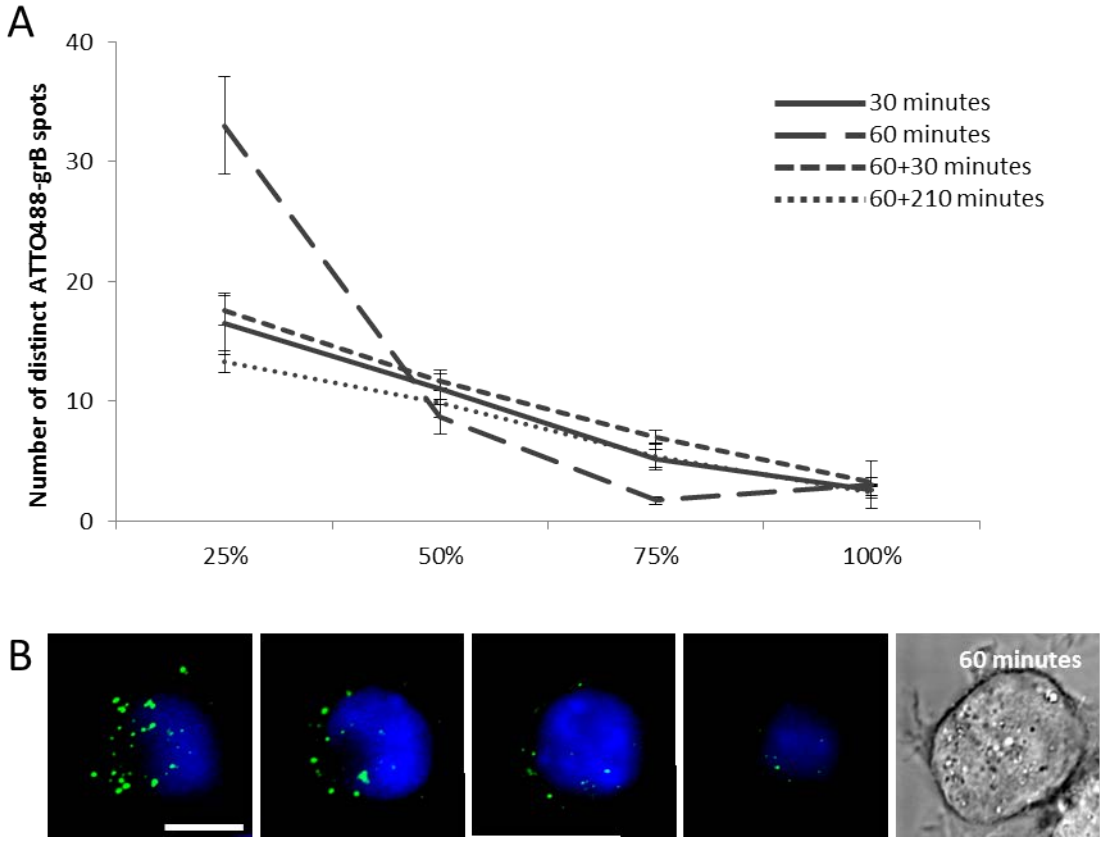

Figure 5.15 Granzyme B is pre-dominantly internalised through the adhered surface of 4T1 cells.

A. Using confocal microscopy z-stack images, the number of distinct fluorescent granzyme B spots was calculated over quartiles of the cell height. At all-time points the quartile containing the most granzyme B was the first, from the adhered surface to 25% of the cells height. The cross-sectional area of adhered cells is always greatest in this quartile and is a possible confounding factor, however due to the difficulty in calculating area accurately from bright-field images obtained on a confocal microscope it was not possible to normalise the results for area. Data are presented as mean ± SEM, n = 37. **B.** Representative images to highlight the difference between the first and last quartile (matching the adhered point and apex of the cell). It is clear to see that the first quartile contains vastly more granzyme B than the top of the cell. Fluorescent images shown are representative composites, formed as a sum of the intensity in all frames within the quartile of interests. Bright-field images are single frames from the middle of the cell. Scale bars are 10µm.

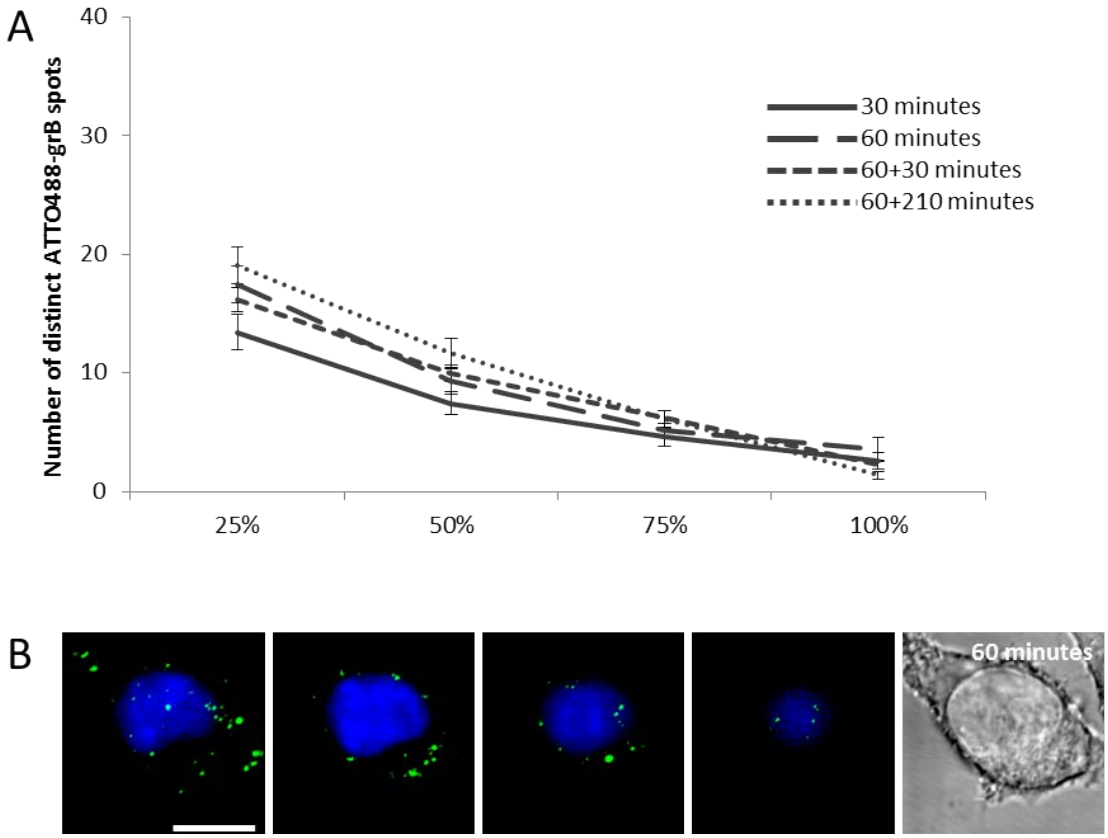

Figure 5.16 Granzyme B is pre-dominantly internalised through the adhered surface of CT26 cells.

A. Using confocal microscopy z-stack images, the number of distinct fluorescent granzyme B spots was calculated over quartiles of the cell height. At all time-points the quartile containing the most granzyme B was the first, from the adhered surface to 25% of the cells height. The cross-sectional area of adhered cells is always greatest in this quartile and is a possible confounding factor, however due to the difficulty in calculating area accurately from bright-field images obtained on a confocal microscope it was not possible to normalise the results for area. Data are presented as mean ± SEM, n = 26. **B.** Representative images to highlight the difference between the first and last quartile (matching the adhered point and apex of the cell). It is clear to see that the first quartile contains vastly more granzyme B than the top of the cell. Fluorescent images shown are representative composites, formed as a sum of the intensity in all frames within the quartile of interests. Bright-field images are single frames from the middle of the cell. Scale bars are 10µm.

5.3.2 Association of internalised granzyme B with intracellular vesicles

In order to better understand the route of memHsp70-mediated granzyme B internalisation, cells which had been incubated with ATTO488-granzyme B were formaldehyde fixed, permeabilised and stained with primary antibodies specific for one of a range of markers of intracellular vesicles and an appropriate fluorescently-labelled secondary antibody. Co-localisation was determined by visualising the overlap of fluorescence channels on the confocal images, as well as calculating Pearson's coefficient and Manders' M1 coefficient, as described above.

There was no evidence of early endosome involvement at any time, with either of the markers used (Rab4a data. MDA-MB-231: 30 min 2.1 ± 0.4%, 60 min 3.9 ± 1.4%. MCF7 30 min 5.3 ±

2.2%, 60 min 3.7 ± 1.6%. T47D 30 min 0.7 ± 0.4%, 60 min 7.2 ± 3.6%. Similar data were obtained for Rab5a) (**Table 5.1**). The initial time point used was 30 minutes; since the flow cytometry data showed that there was no appreciable uptake of granzyme B prior to this time point (**Fig 5.17**). However, this is not conclusive evidence that no internalisation into early endosomes has occurred, as it might be that such small quantities of granzyme B are internalised in each early endosome that the fluorescence is below the detectable level for the microscope.

A. Pearson Coefficient		**30 minutes**	**60 minutes**
MDA-MB-231	Rab4a	0.328 ± 0.049	0.261 ± 0.043
	Rab5a	0.119 ± 0.030	0.262 ± 0.036
MCF7	Rab4a	0.347 ±0.069	0.385 ±0.039
	Rab5a	0.134 ± 0.053	0.341 ± 0.013
T47D	Rab4a	0.398 ± 0.115	0.376 ± 0.050
	Rab5a	-0.124 ± 0.015	-

B. Manders M1 Coefficient		**30 minutes**	**60 minutes**
MDA-MB-231	Rab4a	2.1 ± 0.4 %	3.9 ± 1.4 %
	Rab5a	3.8 ± 1.8 %	5.9 ± 3.1 %
MCF7	Rab4a	5.3 ± 2.2 %	3.7 ± 1.5 %
	Rab5a	3.0 ± 1.0 %	4.3 ± 1.0 %
T47D	Rab4a	0.7 ± 0.4 %	7.2 ± 3.6 %
	Rab5a	1.9 ± 1.4 %	-

Table 5.1 Trafficking of internalised ATTO488-granzyme B to early endosomes in human breast cancer cell lines

A. Pearson coefficient of the correlation between internalised ATTO488-granzyme B and staining for the early endosome markers Rab4a and Rab5a, in human breast cancer cell lines MDA-MB-231, MCF7 and T47D. At all time-points there was a positive correlation suggesting some degree of co-localisation between the markers of interest. **B.** Manders' M1 measurement calculating the percentage of internalised ATTO488-granzyme B which was co-localised with staining for the early endosome markers Rab4a and Rab5a over different time-points. The proportion of co-localisation is low; indicating that at each time very little ATTO488-granzyme B is within early endosomes at any of the measured time-points. Data are presented as mean ± SEM from 5-6 imaged cells, from two independent experiments**.**

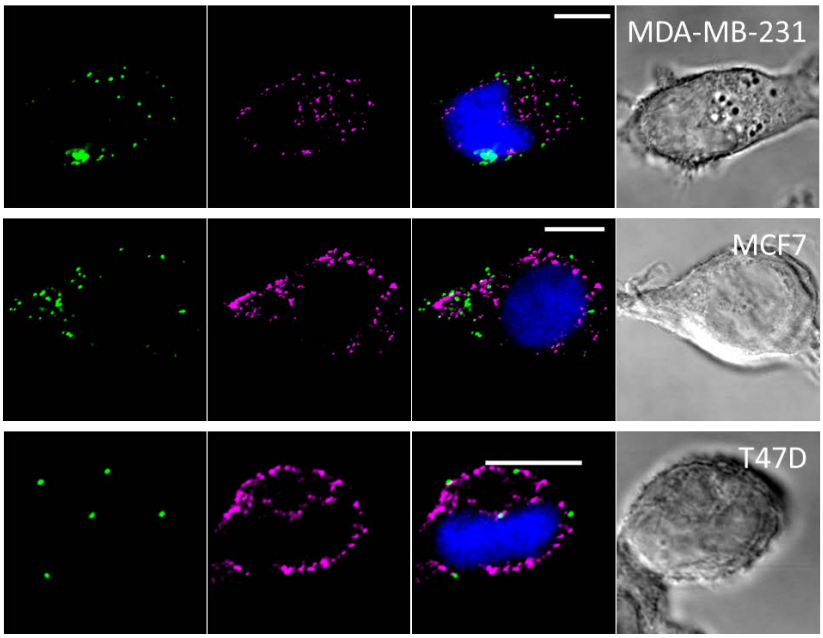

Figure 5.17 Trafficking of internalised ATTO488-granzyme B to early endosomes in human breast cancer cell lines

MDA-MB-231, MCF7 and T47D cells grown in MatTek glass bottom dishes and incubated with granzyme B for either 30 or 60 minutes were fixed, permeabilised and stained for the localisation of early endosomes using Rab4 and Rab5 as markers. Any co-localisation of ATTO488-granzyme B fluorescence (green) and endosome staining (magenta) could confirm the involvement of an early endosome pathway of ATTO488-granzyme B internalisation. Co-localisation was assessed using both Pearson's and Manders' M1 coefficients of co-localisation, as well as visual overlap of the intensity channels. Images shown are representative single frames taken from the middle region of cells incubated with ATTO488-granzyme B for 60 minutes and subsequently stained for the presence of Rab5. No co-localisation was found, nor using the Rab4 marker. After 30 minutes the majority of ATTO488-granzyme B appeared bound to the cell surface and did not co-localise with either early endosome marker. Images shown are representative single frames selected from the middle region of the cells (2nd or 3rd quartile). Scale bars are 10µm.

In contrast to the findings for early endosomes there was a clear trend between the proportion of granzyme B co-localised to Rab7a^{+} late endosomes and the memHsp70 status of the cell line (60+30 minute data. MDA-MB-231: 21.5 ± 6.5%. MCF7: 14.3 ± 4.6%. T47D: 4.7 ± 1.3%) (**Table 5.2 and Fig 5.18**). A similar profile was also seen in the alternative late endosome marker of Rab9 (**Table 5.3 and Fig 5.19**), although the proportion of co-localisation was greater in all cell lines (60+30 minute data. MDA-MB-231: 79.4 ± 5.4%. MCF7: 48.4 ± 7.2%. T47D: 38.2 ± 7.8%). An almost identical profile of co-localisation was observed for Rab11^{+} recycling endosomes (**Table 5.4 and Fig 5.20**) (60+30 minute data. MDA-MB-231: 62.9 ± 10.7%. MCF7: 48.0 ± 4.4%. T47D: 39.7 ± 5.1%).

A. Pearson Coefficient		60+30 minutes
MDA-MB-231	Rab7	0.349 ± 0.046
	Rab9	0.760 ± 0.045
	Rab11	0.400 ± 0.066
MCF7	Rab7	0.383 ± 0.049
	Rab9	0.319 ± 0.124
	Rab11	0.412 ± 0.073
T47D	Rab7	0.451 ± 0.044
	Rab9	0.517 ± 0.028
	Rab11	0.699 ± 0.029

B. Manders M1 Coefficient		60+30 minutes
MDA-MB-231	Rab7	21.5 ± 6.5 %
	Rab9	79.4 ± 5.4 %
	Rab11	62.9 ± 10.7 %
MCF7	Rab7	14.3 ± 4.6 %
	Rab9	48.4 ± 7.2 %
	Rab11	48.0 ± 4.4 %
T47D	Rab7	4.7 ± 1.3 %
	Rab9	38.2 ± 7.8 %
	Rab11	39.7 ± 5.1 %

Table 5.2 Trafficking of internalised ATTO488-granzyme B through late and recycling endosomes in human breast cancer cell lines

A. Pearson coefficient of the correlation between internalised ATTO488-granzyme B and staining for the late endosome markers Rab7 and Rab9 as well the recycling endosome marker Rab11, in human breast cancer cell lines MDA-MB-231, MCF7 and T47D. There was a positive correlation suggesting some degree of co-localisation between the markers of interest. **B.** Manders' M1 measurement calculating the percentage of internalised ATTO488-granzyme B which was co-localised with staining for the late endosome markers Rab7 and Rab9 as well as the recycling endosome marker Rab11. The proportion of co-localisation with both Rab9 and Rab11 in all cell lines positively correlates with the intensity of memHsp70 expression. Data are presented as mean ± SEM from 5-8 imaged cells, from two independent experiments.

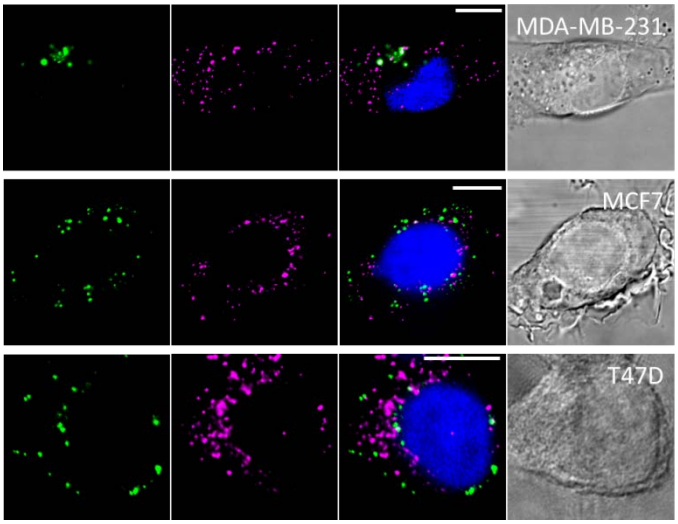

Figure 5.18 Trafficking of internalised ATTO488-granzyme B to Rab7+ late endosomes in human breast cancer cell lines

MDA-MB-231, MCF7 and T47D cells grown in MatTek™ glass bottom dishes and incubated with ATTO488-granzyme B for 60 minutes followed by a further 30 minute incubation period were then fixed, permeabilised and stained for Rab7 to indicate late endosomes. Any co-localisation of ATTO488-granzyme B fluorescence (green) and endosome staining (magenta) could be confirmation of involvement of a late endosome pathway of ATTO488-granzyme B internalisation. Co-localisation was assessed using both Pearson's and Manders' M1 coefficients of co-localisation, as well as visual overlap of the intensity channels. No co-localisation was found in any of the cell lines. Images shown are representative single frames taken from the middle region (2^{nd} or 3^{rd} quartile) of cells. Scale bars are 10µm.

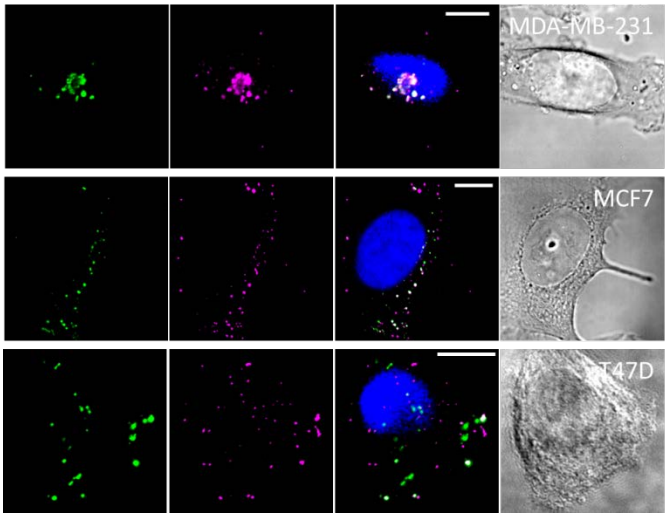

Figure 5.19 Trafficking of internalised ATTO488-granzyme B to Rab9+ recycling endosomes in human breast cancer cell lines

MDA-MB-231, MCF7 and T47D cells grown in MatTek™ glass bottom dishes and incubated with ATTO488-granzyme B for 60 minutes followed by a further 30 minute incubation period were then fixed, permeabilised and stained for Rab9 to indicate late endosomes. Any co-localisation of ATTO488-granzyme B fluorescence (green) and endosome staining (magenta) could be confirmation of involvement of a late endosome pathway of ATTO488-granzyme B internalisation. Co-localisation was assessed using both Pearson's and Manders' M1 coefficients of co-localisation, as well as visual overlap of the intensity channels. Co-localisation was found in all of the cell lines and increased with increasing expression of memHsp70. Images shown are representative single frames taken from the middle region (2^{nd} or 3^{rd} quartile) of cells. Scale bars are 10µm.

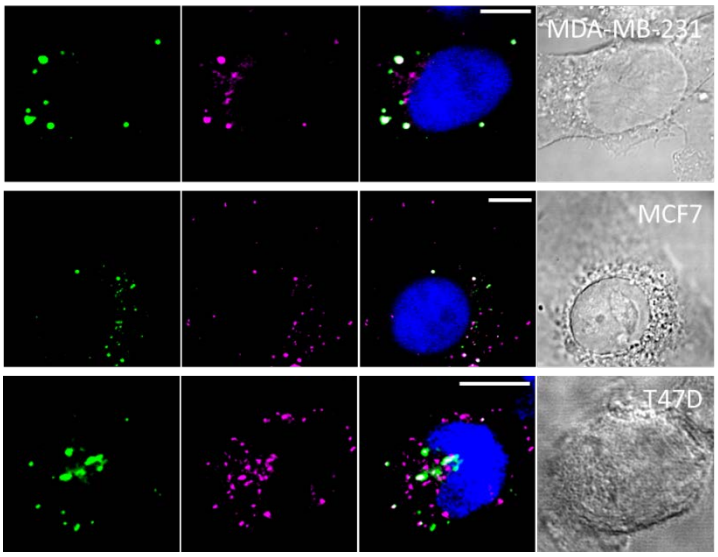

Figure 5.20 Trafficking of internalised ATTO488-granzyme B to Rab11+ recycling endosomes in human breast cancer cell lines

MDA-MB-231, MCF7 and T47D cells grown in MatTek™ glass bottom dishes and incubated with ATTO488-granzyme B for 60 minutes followed by a further 30 minute incubation period were then fixed, permeabilised and stained for Rab11 to indicate late endosomes. Any co-localisation of ATTO488-granzyme B fluorescence (green) and endosome staining (magenta) could be confirmation of involvement of recycling endosomes in the pathway of ATTO488-granzyme B internalisation. Co-localisation was assessed using both Pearson's and Manders' M1 coefficients of co-localisation, as well as visual overlap of the intensity channels. Co-localisation was found in all of the cell lines, with the proportion increasing in line with the expression of memHsp70. Images shown are representative single frames taken from the middle region (2^{nd} or 3^{rd} quartile) of cells. Scale bars are 10µm.

Although co-localisation with LAMP1 and LAMP2 lysosomes was similar, unlike with Rab9 and Rab11 there was a negative trend between co-localisation and memHsp70 status (60+30 minute, LAMP2 data. MDA-MB-231: 9.8 ± 2.5%. MCF7: 18.9 ± 2.2%. T47D: 20.3 ± 7.6%. Similar data for LAMP1 but not shown) (**Table 5.3 and Fig 5.21**).

A. Pearson Coefficient		60+30 minutes
MDA-MB-231	LAMP1	0.134 ± 0.066
	LAMP2	0.212 ± 0.048
MCF7	LAMP1	0.425 ± 0.054
	LAMP2	0.378 ± 0.015
T47D	LAMP1	0.408 ± 0.084
	LAMP2	0.412 ± 0.073

B. Manders M1 Coefficient		60+30 minutes
MDA-MB-231	LAMP1	6.8 ± 6.2 %
	LAMP2	9.8 ± 2.5 %
MCF7	LAMP1	15.7 ± 3.0 %
	LAMP2	18.9 ± 2.2 %
T47D	LAMP1	22.0 ± 7.0 %
	LAMP2	20.3 ± 7.6 %

Table 5.3 Trafficking of internalised ATTO488-granzyme B to lysosomes in human breast cancer cell lines

A. Pearson coefficient of the correlation between internalised ATTO488-granzyme B and staining for the lysosomal markers LAMP1 and LAMP2, in human breast cancer cell lines MDA-MB-231, MCF7 and T47D. There was a positive correlation suggesting some degree of co-localisation between the markers of interest. **B.** Manders' M1 measurement calculating the percentage of internalised ATTO488-granzyme B which was co-localised with staining for the lysosomal markers LAMP1 and LAMP2. The proportion of co-localisation with both markers negatively correlates with the intensity of memHsp70 expression on cell lines. Data are presented as mean ± SEM from 5-6 imaged cells, from two independent experiments.

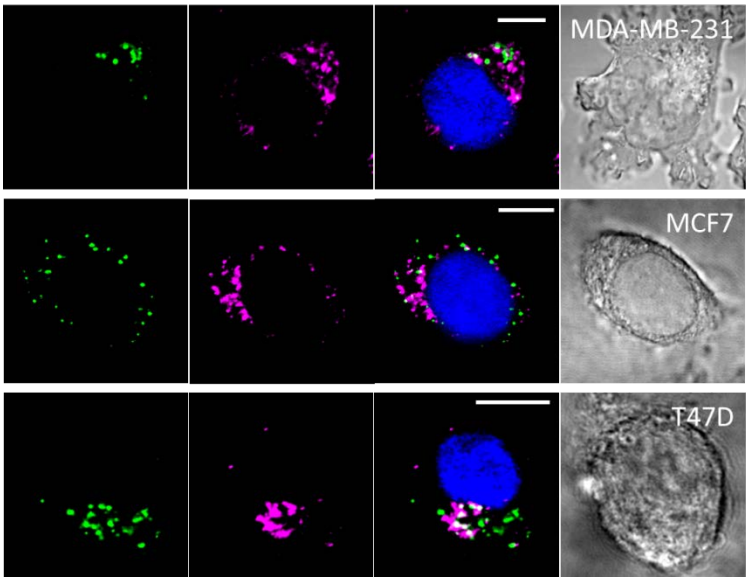

Figure 5.21 Trafficking of internalised ATTO488-granzyme B to lysosomes in human breast cancer cell lines

MDA-MB-231, MCF7 and T47D cells grown in MatTek glass bottom dishes and incubated with ATTO488-granzyme B for 60 minutes followed by a further 30 minutes incubation were then fixed, permeabilised and stained for LAMP1 and LAMP2 to indicate lysosomes endosomes. Any co-localisation (white) of ATTO488-granzyme B fluorescence (green) and lysosome staining (magenta) could be confirmation of involvement of a late endosome pathway of ATTO488-granzyme B internalisation. Co-localisation was assessed using both Pearson's and Manders' M1 coefficients of co-localisation, as well as visual overlap of the intensity channels. Co-localisation was found in all of the cell lines, increasing over time. Images shown are representative single frames taken from the middle region (2^{nd} or 3^{rd} quartile) of cells stained for LAMP2 expression. Scale bars are 10µm.

Co-localisation of granzyme B with mitochondria was also observed, but only at a time point later than that when co-localisation was observed with other markers (MDA-MB-231: 60+30 minutes 5.5 ± 1.7%, 60+210 minutes 23.0 ± 6.2%. MCF7: 60+30 minutes 3.8 ± 2.4%, 60+210 minutes 17.8 ± 3.0%. T47D: 60+30 minutes 0.4 ± 0.2%, 60+210 minutes 15.0 ± 3.1%) (**Table 5.4 and Fig 5.22)**.

A. Pearson Coefficient	60+30 minutes	60+210 minutes
MDA-MB-231	0.384 ± 0.031	0.413 ± 0.031
MCF7	0.365 ± 0.061	0.473 ± 0.053
T47D	0.375 ± 0.060	0.565 ± 0.029

B. Manders M1 Coefficient	60+30 minutes	60+210 minutes
MDA-MB-231	5.5 ± 1.7 %	23.0 ± 6.2 %
MCF7	3.8 ± 2.4 %	17.8 ± 3.0 %
T47D	0.4 ± 0.2 %	15.0 ± 3.1 %

Table 5.4 Trafficking of internalised ATTO488-granzyme B to mitochondria in human breast cancer cell lines

A. Pearson coefficient of the correlation between internalised ATTO488-granzyme B and staining for the mitochondria in breast cancer cell lines MDA-MB-231, MCF7 and T47D after 60 minutes incubation with ATTO488-granzyme B followed by a further 30 or 210 minute incubation. At both time-points there was a positive correlation suggesting some degree of co-localisation between the markers of interest. **B.** Manders' M1 measurement calculating the percentage of internalised ATTO488-granzyme B which was co-localised with staining for the mitochondria over different time-points. The proportion of ATTO488-granzyme B co-localisation with the mitochondria increases over time in all cell lines, and positively correlates to the expression of memHsp70. Data are presented as mean ± SEM from 9-12 imaged cells, from at least two independent experiments.

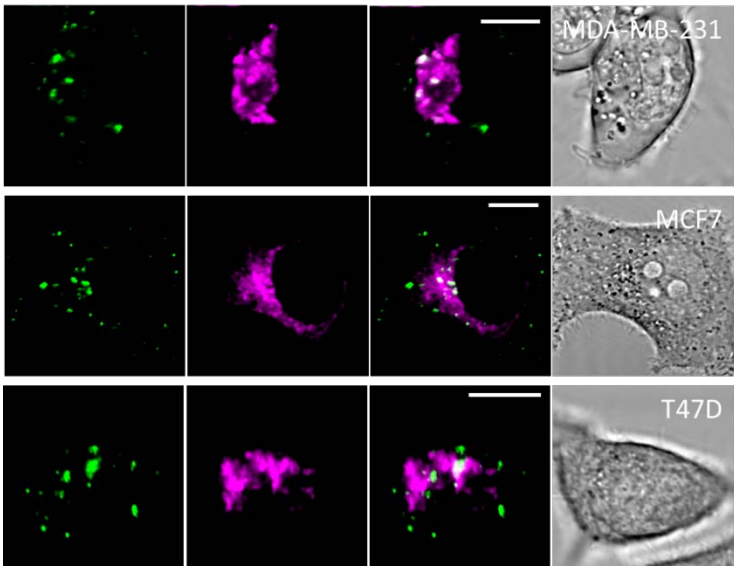

Figure 5.22 Trafficking of internalised ATTO488-granzyme B to mitochondria in human breast cancer cell lines

MDA-MB-231, MCF7 and T47D cells grown in MatTek™ glass bottom dishes and incubated with ATTO488-granzyme B for 60 minutes followed by a further 30 or 210 minute incubation were then stained with MitoID™ red to show the mitochondria. Any co-localisation (white) of ATTO488-granzyme B fluorescence (green) and mitochondrial staining (magenta) could be confirmation of trafficking of ATTO488-granzyme B to mitochondria. Co-localisation was assessed using both Pearson's and Manders' M1 coefficients of co-localisation, as well as visual overlap of the intensity channels. Co-localisation was found in all of the cell lines, increasing over time. Images shown are representative single frames taken from the middle region (2nd or 3rd quartile) of cells incubated with ATTO488-granzyme B for 60+210 minutes. Scale bars are 10µm.

Similar to the situation with the human-derived cell lines, there was negligible co-localisation of granzyme B with Rab4a^{+} and Rab5^{+} early endosomes at any time in 4T1 and CT26 cells (4T1:

30 minutes 2.8 ± 1.3%, 60 minutes 3.1 ± 2.2%. CT26: 30 minutes 5.0 ± 0.8%, 60 minutes 3.8 ± 1.6%) (**Table 5.5 and Fig 5.23**).

A. Pearson Coefficient		**30 minutes**	**60 minutes**
4T1	Rab4a	0.237 ± 0.033	0.300 ± 0.036
	Rab5a	0.292 ± 0.065	0.447 ± 0.092
CT26	Rab4a	0.318 ± 0.033	0.294 ± 0.015
	Rab5a	0.211 ± 0.016	0.220 ± 0.017

B. Manders M1 Coefficient		**30 minutes**	**60 minutes**
4T1	Rab4a	2.8 ± 1.3 %	3.1 ± 2.2 %
	Rab5a	9.9 ± 3.1 %	1.9 ± 0.8 %
CT26	Rab4a	5.0 ± 0.8 %	3.8 ± 1.6 %
	Rab5a	3.1 ± 0.8 %	3.2 ± 1.0 %

Table 5.5 Trafficking of internalised ATTO488-granzyme B to early endosomes in murine cancer cell lines

A. Pearson coefficient of the correlation between internalised and staining for the early endosome markers Rab4a and Rab5a, in mouse cancer cell lines 4T1 and CT26. At both time-points there was a positive correlation suggesting some degree of co-localisation between the markers of interest. **B.** Manders' M1 measurement calculating the percentage of internalised ATTO488-granzyme B which was co-localised with staining for the early endosome markers Rab4a and Rab5a over different time-points. The proportion of co-localisation is low; indicating that at each time very little ATTO488-granzyme B is within early endosomes. Data are presented as mean ± SEM from 6-9 imaged cells, from two independent experiments**.**

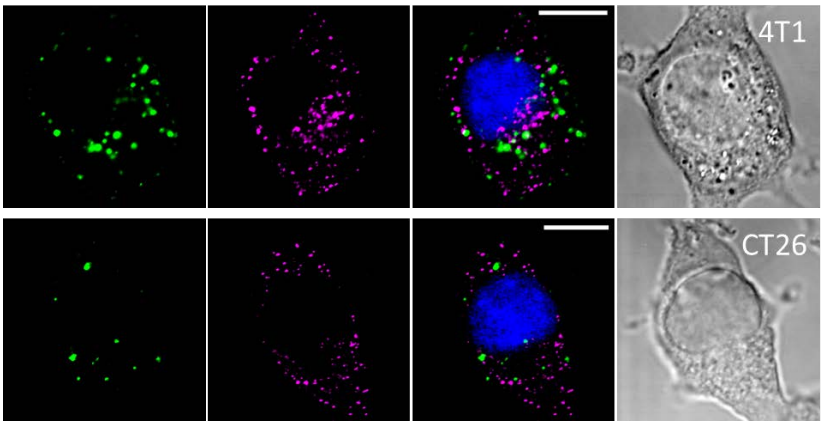

Figure 5.23 Trafficking of internalised ATTO488-granzyme B to early endosomes in murine cancer cell lines

4T1 and CT26 cells grown in MatTek™ glass bottom dishes and incubated with ATTO488-granzyme B for 30 or 60 minutes were fixed, permeabilised and stained for the localisation of early endosomes using Rab4 and Rab5 as markers. Any co-localisation of ATTO488-granzyme B fluorescence (green) and endosome staining (magenta) could be confirmation of involvement of an early endosome pathway of ATTO488-granzyme B internalisation. Co-localisation was assessed using both Pearson's and Manders' M1 coefficients of co-localisation, as well as visual overlap of the intensity channels. Images shown are representative single frames taken from the middle region (2nd or 3rd quartile) of cells incubated with ATTO488-granzyme B for 30 minutes and subsequently stained for the presence of Rab5. No co-localisation was found, nor using the Rab4 marker. Scale bars are 10µm.

As seen with the human-derived cell lines, there was a small degree of granzyme B co-localisation with Rab7$^+$ late endosomes which followed in line with the memHsp70 status of the cell lines (60+30 minute data. 4T1:26.6 ± 5.1%. CT26: 8.5 ± 1.6%) (**Table 5.6 and Fig 5.24**). A similar profile was observed with the alternative late endosomal marker, Rab9 (**Table 5.6 and Fig 5.25**), and a greater proportion of granzyme B co-localised with Rab9$^+$ late endosomes than with Rab7$^+$ late endosomes (60+30 minute data. 4T1: 31.7 ± 4.3%. CT26 26.4 ± 4.3%).

Although granzyme B also co-localised with Rab11$^+$ recycling endosomes the profile in the mouse lines was different to that seen in the human cell lines. All three human cell lines exhibited a smaller proportion of granzyme B co-localised to Rab11$^+$ vesicles than those expressing Rab9, whereas in both mouse lines the situation was reversed, in that the greater proportion of co-localisation was observed in Rab11$^+$ vesicles (60+30 minute data. 4T1: 60.9 ± 4.6%. CT26: 31.4 ± 5.5%) (**Table 5.6 and Fig 5.26**).

A. Pearson Coefficient		**60+30 minutes**
4T1	Rab7	0.413 ± 0.027
	Rab9	0.384 ± 0.026
	Rab11	0.562 ± 0.092
CT26	Rab7	0.363 ± 0.020
	Rab9	0.373 ± 0.096
	Rab11	0.520 ± 0.036

B. Manders M1 Coefficient		**60+30 minutes**
4T1	Rab7	26.6 ± 5.1 %
	Rab9	31.7 ± 4.3 %
	Rab11	60.9 ± 4.6 %
CT26	Rab7	8.5 ± 1.6 %
	Rab9	26.4 ± 4.3 %
	Rab11	31.4 ± 5.5 %

Table 5.6 Trafficking of internalised ATTO488-granzyme B to late and recycling endosomes in murine cancer cell lines

A. Pearson coefficient of the correlation between internalised ATTO488-granzyme B and staining for the late endosome markers Rab7 and Rab9 as well the recycling endosome marker Rab11, in mouse cancer cell lines 4T1 and CT26. Cells were incubated with granzyme B for 60 minutes followed by a further 30 minutes incubation and there was a positive correlation suggesting some degree of co-localisation between the markers of interest. **B.** Manders' M1 measurement calculating the percentage of internalised ATTO488-granzyme B which was co-localised with staining for the late endosome markers Rab7 and Rab9 as well as the recycling endosome marker Rab11. The proportion of co-localisation with both Rab9 and Rab11 in all cell lines positively correlates with the intensity of memHsp70 expression. Data are presented as mean ± SEM for 6-9 imaged cells, from two independent experiments.

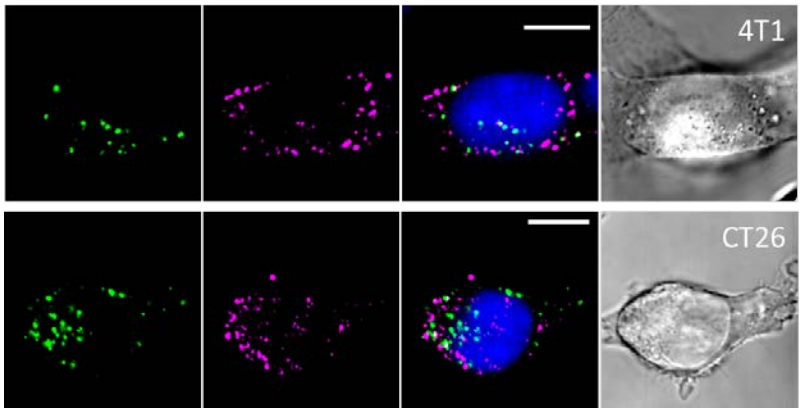

Figure 5.24 Trafficking of internalised ATTO488-granzyme B to Rab7+ late endosomes in murine cancer cell lines

4T1 and CT26 cells grown in MatTek™ glass bottom dishes and incubated with ATTO488-granzyme B for 60 minutes followed by a further 30 minute incubation were fixed, permeabilised and stained for Rab7 to indicate late endosomes. Any co-localisation of ATTO488-granzyme B fluorescence (green) and endosome staining (magenta) could be confirmation of involvement of a late endosome pathway of granzyme B internalisation. Co-localisation was assessed using both Pearson's and Manders' M1 coefficients of co-localisation, as well as visual overlap of the intensity channels. No co-localisation was found in any of the cell lines. Images shown are representative single frames taken from the middle region (2nd or 3rd quartile) of cells. Scale bars are 10µm.

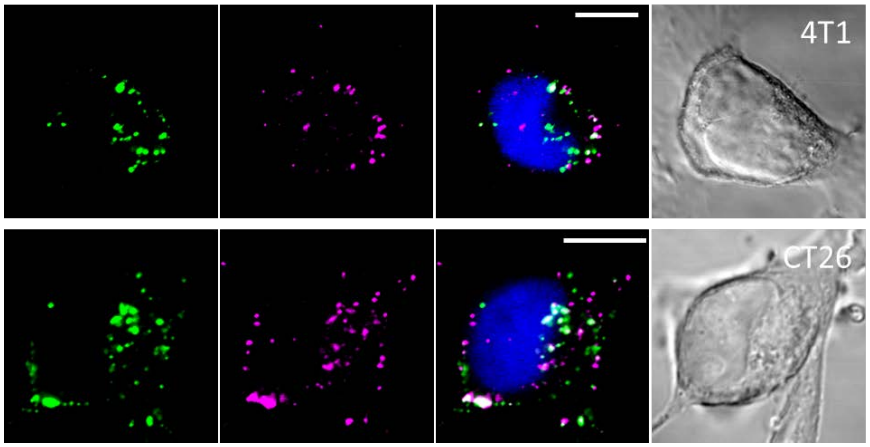

Figure 5.25 Trafficking of internalised ATTO488-granzyme B to Rab9+ late endosomes in murine cancer cell lines

4T1 and CT26 cells grown in MatTek™ glass bottom dishes and incubated with ATTO488-granzyme B for 60 minutes followed by a further 30 minute incubation period were then fixed, permeabilised and stained for Rab9 to indicate late endosomes. Any co-localisation of ATTO488-granzyme B fluorescence (green) and endosome staining (magenta) could be confirmation of involvement of a late endosome pathway of ATTO488-granzyme B internalisation. Co-localisation was assessed using both Pearson's and Manders' M1 coefficients of co-localisation, as well as visual overlap of the intensity channels. Co-localisation was found in all of the cell lines and increased in line with increasing expression of memHsp70. Images shown are representative single frames taken from the middle region (2nd or 3rd quartile) of cells. Scale bars are 10µm.

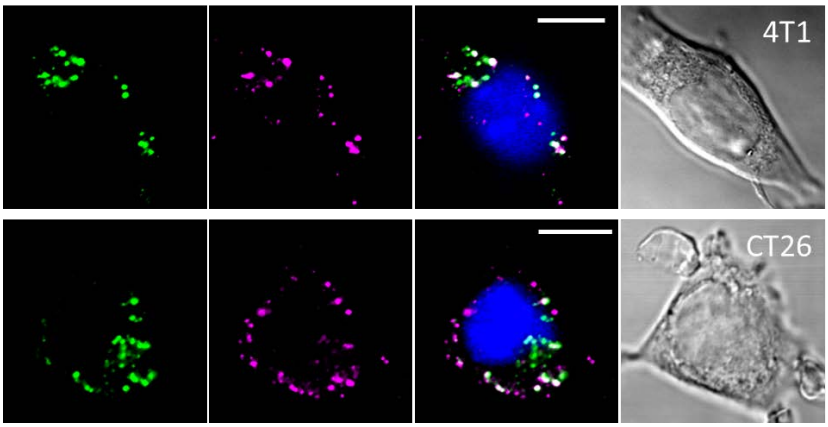

Figure 5.26 Trafficking of internalised ATTO488-granzyme B to Rab11+ recycling endosomes in murine cancer cell lines

4T1 and CT26 cells grown in MatTek™ glass bottom dishes and incubated with ATTO488-granzyme B for 60 minutes followed by a further 30 minute incubation period were then fixed, permeabilised and stained for Rab11 to indicate late endosomes. Any co-localisation of ATTO488-granzyme B fluorescence (green) and endosome staining (magenta) could be confirmation of involvement of recycling endosomes in the pathway of ATTO488-granzyme B internalisation. Co-localisation was assessed using both Pearson's and Manders' M1 coefficients of co-localisation, as well as visual overlap of the intensity channels. Co-localisation was found in all of the cell lines and increased in line with increasing expression of memHsp70. Images shown are representative single frames taken from the middle region (2nd or 3rd quartile) of cells. Scale bars are 10µm.

The two mouse cells lines were also investigated for the possibility of internalised granzyme B co-localising to lysosomes. Granzyme B co-localised with LAMP2^{+} lysosomes in both cells lines at almost identical percentages (60+30 minute data. 4T1: 35.4 ± 5.1%. CT26: 33.7 ± 4.8%) (**Table 5.7 and Fig 5.27**).

A. Pearson Coefficient		**60+30 minutes**
4T1	LAMP2	0.408 ± 0.073
CT26	LAMP2	0.485 ± 0.030
B. Manders M1 Coefficient		**60+30 minutes**
4T1	LAMP2	35.4 ± 5.1 %
CT26	LAMP2	33.7 ± 4.8 %

Table 5.7 Trafficking of internalised ATTO488-granzyme B to lysosomes in murine cancer cell lines

A. Pearson coefficient of the correlation between internalised ATTO488-granzyme B and staining for the lysosome marker LAMP2, in the mouse cancer cell lines 4T1 and CT26 60 minutes incubation with granzyme B followed by a further 30 minute incubation. There was a positive correlation suggesting some degree of co-localisation between the markers of interest. **B.** Manders' M1 measurement calculating the percentage of internalised ATTO488-granzyme B which was co-localised with staining for the lysosome marker LAMP2. There is a similar proportion of internalised ATTO488-granzyme B that co-localises with LAMP2 in both cell lines. Data are presented as mean ± SEM from 5-6 imaged cells, from two independent experiments.

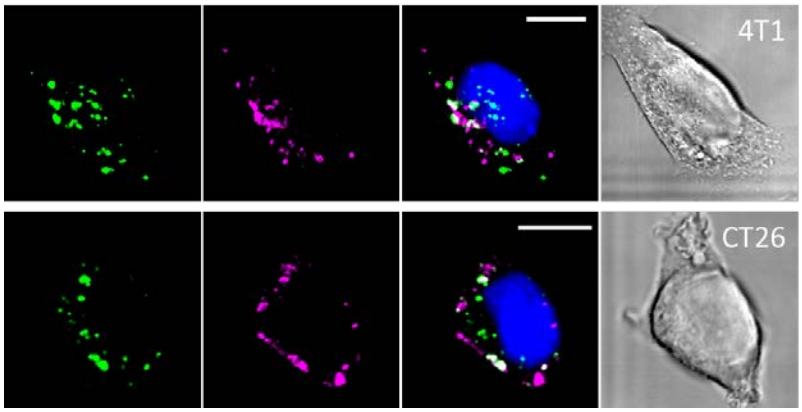

Figure 5.27 Trafficking of internalised ATTO488-granzyme B to lysosomes in murine cancer cell lines

4T1 and CT26 cells grown in MatTek™ glass bottom dishes and incubated with ATTO488-granzyme B for 60 minutes followed by a further 30 minute incubation period were then fixed, permeabilised and stained for LAMP2 to indicate lysosomes. Any co-localisation of ATTO488-granzyme B fluorescence (green) and lysosome staining (magenta) could be confirmation of involvement of lysosome in the internalisation of granzyme B. Co-localisation was assessed using both Pearson's and Manders' M1 coefficients of co-localisation, as well as visual overlap of the intensity channels. Co-localisation was found in both of the cell lines but seemingly independent of memHsp70 expression. Images shown are representative single frames taken from the middle region (2^{nd} or 3^{rd} quartile) of cells. Scale bars are 10µm.

The findings relating to the co-localisation of granzyme B with mitochondria in the mouse cell lines also differed from those that were obtained with the human cell lines. Rather than co-localisation only being evident at the very latest time point, granzyme B co-localisation with mitochondria appeared earlier in both of the mouse cell lines (**Table 5.8 and Fig 5.28**) (4T1: 60+30 min 20.3 ± 2.7%, 60+210 min 33.7 ± 3.6%. CT26: 60+30 min 11.6 ± 4.2%, 60+210 min 21.7 ± 4.7%). The observed co-localisation increased with increasing expression of memHsp70 on the cells.

A. Pearson Coefficient	60+30 minutes	60+210 minutes
4T1	0.650 ± 0.031	0.490 ± 0.022
CT26	0.493 ± 0.071	0.461 ± 0.024

B. Manders M1 Coefficient	60+30 minutes	60+210 minutes
4T1	20.3 ± 2.7 %	33.7 ± 3.6 %
CT26	11.6 ± 4.2 %	21.7 ± 4.7 %

Table 5.8 Trafficking of internalised ATTO488-granzyme B to mitochondria in murine cancer cell lines

A. Pearson coefficient of the correlation between internalised ATTO488-granzyme B and staining for the mitochondria in cancer cell lines 4T1 and CT26 after 60 minutes incubation with granzyme B followed by a further 30 or 210 minutes incubation. At both time-points there was a positive correlation suggesting some degree of co-localisation between the markers of interest. **B.** Manders' M1 measurement calculating the percentage of internalised ATTO488-granzyme B which was co-localised with staining for the mitochondria over different time-points. The proportion of ATTO488-granzyme B co-localisation with the mitochondria increases over time in both cell lines, and positively correlates to the expression of memHsp70. Data are presented as mean ± SEM from 8-9 imaged cells, from two independent experiments.

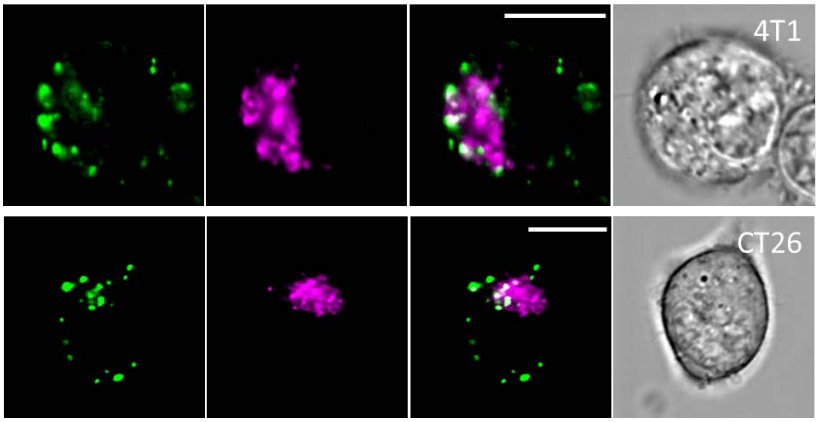

Figure 5.28 Trafficking of internalised ATTO488-granzyme B to mitochondria in murine cancer cell lines

4T1 and CT26 cells grown in MatTek™ glass bottom dishes and incubated with ATTO488-granzyme B for 60 minutes followed by a further 30 or 210 minutes incubation were stained with MitoID™ red to show the mitochondria. Any co-localisation (white) of ATTO488-granzyme B fluorescence (green) and mitochondrial staining (magenta) could be confirmation of trafficking of granzyme B to mitochondria. Co-localisation was assessed using both Pearson's and Manders' M1 coefficients of co-localisation, as well as visual overlap of the intensity channels. Co-localisation was found in both of the cell lines and increased over time. Images shown are representative single frames taken from the middle region (2nd or 3rd quartile) of cells incubated with ATTO488-granzyme B for 60+210 minutes. Scale bars are 10µm.

5.4 Induction of apoptosis

Granzyme B released by NK cells or cytotoxic $CD8^+$ T cells undergoes perforin-mediated internalisation into target cells, after which it cleaves one of a number of substrates within the apoptosis pathway to induce cell death. Although it has herein been clearly demonstrated that memHsp70 can also mediate the internalisation of granzyme B, it is not known whether the subsequent intracellular trafficking route allows granzyme B access to apoptosis-inducing pathways and machinery. Initially, detection of both active caspase-3 and the presence of surface phosphatidylserine (by way of staining with Annexin V) were employed. As activation of caspase-3 is an intracellular process, detection is only possible after fixing and permeabilising the cells, whereas Annexin V staining can only be conducted on live cells.

All cells were grown in 24 well plates and, after seeding, were allowed 48 hours to grow before being incubated with recombinant human granzyme B. As serum has been found to interfere with the binding and uptake of granzyme B, it was necessary to first aspirate the growth medium and wash cells once in PBS. This was also aspirated and replaced with PBS containing 4µg/ml granzyme B. Cells were then incubated for 60 minutes at 37°C. Control cells were washed in the same manner, but the negative controls received PBS only and the positive controls PBS containing camptothecin for the incubation period. After the incubation period was completed, fresh growth medium was administered to all wells. If cells were already undergoing apoptosis during this time, it could have been possible for them to detach from the plate. As it was crucial to ensure that these cells were not removed from the culture, the PBS containing granzyme B was not removed, but the fresh medium simply added to the well. Although the presence of the PBS would serve to dilute the medium, there was such a large disparity in volumes (1 mL medium and 200µL PBS/granzyme B) it was felt that the cells would suffer no adverse effects. This was confirmed on the basis of observations that there was no viability loss in control cultures, in which cells had been incubated in PBS.

The results of the experiments relating to the capacity of granzyme B to induce caspase-3 activation proved to be inconclusive. There were very few significant increases to the levels of active caspase-3 following granzyme B treatment, and the results for the controls that had been incubated with camptothecin were also variable (**Fig 5.29 and 5.30**). There were also no apparent effects on Annexin V binding (data not shown).

That the camptothecin control did not consistently induce activation of caspase-3 reduces confidence in the capacity of this approach to determine the induction of apoptosis. At no time was there significant evidence of caspase-3 activation in T47D cells in response to camptothecin treatment, however there was in both MDA-MB-231 and MCF7 cells. In the

human cell lines there was only instance of granzyme B incubation resulting in significant levels of caspase-3 activation, with MDA-MB-231 cells 4 hours after granzyme B introduction.

A very similar scenario was observed with the mouse cell lines, with the only significant induction of caspase-3 activation being seen in CT26 cells after 4 hours treatment with granzyme B. Whilst the activation of caspase-3 in 4T1 cells at the same time point was approaching significance, it was not achieved. At the later time points of 24 and 48 hours after granzyme B treatment, the activation of caspase-3 was indistinguishable from the level seen in untreated cells. Whilst the mean activation of caspase-3 resulting from camptothecin incubation was always greater than in the untreated cells, the differences were not always significant.

Of the human cell lines, the two which express the greatest amount of memHsp70 were the two found to exhibit significant levels of caspase-3 activation 4 hours after granzyme B introduction, whilst the low memHsp70 expresser T47D did not. Knowing that granzyme B is internalised through memHsp70, this finding is not altogether surprising. The limited expression of memHsp70 on T47D cells may not be capable of internalising sufficient granzyme B within the time frame to induce apoptosis. As earlier optimisation experiments showed, the addition of serum into the system interfered with the memHsp70-mediated uptake of granzyme B into cells. The addition of growth medium after 60 minutes would be sufficient to reduce the internalisation of any remaining granzyme B from this point onwards. The situation in the mouse cell lines does not currently 'track' with the memHsp70 status, as it is the lower memHsp70 expresser, CT26, which was found to activate caspase-3 4 hours post granzyme B introduction. The 4T1 cells, which express more memHsp70, showed no significant activation of caspase-3 at any time after granzyme B introduction. This may simply be an artefact of having data variation in a small sample size, and ideally this could be repeated in the future in order to boost n numbers.

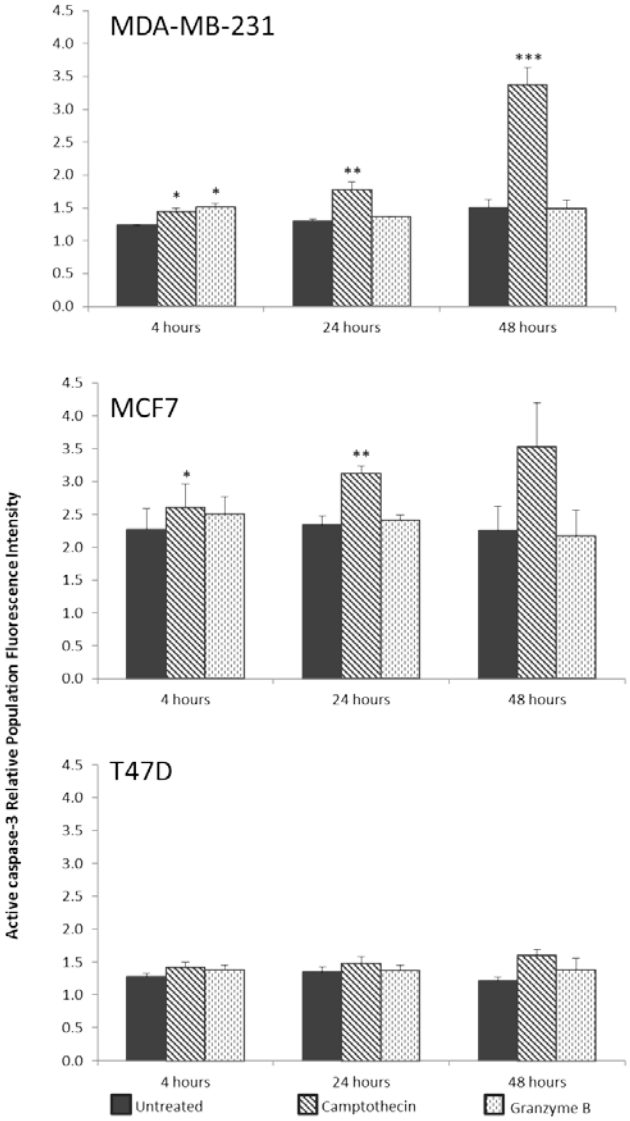

Figure 5.29 Activation of caspase-3 in human breast cancer cell lines after incubation with granzyme B.

Only the MDA-MB-231 cell line, which exhibits the highest level of memHsp70, was found to express significantly increased levels of activated caspase-3 when incubated with granzyme B. This significant difference was only seen 4 hours after introduction of granzyme B, and at later time points there was no difference in activated caspase-3 when compared to the untreated cells (Control: 1.24 ± 0.01, granzyme B: 1.52 ± 0.6. One way ANOVA $F=43.844$, $p=0.001$. Within subject contrast $F=19.401$, $p=0.012$). Other human cell lines (MCF7 and T47D) did not express activated caspase-3 in response to any duration of granzyme B incubation. Activation of caspase-3 was observed in both MDA-MB-231 and MCF7, however due to large variation in the results did not reach significance in MCF7 after 48 hours. T47D cells did not exhibit significant levels of caspase-3 activation at any time, after either granzyme B or camptothecin incubation (MDA-MB-231: 4 hour control 1.24 ± 0.01, camptothecin 1.44 ± 0.06, 24 hour control 1.30 ± 0.03, camptothecin 1.78 ± 0.11, 48 hour control 1.50 ± 0.13, camptothecin 3.37 ± 0.27. One way ANOVA $F=43.844$, $p=0.001$. Within subject contrast 4hr $F=15.201$, $p=0.018$, 24hr $F=25.657$, $p=0.007$, 48hr $F=169.471$, $p=0.0002$; MCF7 4 hour control 2.27 ± 0.31, camptothecin 2.60 ± 0.36, 24 hour control 2.34 ± 0.14, camptothecin 3.12 ± 0.12. One way ANOVA $F=1.172$, $p=0.355$. Within subject contrast 4hr $F=11.486$, $p=0.043$, 24hr $F=67.094$, $p=0.004$). Significance values displayed as * $p<0.05$, ** $p<0.01$. Data are presented as mean ± SEM from three independent experiments.

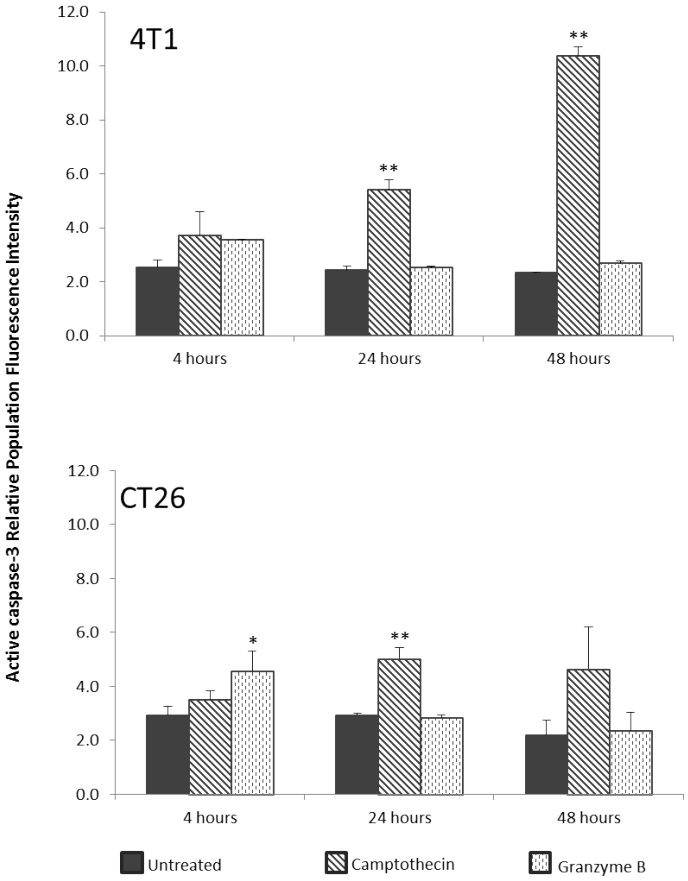

Figure 5.30 Activation of caspase-3 in mouse cancer cell lines after incubation with granzyme B.

The greatest activation of caspase-3 resulting from granzyme B incubation appeared in both CT26 and 4T1 after 4 hours, but only in the CT26 cells was this to a significant level (Control: 2.9 ± 0.3, granzyme B:4.6 ± 0.7. One way ANOVA F=3.784, p=0.005. Within subject contrast F=25.911, p=0.015). Cells that were treated with camptothecin, in an attempt to provide a positive control for caspase-3 activation, were found to exhibit significantly increased levels of caspase-3 activation at 24 hours after treatment, and in the case of 4T1 cells, also at 48 hours (CT26: control 2.9 ± 0.1, camptothecin 5.0 ± 0.4. Within subject contrast F=36.413, p=0.009. 4T1: 24 hour control 2.4 ± 0.2, camptothecin 5.4 ± 0.4. One way ANOVA F=51.041, p=51.041. Within subject contrast F=151.593, p=0.007. 48 hour control 2.3 ± 0.1, camptothecin 10.4 ± 0.3. Within subject contrast F=304.644, p=0.003). Significance values displayed as * p<0.05, ** p<0.01. Data are presented as mean ± SEM from three independent experiments.

The lack of clarity and inconsistency of the caspase-3 activation data were highly surprising. From a morphological perspective, untreated cells retained normal growth morphology, whereas a proportion of the human and mouse cell lines that had been treated with camptothecin or granzyme B were smaller and rounded in appearance. Furthermore, some cells had detached from the plate and were observed to be in suspension within the growth medium. These changes in appearance were observed in all time points, but were more pronounced at later time points. These are characteristics of cells having undergone apoptosis, so it is surprising that the activation of caspase-3, taken as a measurement of apoptosis, was not present. There are a number of possibilities for this discrepancy. Perhaps cells were not analysed at the most appropriate time-point to observe activated caspase-3. Since the

activation is a transient event timing is crucial, and it may be that a shorter incubation time was required. It may be that caspase-3 activation is an inappropriate marker of memHsp70-mediated granzyme B-induced apoptosis, if the uptake and trafficking pathway does not allow for caspase-3 interaction but perhaps instead relies on an alternative method of apoptosis induction. Whilst harvesting the cells from the plates prior to staining it was noticed that those wells with cells incubated with camptothecin or granzyme B appeared to hold fewer cells, and with a smaller proportion adhered to the well surface, than the control wells. This sparked further microscopical image analysis of the cells.

As the selected staining did not provide data to match the observed changes in cell morphology, additional experiments incubated cells in the presence of granzyme B for a variety of time points and then imaged the cultures on the Zeiss 510 inverted microscope. For this, cells were set up in glass bottomed dishes and grown for 48 hours before washing in PBS and applying PBS containing granzyme B for 60 min. After this time, 2 mL of fresh growth medium was added and cells were incubated for the remainder of their respective incubation durations (up to 2, 4 or 24 hours). Cells were washed and mounted onto microscopy slides using VECTASHIELD® containing DAPI, to stain the nucleus. This protocol necessitated the washing of wells before samples were mounted onto microscopy slides for imaging. This process would therefore remove fully detached cells. This compromise was deemed acceptable because even if detached cells were still present, they could not have been imaged easily. Single frame images of the bright-field channel (to show the cell morphology) and DAPI (to place the nucleus) were obtained using a 20x dry objective with representative images shown for human (**Fig 5.31**) and mouse (**Fig 5.32**) cell lines. The control cells show the usual morphology, and although all cell lines have their own typical morphology they all exhibit elongated structures with jagged cell edges. After 2 hours, cells begin to exhibit rounded qualities, with greater space between cells. After 4 hours, the spacing of cell is more pronounced. By 24 hours, there is a marked reduction in cell number, however those which remain have reverted back to a typical growth morphology, as seen in the control panel.

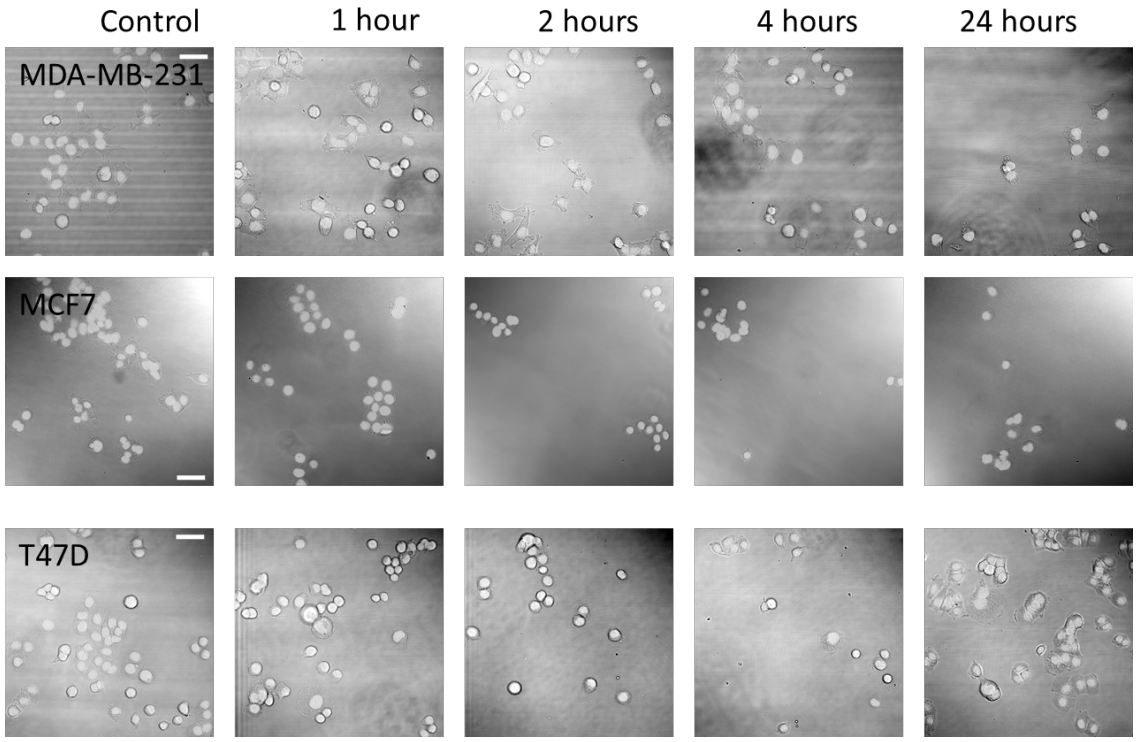

Figure 5.31 Morphology of human breast cancer cell cultures after incubation with granzyme B

Even one hour after the introduction of granzyme B to the cells, their morphology can be seen to change. Cells begin to round up and by 2-4 hours there is a clear reduction in cell number due to detachment and cells being washed away. After 24 hours, the cell number is much reduced, however those cells which remain have returned to a morphology similar to that in the control population.

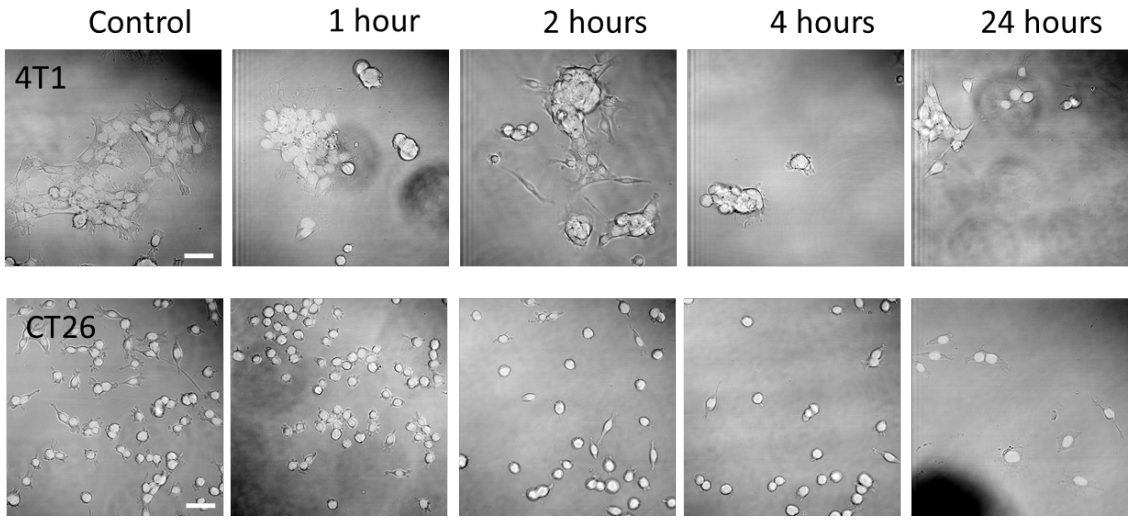

Figure 5.32 Morphology of mouse cancer cell cultures after incubation with granzyme B.

Even one hour after the introduction of granzyme B to the cells, their morphology can be seen to change. Cells begin to round up and by 2-4 hours there is a clear reduction in cell number due to detachment and cells being washed away. After 24 hours, the cell number is much reduced, however those cells which remain have returned to standard adhered morphology like that of the control population.

As a proportion of cells which adhere and grow remain following granzyme B incubation, it would appear that a single dose of granzyme B is insufficient to kill all cells, or that this reflects the heterogeneous nature of memHsp70 expression within these cell lines. In future experiments it may be worth investigating the consequences of re-incubating the remaining cells with granzyme B again, to determine whether the residual observed cell population is due to some inherent degree of granzyme B resistance (due to variable memHsp70 expression for example) or perhaps due to exhaustion of granzyme B in the media before complete killing can occur.

5.5 Involvement of sugars in the binding of granzyme B to memHsp70

Granzyme B uptake was found to be inhibited following deglycosylation (Mathias Gehrmann personal communication followed by [531]) and so to investigate further whether sugars are involved in the binding and subsequent internalisation of granzyme B to cancer cells expressing memHsp70, a variety of sugars were used as potential blocking agents and the results analysed by both flow cytometry and confocal microscopy. To date, these experiments have only been conducted on a single cell line (CT26), and so they need to be repeated using other cell lines in order to confirm the wider applicability of the findings.

For the experiments, CT26 cells were incubated in the presence of staining buffer containing either 10mM or 20mM of fucose, galactose, glucosamine, glucose, mannose, or n-acetyl neuraminic acid (NANA) and incubated at 37°C for 30 minutes. After this time, the buffer was replaced with PBS containing fluorescently-labelled granzyme B and cells were incubated at 37°C for an additional 30 minutes. Cells were then directly analysed via flow cytometry, with any reduction in fluorescence compared to the control being evident of blocking of the granzyme B. Only one of the sugar treatments was found to significantly impair granzyme B uptake; 20mM of n-acetyl neuraminic acid (**Fig 5.33**). This treatment resulted in an almost 40% reduction in detected fluorescence compared to the control cells (relative fluorescence; control 5.2 ± 0.4, 20mM NANA 3.3 ± 0.1).

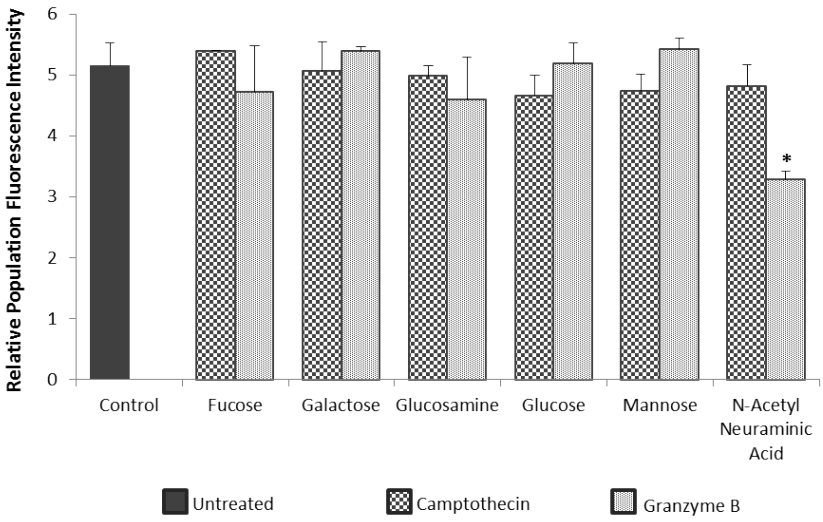

Figure 5.33 Internalisation of ATTO488-granzyme B by CT26 cells can be impaired by the presence of N-acetyl neuraminic acid.

CT26 cells pre-incubated with 10mM or 20mM of a variety of sugars (fucose, galactose, glucosamine, glucose, mannose and N-acetyl neurammininc acid) for 30 minutes were subsequently incubated in the presence of 4µg/mL ATTO488-granzyme B for a further 30 minutes. Whilst most sugars have no effect on the binding and uptake of granzyme B, pre-incubation with 20mM NANA results in a significant reduction in the amount of granzyme B processed by CT26 cells. Data shown are mean + SEM from 3-5 independent experiments. Significance determined by one-way independent ANOVA ($F=2.569$, $p=0.014$) with Games-Howell post-hoc comparison ($p=0.019$)

More information pertaining to the influence of sugars was obtained using confocal microscopy. For this, cells were set up on MatTek™ glass-bottomed dishes and grown for 48 hours, before being treated with 10mM of one of the sugars for 30 minutes at 37°C. Subsequently cells were washed, and incubated with granzyme B in PBS for a further 30 minutes at 37°C. After this time, cells were formaldehyde fixed, permeabilised and stained with antibodies specific for LAMP2, followed by an appropriate Cy3-labelled secondary antibody. LAMP2 was selected as the cells had previously exhibited a measurable co-localisation between internalised ATTO488-granzyme B and LAMP2. If the pre-treatment of the cells with sugars did indeed influence the uptake of granzyme B then a quantifiable variation in co-localisation would be observed. Next, the glass coverslips were detached from the dishes and mounted on microscopy slides using VECTASHIELD® containing DAPI. Slides were stored at 4°C protected from light until imaging could commence. Representative single frame images from the middle of cells treated with each sugar are shown (**Fig 5.34**).

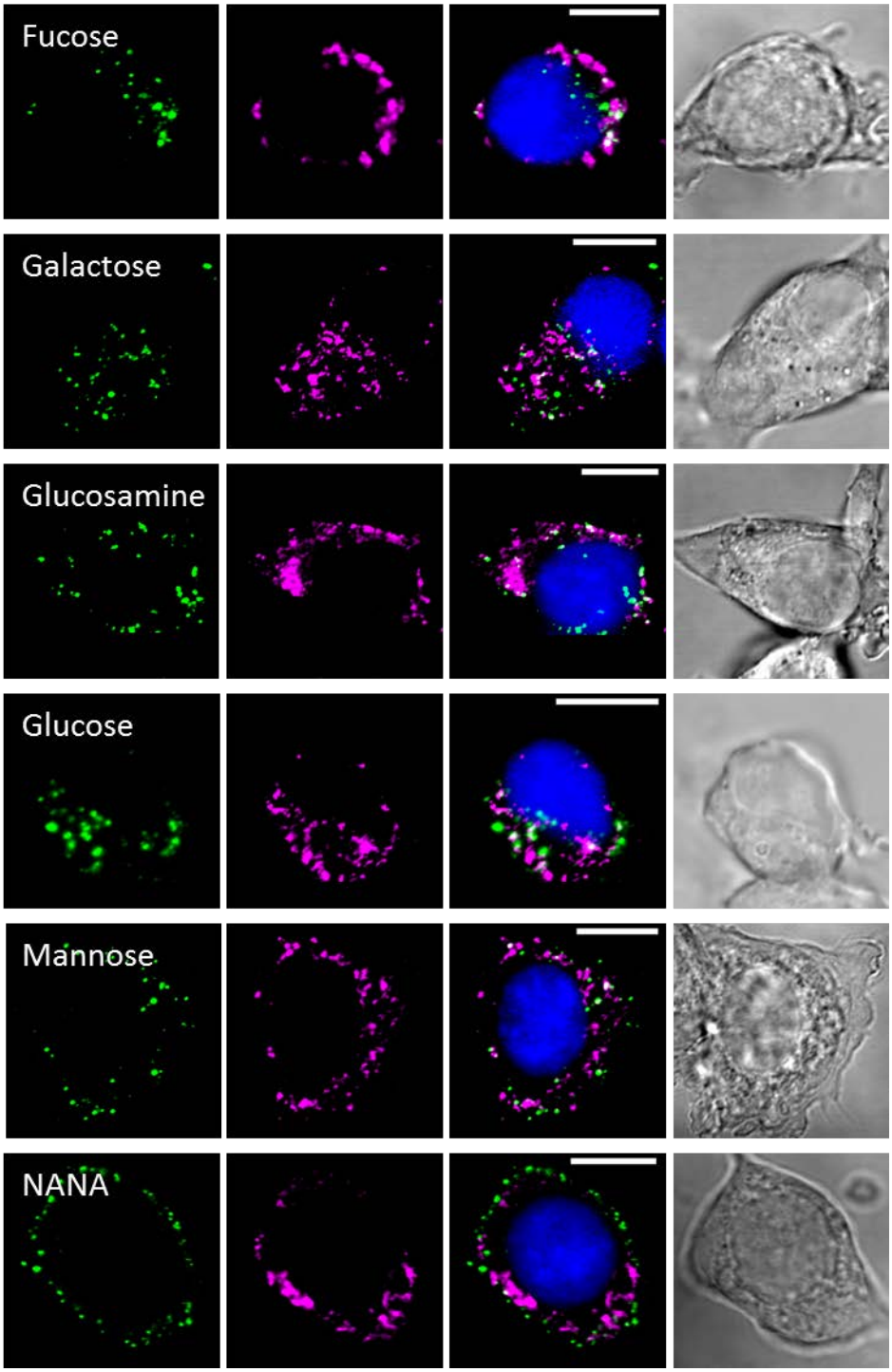

Figure 5.34 Internalisation of ATTO488-granzyme B by CT26 cells can be impaired by the presence of N-acetyl neuraminic acid.

CT26 cells pre-incubated with 10mM of a variety of sugars (fucose, galactose, glucosamine, glucose, mannose and N-acetyl neuramininc acid) for 30 minutes were subsequently incubated in the presence of 4µg/mL ATTO488-granzyme B (green) for a further 30 minutes. Cells were fixed, permeabilised and stained for the presence of LAMP2 (magenta) and mounted in VECTASHIELD™ containing DAPI to stain the nucleus (blue). The majority of sugars did not significantly alter the internalisation of ATTO488-granzyme B, however incubation with 10µM resulted in binding of ATTO488-granzyme B, but virtually no internalisation. Images shown are representative single frames taken from the middle region of the cells. Scale bars represent 10µm.

The profile of ATTO488-granzyme B (green) presents as spots within the cell boundary, and therefore has been internalised, after 5 of the sugar treatments. The cells treated with 10mM of n-acetyl neuraminic acid differed, as the majority of granzyme B was found instead along the cell boundary. These findings suggest that although granzyme B binding is unaffected, its internalisation has somehow been impaired by the presence of NANA. In an effort to provide some quantification on the reduction of internalised granzyme B, one of the vesicle stainings was employed. LAMP2 staining was used as it showed measureable co-localisation with granzyme B in CT26 cells incubated for 30 minutes.

The inclusion of LAMP2 staining (magenta) allowed the co-localisation of granzyme B with $LAMP2^+$ vesicles to be calculated. Previously internalised ATTO488-granzyme B had been shown to co-localise with different intracellular vesicle stainings and any of them could have been used at this point. The results of all treatments, including the control cells which received no sugar incubation, are shown (T**able 5.9**), and the only treatment to significantly reduce the co-localisation of granzyme B with $LAMP2^+$ vesicles was 10mM n-acetyl neuraminic acid (Control: 33.7 ± 4.8%. NANA: 5.6 ± 3.1%). These findings confirm and extend the flow cytometry data.

Treatment	Manders' M1
Control	33.7 ± 4.8
Fucose	29.5 ± 3.8
Galactose	29.4 ± 3.7
Glucosamine	33.3 ± 4.3
Glucose	36.7 ± 1.6
Mannose	31.3 ± 3.8
NANA	5.6 ± 3.1 ***

Table 5.9 Influence of incubation with sugars on the uptake of granzyme B into CT26 cells

CT26 cells pre-treated with one of six different sugars then incubated with ATTO488-granzyme B were analysed by confocal microscopy to calculate the proportion of ATTO488-granzyme B co-localised to lysosomes ($LAMP2^+$). Cells pre-treated with N-acetyl Neuraminic Acid showed a significant reduction in co-localisation indicating that significantly less ATTO488-granzyme B was internalised. One-way ANOVA F=10.002, p=0.000005, Hochberg *post-hoc* test p=0.0001. Data are presented as mean ± SEM from 4-6 imaged cells, from two independent experiments.

Time restraints did not allow for this to be investigated with the breast cancer cell lines however this would be an interesting follow-up in the future.

5.6 Summary

The serine protease granzyme B is a main constituent in the cytotoxic granules of natural killer cells and cytotoxic $CD8^+$ T cells which acts to induce apoptosis. In this setting, granzyme B is able to enter the target cells by way of combined action with the pore-forming protein perforin, however the presence of memHsp70 on the cell surface has been shown to circumvent this need. Recombinant human granzyme B is able to bind directly to memHsp70, an action that is dependent on mammalian post-translational modifications and is not possible if the granzyme B is deglycosylated [531]. MemHsp70 positive breast cancer cell lines were shown to bind and uptake granzyme B, with the rate of uptake increased in line with increasing memHsp70 expression levels. Using fluorescently labelled granzyme B the trafficking of internalised granzyme B could be tracked and was found to involve a late endosome pathway with a proportion co-localising to the mitochondria and some going into lysosome degradation. The uptake of granzyme B occurred predominantly around the adhered surface of cells, suggesting a possible link between memHsp70 and cell adherence. Following on from the finding that mammalian post-translational modifications are required for efficient binding and uptake, it was shown that N-acetyl neuraminic acid could successfully block the majority of granzyme B uptake into CT26 murine colorectal carcinoma cells. This issue needs to be addressed in breast cancer cells to confirm if the same is true in different cell lines and cancer types.

Once internalised, granzyme B induces apoptosis in 4 hours as measured by flow cytometry caspase-3 activation, in MDA-MB-231 and CT26 cells. However, when viewed using microscopy image analysis all memHsp70 positive cell lines were observed to show morphological features apoptosis such as cell rounding, blebbing and detachment. It may be that caspase-3 activation is not the most appropriate measure for memHsp70-mediated granzyme B-induced cell death, either because the granzyme B acts via a different pathway of apoptosis induction or that the activation is transient and the time-points investigated were not the most appropriate.

CHAPTER 6

RESULTS IV – Lymphocytes and memHsp70 expression

6.1 Introduction

Although heat shock protein 70 has been traditionally viewed as being an intracellular protein, the selective expression of a membrane form of Hsp70 on a large proportion (~50%) of tumours has been reported [285]. The development of new molecules that can interact with this membrane form of Hsp70 could therefore provide a platform on which to develop a range of tumour targeting and therapeutic agents. Finding a marker which allows the imaging and/or targeting of primary and metastatic tumours could offer real advances in cancer treatment. However, for this to be the case, it is essential that healthy cells do not, and cannot be induced to, express membrane Hsp70. As the membrane Hsp70 status of peripheral blood immune cells has never been investigated before, the aim of this part of the study is to provide a thorough assessment of any membrane expression of Hsp70 in peripheral blood immune cells at rest and after stresses. If indeed memHsp70 were to be found on peripheral blood immune cells this could prove to be highly important. MemHsp70 has been found to mediate internalisation of granzyme B resulting in cellular apoptosis [530, 532], and granzyme B has also been proposed as one mechanism for regulatory T cells eliciting immunosuppression by way of removal of effector cells [167, 168].

Peripheral blood lymphocytes from healthy volunteers were assessed *ex vivo* for the presence of membrane Hsp70, as well as after a variety of treatments designed to reflect different conditions which could be experienced in a tumour environment. The expression of memHsp70 was assessed using flow cytometric analysis following incubation with FITC-labelled antibodies specific for Hsp70 and appropriate isotype control antibodies. The inclusion of the C92F3A-5 Hsp70 mAb (which is specific for an epitope which is unavailable when the molecule is present on the membrane) in addition to the cmHsp70.1 mAb allows memHsp70 to be distinguished from extracellular Hsp70 which has bound to the cell surface.

6.1.1 Membrane Hsp70 expression on peripheral blood immune cells

The presence of memHsp70 on $CD4^+$ and $CD8^+$ T cells, as well as $CD56^+$ NK cells in whole blood and PBMC preparations was determined. For this, whole blood samples were stained

immediately after venepuncture in order to provide the most accurate estimation of the *in vivo* situation. Complete whole blood was not a suitable medium for the majority of treatment conditions, and so the impact of density gradient separation on the memHsp70 expression of lymphocytes was assessed by staining PBMCs immediately following the separation and also 24 hours later.

The expression of memHsp70 is determined on the basis of positive staining with the FITC-labelled cmHsp70.1 mAb. Membrane Hsp70 is an inducible molecule, and consequently, rather than reporting the results as 'percentage positive' expression can be more accurately described in terms of 'relative intensity'. This is calculated as the median fluorescence intensity (mfi) of the stained cells divided by the mfi of the isotype control. A relative intensity of 1 is indicative of no difference over the isotype (and therefore no memHsp70 expression). As the relative intensity value increases it is indicative more intense staining and therefore greater expression of memHsp70.

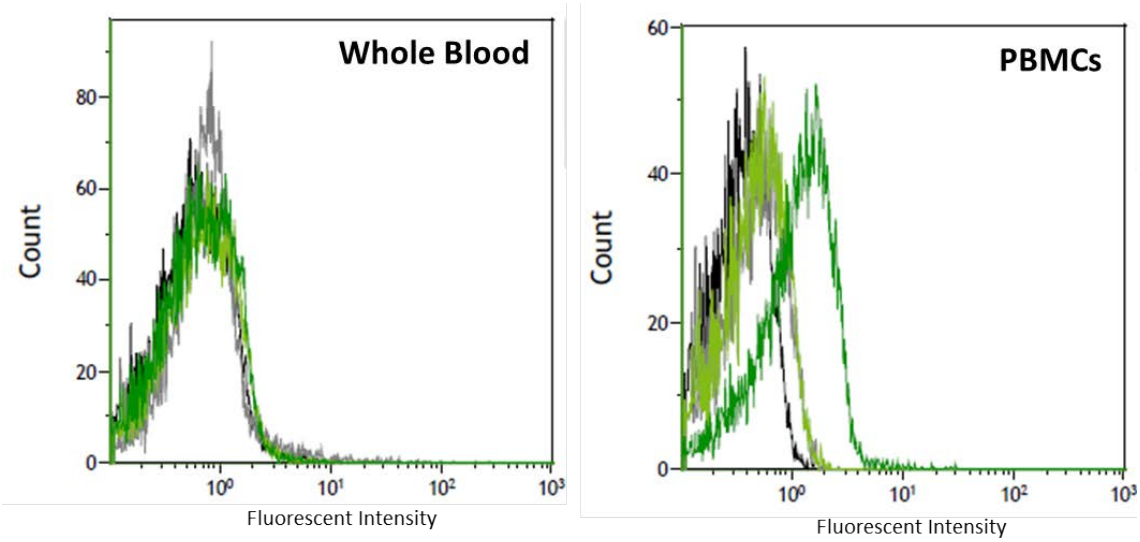

Figure 6.1 Representative memHsp70 staining patterns for whole blood and PBMCs

Representative flow cytometry histograms depicting unstained cells (black line), and cells incubated with isotype (grey line), C92F3A-5 mAb (light green line) and cmHsp70.1 mAb (dark green line), for viable lymphocyte populations in a whole blood sample and a preparation of isolated PBMCs.

The relative intensity of memHsp70 on all lymphocyte subsets in whole blood analysed *ex vivo* was low ($CD4^+$ T cells 1.28 ± 0.12, $CD8^+$ T cells 1.37 ± 0.13, NK cells 1.33 ± 0.37; mean ± SEM, n=7) (**Fig. 6.2**). The staining with the alternative Hsp70 antibody clone C92F3A-5 had relative intensity measurements close to 1 for all of the lymphocytes assessed ($CD4^+$ T cells 0.69 ± 0.13, $CD8^+$ T cells 0.91 ± 0.16, NK cells 0.76 ± 0.14; mean ± SEM, n=5). These results were not significantly different to the isotype control (Multivariate ANOVA, F=0.703, p=0.409).

In contrast to whole blood, the relative intensity of cmHsp70.1 mAb binding to all cell types was increased following density gradient separation. ($CD4^+$ T cells 2.21 ± 0.46, $CD8^+$ T cells 2.67 ± 0.27, NK cells 3.38 ± 1.12; mean ± SEM, n=5, multivariate ANOVA F=11.403, p=0.002). This increase was maintained even after a 24 hour incubation period ($CD4^+$ T cells 2.83 ± 0.37, $CD8^+$ T cells 3.34 ± 0.39, NK cells 4.14 ± 0.80; mean ± SEM, n=5). The relative intensity of C92F3A-5 staining was the same as the isotype control (multivariate ANOVA F=0.426, p=0.517). There was no evidence that venepuncture or density gradient separation had any effect on cellular activation, as there was no expression of either CD69 or CD25 (data not shown).

The level of memHsp70 staining on whole blood lymphocyte populations when examined *ex vivo* is negligible and not significantly different to the isotype control. When cells are examined after PBMC isolation as well as after 24 hours rest period the level of memHsp70 induction is to similar relative levels as on tumour cells.

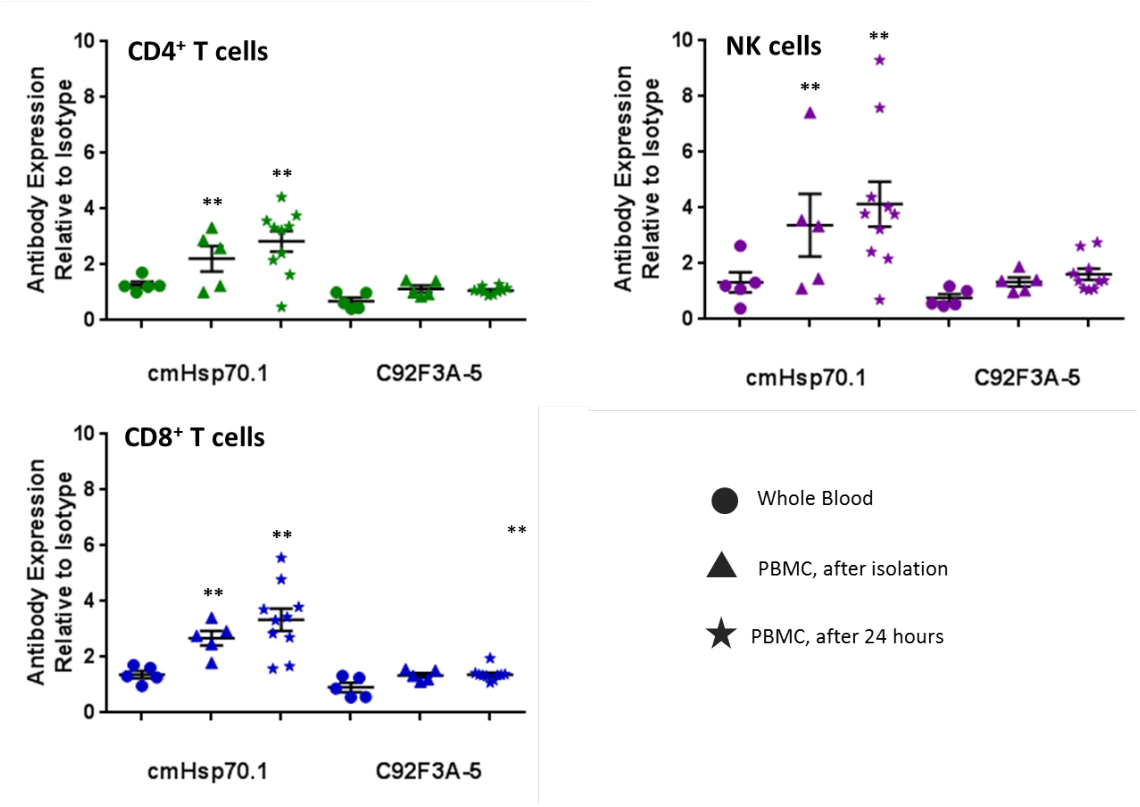

Figure 6.2 Relative intensities of staining with fluorescently-labelled cmHsp70.1 mAb and C92F3A-5 on lymphocyte subsets in whole blood and following density gradient separation

Peripheral blood lymphocytes assessed ex vivo expressed very low levels of memHsp70 (shown by the relative intensities of both cmHsp70.1 mAb and C92F3A-5 binding being close to 1). PBMC isolation promoted the binding of the cmHsp70.1 mAb to $CD4^+$ and $CD8^+$ T cells, as well as NK cells. This binding was retained following a 24 hour period of 37°C incubation. Data are presented as mean + SEM, n = 5. * p<0.05, ** p<0.01.

6.1.2 Effect of different stimuli on memHsp70 expression

Lymphocytes are subjected to numerous different influences and undergo many responses. Tumours provide an immune stress and could be responsible for influences on the lymphocytes. The aim here was to investigate whether any of a variety of possible stimuli / stressors were able to induce the capacity of the cmHsp70.1 mAb to bind to lymphocytes.

6.1.2.1 Heat stress

Although the intracellular increase of Hsp70 in lymphocytes in response to heat stress has been well documented [560, 561] no data regarding the possible influence on the membrane form of the molecule is available. To investigate, isolated PBMCs were incubated at 42°C for two hours, and then allowed to rest at 37°C for either 2 hours or 22 hours (**Fig 6.3**). There was no significant change in cmHsp70.1 mAb binding after heat stress with either the short, 2 hour rest period or the longer 22 hour rest ($CD4^+$ T cells: control 2.93 ± 1.23, 2hr rest 3.09 ± 1.26, 22hr rest 2.79 ± 0.07, one-way ANOVA F = 0.041 p = 0.960; $CD8^+$ T cells: control 4.04 ± 1.26, 2hr rest 3.73 ± 1.25, 22hr rest 3.12 ± 0.07, one-way ANOVA F = 0.230 p = 0.799; NK cells: control 4.11 ± 2.07, 2hr rest 3.89 ± 2.31, 22hr rest 3.74 ± 0.88 one-way ANOVA F = 0.004 p = 0.996; all data presented as mean ± SEM, n = 6).

As the mechanism of Hsp70 appearing on the membrane is not yet known, one simple proposition is that memHsp70 expression is directly dependent on the intracellular Hsp70 content. Alongside the staining for membrane Hsp70, lymphocytes were subjected to fixation/ permeabilisation and stained for intracellular Hsp70. In line with a wealth of published literature, lymphocytes were found to upregulate intracellular Hsp70 levels in response to increasing durations of incubation at 42^{o}C, up to 2 hours. Incubating cells at 37^{o}C had no effect on intracellular Hsp70 (**Fig 6.4**).

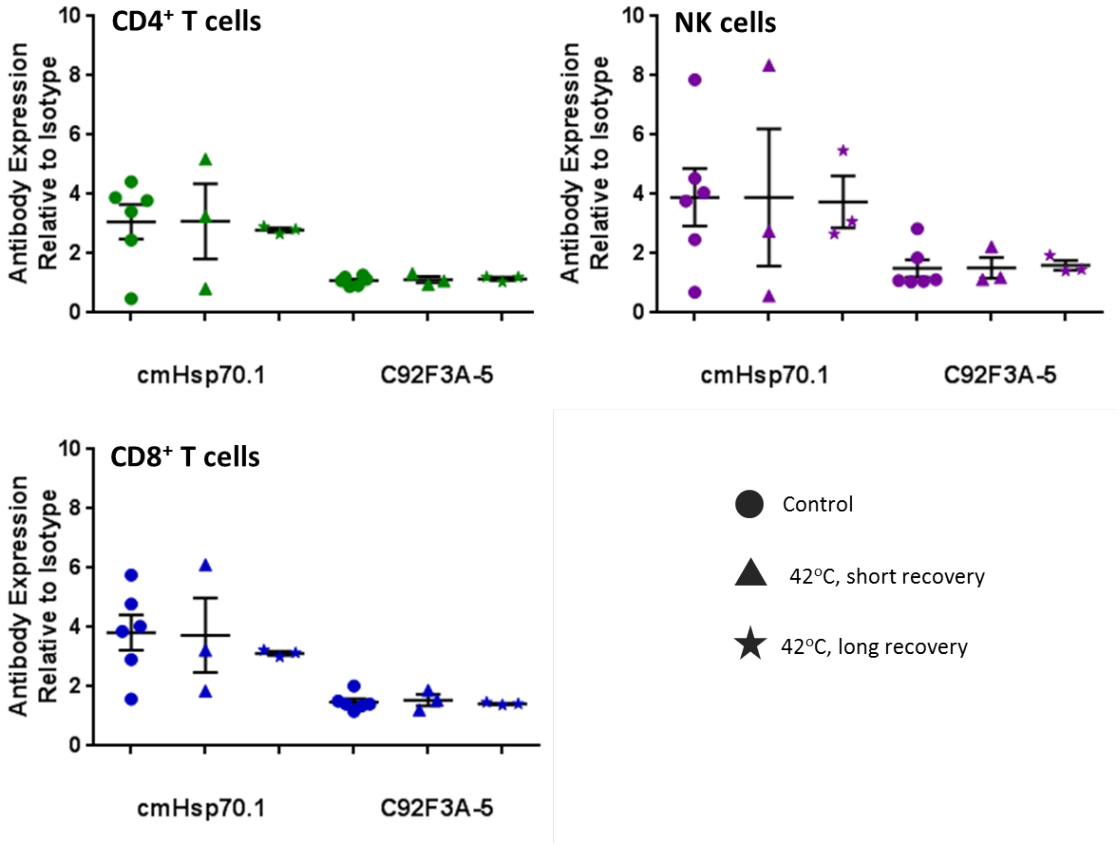

Figure 6.3 Effect of heat stress on the binding of cmHsp70.1 mAb to lymphocytes

Heat stress that was sufficient to increase intracellular expression (data not shown) did not lead to any increase in the binding of cmHsp70.1 mAb over that caused by density gradient isolation of PBMCs. The relative intensity of the binding of the C92F3A-5 clone did not significantly increase over the isotype, confirming the presence of cmHsp70.1 mAb binding rather than the binding of extracellular Hsp70 to the cell surface. Data are presented as mean + SEM, n = 6. * $p<0.05$, ** $p<0.01$.

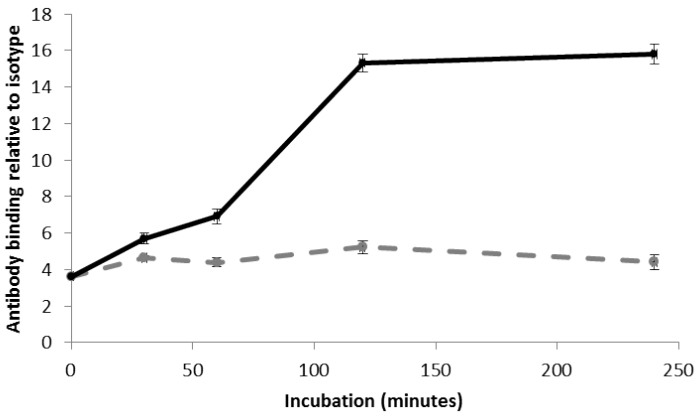

Figure 6.4 Intracellular Hsp70 response of lymphocytes to heat stress

Intracellular Hsp70 content of lymphocytes is stable under optimal incubation conditions (37°C, dashed line), but is increased in response to incubation at 42°C (solid line). This increase peaks after 2 hours and then remains stable. Data presented as mean ± SEM, n = 3.

This would indicate that rather than a simple, direct relationship between intracellular Hsp70 content and memHsp70 expression, there is no relationship between the two. Additionally, none of the cell populations showed any sign of activation following heat stress, as there was no change in their expression of CD69 or CD25 (data not shown).

6.1.2.2 Cellular activation

The influence of activation (concanavalin A and incubation with CD3/CD28 mAb-coated beads) on the binding of cmHsp70.1 mAb to density gradient isolated PBMCs populations was determined (**Fig 6.5**).

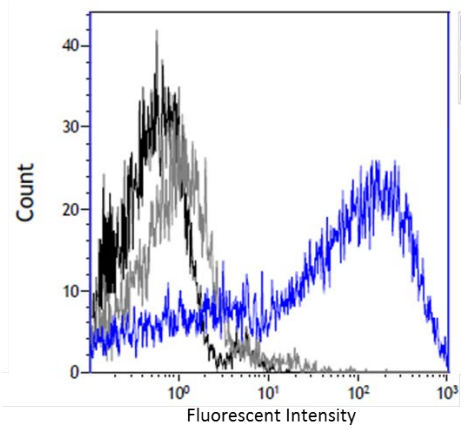

Figure 6.5 Representative CD69 staining pattern

Representative flow cytometry histogram depicting unstained cells (black line), and cells incubated with isotype (grey line) and with anti-CD69 mAb (blue line), for viable lymphocyte populations in a preparation of isolated PBMCs.

6.1.2.2.1 Influence of activation with Concanavalin A on cmHsp70.1 mAb binding to lymphocyte sub-populations

Whole blood and PBMC preparations were stimulated with Concanavalin A (ConA) for 24 hours, after which the activation state and capacity of $CD4^+$ T cells, $CD8^+$ T cells and $CD56^+$ NK cells to bind FITC-cmHsp70.1 mAb were determined by flow cytometry. Although ConA treatment induced a significant activation of $CD4^+$ T cells and $CD56^+$ NK cells in whole blood ($CD4^+$ T cells: control 2.5 ± 1.0 %, ConA 11.3 ± 0.5 %, Student's Paired t test t(3) = -7.495, p = 0.005; NK cells: control 12.5 ± 8.3 %, ConA 33.8 ± 15.5 %, Student's Paired t test t(3) = -3.203, p = 0.049; data presented as mean ± SEM, n = 4). There was no effect on the activation of $CD8^+$ T cells (control 10.0 ± 3.9 %, ConA 10.6 ± 3.0, Student's Paired t test t(3) = -0.242, p = 0.825, data presented as mean ± SEM, n = 4) (**Fig 6.6**).

When cells were examined in the whole blood sample there was a trend for the addition of ConA to reduce FITC-cmHsp70.1 binding to T cells (**Fig 6.7**. $CD4^+$ T cells: control 1.37 ± 0.07, ConA 1.21 ± 0.02; $CD8^+$ T cells: control 1.95 ± 0.20, conA 1.49 ± 0.12, data presented as mean ± SEM, n = 4), however the decrease did not reach significance for either cell type (Student's Paired t test: $CD4^+$ T cells $t(3) = 1.860$, $p = 0.160$; $CD8^+$ T cells $t(3) = 2.240$, $p = 0.111$). The ConA treatment did not result in any such trend in NK cells (**Fig 6.7**), with no change in memHsp70 expression being observed (control 1.53 ± 0.22, ConA 1.52 ± 0.18; Student's Paired T test $t(3) = 0.041$, $p = 0.970$, data presented as mean ± SEM, n = 4).

Cellular activation was achieved to a much greater extent when ConA was used to stimulate isolated PBMCs (**Fig 6.6**). In this situation, activation induced a significant increase in the proportion of cells expressing CD69 ($CD4^+$ T cells: control 3.6 ± 2.4 %, ConA 76.0 ± 6.3 %, Student's Paired t test $t(2) = -8.543$, $p = 0.013$; $CD8^+$ T cells: 4.8 ± 1.9 %, ConA 68.0 ± 6.7 %, Student's Paired t test $t(2) = -7.394$, $p = 0.018$; NK cells: control 11.5 ± 1.5 %, ConA 51.4 ± 6.5 %, Student's Paired t test $t(2) = -5.154$, $p = 0.036$, all data presented as mean ± SEM, n = 3). This difference in activation capability could be attributed to the ConA being 'mopped up' by elements within the blood, such as sugars and other carbohydrates, and by cells with an abundance of these on their surface such as monocytes. ConA is a lectin and binds to cells through sugars on the cell membrane, predominately α-D-mannosyl and α-D-glucosyl groups, both of which are abundant on the surface of monocytes.

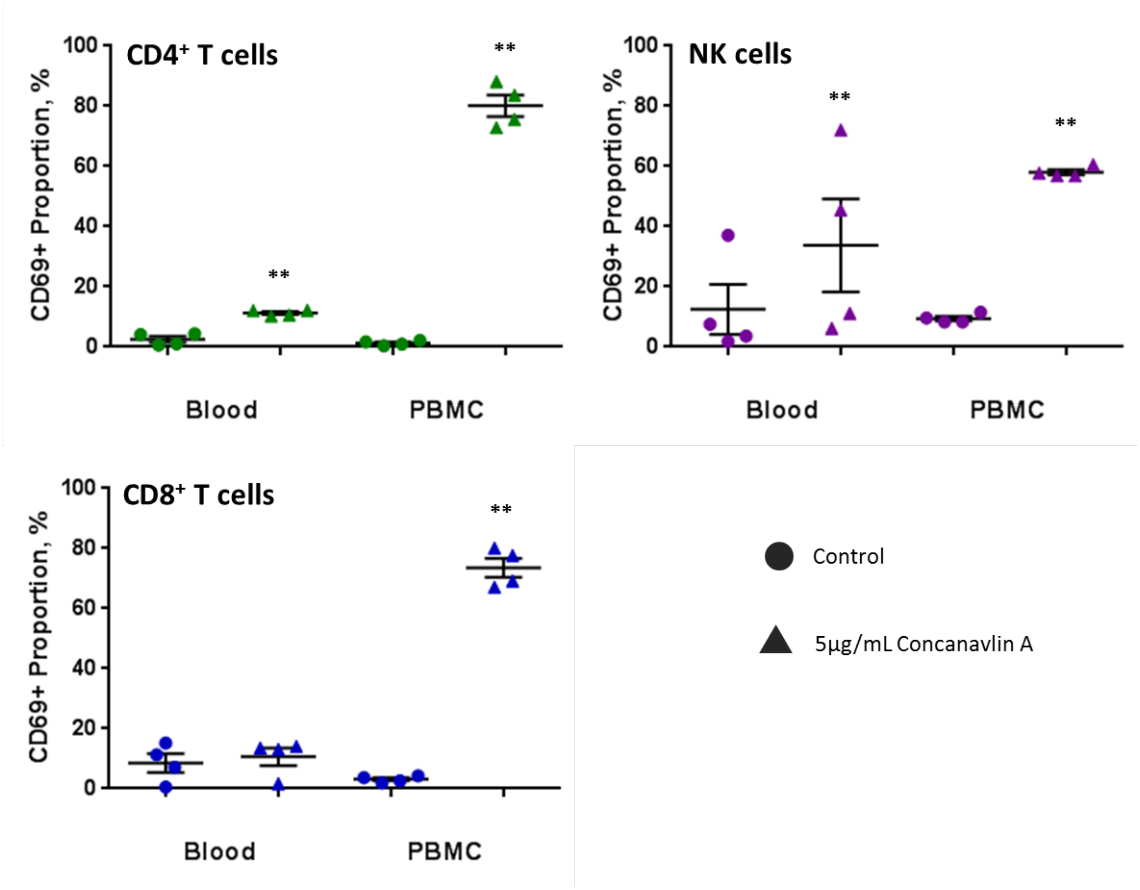

Figure 6.6 Lymphocyte activation following 24 hour stimulation with ConA in whole blood and PBMC preparations.

Incubation with ConA for 24 hours resulted in significant activation of T cell and NK cell populations in isolated PBMCs. In whole blood samples only $CD4^+$ T cells and NK cells were significantly activated, and then to a lesser degree than their counterparts in the PBMC preparation. Data presented as mean + SEM, n = 4. * $p<0.05$, ** $p<0.01$.

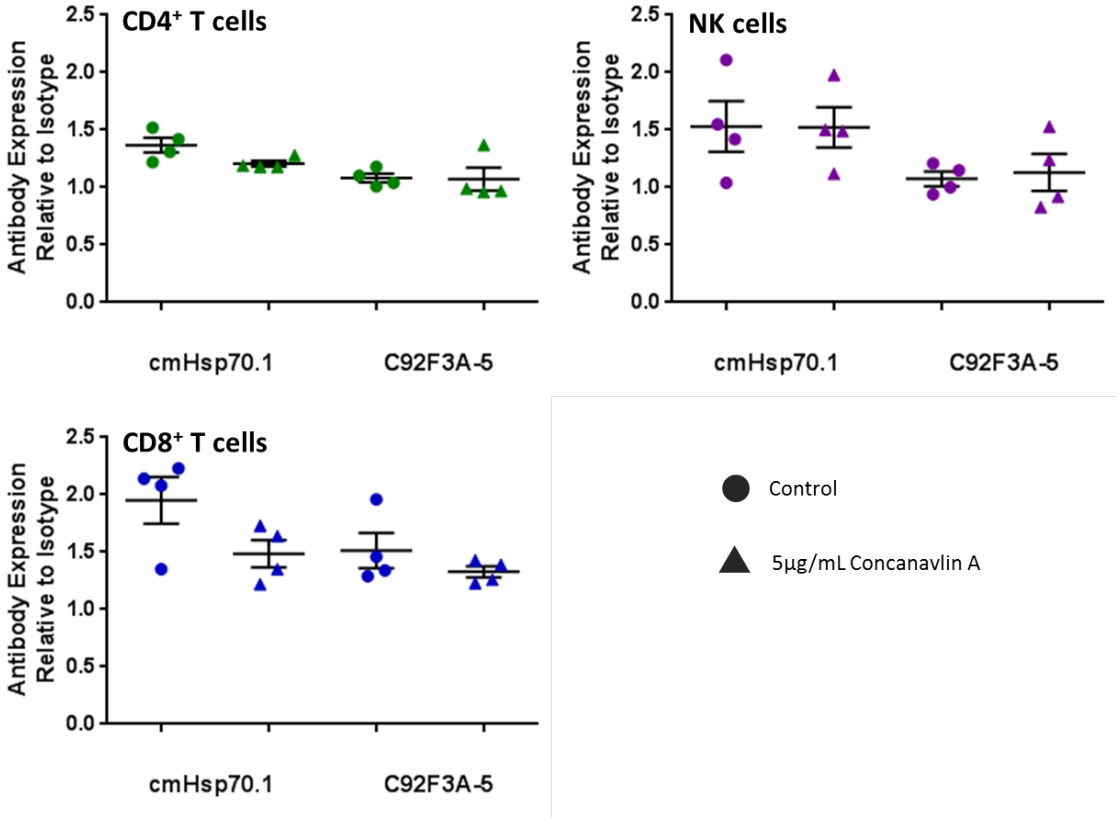

Figure 6.7 The effect of ConA on FITC-cmHsp70.1 mAb binding to lymphocytes in whole blood

A 24 hour incubation with ConA in whole blood did not result in any significant alteration to the cmHsp70.1 mAb binding to T cells or NK. There was no staining with the C92F3A-5 Hsp70 antibody clone over and above that of the isotype control. Data presented mean + SEM, n = 4.

When ConA was used to activate PBMCs there was no obvious trend or significant differences in binding of cmHsp70.1 mAb observed in any cell type (**Fig 6.8**. $CD4^+$ T cells: control 2.38 ± 0.23, ConA 2.57 ± 0.18, Student's Paired T test t(2) = -0.535, p = 0.646; $CD8^+$ T cells: control 3.01 ± 0.48, ConA 2.96 ± 0.47, Student's Paired T test t(2) = 0.325, p = 0.776; NK cells: control 2.42 ± 0.11, ConA 2.31 ± 0.16, Student's Paired T test t(2) = 0.429, p = 0.710; all data presented as mean ± SEM, n = 3).

Even the enhanced activation levels observed when ConA was applied to PBMC preparations did not lead to any significant changes in FITC-cmHsp70.1 mAb binding to T cell or NK populations. This would suggest that there is either no link between cellular activation status and memHsp70 expression in lymphocytes, or that the timeframe for any downstream effects on memHsp70 is a result of activation is longer than that assessed here, or that there is a

critical threshold of activation before memHsp70 is affected that the ConA stimulation was insufficient to achieve.

6.1.2.2.2 Influence of activation with CD3/CD28 mAb-coated beads on cmHsp70.1 mAb binding to lymphocyte sub-populations

In order to assess another route of cellular activation, isolated PBMCs were incubated in the presence of polystyrene beads coated with anti-CD3/CD28 mAb. These beads mimic T cell receptor engagement and the concomitant delivery of co-stimulatory signals. NK cells cannot respond to the beads directly, but are stimulated by the cytokines released from T cells upon their activation. Two bead preparations which offer different levels of stiumulus due to different concentrations of antibodies were used. Human T-Activator CD3/CD28 Expander beads (Dynabeads®, Life Technologies) provide a very strong signal, whereas Treg Suppression Inspector beads (Inspector beads, Miltenyi Biotec) provide a weaker signal. These beads are unsuitable for use in whole blood samples and consequently only isolated PBMCs could be investigated in this way. Using the expression of CD69 as a marker of activation status, both T cell subsets and the NK cells were found to be activated as a result of incubation with both preparations of CD3/CD28 mAb beads ($CD4^+$ T cells: control 1.8 ± 0.4 %, Inspector 28.5 ± 7.4 %, expander beads 86.4 ± 5.7 %; $CD8^+$ T cells: control 3.1 ± 0.7 %, Inspector 29.9 ± 6.0 %, expander beads 95.9 ± 2.1 %; NK cells: control 17.2 ± 7.6 %, Inspector 56.6 ± 15.9, expander beads 97.8 ± 1.2 %; data presented as mean ± SEM, n = 5, **Fig 6.9**). The activation achieved with stimulation using both the Inspector bead and expander bead preparations was significant for all cell subsets ($CD4^+$ T cells: one-way repeated ANOVA $F = 47.625$, $p < 0.001$, Control vs Inspector $p = 0.080$, Control vs expander beads $p < 0.001$ Bonferroni post hoc comparison; $CD8^+$ T cells: one-way ANOVA $F = 198.799$, $p < 0.001$, Control vs Inspector $p = 0.040$, Control vs expander beads $p < 0.001$, Bonferroni post hoc comparison; NK cells: one-way ANOVA $F = 19.887$ $p = 0.002$, Control vs Inspector $p = 0.216$, Control vs expander beads $p = 0.005$, Bonferroni post hoc comparisons).

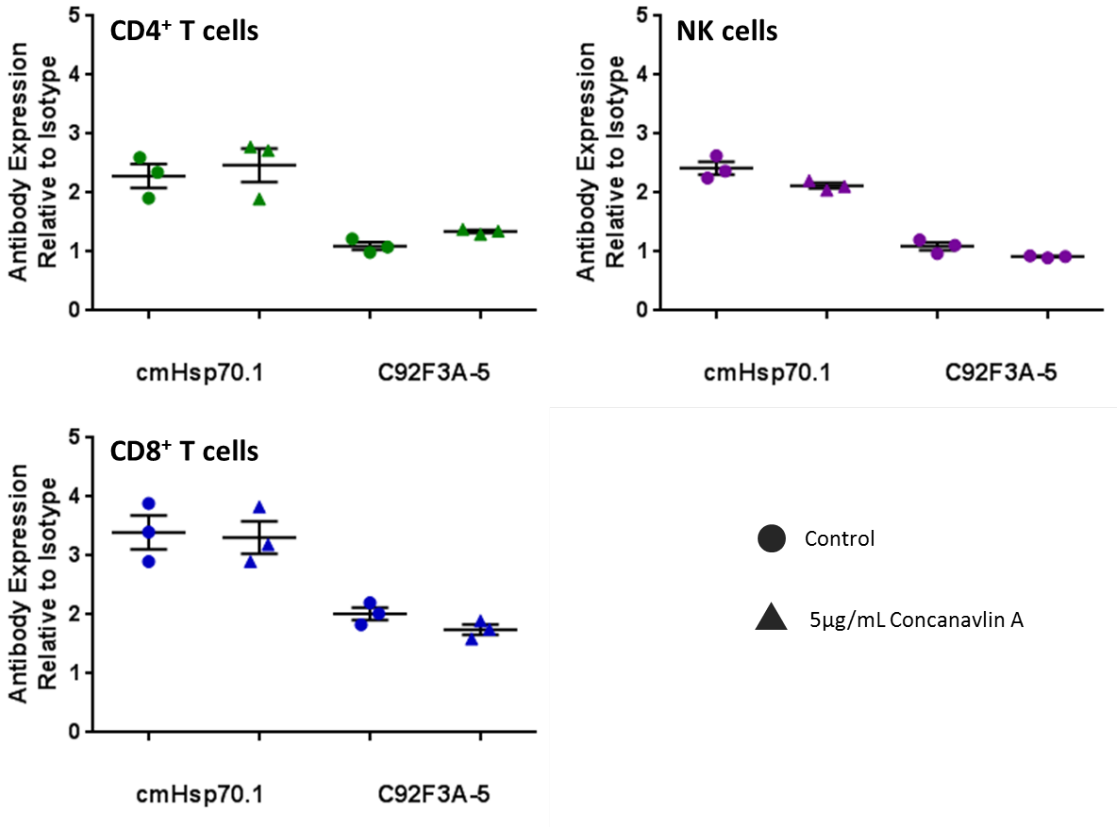

Figure 6.8 Effect of ConA on FITC-cmHsp70.1 mAb binding to lymphocytes in an isolated PBMC preparation

24 hour incubation with ConA in an isolated PBMC preparation did not lead to any significant alterations in FITC-cmHsp70.1 mAb binding to T cell and NK cell populations. There was no staining with the C92F3A-5 Hsp70 antibody clone over and above that of the isotype control. Data presented as mean + SEM, n = 3.

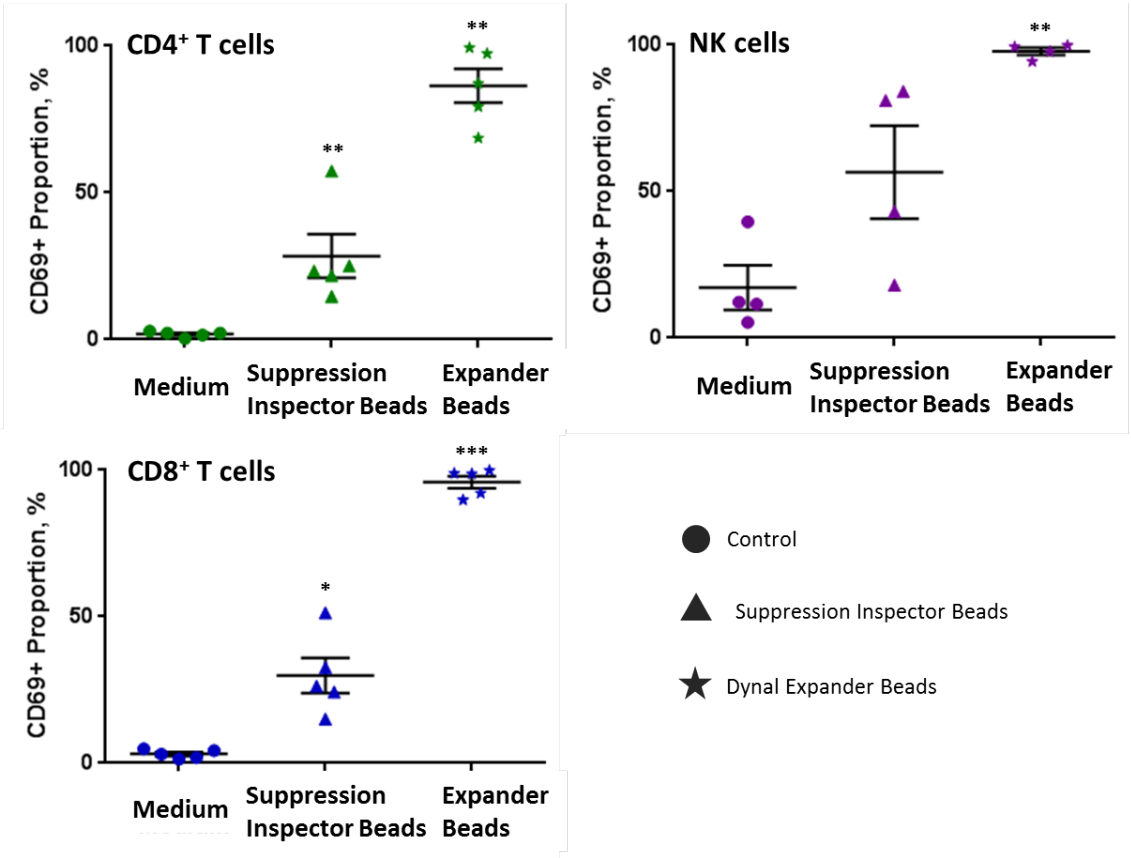

Figure 6.9 Effect of incubation with anti-CD3/CD28 mAB coated beads on the activation status of lymphocyte subsets.

T cells and NK cells exhibited significant activation following incubation with anti-CD3/CD28 mAb coated beads. Whilst the T cells are activated directly through TCR co-stimulation, the NK cells respond instead to the resulting cytokines released from activated T cells. Data presented as mean + SEM, n = 4/5. * $p<0.05$, ** $p<0.01$, *** $p<0.001$.

Although there was a trend for cmHsp70.1 mAb binding to cell subsets to increase after cellular activation ($CD4^+$ T cells: control 2.77 ± 0.41, Inspector 3.49 ± 0.70, expander beads 5.32 ± 1.69; $CD8^+$ T cells: control 3.21 ± 0.37, Inspector 3.91 ± 0.58, expander beads 5.47 ± 1.48; NK cells: control 4.80 ± 1.64, Inspector 6.46 ± 1.92, expander beads 6.73 ± 2.77; data presented as mean ± SEM, n = 5, **Fig 6.10**), none of these effects were found to be of statistical significance ($CD4^+$ T cells: one-way repeated ANOVA $F = 2.719$, $p = 0.174$; $CD8^+$ T cells: one-way repeated ANOVA $F = 2.195$, $p = 0.212$; NK cells: one-way repeated ANOVA $F = 1.261$, $p = 0.349$). This lack of significance is most likely due to the relatively small number of subjects investigated. Using these data, power calculations were preformed to assess the necessary sample size required to detect significant effects with a one-way repeated ANOVA at the 0.05 level. The result was that experimental group sizes of 12 would be needed to confirm whether the trend for memHsp70 to increase following anti-CD3/CD28 coated bead activation of lymphocytes.

Increasing the subject count to this level is something that would be desirable to complete in the future.

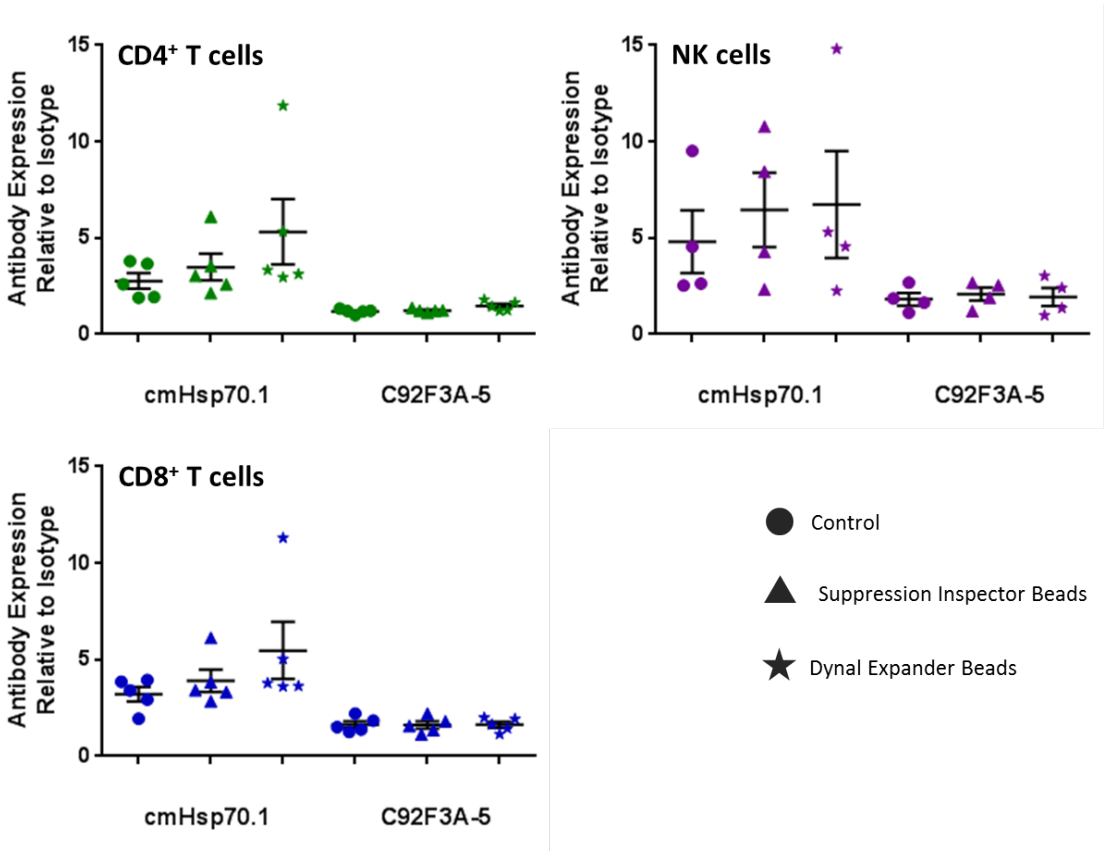

Figure 6.10 Effect of incubation with anti-CD3/CD28 mAB coated beads on cmHsp70.1 mAB binding to PBMC subpopulations

Both T cell subsets and NK cells exhibited an increase of the relative intensity of FITC-cmHsp70.1 mAb binding following 24 hour exposure to anti-CD3/CD28 mAb stimulation. Data are presented as mean + SEM, n = 4/5.

6.1.2.2.3 Supernatants from activated PBMC cultures

To investigate whether T cell and NK cell derived cytokines can influence the binding of cmHsp70.1 mAb, isolated PBMCs were incubated with the supernatant of PBMCs incubated with Inspector or Expander beads, or with supernatants derived from control PBMCs (100% v/v or 50% v/v). The concern with using 100% v/v supernatant was that the medium could be nutrient depleted from already being used to support activated cells for 24 hours, and that it could lead to nutrient starvation stress rather than simply providing released factors from cell activation. However, cells incubated in 100% v/v supernatant exhibited good viability (>95%) and so nutrient deficiency did not appear to pose a problem. The addition of the 50% v/v also allowed for concentration-dependent effects to be observed.

Although $CD8^+$ T cells showed no increase to activation after incubation with supernatants derived from anti-CD3/CD28 mAb activated PBMCs (control: 16.9 ± 6.4%; 50% v/v: control 15.4 ± 5.7 %, inspector 16.8 ± 5.9 %, expander beads 24.1 ± 10.8 %; 100% v/v: control 16.8 ± 6.6 , inspector 15.2 ± 8.0 %, expander beads 22.1 ± 8.7; one-way ANOVA $F = 0.338$, $p = 0.907$, data presented as mean ± SEM, n = 4, **Fig 6.11**), $CD4^+$ T cells did show activation in response to the supernatants, with a trend for increasing activation in a concentration-dependent manner and in line with the strength of activation of the beads themselves (control: 2.9 ± 1.2 %; 50% v/v: control 3.7 ± 0.7 %, inspector 7.8 ± 1.8 %, expander beads 13.5 ± 3.7 %; 100% v/v: control 4.1 ± 0.7 %, inspector 10.7 ± 2.7 %, expander beads 16.4 ± 2.1 %; one-way ANOVA $F = 9.027$, $p < 0.001$, significance differences between Control vs 50% v/v expander beads supernatant ($p = 0.004$) and Control vs 100% v/v expander beads supernatant ($p = 0.001$) determined by Gabriel *post hoc* comparison), data presented as mean ± SEM, n = 4, **Fig 6.11**). NK cells were also activated in response to incubation with supernatants from previously activated PBMCs (control: 12.1 ± 5.5 %; 50% v/v: control 16.1 ± 7.9 %, inspector 62.3 ± 8.7 %, expander beads 95.4 ± 2.1; 100% v/v: control 19.4 ± 6.1 %, 77.7 ± 4.8 %, expander beads 94.7 ± 2.5 %; one-way ANOVA $F = 54.436$, $p < 0.001$, significant differences between Control and all concentrations of both supernatants derived from beads activated lymphocytes ($p < 0.001$) determined by Gabriel *post hoc* comparison, data presented as mean ± SEM, n = 4, **Fig 6.11**). Compared to the control sample, none of the control supernatants were found to have any significant effect on cellular activation for any of the lymphocytes studied, demonstrating that there is no confounding factor within the supernatant that may influence activation.

Whilst there was a concentration dependent activation in conjunction with supernatant derived from incubation with the less potent inspector beads, the activation levels of NK cells in response to supernatant derived from expander bead stimulation were consistent and independent of the concentration of supernatant used. The levels of activation in NK cells were similar to those seen when PBMCs were incubated with the beads, and this is unsurprising as NK cells respond to the released cytokines rather than the beads themselves.

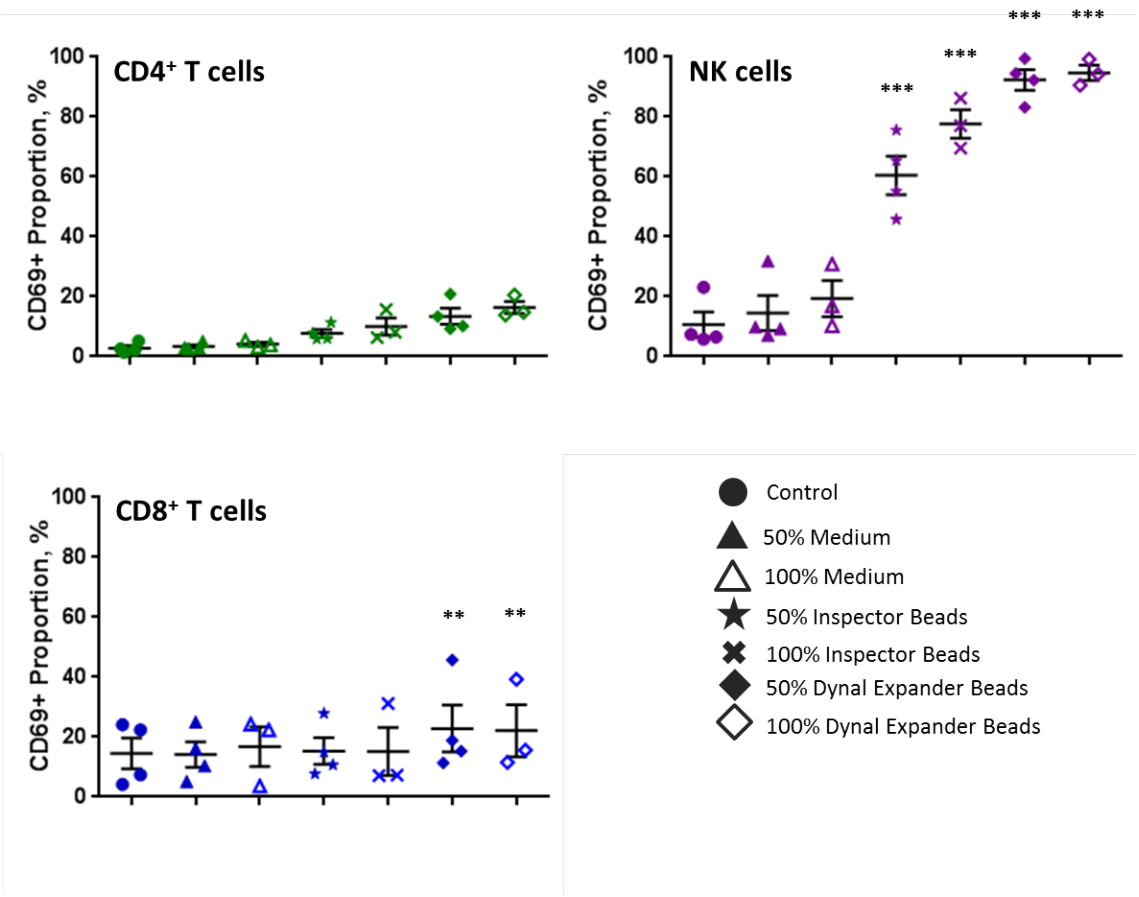

Figure 6.11 Effect of the incubation with supernatants derived from CD3/CD28 mAb activated PBMCs on the activation status of lymphocyte subsets

Incubating PBMCs in supernatant derived from anti-CD3/CD28 mAb activated cells did not lead to any activation of $CD8^+$ T cells, although $CD4^+$ T cells and NK cells did exhibit activation. The most pronounced activation resulted from incubation with the highest concentration of supernatant derived from expander bead (the more potent) stimulation. Data presented as mean + SEM, n = 4. ** $p<0.01$, *** $p<0.001$.

Incubation of PBMCs with supernatants had little effect on cmHsp70.1 mAb binding to T cells, apart from when cells were incubated with 100% v/v supernatant derived from expander bead stimulated PBMCs, but this effect was found not to be of statistical significance ($CD4^+$ T cells – control: 2.86 ± 1.21, 50% v/v: control 2.96 ± 1.12, inspector 2.86 ± 0.85, expander beads 3.26 ± 1.15; 100% v/v control: 2.75 ± 0.73, inspector 2.93 ± 0.81, expander beads 4.41 ± 1.71; one-way ANOVA F = 0.263, p = 0.945. $CD8^+$ T cells – control: 3.93 ± 1.19, 50% v/v: control 4.13 ± 0.95, inspector 3.76 ± 0.79, expander beads 4.09 ± 0.71; 100% v/v control: 3.92 ± 0.52, inspector 3.71 ± 0.60, expander beads 4.73 ± 1.16; one-way ANOVA F = 0.151, p = 0.986. Data presented as mean ± SEM, n = 4, **Fig 6.12**). However, cmHsp70.1 mAb binding to NK cells was increased following incubation with supernatants derived from PBMCs incubated with both inspector and expander beads, although again these effects were not of statistical significance (control: 3.96 ± 1.94 %; 50% v/v: control 3.82 ± 1.72 %, inspector 4.44 ± 2.04 %, expander beads 6.73 ± 2.35; 100% v/v: control 3.55 ± 1.37 %, 4.41 ± 1.73 %, expander beads 8.26 ± 2.93

%; one-way ANOVA F = 0.737, p = 0.628) The results from the using different concentrations of inspector bead supernatant were similar, although the cmHsp70.1 mAb binding following incubation with expander beads supernatant was increased in a concentration-dependent manner.

The magnitude of the relative intensity expression of cmHsp70.1 mAb binding was greater with 100% v/v expander bead derived supernatant than when PBMCs were incubated with expander beads themselves. As NK cells respond to the cytokines released after activation, when beads are used there is a waiting period after addition of the beads and until the T cells begin to release IL-2 and NK cells can respond. When the supernatant is used there is no lag period, as released IL-2 is already present and NKs can respond immediately. If cmHsp70.1 mAb binding is somehow linked to NK activation status, then the increased binding in response to incubation with expander bead-stimulated PBMC-derived supernatant is not surprising.

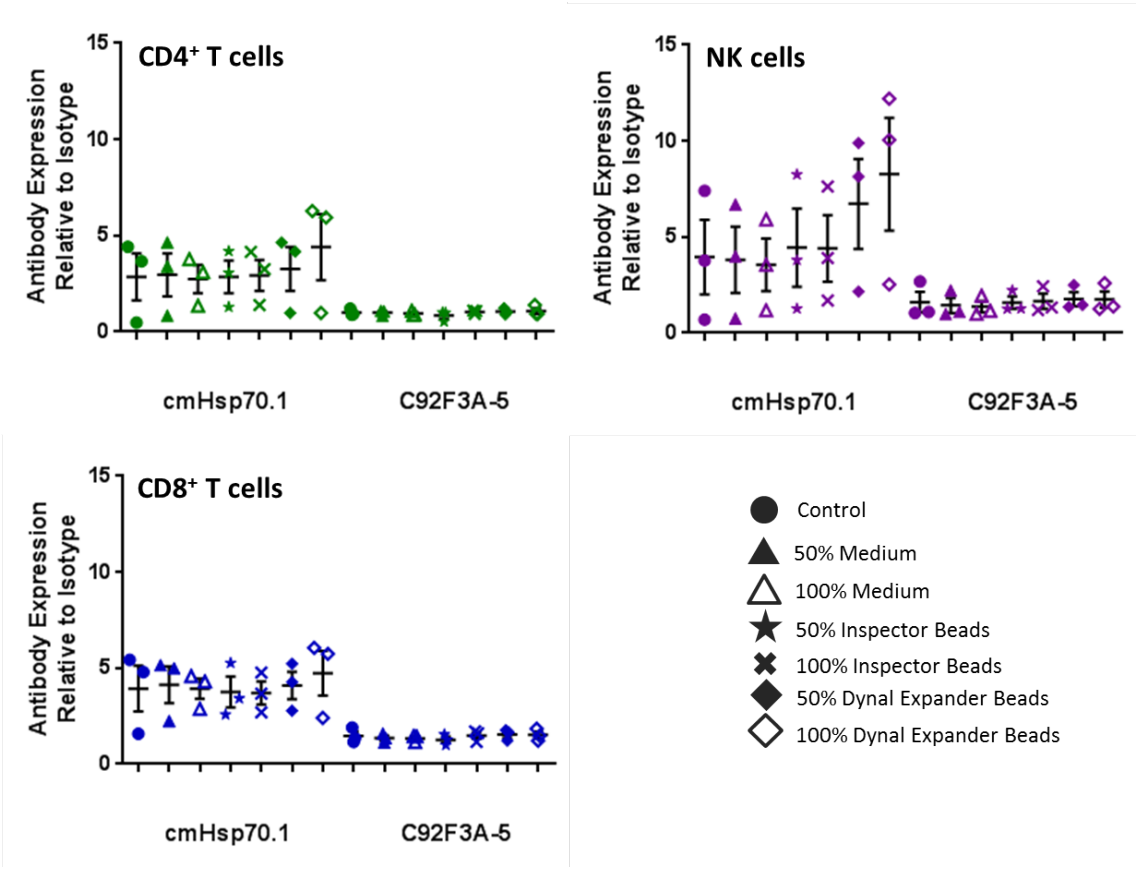

Figure 6.12 Effect of incubation with supernatants derived from CD3/CD28 mAb activated PBMCs on the binding of cmHsp70.1 mAb to lymphocyte subsets

Incubating PBMCs in supernatant derived from bead activated cells did not lead to any change in cmHsp70.1 mAb binding to T cells subsets, only NK cells. The Inspector bead supernatant results in a modest increase in cmHsp70.1 mAb binding, whilst the expander bead-derived supernatant resulted in a concentration dependent increase to the relative intensity of cmHsp70.1 mAb binding up to twice the level of the control. Data presented as mean + SEM, n = 4.

6.1.2.2.4 Relationship between lymphocyte activation status and cmHsp70.1 mAb binding expression

In order to further investigate the possible relationship between activation status and cmHsp70.1 mAb binding, correlation analyses were performed on data relating to the percentage of CD69 expression and the relative intensity of memHsp70 expression for $CD4^+$ T cells, $CD8^+$ T cells and NK cells (**Fig 6.13**). Paired data for percentage of CD69 and relative intensity of cmHsp70.1 mAb binding from all treatments used is presented on scatter plots with linear trendlines applied. For all lymphocyte subsets, there was found to be a significant positive correlation between the expression of CD69 (as a measurement of cellular activation) and the relative intensity of cmHsp70.1 mAb staining (Pearson's Correlation Co-efficient: $CD4^+$ T cells r=0.352, p=0.002; $CD8^+$ T cells r=0.301, p=0.008; NK cells r=0.518, p<0.001). Whilst the correlation is significant for all lymphocyte subsets, the value of the correlation coefficient is fairly low in all instances, suggesting that either activation is just one of many factors that can influence cmHsp70.1 mAb binding.

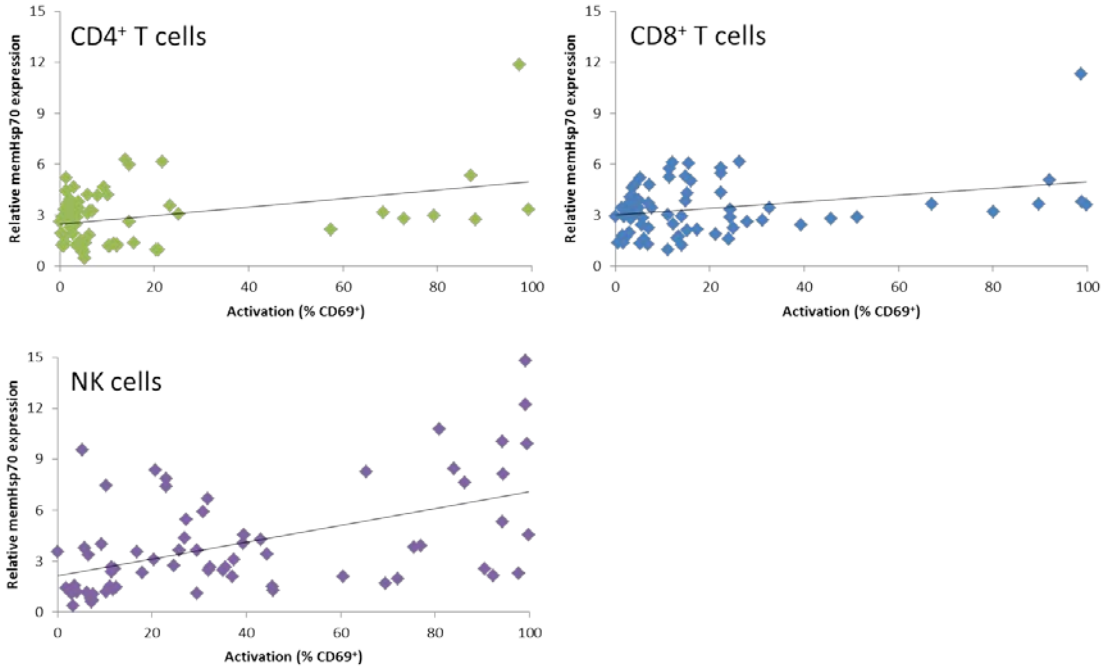

Figure 6.13 Relationship between activation status and cmHsp70.1 mAb binding to lymphocyte subsets.

Regression analysis was conducted to describe the relationship between activation status and cmHsp70.1 mAb binding. Data were combined across all lymphocyte stainings from all treatments (n = 64). Although all lymphocyte subsets were found to exhibit a positive correlation between activation and memHsp70 expression, the magnitude was low indicating that multiple factors in addition to activation could influence cmHsp70.1 mAb binding.

6.1.2.3 Oxidative stress

Using density gradient isolated PBMCs, lymphocytes were assessed for their capacity to bind the cmHsp70.1 mAb following exposure to oxidative stress. This was conducted using two methods; incubation of the cells under 0.1% v/v O_2 in a hypoxic chamber (mimicking the physiological hypoxia in the centre of a tumour) and by incubation in the presence of H_2O_2 (a chemical-induced oxidative stress to investigate whether the mechanism or end result can influence cmHsp70.1 mAb binding).

6.1.2.3.1 Hypoxic chamber

All lymphocyte subsets retained high viability (>85%) after the incubation at 0.1% v/v O_2. Although there appeared to be a trend for the relative intensity of cmHsp70.1 mAb binding to be reduced following exposure to a hypoxic environment, this was not significant for any of the cell subsets ($CD4^+$ T cells: control 2.26 ± 0.34, 0.1% O_2 2.01 ± 0.24; $CD8^+$ T cells: control 3.42 ± 0.52, 0.1% O_2 3.37 ± 0.30; NK cells: control 2.91 ± 0.25, 0.1% O_2 2.38 ± 0.08. Data presented as mean ± SEM, n = 3. Two-tailed Student's paired T test: $CD4^+$ T cells $t(2) = 4.163$, $p = 0.053$; $CD8^+$ T cells $t(2) = 0.420$, $p = 0.715$; NK cells $t(2) = 2.412$, $p = 0.137$. **Fig 6.14**). Power calculations to compute the necessary sample size required to detect significant differences were calculated using G*Power software. $CD4^+$ T cells and NK cells were found to require sample sizes of 31 and 9 respectively, but $CD8^+$ T cells would require 2231. This would suggest that $CD8^+$ T cells do not modulate memHsp70 expression in response to a hypoxic environment. In the future it would be preferable to increase the sample size to 30 to confirm whether memHsp70 expression in $CD4^+$ T cells and NK cells does respond to a hypoxic environment. In addition, as only one time point was assessed and the cell subsets exhibited only a small trend for a reduction in cmHsp70.1 mAb binding following hypoxia, it could be that sustaining a hypoxic environment for a longer duration may result in a greater reduction to cmHsp70.1 mAb binding. However, it would be difficult to apply this environment whilst still maintaining cell viability.

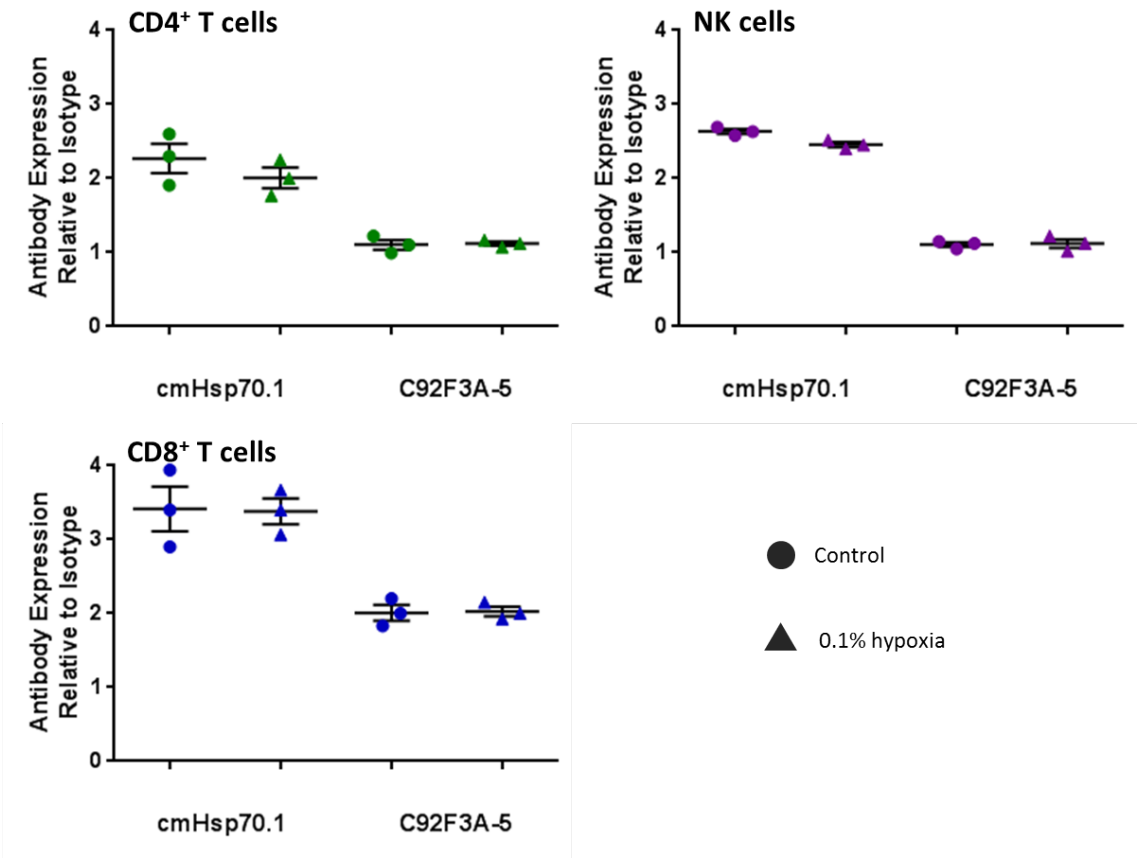

Figure 6.14 Effect of incubation under 0.1% v/v O_2 on the relative intensity of cmHsp70.1 mAb binding

A non-lethal hypoxic environment did not have any significant impact on the relative intensity of cmHsp70.1 mAb binding by lymphocyte subsets, although there was a trend for a reduction. Data are presented as mean + SEM, n = 3.

5.1.2.3.2 Hydrogen peroxide

Density gradient isolated PBMCs were incubated in the presence of H_2O_2. The biggest problem encountered when incubating cells was ensuring a high level of cell viability. Only a 10µM concentration maintained an acceptable level of viability, other concentrations attempted (1000, 100, 50 and 25µM) resulted in only 10-40% of cells remaining viable. To ensure that any results were indeed due to the treatment in question and not an artefact of other stresses within the environment, only the 10µM was selected for investigation. All lymphocyte subsets were found to exhibit a significantly reduced relative intensity of cmHsp70.1 mAb binding following incubation in the presence of 10µM H_2O_2 ($CD4^+$ T cells: control 2.95 ± 0.34, H_2O_2 2.47 ± 0.33; $CD8^+$ T cells: control 3.41 ± 0.29, H_2O_2 2.90 ± 0.25; NK cells: control 3.81 ± 0.29, H_2O_2 3.07 ± 0.34. Data presented as mean ± SEM, n = 3. Two-tailed Student's paired T test: $CD4^+$ T cells $t(2) = 7.021$, $p = 0.020$; $CD8^+$ T cells $t(2) = 13.180$, $p = 0.006$; NK cells $t(2) = 6.712$, $p = 0.021$, **Fig 6.15**).

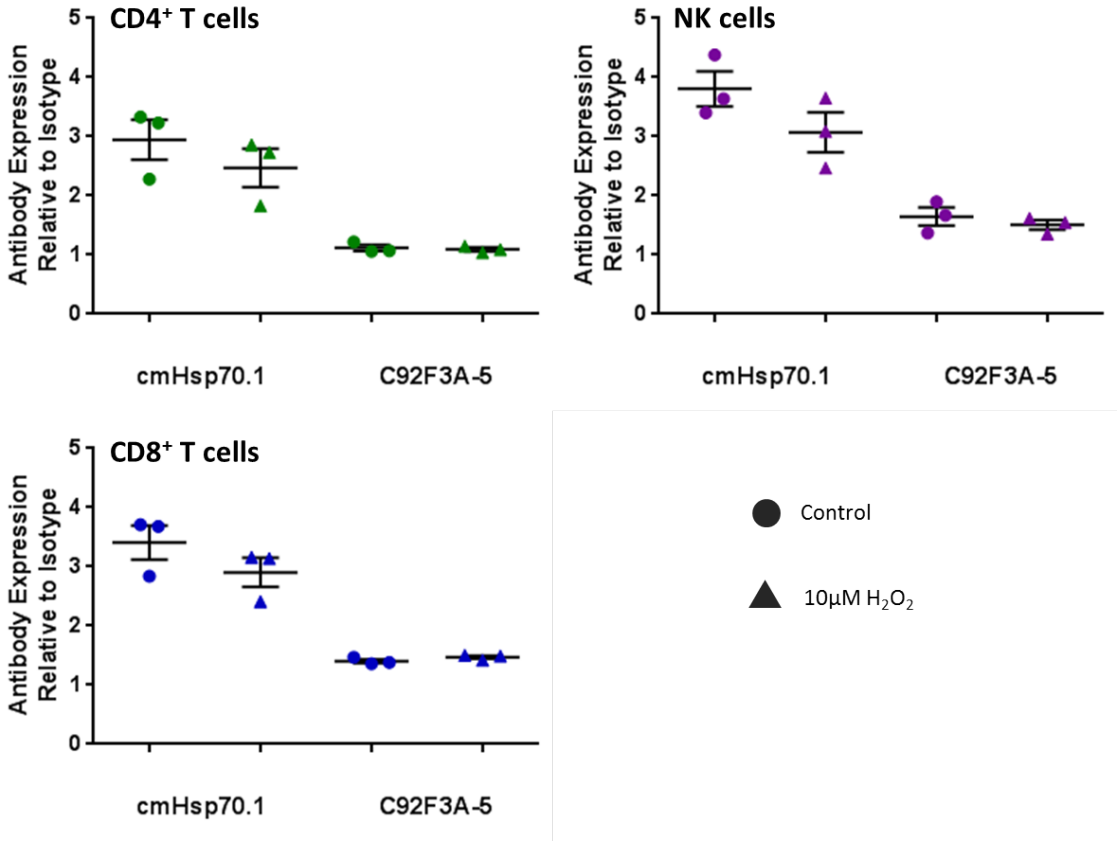

Figure 6.15 Effect of H2O2 incubation on the relative intensity of cmHsp70.1 mAb binding to lymphocyte subsets.

Incubating PBMCs with 10µM H_2O_2 induces a chemical hypoxia and leads to a reduction in cmHsp70.1 mAb binding by T cell populations and NK cells. Due to high levels of non-viability when greater concentrations were used, it was not possible to demonstrate a concentration dependent curve within the results. Data presented as mean + SEM, n =3.

6.2 Summary

None of the peripheral cell populations assessed *ex vivo* were found to express memHsp70, which falls in line with other published data that healthy tissue is memHsp70$^-$ and only tumour tissue is positive for memHsp70. When cellular activation was performed *ex vivo* on whole blood samples then there was also no expression of memHsp70. When PBMCs were isolated via density gradient separation there was the appearance of cmHsp70.1 mAb binding. Whilst this demonstrates that cells have some capacity to exhibit Hsp70 on their membrane it is also worth noting that is a highly artificial scenario and that cellular separation does not have an *in vivo* analogy and it does not mean that cells would memHsp70 in the circulating periphery. Although some regulation of cmHsp70.1 mAb binding to lymphocyte subpopulations in response to certain stimuli (cell activation, hypoxia and tumour-secreted factors) was apparent, it is difficult to assess the relevance of these findings. Since the stimuli were applied to isolated PBMCs which were already binding cmHsp70.1 mAb binding in a somewhat artificial manner, it is unclear whether the same stimuli would have resulted in cmHsp70.1 mAb binding if the cells had not undergone the density gradient separation.

CHAPTER 7 Discussion

Hsp70 is a molecular chaperone which serves a number of cytoprotective and essential 'housekeeping' functions in times of internal and external stress. The upregulation of intracellular Hsp70 expression is a common feature of cancer cells and relates to their highly proliferative state. Importantly, in the context of cancer, the upregulation and elevated expression of heat shock proteins confers protection against the effects of many therapeutic interventions.

The cytoprotective effect of Hsp70 in cancer cells can be deleterious to patients, as illustrated by the observation that the prognosis of patients whose tumours express high levels of intracellular Hsp70 is typically worse [562]. The occurrence of environmental stresses can further upregulate the expression of Hsp70, via the transcription factor heat shock factor 1 (HSF1). HSF1 has also been found to be overexpressed in tumour cells, and is a cause of the constitutive overexpression of Hsp70 [563]. The association of Hsp70 and HSF1 overexpression with poor patient prognosis is related to an increased incidence of metastasis and an enhanced resistance to chemo- and radiotherapies [564]. Since knock-down of Hsp70 or HSF1 leads to enhanced sensitivity of cancer cells to radiotherapy [565], a similar response may be possible via the application of inhibitors. In this regard, the small molecular weight Hsp70/HSF1 inhibitor NZ28 has been reported to reduce Hsp70 and HSF1 levels *in vitro* to such an extent that treated cancer cells subsequently exhibit an increased susceptibility to radiation [566].

Another heat shock protein which has generated interest for therapeutic targeting using inhibitors is Hsp90. A multitude of oncogenic client proteins including HER2, mutant p53, mutant EGFR, surviving and HIF-1α are chaperoned by Hsp90 and consequently the effective inhibition of Hsp90 offers an attractive potential anti-cancer avenue. The use of Hsp90 inhibitors can improve the radiosensitivity of tumour cell lines [567, 568], however one significant hurdle to overcome is that inhibition of hsp90 is one of the stresses which activates HSF1, consequently triggering upregulation of Hsp70 expression and the cells gain back some radioresistance. Experiments performed *in vitro* on breast and lung cancer cells lines have shown that the use of an Hsp90 inhibitor (NVP-AUY922) in addition to the Hsp70/HSF1 inhibitor NZ28 results in lower concentrations of inhibitors (~20 fold) being required in order to see the same increase in tumour radio-sensitivity [566].

In addition to being expressed intracellularly, a large proportion of tumours (~50-80%) have been found to also display Hsp70 on the surface of their plasma membrane (memHsp70) [287,

569]. This membrane-associated localisation of Hsp70 is restricted to tumours, with normal surrounding tissue and other tissues being negative for memHsp70 expression. Ongoing analysis of patient tumour biopsies (currently standing at over 1300 samples) confirms the tumour-specificity of memHsp70 and shows memHsp70-positivity occurs in 40-80% of tumours, depending on the tumour type. When biopsies from primary and secondary tumour tissue are available, the metastases maintain the memHsp70 phenotype of the primary tumour [532]. Analysis of a smaller cohort, comparing biopsies of 150 patients with either colon, gastric, lower rectal or squamous cell carcinomas found that whilst all tumour types expressed similar levels of memHsp70 (37-43%) there was a disparity between memHsp70 status and patient survival. For those patients with colon and gastric carcinoma, the presence of memHsp70 correlated with longer overall survival, but for lower rectal and squamous cell carcinomas the opposite was true with memHsp70^{+} patients having a reduced overall survival [515]. The authors hypothesise that the favoured routes of metastasis may account for the survival differences. Both colon and gastric cancers metastasise through the liver, and the authors propose that hepatic natural killer (NK) cells may better recognise memHsp70^{+} cells and hence patients may gain a survival benefit [515]. This is supported by findings that memHsp70 serves as a target recognition and activation structure for NK cells [288, 570] as well as the increased abundance of NK cells in the liver [571].

The definitive presence of this unique membrane form of Hsp70 is confirmed by staining cells using an anti-Hsp70 mAb (clone C92F3A-5) which recognises an epitope which is not available when Hsp70 is expressed in its membrane, but is available if extracellular Hsp70 has become associated with the cell surface. The mechanism for the presence of memHsp70 has not yet been elucidated, although data from the memHsp70^{+} mouse colorectal carcinoma cell line CT26 has provided evidence for the co-localisation of memHsp70 within cholesterol-rich microdomains [518] [572], based on the observation that cholesterol depletion by methyl-beta cyclodextrin treatment led to a reduction in the membrane expression of hsp70 [518]. The authors observed no change in memHsp70 expression when cells were subject to modifications in environmental salt concentrations or pH, which would have been indicative of associations with proteins, leading to the assumption that memHsp70 interacts with membraneous lipids [518]. Profiling cell membranes of memHsp70^{+} and memHsp70^{-} colon and pancreas carcinoma cell lines by electrospray tandem mass spectrometry found no difference in phosphatidylcholine, sphingomyelin, dihydrosphingomyelin, ceramide, phosphatidylserine, phosphatidylethanolamine or glucosylceramide, however globotriaosylceramide (Gb3/CD77) was found to exhibit at significantly higher levels in memHsp70^{+} cell lines [518]. Performing

vesicle copellation assays showed that Hsp70 bound to vesicles containing Gb3, but not to those with other, physiologically relevant lipid compositions.

From a potential therapeutic perspective, studies have demonstrated that memHsp70 can act as a target recognition structure for NK cells that have been activated (4 days) *in vitro* with low dose IL-2 alone (100IU/mL) [523, 526] or with low-dose IL-2 in addition to a 14-mer peptide which includes the epitope to which the cmHsp70.1 mAb is reactive. Such activated NK cell populations have been shown to selectively kill memHsp70^{+} CT26 cells [533], as well as a range of other murine and human tumour cells that express the membrane form of Hsp70 *in vitro* [523, 573]. The Multhoff group translated these findings into the clinical setting by undertaking a Phase I clinical trial to assess the safety and tolerability of adoptively-transferred 14-mer peptide/IL-2 activated autologous NK cells in 11 patients with colorectal cancer and one with non-small cell lung cancer [528]. The trial showed the procedure to be safe, with no negative side effects in patients. Following the procedure, activated NK cells comprised 8-20% of patients' lymphocytes, and in 10 of the 12 patients *in vitro* cytolytic activity of 14-mer-peptide/IL-2 activated NK cells was enhanced. In a follow-up study of one of the patients with colorectal carcinoma [529], a stable cell line was generated from the patient's own tumour to allow personalised cytotoxicity assays to be performed using the patients NK cells following repeated cycles of infusion following leukapheresis and extrinsically activated with 14-mer peptide and IL-2. The patient received 9 infusions, 6 of which were given monthly, and the remaining 3 being given monthly following a 3-month pause. NK cell responsiveness was increased following activation and infusion, and this was heightened with each cycle [529]. The pause in treatment led to a gradual decline in responsiveness, but this was recovered when treatment resumed. This leukapheresis/activation/re-infusion therapeutic strategy is currently being investigated in a randomised multicentre Phase II clinical trial in patients with non-small cell lung carcinoma lung cancer who have opted for chemo(radio)therapy [574].

NK cell-mediated tumour cell lysis *in vitro* can be enhanced in the presence of cmHsp70.1 mAb, due to the induction NK cell-mediated antibody-dependent cellular cytotoxicity (ADCC) [522]. These findings have been extended and corroborated by *in vivo* observations that mice bearing implanted CT26 tumours that received three doses of cmHsp70.1 mAb exhibited both a significant reduction in tumour size as well as an infiltration of NK cells into the tumour microenvironment [533].

An important feature of membrane Hsp70 expression is that 'standard' therapeutic approaches such as chemotherapy and radiotherapy enhance the cell surface density of Hsp70 on tumours [290, 519, 575, 576], thereby enhancing the potential sensitivity of tumours to

targeting by NK cells, the cmHsp70 mAb and granzyme B, as well as improving the potential to image and define the boundaries of the tumour using appropriately labelled cmHsp70.1 mAb and Hsp70-derived peptides.

7.1 The cmHsp70.1 monoclonal antibody as a theranostic

The term "**theranostics**" has been coined to define the pre-clinical and clinical approaches that are being used to develop more specific, individualised therapies for various diseases, and to combine diagnostic and therapeutic capabilities into a single agent.

In addition to being capable of identifying the expression of memHsp70 by tumour cells and inducing ADCC *in vitro* and *in vivo*, the cmHsp70.1 mAb can also be selectively taken up into tumour cells, as demonstrated by the tumour-specific accumulation of FITC-labelled cmHsp70.1 mAb into memHsp70^{+} CT26 carcinoma cell-derived tumours [533]. These initial studies have been extended and expanded upon in the programme of work which constitutes this thesis. The cmHsp70.1 mAb therefore offers potential platform on which to develop new tumour imaging and targeting strategies, either as a sole reagent, or as part of an imaging / therapeutic complex in the clinical setting. These could be particularly valuable for the visualisation and targeting of metastatic disease, since it would allow for a specific way to pinpoint or treat even small, distant metastases.

With breast cancer being one of the most prevalent malignancies in the world, and one which is responsible for over 500,000 deaths per year worldwide and nearly 15,000 deaths per year in the UK alone (http://www.cancerresearchuk.org/cancer-info/cancerstats), it is vital that novel treatment options are explored [577, 578]. Aggressive and invasive breast cancers have higher mortality rates, so a molecule which allows for metastatic targeting could offer improved prognosis for these patients – approximately 90% of all breast cancer-related deaths result from metastatic disease. Although not yet confirmed for breast cancer, a comparison of memHsp70 expression on biopsy tissue from primary and metastatic sites found that not only was memHsp70 expression retained, but it was actually higher in metastases than the primary tumour [532]. This may result in memHsp70 being an even better candidate for metastatic targeting. A minority of breast cancers are classified as triple negative, meaning that they do not express HER-2, oestrogen receptor or progesterone receptor. As such, currently available targeted strategies cannot be employed so any other specifically expressed molecule that may be able to offer new therapeutic targets should be welcomed. With memHsp70 present on around 50% of breast cancers, and could be exploited for imaging, inducing ADCC or as part of a theranostic and delivery platform, it is therefore a very attractive proposition.

The expression of membrane Hsp70 on a panel of human breast cancer cell lines (MDA-MB-231, MCF7, T47D) having different characteristics that are relevant to clinical outcome was determined, and the internalisation and intracellular trafficking of the cmHsp70.1 mAb into these assessed.

Cell Line	HER2	ER	PR	Classification	Disease severity represented
MDA-MB-231	-	-	-	TNBC	+++
MCF7	-	+	Low	Luminal A	++
T47D	-	+	High	Luminal A	+

Replication of Table 2.1: Characteristics of the human breast cancer cell lines selected
A summary of the key differences between the three human-derived breast cancer cell lines used in this study, in terms of receptors expressed and disease severity represented. HER2 (also HER2/neu) = Human epidermal growth factor receptor 2. ER = Oestrogen receptor. PR = Progesterone receptor.

Similar studies were performed using the mouse mammary carcinoma line 4T1, as this is a widely used murine model of aggressive and metastatic breast cancer [579]. Although no *in vivo* work was carried out in the current study, future work will examine the imaging and therapeutic potential of memHsp70 targeting in this model. It is one of the most widely used animal models of breast cancer, can be grown with ease in the correct anatomical site and as since it develops spontaneous metastases can be used as a model for aggressive disease [579]. As a comparator with previous studies, the mouse colorectal carcinoma line CT26 was also used. In addition to the binding of the cmHsp70.1 mAb to memHsp70$^+$ tumours, this study clearly demonstrates the ability of cmHsp70.1 mAb to be internalised by memHsp70$^+$ tumour cells. *In vitro*, the kinetics of uptake were dependent on the relative expression of memHsp70, with more rapid uptake into MDA-MB-231 and MCF7, those cell lines with high expression. The uptake of cmHsp70.1 mAb into tumours expressing memHsp70 could serve as a specific delivery vessel for cytotoxic agent(s). This could include the coupling of the cmHsp70.1 mAb to nanocarriers containing cytotoxic drugs or as part of an antibody-drug targeting complex.

Nanocarriers are nano-scale transport vessels with no tumour specificity of their own, but which may be coupled to targeting molecules such as antibodies, and can be loaded with anti-tumour agents (such as chemotherapeutic drugs). By packaging the cytotoxic agents in this way specific delivery to the tumour is favoured, resulting in high concentrations intratumourally, but low toxicity throughout the body, especially when compared to systemic administration of the free drug [580-582]. Other benefits are that the drug has protection from peripheral degradation prior to reaching the tumour target, as well as clearance through the kidneys being reduced, with the net result being that more of the drug remains available to

accumulate in the tumour [583, 584]. There are different forms of nanocarriers, including carbon nanotubes (cylindrical structures with ultra-high surface areas able to hold drugs in the cavity and on the surface, but exhibiting some toxicity issues due to their insolubility in all solvents [585-588] liposomes (membraneous lipid-bilayer structures which entirely encapsulate drugs, and can deliver both hydrophilic and hydrophobic compounds and have been highly favoured in pre-clinical investigations, but their administration can result in complement activation-related pseudoallergy and they offer limited control over the release of their contents [589-591]) and polymeric nanocarriers (polymer-based formations which can be presented in different structures and improve on the characteristics of liposomes being more stable, having longer circulation times, have higher capacities for loading and allow more control over content release [592, 593]).

There are numerous studies involving all types of nanocarrier and these have been comprehensively reviewed elsewhere [594]. With regards to breast cancer, ongoing trials are assessing the use of these nanocarriers as drug delivery agents. Two phase I trials looking at doxorubicin in liposomes given to 29 pre-treated patients with recurring breast cancer found the treatment was well-tolerated, with half of patients showing a local response [595]. There has been FDA approval of one polymeric nanocarrier for use in breast cancer; abraxane, albumin–bound paclitaxel [596-599]. Although these strategies use nanocarriers, there is no specific tumour targeting via antibody conjugates however this is also a strategy being investigated. Using a doxorubicin-loaded, iron oxide nanoparticle conjugated to the anti-HER2 monoclonal antibody Herceptin, specific uptake in to $HER2^+$ breast cancer cell lines along with cell cytotoxicity has been demonstrated [600] and could offer a more efficient treatment option to patients in the future. In light of this, it is reasonable to think that a strategy of conjugating the cmHsp70.1 mAb to drug-loaded nanocarriers may be a viable one.

The cmHsp70.1 mAb could also have a use in imaging tumours. As demonstrated herein, fluorescently-labelled cmHsp70.1 mAb is readily taken up into $memHsp70^+$ tumour cells and the same has been shown to be true for $memHsp70^+$ CT26 tumours implanted into mice. Given the broad expression of memHsp70 across a range of tumours this could prove useful for a large number of patients. Since fluorescence imaging is best conducted through short distances and will not be effective for imaging deep tumours in humans, this idea may be best translated by finding more appropriate labels for the antibody.

7.2 The TKDNNLLGRFELSG peptide as a theranostic

There has been an increased interest in the use of peptides in cancer therapeutics [558, 601-604] due to their ability to penetrate tissue well, and their better biodistribution profiles over

alternatives such as antibodies. Furthermore, peptides can be produced at a relatively lower cost. One benefit of specific tumour-targeting peptides is their use as delivery vectors for anti-tumour agents such as cytotoxic drugs. A 15-mer peptide derived from follicle stimulating hormone β specifically binds with high affinity to the follicle stimulating hormone receptor (FSHR) in the ovaries [605] and is subsequently taken up into cells. The specificity of binding and uptake led the authors to generate peptide-nanoparticle conjugates, with the nanoparticles containing paclitaxel, as a route to allow drug delivery specifically to cancer cells [606]. Between 50-70% of ovarian cancers express FSHR making this a treatment strategy of benefit to a large proportion of patients with this disease. However, this benefit is likely to be greater in patients with early stage disease, since secondary metastases have been found to be FSHR negative, despite the presence of FSHR on the patients primary tumour [606].

Another example is the 17-mer peptide (termed BR2) [607] derived from buforin llb, itself a peptide derivative from histone H2A [608]. The peptide is known to interact with cells via surface gangliosides and is taken up into cells by lipid-mediated macropinocytosis. The authors have been developing the peptide as a drug delivery vehicle, using a fusion to a single-chain variable fragment directed to mutated K-ras, which is able to suppress Ras activity and induce cell death. Although this targeting is not restricted to one cancer type, the cancer specific cytotoxicity is very much determined by concentration. Increasing the peptide concentration eventually reaches a level where normal cells are affected, and this is obviously a concern when thinking of translating this into the clinic.

Peptides may also themselves give direct anti-tumour effects, as seen *in vitro* with a (12-mer) peptide which, when taken up into SKOV3 cells down-regulates Bcl-2 in a caspase-dependent manner thereby inducing apoptosis [609] and in an *in vivo* breast cancer model using a 9-mer peptide which accumulates in MDA-MB-435 implanted tumours and induces cell death. However, the mechanism for this cytotoxic is unknown [610]. Targets currently under investigation for peptide-based tumour therapies typically express on specific tumour types and therefore are of potential benefit to a niche group of cancer patients.

A 14-mer peptide derived from the region of Hsp70 that is available at the cell surface when it is in the membrane (TKDNNLLGRFELSG) form has already been used in a phase I clinical trial, whereby NK cells activated *ex vivo* in the presence of the TKDNNLLGRFELSG peptide in conjunction with low dose (100 IU/mL) IL-2 were investigated for their ability to target patient tumours [528]. The TKDNNLLGRFELSG peptide is now being used in a similar strategy in a phase II trial involving patients with memHsp70^{+} lung cancer [574]. As well being used in the activation of NK cells, the peptide can also be used directly where it can bind to, and be taken

up by memHsp70 on tumour cells [535], as has been demonstrated herein. The specificity of the binding and internalisation of TKDNNLLGRFELSG peptide has been further confirmed using an Hsp70 knockout ($Hsp70^{-/-}$) 4T1 model, in which the proportion of cells taking up the TKDNNLLGRFELSG peptide falls from 49% for wild type cells to 1% in the knockout [535]. A key advantage of the TKDNNLLGRFELSG peptide over others that are currently available in the clinical setting, either as an imaging agent or drug delivery enhancer is that memHsp70 is selectively expressed on a broad range of tumour types, and therefore the profile potential recipients for whom this approach will be effective is markedly greater than that for other peptides whose targeting molecules are more restrictively expressed [557, 558, 601, 611, 612]. Furthermore, the expression of memHsp70 can be induced, enhanced by chemotherapy [290] and radiotherapy [613].

Data shown herein confirm that the TKDNNLLGRFELSG peptide is able to bind to and be internalised by memHsp70. The fluorescently-labelled TKDNNLLGRFELSG peptide accumulates in the cells over time, at levels which correlate with the amount of memHsp70 expressed. Internalised TKDNNLLGRFELSG peptide is observed to be present in the cytoplasm of cells, as seen in confocal microscope imagery, as well as in distinct regions which appear to be vesicular structures. However, fixation and permeabilisation resulted in the TKDNNLLGRFELSG peptide being lost from cells and so the co-localisation of TKDNNLLGRFELSG peptide could not be determined. It was possible to determine the co-localisation of the TKDNNLLGRFELSG peptide with mitochondria, as these could be stained using a passively diffusing dye which can enter live cells without the need for fixation and permeabilisation steps. In future experiments, similar 'live dyes' could be employed to stain other intracellular structures in order to allow for a more comprehensive profile of TKDNNLLGRFELSG peptide trafficking.

In all human and mouse cell lines studied, the TKDNNLLGRFELSG peptide was found to co-localise with the mitochondria, with proportion of co-localisation increasing with increased memHsp70 expression levels. There have been reports of peptides and small molecules which exhibit anti-tumour effects by targeting the mitochondrial membrane. For example, take up of the 14-mer cationic α-helix forming peptide by breast cancer cell lines MCF7 and MDA-MB-231 has been shown to result in a proportion of cells dying by apoptosis which is associated with a disruption of the mitochondrial membrane, as determined by Mitotracker Red staining [614]. Following compound screening, a small molecule within the class of triphenylphosphonium salts was found to induce G_0/G_1 cell cycle arrest following accumulation in the mitochondria of a number of pancreatic cancer cell lines, leading to an increase in reactive oxygen species (ROS) as well as cleavage of caspases and PARP-1 indicating apoptosis [615]. However, the TKDNNLLGRFELSG peptide does not appear to have a direct anti-tumour effect. Cell lines

treated with TKDNNLLGRFELSG peptide (up to 750mg/mL, equivalent to 2M) showed no evidence of apoptosis on the basis of morphology, microscopy, cytochrome c release or caspase-3 activation [535]. Although not having any apparent direct anti-tumour effects, the TKDNNLLGRFELSG peptide still has potential for use in tumour imaging, or to aid the specific delivery of apoptotic agents to tumour cells, for example through the coupling of TKDNNLLGRFELSG peptide to cytotoxic drugs or to radionuclides [602].

The TKDNNLLGRFELSG peptide exhibits a rapid and progressive internalisation into memHsp70^{+} tumour cells. Unfortunately the current experimental setup makes direct comparison between the uptake kinetics of TKDNNLLGRFELSG peptide and cmHsp70.1 mAb highly problematic. The TKDNNLLGRFELSG peptide is conjugated during synthesis, whereby each 14-mer TKDNNLLGRFELSG peptide is labelled with one molecule of fluorescein. The cmHsp70.1 mAb used in the flow cytometric analyses is labelled with FITC in a post-synthesis conjugation reaction, with each antibody having an average of 3-4 FITC molecules. Without a directly comparable fluorescent label it is therefore not possible to accurately compare the internalisation kinetics of both molecules. This would be something to consider as a future extension to this work.

The potential value of the TKDNNLLGRFELSG peptide in the management and treatment of cancers expressing the membrane form of Hsp70 is multifaceted. The specificity of peptide binding as well as the rapid uptake kinetics into memHsp70^{+} tumour cells means that the TKDNNLLGRFELSG peptide could be used for better tumour imaging, of both primary and metastatic tumours. Fluorescently labelled TKDNNLLGRFELSG peptide administered to mice with implanted memHsp70^{+} CT26 tumours has been shown to accumulate in the tumour site and was maintained for at least 24 hours [535]. Due to the specificity of binding and well characterised internalisation pathway of TKDNNLLGRFELSG peptide, the peptide could be coupled to other agents (such as nanocarriers for example) and used as a delivery vector, facilitating the delivering of cytotoxic or radiotherapeutic agents, for example.

Key elements of this study have now been published [535], in which the TKDNNLLGRFELSG peptide has been termed, on the basis of the results, a tumour-penetrating peptide (TPP) and have underpinned further investigation of the peptide as a tool for *in vivo* tumour imaging [616]. A variety of tumour models (including those of colon, breast, pancreas, small-cell and non-small cell lung cancer, head and neck carcinoma and cervical cancer origin) and covering syngeneic, spontaneous, chemically-induced and xenograft models which were memHsp70^{+} were found to take up and accumulate the TPP in a highly tumour-specific manner. This occurred with greater specificity than the commercially available tumour targeting small

molecule IntegriSense (Perkin Elmer), which is marketed for *in vivo* tumour imaging and acts through binding $\alpha_v\beta_3$-integrin.

Importantly, these approaches would work in conjunction with standard therapies such as chemotherapy or radiotherapy, since they are dependent only on the presence of memHsp70, the expression of which is can be enhanced following standard cancer therapies. This contrasts to potential considerations for peptides to be used in vaccination strategies, where effectiveness has been seen to be hampered by previous treatments efforts. For example, in a phase II clinical trial involving 42 patients with progressive, castrate-resistant prostate adenocarcinoma treated with a personalised peptide vaccine (formed as a combination of 2-4 peptides selected from a list of 31 candidates depending on patient responsiveness), those patients who had received no prior docetaxel-based chemotherapy showed a significant overall survival benefit of 8 months [617].

7.3 Granzyme B

Granzyme B is a serine protease which causes apoptosis by cleaving substrates within apoptotic pathways (including Bid, Bax and caspases). Granzyme B is a primary constituent of the cytotoxic granules of NK cells and T cells. Common understanding is that granzyme B acts in concert with perforin, a pore-forming protein, in order to allow uptake and subsequent cytoplasmic release [618]. Perforin is highly conserved within mammalian species and is encoded for by a single gene, *PRF1*.

The ability of granzyme B to induce apoptosis in the absence of perforin is controversial. The concept is not widely accepted, and has at times been dismissed as an artefact of too high a granzyme B concentration. However there are published data to support the proposition that granzyme B can elicit cytotoxicity in the absence of perforin. Hagn et al [619] found that B cells can differentiate into cytotoxic plasma cells that are capable of secreting granzyme B in response to IL-21 produced by $CD4^+$ T cell which lack co-stimulation and therefore do not express CD40L. However, these 'cytotoxic B cells' lack the perforin thought to be necessary for granzyme B uptake. Interestingly the authors found that over a co-incubation period of 3 days the B cell derived granzyme B was observed to transfer to and be taken up by HeLa cervical cancer cells and the malignant melanoma cell line G-361. The result is a reduction in cell viability by 41% and 21% respectively. Although the authors do not offer memHsp70 as a potential explanation for this, it was not an avenue that they explored and may offer an explanation for this phenomenon.

Perforin causes pore formation in cell membranes in a calcium-dependent manner [620], although there remains some discussion as to the exact mechanism of action by perforin in

combination with granzymes. Two favoured hypotheses are that perforin punctures holes directly in the plasma membrane of target cells which are large enough to permit the influx of granzymes [621, 622]. An alternative mechanism is that both perforin and granzymes are endocytosed together into target cells, and perforin punctures the membrane of the endocytic vesicles allowing granzyme escape into the cytoplasm [623]. A third hypothesis is that perforin causes damage to the outer membrane of target cells and that during the process of membrane repair, granzymes can be taken up into vesicles [83]. This latter mechanism is a less favoured, as it offers no explanation for how granzymes may leave the vesicles and exert their effect [624]. Furthermore, previous studies have shown that recombinant Granzyme B generated in *E. coli* can only induce apoptosis in tumour cells in the presence of perforin [625].

Five granzymes have been described in humans, with granzyme B being the most abundant and the most widely studied. Granzyme B is highly pro-apoptotic and has multiple substrates within apoptosis pathways [626]. One is the BH3 interacting-domain death agonist BID, upon proteolysis by granzyme B BID goes on to activate the apoptosis regulator Bax (bcl-2-like protein 4) and/or Bak (Bcl-2 homologous antagonist killer and consequently they oligomerise within the mitochondrial outer membrane [627-631]. This causes membrane permeabilisation which can directly induce apoptosis, but also leads to the subsequent escape of the mitochondrial protein cytochrome c into the cytoplasm [632] which triggers downstream effects in the form of formation of an Apaf-1/caspase-9 complex and cellular apoptosis [633-635]. Granzyme B can also activate caspase-8 through the cleavage of procaspase-8, triggering caspase-7 activation as a precursor to apoptosis as well activation of caspase-3 (which can also occur directly through cleavage of procaspase-3 by granzyme B) which causes the inhibition of PARP and therefore apoptosis, and the cleavage of ICAD to CAD leading to DNA fragmentation and apoptosis [60, 559]. Another result of caspase-8 activation is the cleavage of BID into truncated BID (tBID) which can insert into, and permeabilise, the mitochondrial outer membrane as well as activating Bax and/or Bak causing the same. This intertwining of pathways containing multiple granzyme B substrates makes the situation a little confusing. For many years the mechanism of action has been difficult to decipher due a number of confounding factors such as the significance of difference substrates, the method of granzyme delivery in experiments, whether *in vivo* or *in vitro* experiments were performed, whether recombinant or purified protein was used, including taking into account species variations [624]. It is now clear that when human granzyme B is used in a human system, BID is a highly favoured substrate. However, if mouse granzyme B is used, then direct activation of caspase-3 and caspase-8 is preferred [636].

Granzyme B has been found to bind to Hsp70 [530] and the memHsp70$^+$ cancer cell line CT26 exhibited a degree of cell killing when incubated in the presence of granzyme B. However, an important finding has been that recombinant granzyme B can only kill membrane Hsp70 positive tumour cells if it has been produced in a mammalian system; recombinant granzyme B generated in *E. coli* and *Pischa pastoris* [637] expression systems cannot induce apoptosis in memHsp70$^+$ tumour cells in the absence of perforin. Mammalian posttranslational modifications and glycosylation are therefore crucial for effective memHsp70 mediated granzyme B uptake [531]. When administered i.v. to mice with implanted memHsp70$^+$ CT26 tumours, human recombinant granzyme B was found to reduce tumour burden via the induction of apoptosis of tumour cells, whereas no effect was seen on surrounding normal tissues and no adverse effects were observed in the mice [532]. The apoptotic regions were observed in areas of the tumours in close proximity to blood vessels, a finding which is consistent with the i.v. route of granzyme B administration which was used in this study. The human recombinant granzyme B used for these *in vivo* studies was produced using transfected HEK293 cells engineered to secrete inactive granzyme B into the supernatant with subsequent activation of the molecule being possible by way of enterokinase digestion cleaving the inactivation site. The same method was used to produce the granzyme B in this study. Whilst the CT26 cell line was included to allow comparisons with published data, the current study focussed on the uptake of granzyme B in breast cancer cell lines and its effects.

The use of recombinant human granzyme B to directly induce the apoptosis of memHsp70$^+$ tumour cells makes for a highly attractive platform on which to base new and/or enhance existing therapeutic approaches. As demonstrated herein, granzyme B is readily taken up into memHsp70$^+$ tumour cells and causes death in a proportion of cells. Cell death was observed on the basis of cell numbers as well as morphological changes. However, in contrast to previous studies which used CT26 colon carcinoma cells [532], caspase-3 activation was not observed in the current study. This may be explained by the observation that granzyme B in a mouse system (as in the mouse colorectal carcinoma cell line CT26) favours caspase-3 activation [636]. In fact, the lack of caspase-3 involvement presented herein is supported by other published literature showing that the predominant route of action of granzyme B in a human system is in fact through the truncation of Bid and Bax, which leads to an alteration in the mitochondrial membrane potential and therefore the release of cytochrome c [638].

The confocal microscopical analysis of cells stained with Mito ID red (to visualise the mitochondria) and incubated with fluorescently labelled granzyme B provides evidence that granzyme B which is taken up via memHsp70 locates to the mitochondria. This is the first study to demonstrate the localisation of granzyme B to mitochondria. When granzyme B acts in

conjunction with perforin, the granzyme B is internalised into early endosomes and then released into the cell cytoplasm [83]. Although some granzyme B locates to the nucleus, it is not known to directly traffic to the mitochondria [639]. However, in contrast to granzyme B, there is evidence that granzyme A can induce cell death with direct mitochondrial involvement. This process appears to involve the binding of granzyme A to the cytosolic chaperones hsp70 and hsp90 and subsequent docking to the mitochondrial membrane molecule Tom70 and this, in turn, mediating import into the mitochondria itself [66]. Granzyme A induced cell death can also occur in the absence of caspase involvement [67]. It might therefore be that the mechanism for granzyme A induced cell death may hold clues as to the mechanism of perforin-independent, memHsp70-mediated granzyme B induced apoptosis.

A key and defining occurrence of the intrinsic (not surface death-receptor mediated) pathway of apoptosis is mitochondrial outer membrane permeabilisation, MOMP [640]. The fine details surrounding the instigation of MOMP are not yet completely elucidated although it involves activation of BAX and/or BAK, which itself often requires interaction with a member of the BH3-only protein family, or truncation of Bid (to tBid), all of which can be driven directly or through the upsteam activation of caspases [641]. Conformational changes allow activated BAX or BAK, or tBid oligomerisation into the mitochondrial outer membrane, triggering permeabilisation [642]. This is generally considered a point-of-no-return in apoptosis, with intra-mitochondrial proteins (including cytochrome c, Smac and HtrA2 amongst others) released into the cytosol, rapidly acting on a variety of substrates including numerous caspases, which quickly leads to cell death. That granzyme B internalised through memHsp70 has been shown to traffic to the mitochondria, coupled with the knowledge that Bid is one of many possible substrates of human granzyme [636] begs the question of whether memHsp70-mediated internalisation of granzyme B results directly in MOMP. Since intrinsic apoptosis and MOMP can occur in the absence of caspase activity [643], and very little caspase-3 activation was observed here, it would be useful to know whether memHsp70-mediated internalisation of granzyme B leads to caspase-independent intrinsic apoptosis.

The use of mitochondrial stains which reveal mitochondrial membrane potential (such as JC-1) would be a useful next step to confirm whether permeabilisation is occurring. Since intrinsic apoptosis and MOMP can occur in the absence of caspase activity, and very little caspase-3 activation was observed here, it would be useful to know whether this

One concern for the therapeutic application of granzyme B is the potential systemic effects of administering a serine protease directly into the periphery. Granzyme B has shown high specificity to memHsp70 and should bind to and be taken up by only memHsp70^{+} cells.

Furthermore, the administration of granzyme B into mice bearing memHsp70^{+} CT26 tumours has been found to be well tolerated and did not result in adverse side-effects [532]. It is also worth noting that soluble granzyme B is readily detected in humans, the concentration of which can be used as a proxy measurement for NK cell and cytotoxic T cell activity. Spaeny-Dekking and colleagues reported that soluble granzyme B is present in the circulation of healthy control subjects (median 11.5 pg/mL), and that levels were markedly elevated in patients with chronic inflammatory disorders (EBV patients 60 pg/mL, HIV patients 20 pg/mL, RA patients 20 pg/mL in plasma but over 3000 pg/mL in the synovial fluid of affected joints) [644]]. Similar patterns of increased concentrations of soluble granzyme B have also been observed in patients with breast cancer, with the increased concentration of granzyme B in patients potentially being evident of some anti-cancer immune response [645]. Interestingly, when granzyme B concentration was reassessed following chemotherapy, there was a near doubling in concentration (up to around 100pg/ml, or around 0.5ug per person) as well as there being a detectable presence of soluble cytochrome c and FasL. Although the concentration observed is much lower than that administered to mice [4ug/kg [532], it does highlight that granzyme B, as a naturally-occurring molecule, is tolerated within the periphery.

Although there is much further study to be done, the concept of using granzyme B as a cancer therapeutic is an attractive one. Granzyme B itself acts directly on tumour cells to kill them without the immediate need for an effective immune system. This is important, as the majority of patients receive radiation therapy or chemotherapeutic as standard, both of which have long since been known to suppress the efficacy of protective anti-tumour immunity [646, 647]. This is one issue which has the potential to limit the protective effects of peptide-based anti-cancer vaccines. In addition, if the resulting tumour cell death following granzyme B treatment could lead release of tumour antigen then it could potentially induce a subsequent increased anti-tumour immune response. Further study is necessary to demonstrate memHsp70-mediated granzyme B-induced cell death is an immunogenic cell death conducive to eliciting an immune response [648].

One point to consider is the issue of granzyme B inhibitors. In humans the action of granzyme is blocked by serpinB9 (also known as protease inhibitor 9 or simply PI9) [649], a protease abundantly expressed by T cells and NK cells as protection from granzyme B mediated apoptosis. The expression of serpinB9 in tumour cells is less well characterised, although published data has been shown that MDA-MB-231 cells have some expression (to a level around 300-fold less than that in T cells or NK cells) while MCF7 cells do not express it [650]. In an attempt to replicate these data, cell lysates from the three human breast cancer cell lines

produced using RIPA buffer were subjected to western blot analyses for serpin B9 expression, along with lysates from PBMC preparations as a positive control.

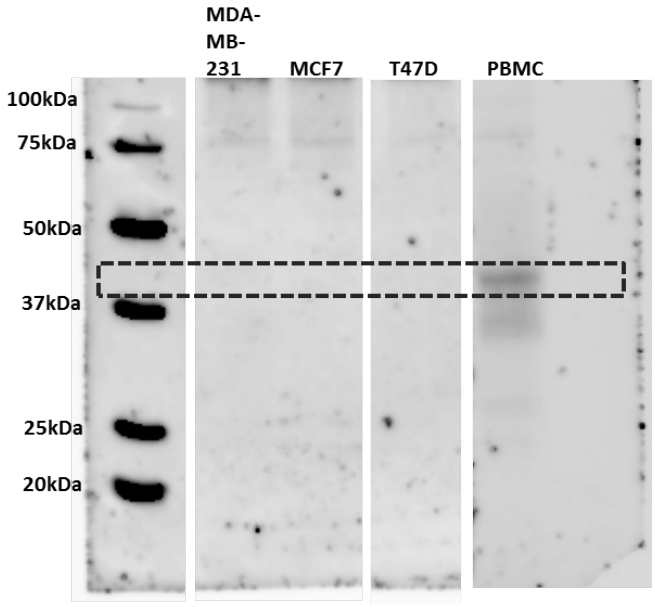

Figure 7.1 Western blot analysis of serpin B9 expression in human breast cancer cell lines.
Cell lysate containing 50µg of protein was used in SDS-page electrophoresis and transferred to PvDF membrane via semi-dry western blotting before staining for serpin B9 expression using mouse monoclonal (PI9-17) anti-serpin B9 antibody (Abcam, used 1:500) followed by HRP anti-mouse antibody (Dako, 1:2000) with non-specific binding blocked using 5% milk powder and 0.5% Tween 20 in TBS. Expression was detected in the PBMC lysate but not in any of the human breast cancer cell lines.

No serpin B9 expression was observed in the human breast cancer cell lines although it was present in the PBMC lysate. Previously published data showed that MDA-MB-231 cells do express serpin B9, but around 300 fold lower than in the T cells and NK cells found in PBMCs. The expression seen here in the PBMC preparation is weak so it is unlikely that a lower expression would be picked up. Use of a different serpin B9 antibody may result in clearer staining and thus may enable lower expressions to be seen. Even if low serpin B9 expression is present in MDA-MB-231 cells they still exhibited morphological characteristics associated with apoptosis, suggesting that either the level of serpinB9 expression was insufficient to inhibit all of the internalised granzyme B or that granzyme B internalised through memHsp70 is somehow able to exert its effects in a way which bypasses any potential blocking by serpinB9. This is an interesting mechanistic point and should be further investigated in the future.

Of interest is to compare the kinetic of uptake of the three molecules – cmHsp70.1 antibody, TKDNNLLGRFELSG peptide and granzyme B. This is made more difficult since each is conjugated to a different fluorescent molecule and hence the brightness of any one of the molecules will vary. In this situation the most appropriate comparison to make is to look at the number of fluorescent spots observed to be internalised at different time-points (**Figure 7.2,**

see over). In all cell lines, although the antibody and granzyme B exhibited a similar number of fluorescent spots at each time-point internalisation of the TKDNNLLGRFELSG peptide resulted in around double the number of spots. This would suggest a more effective and efficient uptake of TKDNNLLGRFELSG peptide and would make this the molecule the main choice of the three to translate for tumour imaging, and potential drug delivery to memHsp70^{+} tumours.

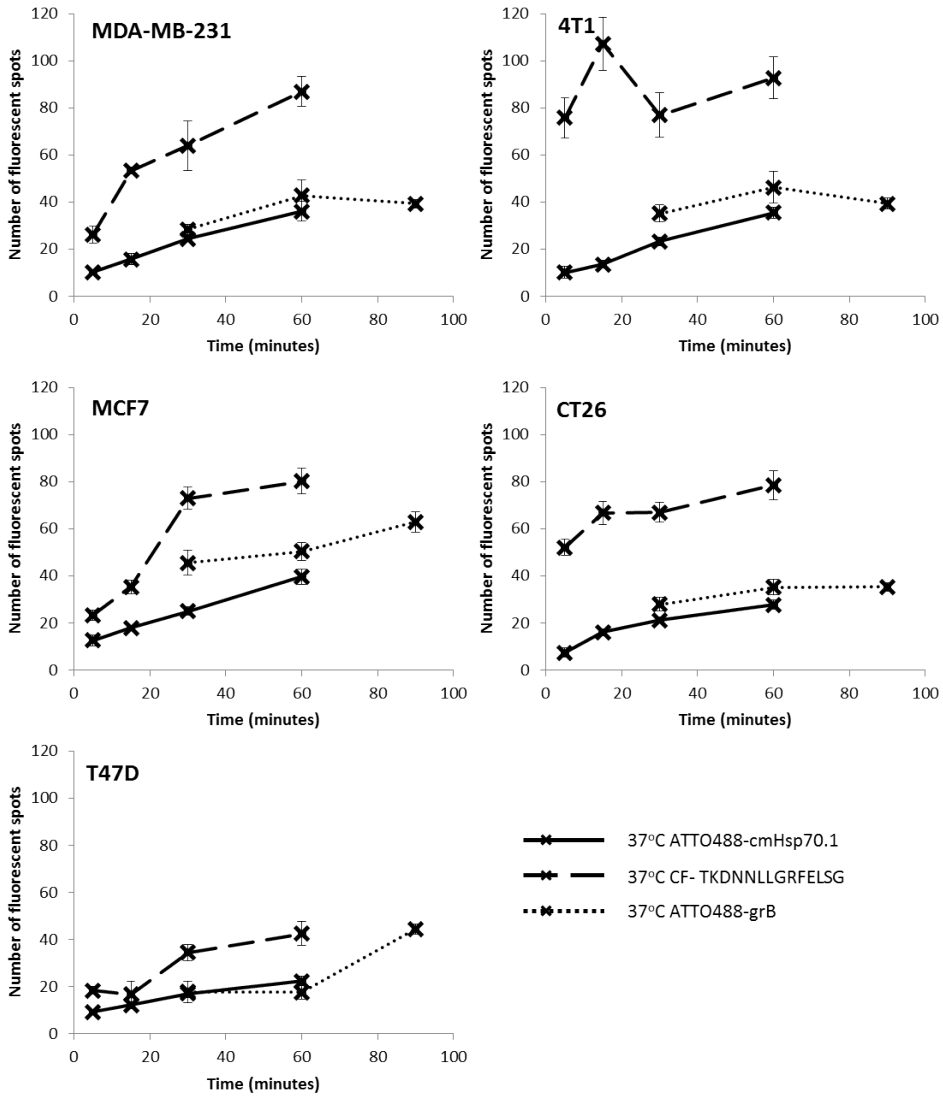

Figure 7.2 Comparing the kinetics of internalisation of cmHsp70.1, TKDNNLLGRFELSG and granzyme B into memHsp70+ cancer cell lines.

Using the count of fluorescent spots following incubation with fluorescently labelled cmHsp70.1, TKDNNLLGRFELSG peptide and granzyme B, the rate of each uptake could be compared. The larger molecules were internalised at similar rates although the small peptide was internalised at double the rate.

7.4 Lymphocytes and memHsp70

Whilst the potential to target a large proportion of tumours through their memHsp70 expression (be it via the cmHsp70.1 antibody, the TTP peptide or granzyme B) is highly exciting, the strategy will only be viable if the expression of memHsp70 is highly tumour

specific. When assessing the memHsp70 expression on tumour biopsies, Hantschel et al [569] also assessed the memHsp70 expression on cells from the surrounding healthy tissue and found it to be negative. This has been the case for all 1300+ patients that the Multhoff laboratory has assessed, and is also true for areas surrounding primary tumours and distant metastases. In terms of memHsp70 being present in other diseases states, the only finding thus far has been in arthritis. A link between rheumatoid arthritis (RA) and Hsp70 has been known for nearly two decades, with increased levels of circulating anti-Hsc70 antibodies [651], raised levels of released Hsp70 in synovial fluid, but not serum [652] and an increased expression of cytoplasmic Hsp70 in synovial tissue [653] in patients with RA. These findings prompted an investigation into whether RA patients also exhibited raised levels of membrane bound Hsp70. Nguyen *et al* used fluorescently-labelled cmHsp70.1 mAb to assess membrane Hsp70 expression on fibroblast-like synovial cells and found that around 40% were positive in patients with RA and JIA (juvenile idiopathic arthritis) [654], whereas there was no expression by synovial cells of healthy volunteers. Skin fibroblasts and peripheral blood lymphocytes served as a negative control, with less than 10% showing positive staining with cmHsp70.1 mAb in either patient group. The authors also looked at other peripheral blood populations and the stand-out finding was that there was a high level of staining with cmHsp70.1 on monocytes (around 80% of cells) in healthy volunteers and patient populations. Whilst these could be interesting findings, the results are flawed due to a lack of an appropriate control antibody. The authors only used one Hsp70 antibody clone, cmHsp70.1, which is able to detect Hsp70 that is both in the membrane and bound to the cell surface. This lack of distinction means that the authors cannot claim to have shown memHsp70 expression with these data. Consequently further investigation is required in order to confirm the presence of memHsp70 in RA and JIA patients, as well as on monocytes.

There has been no other report of memHsp70 expression in non-cancer disease states or on healthy cells in the published literature. However, previous studies in the Immunobiology Research Group at University of Sheffield have observed that $CD4^+CD25^+$ immunoregulatory T (Treg) cells isolated from mouse splenocytes using a magnetic column protocol could be labelled with the cmHsp70.1 mAb (Sarah Haywood-Small, personal communication). This finding led us to enquire if this was an artefact or whether lymphocyte populations could indeed bind the cmHsp70.1 mAb, and if so, under what circumstances this could occur.

Through the use of two Hsp70 antibody clones, no lymphocyte population was found to be reactive with the cmHsp70.1 mAb in peripheral blood when samples were stained using a whole blood technique. As previous investigations with mouse Treg cells have shown that reactivity with the cmHsp70.1 mAb could apparently be induced. PBMCs were isolated using

density gradient centrifugation and their reactivity with the cmHsp70.1 mAb determined by flow cytometry. This demonstrated that the process of density gradient separation induced a capacity for the cmHsp70.1 mAb to bind to T cell and NK cell populations. The capacity of cell activation using the polyclonal mitogen ConA and anti-CD3/CD28 mAb-coated beads, heat and hypoxia was also investigated. Although cells were confirmed to be activated following polyclonal stimulation (on the basis of CD69 and CD25 expression) they showed no reactivity with the cmHsp70.1 mAb. Nor did heat or hypoxia have any effect. It appears that the induction of reactivity to cmHsp70.1 mAb is an artefact of the density gradient centrifugation process, for reasons that are currently unclear.

7.5 Conclusion

MemHsp70 serves as a tumour specific marker and is present on around 50% of malignancies. As such it is a highly desirable candidate for the development of novel cancer therapeutics, as it could potentially be used to treat a large number of patients. The specific targeting of memHsp70 could come from the use of an antibody (cmHsp70.1), the 14-mer TTP peptide or granzyme B.

A key advantage of developing therapeutic platforms on the basis of membrane Hsp70 expression is the fact that the expression of this molecule is enhanced following standard radio(chemo)therapy.

The fact that this specific targeting of memHsp70^{+} tumours could be conducted alongside the administration of standard cancer therapies would be a big advantage to patients, since this would form an additional, complimentary therapy and patient treatment would not be compromised. In fact additional benefits could be gained by delivering a cmHsp70.1 mAb-based therapy concurrently with standard therapy. A side effect of the standard chemo-or radio-therapies is that memHsp70^{+} tumours upregulate that expression, but this could actually boost the effectiveness of a memHsp70-targeted therapeutic through increased availability of target molecules. Moreover, any direct killing of tumours can serve to facilitate the release of tumour antigens which can trigger an immune response. It has previously been shown that non-lethal chemotherapy and radiotherapy can increase the susceptibility of malignant cells to T cell mediated lysis [655-657] so this coupled with increased susceptibility to memHsp70 directed therapies could result in a more efficient anti-tumour immune response.

The use of the antibody and the peptide could be two fold, either as an imaging tool or a delivery vector for cytotoxic agents. The kinetics of uptake of antibody and peptide are reliant on the density of memHsp70, but this can be increased following standard cancer therapies. Granzyme B can be employed as a direct cytotoxic agent that will induce apoptosis in

memHsp70^{+} tumour cells. The killing of tumour cells may have a secondary result of boosting the patients' anti-tumour immune response, if tumour cell death results in the release of tumour antigens.

The next step is to further investigate the potential usage of antibody, peptide and granzyme B in mouse model of breast cancer with a view to moving into human clinical trials in the future.

Future Work

When imaging the uptake of the cmHsp70.1 mAb, the TKDNNLLGRFELSG 14-mer peptide and granzyme B, the potential involvement of early endosomes was not clear, possibly due to the short amount of time that the molecules would co-localise with the early endosome compartment. Rather than imaging this point in the internalisation, involvement could be confirmed another way, by ultracentrifugation separation of the early endosomes following by Western blot analysis, or simply by fluorescent analysis using flow cytometry. Another possible method is to use a protein protection assay such as that described by Cihil *et al* allowing for the endocytic uptake of molecules and their subsequent recycling to the plasma membrane to be tracked [658].

With particular reference to the granzyme B uptake by memHsp70$^+$ tumour cells, further study is required in order to fully elicit the action of granzyme B following memHsp70-mediated uptake. Granzyme B has many substrates and it is not clear which, or how many, are involved when granzyme B is taken up this way. One way could be through the use of proteomic analysis, using mass spectrometry, to study protein modifications (e.g. cleavage) and activation at different time-points following granzyme B internalisation.

Although the use of the cmHsp70.1 antibody, the TKDNNLLGRFELSG peptide or granzyme B as targeting molecules for Hsp70$^+$ breast cancer could offer new treatment avenues for patients, the current studies have been confined to *in vitro* experiments. The next step is to move into looking *in vivo*, starting with mouse models of breast cancer. Using implanted memHsp70$^+$ tumour cell lines, the specificity of binding of the cmHsp70.1 antibody and the TKDNNLLGRFELSG peptide to tumours could be examined using *in vivo* imaging of the animals. The capacity of granzyme B to inhibit the growth of primary tumours and, in the appropriate models, metastatic disease will be examined, either in the presence or absence of existing therapies such as chemotherapy, radiotherapy or therapeutic antibody treatments. Allied to these studies would be to determine whether granzyme B promotes the release of tumour-related antigens, against which protective, adaptive immune responses can be induced. This proposition could be examined on the basis of antigen/peptide-specific proliferation and activation assays, cytokine and granzyme B release from using multiplex bead and ELISpot assays, the identification of peptide-specific T cells using flow cytometric multimer platforms and the ability of cells from treated animals to kill appropriate tumour cells *in vitro*.

The ultimate aim is to translate this research into the clinical setting and use the targeting of memHsp70 to improve tumour imaging and the management and treatments of patients with memHsp70$^+$ cancers.

References

1. Oliveira Cobucci, R.N., et al., *Comparative incidence of cancer in HIV-AIDS patients and transplant recipients.* Cancer Epidemiol, 2012. **36**(2): p. e69-73.
2. Grulich, A.E., et al., *Incidence of cancers in people with HIV/AIDS compared with immunosuppressed transplant recipients: a meta-analysis.* Lancet, 2007. **370**(9581): p. 59-67.
3. Vajdic, C.M., et al., *Cancer incidence before and after kidney transplantation.* JAMA, 2006. **296**(23): p. 2823-31.
4. Taylor, D.O., et al., *Registry of the International Society for Heart and Lung Transplantation: twenty-third official adult heart transplantation report--2006.* J Heart Lung Transplant, 2006. **25**(8): p. 869-79.
5. Biggar, R.J., et al., *AIDS-related cancer and severity of immunosuppression in persons with AIDS.* J Natl Cancer Inst, 2007. **99**(12): p. 962-72.
6. Bouvard, V., et al., *A review of human carcinogens--Part B: biological agents.* Lancet Oncol, 2009. **10**(4): p. 321-2.
7. Lyronis, I.D., et al., *K-ras mutation, HPV infection and smoking or alcohol abuse positively correlate with esophageal squamous carcinoma.* Pathol Oncol Res, 2008. **14**(3): p. 267-73.
8. Sarchianaki, E., et al., *Detection and genotype analysis of human papillomavirus in non-small cell lung cancer patients.* Tumour Biol, 2014. **35**(4): p. 3203-9.
9. Zaravinos, A., P. Kanellou, and D.A. Spandidos, *Viral DNA detection and RAS mutations in actinic keratosis and nonmelanoma skin cancers.* Br J Dermatol, 2010. **162**(2): p. 325-31.
10. Neparidze, N. and J. Lacy, *Malignancies associated with epstein-barr virus: pathobiology, clinical features, and evolving treatments.* Clin Adv Hematol Oncol, 2014. **12**(6): p. 358-71.
11. Hanahan, D. and R.A. Weinberg, *The hallmarks of cancer.* Cell, 2000. **100**(1): p. 57-70.
12. Hanahan, D. and R.A. Weinberg, *Hallmarks of cancer: the next generation.* Cell, 2011. **144**(5): p. 646-74.
13. Cavallo, F., et al., *2011: the immune hallmarks of cancer.* Cancer Immunol Immunother, 2011. **60**(3): p. 319-26.
14. Lanier, L.L., et al., *The relationship of CD16 (Leu-11) and Leu-19 (NKH-1) antigen expression on human peripheral blood NK cells and cytotoxic T lymphocytes.* J Immunol, 1986. **136**(12): p. 4480-6.
15. Cooper, M.A., T.A. Fehniger, and M.A. Caligiuri, *The biology of human natural killer-cell subsets.* Trends Immunol, 2001. **22**(11): p. 633-40.
16. Ferlazzo, G., et al., *The abundant NK cells in human secondary lymphoid tissues require activation to express killer cell Ig-like receptors and become cytolytic.* J Immunol, 2004. **172**(3): p. 1455-62.
17. Nagler, A., et al., *Comparative studies of human FcRIII-positive and negative natural killer cells.* J Immunol, 1989. **143**(10): p. 3183-91.
18. Gottschalk, L.R., et al., *Two populations of CD56 (Leu-19)+/CD16+ cells in bone marrow transplant recipients.* Bone Marrow Transplant, 1990. **5**(4): p. 259-64.
19. Jacobs, R., et al., *CD16- CD56+ natural killer cells after bone marrow transplantation.* Blood, 1992. **79**(12): p. 3239-44.
20. Farag, S.S. and M.A. Caligiuri, *Human natural killer cell development and biology.* Blood Rev, 2006. **20**(3): p. 123-37.
21. Freud, A.G., et al., *A human CD34(+) subset resides in lymph nodes and differentiates into CD56bright natural killer cells.* Immunity, 2005. **22**(3): p. 295-304.

22. Fehniger, T.A., et al., *CD56bright natural killer cells are present in human lymph nodes and are activated by T cell-derived IL-2: a potential new link between adaptive and innate immunity.* Blood, 2003. **101**(8): p. 3052-7.
23. King, A., et al., *CD3- leukocytes present in the human uterus during early placentation: phenotypic and morphologic characterization of the CD56++ population.* Dev Immunol, 1991. **1**(3): p. 169-90.
24. Koopman, L.A., et al., *Human decidual natural killer cells are a unique NK cell subset with immunomodulatory potential.* J Exp Med, 2003. **198**(8): p. 1201-12.
25. Kammerer, U., et al., *Immunocompetent cells in the endometrium of fetuses and children.* Hum Reprod, 2003. **18**(5): p. 969-75.
26. Hickey, M., et al., *Menopausal hormone therapy and irregular endometrial bleeding: a potential role for uterine natural killer cells?* J Clin Endocrinol Metab, 2005. **90**(10): p. 5528-35.
27. Moffett, A., L. Regan, and P. Braude, *Natural killer cells, miscarriage, and infertility.* BMJ, 2004. **329**(7477): p. 1283-5.
28. Keskin, D.B., et al., *TGFbeta promotes conversion of CD16+ peripheral blood NK cells into CD16- NK cells with similarities to decidual NK cells.* Proc Natl Acad Sci U S A, 2007. **104**(9): p. 3378-83.
29. Matsuura-Sawada, R., et al., *Reproduction of menstrual changes in transplanted human endometrial tissue in immunodeficient mice.* Hum Reprod, 2005. **20**(6): p. 1477-84.
30. Trundley, A. and A. Moffett, *Human uterine leukocytes and pregnancy.* Tissue Antigens, 2004. **63**(1): p. 1-12.
31. Bulmer, J.N. and G.E. Lash, *Human uterine natural killer cells: a reappraisal.* Mol Immunol, 2005. **42**(4): p. 511-21.
32. Acar, N., I. Ustunel, and R. Demir, *Uterine natural killer (uNK) cells and their missions during pregnancy: a review.* Acta Histochem, 2011. **113**(2): p. 82-91.
33. Jones, R.K., et al., *Apoptosis, bcl-2 expression, and proliferative activity in human endometrial stroma and endometrial granulated lymphocytes.* Biol Reprod, 1998. **58**(4): p. 995-1002.
34. Jokhi, P.P., A. King, and Y.W. Loke, *Cytokine production and cytokine receptor expression by cells of the human first trimester placental-uterine interface.* Cytokine, 1997. **9**(2): p. 126-37.
35. Li, X.F., et al., *Angiogenic growth factor messenger ribonucleic acids in uterine natural killer cells.* J Clin Endocrinol Metab, 2001. **86**(4): p. 1823-34.
36. Clifford, K., A.M. Flanagan, and L. Regan, *Endometrial CD56+ natural killer cells in women with recurrent miscarriage: a histomorphometric study.* Hum Reprod, 1999. **14**(11): p. 2727-30.
37. Quenby, S., et al., *Pre-implantation endometrial leukocytes in women with recurrent miscarriage.* Hum Reprod, 1999. **14**(9): p. 2386-91.
38. Lachapelle, M.H., et al., *Endometrial T, B, and NK cells in patients with recurrent spontaneous abortion. Altered profile and pregnancy outcome.* J Immunol, 1996. **156**(10): p. 4027-34.
39. Fukui, A., et al., *Natural killer cell subpopulations and cytotoxicity for infertile patients undergoing in vitro fertilization.* Am J Reprod Immunol, 1999. **41**(6): p. 413-22.
40. Campbell, K.S. and J. Hasegawa, *Natural killer cell biology: an update and future directions.* J Allergy Clin Immunol, 2013. **132**(3): p. 536-44.
41. Orange, J.S., et al., *The mature activating natural killer cell immunologic synapse is formed in distinct stages.* Proc Natl Acad Sci U S A, 2003. **100**(24): p. 14151-6.
42. Rak, G.D., et al., *Natural killer cell lytic granule secretion occurs through a pervasive actin network at the immune synapse.* PLoS Biol, 2011. **9**(9): p. e1001151.
43. Orange, J.S., *Formation and function of the lytic NK-cell immunological synapse.* Nat Rev Immunol, 2008. **8**(9): p. 713-25.

44. Warren, H.S., et al., *A carbohydrate structure associated with CD15 (Lewis x) on myeloid cells is a novel ligand for human CD2.* J Immunol, 1996. **156**(8): p. 2866-73.
45. Inoue, H., et al., *Lipid rafts as the signaling scaffold for NK cell activation: tyrosine phosphorylation and association of LAT with phosphatidylinositol 3-kinase and phospholipase C-gamma following CD2 stimulation.* Eur J Immunol, 2002. **32**(8): p. 2188-98.
46. Chen, S., et al., *Suppression of tumor formation in lymph nodes by L-selectin-mediated natural killer cell recruitment.* J Exp Med, 2005. **202**(12): p. 1679-89.
47. Barber, D.F., M. Faure, and E.O. Long, *LFA-1 contributes an early signal for NK cell cytotoxicity.* J Immunol, 2004. **173**(6): p. 3653-9.
48. Bryceson, Y.T., et al., *Cytolytic granule polarization and degranulation controlled by different receptors in resting NK cells.* J Exp Med, 2005. **202**(7): p. 1001-12.
49. Giurisato, E., et al., *Phosphatidylinositol 3-kinase activation is required to form the NKG2D immunological synapse.* Mol Cell Biol, 2007. **27**(24): p. 8583-99.
50. Graham, D.B., et al., *Vav1 controls DAP10-mediated natural cytotoxicity by regulating actin and microtubule dynamics.* J Immunol, 2006. **177**(4): p. 2349-55.
51. Chen, X., et al., *CD28-stimulated ERK2 phosphorylation is required for polarization of the microtubule organizing center and granules in YTS NK cells.* Proc Natl Acad Sci U S A, 2006. **103**(27): p. 10346-51.
52. Sancho, D., et al., *The tyrosine kinase PYK-2/RAFTK regulates natural killer (NK) cell cytotoxic response, and is translocated and activated upon specific target cell recognition and killing.* J Cell Biol, 2000. **149**(6): p. 1249-62.
53. Roda-Navarro, P., et al., *Dynamic redistribution of the activating 2B4/SAP complex at the cytotoxic NK cell immune synapse.* J Immunol, 2004. **173**(6): p. 3640-6.
54. Andzelm, M.M., et al., *Myosin IIA is required for cytolytic granule exocytosis in human NK cells.* J Exp Med, 2007. **204**(10): p. 2285-91.
55. Odake, S., et al., *Human and murine cytotoxic T lymphocyte serine proteases: subsite mapping with peptide thioester substrates and inhibition of enzyme activity and cytolysis by isocoumarins.* Biochemistry, 1991. **30**(8): p. 2217-27.
56. Darmon, A.J., D.W. Nicholson, and R.C. Bleackley, *Activation of the apoptotic protease CPP32 by cytotoxic T-cell-derived granzyme B.* Nature, 1995. **377**(6548): p. 446-8.
57. Quan, L.T., et al., *Proteolytic activation of the cell death protease Yama/CPP32 by granzyme B.* Proc Natl Acad Sci U S A, 1996. **93**(5): p. 1972-6.
58. Martin, S.J., et al., *The cytotoxic cell protease granzyme B initiates apoptosis in a cell-free system by proteolytic processing and activation of the ICE/CED-3 family protease, CPP32, via a novel two-step mechanism.* EMBO J, 1996. **15**(10): p. 2407-16.
59. Medema, J.P., et al., *Cleavage of FLICE (caspase-8) by granzyme B during cytotoxic T lymphocyte-induced apoptosis.* Eur J Immunol, 1997. **27**(12): p. 3492-8.
60. Thomas, D.A., et al., *DFF45/ICAD can be directly processed by granzyme B during the induction of apoptosis.* Immunity, 2000. **12**(6): p. 621-32.
61. Andrade, F., et al., *Granzyme B directly and efficiently cleaves several downstream caspase substrates: implications for CTL-induced apoptosis.* Immunity, 1998. **8**(4): p. 451-60.
62. Barry, M., et al., *Granzyme B short-circuits the need for caspase 8 activity during granule-mediated cytotoxic T-lymphocyte killing by directly cleaving Bid.* Mol Cell Biol, 2000. **20**(11): p. 3781-94.
63. Adrain, C., B.M. Murphy, and S.J. Martin, *Molecular ordering of the caspase activation cascade initiated by the cytotoxic T lymphocyte/natural killer (CTL/NK) protease granzyme B.* J Biol Chem, 2005. **280**(6): p. 4663-73.
64. Bredemeyer, A.J., R.R. Townsend, and T.J. Ley, *Use of protease proteomics to discover granzyme B substrates.* Immunol Res, 2005. **32**(1-3): p. 143-53.
65. Beresford, P.J., et al., *Granzyme A loading induces rapid cytolysis and a novel form of DNA damage independently of caspase activation.* Immunity, 1999. **10**(5): p. 585-94.

66. Martinvalet, D., et al., *Granzyme A cleaves a mitochondrial complex I protein to initiate caspase-independent cell death.* Cell, 2008. **133**(4): p. 681-92.
67. Martinvalet, D., P. Zhu, and J. Lieberman, *Granzyme A induces caspase-independent mitochondrial damage, a required first step for apoptosis.* Immunity, 2005. **22**(3): p. 355-70.
68. Hou, Q., et al., *Granzyme H induces apoptosis of target tumor cells characterized by DNA fragmentation and Bid-dependent mitochondrial damage.* Mol Immunol, 2008. **45**(4): p. 1044-55.
69. Zhao, T., et al., *Granzyme K cleaves the nucleosome assembly protein SET to induce single-stranded DNA nicks of target cells.* Cell Death Differ, 2007. **14**(3): p. 489-99.
70. Lu, H., et al., *Granzyme M directly cleaves inhibitor of caspase-activated DNase (CAD) to unleash CAD leading to DNA fragmentation.* J Immunol, 2006. **177**(2): p. 1171-8.
71. Ewen, C.L., K.P. Kane, and R.C. Bleackley, *Granzyme H induces cell death primarily via a Bcl-2-sensitive mitochondrial cell death pathway that does not require direct Bid activation.* Mol Immunol, 2013. **54**(3-4): p. 309-18.
72. Fellows, E., et al., *Natural killer cell-derived human granzyme H induces an alternative, caspase-independent cell-death program.* Blood, 2007. **110**(2): p. 544-52.
73. Zhao, T., et al., *Granzyme K directly processes bid to release cytochrome c and endonuclease G leading to mitochondria-dependent cell death.* J Biol Chem, 2007. **282**(16): p. 12104-11.
74. MacDonald, G., et al., *Mitochondria-dependent and -independent regulation of Granzyme B-induced apoptosis.* J Exp Med, 1999. **189**(1): p. 131-44.
75. Guo, Y., et al., *Valosin-containing protein cleavage by granzyme K accelerates an endoplasmic reticulum stress leading to caspase-independent cytotoxicity of target tumor cells.* J Immunol, 2010. **185**(9): p. 5348-59.
76. Kelly, J.M., et al., *Granzyme M mediates a novel form of perforin-dependent cell death.* J Biol Chem, 2004. **279**(21): p. 22236-42.
77. Hu, D., et al., *Cleavage of survivin by Granzyme M triggers degradation of the survivin-X-linked inhibitor of apoptosis protein (XIAP) complex to free caspase activity leading to cytolysis of target tumor cells.* J Biol Chem, 2010. **285**(24): p. 18326-35.
78. Millard, P.J., et al., *Purification and properties of cytoplasmic granules from cytotoxic rat LGL tumors.* J Immunol, 1984. **132**(6): p. 3197-204.
79. Tschopp, J., D. Masson, and K.K. Stanley, *Structural/functional similarity between proteins involved in complement- and cytotoxic T-lymphocyte-mediated cytolysis.* Nature, 1986. **322**(6082): p. 831-4.
80. Pinkoski, M.J., et al., *Entry and trafficking of granzyme B in target cells during granzyme B-perforin-mediated apoptosis.* Blood, 1998. **92**(3): p. 1044-54.
81. Froelich, C.J., et al., *New paradigm for lymphocyte granule-mediated cytotoxicity. Target cells bind and internalize granzyme B, but an endosomolytic agent is necessary for cytosolic delivery and subsequent apoptosis.* J Biol Chem, 1996. **271**(46): p. 29073-9.
82. Pipkin, M.E. and J. Lieberman, *Delivering the kiss of death: progress on understanding how perforin works.* Curr Opin Immunol, 2007. **19**(3): p. 301-8.
83. Keefe, D., et al., *Perforin triggers a plasma membrane-repair response that facilitates CTL induction of apoptosis.* Immunity, 2005. **23**(3): p. 249-62.
84. Veugelers, K., et al., *The granzyme B-serglycin complex from cytotoxic granules requires dynamin for endocytosis.* Blood, 2004. **103**(10): p. 3845-53.
85. Sweitzer, S.M. and J.E. Hinshaw, *Dynamin undergoes a GTP-dependent conformational change causing vesiculation.* Cell, 1998. **93**(6): p. 1021-9.
86. Conner, S.D. and S.L. Schmid, *Differential requirements for AP-2 in clathrin-mediated endocytosis.* J Cell Biol, 2003. **162**(5): p. 773-9.
87. Sun, J.C., et al., *NK cells and immune "memory".* J Immunol, 2011. **186**(4): p. 1891-7.

88. Moretta, L., F. Locatelli, and A. Moretta, *Alloreactive natural killer cells in targeting high-risk leukaemias.* Ann Rheum Dis, 2008. **67 Suppl 3**: p. iii39-43.
89. Cooper, M.A., et al., *Cytokine-induced memory-like natural killer cells.* Proc Natl Acad Sci U S A, 2009. **106**(6): p. 1915-9.
90. Netea, M.G., *Training innate immunity: the changing concept of immunological memory in innate host defence.* Eur J Clin Invest, 2013. **43**(8): p. 881-4.
91. Vivier, E., et al., *Innate or adaptive immunity? The example of natural killer cells.* Science, 2011. **331**(6013): p. 44-9.
92. Sun, J.C. and L.L. Lanier, *Natural killer cells remember: an evolutionary bridge between innate and adaptive immunity?* Eur J Immunol, 2009. **39**(8): p. 2059-64.
93. O'Leary, J.G., et al., *T cell- and B cell-independent adaptive immunity mediated by natural killer cells.* Nat Immunol, 2006. **7**(5): p. 507-16.
94. Sun, J.C., J.N. Beilke, and L.L. Lanier, *Adaptive immune features of natural killer cells.* Nature, 2009. **457**(7229): p. 557-61.
95. Guma, M., et al., *Imprint of human cytomegalovirus infection on the NK cell receptor repertoire.* Blood, 2004. **104**(12): p. 3664-71.
96. Lopez-Verges, S., et al., *CD57 defines a functionally distinct population of mature NK cells in the human CD56dimCD16+ NK-cell subset.* Blood, 2010. **116**(19): p. 3865-74.
97. Tilden, A.B., et al., *Subpopulation analysis of human granular lymphocytes: associations with age, gender and cytotoxic activity.* Nat Immun Cell Growth Regul, 1986. **5**(2): p. 90-9.
98. Merino, J., et al., *Progressive decrease of CD8high+ CD28+ CD57- cells with ageing.* Clin Exp Immunol, 1998. **112**(1): p. 48-51.
99. Le Priol, Y., et al., *High cytotoxic and specific migratory potencies of senescent CD8+ CD57+ cells in HIV-infected and uninfected individuals.* J Immunol, 2006. **177**(8): p. 5145-54.
100. Lin, X., et al., *Advances in distinguishing natural from induced Foxp3(+) regulatory T cells.* Int J Clin Exp Pathol, 2013. **6**(2): p. 116-23.
101. Mosmann, T.R., et al., *Two types of murine helper T cell clone. I. Definition according to profiles of lymphokine activities and secreted proteins.* J Immunol, 1986. **136**(7): p. 2348-57.
102. Thieu, V.T., et al., *Signal transducer and activator of transcription 4 is required for the transcription factor T-bet to promote T helper 1 cell-fate determination.* Immunity, 2008. **29**(5): p. 679-90.
103. Djuretic, I.M., et al., *Transcription factors T-bet and Runx3 cooperate to activate Ifng and silence Il4 in T helper type 1 cells.* Nat Immunol, 2007. **8**(2): p. 145-53.
104. Weaver, C.T. and K.M. Murphy, *T-cell subsets: the more the merrier.* Curr Biol, 2007. **17**(2): p. R61-3.
105. Ansel, K.M., et al., *Regulation of Th2 differentiation and Il4 locus accessibility.* Annu Rev Immunol, 2006. **24**: p. 607-56.
106. Mowen, K.A. and L.H. Glimcher, *Signaling pathways in Th2 development.* Immunol Rev, 2004. **202**: p. 203-22.
107. Agarwal, S., O. Avni, and A. Rao, *Cell-type-restricted binding of the transcription factor NFAT to a distal IL-4 enhancer in vivo.* Immunity, 2000. **12**(6): p. 643-52.
108. Wan, Y.Y., *GATA3: a master of many trades in immune regulation.* Trends Immunol, 2014. **35**(6): p. 233-42.
109. Naoe, Y., et al., *Repression of interleukin-4 in T helper type 1 cells by Runx/Cbf beta binding to the Il4 silencer.* J Exp Med, 2007. **204**(8): p. 1749-55.
110. Harrington, L.E., et al., *Interleukin 17-producing CD4+ effector T cells develop via a lineage distinct from the T helper type 1 and 2 lineages.* Nat Immunol, 2005. **6**(11): p. 1123-32.
111. Park, H., et al., *A distinct lineage of CD4 T cells regulates tissue inflammation by producing interleukin 17.* Nat Immunol, 2005. **6**(11): p. 1133-41.

112. Yang, J., et al., *Unphosphorylated STAT3 accumulates in response to IL-6 and activates transcription by binding to NFkappaB.* Genes Dev, 2007. **21**(11): p. 1396-408.
113. Naka, T., N. Nishimoto, and T. Kishimoto, *The paradigm of IL-6: from basic science to medicine.* Arthritis Res, 2002. **4 Suppl 3**: p. S233-42.
114. Kishimoto, T., et al., *Interleukin-6 family of cytokines and gp130.* Blood, 1995. **86**(4): p. 1243-54.
115. Mangan, P.R., et al., *Transforming growth factor-beta induces development of the T(H)17 lineage.* Nature, 2006. **441**(7090): p. 231-4.
116. Durant, L., et al., *Diverse targets of the transcription factor STAT3 contribute to T cell pathogenicity and homeostasis.* Immunity, 2010. **32**(5): p. 605-15.
117. McGeachy, M.J., et al., *The interleukin 23 receptor is essential for the terminal differentiation of interleukin 17-producing effector T helper cells in vivo.* Nat Immunol, 2009. **10**(3): p. 314-24.
118. Laurence, A., et al., *Interleukin-2 signaling via STAT5 constrains T helper 17 cell generation.* Immunity, 2007. **26**(3): p. 371-81.
119. Hirota, K., et al., *Fate mapping of IL-17-producing T cells in inflammatory responses.* Nat Immunol, 2011. **12**(3): p. 255-63.
120. Marks, B.R., et al., *Thymic self-reactivity selects natural interleukin 17-producing T cells that can regulate peripheral inflammation.* Nat Immunol, 2009. **10**(10): p. 1125-32.
121. Jordan, M.S., et al., *Thymic selection of CD4+CD25+ regulatory T cells induced by an agonist self-peptide.* Nat Immunol, 2001. **2**(4): p. 301-6.
122. Zuniga, L.A., et al., *Th17 cell development: from the cradle to the grave.* Immunol Rev, 2013. **252**(1): p. 78-88.
123. Tosolini, M., et al., *Clinical impact of different classes of infiltrating T cytotoxic and helper cells (Th1, th2, treg, th17) in patients with colorectal cancer.* Cancer Res, 2011. **71**(4): p. 1263-71.
124. Maruyama, T., et al., *Distribution of Th17 cells and FoxP3(+) regulatory T cells in tumor-infiltrating lymphocytes, tumor-draining lymph nodes and peripheral blood lymphocytes in patients with gastric cancer.* Cancer Sci, 2010. **101**(9): p. 1947-54.
125. Kesselring, R., et al., *Human Th17 cells can be induced through head and neck cancer and have a functional impact on HNSCC development.* Br J Cancer, 2010. **103**(8): p. 1245-54.
126. Chen, X., et al., *Role of interleukin-17 in lymphangiogenesis in non-small-cell lung cancer: Enhanced production of vascular endothelial growth factor C in non-small-cell lung carcinoma cells.* Cancer Sci, 2010. **101**(11): p. 2384-90.
127. Derhovanessian, E., et al., *Pretreatment frequency of circulating IL-17+ CD4+ T-cells, but not Tregs, correlates with clinical response to whole-cell vaccination in prostate cancer patients.* Int J Cancer, 2009. **125**(6): p. 1372-9.
128. Horlock, C., et al., *The effects of trastuzumab on the CD4+CD25+FoxP3+ and CD4+IL17A+ T-cell axis in patients with breast cancer.* Br J Cancer, 2009. **100**(7): p. 1061-7.
129. Lanca, T. and B. Silva-Santos, *The split nature of tumor-infiltrating leukocytes: Implications for cancer surveillance and immunotherapy.* Oncoimmunology, 2012. **1**(5): p. 717-725.
130. Dai, Y., et al., *Embelin reduces colitis-associated tumorigenesis through limiting IL-6/STAT3 signaling.* Mol Cancer Ther, 2014. **13**(5): p. 1206-16.
131. Bailey, S.R., et al., *Th17 cells in cancer: the ultimate identity crisis.* Front Immunol, 2014. **5**: p. 276.
132. Karin, M., T. Lawrence, and V. Nizet, *Innate immunity gone awry: linking microbial infections to chronic inflammation and cancer.* Cell, 2006. **124**(4): p. 823-35.
133. Wu, S., et al., *A human colonic commensal promotes colon tumorigenesis via activation of T helper type 17 T cell responses.* Nat Med, 2009. **15**(9): p. 1016-22.

134. Numasaki, M., et al., *Interleukin-17 promotes angiogenesis and tumor growth.* Blood, 2003. **101**(7): p. 2620-7.
135. Tong, Z., et al., *A protective role by interleukin-17F in colon tumorigenesis.* PLoS One, 2012. **7**(4): p. e34959.
136. Weber, G.F., et al., *IL-22-mediated tumor growth reduction correlates with inhibition of ERK1/2 and AKT phosphorylation and induction of cell cycle arrest in the G2-M phase.* J Immunol, 2006. **177**(11): p. 8266-72.
137. Castermans, K., et al., *Angiostatic activity of the antitumor cytokine interleukin-21.* Blood, 2008. **112**(13): p. 4940-7.
138. Thornton, A.M. and E.M. Shevach, *Suppressor effector function of CD4+CD25+ immunoregulatory T cells is antigen nonspecific.* J Immunol, 2000. **164**(1): p. 183-90.
139. Sakaguchi, S., *Naturally arising CD4+ regulatory t cells for immunologic self-tolerance and negative control of immune responses.* Annu Rev Immunol, 2004. **22**: p. 531-62.
140. Jonuleit, H., et al., *Identification and functional characterization of human CD4(+)CD25(+) T cells with regulatory properties isolated from peripheral blood.* J Exp Med, 2001. **193**(11): p. 1285-94.
141. Ralainirina, N., et al., *Control of NK cell functions by CD4+CD25+ regulatory T cells.* J Leukoc Biol, 2007. **81**(1): p. 144-53.
142. Lim, H.W., et al., *Cutting edge: direct suppression of B cells by CD4+ CD25+ regulatory T cells.* J Immunol, 2005. **175**(7): p. 4180-3.
143. Taams, L.S., et al., *Modulation of monocyte/macrophage function by human CD4+CD25+ regulatory T cells.* Hum Immunol, 2005. **66**(3): p. 222-30.
144. Fallarino, F., et al., *Modulation of tryptophan catabolism by regulatory T cells.* Nat Immunol, 2003. **4**(12): p. 1206-12.
145. Piccirillo, C.A. and E.M. Shevach, *Naturally-occurring CD4+CD25+ immunoregulatory T cells: central players in the arena of peripheral tolerance.* Semin Immunol, 2004. **16**(2): p. 81-8.
146. Apostolou, I. and H. von Boehmer, *In vivo instruction of suppressor commitment in naive T cells.* J Exp Med, 2004. **199**(10): p. 1401-8.
147. Zheng, S.G., et al., *TGF-beta requires CTLA-4 early after T cell activation to induce FoxP3 and generate adaptive CD4+CD25+ regulatory cells.* J Immunol, 2006. **176**(6): p. 3321-9.
148. Zheng, S.G., et al., *IL-2 is essential for TGF-beta to convert naive CD4+CD25- cells to CD25+Foxp3+ regulatory T cells and for expansion of these cells.* J Immunol, 2007. **178**(4): p. 2018-27.
149. Barrat, F.J., et al., *In vitro generation of interleukin 10-producing regulatory CD4(+) T cells is induced by immunosuppressive drugs and inhibited by T helper type 1 (Th1)- and Th2-inducing cytokines.* J Exp Med, 2002. **195**(5): p. 603-16.
150. Zheng, S.G., et al., *Generation ex vivo of TGF-beta-producing regulatory T cells from CD4+CD25- precursors.* J Immunol, 2002. **169**(8): p. 4183-9.
151. Lan, Q., et al., *Induced Foxp3(+) regulatory T cells: a potential new weapon to treat autoimmune and inflammatory diseases?* J Mol Cell Biol, 2012. **4**(1): p. 22-8.
152. Curotto de Lafaille, M.A. and J.J. Lafaille, *Natural and adaptive foxp3+ regulatory T cells: more of the same or a division of labor?* Immunity, 2009. **30**(5): p. 626-35.
153. Yadav, M., et al., *Neuropilin-1 distinguishes natural and inducible regulatory T cells among regulatory T cell subsets in vivo.* J Exp Med, 2012. **209**(10): p. 1713-22, S1-19.
154. Sugimoto, N., et al., *Foxp3-dependent and -independent molecules specific for CD25+CD4+ natural regulatory T cells revealed by DNA microarray analysis.* Int Immunol, 2006. **18**(8): p. 1197-209.
155. Getnet, D., et al., *A role for the transcription factor Helios in human CD4(+)CD25(+) regulatory T cells.* Mol Immunol, 2010. **47**(7-8): p. 1595-600.
156. Akimova, T., et al., *Helios expression is a marker of T cell activation and proliferation.* PLoS One, 2011. **6**(8): p. e24226.

157. Josefowicz, S.Z., L.F. Lu, and A.Y. Rudensky, *Regulatory T cells: mechanisms of differentiation and function.* Annu Rev Immunol, 2012. **30**: p. 531-64.
158. von Boehmer, H., *Mechanisms of suppression by suppressor T cells.* Nat Immunol, 2005. **6**(4): p. 338-44.
159. Li, M.O., Y.Y. Wan, and R.A. Flavell, *T cell-produced transforming growth factor-beta1 controls T cell tolerance and regulates Th1- and Th17-cell differentiation.* Immunity, 2007. **26**(5): p. 579-91.
160. Asseman, C., et al., *An essential role for interleukin 10 in the function of regulatory T cells that inhibit intestinal inflammation.* J Exp Med, 1999. **190**(7): p. 995-1004.
161. Collison, L.W., et al., *Regulatory T cell suppression is potentiated by target T cells in a cell contact, IL-35- and IL-10-dependent manner.* J Immunol, 2009. **182**(10): p. 6121-8.
162. Feng, L.L., et al., *IL-9 contributes to immunosuppression mediated by regulatory T cells and mast cells in B-cell non-hodgkin's lymphoma.* J Clin Immunol, 2011. **31**(6): p. 1084-94.
163. Liu, V.C., et al., *Tumor evasion of the immune system by converting CD4+CD25- T cells into CD4+CD25+ T regulatory cells: role of tumor-derived TGF-beta.* J Immunol, 2007. **178**(5): p. 2883-92.
164. Bopp, T., et al., *Cyclic adenosine monophosphate is a key component of regulatory T cell-mediated suppression.* J Exp Med, 2007. **204**(6): p. 1303-10.
165. Deaglio, S., et al., *Adenosine generation catalyzed by CD39 and CD73 expressed on regulatory T cells mediates immune suppression.* J Exp Med, 2007. **204**(6): p. 1257-65.
166. Bachmann, M.F., et al., *Cutting edge: lymphoproliferative disease in the absence of CTLA-4 is not T cell autonomous.* J Immunol, 1999. **163**(3): p. 1128-31.
167. Grossman, W.J., et al., *Human T regulatory cells can use the perforin pathway to cause autologous target cell death.* Immunity, 2004. **21**(4): p. 589-601.
168. Grossman, W.J., et al., *Differential expression of granzymes A and B in human cytotoxic lymphocyte subsets and T regulatory cells.* Blood, 2004. **104**(9): p. 2840-8.
169. Pandiyan, P., et al., *CD4+CD25+Foxp3+ regulatory T cells induce cytokine deprivation-mediated apoptosis of effector CD4+ T cells.* Nat Immunol, 2007. **8**(12): p. 1353-62.
170. Jung, Y.J. and J.Y. Seoh, *Feedback loop of immune regulation by CD4+CD25+ Treg.* Immunobiology, 2009. **214**(4): p. 291-302.
171. Morales-Sanchez, A. and E.M. Fuentes-Panana, *Human Viruses and Cancer.* Viruses, 2014. **6**(10): p. 4047-4079.
172. Bruno, A., et al., *Orchestration of angiogenesis by immune cells.* Front Oncol, 2014. **4**: p. 131.
173. Allan, D.S., et al., *TGF-beta affects development and differentiation of human natural killer cell subsets.* Eur J Immunol, 2010. **40**(8): p. 2289-95.
174. Mantovani, A. and A. Sica, *Macrophages, innate immunity and cancer: balance, tolerance, and diversity.* Curr Opin Immunol, 2010. **22**(2): p. 231-7.
175. Sica, A., et al., *Tumour-associated macrophages are a distinct M2 polarised population promoting tumour progression: potential targets of anti-cancer therapy.* Eur J Cancer, 2006. **42**(6): p. 717-27.
176. Crowther, M., et al., *Microenvironmental influence on macrophage regulation of angiogenesis in wounds and malignant tumors.* J Leukoc Biol, 2001. **70**(4): p. 478-90.
177. Scapini, P., et al., *The neutrophil as a cellular source of chemokines.* Immunol Rev, 2000. **177**: p. 195-203.
178. Hanahan, D. and L.M. Coussens, *Accessories to the crime: functions of cells recruited to the tumor microenvironment.* Cancer Cell, 2012. **21**(3): p. 309-22.
179. Strieter, R.M., et al., *CXC chemokines in angiogenesis.* Cytokine Growth Factor Rev, 2005. **16**(6): p. 593-609.
180. Santoni, A., et al., *Natural killer (NK) cells from killers to regulators: distinct features between peripheral blood and decidual NK cells.* Am J Reprod Immunol, 2007. **58**(3): p. 280-8.

181. Vacca, P., et al., *Origin, phenotype and function of human natural killer cells in pregnancy.* Trends Immunol, 2011. **32**(11): p. 517-23.
182. Bruno, A., et al., *The proangiogenic phenotype of natural killer cells in patients with non-small cell lung cancer.* Neoplasia, 2013. **15**(2): p. 133-42.
183. Facciabene, A., et al., *Tumour hypoxia promotes tolerance and angiogenesis via CCL28 and T(reg) cells.* Nature, 2011. **475**(7355): p. 226-30.
184. Murdoch, C., et al., *The role of myeloid cells in the promotion of tumour angiogenesis.* Nat Rev Cancer, 2008. **8**(8): p. 618-31.
185. Bunt, S.K., et al., *Inflammation induces myeloid-derived suppressor cells that facilitate tumor progression.* J Immunol, 2006. **176**(1): p. 284-90.
186. Martin-Orozco, N. and C. Dong, *Inhibitory costimulation and anti-tumor immunity.* Semin Cancer Biol, 2007. **17**(4): p. 288-98.
187. Seliger, B. and D. Quandt, *The expression, function, and clinical relevance of B7 family members in cancer.* Cancer Immunol Immunother, 2012. **61**(8): p. 1327-41.
188. Nakanishi, J., et al., *Overexpression of B7-H1 (PD-L1) significantly associates with tumor grade and postoperative prognosis in human urothelial cancers.* Cancer Immunol Immunother, 2007. **56**(8): p. 1173-82.
189. Ohigashi, Y., et al., *Clinical significance of programmed death-1 ligand-1 and programmed death-1 ligand-2 expression in human esophageal cancer.* Clin Cancer Res, 2005. **11**(8): p. 2947-53.
190. Wu, C., et al., *Immunohistochemical localization of programmed death-1 ligand-1 (PD-L1) in gastric carcinoma and its clinical significance.* Acta Histochem, 2006. **108**(1): p. 19-24.
191. Ghebeh, H., et al., *Expression of B7-H1 in breast cancer patients is strongly associated with high proliferative Ki-67-expressing tumor cells.* Int J Cancer, 2007. **121**(4): p. 751-8.
192. Hamanishi, J., et al., *Programmed cell death 1 ligand 1 and tumor-infiltrating CD8+ T lymphocytes are prognostic factors of human ovarian cancer.* Proc Natl Acad Sci U S A, 2007. **104**(9): p. 3360-5.
193. Yao, Y., et al., *B7-H1 is correlated with malignancy-grade gliomas but is not expressed exclusively on tumor stem-like cells.* Neuro Oncol, 2009. **11**(6): p. 757-66.
194. Geng, L., et al., *B7-H1 up-regulated expression in human pancreatic carcinoma tissue associates with tumor progression.* J Cancer Res Clin Oncol, 2008. **134**(9): p. 1021-7.
195. Thompson, R.H., et al., *Costimulatory molecule B7-H1 in primary and metastatic clear cell renal cell carcinoma.* Cancer, 2005. **104**(10): p. 2084-91.
196. Tamura, H., et al., *Expression of functional B7-H2 and B7.2 costimulatory molecules and their prognostic implications in de novo acute myeloid leukemia.* Clin Cancer Res, 2005. **11**(16): p. 5708-17.
197. Sun, J., et al., *Clinical significance and regulation of the costimulatory molecule B7-H3 in human colorectal carcinoma.* Cancer Immunol Immunother, 2010. **59**(8): p. 1163-71.
198. Roth, T.J., et al., *B7-H3 ligand expression by prostate cancer: a novel marker of prognosis and potential target for therapy.* Cancer Res, 2007. **67**(16): p. 7893-900.
199. Jiang, J., et al., *Tumor expression of B7-H4 predicts poor survival of patients suffering from gastric cancer.* Cancer Immunol Immunother, 2010. **59**(11): p. 1707-14.
200. Sun, Y., et al., *B7-H3 and B7-H4 expression in non-small-cell lung cancer.* Lung Cancer, 2006. **53**(2): p. 143-51.
201. Chen, L.J., et al., *B7-H4 expression associates with cancer progression and predicts patient's survival in human esophageal squamous cell carcinoma.* Cancer Immunol Immunother, 2011. **60**(7): p. 1047-55.
202. Quandt, D., et al., *B7-h4 expression in human melanoma: its association with patients' survival and antitumor immune response.* Clin Cancer Res, 2011. **17**(10): p. 3100-11.

203. Zang, X., et al., *B7-H3 and B7x are highly expressed in human prostate cancer and associated with disease spread and poor outcome.* Proc Natl Acad Sci U S A, 2007. **104**(49): p. 19458-63.
204. Krambeck, A.E., et al., *B7-H4 expression in renal cell carcinoma and tumor vasculature: associations with cancer progression and survival.* Proc Natl Acad Sci U S A, 2006. **103**(27): p. 10391-6.
205. Chen, L., et al., *Costimulation of antitumor immunity by the B7 counterreceptor for the T lymphocyte molecules CD28 and CTLA-4.* Cell, 1992. **71**(7): p. 1093-102.
206. Townsend, S.E. and J.P. Allison, *Tumor rejection after direct costimulation of CD8+ T cells by B7-transfected melanoma cells.* Science, 1993. **259**(5093): p. 368-70.
207. Curran, M.A., et al., *PD-1 and CTLA-4 combination blockade expands infiltrating T cells and reduces regulatory T and myeloid cells within B16 melanoma tumors.* Proc Natl Acad Sci U S A, 2010. **107**(9): p. 4275-80.
208. Garrido, F., H. Festenstein, and V. Schirrmacher, *Further evidence for depression of H-2 and Ia-like specificities of foreign haplotypes in mouse tumour cell lines.* Nature, 1976. **261**(5562): p. 705-7.
209. Pellegrino, M.A., et al., *Expression of histocompatibility (HLA) antigens on tumor cells and normal cells from patients with melanoma.* Cancer, 1977. **40**(1): p. 36-41.
210. Garrido, F. and I. Algarra, *MHC antigens and tumor escape from immune surveillance.* Adv Cancer Res, 2001. **83**: p. 117-58.
211. Koopmann, J.O., et al., *Export of antigenic peptides from the endoplasmic reticulum intersects with retrograde protein translocation through the Sec61p channel.* Immunity, 2000. **13**(1): p. 117-27.
212. Garrido, F., et al., *Implications for immunosurveillance of altered HLA class I phenotypes in human tumours.* Immunol Today, 1997. **18**(2): p. 89-95.
213. Bukur, J., S. Jasinski, and B. Seliger, *The role of classical and non-classical HLA class I antigens in human tumors.* Semin Cancer Biol, 2012. **22**(4): p. 350-8.
214. Garrido, F., T. Cabrera, and N. Aptsiauri, *"Hard" and "soft" lesions underlying the HLA class I alterations in cancer cells: implications for immunotherapy.* Int J Cancer, 2010. **127**(2): p. 249-56.
215. Maleno, I., et al., *Multiple mechanisms generate HLA class I altered phenotypes in laryngeal carcinomas: high frequency of HLA haplotype loss associated with loss of heterozygosity in chromosome region 6p21.* Cancer Immunol Immunother, 2002. **51**(7): p. 389-96.
216. Paschen, A., et al., *The coincidence of chromosome 15 aberrations and beta2-microglobulin gene mutations is causative for the total loss of human leukocyte antigen class I expression in melanoma.* Clin Cancer Res, 2006. **12**(11 Pt 1): p. 3297-305.
217. Zhu, K., et al., *p53 induces TAP1 and enhances the transport of MHC class I peptides.* Oncogene, 1999. **18**(54): p. 7740-7.
218. Mimura, K., et al., *T cell recognition of HLA-A2 restricted tumor antigens is impaired by the oncogene HER2.* Int J Cancer, 2011. **128**(2): p. 390-401.
219. Carretero, R., et al., *Analysis of HLA class I expression in progressing and regressing metastatic melanoma lesions after immunotherapy.* Immunogenetics, 2008. **60**(8): p. 439-47.
220. Watson, N.F., et al., *Immunosurveillance is active in colorectal cancer as downregulation but not complete loss of MHC class I expression correlates with a poor prognosis.* Int J Cancer, 2006. **118**(1): p. 6-10.
221. Kasajima, A., et al., *Down-regulation of the antigen processing machinery is linked to a loss of inflammatory response in colorectal cancer.* Hum Pathol, 2010. **41**(12): p. 1758-69.
222. Halama, N., et al., *Natural killer cells are scarce in colorectal carcinoma tissue despite high levels of chemokines and cytokines.* Clin Cancer Res, 2011. **17**(4): p. 678-89.

223. Platonova, S., et al., *Profound coordinated alterations of intratumoral NK cell phenotype and function in lung carcinoma.* Cancer Res, 2011. **71**(16): p. 5412-22.
224. Imai, K., et al., *Natural cytotoxic activity of peripheral-blood lymphocytes and cancer incidence: an 11-year follow-up study of a general population.* Lancet, 2000. **356**(9244): p. 1795-9.
225. Ito, M., et al., *NOD/SCID/gamma(c)(null) mouse: an excellent recipient mouse model for engraftment of human cells.* Blood, 2002. **100**(9): p. 3175-82.
226. Dewan, M.Z., et al., *Role of natural killer cells in hormone-independent rapid tumor formation and spontaneous metastasis of breast cancer cells in vivo.* Breast Cancer Res Treat, 2007. **104**(3): p. 267-75.
227. Saito, H., T. Osaki, and M. Ikeguchi, *Decreased NKG2D expression on NK cells correlates with impaired NK cell function in patients with gastric cancer.* Gastric Cancer, 2011. **15**(1): p. 27-33.
228. Garcia-Iglesias, T., et al., *Low NKp30, NKp46 and NKG2D expression and reduced cytotoxic activity on NK cells in cervical cancer and precursor lesions.* BMC Cancer, 2009. **9**: p. 186.
229. Sanchez-Correa, B., et al., *Human NK cells in acute myeloid leukaemia patients: analysis of NK cell-activating receptors and their ligands.* Cancer Immunol Immunother, 2011. **60**(8): p. 1195-205.
230. Watanabe, M., et al., *NK cell dysfunction with down-regulated CD16 and up-regulated CD56 molecules in patients with esophageal squamous cell carcinoma.* Dis Esophagus, 2010. **23**(8): p. 675-81.
231. Al Omar, S.Y., et al., *Increased killer immunoglobulin-like receptor expression and functional defects in natural killer cells in lung cancer.* Immunology, 2011. **133**(1): p. 94-104.
232. de Kruijf, E.M., et al., *NKG2D ligand tumor expression and association with clinical outcome in early breast cancer patients: an observational study.* BMC Cancer, 2012. **12**: p. 24.
233. Mamessier, E., et al., *Human breast cancer cells enhance self tolerance by promoting evasion from NK cell antitumor immunity.* J Clin Invest, 2011. **121**(9): p. 3609-22.
234. Hao, S., et al., *Modulation of 17beta-estradiol on the number and cytotoxicity of NK cells in vivo related to MCM and activating receptors.* Int Immunopharmacol, 2007. **7**(13): p. 1765-75.
235. Dewan, M.Z., et al., *Natural killer activity of peripheral-blood mononuclear cells in breast cancer patients.* Biomed Pharmacother, 2009. **63**(9): p. 703-6.
236. Jimenez-Perez, M.I., et al., *Cervical cancer cell lines expressing NKG2D-ligands are able to down-modulate the NKG2D receptor on NKL cells with functional implications.* BMC Immunol, 2012. **13**: p. 7.
237. Parham, P., *Killer cell immunoglobulin-like receptor diversity: balancing signals in the natural killer cell response.* Immunol Lett, 2004. **92**(1-2): p. 11-3.
238. Yawata, M., et al., *Variation within the human killer cell immunoglobulin-like receptor (KIR) gene family.* Crit Rev Immunol, 2002. **22**(5-6): p. 463-82.
239. Valiante, N.M., et al., *Functionally and structurally distinct NK cell receptor repertoires in the peripheral blood of two human donors.* Immunity, 1997. **7**(6): p. 739-51.
240. Chan, H.W., et al., *DNA methylation maintains allele-specific KIR gene expression in human natural killer cells.* J Exp Med, 2003. **197**(2): p. 245-55.
241. Santourlidis, S., et al., *Crucial role of DNA methylation in determination of clonally distributed killer cell Ig-like receptor expression patterns in NK cells.* J Immunol, 2002. **169**(8): p. 4253-61.
242. Moretta, A., et al., *Identification of four subsets of human CD3-CD16+ natural killer (NK) cells by the expression of clonally distributed functional surface molecules: correlation between subset assignment of NK clones and ability to mediate specific alloantigen recognition.* J Exp Med, 1990. **172**(6): p. 1589-98.

243. Curiel, T.J., et al., *Specific recruitment of regulatory T cells in ovarian carcinoma fosters immune privilege and predicts reduced survival.* Nat Med, 2004. **10**(9): p. 942-9.
244. Ishigami, S., et al., *Cancerous HLA class I expression and regulatory T cell infiltration in gastric cancer.* Cancer Immunol Immunother, 2012. **61**(10): p. 1663-9.
245. Kang, M.J., et al., *Tumor-infiltrating PD1-Positive Lymphocytes and FoxP3-Positive Regulatory T Cells Predict Distant Metastatic Relapse and Survival of Clear Cell Renal Cell Carcinoma.* Transl Oncol, 2013. **6**(3): p. 282-9.
246. Hanakawa, H., et al., *Regulatory T-cell infiltration in tongue squamous cell carcinoma.* Acta Otolaryngol, 2014. **134**(8): p. 859-64.
247. Guo, C.L., et al., *Associations between infiltrating lymphocyte subsets and hepatocellular carcinoma.* Asian Pac J Cancer Prev, 2012. **13**(11): p. 5909-13.
248. Ino, Y., et al., *Immune cell infiltration as an indicator of the immune microenvironment of pancreatic cancer.* Br J Cancer, 2013. **108**(4): p. 914-23.
249. Katz, S.C., et al., *Regulatory T cell infiltration predicts outcome following resection of colorectal cancer liver metastases.* Ann Surg Oncol, 2013. **20**(3): p. 946-55.
250. Pircher, A., et al., *Neoadjuvant chemo-immunotherapy modifies CD4(+)CD25(+) regulatory T cells (Treg) in non-small cell lung cancer (NSCLC) patients.* Lung Cancer, 2014. **85**(1): p. 81-7.
251. Li, Y.Q., et al., *Tumor secretion of CCL22 activates intratumoral Treg infiltration and is independent prognostic predictor of breast cancer.* PLoS One, 2013. **8**(10): p. e76379.
252. Mizukami, Y., et al., *CCL17 and CCL22 chemokines within tumor microenvironment are related to accumulation of Foxp3+ regulatory T cells in gastric cancer.* Int J Cancer, 2008. **122**(10): p. 2286-93.
253. Gobert, M., et al., *Regulatory T cells recruited through CCL22/CCR4 are selectively activated in lymphoid infiltrates surrounding primary breast tumors and lead to an adverse clinical outcome.* Cancer Res, 2009. **69**(5): p. 2000-9.
254. Cao, X., et al., *Granzyme B and perforin are important for regulatory T cell-mediated suppression of tumor clearance.* Immunity, 2007. **27**(4): p. 635-46.
255. Li, C.H., et al., *Activation of regulatory T cells instigates functional down-regulation of cytotoxic T lymphocytes in human breast cancer.* Immunol Res, 2011. **51**(1): p. 71-9.
256. Bonertz, A., et al., *Antigen-specific Tregs control T cell responses against a limited repertoire of tumor antigens in patients with colorectal carcinoma.* J Clin Invest, 2009. **119**(11): p. 3311-21.
257. Takahashi, T., et al., *Immunologic self-tolerance maintained by CD25+CD4+ naturally anergic and suppressive T cells: induction of autoimmune disease by breaking their anergic/suppressive state.* Int Immunol, 1998. **10**(12): p. 1969-80.
258. Liyanage, U.K., et al., *Prevalence of regulatory T cells is increased in peripheral blood and tumor microenvironment of patients with pancreas or breast adenocarcinoma.* J Immunol, 2002. **169**(5): p. 2756-61.
259. Wolf, A.M., et al., *Increase of regulatory T cells in the peripheral blood of cancer patients.* Clin Cancer Res, 2003. **9**(2): p. 606-12.
260. Jaberipour, M., et al., *Increased CTLA-4 and FOXP3 transcripts in peripheral blood mononuclear cells of patients with breast cancer.* Pathol Oncol Res, 2010. **16**(4): p. 547-51.
261. Gershwin, M.E., E.J. Goetzl, and A.D. Steinberg, *Cyclophosphamide: use in practice.* Ann Intern Med, 1974. **80**(4): p. 531-40.
262. Brode, S. and A. Cooke, *Immune-potentiating effects of the chemotherapeutic drug cyclophosphamide.* Crit Rev Immunol, 2008. **28**(2): p. 109-26.
263. Mackall, C.L., et al., *Distinctions between CD8+ and CD4+ T-cell regenerative pathways result in prolonged T-cell subset imbalance after intensive chemotherapy.* Blood, 1997. **89**(10): p. 3700-7.
264. Rosental, B., et al., *The effect of chemotherapy/radiotherapy on cancerous pattern recognition by NK cells.* Curr Med Chem, 2012. **19**(12): p. 1780-91.

265. Ménard, C., et al., *Cancer chemotherapy: not only a direct cytotoxic effect, but also an adjuvant for antitumor immunity.* Cancer Immunol Immunother, 2008. **57**(11): p. 1579-87.
266. Polak, L. and J.L. Turk, *Reversal of immunological tolerance by cyclophosphamide through inhibition of suppressor cell activity.* Nature, 1974. **249**(458): p. 654-6.
267. Ghiringhelli, F., et al., *CD4+CD25+ regulatory T cells suppress tumor immunity but are sensitive to cyclophosphamide which allows immunotherapy of established tumors to be curative.* Eur J Immunol, 2004. **34**(2): p. 336-44.
268. Ghiringhelli, F., et al., *Metronomic cyclophosphamide regimen selectively depletes CD4+CD25+ regulatory T cells and restores T and NK effector functions in end stage cancer patients.* Cancer Immunol Immunother, 2007. **56**(5): p. 641-8.
269. Walter, S., et al., *Multipeptide immune response to cancer vaccine IMA901 after single-dose cyclophosphamide associates with longer patient survival.* Nat Med, 2012. **18**(8): p. 1254-61.
270. Hengartner, M.O., *The biochemistry of apoptosis.* Nature, 2000. **407**(6805): p. 770-6.
271. Rödel, F., et al., *Immunomodulatory properties and molecular effects in inflammatory diseases of low-dose x-irradiation.* Front Oncol, 2012. **2**: p. 120.
272. Foulds, G.A., et al., *Influence of tumors on protective anti-tumor immunity and the effects of irradiation.* Front Oncol, 2013. **3**: p. 14.
273. Shakhov, A.N., et al., *Kappa B-type enhancers are involved in lipopolysaccharide-mediated transcriptional activation of the tumor necrosis factor alpha gene in primary macrophages.* J Exp Med, 1990. **171**(1): p. 35-47.
274. Mori, N. and D. Prager, *Transactivation of the interleukin-1alpha promoter by human T-cell leukemia virus type I and type II Tax proteins.* Blood, 1996. **87**(8): p. 3410-7.
275. Shan, Y.X., et al., *Ionizing radiation stimulates secretion of pro-inflammatory cytokines: dose-response relationship, mechanisms and implications.* Radiat Environ Biophys, 2007. **46**(1): p. 21-9.
276. Matsumura, S., et al., *Radiation-induced CXCL16 release by breast cancer cells attracts effector T cells.* J Immunol, 2008. **181**(5): p. 3099-107.
277. Handschel, J., et al., *Irradiation induces increase of adhesion molecules and accumulation of beta2-integrin-expressing cells in humans.* Int J Radiat Oncol Biol Phys, 1999. **45**(2): p. 475-81.
278. Bianchi, M.E., *DAMPs, PAMPs and alarmins: all we need to know about danger.* J Leukoc Biol, 2007. **81**(1): p. 1-5.
279. Apetoh, L., et al., *The interaction between HMGB1 and TLR4 dictates the outcome of anticancer chemotherapy and radiotherapy.* Immunol Rev, 2007. **220**: p. 47-59.
280. Pockley, A.G., J. Shepherd, and J.M. Corton, *Detection of heat shock protein 70 (Hsp70) and anti-Hsp70 antibodies in the serum of normal individuals.* Immunol Invest, 1998. **27**(6): p. 367-77.
281. Pockley, A.G., B. Henderson, and G. Multhoff, *Extracellular cell stress proteins as biomarkers of human disease.* Biochem Soc Trans, 2014. **42**(6): p. 1744-51.
282. Theriault, J.R., et al., *Extracellular HSP70 binding to surface receptors present on antigen presenting cells and endothelial/epithelial cells.* FEBS Lett, 2005. **579**(9): p. 1951-60.
283. Asea, A., et al., *Novel signal transduction pathway utilized by extracellular HSP70: role of toll-like receptor (TLR) 2 and TLR4.* J Biol Chem, 2002. **277**(17): p. 15028-34.
284. Sutmuller, R., A. Garritsen, and G.J. Adema, *Regulatory T cells and toll-like receptors: regulating the regulators.* Ann Rheum Dis, 2007. **66 Suppl 3**: p. iii91-5.
285. Multhoff, G., *Heat shock protein 70 (Hsp70): membrane location, export and immunological relevance.* Methods, 2007. **43**(3): p. 229-37.
286. Vega, V.L., et al., *Hsp70 translocates into the plasma membrane after stress and is released into the extracellular environment in a membrane-associated form that activates macrophages.* J Immunol, 2008. **180**(6): p. 4299-307.

287. Multhoff, G., et al., *A stress-inducible 72-kDa heat-shock protein (HSP72) is expressed on the surface of human tumor cells, but not on normal cells.* Int J Cancer, 1995. **61**(2): p. 272-9.
288. Multhoff, G., et al., *Heat shock protein 72 on tumor cells: a recognition structure for natural killer cells.* J Immunol, 1997. **158**(9): p. 4341-50.
289. Botzler, C., et al., *Definition of extracellular localized epitopes of Hsp70 involved in an NK immune response.* Cell Stress Chaperones, 1998. **3**(1): p. 6-11.
290. Gehrmann, M., et al., *The therapeutic implications of clinically applied modifiers of heat shock protein 70 (Hsp70) expression by tumor cells.* Cell Stress Chaperones, 2008. **13**(1): p. 1-10.
291. Berkowitz, N., S. Gupta, and G. Silberman, *Estimates of the lifetime direct costs of treatment for metastatic breast cancer.* Value Health, 2000. **3**(1): p. 23-30.
292. Cardoso, F., et al., *Locally recurrent or metastatic breast cancer: ESMO Clinical Practice Guidelines for diagnosis, treatment and follow-up.* Ann Oncol, 2010. **21 Suppl 5**: p. v15-9.
293. Cardoso, F., et al., *1st International consensus guidelines for advanced breast cancer (ABC 1).* Breast, 2012. **21**(3): p. 242-52.
294. Andre, F., et al., *Breast cancer with synchronous metastases: trends in survival during a 14-year period.* J Clin Oncol, 2004. **22**(16): p. 3302-8.
295. Largillier, R., et al., *Prognostic factors in 1,038 women with metastatic breast cancer.* Ann Oncol, 2008. **19**(12): p. 2012-9.
296. Paget, S., *The Distribution of Secondary Growths in Cancer of the Breast.* The Lancet, 1889. **133**(3421): p. 571-573.
297. Fidler, I.J., *The pathogenesis of cancer metastasis: the 'seed and soil' hypothesis revisited.* Nat Rev Cancer, 2003. **3**(6): p. 453-8.
298. Bonnet, D. and J.E. Dick, *Human acute myeloid leukemia is organized as a hierarchy that originates from a primitive hematopoietic cell.* Nat Med, 1997. **3**(7): p. 730-7.
299. Al-Hajj, M., et al., *Prospective identification of tumorigenic breast cancer cells.* Proc Natl Acad Sci U S A, 2003. **100**(7): p. 3983-8.
300. Iqbal, J., P.Y. Chong, and P.H. Tan, *Breast cancer stem cells: an update.* J Clin Pathol, 2013. **66**(6): p. 485-90.
301. Allan, A.L., et al., *Tumor dormancy and cancer stem cells: implications for the biology and treatment of breast cancer metastasis.* Breast Dis, 2006. **26**: p. 87-98.
302. Dontu, G., D. El-Ashry, and M.S. Wicha, *Breast cancer, stem/progenitor cells and the estrogen receptor.* Trends Endocrinol Metab, 2004. **15**(5): p. 193-7.
303. Li, F., et al., *Beyond tumorigenesis: cancer stem cells in metastasis.* Cell Res, 2007. **17**(1): p. 3-14.
304. Yu, J., et al., *Induced pluripotent stem cell lines derived from human somatic cells.* Science, 2007. **318**(5858): p. 1917-20.
305. Ginestier, C., et al., *ALDH1 is a marker of normal and malignant human mammary stem cells and a predictor of poor clinical outcome.* Cell Stem Cell, 2007. **1**(5): p. 555-67.
306. Patrawala, L., et al., *Side population is enriched in tumorigenic, stem-like cancer cells, whereas ABCG2+ and ABCG2- cancer cells are similarly tumorigenic.* Cancer Res, 2005. **65**(14): p. 6207-19.
307. Ponti, D., et al., *Isolation and in vitro propagation of tumorigenic breast cancer cells with stem/progenitor cell properties.* Cancer Res, 2005. **65**(13): p. 5506-11.
308. Gangopadhyay, S., et al., *Breast cancer stem cells: a novel therapeutic target.* Clin Breast Cancer, 2013. **13**(1): p. 7-15.
309. Li, H.Z., T.B. Yi, and Z.Y. Wu, *Suspension culture combined with chemotherapeutic agents for sorting of breast cancer stem cells.* BMC Cancer, 2008. **8**: p. 135.
310. Eyler, C.E. and J.N. Rich, *Survival of the fittest: cancer stem cells in therapeutic resistance and angiogenesis.* J Clin Oncol, 2008. **26**(17): p. 2839-45.

311. Woodward, J.K., et al., *The roles of proteolytic enzymes in the development of tumour-induced bone disease in breast and prostate cancer.* Bone, 2007. **41**(6): p. 912-27.
312. Diehn, M., et al., *Association of reactive oxygen species levels and radioresistance in cancer stem cells.* Nature, 2009. **458**(7239): p. 780-3.
313. Hugh, J., et al., *Breast cancer subtypes and response to docetaxel in node-positive breast cancer: use of an immunohistochemical definition in the BCIRG 001 trial.* J Clin Oncol, 2009. **27**(8): p. 1168-76.
314. Carey, L.A., et al., *The triple negative paradox: primary tumor chemosensitivity of breast cancer subtypes.* Clin Cancer Res, 2007. **13**(8): p. 2329-34.
315. Perou, C.M., et al., *Molecular portraits of human breast tumours.* Nature, 2000. **406**(6797): p. 747-52.
316. Sorlie, T., et al., *Gene expression patterns of breast carcinomas distinguish tumor subclasses with clinical implications.* Proc Natl Acad Sci U S A, 2001. **98**(19): p. 10869-74.
317. Cheang, M.C., et al., *Ki67 index, HER2 status, and prognosis of patients with luminal B breast cancer.* J Natl Cancer Inst, 2009. **101**(10): p. 736-50.
318. Parker, J.S., et al., *Supervised risk predictor of breast cancer based on intrinsic subtypes.* J Clin Oncol, 2009. **27**(8): p. 1160-7.
319. Prat, A., et al., *Phenotypic and molecular characterization of the claudin-low intrinsic subtype of breast cancer.* Breast Cancer Res, 2010. **12**(5): p. R68.
320. Slamon, D.J., et al., *Human breast cancer: correlation of relapse and survival with amplification of the HER-2/neu oncogene.* Science, 1987. **235**(4785): p. 177-82.
321. Pegram, M.D., G. Pauletti, and D.J. Slamon, *HER-2/neu as a predictive marker of response to breast cancer therapy.* Breast Cancer Res Treat, 1998. **52**(1-3): p. 65-77.
322. Witton, C.J., et al., *Expression of the HER1-4 family of receptor tyrosine kinases in breast cancer.* J Pathol, 2003. **200**(3): p. 290-7.
323. Kassam, F., et al., *Survival outcomes for patients with metastatic triple-negative breast cancer: implications for clinical practice and trial design.* Clin Breast Cancer, 2009. **9**(1): p. 29-33.
324. Bertucci, F., et al., *How basal are triple-negative breast cancers?* Int J Cancer, 2008. **123**(1): p. 236-40.
325. Valentin, M.D., et al., *Molecular insights on basal-like breast cancer.* Breast Cancer Res Treat, 2012. **134**(1): p. 21-30.
326. Elsawaf, Z., et al., *Biological subtypes of triple-negative breast cancer are associated with distinct morphological changes and clinical behaviour.* Breast, 2013. **22**(5): p. 986-92.
327. Prat, A., et al., *Molecular characterization of basal-like and non-basal-like triple-negative breast cancer.* Oncologist, 2013. **18**(2): p. 123-33.
328. Kreike, B., et al., *Gene expression profiling and histopathological characterization of triple-negative/basal-like breast carcinomas.* Breast Cancer Res, 2007. **9**(5): p. R65.
329. Shastry, M. and D.A. Yardley, *Updates in the treatment of basal/triple-negative breast cancer.* Curr Opin Obstet Gynecol, 2013. **25**(1): p. 40-8.
330. Herschkowitz, J.I., et al., *Identification of conserved gene expression features between murine mammary carcinoma models and human breast tumors.* Genome Biol, 2007. **8**(5): p. R76.
331. Curtis, C., et al., *The genomic and transcriptomic architecture of 2,000 breast tumours reveals novel subgroups.* Nature, 2012. **486**(7403): p. 346-52.
332. Bayraktar, S. and S. Gluck, *Systemic therapy options in BRCA mutation-associated breast cancer.* Breast Cancer Res Treat, 2012. **135**(2): p. 355-66.
333. Farmer, H., et al., *Targeting the DNA repair defect in BRCA mutant cells as a therapeutic strategy.* Nature, 2005. **434**(7035): p. 917-21.
334. Bryant, H.E., et al., *Specific killing of BRCA2-deficient tumours with inhibitors of poly(ADP-ribose) polymerase.* Nature, 2005. **434**(7035): p. 913-7.

335. Kimbung, S., et al., *Co-targeting of the PI3K pathway improves the response of BRCA1 deficient breast cancer cells to PARP1 inhibition.* Cancer Lett, 2012. **319**(2): p. 232-41.
336. Rakha, E.A., et al., *Nottingham Prognostic Index Plus (NPI+): a modern clinical decision making tool in breast cancer.* Br J Cancer, 2014. **110**(7): p. 1688-97.
337. Abd El-Rehim, D.M., et al., *High-throughput protein expression analysis using tissue microarray technology of a large well-characterised series identifies biologically distinct classes of breast cancer confirming recent cDNA expression analyses.* Int J Cancer, 2005. **116**(3): p. 340-50.
338. Soria, D., et al., *A methodology to identify consensus classes from clustering algorithms applied to immunohistochemical data from breast cancer patients.* Comput Biol Med, 2010. **40**(3): p. 318-30.
339. Haybittle, J.L., et al., *A prognostic index in primary breast cancer.* Br J Cancer, 1982. **45**(3): p. 361-6.
340. Galea, M.H., et al., *The Nottingham Prognostic Index in primary breast cancer.* Breast Cancer Res Treat, 1992. **22**(3): p. 207-19.
341. Murphy, C.G. and P.G. Morris, *Recent advances in novel targeted therapies for HER2-positive breast cancer.* Anticancer Drugs, 2012. **23**(8): p. 765-76.
342. Awada, A., I. Bozovic-Spasojevic, and L. Chow, *New therapies in HER2-positive breast cancer: a major step towards a cure of the disease?* Cancer Treat Rev, 2012. **38**(5): p. 494-504.
343. Glass, A.G., et al., *Breast cancer incidence, 1980-2006: combined roles of menopausal hormone therapy, screening mammography, and estrogen receptor status.* J Natl Cancer Inst, 2007. **99**(15): p. 1152-61.
344. Boswell, K.A., et al., *Disease burden and treatment outcomes in second-line therapy of patients with estrogen receptor-positive (ER+) advanced breast cancer: a review of the literature.* Breast, 2012. **21**(6): p. 701-6.
345. Stokes, M.E., et al., *Ten-year survival and cost following breast cancer recurrence: estimates from SEER-medicare data.* Value Health, 2008. **11**(2): p. 213-20.
346. Horwitz, K.B. and W.L. McGuire, *Predicting response to endocrine therapy in human breast cancer: a hypothesis.* Science, 1975. **189**(4204): p. 726-7.
347. Perrault, D., et al., *Phase II study of the progesterone antagonist mifepristone in patients with untreated metastatic breast carcinoma: a National Cancer Institute of Canada Clinical Trials Group study.* J Clin Oncol, 1996. **14**(10): p. 2709-12.
348. Robertson, J.F., et al., *Onapristone, a progesterone receptor antagonist, as first-line therapy in primary breast cancer.* Eur J Cancer, 1999. **35**(2): p. 214-8.
349. Afhuppe, W., et al., *In vitro characterization of ZK 230211--A type III progesterone receptor antagonist with enhanced antiproliferative properties.* J Steroid Biochem Mol Biol, 2010. **119**(1-2): p. 45-55.
350. Attardi, B.J., et al., *In vitro antiprogestational/antiglucocorticoid activity and progestin and glucocorticoid receptor binding of the putative metabolites and synthetic derivatives of CDB-2914, CDB-4124, and mifepristone.* J Steroid Biochem Mol Biol, 2004. **88**(3): p. 277-88.
351. Piccart-Gebhart, M.J., et al., *Trastuzumab after adjuvant chemotherapy in HER2-positive breast cancer.* N Engl J Med, 2005. **353**(16): p. 1659-72.
352. Dawood, S., et al., *Prognosis of women with metastatic breast cancer by HER2 status and trastuzumab treatment: an institutional-based review.* J Clin Oncol, 2010. **28**(1): p. 92-8.
353. Junttila, T.T., et al., *Ligand-independent HER2/HER3/PI3K complex is disrupted by trastuzumab and is effectively inhibited by the PI3K inhibitor GDC-0941.* Cancer Cell, 2009. **15**(5): p. 429-40.
354. Lane, H.A., et al., *ErbB2 potentiates breast tumor proliferation through modulation of p27(Kip1)-Cdk2 complex formation: receptor overexpression does not determine growth dependency.* Mol Cell Biol, 2000. **20**(9): p. 3210-23.

355. Le, X.F., et al., *Anti-HER2 antibody and heregulin suppress growth of HER2-overexpressing human breast cancer cells through different mechanisms.* Clin Cancer Res, 2000. **6**(1): p. 260-70.
356. Park, S., et al., *The therapeutic effect of anti-HER2/neu antibody depends on both innate and adaptive immunity.* Cancer Cell, 2010. **18**(2): p. 160-70.
357. Lewis, G.D., et al., *Differential responses of human tumor cell lines to anti-p185HER2 monoclonal antibodies.* Cancer Immunol Immunother, 1993. **37**(4): p. 255-63.
358. Clynes, R.A., et al., *Inhibitory Fc receptors modulate in vivo cytotoxicity against tumor targets.* Nat Med, 2000. **6**(4): p. 443-6.
359. Gianni, L., et al., *Neoadjuvant and adjuvant trastuzumab in patients with HER2-positive locally advanced breast cancer (NOAH): follow-up of a randomised controlled superiority trial with a parallel HER2-negative cohort.* Lancet Oncol, 2014. **15**(6): p. 640-7.
360. Baselga, J., et al., *Phase II study of efficacy, safety, and pharmacokinetics of trastuzumab monotherapy administered on a 3-weekly schedule.* J Clin Oncol, 2005. **23**(10): p. 2162-71.
361. Nielsen, D.L., et al., *Efficacy of HER2-targeted therapy in metastatic breast cancer. Monoclonal antibodies and tyrosine kinase inhibitors.* Breast, 2013. **22**(1): p. 1-12.
362. Boix-Perales, H., et al., *The European Medicines Agency Review of Pertuzumab for the treatment of adult patients with HER2-positive metastatic or locally recurrent unresectable breast cancer: summary of the scientific assessment of the committee for medicinal products for human use.* Oncologist, 2014. **19**(7): p. 766-73.
363. Scheuer, W., et al., *Strongly enhanced antitumor activity of trastuzumab and pertuzumab combination treatment on HER2-positive human xenograft tumor models.* Cancer Res, 2009. **69**(24): p. 9330-6.
364. Baselga, J., et al., *Pertuzumab plus trastuzumab plus docetaxel for metastatic breast cancer.* N Engl J Med, 2012. **366**(2): p. 109-19.
365. Amiri-Kordestani, L., et al., *FDA approval: ado-trastuzumab emtansine for the treatment of patients with HER2-positive metastatic breast cancer.* Clin Cancer Res, 2014. **20**(17): p. 4436-41.
366. Lewis Phillips, G.D., et al., *Targeting HER2-positive breast cancer with trastuzumab-DM1, an antibody-cytotoxic drug conjugate.* Cancer Res, 2008. **68**(22): p. 9280-90.
367. Junttila, T.T., et al., *Trastuzumab-DM1 (T-DM1) retains all the mechanisms of action of trastuzumab and efficiently inhibits growth of lapatinib insensitive breast cancer.* Breast Cancer Res Treat, 2011. **128**(2): p. 347-56.
368. Verma, S., et al., *Trastuzumab emtansine for HER2-positive advanced breast cancer.* N Engl J Med, 2012. **367**(19): p. 1783-91.
369. Perez, E.A., et al., *Relationship between HER2 expression and efficacy with first-line trastuzumab emtansine compared with trastuzumab plus docetaxel in TDM4450g: a randomized phase II study of patients with previously untreated HER2-positive metastatic breast cancer.* Breast Cancer Res, 2014. **16**(3): p. R50.
370. Xia, W., et al., *Anti-tumor activity of GW572016: a dual tyrosine kinase inhibitor blocks EGF activation of EGFR/erbB2 and downstream Erk1/2 and AKT pathways.* Oncogene, 2002. **21**(41): p. 6255-63.
371. Ahn, E.R. and C.L. Vogel, *Dual HER2-targeted approaches in HER2-positive breast cancer.* Breast Cancer Res Treat, 2012. **131**(2): p. 371-83.
372. Kroep, J.R., et al., *Lapatinib: clinical benefit in patients with HER 2-positive advanced breast cancer.* Neth J Med, 2010. **68**(9): p. 371-6.
373. Cameron, D., et al., *Lapatinib plus capecitabine in women with HER-2-positive advanced breast cancer: final survival analysis of a phase III randomized trial.* Oncologist, 2010. **15**(9): p. 924-34.
374. Thery, J.C., et al., *Resistance to human epidermal growth factor receptor type 2-targeted therapies.* Eur J Cancer, 2014. **50**(5): p. 892-901.

375. Baselga, J., et al., *Lapatinib with trastuzumab for HER2-positive early breast cancer (NeoALTTO): a randomised, open-label, multicentre, phase 3 trial.* Lancet, 2012. **379**(9816): p. 633-40.
376. Mohit, E., A. Hashemi, and M. Allahyari, *Breast cancer immunotherapy: monoclonal antibodies and peptide-based vaccines.* Expert Rev Clin Immunol, 2014. **10**(7): p. 927-61.
377. Emens, L.A., *Re-purposing cancer therapeutics for breast cancer immunotherapy.* Cancer Immunol Immunother, 2012. **61**(8): p. 1299-305.
378. Schlom, J., *Therapeutic cancer vaccines: current status and moving forward.* J Natl Cancer Inst, 2012. **104**(8): p. 599-613.
379. Knutson, K.L., et al., *Immunization of cancer patients with a HER-2/neu, HLA-A2 peptide, p369-377, results in short-lived peptide-specific immunity.* Clin Cancer Res, 2002. **8**(5): p. 1014-8.
380. Mittendorf, E.A., et al., *CD4+ T cells in antitumor immunity: utility of an li-key HER2/neu hybrid peptide vaccine (AE37).* Expert Opin Biol Ther, 2009. **9**(1): p. 71-8.
381. Pardoll, D.M. and S.L. Topalian, *The role of CD4+ T cell responses in antitumor immunity.* Curr Opin Immunol, 1998. **10**(5): p. 588-94.
382. Zwaveling, S., et al., *Established human papillomavirus type 16-expressing tumors are effectively eradicated following vaccination with long peptides.* J Immunol, 2002. **169**(1): p. 350-8.
383. Bijker, M.S., et al., *CD8+ CTL priming by exact peptide epitopes in incomplete Freund's adjuvant induces a vanishing CTL response, whereas long peptides induce sustained CTL reactivity.* J Immunol, 2007. **179**(8): p. 5033-40.
384. Reddish, M., et al., *Anti-MUC1 class I restricted CTLs in metastatic breast cancer patients immunized with a synthetic MUC1 peptide.* Int J Cancer, 1998. **76**(6): p. 817-23.
385. Gilewski, T., et al., *Vaccination of high-risk breast cancer patients with mucin-1 (MUC1) keyhole limpet hemocyanin conjugate plus QS-21.* Clin Cancer Res, 2000. **6**(5): p. 1693-701.
386. Disis, M.L., et al., *Generation of T-cell immunity to the HER-2/neu protein after active immunization with HER-2/neu peptide-based vaccines.* J Clin Oncol, 2002. **20**(11): p. 2624-32.
387. Murray, J.L., et al., *Toxicity, immunogenicity, and induction of E75-specific tumor-lytic CTLs by HER-2 peptide E75 (369-377) combined with granulocyte macrophage colony-stimulating factor in HLA-A2+ patients with metastatic breast and ovarian cancer.* Clin Cancer Res, 2002. **8**(11): p. 3407-18.
388. Morse, M.A., et al., *Phase I study of immunization with dendritic cells modified with fowlpox encoding carcinoembryonic antigen and costimulatory molecules.* Clin Cancer Res, 2005. **11**(8): p. 3017-24.
389. Miles, D., et al., *Phase III multicenter clinical trial of the sialyl-TN (STn)-keyhole limpet hemocyanin (KLH) vaccine for metastatic breast cancer.* Oncologist, 2011. **16**(8): p. 1092-100.
390. Madan, R.A., P.M. Arlen, and J.L. Gulley, *PANVAC-VF: poxviral-based vaccine therapy targeting CEA and MUC1 in carcinoma.* Expert Opin Biol Ther, 2007. **7**(4): p. 543-54.
391. Mohebtash, M., et al., *A pilot study of MUC-1/CEA/TRICOM poxviral-based vaccine in patients with metastatic breast and ovarian cancer.* Clin Cancer Res, 2011. **17**(22): p. 7164-73.
392. Gulley, J.L., et al., *Pilot study of vaccination with recombinant CEA-MUC-1-TRICOM poxviral-based vaccines in patients with metastatic carcinoma.* Clin Cancer Res, 2008. **14**(10): p. 3060-9.
393. Peoples, G.E., et al., *Clinical trial results of a HER2/neu (E75) vaccine to prevent recurrence in high-risk breast cancer patients.* J Clin Oncol, 2005. **23**(30): p. 7536-45.

394. Peoples, G.E., et al., *Combined clinical trial results of a HER2/neu (E75) vaccine for the prevention of recurrence in high-risk breast cancer patients: U.S. Military Cancer Institute Clinical Trials Group Study I-01 and I-02.* Clin Cancer Res, 2008. **14**(3): p. 797-803.
395. Mittendorf, E.A., et al., *Final report of the phase I/II clinical trial of the E75 (nelipepimut-S) vaccine with booster inoculations to prevent disease recurrence in high-risk breast cancer patients.* Ann Oncol, 2014. **25**(9): p. 1735-42.
396. Carmichael, M.G., et al., *Results of the first phase 1 clinical trial of the HER-2/neu peptide (GP2) vaccine in disease-free breast cancer patients: United States Military Cancer Institute Clinical Trials Group Study I-04.* Cancer, 2010. **116**(2): p. 292-301.
397. Domchek, S.M., et al., *Telomerase-specific T-cell immunity in breast cancer: effect of vaccination on tumor immunosurveillance.* Cancer Res, 2007. **67**(21): p. 10546-55.
398. Relf, M., et al., *Expression of the angiogenic factors vascular endothelial cell growth factor, acidic and basic fibroblast growth factor, tumor growth factor beta-1, platelet-derived endothelial cell growth factor, placenta growth factor, and pleiotrophin in human primary breast cancer and its relation to angiogenesis.* Cancer Res, 1997. **57**(5): p. 963-9.
399. Elbauomy Elsheikh, S., et al., *FGFR1 amplification in breast carcinomas: a chromogenic in situ hybridisation analysis.* Breast Cancer Res, 2007. **9**(2): p. R23.
400. Reis-Filho, J.S., et al., *FGFR1 emerges as a potential therapeutic target for lobular breast carcinomas.* Clin Cancer Res, 2006. **12**(22): p. 6652-62.
401. Dark, G.G., et al., *Combretastatin A-4, an agent that displays potent and selective toxicity toward tumor vasculature.* Cancer Res, 1997. **57**(10): p. 1829-34.
402. Li, L., A. Rojiani, and D.W. Siemann, *Targeting the tumor vasculature with combretastatin A-4 disodium phosphate: effects on radiation therapy.* Int J Radiat Oncol Biol Phys, 1998. **42**(4): p. 899-903.
403. Parihar, S., et al., *Synthesis of combretastatin A4 analogues on steroidal framework and their anti-breast cancer activity.* J Steroid Biochem Mol Biol, 2013.
404. McKeage, M.J., et al., *Randomised phase II study of ASA404 combined with carboplatin and paclitaxel in previously untreated advanced non-small cell lung cancer.* Br J Cancer, 2008. **99**(12): p. 2006-12.
405. McKeage, M.J., et al., *Phase II study of ASA404 (vadimezan, 5,6-dimethylxanthenone-4-acetic acid/DMXAA) 1800mg/m(2) combined with carboplatin and paclitaxel in previously untreated advanced non-small cell lung cancer.* Lung Cancer, 2009. **65**(2): p. 192-7.
406. Siemann, D.W., et al., *Vascular targeting agents enhance chemotherapeutic agent activities in solid tumor therapy.* Int J Cancer, 2002. **99**(1): p. 1-6.
407. Boyle, P., *Triple-negative breast cancer: epidemiological considerations and recommendations.* Ann Oncol, 2012. **23 Suppl 6**: p. vi7-12.
408. Kestell, P., et al., *Plasma disposition, metabolism and excretion of the experimental antitumour agent 5,6-dimethylxanthenone-4-acetic acid in the mouse, rat and rabbit.* Cancer Chemother Pharmacol, 1999. **43**(4): p. 323-30.
409. Hasani, A. and N. Leighl, *Classification and toxicities of vascular disrupting agents.* Clin Lung Cancer, 2011. **12**(1): p. 18-25.
410. LoRusso, P.M., et al., *Phase I clinical evaluation of ZD6126, a novel vascular-targeting agent, in patients with solid tumors.* Invest New Drugs, 2008. **26**(2): p. 159-67.
411. McKeage, M.J., et al., *5,6-Dimethylxanthenone-4-acetic acid in the treatment of refractory tumors: a phase I safety study of a vascular disrupting agent.* Clin Cancer Res, 2006. **12**(6): p. 1776-84.
412. Delmonte, A. and C. Sessa, *AVE8062: a new combretastatin derivative vascular disrupting agent.* Expert Opin Investig Drugs, 2009. **18**(10): p. 1541-8.

413. Cooney, M.M., et al., *Cardiovascular safety profile of combretastatin a4 phosphate in a single-dose phase I study in patients with advanced cancer.* Clin Cancer Res, 2004. **10**(1 Pt 1): p. 96-100.
414. Jameson, M.B., et al., *Clinical aspects of a phase I trial of 5,6-dimethylxanthenone-4-acetic acid (DMXAA), a novel antivascular agent.* Br J Cancer, 2003. **88**(12): p. 1844-50.
415. Patel, A.G., et al., *Failure of iniparib to inhibit poly(ADP-Ribose) polymerase in vitro.* Clin Cancer Res, 2012. **18**(6): p. 1655-62.
416. Janakiram, M., et al., *T cell coinhibition and immunotherapy in human breast cancer.* Discov Med, 2012. **14**(77): p. 229-36.
417. McCoy, K.D. and G. Le Gros, *The role of CTLA-4 in the regulation of T cell immune responses.* Immunol Cell Biol, 1999. **77**(1): p. 1-10.
418. Harper, K., et al., *CTLA-4 and CD28 activated lymphocyte molecules are closely related in both mouse and human as to sequence, message expression, gene structure, and chromosomal location.* J Immunol, 1991. **147**(3): p. 1037-44.
419. Balzano, C., et al., *CTLA-4 and CD28: similar proteins, neighbouring genes.* Int J Cancer Suppl, 1992. **7**: p. 28-32.
420. Freeman, G.J., et al., *Uncovering of functional alternative CTLA-4 counter-receptor in B7-deficient mice.* Science, 1993. **262**(5135): p. 907-9.
421. Azuma, M., et al., *B70 antigen is a second ligand for CTLA-4 and CD28.* Nature, 1993. **366**(6450): p. 76-9.
422. Linsley, P.S., et al., *CTLA-4 is a second receptor for the B cell activation antigen B7.* J Exp Med, 1991. **174**(3): p. 561-9.
423. Ghebeh, H., et al., *The B7-H1 (PD-L1) T lymphocyte-inhibitory molecule is expressed in breast cancer patients with infiltrating ductal carcinoma: correlation with important high-risk prognostic factors.* Neoplasia, 2006. **8**(3): p. 190-8.
424. Hasan, A., et al., *Therapeutic targeting of B7-H1 in breast cancer.* Expert Opin Ther Targets, 2011. **15**(10): p. 1211-25.
425. Zhang, P., et al., *Chemopreventive agents induce programmed death-1-ligand 1 (PD-L1) surface expression in breast cancer cells and promote PD-L1-mediated T cell apoptosis.* Mol Immunol, 2008. **45**(5): p. 1470-6.
426. Hurwitz, A.A., et al., *CTLA-4 blockade synergizes with tumor-derived granulocyte-macrophage colony-stimulating factor for treatment of an experimental mammary carcinoma.* Proc Natl Acad Sci U S A, 1998. **95**(17): p. 10067-71.
427. Vonderheide, R.H., et al., *Tremelimumab in combination with exemestane in patients with advanced breast cancer and treatment-associated modulation of inducible costimulator expression on patient T cells.* Clin Cancer Res, 2010. **16**(13): p. 3485-94.
428. Topalian, S.L., et al., *Safety, activity, and immune correlates of anti-PD-1 antibody in cancer.* N Engl J Med, 2012. **366**(26): p. 2443-54.
429. Brahmer, J.R., et al., *Safety and activity of anti-PD-L1 antibody in patients with advanced cancer.* N Engl J Med, 2012. **366**(26): p. 2455-65.
430. Ritossa, F., *A new puffing pattern induced by temperature shock and DNP in Drosophila.* Experimentia, 1962. **18**: p. 571-73.
431. Tissieres, A., H.K. Mitchell, and U.M. Tracy, *Protein synthesis in salivary glands of Drosophila melanogaster: Relation to chromosome puffs.* J Mol Biol, 1974. **85**(3): p. 389-98.
432. Donati, Y.R., D.O. Slosman, and B.S. Polla, *Oxidative injury and the heat shock response.* Biochem Pharmacol, 1990. **40**(12): p. 2571-7.
433. Shipp, C., E. Derhovanessian, and G. Pawelec, *Effect of culture at low oxygen tension on the expression of heat shock proteins in a panel of melanoma cell lines.* PLoS One, 2012. **7**(6): p. e37475.
434. Khassaf, M., et al., *Effect of vitamin C supplements on antioxidant defence and stress proteins in human lymphocytes and skeletal muscle.* J Physiol, 2003. **549**(Pt 2): p. 645-52.

435. La Thangue, N.B. and D.S. Latchman, *A cellular protein related to heat-shock protein 90 accumulates during herpes simplex virus infection and is overexpressed in transformed cells.* Exp Cell Res, 1988. **178**(1): p. 169-79.
436. Trautinger, F., et al., *Expression of the 72-kD heat shock protein is induced by ultraviolet A radiation in a human fibrosarcoma cell line.* Exp Dermatol, 1999. **8**(3): p. 187-92.
437. Vargas-Roig, L.M., et al., *Heat shock protein expression and drug resistance in breast cancer patients treated with induction chemotherapy.* Int J Cancer, 1998. **79**(5): p. 468-75.
438. Kampinga, H.H., et al., *Guidelines for the nomenclature of the human heat shock proteins.* Cell Stress Chaperones, 2009. **14**(1): p. 105-11.
439. Bukau, B., et al., *Getting newly synthesized proteins into shape.* Cell, 2000. **101**(2): p. 119-22.
440. Mayer, M.P. and B. Bukau, *Hsp70 chaperones: cellular functions and molecular mechanism.* Cell Mol Life Sci, 2005. **62**(6): p. 670-84.
441. Stolz, A. and D.H. Wolf, *Endoplasmic reticulum associated protein degradation: a chaperone assisted journey to hell.* Biochim Biophys Acta, 2010. **1803**(6): p. 694-705.
442. Kampinga, H.H. and E.A. Craig, *The HSP70 chaperone machinery: J proteins as drivers of functional specificity.* Nat Rev Mol Cell Biol, 2010. **11**(8): p. 579-92.
443. Hartl, F.U. and M. Hayer-Hartl, *Molecular chaperones in the cytosol: from nascent chain to folded protein.* Science, 2002. **295**(5561): p. 1852-8.
444. Shi, Y. and J.O. Thomas, *The transport of proteins into the nucleus requires the 70-kilodalton heat shock protein or its cytosolic cognate.* Mol Cell Biol, 1992. **12**(5): p. 2186-92.
445. Jaattela, M., *Escaping cell death: survival proteins in cancer.* Exp Cell Res, 1999. **248**(1): p. 30-43.
446. Jaattela, M., et al., *Hsp70 exerts its anti-apoptotic function downstream of caspase-3-like proteases.* EMBO J, 1998. **17**(21): p. 6124-34.
447. Mosser, D.D., et al., *Role of the human heat shock protein hsp70 in protection against stress-induced apoptosis.* Mol Cell Biol, 1997. **17**(9): p. 5317-27.
448. Stankiewicz, A.R., et al., *Hsp70 inhibits heat-induced apoptosis upstream of mitochondria by preventing Bax translocation.* J Biol Chem, 2005. **280**(46): p. 38729-39.
449. Beere, H.M., et al., *Heat-shock protein 70 inhibits apoptosis by preventing recruitment of procaspase-9 to the Apaf-1 apoptosome.* Nat Cell Biol, 2000. **2**(8): p. 469-75.
450. Park, H.S., et al., *Hsp72 functions as a natural inhibitory protein of c-Jun N-terminal kinase.* EMBO J, 2001. **20**(3): p. 446-56.
451. Milarski, K.L. and R.I. Morimoto, *Expression of human HSP70 during the synthetic phase of the cell cycle.* Proc Natl Acad Sci U S A, 1986. **83**(24): p. 9517-21.
452. Taira, T., et al., *A novel G1-specific enhancer identified in the human heat shock protein 70 gene.* Nucleic Acids Res, 1997. **25**(10): p. 1975-83.
453. Tsutsumi-Ishii, Y., et al., *Response of heat shock element within the human HSP70 promoter to mutated p53 genes.* Cell Growth Differ, 1995. **6**(1): p. 1-8.
454. Taira, T., et al., *Cell cycle-dependent switch of up-and down-regulation of human hsp70 gene expression by interaction between c-Myc and CBF/NF-Y.* J Biol Chem, 1999. **274**(34): p. 24270-9.
455. Williams, G.T., T.K. McClanahan, and R.I. Morimoto, *E1a transactivation of the human HSP70 promoter is mediated through the basal transcriptional complex.* Mol Cell Biol, 1989. **9**(6): p. 2574-87.
456. Barnes, J.A., et al., *Expression of inducible Hsp70 enhances the proliferation of MCF-7 breast cancer cells and protects against the cytotoxic effects of hyperthermia.* Cell Stress Chaperones, 2001. **6**(4): p. 316-25.
457. Schmitt, E., et al., *Intracellular and extracellular functions of heat shock proteins: repercussions in cancer therapy.* J Leukoc Biol, 2007. **81**(1): p. 15-27.

458. Ciocca, D.R. and S.K. Calderwood, *Heat shock proteins in cancer: diagnostic, prognostic, predictive, and treatment implications.* Cell Stress Chaperones, 2005. **10**(2): p. 86-103.
459. Takahashi, S., et al., *Correlation of heat shock protein 70 expression with estrogen receptor levels in invasive human breast cancer.* Am J Clin Pathol, 1994. **101**(4): p. 519-25.
460. Vargas-Roig, L.M., et al., *Heat shock proteins and cell proliferation in human breast cancer biopsy samples.* Cancer Detect Prev, 1997. **21**(5): p. 441-51.
461. Ciocca, D.R., et al., *Heat shock protein hsp70 in patients with axillary lymph node-negative breast cancer: prognostic implications.* J Natl Cancer Inst, 1993. **85**(7): p. 570-4.
462. Thanner, F., et al., *Heat-shock protein 70 as a prognostic marker in node-negative breast cancer.* Anticancer Res, 2003. **23**(2A): p. 1057-62.
463. Mestiri, S., et al., *Genetic variation in the tumor necrosis factor-alpha promoter region and in the stress protein hsp70-2: susceptibility and prognostic implications in breast carcinoma.* Cancer, 2001. **91**(4): p. 672-8.
464. Hunter-Lavin, C., et al., *Hsp70 release from peripheral blood mononuclear cells.* Biochem Biophys Res Commun, 2004. **324**(2): p. 511-7.
465. Lancaster, G.I. and M.A. Febbraio, *Exosome-dependent trafficking of HSP70: a novel secretory pathway for cellular stress proteins.* J Biol Chem, 2005. **280**(24): p. 23349-55.
466. Anand, P.K., et al., *Exosomal Hsp70 induces a pro-inflammatory response to foreign particles including mycobacteria.* PLoS One, 2010. **5**(4): p. e10136.
467. Wright, B.H., et al., *Elevated levels of circulating heat shock protein 70 (Hsp70) in peripheral and renal vascular disease.* Heart Vessels, 2000. **15**(1): p. 18-22.
468. Krepuska, M., et al., *Serum level of soluble Hsp70 is associated with vascular calcification.* Cell Stress Chaperones, 2011. **16**(3): p. 257-65.
469. Kocsis, J., et al., *Serum level of soluble 70-kD heat shock protein is associated with high mortality in patients with colorectal cancer without distant metastasis.* Cell Stress Chaperones, 2010. **15**(2): p. 143-51.
470. Abe, M., et al., *Plasma levels of heat shock protein 70 in patients with prostate cancer: a potential biomarker for prostate cancer.* Clin Prostate Cancer, 2004. **3**(1): p. 49-53.
471. Yeh, C.H., et al., *Clinical correlation of circulating heat shock protein 70 in acute leukemia.* Leuk Res, 2009. **34**(5): p. 605-9.
472. Yeh, C.H., et al., *Circulating heat shock protein 70 and progression in patients with chronic myeloid leukemia.* Leuk Res, 2009. **33**(2): p. 212-7.
473. Bayer, C., et al., *Validation of heat shock protein 70 as a tumor-specific biomarker for monitoring the outcome of radiation therapy in tumor mouse models.* Int J Radiat Oncol Biol Phys, 2014. **88**(3): p. 694-700.
474. Hightower, L.E. and P.T. Guidon, Jr., *Selective release from cultured mammalian cells of heat-shock (stress) proteins that resemble glia-axon transfer proteins.* J Cell Physiol, 1989. **138**(2): p. 257-66.
475. Mambula, S.S., et al., *Mechanisms for Hsp70 secretion: crossing membranes without a leader.* Methods, 2007. **43**(3): p. 168-75.
476. Arispe, N., M. Doh, and A. De Maio, *Lipid interaction differentiates the constitutive and stress-induced heat shock proteins Hsc70 and Hsp70.* Cell Stress Chaperones, 2002. **7**(4): p. 330-8.
477. Arispe, N., et al., *Hsc70 and Hsp70 interact with phosphatidylserine on the surface of PC12 cells resulting in a decrease of viability.* FASEB J, 2004. **18**(14): p. 1636-45.
478. Binder, R.J., R. Vatner, and P. Srivastava, *The heat-shock protein receptors: some answers and more questions.* Tissue Antigens, 2004. **64**(4): p. 442-51.
479. Basu, S., et al., *CD91 is a common receptor for heat shock proteins gp96, hsp90, hsp70, and calreticulin.* Immunity, 2001. **14**(3): p. 303-13.

480. Chen, T., et al., *Heat shock protein 70, released from heat-stressed tumor cells, initiates antitumor immunity by inducing tumor cell chemokine production and activating dendritic cells via TLR4 pathway.* J Immunol, 2009. **182**(3): p. 1449-59.
481. Pockley, A.G., S.K. Calderwood, and G. Multhoff, *The atheroprotective properties of Hsp70: a role for Hsp70-endothelial interactions?* Cell Stress Chaperones, 2009. **14**(6): p. 545-53.
482. Zitzler, S., et al., *Distinct binding sites for the ATPase and substrate-binding domain of human Hsp70 on the cell surface of antigen presenting cells.* Mol Immunol, 2008. **45**(15): p. 3974-83.
483. Srivastava, P.K., A.B. DeLeo, and L.J. Old, *Tumor rejection antigens of chemically induced sarcomas of inbred mice.* Proc Natl Acad Sci U S A, 1986. **83**(10): p. 3407-11.
484. Udono, H. and P.K. Srivastava, *Heat shock protein 70-associated peptides elicit specific cancer immunity.* J Exp Med, 1993. **178**(4): p. 1391-6.
485. Srivastava, P.K., et al., *Heat shock proteins transfer peptides during antigen processing and CTL priming.* Immunogenetics, 1994. **39**(2): p. 93-8.
486. Tamura, Y., et al., *Immunotherapy of tumors with autologous tumor-derived heat shock protein preparations.* Science, 1997. **278**(5335): p. 117-20.
487. Srivastava, P., *Roles of heat-shock proteins in innate and adaptive immunity.* Nat Rev Immunol, 2002. **2**(3): p. 185-94.
488. Blachere, N.E., et al., *Heat shock protein-peptide complexes, reconstituted in vitro, elicit peptide-specific cytotoxic T lymphocyte response and tumor immunity.* J Exp Med, 1997. **186**(8): p. 1315-22.
489. Srivastava, P., *Interaction of heat shock proteins with peptides and antigen presenting cells: chaperoning of the innate and adaptive immune responses.* Annu Rev Immunol, 2002. **20**: p. 395-425.
490. Berwin, B. and C.V. Nicchitta, *To find the road traveled to tumor immunity: the trafficking itineraries of molecular chaperones in antigen-presenting cells.* Traffic, 2001. **2**(10): p. 690-7.
491. Fischer, N., et al., *Involvement of CD91 and scavenger receptors in Hsp70-facilitated activation of human antigen-specific CD4+ memory T cells.* Eur J Immunol, 2010. **40**(4): p. 986-97.
492. Castelli, C., et al., *Heat shock proteins: biological functions and clinical application as personalized vaccines for human cancer.* Cancer Immunol Immunother, 2004. **53**(3): p. 227-33.
493. Srivastava, P.K., *Immunotherapy for human cancer using heat shock protein-peptide complexes.* Curr Oncol Rep, 2005. **7**(2): p. 104-8.
494. Testori, A., et al., *Phase III comparison of vitespen, an autologous tumor-derived heat shock protein gp96 peptide complex vaccine, with physician's choice of treatment for stage IV melanoma: the C-100-21 Study Group.* J Clin Oncol, 2008. **26**(6): p. 955-62.
495. Mazzaferro, V., et al., *Vaccination with autologous tumor-derived heat-shock protein gp96 after liver resection for metastatic colorectal cancer.* Clin Cancer Res, 2003. **9**(9): p. 3235-45.
496. Wood, C., et al., *An adjuvant autologous therapeutic vaccine (HSPPC-96; vitespen) versus observation alone for patients at high risk of recurrence after nephrectomy for renal cell carcinoma: a multicentre, open-label, randomised phase III trial.* Lancet, 2008. **372**(9633): p. 145-54.
497. Chandawarkar, R.Y., M.S. Wagh, and P.K. Srivastava, *The dual nature of specific immunological activity of tumor-derived gp96 preparations.* J Exp Med, 1999. **189**(9): p. 1437-42.
498. Slack, L.K., et al., *Administration of the stress protein gp96 prolongs rat cardiac allograft survival, modifies rejection-associated inflammatory events, and induces a state of peripheral T-cell hyporesponsiveness.* Cell Stress Chaperones, 2007. **12**(1): p. 71-82.

499. Kovalchin, J.T., et al., *In vivo treatment of mice with heat shock protein, gp 96, improves survival of skin grafts with minor and major antigenic disparity.* Transpl Immunol, 2006. **15**(3): p. 179-85.
500. Enomoto, Y., et al., *Enhanced immunogenicity of heat shock protein 70 peptide complexes from dendritic cell-tumor fusion cells.* J Immunol, 2006. **177**(9): p. 5946-55.
501. Gong, J., et al., *A heat shock protein 70-based vaccine with enhanced immunogenicity for clinical use.* J Immunol, 2009. **184**(1): p. 488-96.
502. Kuppner, M.C., et al., *The role of heat shock protein (hsp70) in dendritic cell maturation: hsp70 induces the maturation of immature dendritic cells but reduces DC differentiation from monocyte precursors.* Eur J Immunol, 2001. **31**(5): p. 1602-9.
503. Bausinger, H., et al., *Endotoxin-free heat-shock protein 70 fails to induce APC activation.* Eur J Immunol, 2002. **32**(12): p. 3708-13.
504. Henderson, B., et al., *Caught with their PAMPs down? The extracellular signalling actions of molecular chaperones are not due to microbial contaminants.* Cell Stress Chaperones, 2010. **15**(2): p. 123-41.
505. Mizzen, L., *Immune responses to stress proteins: applications to infectious disease and cancer.* Biotherapy, 1998. **10**(3): p. 173-89.
506. Ciupitu, A.M., et al., *Immunization with a lymphocytic choriomeningitis virus peptide mixed with heat shock protein 70 results in protective antiviral immunity and specific cytotoxic T lymphocytes.* J Exp Med, 1998. **187**(5): p. 685-91.
507. Zugel, U., et al., *gp96-peptide vaccination of mice against intracellular bacteria.* Infect Immun, 2001. **69**(6): p. 4164-7.
508. Suzue, K. and R.A. Young, *Adjuvant-free hsp70 fusion protein system elicits humoral and cellular immune responses to HIV-1 p24.* J Immunol, 1996. **156**(2): p. 873-9.
509. De Graeff-Meeder, E.R., et al., *Recognition of human 60 kD heat shock protein by mononuclear cells from patients with juvenile chronic arthritis.* Lancet, 1991. **337**(8754): p. 1368-72.
510. Elias, D., et al., *Induction and therapy of autoimmune diabetes in the non-obese diabetic (NOD/Lt) mouse by a 65-kDa heat shock protein.* Proc Natl Acad Sci U S A, 1990. **87**(4): p. 1576-80.
511. van Eden, I., *Stress proteins as targets for anti-inflammatory therapies.* Drug Discov Today, 2000. **5**(3): p. 115-120.
512. Liu, Z., et al., *Treg suppress CTL responses upon immunization with HSP gp96.* Eur J Immunol, 2009. **39**(11): p. 3110-20.
513. Wachstein, J., et al., *HSP70 enhances immunosuppressive function of CD4(+)CD25(+)FoxP3(+) T regulatory cells and cytotoxicity in CD4(+)CD25(-) T cells.* PLoS One, 2012. **7**(12): p. e51747.
514. Todorova, V.K., et al., *Immunomodulatory effects of radiofrequency ablation in a breast cancer model.* Immunol Invest, 2010. **39**(1): p. 74-92.
515. Pfister, K., et al., *Patient survival by Hsp70 membrane phenotype: association with different routes of metastasis.* Cancer, 2007. **110**(4): p. 926-35.
516. Multhoff, G., et al., *Heat shock protein 70 (Hsp70) stimulates proliferation and cytolytic activity of natural killer cells.* Exp Hematol, 1999. **27**(11): p. 1627-36.
517. Broquet, A.H., et al., *Expression of the molecular chaperone Hsp70 in detergent-resistant microdomains correlates with its membrane delivery and release.* J Biol Chem, 2003. **278**(24): p. 21601-6.
518. Gehrmann, M., et al., *Tumor-specific Hsp70 plasma membrane localization is enabled by the glycosphingolipid Gb3.* PLoS One, 2008. **3**(4): p. e1925.
519. Gehrmann, M., et al., *Dual function of membrane-bound heat shock protein 70 (Hsp70), Bag-4, and Hsp40: protection against radiation-induced effects and target structure for natural killer cells.* Cell Death Differ, 2005. **12**(1): p. 38-51.
520. Gehrmann, M., et al., *Retinoid- and sodium-butyrate-induced decrease in heat shock protein 70 membrane-positive tumor cells is associated with reduced sensitivity to*

natural killer cell lysis, growth delay, and altered growth morphology. Cell Stress Chaperones, 2005. **10**(2): p. 136-46.
521. Gross, C., et al., *Interaction of heat shock protein 70 peptide with NK cells involves the NK receptor CD94.* Biol Chem, 2003. **384**(2): p. 267-79.
522. Gross, C., et al., *Heat shock protein 70-reactivity is associated with increased cell surface density of CD94/CD56 on primary natural killer cells.* Cell Stress Chaperones, 2003. **8**(4): p. 348-60.
523. Multhoff, G., et al., *A 14-mer Hsp70 peptide stimulates natural killer (NK) cell activity.* Cell Stress Chaperones, 2001. **6**(4): p. 337-44.
524. Elsner, L., et al., *The endogenous danger signals HSP70 and MICA cooperate in the activation of cytotoxic effector functions of NK cells.* J Cell Mol Med, 2010. **14**(4): p. 992-1002.
525. Gastpar, R., et al., *The cell surface-localized heat shock protein 70 epitope TKD induces migration and cytolytic activity selectively in human NK cells.* J Immunol, 2004. **172**(2): p. 972-80.
526. Stangl, S., et al., *Control of metastasized pancreatic carcinomas in SCID/beige mice with human IL-2/TKD-activated NK cells.* J Immunol, 2006. **176**(10): p. 6270-6.
527. Gross, C., et al., *An Hsp70 peptide initiates NK cell killing of leukemic blasts after stem cell transplantation.* Leuk Res, 2008. **32**(4): p. 527-34.
528. Krause, S.W., et al., *Treatment of colon and lung cancer patients with ex vivo heat shock protein 70-peptide-activated, autologous natural killer cells: a clinical phase i trial.* Clin Cancer Res, 2004. **10**(11): p. 3699-707.
529. Milani, V., et al., *Anti-tumor activity of patient-derived NK cells after cell-based immunotherapy--a case report.* J Transl Med, 2009. **7**: p. 50.
530. Gross, C., et al., *Cell surface-bound heat shock protein 70 (Hsp70) mediates perforin-independent apoptosis by specific binding and uptake of granzyme B.* J Biol Chem, 2003. **278**(42): p. 41173-81.
531. Gehrmann, M., et al., *A novel expression and purification system for the production of enzymatic and biologically active human granzyme B.* J Immunol Methods, 2011. **371**(1-2): p. 8-17.
532. Gehrmann, M., et al., *Immunotherapeutic targeting of membrane Hsp70-expressing tumors using recombinant human granzyme B.* PLoS One, 2012. **7**(7): p. e41341.
533. Stangl, S., et al., *Targeting membrane heat-shock protein 70 (Hsp70) on tumors by cmHsp70.1 antibody.* Proc Natl Acad Sci U S A, 2010.
534. Stangl, S., et al., *In vivo imaging of CT26 mouse tumors by using cmHsp70.1 monoclonal antibody.* J Cell Mol Med, 2010.
535. Gehrmann, M., et al., *Tumor imaging and targeting potential of an Hsp70-derived 14-mer peptide.* PLoS One, 2014. **9**(8): p. e105344.
536. Foy, K.C., et al., *Combined vaccination with HER-2 peptide followed by therapy with VEGF peptide mimics exerts effective anti-tumor and anti-angiogenic effects in vitro and in vivo.* Oncoimmunology, 2012. **1**(7): p. 1048-1060.
537. Cailleau, R., M. Olive, and Q.V. Cruciger, *Long-term human breast carcinoma cell lines of metastatic origin: preliminary characterization.* In Vitro, 1978. **14**(11): p. 911-5.
538. Soule, H.D., et al., *A human cell line from a pleural effusion derived from a breast carcinoma.* J Natl Cancer Inst, 1973. **51**(5): p. 1409-16.
539. Brooks, S.C., E.R. Locke, and H.D. Soule, *Estrogen receptor in a human cell line (MCF-7) from breast carcinoma.* J Biol Chem, 1973. **248**(17): p. 6251-3.
540. Keydar, I., et al., *Establishment and characterization of a cell line of human breast carcinoma origin.* Eur J Cancer, 1979. **15**(5): p. 659-70.
541. Aslakson, C.J. and F.R. Miller, *Selective events in the metastatic process defined by analysis of the sequential dissemination of subpopulations of a mouse mammary tumor.* Cancer Res, 1992. **52**(6): p. 1399-405.

542. Brattain, M.G., et al., *Establishment of mouse colonic carcinoma cell lines with different metastatic properties.* Cancer Res, 1980. **40**(7): p. 2142-6.
543. Botzler, C., R. Issels, and G. Multhoff, *Heat-shock protein 72 cell-surface expression on human lung carcinoma cells in associated with an increased sensitivity to lysis mediated by adherent natural killer cells.* Cancer Immunol Immunother, 1996. **43**(4): p. 226-30.
544. Gehrmann, M., et al., *Membrane-bound heat shock protein 70 (Hsp70) in acute myeloid leukemia: a tumor specific recognition structure for the cytolytic activity of autologous NK cells.* Haematologica, 2003. **88**(4): p. 474-6.
545. Gatignol, A., H. Durand, and G. Tiraby, *Bleomycin resistance conferred by a drug-binding protein.* FEBS Lett, 1988. **230**(1-2): p. 171-5.
546. Dumas, P., et al., *Crystal structure and site-directed mutagenesis of a bleomycin resistance protein and their significance for drug sequestering.* EMBO J, 1994. **13**(11): p. 2483-92.
547. Hinkeldey, B., A. Schmitt, and G. Jung, *Comparative photostability studies of BODIPY and fluorescein dyes by using fluorescence correlation spectroscopy.* Chemphyschem, 2008. **9**(14): p. 2019-27.
548. Manders, E.M.M., F.J. Verbeek, and J.A. Aten, *Measurement of co-localization of objects in dual-colour confocal images.* Journal of Microscopy, 1993. **169**(3): p. 375-382.
549. Bolte, S. and F.P. Cordelieres, *A guided tour into subcellular colocalization analysis in light microscopy.* J Microsc, 2006. **224**(Pt 3): p. 213-32.
550. Zhang, H., R. Liu, and W. Huang, *A 14-mer peptide from HSP70 protein is the critical epitope which enhances NK activity against tumor cells in vivo.* Immunol Invest, 2007. **36**(3): p. 233-46.
551. Shetty, A., et al., *The neural cell adhesion molecule promotes maturation of the presynaptic endocytotic machinery by switching synaptic vesicle recycling from adaptor protein 3 (AP-3)- to AP-2-dependent mechanisms.* J Neurosci, 2013. **33**(42): p. 16828-45.
552. Xin, L., et al., *Human monoclonal antibodies in cancer therapy: a review of recent developments.* Front Biosci (Landmark Ed), 2013. **18**: p. 765-72.
553. Barbet, J., et al., *Radiolabeled antibodies for cancer imaging and therapy.* Methods Mol Biol, 2012. **907**: p. 681-97.
554. Baeuerle, P.A. and C. Itin, *Clinical experience with gene therapy and bispecific antibodies for T cell-based therapy of cancer.* Curr Pharm Biotechnol, 2012. **13**(8): p. 1399-408.
555. Vacchelli, E., et al., *Trial watch: Monoclonal antibodies in cancer therapy.* Oncoimmunology, 2013. **2**(1): p. e22789.
556. Copeland, A. and A. Younes, *Current treatment strategies in Hodgkin lymphomas.* Curr Opin Oncol, 2012. **24**(5): p. 466-74.
557. Kaumaya, P.T. and K.C. Foy, *Peptide vaccines and targeting HER and VEGF proteins may offer a potentially new paradigm in cancer immunotherapy.* Future Oncol, 2012. **8**(8): p. 961-87.
558. Bidwell, G.L., *Peptides for cancer therapy: a drug-development opportunity and a drug-delivery challenge.* Ther Deliv, 2012. **3**(5): p. 609-21.
559. Sharif-Askari, E., et al., *Direct cleavage of the human DNA fragmentation factor-45 by granzyme B induces caspase-activated DNase release and DNA fragmentation.* EMBO J, 2001. **20**(12): p. 3101-13.
560. Kim, D., et al., *Expression of hsp 27, hsp 60, hsc 70, and hsp 70 by immortalized human proximal tubule cells (HK-2) following exposure to heat shock, sodium arsenite, or cadmium chloride.* J Toxicol Environ Health A, 2001. **63**(7): p. 475-93.

561. Jornot, L., M.E. Mirault, and A.F. Junod, *Differential expression of hsp70 stress proteins in human endothelial cells exposed to heat shock and hydrogen peroxide.* Am J Respir Cell Mol Biol, 1991. **5**(3): p. 265-75.
562. Juhasz, K., et al., *The complex function of hsp70 in metastatic cancer.* Cancers (Basel), 2013. **6**(1): p. 42-66.
563. Santagata, S., et al., *High levels of nuclear heat-shock factor 1 (HSF1) are associated with poor prognosis in breast cancer.* Proc Natl Acad Sci U S A, 2011. **108**(45): p. 18378-83.
564. Ciocca, D.R., A.P. Arrigo, and S.K. Calderwood, *Heat shock proteins and heat shock factor 1 in carcinogenesis and tumor development: an update.* Arch Toxicol, 2013. **87**(1): p. 19-48.
565. Du, X.L., et al., *Silencing of heat shock protein 70 expression enhances radiotherapy efficacy and inhibits cell invasion in endometrial cancer cell line.* Croat Med J, 2009. **50**(2): p. 143-50.
566. Schilling, D., et al., *Sensitizing tumor cells to radiation by targeting the heat shock response.* Cancer Lett, 2015. **360**(2): p. 294-301.
567. Zaidi, S., et al., *The HSP90 inhibitor NVP-AUY922 radiosensitizes by abrogation of homologous recombination resulting in mitotic entry with unresolved DNA damage.* PLoS One, 2012. **7**(4): p. e35436.
568. Schilling, D., et al., *Radiosensitization of normoxic and hypoxic h1339 lung tumor cells by heat shock protein 90 inhibition is independent of hypoxia inducible factor-1alpha.* PLoS One, 2012. **7**(2): p. e31110.
569. Hantschel, M., et al., *Hsp70 plasma membrane expression on primary tumor biopsy material and bone marrow of leukemic patients.* Cell Stress Chaperones, 2000. **5**(5): p. 438-42.
570. Multhoff, G., *Activation of natural killer cells by heat shock protein 70.* Int J Hyperthermia, 2002. **18**(6): p. 576-85.
571. Gao, B., S. Radaeva, and O. Park, *Liver natural killer and natural killer T cells: immunobiology and emerging roles in liver diseases.* J Leukoc Biol, 2009. **86**(3): p. 513-28.
572. Sugawara, S., et al., *Binding of Silurus asotus lectin to Gb3 on Raji cells causes disappearance of membrane-bound form of HSP70.* Biochim Biophys Acta, 2009. **1790**(2): p. 101-9.
573. Multhoff, G., et al., *Adoptive transfer of human natural killer cells in mice with severe combined immunodeficiency inhibits growth of Hsp70-expressing tumors.* Int J Cancer, 2000. **88**(5): p. 791-7.
574. Specht, H.M., et al., *Heat Shock Protein 70 (Hsp70) Peptide Activated Natural Killer (NK) Cells for the Treatment of Patients with Non-Small Cell Lung Cancer (NSCLC) after Radiochemotherapy (RCTx) - From Preclinical Studies to a Clinical Phase II Trial.* Front Immunol, 2015. **6**: p. 162.
575. Farkas, B., et al., *Heat shock protein 70 membrane expression and melanoma-associated marker phenotype in primary and metastatic melanoma.* Melanoma Res, 2003. **13**(2): p. 147-52.
576. Kleinjung, T., et al., *Heat shock protein 70 (Hsp70) membrane expression on head-and-neck cancer biopsy-a target for natural killer (NK) cells.* Int J Radiat Oncol Biol Phys, 2003. **57**(3): p. 820-6.
577. Clarke, M., et al., *Effects of radiotherapy and of differences in the extent of surgery for early breast cancer on local recurrence and 15-year survival: an overview of the randomised trials.* Lancet, 2005. **366**(9503): p. 2087-106.
578. Li, S., et al., *Heat shock protein 72 enhances autophagy as a protective mechanism in lipopolysaccharide-induced peritonitis in rats.* Am J Pathol, 2011. **179**(6): p. 2822-34.
579. Pulaski, B.A. and S. Ostrand-Rosenberg, *Mouse 4T1 breast tumor model.* Curr Protoc Immunol, 2001. **Chapter 20**: p. Unit 20 2.

580. Danhier, F., O. Feron, and V. Preat, *To exploit the tumor microenvironment: Passive and active tumor targeting of nanocarriers for anti-cancer drug delivery.* J Control Release, 2010. **148**(2): p. 135-46.
581. Northfelt, D.W., et al., *Doxorubicin encapsulated in liposomes containing surface-bound polyethylene glycol: pharmacokinetics, tumor localization, and safety in patients with AIDS-related Kaposi's sarcoma.* J Clin Pharmacol, 1996. **36**(1): p. 55-63.
582. Iyer, A.K., et al., *Exploiting the enhanced permeability and retention effect for tumor targeting.* Drug Discov Today, 2006. **11**(17-18): p. 812-8.
583. Davis, M.E., Z.G. Chen, and D.M. Shin, *Nanoparticle therapeutics: an emerging treatment modality for cancer.* Nat Rev Drug Discov, 2008. **7**(9): p. 771-82.
584. Peer, D., et al., *Nanocarriers as an emerging platform for cancer therapy.* Nat Nanotechnol, 2007. **2**(12): p. 751-60.
585. Ajima, K., et al., *Enhancement of in vivo anticancer effects of cisplatin by incorporation inside single-wall carbon nanohorns.* ACS Nano, 2008. **2**(10): p. 2057-64.
586. Bianco, A., K. Kostarelos, and M. Prato, *Making carbon nanotubes biocompatible and biodegradable.* Chem Commun (Camb), 2011. **47**(37): p. 10182-8.
587. Ali-Boucetta, H., et al., *Cellular uptake and cytotoxic impact of chemically functionalized and polymer-coated carbon nanotubes.* Small, 2011. **7**(22): p. 3230-8.
588. Vardharajula, S., et al., *Functionalized carbon nanotubes: biomedical applications.* Int J Nanomedicine, 2012. **7**: p. 5361-74.
589. Malam, Y., M. Loizidou, and A.M. Seifalian, *Liposomes and nanoparticles: nanosized vehicles for drug delivery in cancer.* Trends Pharmacol Sci, 2009. **30**(11): p. 592-9.
590. Blanco, E., et al., *Nanomedicine in cancer therapy: innovative trends and prospects.* Cancer Sci, 2011. **102**(7): p. 1247-52.
591. Szebeni, J., *Complement activation-related pseudoallergy: a new class of drug-induced acute immune toxicity.* Toxicology, 2005. **216**(2-3): p. 106-21.
592. Panyam, J. and V. Labhasetwar, *Biodegradable nanoparticles for drug and gene delivery to cells and tissue.* Adv Drug Deliv Rev, 2003. **55**(3): p. 329-47.
593. Panyam, J., et al., *Polymer degradation and in vitro release of a model protein from poly(D,L-lactide-co-glycolide) nano- and microparticles.* J Control Release, 2003. **92**(1-2): p. 173-87.
594. Perez-Herrero, E. and A. Fernandez-Medarde, *Advanced targeted therapies in cancer: Drug nanocarriers, the future of chemotherapy.* Eur J Pharm Biopharm, 2015. **93**: p. 52-79.
595. Zagar, T.M., et al., *Two phase I dose-escalation/pharmacokinetics studies of low temperature liposomal doxorubicin (LTLD) and mild local hyperthermia in heavily pretreated patients with local regionally recurrent breast cancer.* Int J Hyperthermia, 2014. **30**(5): p. 285-94.
596. Ibrahim, N.K., et al., *Multicenter phase II trial of ABI-007, an albumin-bound paclitaxel, in women with metastatic breast cancer.* J Clin Oncol, 2005. **23**(25): p. 6019-26.
597. Gradishar, W.J., et al., *Phase III trial of nanoparticle albumin-bound paclitaxel compared with polyethylated castor oil-based paclitaxel in women with breast cancer.* J Clin Oncol, 2005. **23**(31): p. 7794-803.
598. Gradishar, W.J., *Albumin-bound nanoparticle paclitaxel.* Clin Adv Hematol Oncol, 2005. **3**(5): p. 348-9.
599. Harries, M., P. Ellis, and P. Harper, *Nanoparticle albumin-bound paclitaxel for metastatic breast cancer.* J Clin Oncol, 2005. **23**(31): p. 7768-71.
600. Choi, W.I., et al., *Targeted antitumor efficacy and imaging via multifunctional nano-carrier conjugated with anti-HER2 trastuzumab.* Nanomedicine, 2015. **11**(2): p. 359-68.
601. Okarvi, S.M., *Peptide-based radiopharmaceuticals and cytotoxic conjugates: potential tools against cancer.* Cancer Treat Rev, 2008. **34**(1): p. 13-26.
602. Thundimadathil, J., *Cancer treatment using peptides: current therapies and future prospects.* J Amino Acids, 2012. **2012**: p. 967347.

603. Condeelis, J. and R. Weissleder, *In vivo imaging in cancer.* Cold Spring Harb Perspect Biol, 2010. **2**(12): p. a003848.
604. Fani, M., H.R. Maecke, and S.M. Okarvi, *Radiolabeled peptides: valuable tools for the detection and treatment of cancer.* Theranostics, 2012. **2**(5): p. 481-501.
605. Zhang, X.Y., et al., *[Preparation and in vitro targeting of follicle stimulating hormone polypeptide modified nanoparticles].* Zhonghua Fu Chan Ke Za Zhi, 2008. **43**(7): p. 533-7.
606. Zhang, X., et al., *Targeted paclitaxel nanoparticles modified with follicle-stimulating hormone beta 81-95 peptide show effective antitumor activity against ovarian carcinoma.* Int J Pharm, 2013. **453**(2): p. 498-505.
607. Lim, K.J., et al., *A cancer specific cell-penetrating peptide, BR2, for the efficient delivery of an scFv into cancer cells.* PLoS One, 2013. **8**(6): p. e66084.
608. Lee, H.S., et al., *Mechanism of anticancer activity of buforin IIb, a histone H2A-derived peptide.* Cancer Lett, 2008. **271**(1): p. 47-55.
609. Ma, C., et al., *A specific cell-penetrating peptide induces apoptosis in SKOV3 cells by down-regulation of Bcl-2.* Biotechnol Lett, 2013. **35**(11): p. 1791-7.
610. Laakkonen, P., et al., *Antitumor activity of a homing peptide that targets tumor lymphatics and tumor cells.* Proc Natl Acad Sci U S A, 2004. **101**(25): p. 9381-6.
611. Askoxylakis, V., et al., *Characterization and development of a peptide (p160) with affinity for neuroblastoma cells.* J Nucl Med, 2006. **47**(6): p. 981-8.
612. Zitzmann, S., et al., *Identification and evaluation of a new tumor cell-binding peptide, FROP-1.* J Nucl Med, 2007. **48**(6): p. 965-72.
613. Gehrmann, M., et al., *Radiation induced stress proteins.* Int J Clin Pharmacol Ther, 2010. **48**(7): p. 492-3.
614. Moktan, S. and D. Raucher, *Anticancer activity of proapoptotic peptides is highly improved by thermal targeting using elastin-like polypeptides.* Int J Pept Res Ther, 2012. **18**(3): p. 227-237.
615. Shabaik, Y.H., M. Millard, and N. Neamati, *Mechanistic evaluation of a novel small molecule targeting mitochondria in pancreatic cancer cells.* PLoS One, 2013. **8**(1): p. e54346.
616. Stangl, S., et al., *Selective in vivo imaging of syngeneic, spontaneous, and xenograft tumors using a novel tumor cell-specific hsp70 peptide-based probe.* Cancer Res, 2014. **74**(23): p. 6903-12.
617. Noguchi, M., et al., *Phase II study of personalized peptide vaccination for castration-resistant prostate cancer patients who failed in docetaxel-based chemotherapy.* Prostate, 2012. **72**(8): p. 834-45.
618. Thiery, J., et al., *Perforin pores in the endosomal membrane trigger the release of endocytosed granzyme B into the cytosol of target cells.* Nat Immunol, 2011. **12**(8): p. 770-7.
619. Hagn, M., et al., *Human B cells differentiate into granzyme B-secreting cytotoxic B lymphocytes upon incomplete T-cell help.* Immunol Cell Biol, 2012. **90**(4): p. 457-67.
620. Voskoboinik, I., et al., *Calcium-dependent plasma membrane binding and cell lysis by perforin are mediated through its C2 domain: A critical role for aspartate residues 429, 435, 483, and 485 but not 491.* J Biol Chem, 2005. **280**(9): p. 8426-34.
621. Young, J.D., et al., *Purification and characterization of a cytolytic pore-forming protein from granules of cloned lymphocytes with natural killer activity.* Cell, 1986. **44**(6): p. 849-59.
622. Kurschus, F.C., et al., *Granzyme B delivery via perforin is restricted by size, but not by heparan sulfate-dependent endocytosis.* Proc Natl Acad Sci U S A, 2008. **105**(37): p. 13799-804.
623. Browne, K.A., et al., *Cytosolic delivery of granzyme B by bacterial toxins: evidence that endosomal disruption, in addition to transmembrane pore formation, is an important function of perforin.* Mol Cell Biol, 1999. **19**(12): p. 8604-15.

624. Hoves, S., J.A. Trapani, and I. Voskoboinik, *The battlefield of perforin/granzyme cell death pathways.* J Leukoc Biol, 2010. **87**(2): p. 237-43.
625. Kurschus, F.C., et al., *Membrane receptors are not required to deliver granzyme B during killer cell attack.* Blood, 2005. **105**(5): p. 2049-58.
626. Cullen, S.P., et al., *Human and murine granzyme B exhibit divergent substrate preferences.* J Cell Biol, 2007. **176**(4): p. 435-44.
627. Heibein, J.A., et al., *Granzyme B-mediated cytochrome c release is regulated by the Bcl-2 family members bid and Bax.* J Exp Med, 2000. **192**(10): p. 1391-402.
628. Sutton, V.R., et al., *Initiation of apoptosis by granzyme B requires direct cleavage of bid, but not direct granzyme B-mediated caspase activation.* J Exp Med, 2000. **192**(10): p. 1403-14.
629. Alimonti, J.B., et al., *Granzyme B induces BID-mediated cytochrome c release and mitochondrial permeability transition.* J Biol Chem, 2001. **276**(10): p. 6974-82.
630. Pinkoski, M.J., et al., *Granzyme B-mediated apoptosis proceeds predominantly through a Bcl-2-inhibitable mitochondrial pathway.* J Biol Chem, 2001. **276**(15): p. 12060-7.
631. Waterhouse, N.J., et al., *A central role for Bid in granzyme B-induced apoptosis.* J Biol Chem, 2005. **280**(6): p. 4476-82.
632. Kuwana, T., et al., *Bid, Bax, and lipids cooperate to form supramolecular openings in the outer mitochondrial membrane.* Cell, 2002. **111**(3): p. 331-42.
633. Li, P., et al., *Cytochrome c and dATP-dependent formation of Apaf-1/caspase-9 complex initiates an apoptotic protease cascade.* Cell, 1997. **91**(4): p. 479-89.
634. Slee, E.A., et al., *Ordering the cytochrome c-initiated caspase cascade: hierarchical activation of caspases-2, -3, -6, -7, -8, and -10 in a caspase-9-dependent manner.* J Cell Biol, 1999. **144**(2): p. 281-92.
635. Hill, M.M., et al., *Analysis of the composition, assembly kinetics and activity of native Apaf-1 apoptosomes.* EMBO J, 2004. **23**(10): p. 2134-45.
636. Kaiserman, D., et al., *The major human and mouse granzymes are structurally and functionally divergent.* J Cell Biol, 2006. **175**(4): p. 619-30.
637. Giesubel, U., et al., *Cell binding, internalization and cytotoxic activity of human granzyme B expressed in the yeast Pichia pastoris.* Biochem J, 2006. **394**(Pt 3): p. 563-73.
638. Ben Safta, T., et al., *Granzyme B-activated p53 interacts with Bcl-2 to promote cytotoxic lymphocyte-mediated apoptosis.* J Immunol, 2015. **194**(1): p. 418-28.
639. Chowdhury, D. and J. Lieberman, *Death by a thousand cuts: granzyme pathways of programmed cell death.* Annu Rev Immunol, 2008. **26**: p. 389-420.
640. Tait, S.W. and D.R. Green, *Mitochondria and cell death: outer membrane permeabilization and beyond.* Nat Rev Mol Cell Biol, 2010. **11**(9): p. 621-32.
641. Ola, M.S., M. Nawaz, and H. Ahsan, *Role of Bcl-2 family proteins and caspases in the regulation of apoptosis.* Mol Cell Biochem, 2011. **351**(1-2): p. 41-58.
642. Lopez, J. and S.W. Tait, *Mitochondrial apoptosis: killing cancer using the enemy within.* Br J Cancer, 2015. **112**(6): p. 957-62.
643. Lartigue, L., et al., *Caspase-independent mitochondrial cell death results from loss of respiration, not cytotoxic protein release.* Mol Biol Cell, 2009. **20**(23): p. 4871-84.
644. Spaeny-Dekking, E.H., et al., *Extracellular granzymes A and B in humans: detection of native species during CTL responses in vitro and in vivo.* J Immunol, 1998. **160**(7): p. 3610-6.
645. Kadam, C.Y. and S.A. Abhang, *Serum levels of soluble Fas ligand, granzyme B and cytochrome c during adjuvant chemotherapy of breast cancer.* Clin Chim Acta, 2015. **438**: p. 98-102.
646. Wara, W.M., et al., *Immunosuppression following radiation therapy for carcinoma of the nasopharynx.* Am J Roentgenol Radium Ther Nucl Med, 1975. **123**(3): p. 482-5.
647. Rasmussen, L. and A. Arvin, *Chemotherapy-induced immunosuppression.* Environ Health Perspect, 1982. **43**: p. 21-5.

648. Kepp, O., et al., *Consensus guidelines for the detection of immunogenic cell death.* Oncoimmunology, 2014. **3**(9): p. e955691.
649. Cunningham, T.D., X. Jiang, and D.J. Shapiro, *Expression of high levels of human proteinase inhibitor 9 blocks both perforin/granzyme and Fas/Fas ligand-mediated cytotoxicity.* Cell Immunol, 2007. **245**(1): p. 32-41.
650. Medema, J.P., et al., *Blockade of the granzyme B/perforin pathway through overexpression of the serine protease inhibitor PI-9/SPI-6 constitutes a mechanism for immune escape by tumors.* Proc Natl Acad Sci U S A, 2001. **98**(20): p. 11515-20.
651. Hayem, G., et al., *Anti-heat shock protein 70 kDa and 90 kDa antibodies in serum of patients with rheumatoid arthritis.* Ann Rheum Dis, 1999. **58**(5): p. 291-6.
652. Martin, C.A., et al., *Aberrant extracellular and dendritic cell (DC) surface expression of heat shock protein (hsp)70 in the rheumatoid joint: possible mechanisms of hsp/DC-mediated cross-priming.* J Immunol, 2003. **171**(11): p. 5736-42.
653. Schett, G., et al., *Enhanced expression of heat shock protein 70 (hsp70) and heat shock factor 1 (HSF1) activation in rheumatoid arthritis synovial tissue. Differential regulation of hsp70 expression and hsf1 activation in synovial fibroblasts by proinflammatory cytokines, shear stress, and antiinflammatory drugs.* J Clin Invest, 1998. **102**(2): p. 302-11.
654. Nguyen, T.T., et al., *Heat shock protein 70 membrane expression on fibroblast-like synovial cells derived from synovial tissue of patients with rheumatoid and juvenile idiopathic arthritis.* Scand J Rheumatol, 2006. **35**(6): p. 447-53.
655. Garnett, G.P., et al., *The potential epidemiological impact of a genital herpes vaccine for women.* Sex Transm Infect, 2004. **80**(1): p. 24-9.
656. Reits, E.A., et al., *Radiation modulates the peptide repertoire, enhances MHC class I expression, and induces successful antitumor immunotherapy.* J Exp Med, 2006. **203**(5): p. 1259-71.
657. Hodge, J.W., et al., *The tipping point for combination therapy: cancer vaccines with radiation, chemotherapy, or targeted small molecule inhibitors.* Semin Oncol, 2012. **39**(3): p. 323-39.
658. Cihil, K.M. and A. Swiatecka-Urban, *The cell-based L-glutathione protection assays to study endocytosis and recycling of plasma membrane proteins.* J Vis Exp, 2013(82): p. e50867.

Appendix

i. Reagents and Suppliers

0.22µm filter *Sarstedt AG & Co*
12x75mm polypropylene tubes *Sarstedt AG & Co*
35mm glass bottom dishes *MatTek Corporation*
5mL Bijous tubes *Star Lab UK Ltd*
96 well plates *Sarstedt AG & Co*
Ab anti-CD3 UCHT1 Qdot605 *Molecular Probes®, Life Technologies*
Ab anti-CD3 UCHT1 Alexa Fluor 700 *Biolegend, Inc*
Ab anti-CD4 RPA-T4 Pacific Blue *Biolegend, Inc*
Ab anti-CD8 RPA-T8 V500 *BD Bioscience*
Ab anti-CD8 RPA-T8 Alexa Fluor 700 *Biolegend, Inc*
Ab anti-CD56 MEM-188 R-PE *Biolegend, Inc*
Ab anti-CD69 FN50 PE/Cy7 *Biolegend, Inc*
Ab anti-CD25 BC96 PerCP/Cy5.5 *Biolegend, Inc*
Ab C92F3A-5 *Stressgen®, Enzo Life Sciences Inc*
Ab cmHsp70.1 *Multimmune Gmbh*
Ab Cy3 goat anti-rabbit *Jackson ImmunoResearch Inc*
Ab Cy3 rabbit anti-goat *Jackson ImmunoResearch Inc*
Ab HRP rabbit anti-mouse secondary *Dako UK Ltd*
Ab Mouse IgG1 Isotypes *Biolegend, Inc*
Ab Purified mouse anti-human Granzyme B primary *BD Biosciences*
Ab Purified mouse anti-LAMP1 *Biolegend, Inc*
Ab Purified mouse anti-phosphatidylserine 1H6 *Merck Millipore*
Ab Purified Mouse IgG *Invitrogen™, Life Technologies*
Ab Rab4a sc312 *Santa Cruz Biotechnology Inc*
Ab Rab5a sc309 *Santa Cruz Biotechnology Inc*
Ab Rab7 sc10767 *Santa Cruz Biotechnology Inc*
Ab Rab9a sc6562 *Santa Cruz Biotechnology Inc*
Ab Rab11 sc6565 *Santa Cruz Biotechnology Inc*
Ab Purified rabbit anti-LAMP2 *Sigma-Aldrich Co LLC*
Amersham Rainbow Marker *GE Healthcare Life Sciences*
Amicon Ultra Centrifugal filter tubes *Merck Millipore*
Ammonium sulphate *Sigma-Aldrich Co LLC*
Annexin V Alexa Fluor 647 *Biolegend, Inc*
ArC Beads *Molecular Probes®, Life Technologies*
BCA protein kit *Pierce™, Thermo Fisher Scientific Inc*
BD™ CompBeads *BD Biosciences*
Blotting Paper *GE Healthcare Life Sciences*
Bradford Solution *Sigma-Aldrich Co LLC*
Bromide Blue *Sigma-Aldrich Co LLC*
Calcium Chloride *Sigma-Aldrich Co LLC*
Caspase-3 Assay Kit *BD Biosciences*
Cell Fix *BD Biosciences*
Concanavalin A *Sigma-Aldrich Co LLC*
Cover Slip Removal Fluid *MatTek Corporation*
Culture Flasks *Sarstedt AG & Co*
Culture Medium – OptiMem *Life Technologies*
Culture Medium – RPMI 1640 *Lonza, Ltd*
Dimethyl sulfoxide *Sigma-Aldrich Co LLC*
Dynal Expander Beads *Life Technologies*
ECL Substrate *Pierce ™, Thermo Fisher Scientific Inc*
Enterokinase *Sigma-Aldrich Co LLC*
Ethanol *Thermo Fisher Scientific Inc*
Falcon tubes *BD Biosciences*
Film *GE Healthcare Life Sciences*
FIX & PERM® Cell permeabilisation kit *Life Technologies*
Foetal Bovine Serum *Lonza, Ltd*
Fucose *Sigma-Aldrich Co LLC*
Galactose *Sigma-Aldrich Co LLC*
Glucosamine *Sigma-Aldrich Co LLC*
Glucose *Sigma-Aldrich Co LLC*
Glycine *Sigma-Aldrich Co LLC*
HEPES *Sigma-Aldrich Co LLC*
HiTrap™ Heparin HP column *GE Healthcare Life Sciences*
HisTrap™ FF Nickel column *GE Healthcare Life Sciences*
Hydrogen Peroxide *Sigma-Aldrich Co LLC*
I-Glutamine *Lonza, Ltd*
Imidazole *Sigma-Aldrich Co LLC*
Lightning Link conjugation kits *Innova Bioscience Ltd*
Lithium-heparin vacutainer® tubes *BD Biosciences*
Live/Dead Cell Stain *Molecular Probes®, Life Technologies*
Lymphocyte Separation Medium 1077 *PAA Laboratories GmbH*
Lysis Buffer *BD Biosciences*
Magnesium Chloride *Sigma-Aldrich Co LLC*
Mannose *Sigma-Aldrich Co LLC*
Methanol *Thermo Fisher Scientific Inc*
Microfuge Tubes *Sarstedt AG & Co*
Microscopy Slides *VWR International*
Milk Powder *Co-operative Group Ltd*
MitoID ™®Red *Enzo Life Sciences Inc*
MitoTracker ®Green *Molecular Probes®, Life Technologies*
Mouse Serum *Sigma-Aldrich Co LLC*
N-acetyl-Ile-Glu-Pro-Asp-p-nitroanilide *Merck KGaA*
N-acetyl neuraminic acid *Sigma-Aldrich Co LLC*
Nail varnish *Boots plc*
Needles *Terumo Medical Corporation*
NycoPrep™ 1.077 *Axis-Shield plc*
Paraformaldehyde *Sigma-Aldrich Co LLC*
PBS *Lonza, Ltd*
Penicillin *Lonza, Ltd*
Peptide NGLTLKNDFSRLEG *EMC Microcollections*
Peptide TKDNNLLGRFELSG *EMC Microcollections*
Propidium Iodide *Sigma-Aldrich Co LLC*
PVDF membrane *GE Healthcare Life Sciences*
Radi-Blue dye *BioRad Laboratories Ltd*
Scalpels *Swann Morton*
SFCA filter *Nalgene™, Thermo Fisher Scientific Inc*
Sodium chloride *Sigma-Aldrich Co LLC*
Sodium dodecyl sulphate *Sigma-Aldrich Co LLC*
Sodium Pyruvate *Sigma-Aldrich Co LLC*
Streptomycin *Lonza, Ltd*
Suppression Inspector Beads *Miltenyi Biotec Ltd*
Syringes *Terumo Medical Corporation*
Tris-HCl *Sigma-Aldrich Co LLC*
Trypan Blue *Sigma-Aldrich Co LLC*
Trypsin-EDTA *Lonza, Ltd*
Tween *Sigma-Aldrich Co LLC*
VECTASHIELD mounting medium with DAPI *Vector Laboratories*
Zeocin *InvivoGen*

ii. Publications arising from data herein

A novel expression and purification system for the production of enzymatic and biologically active human granzyme B

Gehrmann, M, Doss, B. T, Wagner, M, Zettlitz, K. A, Kontermann, R. E, .Foulds, G, Pockley, A. G, Multhoff, G. *J Immunol Methods 2011 371 (1-2) 8-17*

The serine protease granzyme B (grB) has previously been shown to induce perforin-independent apoptosis in membrane Hsp70 positive tumor cells in a number of in vitro experimental systems. Ongoing studies that are investigating the in vivo relevance of these findings by assessing the therapeutic potential of grB in a human xenograft tumor mouse model required the development of an expression system for the production of high yields of enzymatic and biologically active human grB. In order to maintain potentially important posttranslational modifications that occur in mammalian cells, human embryonal kidney cells (HEK293) were stably transfected with human grB. The HEK293 host cells were protected from apoptotic cell death by fusing an inactivation site coupled to a (His)(6) tag to the gene sequence of GrB. Inactive grB which was actively released from HEK293 cells by insertion of a Igkappa leader sequence was purified on a nickel column utilizing the (His)(6) tag. After enterokinase digestion and heparin affinity chromatography, high yields of enzymatic and biologically active human grB were obtained. The perforin-independent interaction of grB with membrane Hsp70 positive tumor cells appeared to be associated with mammalian glycosylation and mediated by the oligosaccharide moiety of neuraminic acid (NANA).

Immunotherapeutic targeting of membrane Hsp70-expressing tumors using recombinant human granzyme B

Gehrmann, M, Stangl, S, Kirschner, A, Foulds, G. A, Sievert, W, Doss, B. T, Walch, A, Pockley, A. G, Multhoff, G. *PLoS One 2012 7(7) e41341*

BACKGROUND: We have previously reported that human recombinant granzyme B (grB) mediates apoptosis in membrane heat shock protein 70 (Hsp70)-positive tumor cells in a perforin-independent manner. METHODOLOGY/PRINCIPAL FINDINGS: Optical imaging of uptake kinetics revealed co-localization of grB with recycling endosomes (Rab9/11) as early as 5 min after internalization, with late endosomes (Rab7) after 30 min, and the lysosomal compartment (LAMP1/2) after 60 to 120 min. Active caspase-3-mediated apoptosis was induced in mouse CT26 monolayer cells and 3D tumor spheroids, but not in normal mouse endothelial cells. Granzyme B selectively reduced the proportion of membrane Hsp70-positive cells in CT26 tumor spheroids. Consecutive i.v. injections of recombinant human grB into mice bearing membrane Hsp70-positive CT26 tumors resulted in significant tumor suppression, and a detailed inspection of normal mouse organs revealed that the administration of anti-tumoral concentrations of grB elicited no clinicopathological changes. CONCLUSIONS/SIGNIFICANCE: These findings support the future clinical evaluation of human grB as a potential adjuvant therapeutic agent, especially for treating immunosuppressed patients that bear membrane Hsp70-positive tumors.

Tumor imaging and targeting potential of an Hsp70-derived 14-mer peptide

Gehrmann, M, Stangl, S, Foulds, G. A, Oellinger, R, Breuninger, S, Rad, R, Pockley, A. G, Multhoff, G. *PLoS One 2014 9 (8) e105344*

BACKGROUND: We have previously used a unique mouse monoclonal antibody cmHsp70.1 to demonstrate the selective presence of a membrane-bound form of Hsp70 (memHsp70) on a variety of leukemia cells and on single cell suspensions derived from solid tumors of different entities, but not on non-transformed cells or cells from corresponding 'healthy' tissue. This antibody can be used to image tumors in vivo and target them for antibody-dependent cellular cytotoxicity. Tumor-specific expression of memHsp70 therefore has the potential to be exploited for theranostic purposes. Given the advantages of peptides as imaging and targeting agents, this study assessed whether a 14-mer tumor penetrating peptide (TPP; TKDNNLLGRFELSG), the sequence of which is derived from the oligomerization domain of Hsp70 which is expressed on the cell surface of tumor cells, can also be used for targeting membrane Hsp70 positive (memHsp70+) tumor cells, in vitro. METHODOLOGY/PRINCIPAL FINDINGS: The specificity of carboxy-fluorescein (CF-) labeled TPP (TPP) to Hsp70 was proven in an Hsp70 knockout mammary tumor cell system. TPP specifically binds to different memHsp70+ mouse and human tumor cell lines and is rapidly taken up via endosomes. Two to four-fold higher levels of CF-labeled TPP were detected in MCF7 (82% memHsp70+) and MDA-MB-231 (75% memHsp70+) cells compared to T47D cells (29% memHsp70+) that exhibit a lower Hsp70 membrane positivity. After 90 min incubation, TPP co-localized with mitochondrial membranes in memHsp70+ tumors. Although there was no evidence that any given vesicle population was specifically localized, fluorophore-labeled cmHsp70.1 antibody and TPP preferentially accumulated in the proximity of the adherent surface of cultured cells. These findings suggest a potential association between membrane Hsp70 expression and cytoskeletal elements that are involved in adherence, the establishment of intercellular synapses and/or membrane reorganization. CONCLUSIONS/SIGNIFICANCE: This study demonstrates the specific binding and rapid internalization of TPP by tumor cells with a memHsp70+ phenotype. TPP might therefore have potential for targeting and imaging the large proportion of tumors (approximately 50%) that express memHsp70.